NATIONAL AERONAUTICS AND SPACE ADMINISTRATION

MSC APOLLO 13 INVESTIGATION TEAM

PANEL 1

SPACECRAFT INCIDENT INVESTIGATION

VOLUME III

SPECIAL ANALYSES AND TESTS IN SUPPORT OF INVESTIGATION

SEPTEMBER 1970

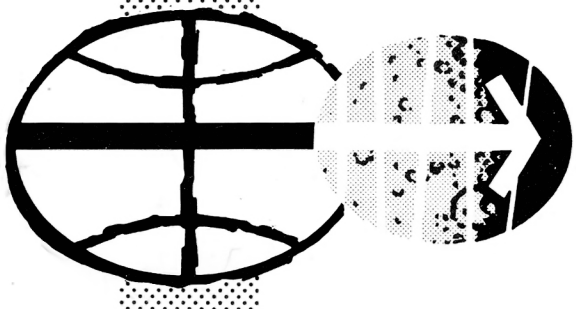

MANNED SPACECRAFT CENTER
HOUSTON, TEXAS

MSC APOLLO 13 INVESTIGATION TEAM

FINAL REPORT

PANEL 1

SPACECRAFT INCIDENT INVESTIGATION

September 1970

VOLUME III

REPORTS OF ANALYSES AND TESTS PERFORMED IN SUPPORT OF THE CRYOGENIC OXYGEN TANK 2 ANOMALY INVESTIGATION

APPROVED BY

Donald D. Arabian
Chief, Test Division

NATIONAL AERONAUTICS AND SPACE ADMINISTRATION
MANNED SPACECRAFT CENTER
HOUSTON, TEXAS

TABLE OF CONTENTS

TABLE OF CONTENTS

Preface

Part A summarizes the various analysis tasks performed during the course of the investigation in areas related to thermodynamics, heat transfer, and fluid flow. Of the many analyses performed in support of the investigation, only the most pertinent are included in this report.

It must be emphasized that these analyses are very preliminary in nature, being performed in most cases on extremely short notice. As such, any information derived from them should be taken in this context and any conclusions drawn should also be influenced by tests performed subsequent to these analyses.

Part B summarizes the various tests performed during the course of the investigation of the Apollo 13 cryogenic oxygen tank anomaly. The complete test evaluation reports may be obtained from the Apollo Test Division, PT2, Manned Spacecraft Center, Houston, Texas 77058.

PART A

REPORTS OF ANALYSES PERFORMED IN SUPPORT OF THE CRYOGENIC OXYGEN TANK 2 ANOMALY INVESTIGATION

A.1 THERMODYNAMIC ANALYSIS OF APOLLO 13 OXYGEN TANK 2 PRESSURE VESSEL BASED ON HOT-GAS EXPULSION MODEL

A.1.1 Statement of Problem

A thermodynamic analysis is required to describe the stratification phenomenon occurring in oxygen tank 2 between 55:53:21 and 55:54:53. More specifically, it is required to:

(a) Calculate the total heat input and heat input rates required to produce the observed pressure trace

(b) Calculate the hot-gas volumes and masses required for the observed pressure trace (as a function of assumed hot-gas temperatures)

(c) Determine whether or not a premature opening of the relief valve at 955 psia could have occurred to produce the relatively flat (4 psi/15 sec) pressure plateau at the beginning of region II

(d) Using an extrapolated heat rate at the beginning of region III, determine the expulsion rate required to produce the observed pressure decay.

A.1.2 Description of Analytical Model and Assumptions

The formulation of the analytical model was based on the existence of a heat source within the tank, located in the upper region of the capacitance probe. In the absence of a gravity field, this heat source creates a localized hot-gas mass in the fluid-exit region of the tank, which grows with the addition of heat and contracts with fluid expulsion from the tank. In the event the hot-gas mass becomes completely exhausted, cold fluid begins flowing from the tank.

Two thermodynamic boundaries are considered in the analysis. One is the interface between the hot-gas mass and the cold fluid; the other is

the pressure-vessel inside wall. For analytical purposes, a distinct interface is assumed between the hot and cold fluids. It is assumed that the hot-gas mass is at a constant temperature and is thermally insulated from the bulk cold fluid; therefore, a sharp temperature gradient exists between the stratified gas mass and the cold fluid. Due to the low thermal conductivity of supercritical oxygen under these conditions of temperature and pressure and the short times involved (less than 100 seconds) this assumption is reasonable. To further illustrate this point, figure A.1-1 shows the temperature distribution as a function of time through an idealized wall of supercritical oxygen, as calculated from the error function solution of Schneider (ref. 1). It is seen from figure A.1-1 that for a 347-degree temperature difference between the heat source and the cold fluid at a pressure of 900 psia, after 5 minutes 90 percent of the temperature drop in the fluid takes place less than 1/2-inch from the heat source.

The internal heat (ignition) source within the hot-gas mass causes mass to be transferred into the hot-gas region from the cold bulk fluid. The ignition heat source heats the cold fluid from cryogen temperature to "flame" or hot-gas temperature. The cryogenic temperature is known, but a hot-gas temperature must be assumed. This temperature then becomes a parameter in the study.

Mass leaves the hot-gas region via expulsion through the system supply line. Since the hot-gas mass is assumed to be at the top of the tank in the exit region, this gas mass must be completely exhausted before cold fluid can flow out of the tank. Pressure equilibrium between the hot and cold regions is assumed at all times. Mass diffusion between the hot-and cold-gas regions is not considered in the analysis.

Assumed thermodynamic processes for the two regions are as follows: the hot-gas mass expands and contracts isothermally; the cold gas (bulk fluid) expands and contracts isentropically.

Figure A.1-2 shows a mechanical analog of the system model. The hot-gas and cold-gas regions are separated by a piston which moves to the left or right depending on whether the hot-gas mass is contracting or expanding. In the event the hot gas is totally depleted, cold gas then is expelled from the tank. This can only happen if the growth rate of the hot-gas mass falls below the tank explulsion rate and remains there for a long period of time. If burning continues after the hot gas is exhausted, the heat released in the combustion process merely heats the cold gas as it leaves the tank. At the opposite extreme, for very large burn rates the hot-gas mass could conceivably grow until it occupies the entire volume of the tank.

A.1.3 Analysis

In order to handle the tedious computations involved in calculating heat input rates and stratified hot-gas mass growth histories, a machine program was developed for the case of hot-gas expulsion. The logic chart for this program is shown in figure A.1-3. Inputs to the program are the relief valve flow characteristic as a function of temperature, tank 2 pressure profile for regions I, II, and III, normal usage flow profile, maximum time, and other miscellaneous data (these are all punched-card inputs). Oxygen property data (ref. 2) was stored on a magnetic tape and was input to the machine with a calling routine which assembled the data into pressure and temperature vectors, with their associated entropy, enthalpy, internal energy, and specific volume arrays.

After all data are read in, the fluid property data are then printed for post-execution reference. The machine begins the computation procedure by setting a flame or hot-gas temperature, and initializing tank conditions (time, flow rates, mass of supercritical oxygen, tank volume, etc.). Pressure vessel volume variations are accounted for as a function of pressure at cryogenic temperature from expansion and contraction data (ref 3). Hot-gas temperature is a parameter in the analysis. Computations are performed in small time increments for the input pressure

profile throughout regions I and II. In the event the pressure begins to drop, the program switches to the logic branch for region III. A linear interpolation subroutine ("ULOOK") then calculates an initial pressure from the elements of the pressure-time array, and from this, a final pressure for the incremental time step is obtained. The same interpolation routine is then used for table lookup of the system flow rate. Leak rates can be introduced in addition to normal flows at the region II pressure plateau, if desired. Knowing an initial pressure and temperature for that time step and a final pressure, subroutine "ISEN" is called to compute cold-gas fluid properties at the initial and final thermodynamic states for isentropic compression (or expansion). Initial properties are calculated using a bi-variate linear interpolation subroutine (independent variables are pressure and temperature). Knowing the initial entropy and holding this constant, a final temperature for the isentropic compression (or expansion) is computed using a Newton-Raphson iterative convergence technique (ref. 4) embodied in a subroutine named "RNEWT." Computation then returns to the subroutine "BIVINT," where properties (s, h, u, and v) are computed for the final state (p_f) using the isentropic final temperature T_f calculated in "RNEWT." Then, with all initial and final properties known, control returns to the main program, where a new hot-gas mass and volume are calculated, along with heat input rates, cumulative heat input to the hot-gas mass, total cumulative energy released at the ignition source, etc. The total energy released will be somewhat higher when the mass of the stratified hot-gas mass is not neglected, as is the case in this analysis. Other analyses, neglecting the mass of the hot gas, have resulted in energies of less than 50 percent of those computed in this analysis.

The calculation procedure is then repeated for a new time (pressure) step, and this continues until the new pressure is less than that of the previous step. This signifies the beginning of region III, and at this pressure (approximately 1008 psia), the relief valve opens, and the flow from this valve (a function of hot-gas temperature) is added to the normal

usage profile. The calculated flow from the ideal gas law for an orifice diameter of 0.038 inch and an orifice coefficient of 1 is shown in figure A.1-4. Two test data points from a test at the Manned Spacecraft Center are also shown in this figure, as well as three test points from the Parker test.

For region III calculations, a linear extrapolated heat release rate is used throughout region III and is based on the heat input at the end of region II and 10 seconds prior to that point. Blowdown times for chosen pressure are calculated within this logic branch, and in this manner a blowdown profile is generated for any assumed hot-gas temperature which can be compared to the flight data. Computation stops when either the maximum time is reached or the hot-gas mass is completely expelled from the tank.

A.1.4 Results and Conclusions

The results of analysis runs with the program are summarized in figures A.1-5, A.1-6, and A.1-7.

Figure A.1-5 shows the flight data pressure profile for regions I, II, and III and below that the growth history of the hot-gas volume, as well as the total heat input for regions I and II. This case was run for a normal usage flow rate of 1.5 lb/hr. The effects of flame temperature are to decrease the volume of hot gas within the tank as the flame temperature increases and to increase with increasing flame temperature the total heat input required to maintain the flight pressure trace. For a nominal 1200° F flame temperature the total heat input to the tank at the end of region II is approximately 35 Btu. This corresponds to a hot-gas volume of about 46 in^3. It should be emphasized that these calculations are for hot-gas expulsion only, and the expulsion of cold gas would require significantly less heat.

The left-hand curve of figure A.1-6 shows maximum possible leak rates at the region II pressure plateau as a function of flame temperature. For

comparison, the relief valve characteristic is again shown. This plot indicates that the relief valve could not have been in a full-open position during the time period of the pressure plateau if hot gas were being expelled from the tank, since the maximum possible expulsion rate to maintain the flight pressure trace is at all temperatures below the relief valve capability.

Figure A.1-7 shows the results of the region III blowdown analysis. The shaded squares are flight data, and the solid curves indicate that even a very low-temperature hot-gas mass would have been expelled by the relief valve (had it opened) much faster than the flight pressure trace indicated.

REFERENCES

1. Conduction Heat Transfer, by P. J. Schneider, Addison-Wesley, 1957, pp. 240-243.

2. "Thermodynamic and Related Properties of Oxygen from the Triple Point to 300 K at Pressures to 330 Atmospheres - Supplement A (British Units)," by L. A. Weber; NBS Report 9710 A; August 29, 1968.

3. Apollo Fuel Cell and Cryogenic Gas Storage System Flight Support Handbook, prepared by Propulsion and Power Division, Manned Spacecraft Center; February 18, 1970, pp. 7-59.

4. Applied Numerical Methods, Vol. I, by Carnahan, Luther, and Wilkes; Wiley, 1964, pp. 213-216.

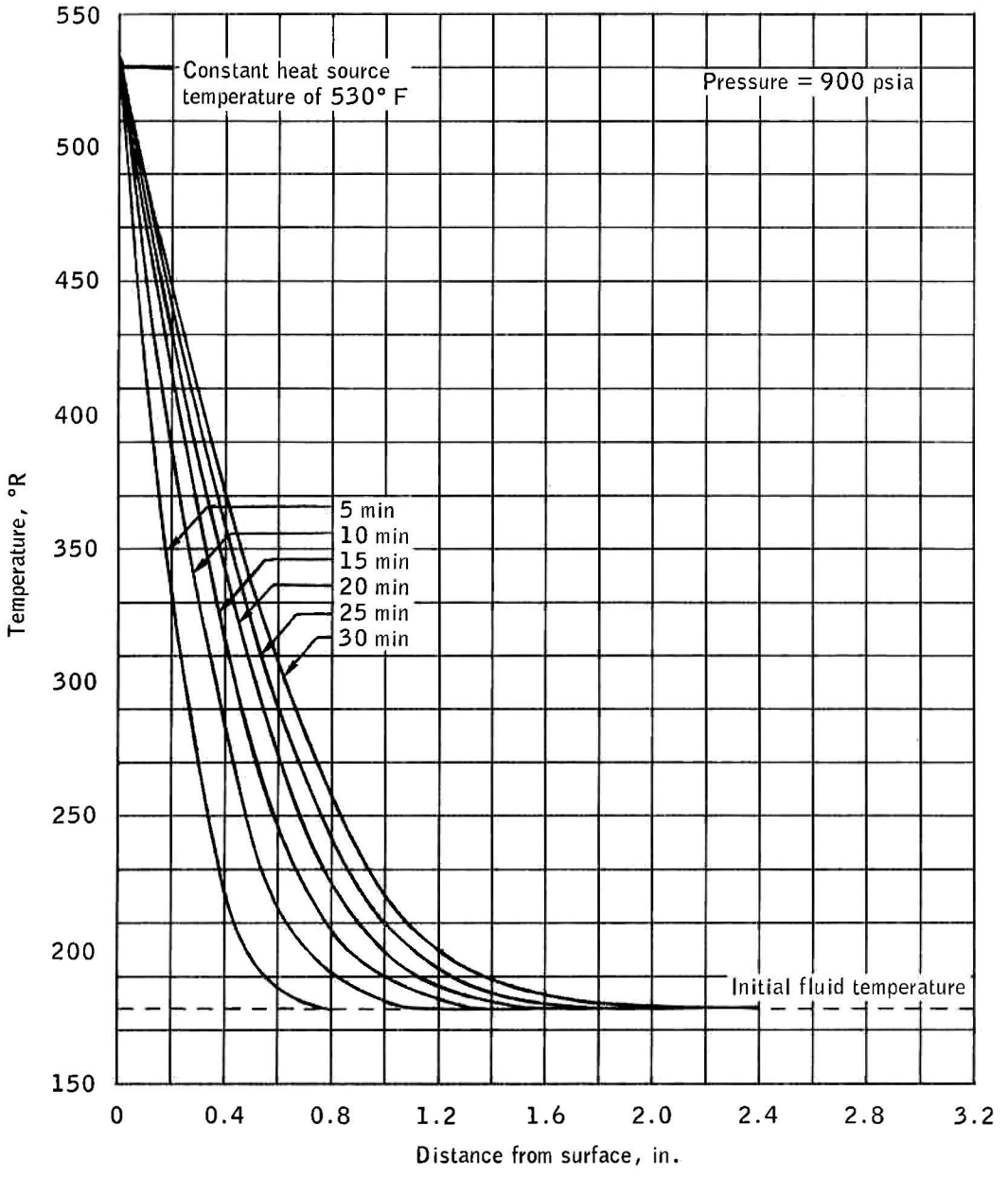

Figure A.1-1.- Temperature distribution in oxygen near a heated wall.

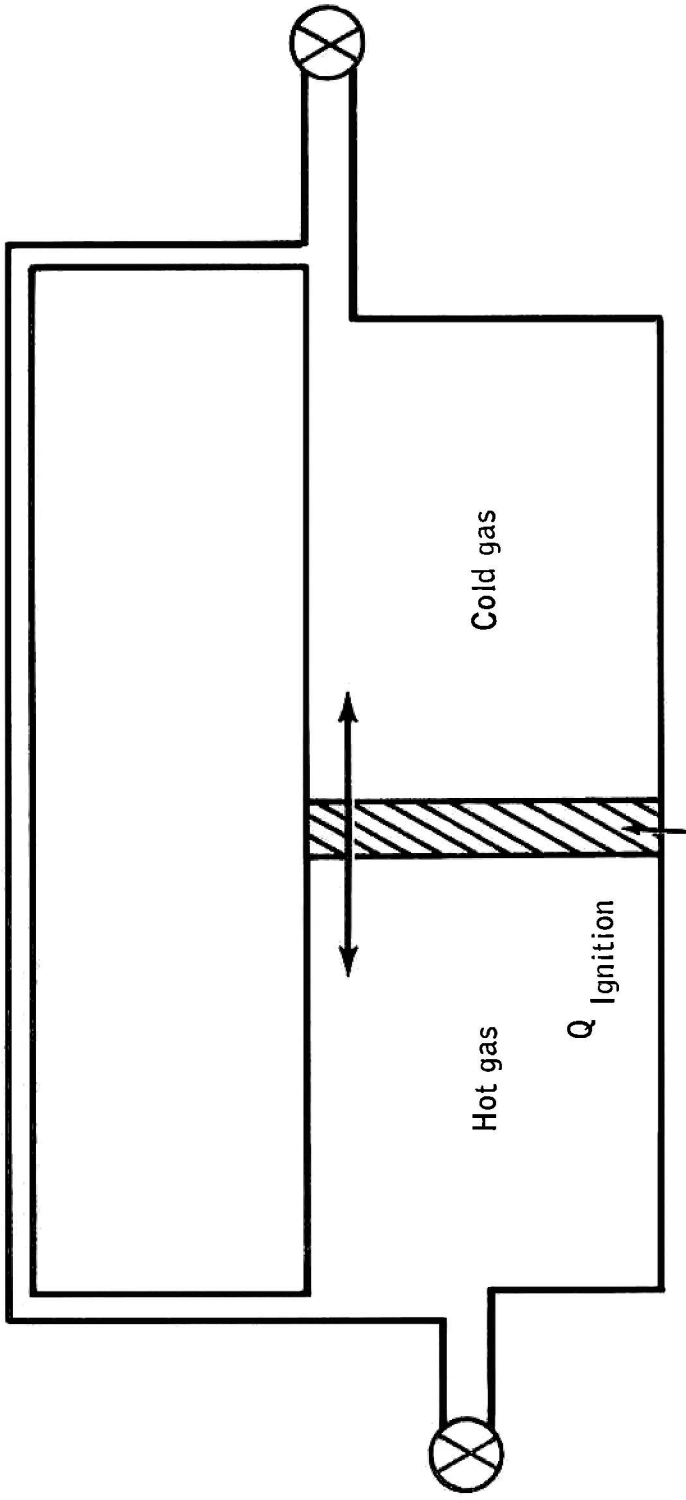

Figure A.1.2.- Mechanical analog.

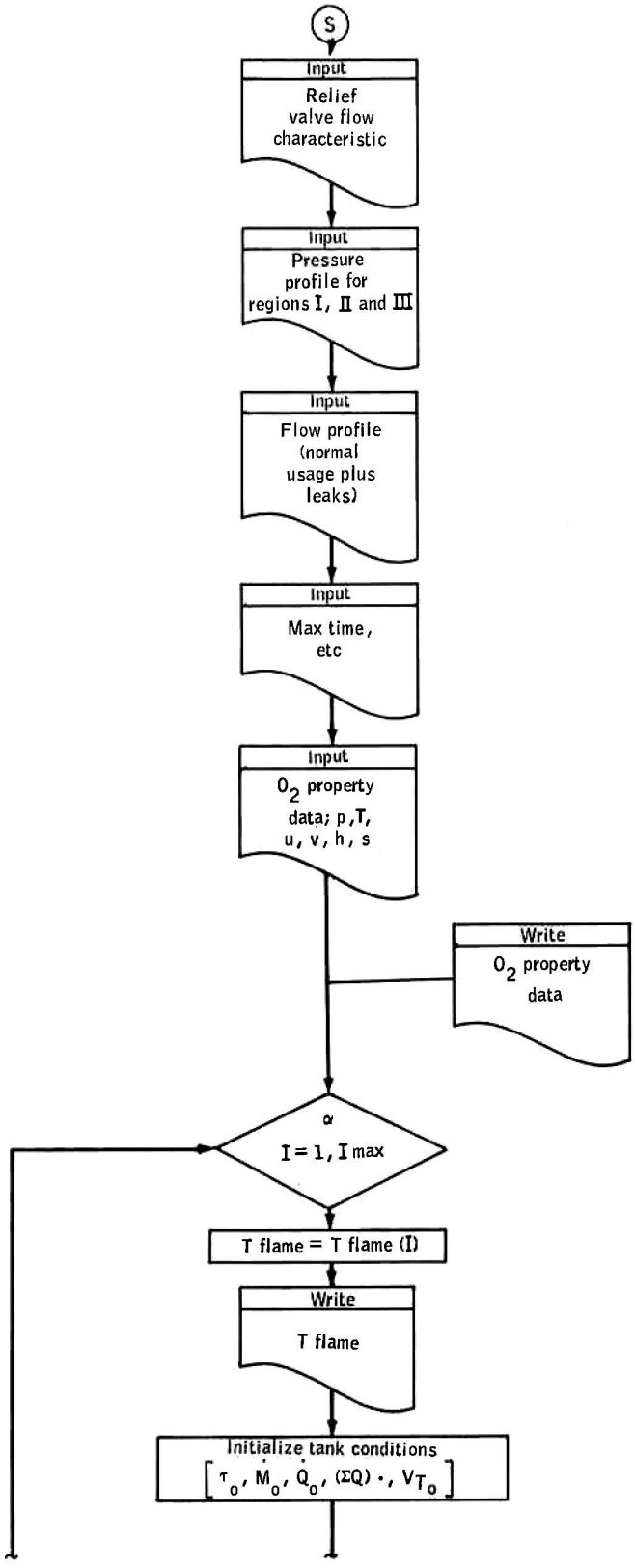

Figure A.1-3.- Logic chart.

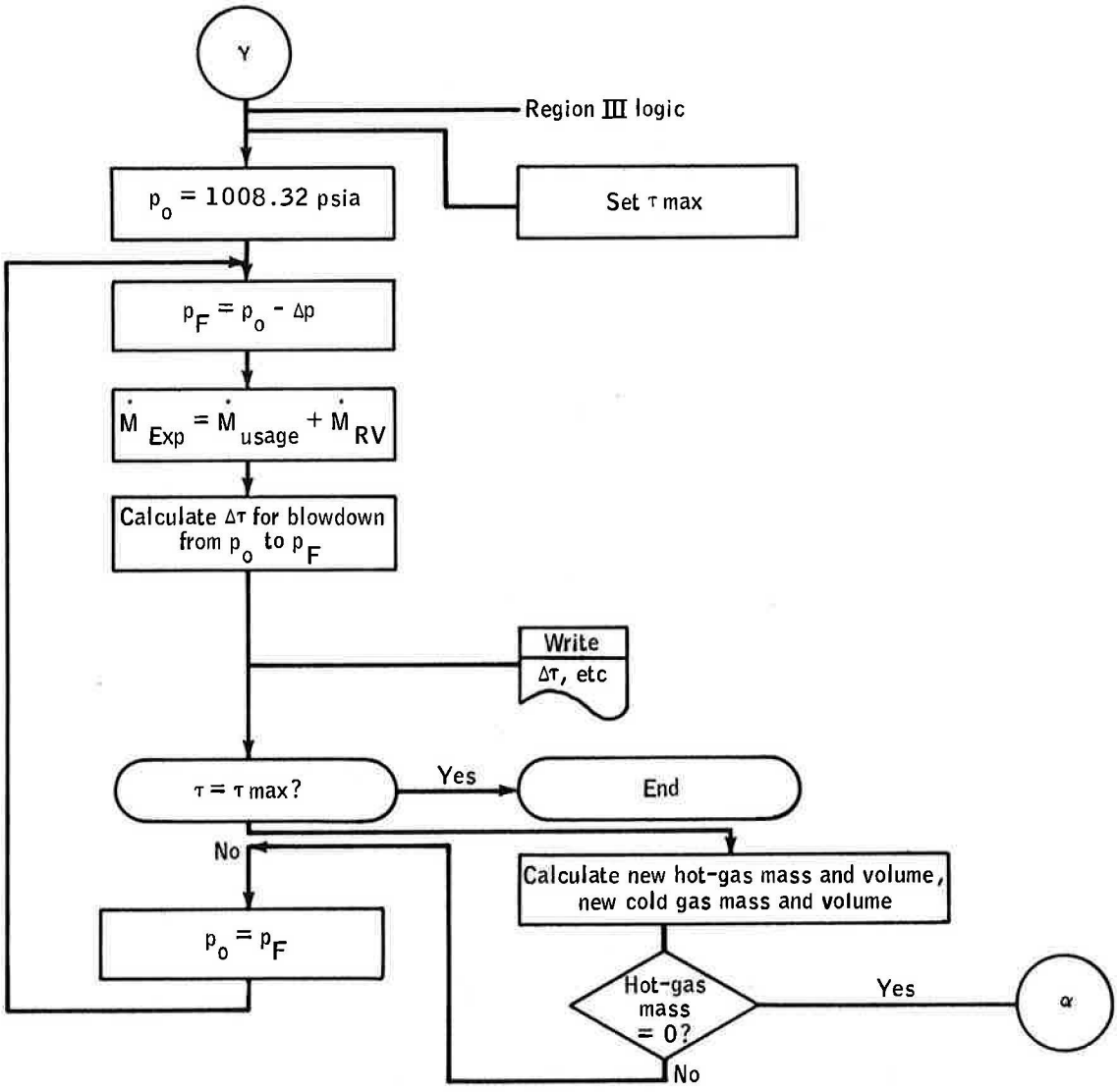

Figure A.1-3.- Continued.

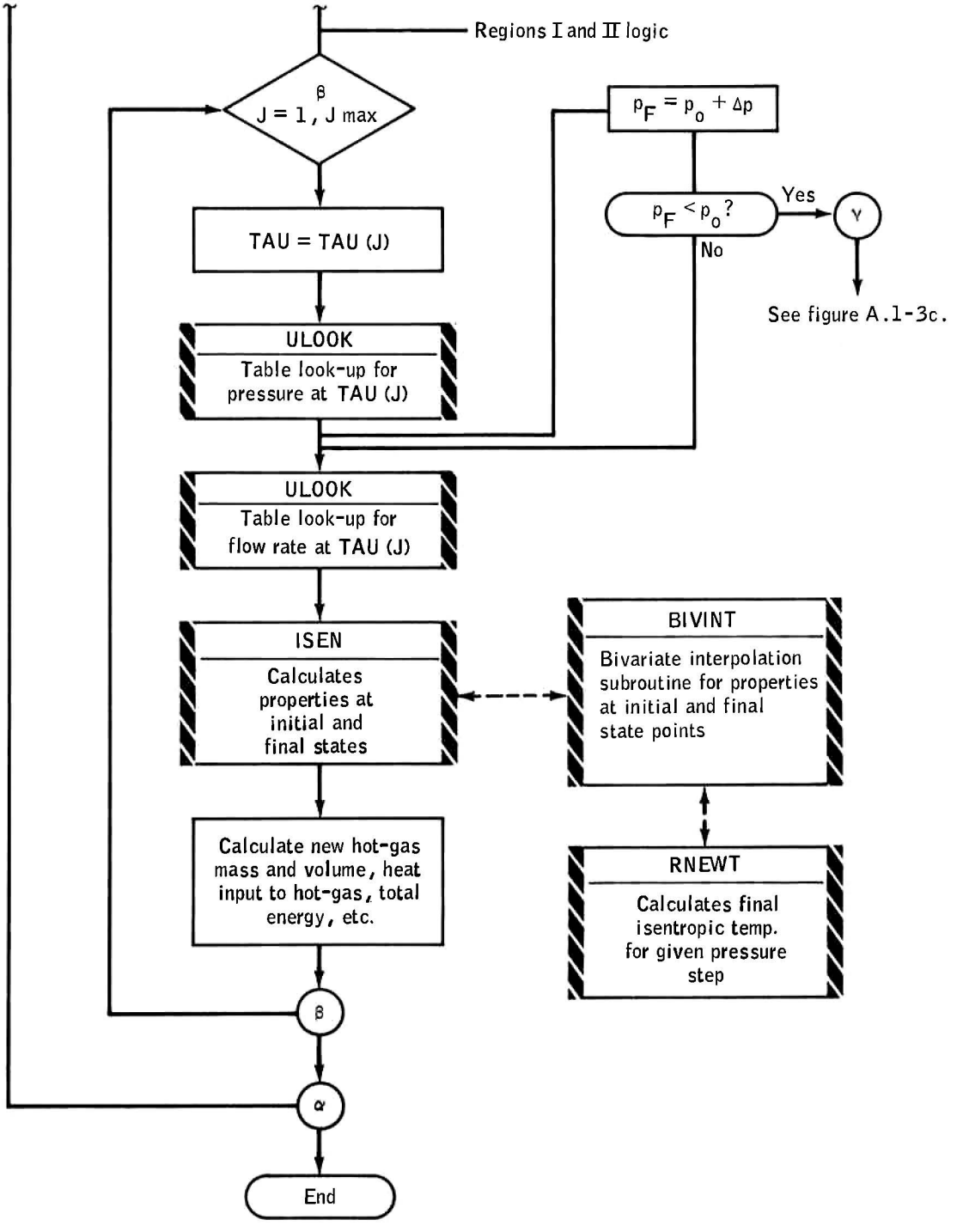

Figure A.1-3.- Concluded.

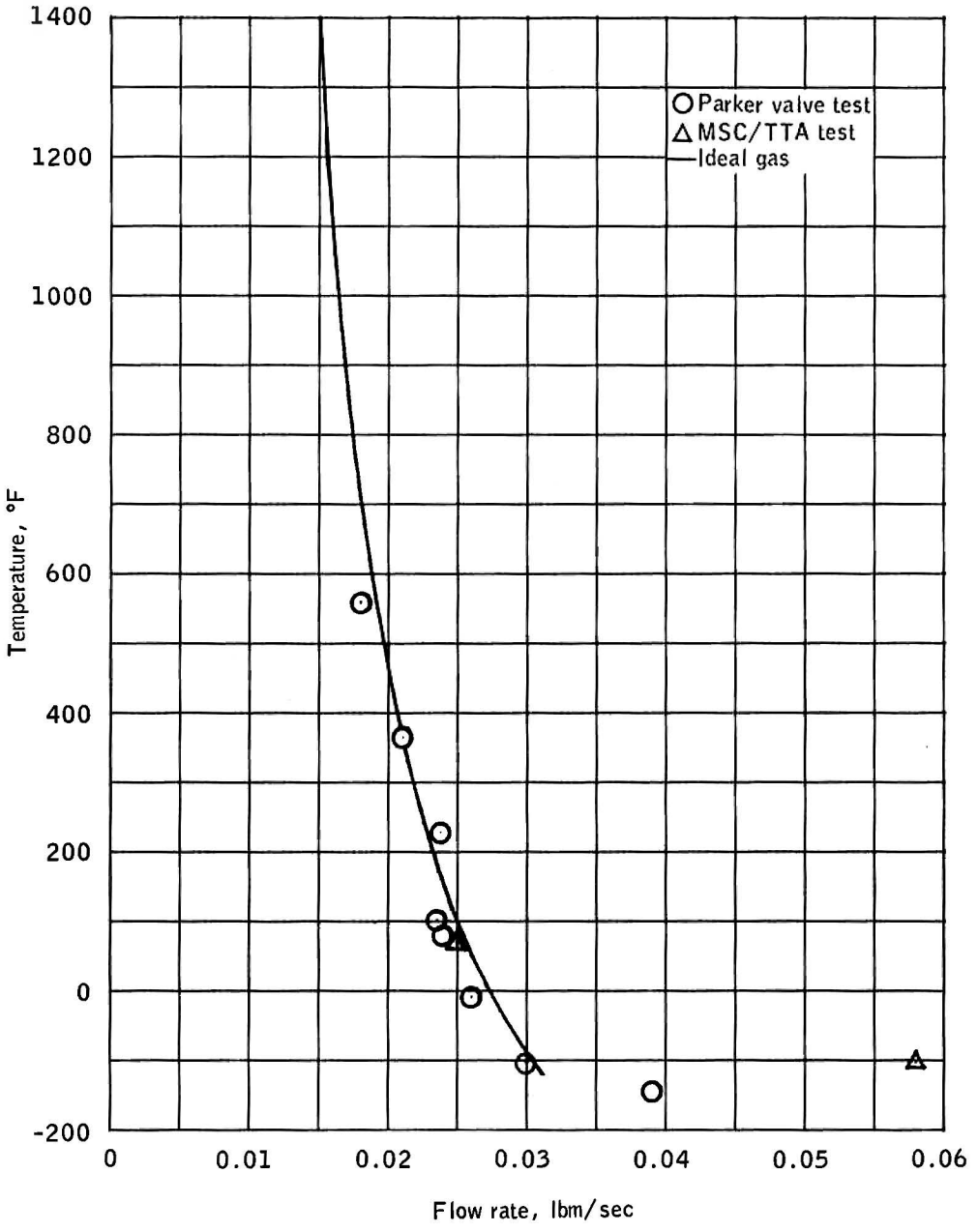

Figure A.1-4.- Oxygen relief valve flow rate as a function of inlet gas temperature.

NASA-S-70-2954

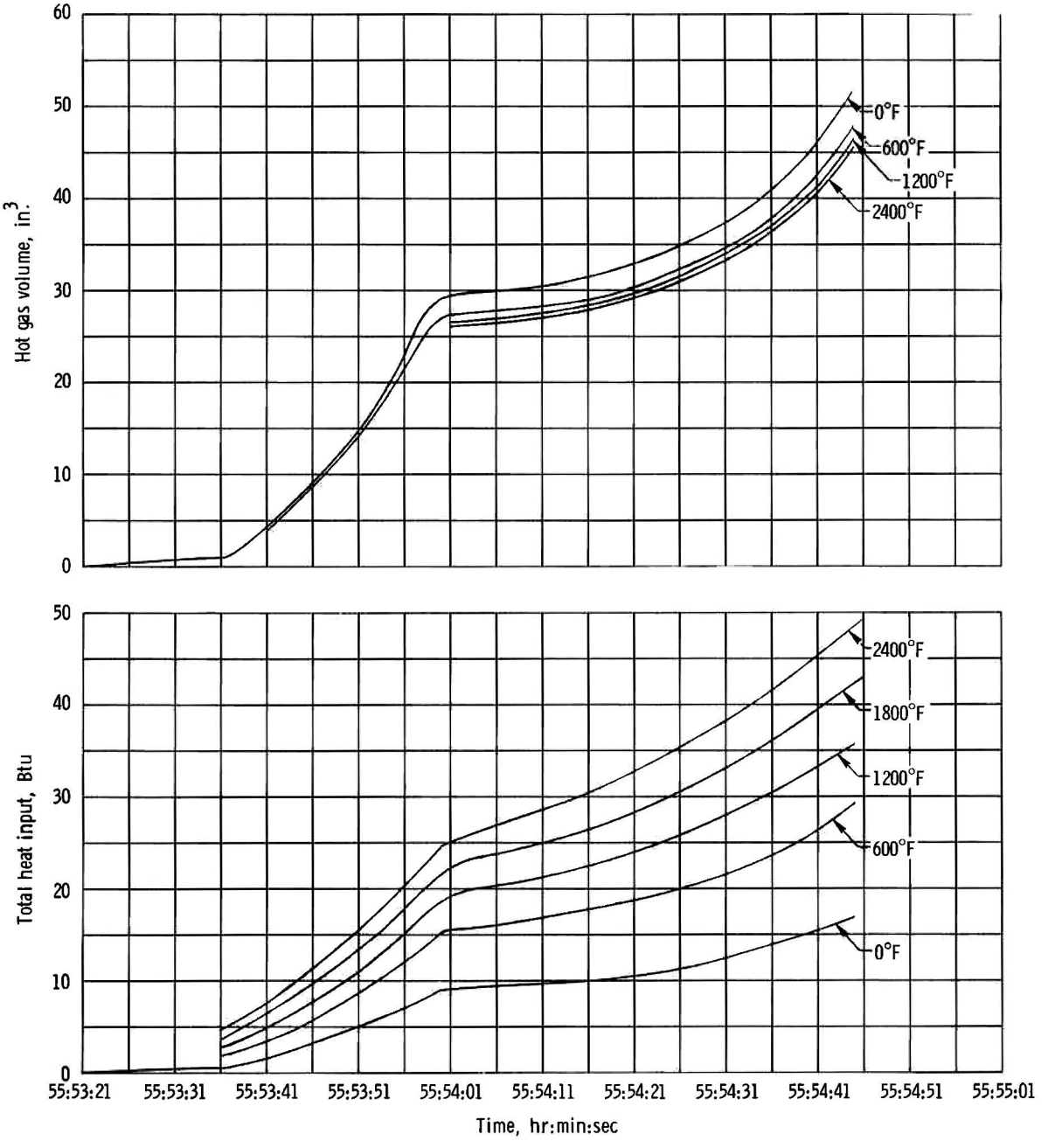

Figure A.1-5. - Computed total heat input and hot gas volume.

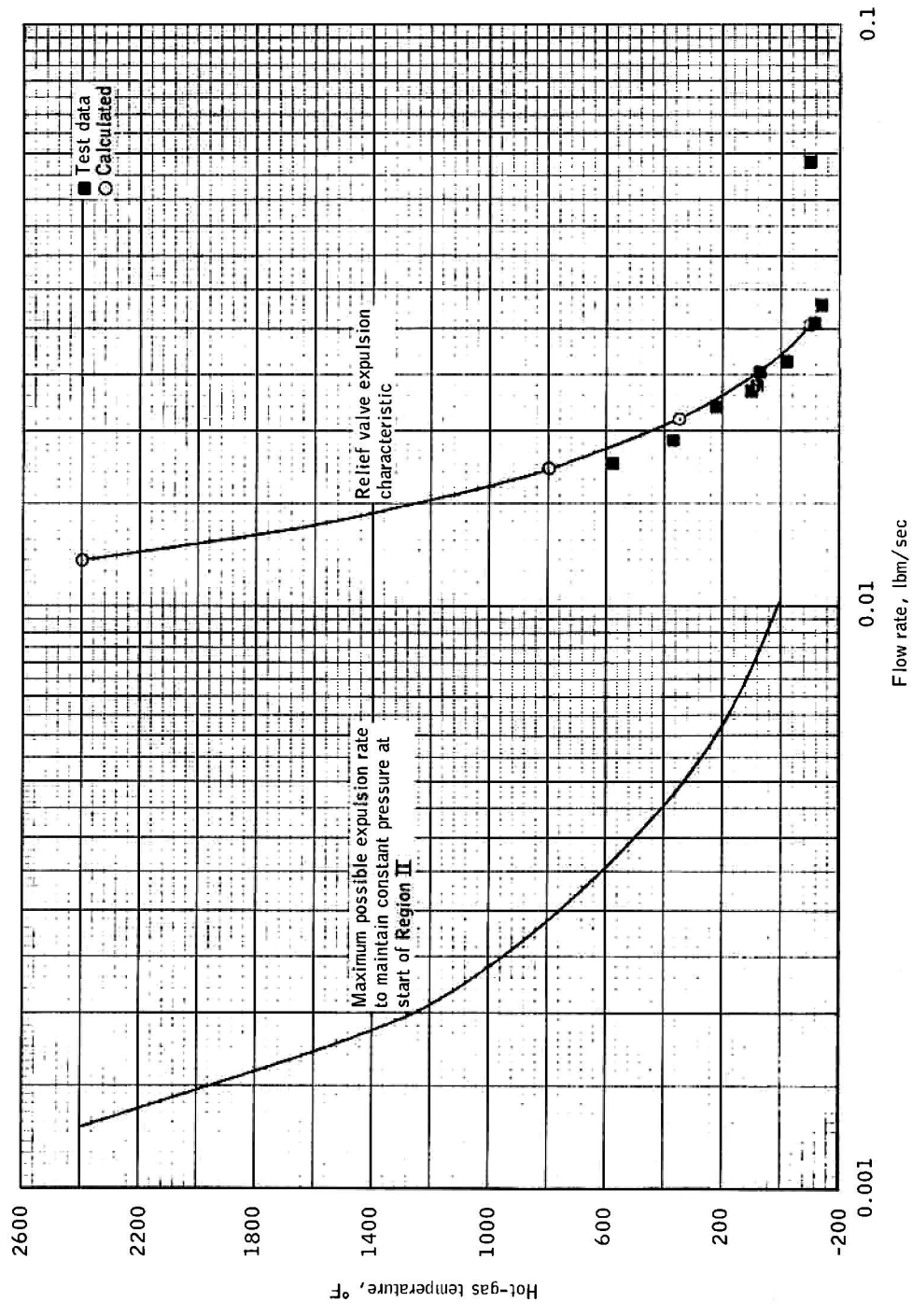

Figure A.1-6.- Region II relief valve analysis.

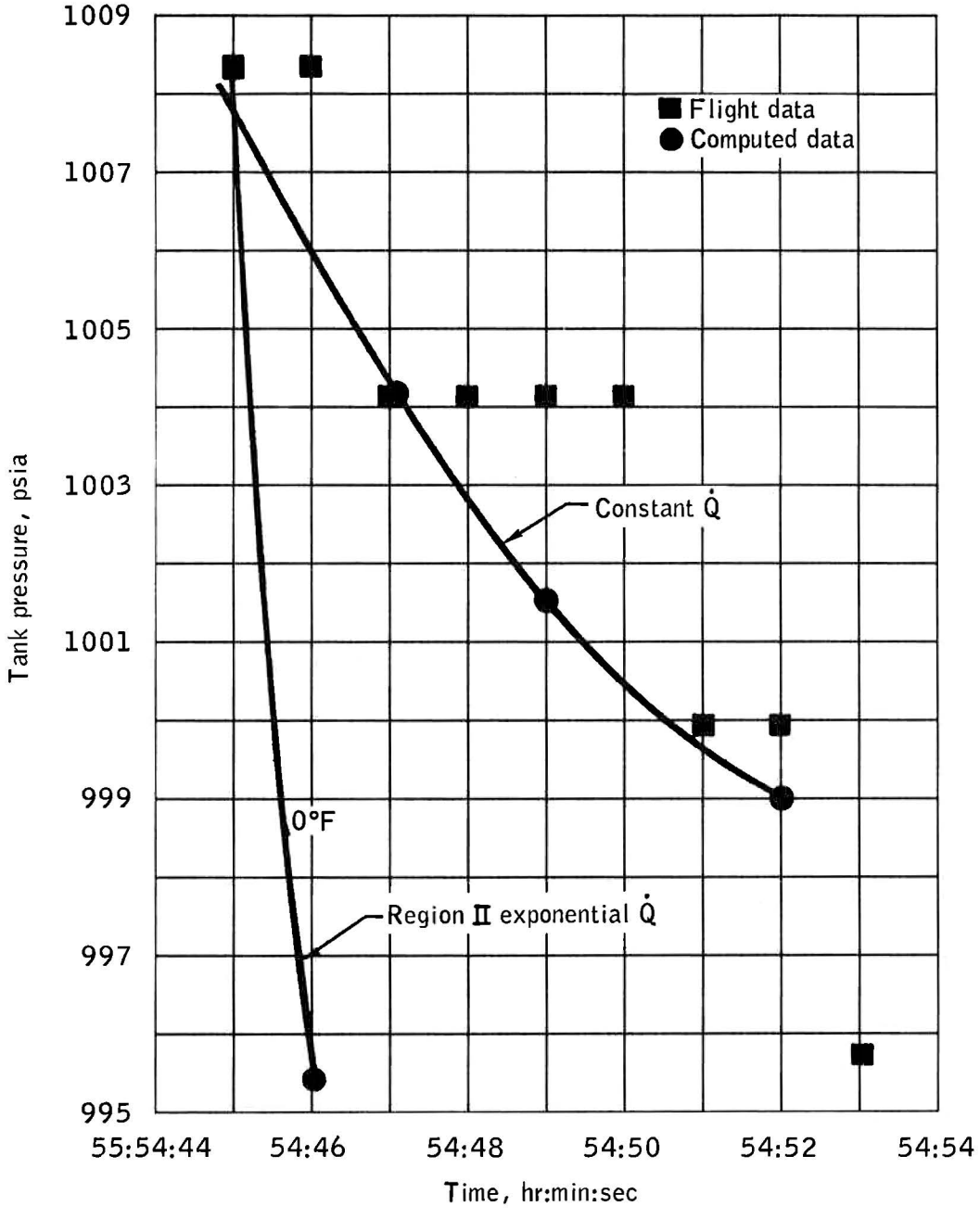

Figure A.1-7.- Relief valve response in region III.

A.2 THERMODYNAMIC RESTRICTIONS ON ENERGY PROCESSES IN THE APOLLO 13 CRYOGENIC OXYGEN TANK 2

A.2.1 Purpose

The purpose of this analysis is to specify the limitations on energy processes which may have occurred in the Apollo 13 cryogenic oxygen tank 2 prior to the incident of apparent tank failure. The limitations are established on the basis of thermodynamics and the recorded pressure history. The primary conclusion of this analysis is that the electrical energy supplied to the tank is insufficient to explain the pressure rise and that therefore a chemical reaction must have occurred within the tank. It is felt that the mechanism for initiation of potential chemical reactions requires experimental verification at simulated conditions.

A.2.2 Assumption

The pressure data during the time of interest are shown in figure A.2-1. It has been assumed on the basis of available information that this pressure history corresponds to the tank pressure.

A.2.3 Analysis and Results

The maximum and minimum energy addition to the fluid is shown as a function of time in figure A.2-2. These calculations include nominal heat leakage and nominal oxygen usage from tank 2 and also the work of the fluid on the tank as the tank expands. The mass at time t_o was taken as 242 pounds of oxygen and the calculations on figure A.2-2 neglect any potential fluid leakage. The minimum energy addition was obtained by assuming that the energy was supplied through a point source, zero mass bubble of fluid. This bubble of fluid then expands, compressing the bulk of the fluid isentropically. The maximum energy addition requires that the fluid is uniformly heated. The real case is bounded by these two

extremes, depending on the volume of the reacting gas, the chemical composition, the degree of mixing, the extent of internal heat transfer, the geometry of the reaction zone and the detailed gas dynamics of the fluid mixture.

The explicit influence of the reaction zone, or bubble mass is depicted in figure A.2-3. Input energies required for these bubbles are normalized with respect to the constant density thermodynamic process, and the bubble masses are normalized by the total fluid mass. The basic conclusion to be drawn from this figure is that the efficiency of compression increases as the bubble size decreases. The limiting case is, of course, the point source isentropic compression previously described.

Figure A.2-4 shows the average bubble temperature which corresponds to the range of bubble sizes just considered. Here it is noted that as the bubble size decreases, the temperature required to carry out the prescribed compression increases.

Due to the short compression times experienced during this incident, a relatively small mass of the compressed fluid will be heated by the relatively hot bubble. Therefore, the vast majority at the fluid experiences a near isentropic compression. Thus, the actual compression process will be near the isentropic energy limit history proposed in figure A.2-2. A detailed heat transfer analysis for a proposed heat source is required in order to establish the actual energy history.

The energy addition rates associated with the two thermodynamic processes are shown in figure A.2-5. At the times T_2 and T_5, there are rapid drops in the rate of energy addition. The calculations to this point have neglected mass loss above the level of a nominal usage rate; however, the rapid change in energy addition rate could be explained by a mass loss. If the energy addition rates are extrapolated exponentially as shown in figure A.2-5, the maximum resulting mass loss rate requirement can be obtained from an energy balance. The maximum mass loss rates for times T_2 and T_5 are shown in figure A.2-6 and A.2-7, respectively, for the two

limiting thermodynamic processes. It is noted that, for the isentropic energy addition case, the required flow rates are comparable to the calculated capability of the vent valve. In addition, if the gas flowing out of the tank is at a higher temperature than the bulk fluid, the mass loss rates required to cause the pressure transients at these times would be reduced due to the higher energy content of this hot venting gas. This effect is also depicted in these two figures.

The bulk fluid temperature history for the two limiting processes is shown in figure A.2-8. There is reasonably good agreement between the calculated temperatures and the data until 55:54:32, at which time the temperature data deviates seriously from the calculated temperatures. Currently, this deviation is best explained by local heat transfer associated with the energy source.

A refined analysis of the thermodynamic restrictions and the heat transfer processes associated with this problem is being conducted.

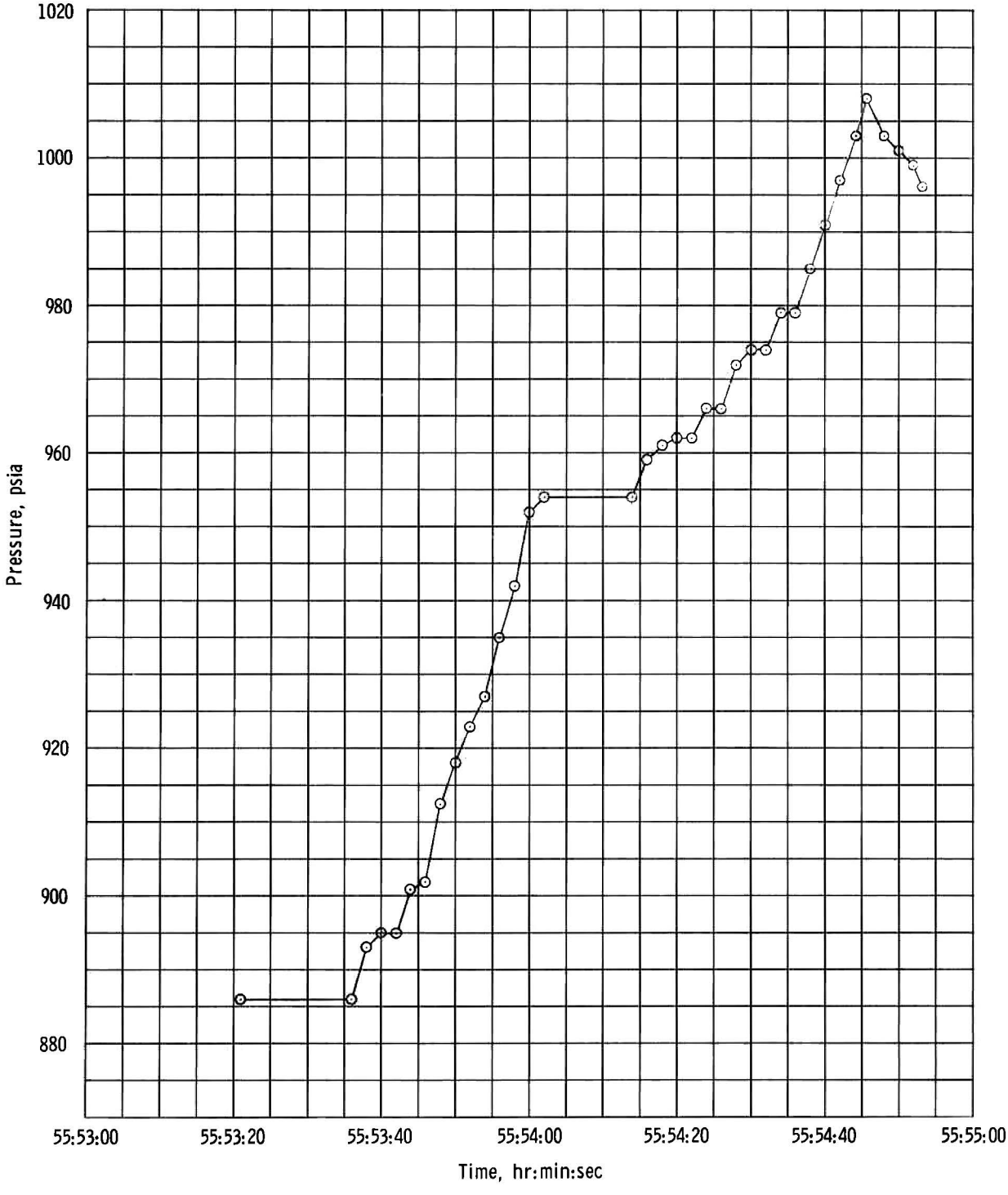

Figure A. 2-1. - Tank 2 oxygen pressure history.

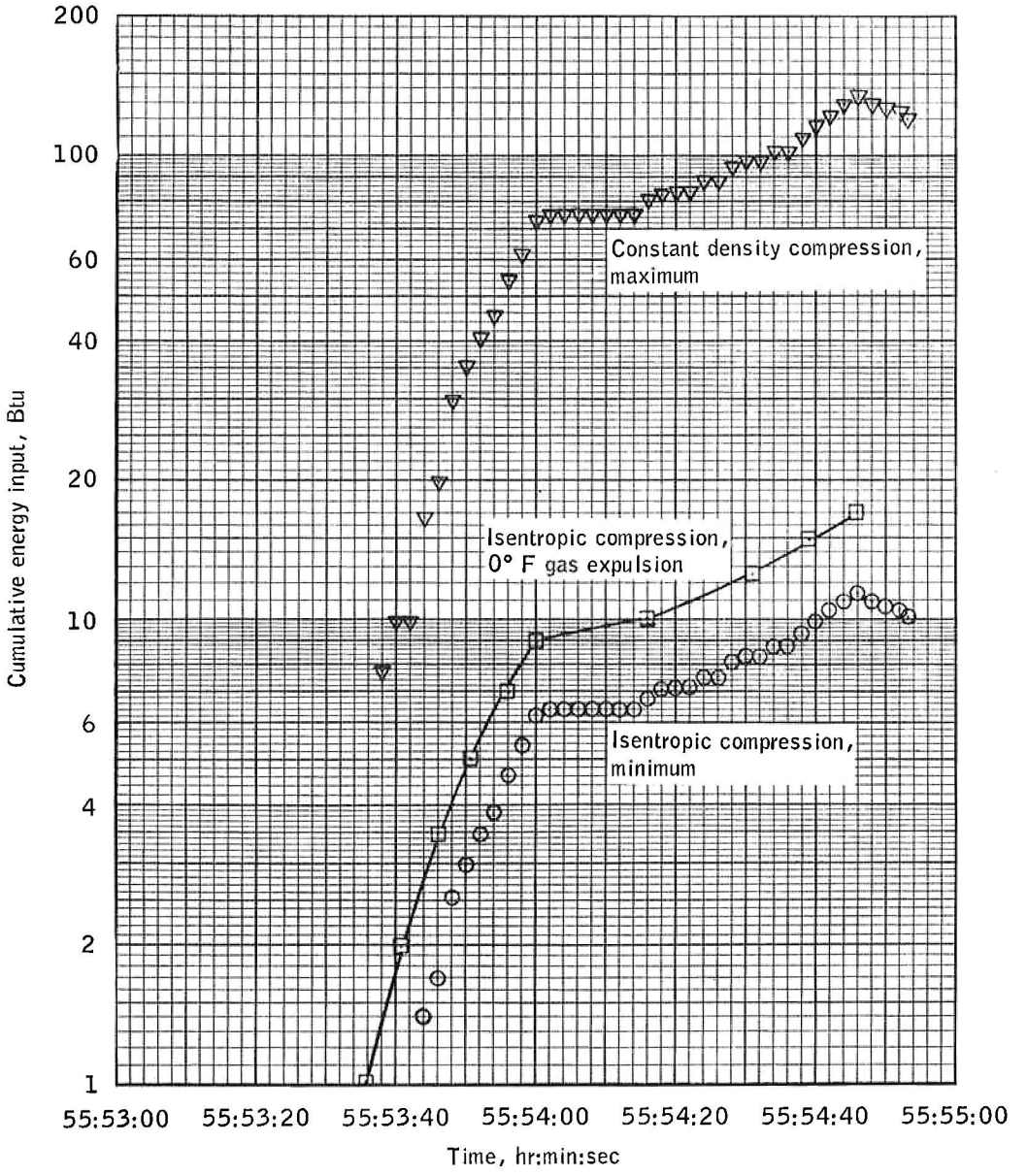

Figure A.2-2.- Cryogenic oxygen tank 2 energy addition.

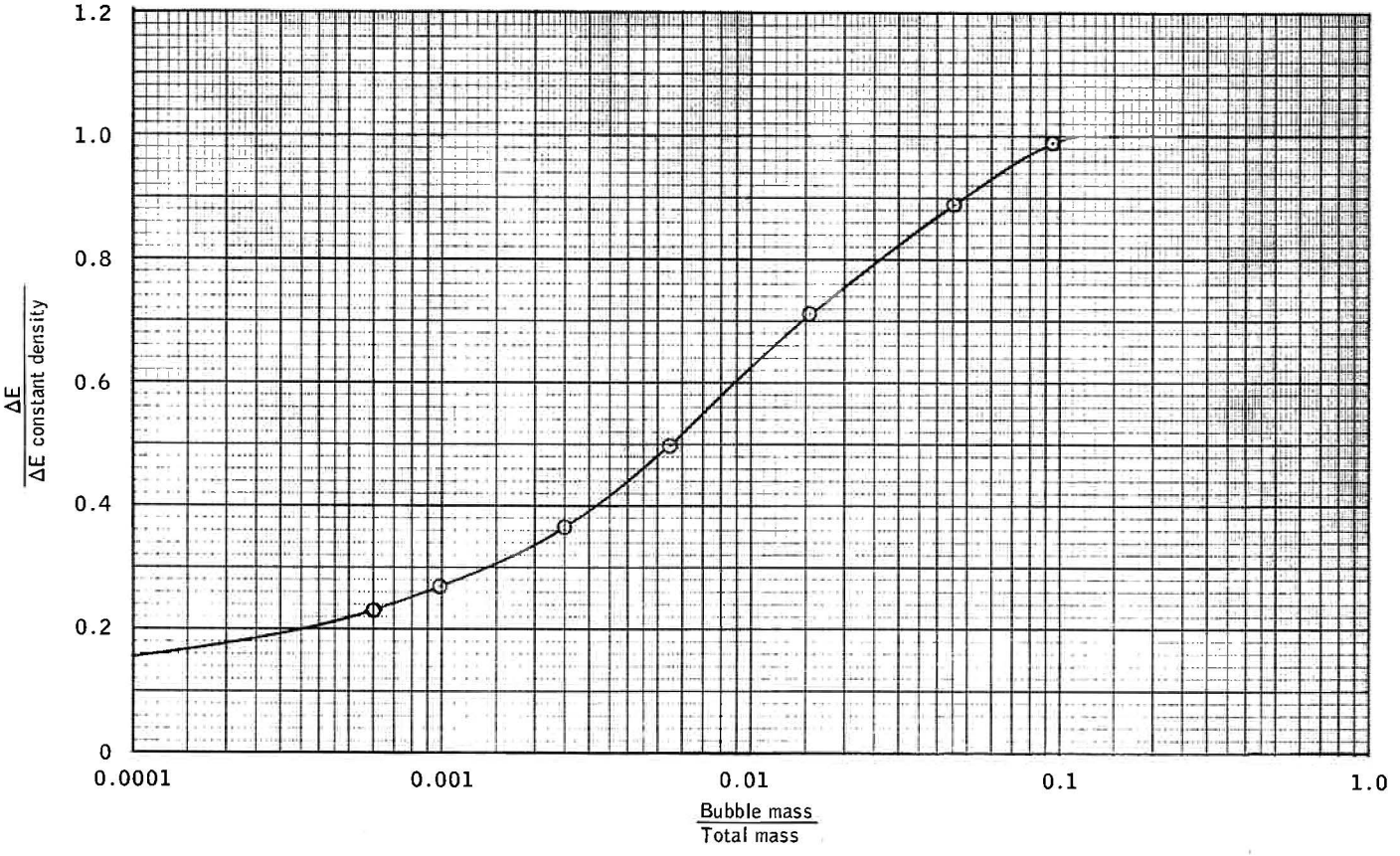

Figure A.2-3.- Input energies associated with bubble masses.

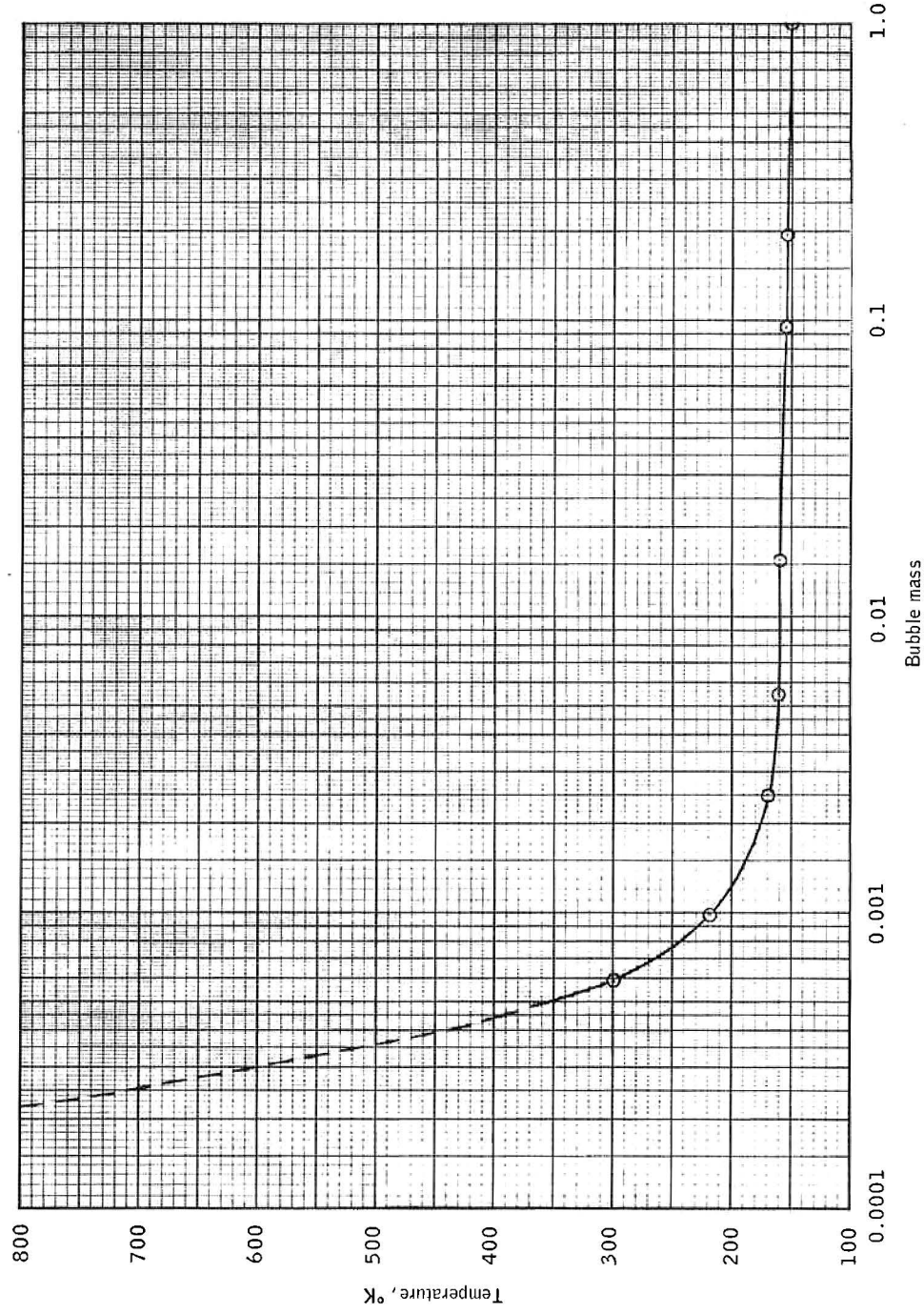

Figure A.2-4.- Average bubble temperature required versus bubble masses.

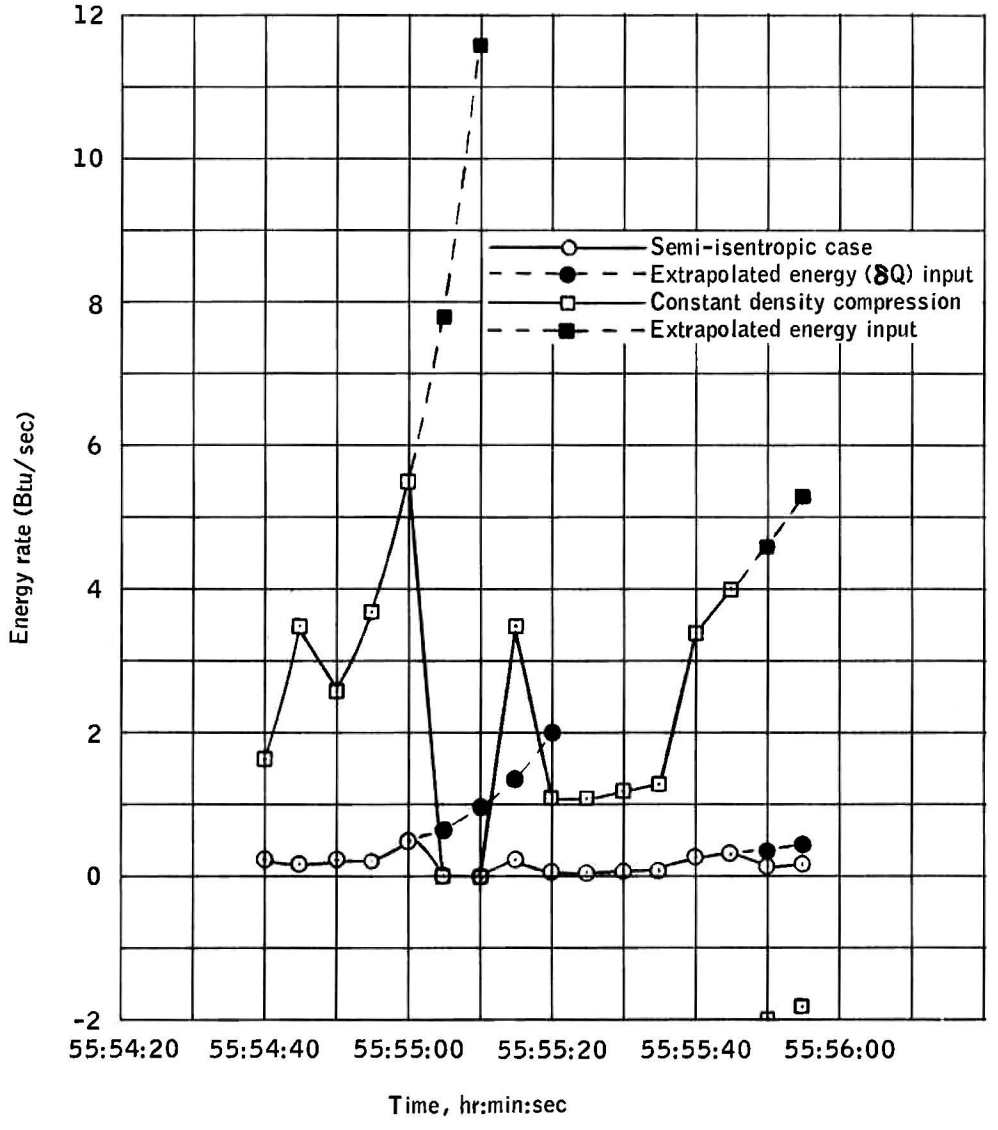

Figure A.2-5.- Energy addition rate.

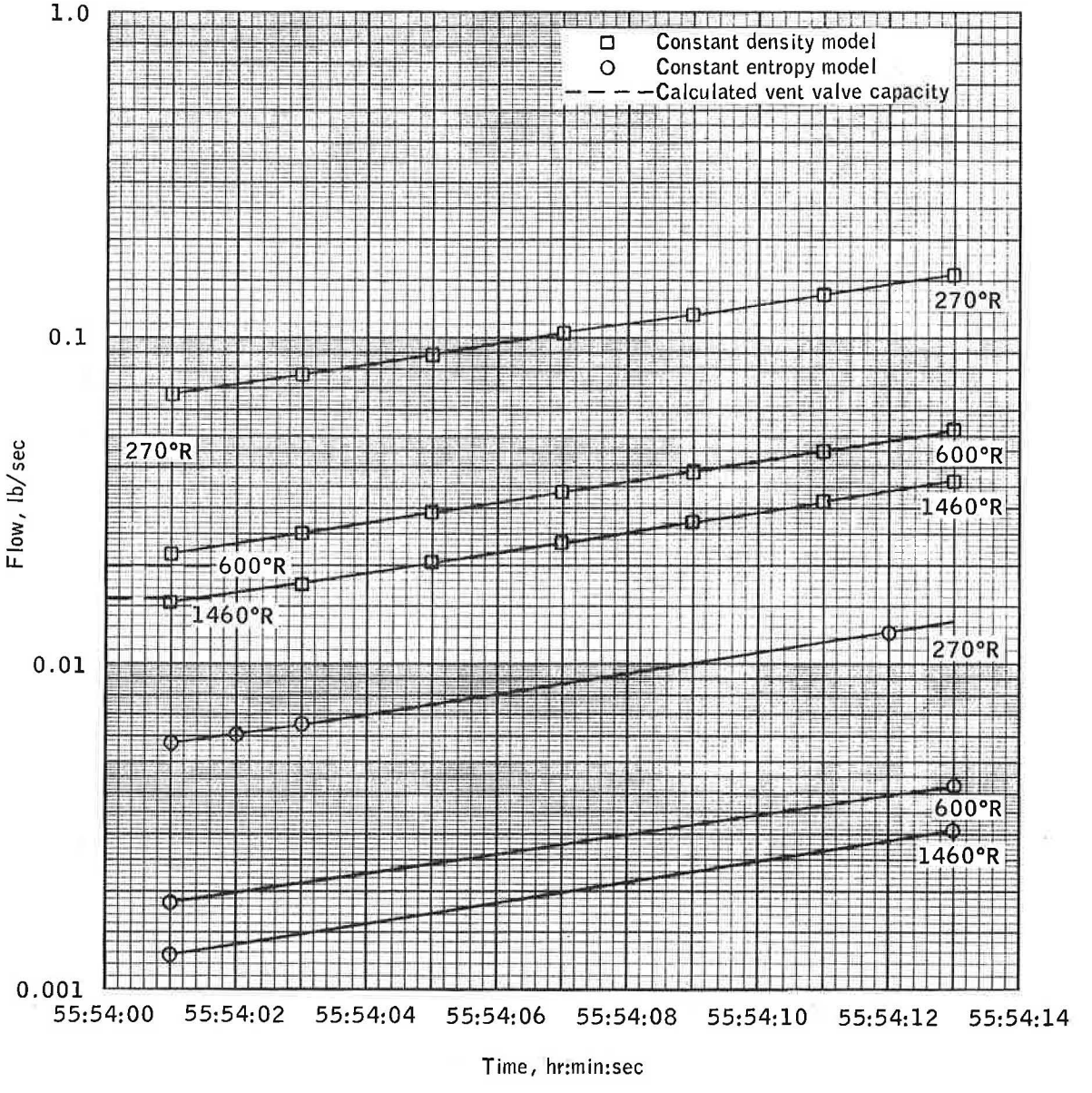

Figure A.2-6.- Oxygen mass flow requirements versus oxygen temperature at first pressure plateau.

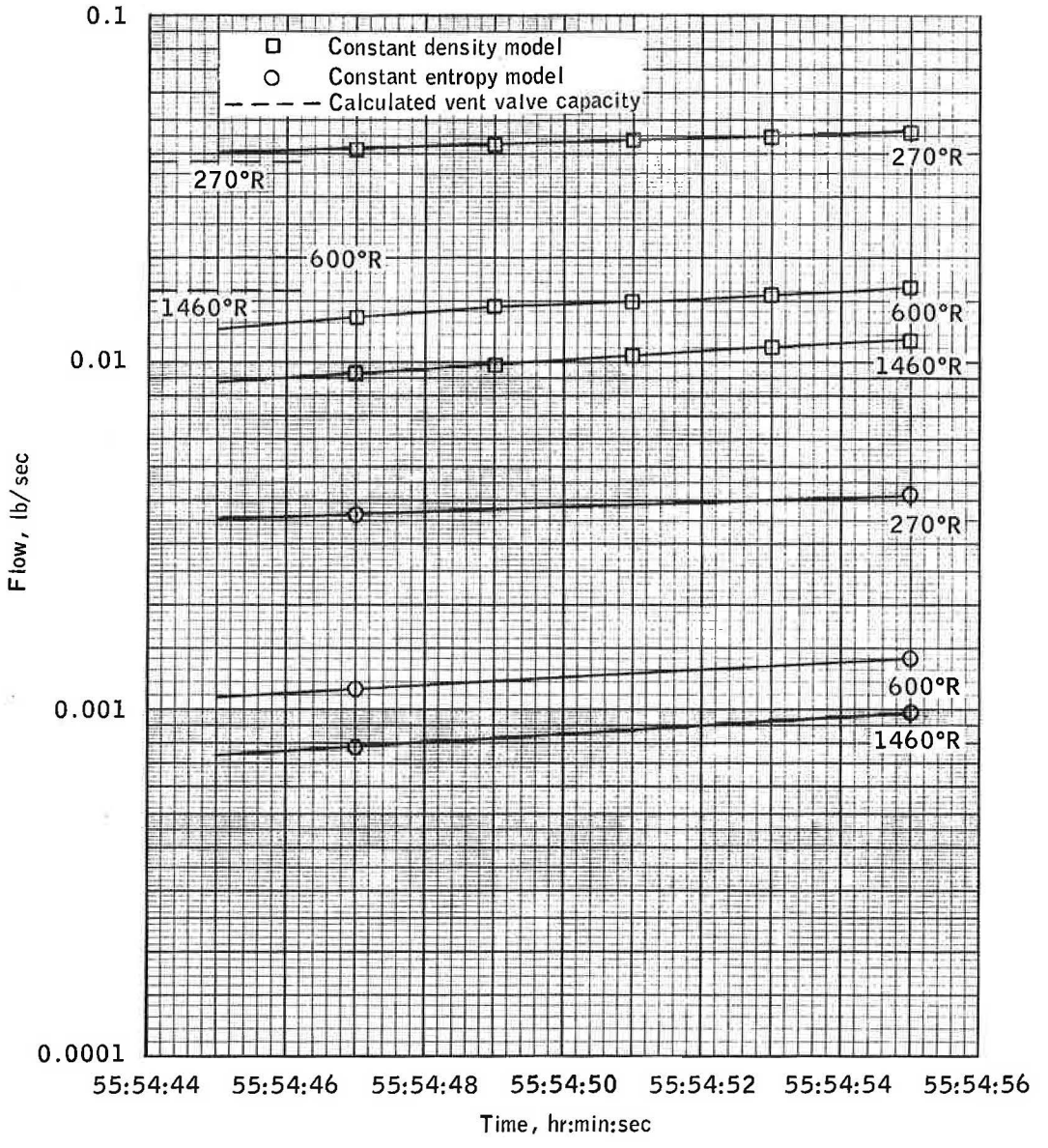

Figure A.2-7.- Oxygen flow requirements, at second pressure plateau.

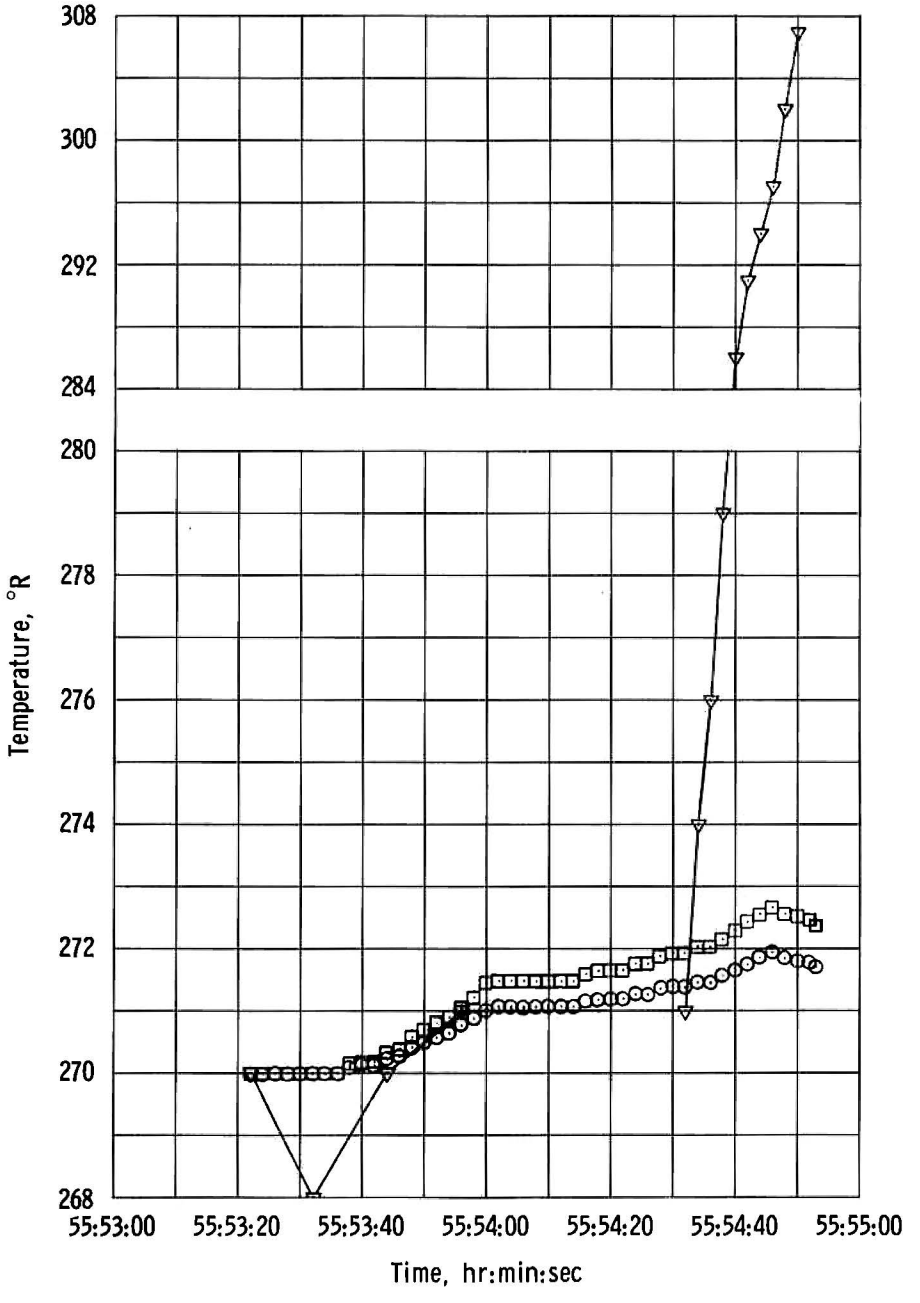

Figure A.2-8. - Bulk fluid temperature history.

A.3 CRYOGENIC OXYGEN TANK 1 BLOWDOWN ANALYSIS

A.3.1 Purpose

Analyze the oxygen tank no. 1 to determine if the flow from this tank was higher than normal after the loss of tank no. 2.

A.3.2 Assumptions

1. Entropy = constant

2. Heat input = negligible during the 72 seconds of the blowdown; only 10 to 15 Btu's total could have been added to the system. This would only change the internal energy by .05 Btu/lb, or, about 0.23 percent. This will not affect the results of this analysis.

A.3.3 Analysis

Quantity at start = 78.03 percent (gage)

Quantity at end = 75.00 percent (gage)

Density at start $= \frac{(323.45)(.7803) + 6.65}{4.7532}$

$= 54.4976 \text{ lb/ft}^3$

Density at end $= \frac{(323.45)(.7500) + 6.65}{4.7532}$

$= 52.4357 \text{ lb/ft}^3$

Mass loss $= 4.7532 (54.4976 - 52.4357$

$= \underline{9.80}$ lb-mass (by gage)

For S = constant

S = 2.92015 at 900 psia and 54.4976 lb/ft^3

Density at end = 53.5522 at 400 psia

Mass loss = 4.7532 (54.4976 - 53.5522)

= 4.50 lb mass (theory)

Time = 72 seconds

M = 0.0624 lb/sec to 0.1360 lb/sec

= 224.64 lb/hr to 490.00 lb/hr

A.3.4 Conclusions

The normal flow from this tank would have been 2.0 lb/hr after the loss of tank 2. The actual flow was between 224.64 and 490.00 lb/hr. This indicates that tank 1 was flowing a higher mass flow than normal.

A.4 TEMPERATURE SENSOR ANALYSIS

A.4.1 Purpose

Using observed flight temperature-time data during tank 1 blowdown and Beech temperature sensor (time constant) test data, calculate the fluid temperature required to produce the observed temperature decrease in tank 1.

A.4.2 Analysis

Flight Data (tank 1): (As shown in figure A.4-1)

Beech Data: Probe-sensor time constant = 23 seconds.

Results: Calculated T_f = 263.1° R
Observed T_2 = 264.7° R
Difference = 1.6° R

A.4.3 Conclusions

Probe time constant calculations for oxygen tank 2 based on Beech data are correct.

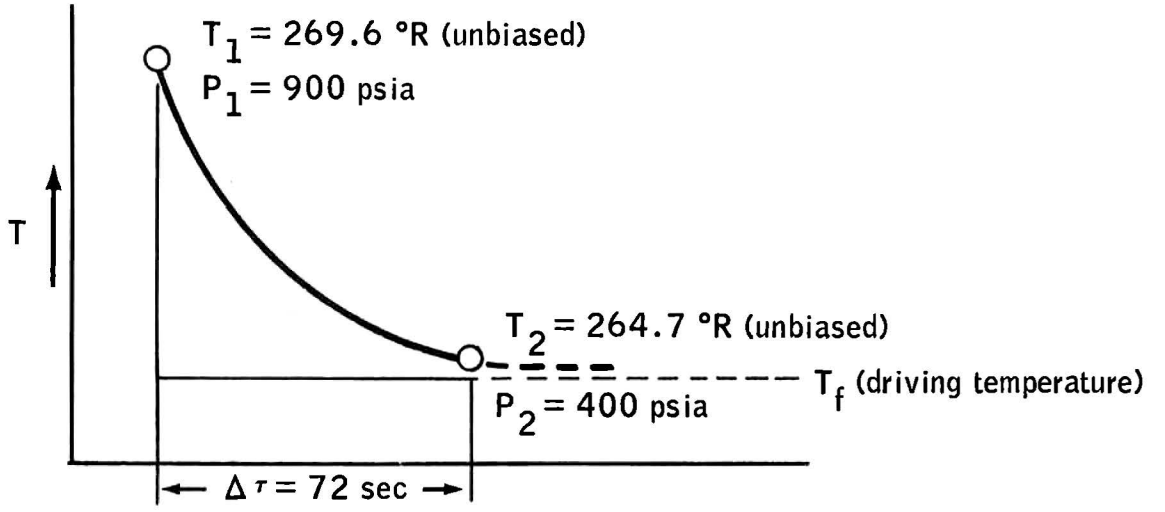

Figure A.4-1.- Flight data for temperature sensor analysis.

A.5 CALCULATION OF REQUIRED HEAT FLUX AND SOURCE TEMPERATURE TO PRODUCE OBSERVED TEMPERATURE TRANSIENTS IN OXYGEN TANK 2

A.5.1 Purpose

Determine the heat flux and source temperature in the vicinity of a sensor to produce observed transient data.

A.5.2 Assumptions

The following assumptions were made:

a. The area for conduction into sensor was taken as total exposed surface area of sensor; that is, assumed hot fluid engulfs sensor completely.

b. Materials, dimensions and physical characteristics, as well as probe/sensor temperature response, were obtained from Beech data.

c. Ignition had a point source on the heater tube radius.

d. The thermal emission from sensor to ignition source was neglected.

e. The thermal capacity C_p of oxygen between source and sensor was neglected.

A.5.3 Analysis

The following procedures were followed for the analysis:

a. Dimensions, mass specific heat, thermal response, and relative positions of all components inside tank, as well as response characteristics of probe, were obtained from Beech.

b. Three models were set up as shown in figure A.5-1. Results shown are for the combined radiation-conduction model.

c. Flight data shows an essentially linear temperature rise with time of 1.7° F/sec.

d. For radiation model and radiation-conduction model, flame emissivities ε_F of 0.5 to 1.0 were investigated.

A.5.4 Conclusions

The following conclusions were made (fig. A.5-1):

a. The required source temperature increases with an increasing sensor angle from the heater tube.

b. The required source temperature increased as ignition source moves toward fan motor.

c. The source temperature could have reached 2900° F if the ignition began at the fan motor.

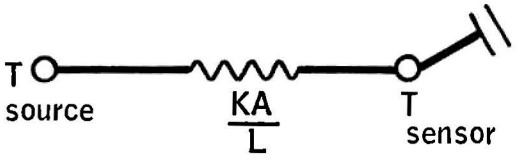

(a) Conduction only.

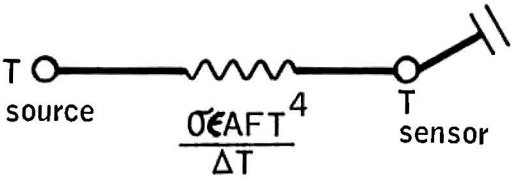

(b) Radiation only.

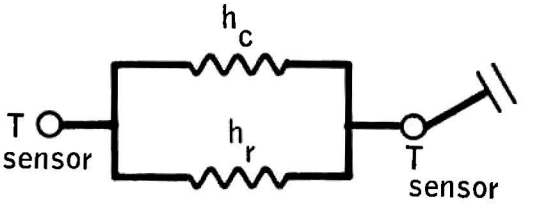

(c) Combined radiation - conduction.

Figure A.5-1.- Analytical models for heat transfer.

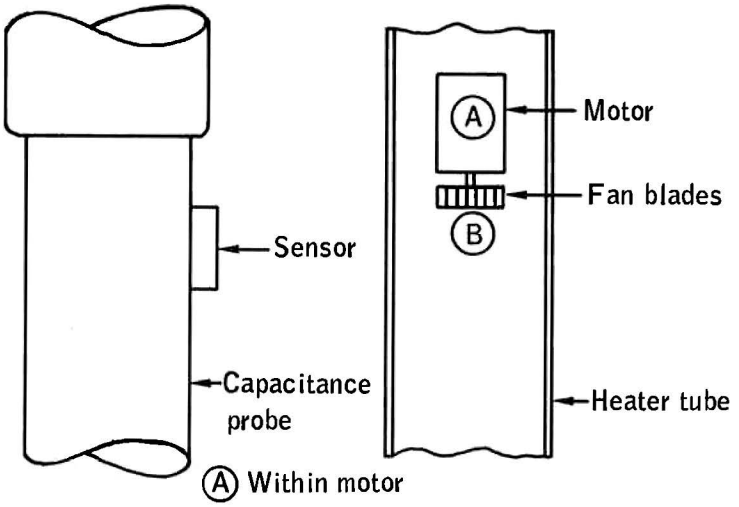

Two ignition sources investigated

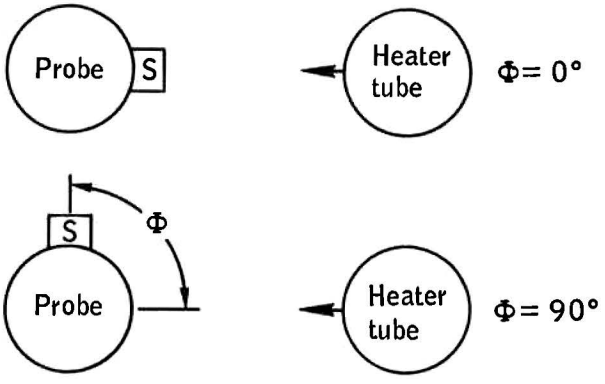

1) Φ= 0°; Source opposite sensor

2) Φ= 90°; Source at right angle to sensor

Two orientations investigated for each source

Figure A.5-1.- Concluded.

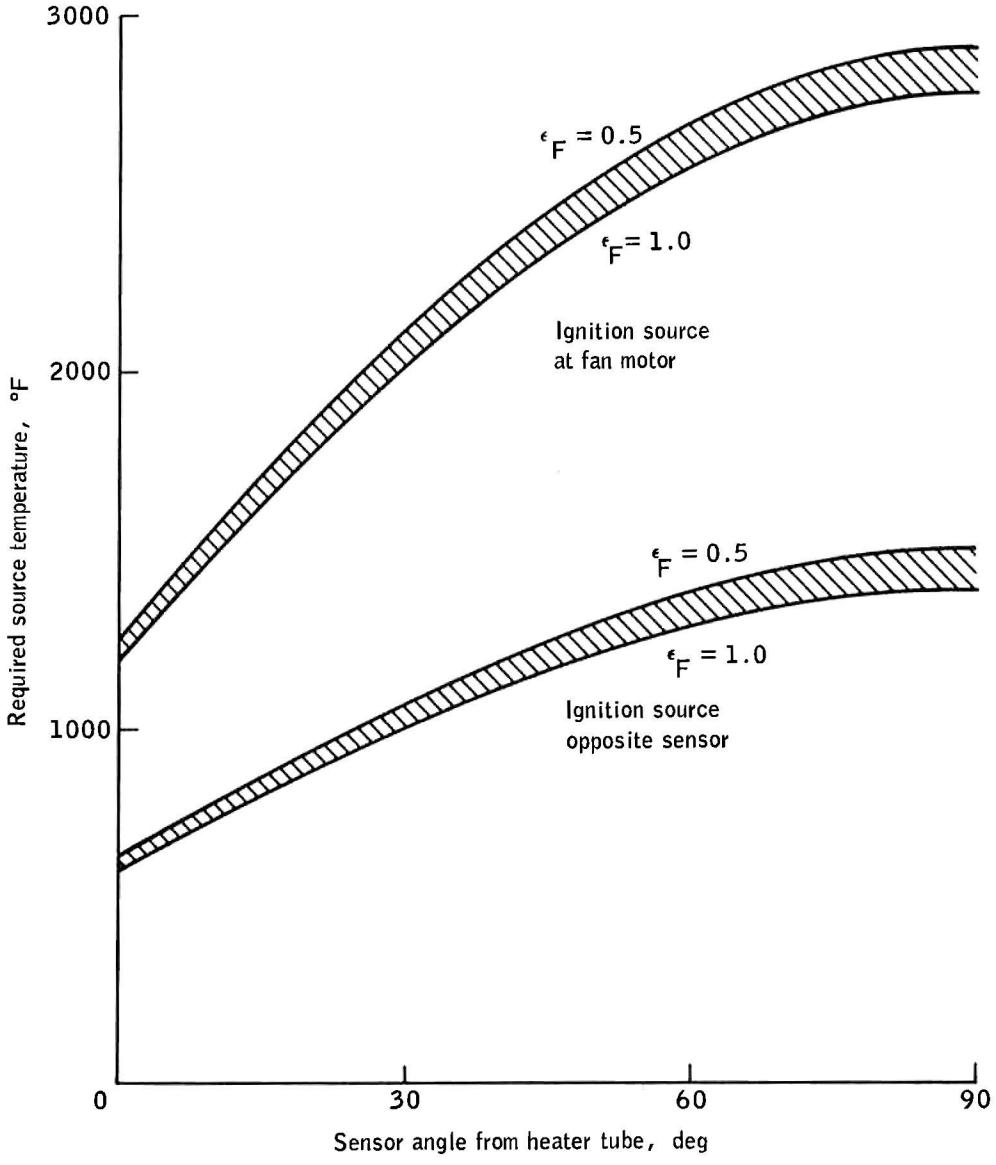

Figure A.5-2.- Source temperature as a function of sensor angle from heater tube.

A.6 TEMPERATURE SENSOR ANALYSIS

A.6.1 Purpose

Assuming a fire burns down the fan/heater leads and through the hole in the polytetrafluoroethylene portion of the probe, calculate the required flame temperature to produce observed flight data. Show variation in flame temperature with wire position.

A.6.2 Assumptions

The following assumptions were made:

a. Flight data on temperature sensor.

b. Conduction path varies with wire angle.

c. Effective conductive area 0.72 square inch.

d. Neglect radiation, since previous calculations show it to be less than 10 percent of total heat transfer.

A.6.3 Analysis

The model used in the analysis is shown in figure A.6-1. Three lead wire positions investigated:

Case A: Effective conduction path 0.4 inch

Case B: Effective conduction path 0.6 inch

Cace C: Effective conduction path 1.4 inches

A.6.4 Conclusions

Flame temperature variations from 672° to 2560° F were calculated, depending on wire position (fig. A.6-2).

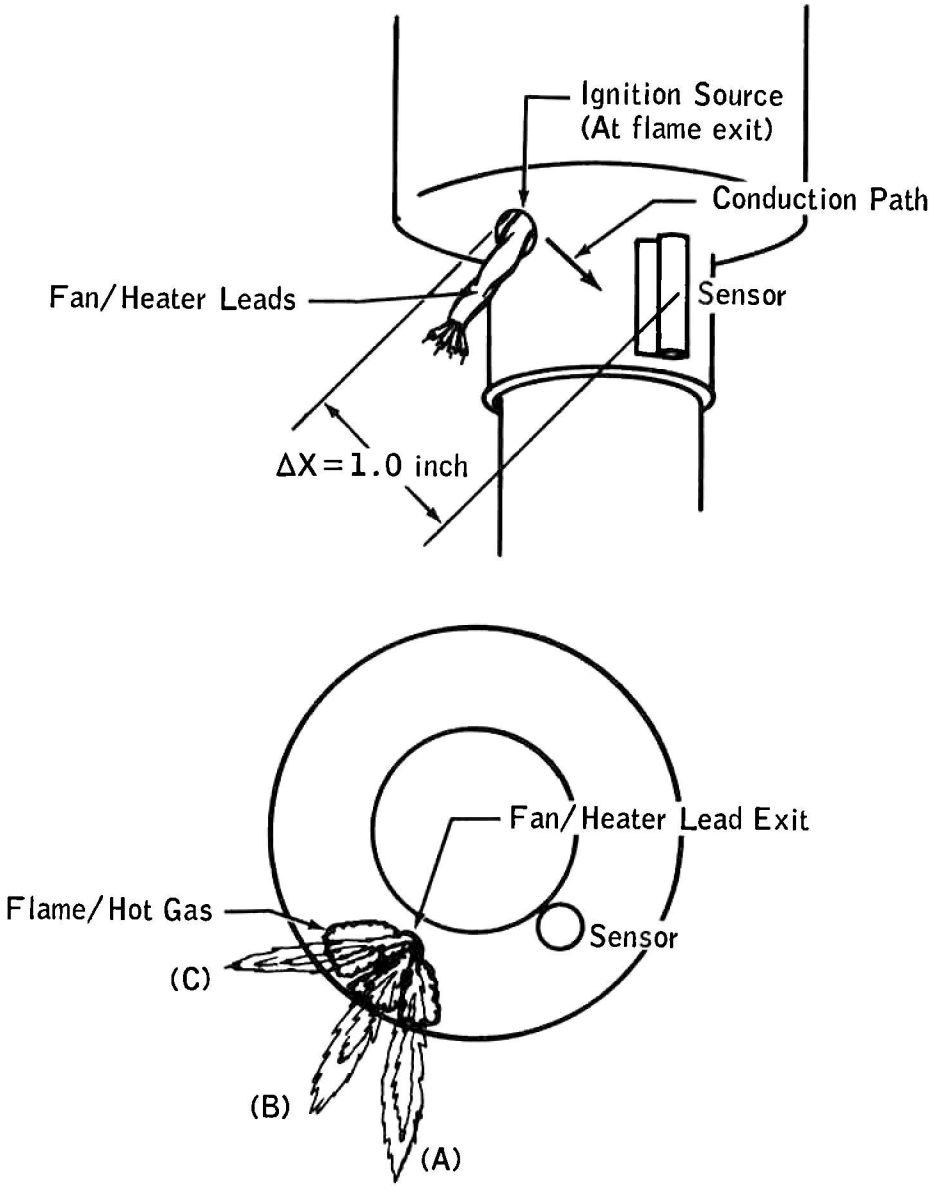

Figure A.6-1.- Model used for temperature sensor analysis.

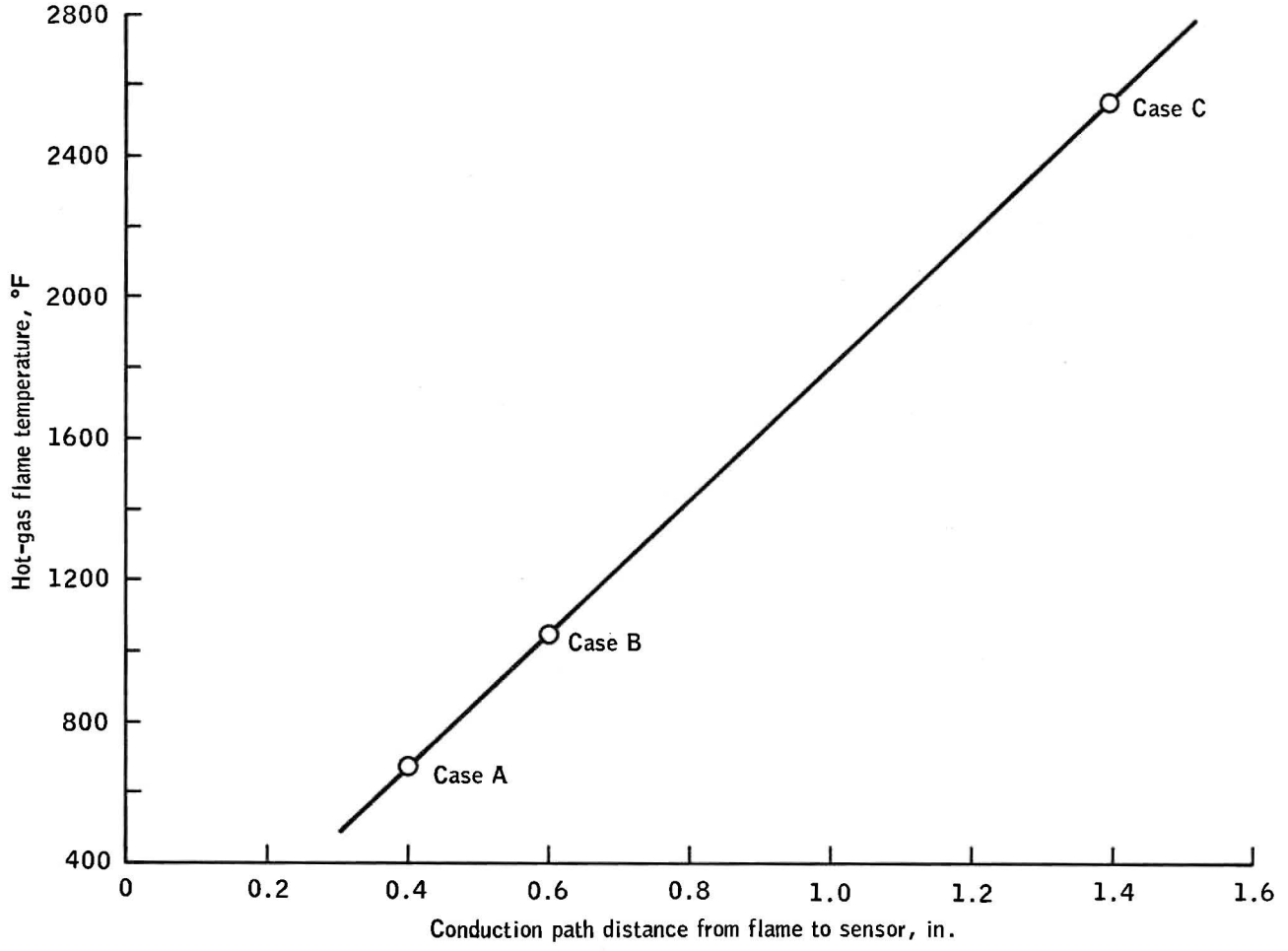

Figure A.6-2- Variation of flame temperature with conduction path distance.

A.7 TEMPERATURE SENSOR ANALYSIS

A.7.1 Purpose

Assuming an ignition source (gas bubble) at the top of the probe assembly, calculate lag time as a function of source temperature to correlate delay in temperature rise after beginning of pressure rise in tank 2.

A.7.2 Assumptions

The following assumptions were made:

a. No radiation

b. Transient conduction through oxygen, aluminum, and polytetrafluoroethylene as shown in figure A.7-1

c. Total conduction path of 5.4 inches

d. Semi-infinite composite slab.

$$\text{Ŧ} = \frac{T-T_f}{T_o-T_f} = \text{erf}\left(\frac{X}{2\sqrt{\alpha\tau}}\right)$$

where: Ŧ = Dimensionless temperature

T = Sensor temperature at any time τ

T_f = Flame temperature (ignition)

T_o = Initial sensor temperature (minus 187° F)

$$\text{erf} = \text{Error function} \equiv \frac{2}{\sqrt{\pi}} \int_0^{\frac{X}{2\sqrt{\alpha\tau}}} e^{-\lambda^2}\, d\lambda$$

X = Conduction path length

α = Composite thermal diffusivity ft^2/hr

τ = Time from ignition

A.7.3 Flight data

Data obtained from the flight showed the following:

a. First observed pressure rise at 55:53:36

b. First observed temperature rise at 55:54:30

c. Observed time lag of 54 seconds.

A.7.4 Analysis

During tank 2 pressure and temperature transients, investigation of thermodynamic properties of oxygen shows extreme variations in oxygen properties from flame source temperatures to cryo temperatures. Analysis indicates a definite time lag associated with this process and this would cause the trend seen in flight to be expected. The magnitude of the time lag is critically dependent on oxygen properties. A critical parameter is thermal diffusivity $\alpha \equiv \frac{\kappa}{\rho C_p}$. A range of thermal diffusivity of oxygen under these conditions is 0.0024 to 0.013 ft^2/hr. For a nominal thermal diffusivity of 0.006 ft^2/hr and a flame source temperature of 1000° F, a time lag of approximately 54 seconds is calculated, which was observed in flight data. Variation of time lag with flame temperature is as shown in figure A.7-2.

A.7.5 Conclusions

The following conclusions were made:

a. The existence of a time lag is to be expected for a process such as this.

b. The observed magnitude of the time lag is within reason for the known extreme variations in cryogenic oxygen properties.

c. Calculation of exact time lag is impossible due to the crudeness of the analytical model.

d. Due to the many unknowns involved in the real process (for example, flame/hot gas temperature and flame/hot gas propagation paths), an extremely sophisticated model, coupled with experimental data, would be needed to adequately describe this process.

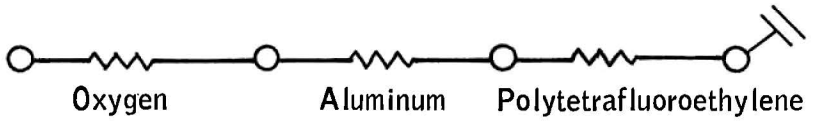

Figure A.7-1- Model for transient conduction through oxygen, aluminum and polytetrafluoroethylene.

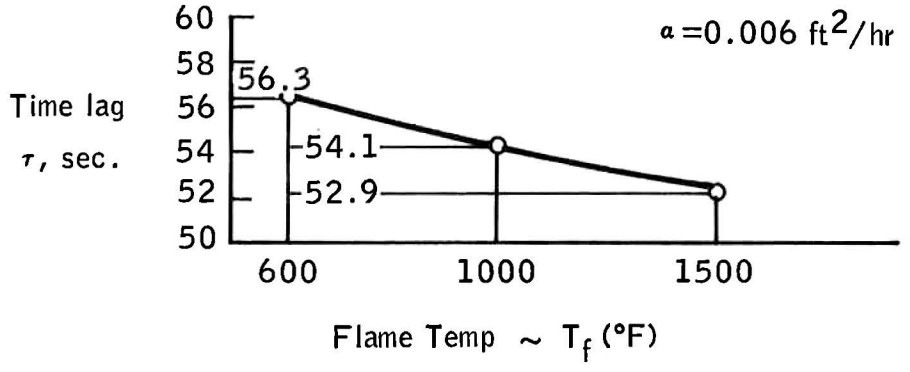

Figure A.7-2- Variation of time lag with flame temperature.

A.8 PRESSURE DROP ANALYSIS AND TESTING

A.8.1 Purpose

According to the pressure transducer, oxygen tank 2 never reached a pressure over 1010 psia before data loss occurred at 55:54:54. However, the tank is rated to burst at 2200 psia by actual test. Hence, the purpose of this analysis and testing was to determine whether frictional pressure drop could account for the pressure transducer reading as much as 1000 psi below actual tank pressure.

A.8.2 Assumptions

The following assumptions were made:

a. Neglect heat transfer from surroundings to flowing fluid.

b. The friction factor is invariant with length and fluid properties and is equal to 0.004.

c. The filter's flow versus pressure drop characteristic will have to be determined by test. Any estimate of pressure drop in the filter used in the test reflects the preliminary nature of these calculations.

d. Sonic flow occurs in at least one point in the piping.

Calculating back to entry into the 115- by 0.1575-inch section gives:

M entry to 0.1575 inch = 0.208

These Mach numbers and the observed pressure of 1000 psia at the end of the 98- by 0.206-inch duct give:

P tank, psia	Assumed ΔP filter	ΔP (0.1575-inch section)	ΔP (0.206-inch section)	P exit psia	M lb/sec
1500	250	715	did not converge	1000	2.09
2000	300	972	did not converge	1000	2.42

A ΔP in the 98- by 0.206-inch section could not be determined such that it would satisfy the Mach number, exit pressure, and mass flow constraints shown. However, the mass flows are in fairly close agreement with quantity gage readings from 55:54:32 to 55:54:48 which indicated a mass flow of 1.71 lb/sec. Notice that the pressure drops even at velocities below sonic in the 0.1575-inch section are sufficient to explain no indication of severe overpressure at these mass flows.

At that time the following test data were obtained from Parker Aircraft, the relief valve manufacturer:

Temperature, °F	ΔP	Flow, lb/sec
-148	1000 psia - 1 atm	0.039
70	1000 psia - 1 atm	≥0.007 (specification of Beech)

The tested mass flow under cryogenic conditions is only about 2 percent of that calculated from the quantity gage reading but, on the other hand, about 100 times the normal flow in this piping. Since the calculations account reliably only for the straight pipe loss, the filter ΔP and possibly the sudden contraction ΔP remained an open question, especially under cryogenic conditions.

A.8.4 Testing

A test flow plan was established whereby the Apollo 13 piping system was simulated, including the actual filter and relief valve. Tests made were:

a. Establish full flow through piping and relief valve to atmosphere with oxygen gas at 70° F and 1000 psia. Increase upstream pressure slowly until downstream pressure reaches 1050 psia (limit of Apollo 13 pressure transducer), while recording upstream and downstream pressures and flow.

b. Same as (a) except that when full flow is established, make step change in upstream pressure to 1500 psia and hold. Record upstream and downstream pressures and flow.

If either of these tests had shown a very high pressure drop or a slow response time, a flow test with cryogenic oxygen could have been deleted, since the cryogenic would show a higher pressure drop than the oxygen gas. However, the tests indicated pressure drops of 5 to 10 psi and a response time of 100 milliseconds.

c. Using simulated Apollo 13 tank and piping and oxygen at 170° F, 1008 psia, establish full flow through relief valve, and raise tank pressure. Record both pressures and flow.

The maximum upstream pressure attainable, as limited by system leakage, was 1050 psia. At this condition the pressure difference between tank and transducer was never greater than 35 psi and response times were similar to those obtained at ambient temperature.

A.8.5 Conclusions

From these flow tests the conclusions are:

a. With the relief valve fully open, neither pressure drop nor time lag between tank and transducer would have been large enough to explain the transducer's reading significantly below the tank pressure.

A.8.3 Analysis

The piping system is shown in figure A.8-1.

Case 1 Mach number = 1.0 at end of the 0.1575-inch inside diameter section

$$F = \int_0^L \frac{4f}{D}\,dx = \frac{4fL}{D}$$

L = 115 inches in the 0.1575 inch section

F = 11.7

From P_1 $\frac{M \text{ at entry}}{M \text{ at exit}} = 0.219$ (based on equations in reference 1)

$\gamma = 3.3$ for approximate entry conditions of 950 psia and 270° R.

$$\frac{P \text{ exit}}{P \text{ entry}} = \frac{M \text{ entry}}{M \text{ exit}} \left[\frac{1 + \frac{\gamma - 1}{2} \left(M \text{ entry}\right)^2}{1 + \frac{\gamma - 1}{2} \left(M \text{ exit}\right)^2} \right]^{1/2} = 0.153$$

where $\gamma = \frac{C_p}{C_v}$

It was necessary to assume some value of ΔP across the filter to arrive at P entry, and oxygen tank 2 pressures of 1000, 1500, and 2000 psia were used as follows:

Assumed		115 by 0.1575-inch section		
P tank, psia	ΔP filter + 14 by 0.206 inch line, psi	P entry, psia	P exit, psia	ΔP, psi
1000	200	800	122	678
1500	250	1250	191	1059
2000	300	1700	260	1440

Also, by referring to P_1:

$$\frac{T \text{ exit}}{T \text{ entry}} = \frac{1 + \frac{\gamma - 1}{2}\left(M \text{ entry}\right)^2}{1 + \frac{\gamma - 1}{2}\left(M \text{ exit}\right)^2}$$

which leads to:

P tank, psia	P exit, psia	T exit, °F
1000	122	-328
1500	191	-328
2000	260	-328

All of these exit pressures and temperatures fall in the two phase region. Accordingly, it was judged to be more productive to do the calculation for the 98 by 0.206-inch section, where sonic flow certainly occurs at the end, rather than attempting to discover where M = 1.0 and where condensation would begin in the 0.1575-inch section.

Case 2 Mach number = 1.0 at end of 98 by 0.206-inch section.

$F = \frac{4fL}{D}$ = 7.61, which gives: M entry = 0.26

A discontinuity and pressure recovery would exist at the sudden expansion from 0.1575 inch to the 0.206-inch line. Hence, a higher Mach number is expected just at the end of the 0.1575-inch line (see detail on fig. A.8-1).

If continuity is postulated for the thermodynamic properties - no infinite gradients, the speed of sound will not change from (1) to (2). This is quite a rough approximation to the true situation.

$$M_1A_1 = M_2A_2 \quad \text{so} \quad M_2 = 0.448$$

b. Unless the tank became isolated from the transducer by some means (such as plugged filter or ruptured line) the transducer was reading close to actual tank pressure until data loss.

REFERENCE

1. "Nonisentropic Finite-Amplitude Wave Generation," by A. C. Peter, North American Rockwell Report SD 69-722, December 1969, Eqtns. (22) and (23-b), pp. 12-13.

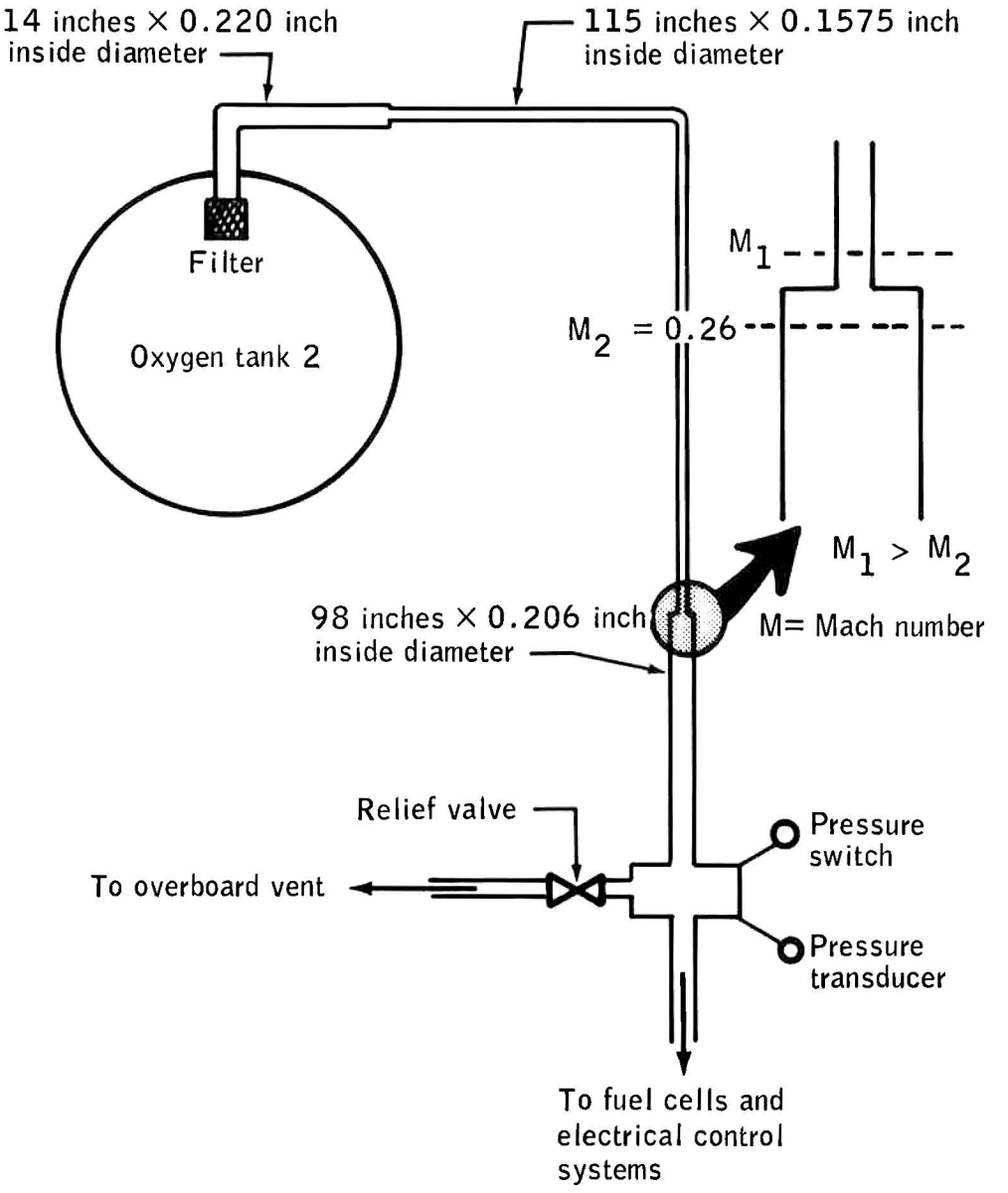

Figure A.8-1.- Cryogenic oxygen tank 2 plumbing.

A.9 EXTENSION OF PRESSURE DATA BY CORRELATION WITH FLOWMETER DATA

A.9.1 Purpose

The oxygen flow to all three fuel cells is sampled 10 times per second while the oxygen tank pressures are sampled only once per second. This fact is used to try to extend the observed pressure data for a fraction of a second past the last recorded point.

A.9.2 Assumptions

The following assumptions were made:

a. Fuel cell 1 flowmeter data are valid until data loss.

b. The line volume from one flowmeter to the oxygen regulator can be treated as an isothermal (70° F) capacity of volume 5.40 in^3 which is at thermodynamic equilibrium all the time.

c. Oxygen is ideal at 70° F and system pressure of about 996 psia

d. The theoretical oxygen demand for the fuel cells can be extrapolated for 0.7 second at a constant value representing the average current for the last 3.5 seconds before data loss.

A.9.3 Analysis

Because of the small time spans involved, it is necessary to correct all tab data times to the actual time the measurement was taken. This was done for flow, pressure, and fuel cell current measurements. The fuel cell current was then extrapolated for 0.7 second at 22.5372 amperes from 55:54:52.763, the time of the last pressure data. This was converted to an oxygen usage of 0.46 lb/hr. Figure A.9-1 shows the extrapolated theoretical oxygen flow to fuel cell 1 and the actual flowmeter data. The area between these graphs from 55:54:52.763 to 55:54:53:463 represents

the change in mass contained in the volume between flowmeter and regulator during this time. This area in 15.179×10^{-6} lbm oxygen and the corresponding density change is $\Delta P = -2.62 \times 10^{-3}$ lbm/ft^3. From the ideal gas law and assumed temperature of 70° F the pressure change is found to be -0.465 psi. This gives the additional calculated pressure point of 995.5 psia at 55:54:52.763 actual time.

A.9.4 Conclusions

A 0.7 second extrapolation of pressure data based on measured flows shows a tank 2 pressure of 995.5 psia at data loss.

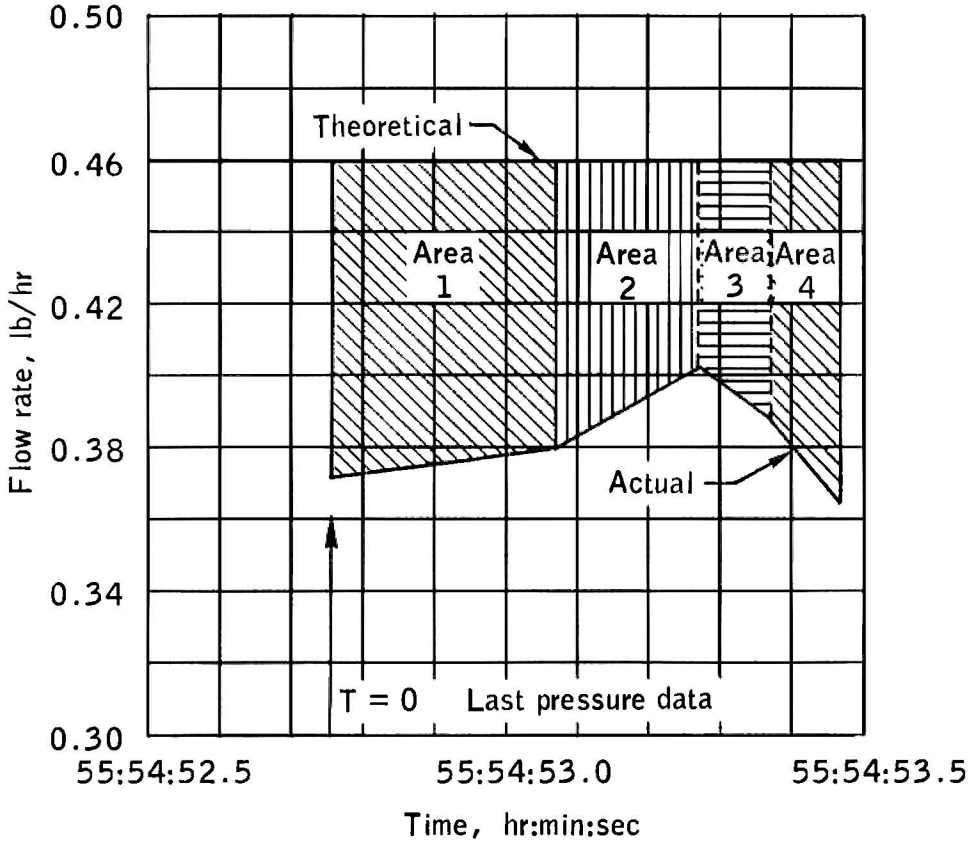

Figure A.9-1.- Oxygen flow to fuel cell 1.

A.10 TEMPERATURE AND PRESSURE VERSUS QUANTITY CORRELATION

A.10.1 Purpose

Attempt to correlate the temperature and quantity data during the time of the incident. This will be done in order to establish the location of the energy source that was responsible.

A.10.2 Analysis

Figure A.10-1 shows the historical data calculated for Apollo 10, 11, and 12. These data consist of quantities calculated from the pressure and temperature data plotted against the quantity gage readings. It was found that if the temperature is biased with a minus 17° F value, the two quantities will agree within a reasonable accuracy (fig. A.10-1). The following data are shown for the case of tank 2:

Time	55:54:32	55:54:50
Quantity, percent	75	72
Temperature, °F	-187	-154 to -151
Pressure, psia	975 psia	1004
Calculated temperature, °F	-205	-195
Bias, °F	-17	-14 to -44

As can be seen, the initial temperature bias at time 55:54:32 is about at the expected minus 17° F, and that 18 seconds later a minus 41° to minus 44° F bias is required to correct the temperature to the quantity data. This increasing bias is indicative of an increasing error and is caused by the temperature increase of the adjacent fluid. The reason for this is that the temperature sensor measures the condition at a single point in the tank while the capacitance probe samples and integrates a cylindrical portion of fluid across the diameter of the spherical tank. If the fluid is stratified and the hot region is located at the top of the capacitance probe the observed data can be explained.

An energy source at any other location in the tank cannot explain these data.

A.10.3 Conclusion

High energy was being released near the top of the tank adjacent to the temperature sensor at the time the temperature was increasing.

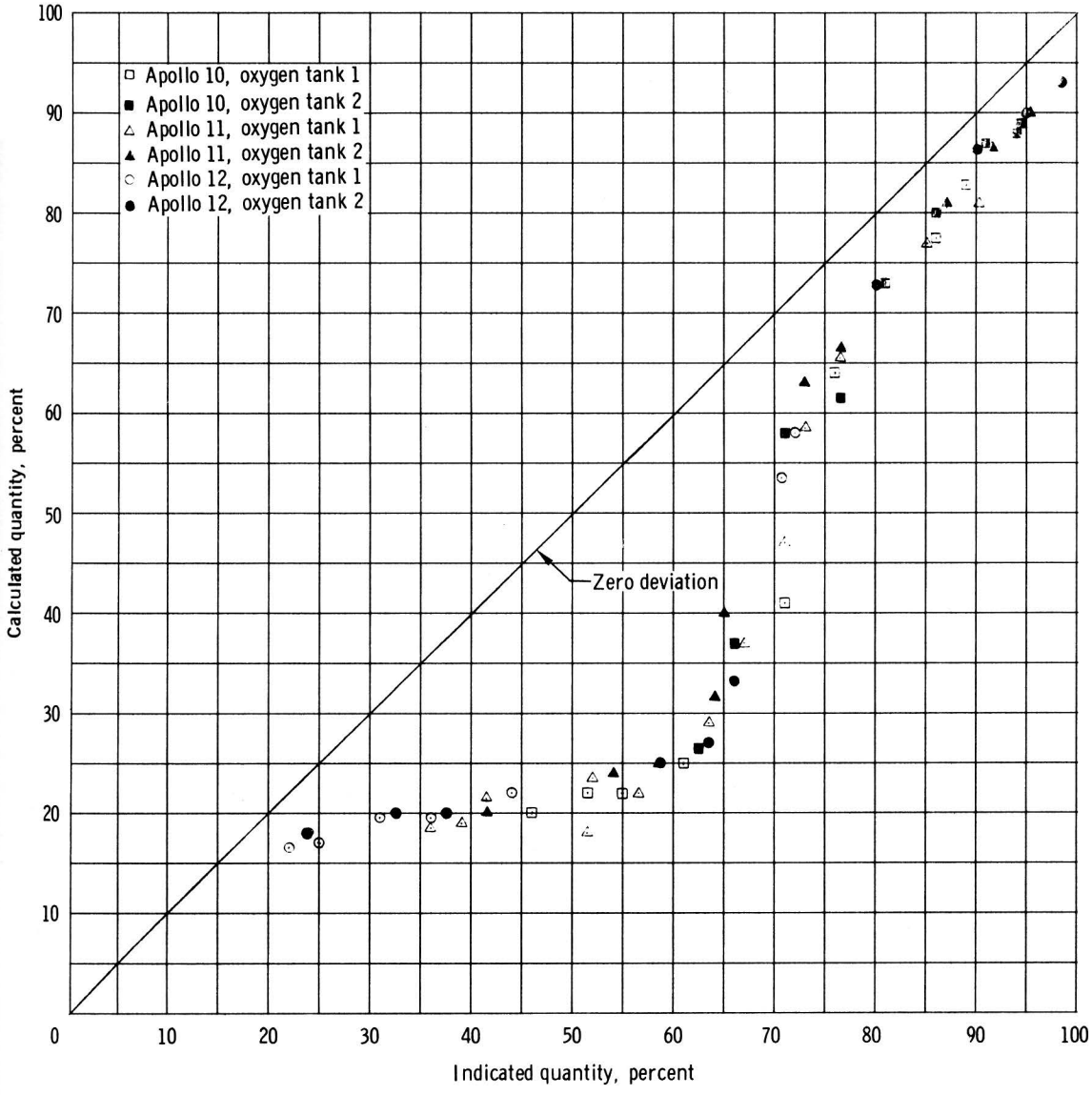

Figure A.10-1. - Correlation of quantity gage with temperature and pressure sensors.

A.11 FUEL CELL ERRATIC OXYGEN FLOW RATE

A.11.1 Purpose

Explain the observed fuel cell oxygen flow data, and correlate it with oxygen tank 2 pressure data.

A.11.2 Analysis

Prior to the oxygen tank 2 failure, flight data had shown a sudden increase in the three fuel cell flow rates. The flow excursions were identical for all three fuel cell flowmeters. The flow increase can be seen from figure A.11-1 to be most pronounced during the rapid increase in oxygen tank 2 pressure and returning to normal flow rates at the pressure plateau (955 psia).

Analysis has shown the flow rate excursions were in response to the oxygen tank 2 pressure increase. The tank pressure increase results in an increase in density downstream of the flowmeter (fig. A.11-2), requiring mass to flow through the flowmeter faster than the fuel cell and environmental control system usage rate. The flowmeter is a capillary tube hot wire anemometer (fig. A.11-3); therefore, it is very sensitive to flow stream changes. The pressure, volume, and temperature relationship for a pressure change from 890 psia to 1008 psia requires that a 0.0036 pound-mass be added to the volume downstream of the flowmeter, as shown in the following calculations.

MASS INCREASE DOWNSTREAM OF FLOWMETER DUE TO

INCREASING PRESSURE FROM 890 TO 1008 PSIA

SOLVE FOR MASS X

$$P_1V_1 = M_1RT_1$$

$$V_2 = V_1 = \frac{M_2RT_2}{P_2}$$

$$V_1 = \frac{M_1 + X \quad RT_1}{P_2}$$

$$P_1 \frac{M_1 + X \quad RT_1}{P_2} = M_1RT$$

$$M_1 + X \; RT_1 = \frac{N_1RT_1P_2}{P_1}$$

$$M_1 + X = \frac{M_1RT_1P_2}{RT_1P_1}$$

$$X = \frac{M_1P_2}{P_1} - M_1$$

$$X = \frac{0.01570(1008)}{890} - 0.01545$$

$$X = 0.0190 - 0.01545$$

$$X = 0.0036 \text{ pound}$$

ASSUME - CONSTANT TEMPERATURE

$$T_1 = T_2 = 70^\circ \text{ F} = 530^\circ \text{ R}$$

$$M_2 = M_1 + X$$

$$V_1 = V_2 = 5.32 \text{ in}^3$$

Volume - Flowmeter to regulator

$$= 5.4 \text{ in}^3$$

$$P_1 = 390 \text{ psia}$$

$$P_2 = 1008 \text{ psia}$$

SOLVING FOR M_1

$$M_1 = \frac{P_1V_1}{RT_1} = \frac{890(144)(5.40)}{(48.3)530(1728)}$$

$$M_1 = 1.57 \times 10^{-2}$$

$$M_1 = 0.01570 \text{ pound}$$

A.11.3 Conclusions

The shaded area in figure A.11-1 represents 0.0034 pound between the flight data flow curve and the theoretical fuel cell oxygen consumption

flow curve, based on fuel cell current during the same time period. The conclusion based on this correlation is that the flow excursions were caused by the response of flowmeters to the increase in oxygen tank 2 pressure.

The initial flow decrease at point A (fig. A.11-1) was caused by the oxygen tank pressure dropping as fan-stirring destratified the fluid. The flow through the flowmeter stops instantaneously as the pressure downstream of the check valve, area B (fig. A.11-2), exceeds the decreasing tank pressure. The flow recovers as the pressure in oxygen tank 2 begins to increase (the pressure in area B also drops due to fuel cell demand) equalizing the pressure upstream and downstream of the check valves, areas A and B, (fig. A.11-2). A flow surge is caused as the check valve opens (check valve cracking pressure is 2.7 psid per acceptance test data) causing the first flow increase at point B (fig. A.11-1).

Test results of flowmeter transient investigation are shown in Volume III. The test further substantiated these conclusions.

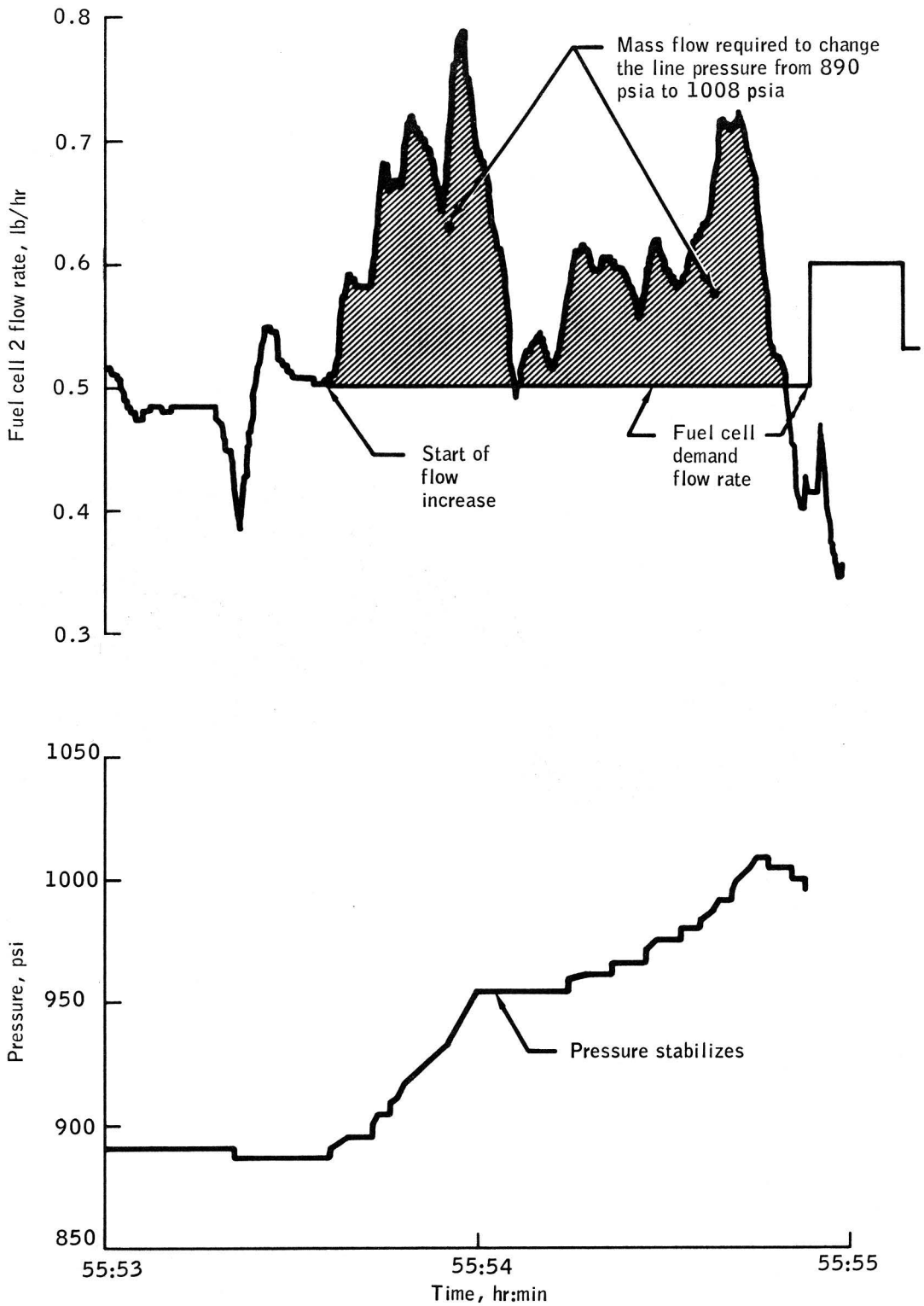

Figure A.11-1.- Effect of oxygen pressure on fuel cell flow rates.

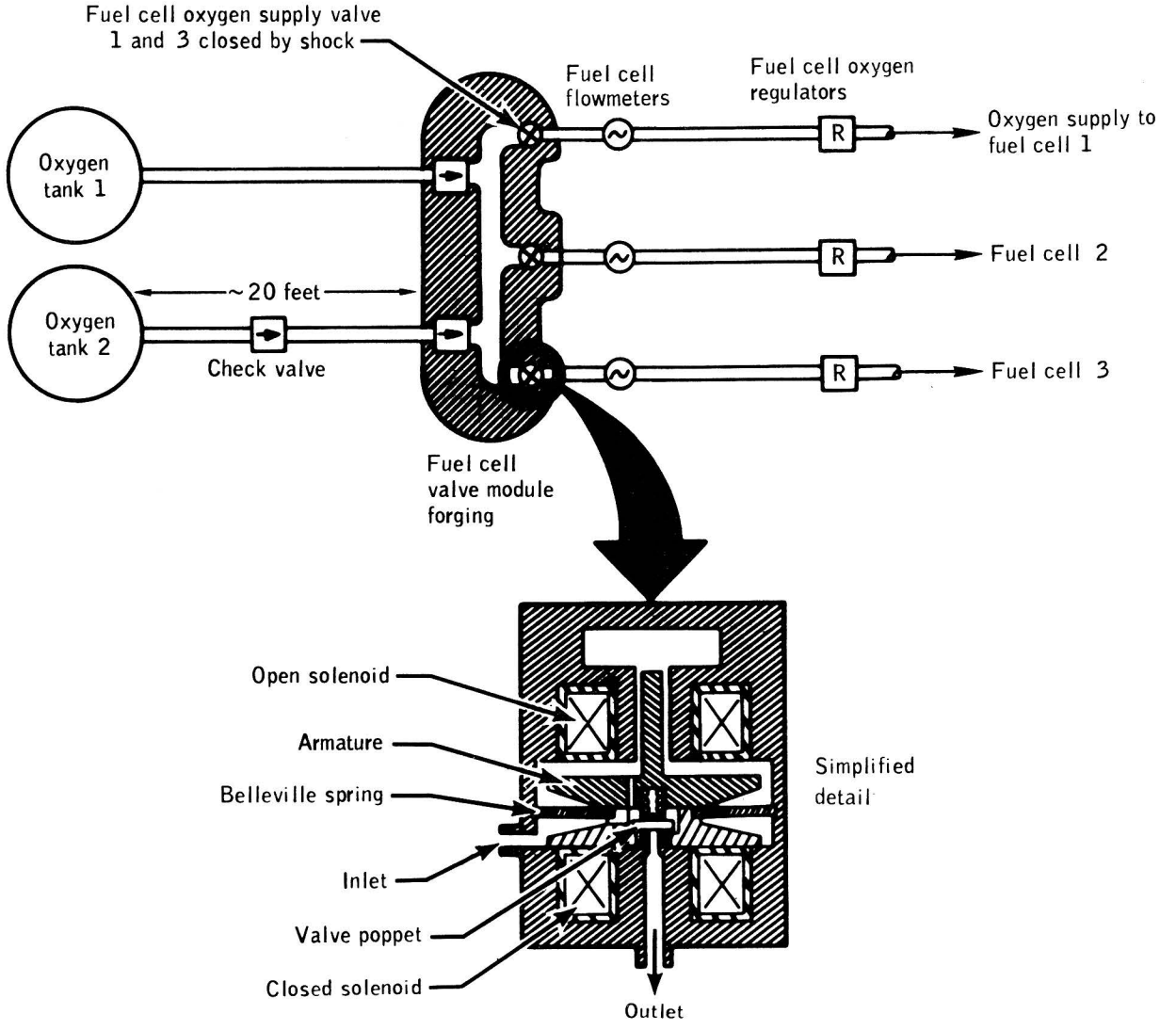

Figure A.11-2.- Solenoid valves for oxygen supply.

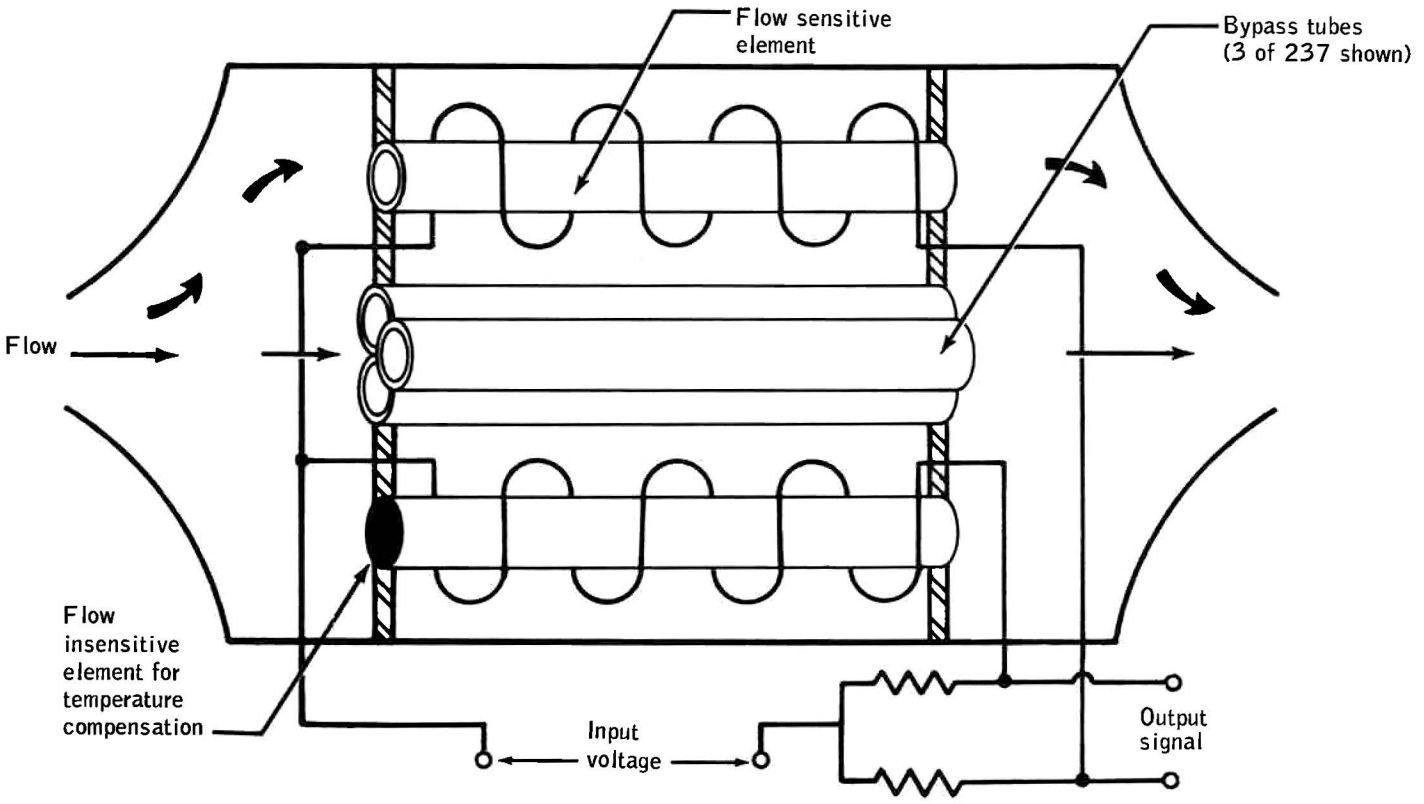

Figure A.11-3.- Flowmeter schematic.

A.12 CALCULATION OF PERFORMANCE LOSS BY FUEL CELLS 1 AND 3

A.12.1 Purpose

Determine if loss of the oxygen supply by closure of the fuel cell reactant shutoff valve caused the fuel cell 1 and 3 performance degradation.

A.12.2 Assumptions

The following assumptions were made:

a. Closure of the fuel cell 1 and 3 oxygen shutoff valves.

b. The temperature in the high pressure system (900 psia), oxygen shutoff valve to fuel cell regulator, was 70° F (530° R).

c. The temperature in the low pressure system (61.5 psia), fuel cell regulator to fuel cell stack, was 70° F for 14.99 in^3 and in the fuel cell stack was 400° F for 67.7 in^3.

d. Performance dropoff becomes evident at a reactant to nitrogen differential pressure of 4 psi. The normal pressure differential is 8.5 psi; therefore, at 57 psia, oxygen pressure performance dropoff should be evident.

e. Fuel cells 1 and 2 operated at 23 and 26 amperes, respectively, from valve closure to performance loss.

A.12.3 Analysis

In performing the analysis, the following facts were known:

a. The oxygen high pressure system volume, solenoid valve to fuel cell regulator, was 6.37 in^3.

b. The oxygen low pressure system volume, fuel cell regulator to stack, was 82.69 in^3.

c. At the time of failure, the oxygen high pressure was 1008 psia and the low pressure was approximately 61.5 psia.

d. The high pressure system will supply oxygen until pressure drops to 61.5 psia.

1. Oxygen initially in high pressure system, M_1:

$$M_{hp} = M_1 = \frac{P_1 V_1}{RT_1} = \frac{1008(144)(6.37)32}{1545(530)1728} = 0.0209 \text{ pound}$$

2. Oxygen at 61.5 psia:

$$M_2 = \frac{61.5}{1008}(0.0209) = 0.0013 \text{ pound}$$

3. Oxygen used to drop pressure from 1008 to 61.5 psia:

$$\Delta M_1 = M_1 - M_2 = 0.0196 \text{ pound}$$

4. Afterwards, all oxygen downstream of solenoid shutoff valve:

61.5 psia

5. Portion of low pressure system at 70° F:

$$V_3 = 6.37 \text{ in}^3 + 14.99 \text{ in}^3 = 21.36 \text{ in}^3$$

6. Oxygen in low pressure system at 70° F and 61.5 psia:

$$M_3 = \frac{P_3 V_3}{RT_3} = \frac{61.5(144)21.36)32}{1545(530)1728} = 0.00426 \text{ pound}$$

7. Oxygen in low pressure system at 400° F and 61.5 psia:

$$M_4 = \frac{P_4 V_4}{RT_4} = \frac{(61.5)(144)(67.7)32}{1545(860)1728} = 0.00835 \text{ pound}$$

8. Total oxygen in low pressure at 61.5 psia:

$$M_{lp} = M_3 + M_4 = 0.01261 \text{ pound}$$

9. Oxygen in total low pressure system at 57 psia:

$$M_5 = \frac{57}{61.5}(0.01261) = 0.0121 \text{ pound}$$

10. Oxygen used to drop pressure from 61.5 to 57 psia:

$$\Delta M_2 = M_{1p} - M_5 = 0.0005 \text{ pound}$$

NOTE: ΔP where performance drop occurs is not significant (0.0005 pound) compared to mass for drop from high pressure (1008 psia) to low pressure (61.5 psia).

11. Total oxygen mass used from reactant shutoff valve closure to oxygen system pressure of 57 psia (oxygen to nitrogen pressure differential is approximately 4 psi)

$$M_t = \Delta M_1 + \Delta M_2 = 0.0196 + 0.0005$$

$$M_t = 0.0201 \text{ pound}$$

12. Calculate time from reactant valve closure to evidence of performance dropoff:

Assume: Fuel cell 3 operated at 26 amperes
Fuel cell 1 operated at 23 amperes

$$T_{\text{Fuel cell 3}} = \frac{(0.0201 \text{ pound})(3600 \text{ sec/hr})}{(2.04 \times 10^{-2} \text{ lb/hr-amp})(26 \text{ amperes})} = 136 \text{ seconds}$$

Time for fuel cell 3 = 2 minutes 16 seconds

$$T_{\text{Fuel cell 1}} = \frac{26 \text{ amperes}}{23 \text{ amperes}} 136 \text{ seconds} = 154 \text{ seconds}$$

Time for fuel cell 1 = 2 minutes 34 seconds

13. Actual times from data review for fuel cell 3 is 2 minutes 29 seconds and for fuel cell 1 is 2 minutes 51 seconds.

A.12.4 Conclusions

A comparison of steps 12 and 13 of the analysis shows close agreement between the calculated and actual data performance loss times. The close agreement confirms that the operating times of fuel cells 1 and 3 were limited by the volume of oxygen trapped between the oxygen shutoff valve and fuel cell regulator. Therefore, the fuel cells 1 and 3 performance loss were caused by oxygen starvation due to closure of the oxygen shut-off valves located in the fuel cell valve module.

A.13 HEATER ENERGY ANALYSIS

A.13.1 Purpose

Examine the heater cycle prior to the anomaly to determine if an unknown energy source was present in the tank.

A.13.2 Analysis

The following data were used for the analysis:

a. Heater duty cycles from pressure plots:

Time switch opened, hr:min	Time switch closed, hr:min	Time on, minutes
53:39		
53:07	53:45	8
54:07	53:59	8
54:21	54:16	5
54:43.5	54:40	3.5

1. Total heater on time was 24.5 minutes.
2. Total heater time was 64.5 minutes (1.075).
3. Fuel cell oxygen usage was 1.53 pounds for 70 amperes.
4. Environmental control system oxygen usage was 2.415 pound.
5. Total oxygen usage was 3.945 pound.
6. Total heat input 463 Btu (heat leak plus heaters).
7. Heat required to expel 1.0 pound was approximately 97 Btu.
8. Total heat required was 382 Btu.
9. An additional 81 Btu was required due to the warmer than equilibrium fluid being expelled under high flow rate conditions.

b. From 55 hours 13.2 minutes to 55 hours 41 minutes, the heaters were on 5 minutes.

1. Fuel cell usage was 0.658 pound.

2. Environmental control system oxygen usage was 0.093 pound.

3. Total oxygen usage was 0.751 pound.

4. Total energy input was 89 Btu.

5. Required energy was (0.751) × (97) = 73 Btu.

6. An additional 16 Btu was required due to warmer than average fluid being expelled.

A.13.3 Conclusions

There is no evidence of a significant unknown energy source in the tank prior to the anomalous pressure excursion.

A.14 LOCKED ROTOR IN ZERO-G

A.14.1 Purpose

Determine if the fan motor would overheat (resistance heating) and become a source of ignition energy if the rotor is locked in the zero-g heat transfer situation.

A.14.2 Assumptions

The following assumptions were made:

a. No heat leaves the motor proper.

b. W = weight of motor = 0.88 lb

c. C_p = approximate specific heat = 0.2 $\frac{\text{Btu}}{\text{lb}\ ^\circ\text{R}}$ at 70° F

d. Q = heat input (28 watts) = 95.6 $\frac{\text{Btu}}{\text{hr}}$

e. Δt = heat-up time (30 to 100 sec) = 0.00833 to 0.0278 hr

f. ΔT = temperature rise

$$\Delta T = \frac{Q\ \Delta t}{C_p\ W} = {}^\circ\text{R}$$

A.14.3 Analysis

The temperature rise from room temperature was estimated for the following conditions:

	Approximate temperature rise, °R	
	In 30 seconds	In 100 seconds
100 percent of motor affected	4.5	15.1
10 percent of motor affected	45.2	151

A.14.4 Conclusions

From this calculation it is concluded that pure resistance heating would not produce ignition temperatures unless the heat is concentrated in much less than 10 percent of the motor. Figure A.14-1 shows the temperature rise that would occur as a function of the fraction of the motor's mass that absorbs energy for heat-up times of 30 and 100 seconds.

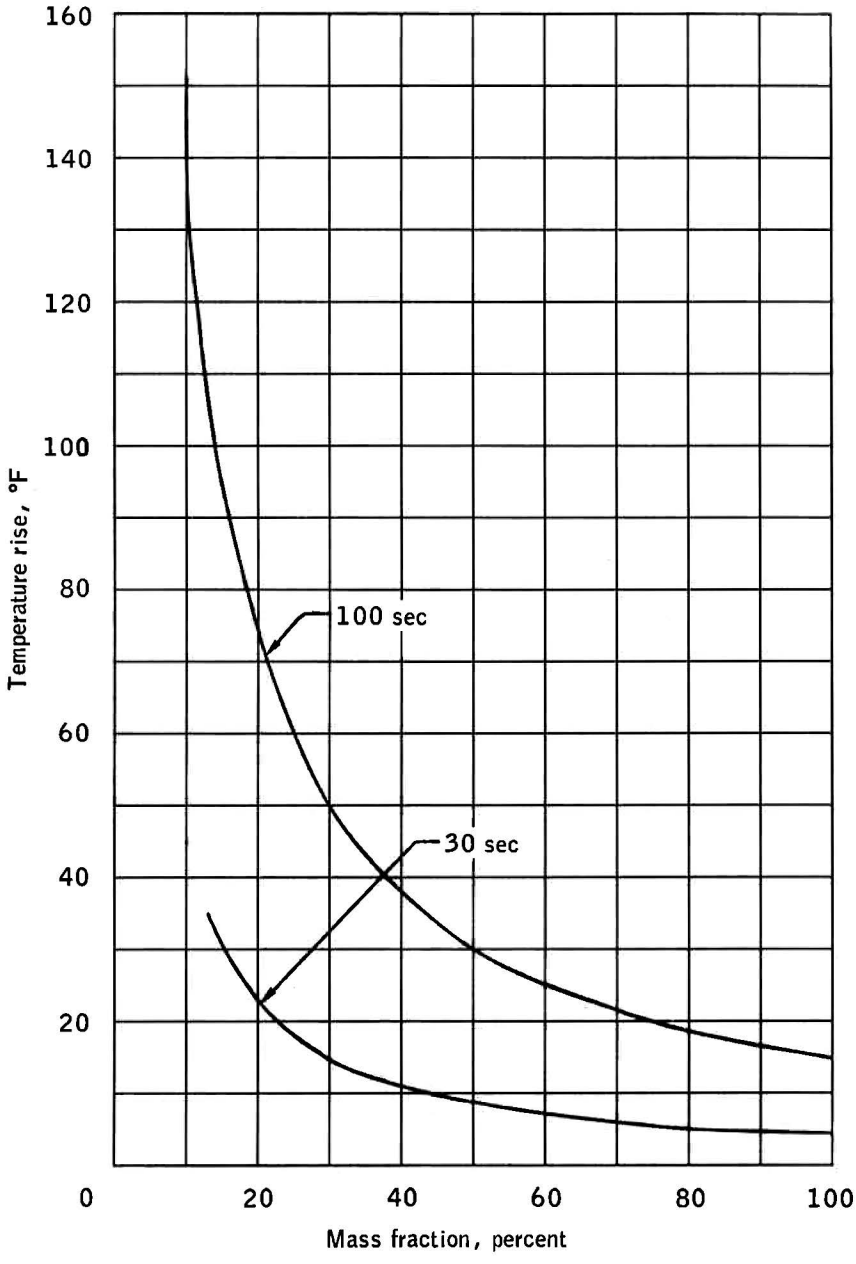

Figure A.14-1.- Heating rates for stalled fan motor in zero g. (no heat loss from the motor)

A.15 ANALYSES OF TWO POSSIBLE IGNITION MECHANISMS

A.15.1 Purpose

Provide information on the reactions from possible contaminants in the oxygen pressure vessel and the reaction from high pressure oxygen leaking into the vacuum jacket.

A.15.2 Analyses

The two following analysis were conducted.

A.15.2.1 Contaminants and Detached Solids in the Tank

In examining possible contaminants or deteched solids, it is necessary to include some aspects of the ground support equipment used in the fill and detanking procedures as well as the components internal to the pressure vessel. Examples of detached solids include contaminants added to the tank during filling, inadvertent cryogenic pumping of air after detanking, and solids detached from internal components by chafing, stress, vibration, detanking, etc. The mechanism postulated involves heat addition due to detached solids impacting the fan vanes or surfaces in close proximity after being accelerated by the fan. Another mode of adding heat is by friction induced from detached solids between rotating parts.

Lead-tin solder, a lubricant (Drilube 822), and tin-plated copper clips are specific materials in the system which have demonstrated sensitivity at low impact energy levels in liquid oxygen. Impact-initiated reactions normally occur very rapidly and very frequently at explosive rates. On the other hand, many examples of impact sensitivity are found where a flash occurs but does not propagate. Long duration, slow burning processes such as are required to satisfy the observed rate of pressure rise in tank 2 have not been observed in liquid oxygen tests. This may be due to the nature of the test rather than to the nature of the material.

The tank probe, heater, and fan assembly have been examined for sources of deteched solids, which could be accelerated by the fans and could have impacted with impact-sensitive materials. Two possibilities were examined. One was a particle which could have passed through the ground support filter. From filter backwash tests, about a 250-micron diameter particle was considered maximum. Using a density for aluminum (0.1 pound per cubic inch) and a tip velocity of 10 ft/sec, assuming no drag loss through the fluid and total conversion of kinetic energy to heat, a value of 10^{-7} joules was obtained. A second possibility considered was the detachment of the center pin from one of the 1/8-inch diameter blind rivets in the probe assembly. The analysis previously described was used except that the pin dimensions gave a particle of 1.7×10^{-3} pounds and resulted in energy of 4×10^{-4} joules. These energy levels are well below the energies demonstrated by test to be necessary for ignition.

This review also revealed two component parts which differ only by dash number designation between the oxygen tank and the hydrogen tank (Beech Aircraft Company part numbers 13532-3132 and 13532-3134). The part for the hydrogen tank is made of a titanium alloy, and the one for oxygen storage is Inconel. No evidence exists for an inadvertent substitution since data and inspection records show correct dash numbers were installed. Even if a substitution had been made, an impact of about 70 ft-lb would be required to cause a problem, and again, no explanation of the "slow" nature of the event is available, assuming impact sensitivity.

A.15.2.2 Ignition of Thermal Blanket in Vacuum Jacket

The insulation in the vacuum jacket consists of fiberglass and aluminum foil (0.00018 inch thick) in alternate layers. Aluminized insulation material is used in the dome region around the discharge lines. An adhesive in the fiberglass mat is used as a binder for the glass, and its

composition would indicate incompatibility with liquid oxygen. Under impact conditions, aluminized Mylar is unacceptable for liquid oxygen usage.

If a high pressure leak of oxygen from the pressure vessel impinged on the insulation, some material reaction could occur, but literature data on impinging oxygen at 1500 psi onto aluminized Mylar show that this type of test did not cause ignition. Therefore, it would appear that hot oxygen (at a temperature to be determined by test) would be required to promote ignition of the insulation in the annulus. This would indicate that this reaction would be a second-order effect but could provide additional heat and pressure to explain the loss of the service module panel or damage to cryogenic oxygen tank 1 lines or components.

This mechanism could not explain the electrical anomalies including the quantity gage behavior and current spikes observed in the electrical data.

A.16 INVESTIGATION OF DETANKING PROCEDURE

A.16.1 Purpose

Determine if cavitation could have occurred at the fan impellers in oxygen tank 2 during detanking at the launch site.

A.16.2 Assumptions

A fan blade may be represented as an elongated ellipse whose major to minor axis ratio a:b is 10:1. The angle of attack of a blade was assumed to be 45 degrees.

A.16.3 Analysis

The effects of cavitation are the introduction of vibration to the rotor assembly and pitting due to material erosion, caused by cavitational shocks. Such shocks result from a sudden collapse of the gas bubbles generated by local expansion of the fluid upon passage of the fan blade.

At one time, the fans and heaters operated continuously for 6 hours submerged in liquid oxygen at its boiling point. Under these conditions, the only pressure differential acting to prevent cavitation was provided by the gravitational head of the liquid. Cavitation will occur for the ellipsoidal model used if the static head h is:

$$\rho h < \frac{\rho u^2}{2g_c} \left[1 + \left(\frac{b}{a}\right)^2 \cos^2\alpha + \frac{a^2}{b^2} \sin^2\alpha \right] - 1$$

With the model parameters and oxygen properties during the 6 hour boil off this gives

$$h < 4.32 \text{ feet}$$

A.16.4 Conclusions

Since the tank has a diameter of about 26 inches, it is apparent that cavitation could have occurred at both fans throughout the 6 hour boil off. This may have produced detrimental fatigue properties on both fan impellers and shafts.

A.17 PROPOSED MECHANISM FOR PRESSURE RISE IN CRYOGENIC OXYGEN TANK 2

A.17.1 Purpose

Develop combustion mechanism to explain the flight data on tank 2 pressure, temperature, and quantity. This mechanism will attempt to identify the initiation point, propagation path, and heat transfer to fit the flight data.

A.17.2 Assumptions

The following assumptions were made:

a. Combustion is initiated near the center of the electrical conduit.

b. Propagation is along a single strand of fuel, the polytetrafluoroethylene sleeve on one of the motor lead cables, and proceeds in both directions without ignition of any other material in the conduit.

c. One flame front traverses the conduit length from the initiation point to the electrical connector in 26.3 seconds, the time to the beginning of the pressure plateau. The other reaches the tank end of the conduit in 40.3 seconds. This implies a propagation rate of 0.479 in/sec.

d. Tank fluid density just prior to the first pressure rise was 54.3 lb/ft^3.

e. Heat transfer from hot gas in the conduit occurs by conduction only. The heat transfer rate is independent of conduit and wire bundle temperatures.

f. Burning rate is constant (due to the absence of data on its variation with environmental conditions).

A.17.3 Analysis

If combustion begins near the center of the conduit, the flame will propagate in both directions along the strand of fuel. When one of the two flame fronts reaches the electrical connector, it will be extinguished, reducing the total rate of combustion by one-half. This is assumed to be the beginning of the pressure plateau at 26.3 seconds after ignition (fig. A.17-1, points A and B). The other flame front continues and is assumed to reach the tank end of the conduit at the end of the plateau, 40.3 seconds after ignition (fig. A.17-1, point C). These two time points and the overall conduit length of 31.9 inches allow a solution for the required propagation rate and ignition site, which are 0.479 in/sec and 12.6 inches from the electrical connector (fig. A.17-2).

During this first 40.3 seconds, the hot gas around the burning insulation is exposed to a heat sink consisting of the conduit and the wire bundles within it. The 14-second pressure plateau is explained by the combustion rate being reduced by one-half while the heat transfer to this sink continues at a rate comparable to the first 26 seconds. At the end of the period the pressure begins rising again (point C on fig. A.17-1) because the combustion has reached the tank volume and the upper end of the quantity probe does not significantly add to the continuing heat sink effect of the conduit materials.

Certain other data support an energy input history such as this. The abrupt rise of the temperature sensor probe occurs shortly after the combustion is postulated to have reached the temperature sensor probe (fig. A.17-1). Figure A.17-2 shows the sensor location, and its rapid response indicates the sudden proximity of very high temperature material. Also, on figure A.17-1 the quantity probe begins indicating an abnormally low value almost coincident in time with the temperature response. This reading decreased rapidly, which could have been caused by a continuing increase in the fluid temperature near or within the quantity probe.

The pressure rise is explained by stratification and the piston effect of the hot gas resulting from combustion. This gas expands as energy is added to it and isentropically compresses the cold cryogenic fluid. Calculated pressures for an assumed hot bubble average temperature of 1200° F are compared with the flight data in figure A.17-1. Sensitivity of bubble properties and consequent energy input requirements to assumed bubble temperatures can be seen from figures A.17-3 and A.17-4. Figure A.17-5 presents the cumulative net energy input required to reach a given tank pressure for a bubble temperature of 1200° F. These calculations account for tank stretch due to pressure rise but neglets energy loss due to normal oxygen usage.

Heat transfer to the conduit and wiring was calculated by a basically one-dimensional conduction model. Propagation was treated by breaking the time span into four steps and the axial distance along the conduit into four zones. One constant representing energy potential for heat transfer per unit time was evaluated based on the pressures at the end points of the first pressure ramp and the selected fuel. Cumulative heat transferred to the conduit is plotted versus time in figure A.17-6.

A.17.4 Conclusions

A combustion process beginning near the center of the conduit and burning only the sleeve of one of the motor lead cables will fit the flight data for pressure rise and temperature and for quantity sensor behavior. Verification of this mechanism would require experimental determination of the combustion rates, the actual heat transfer rate, and the possibility of burning only a limited amount of the polytetrafluoroethylene in the conduit.

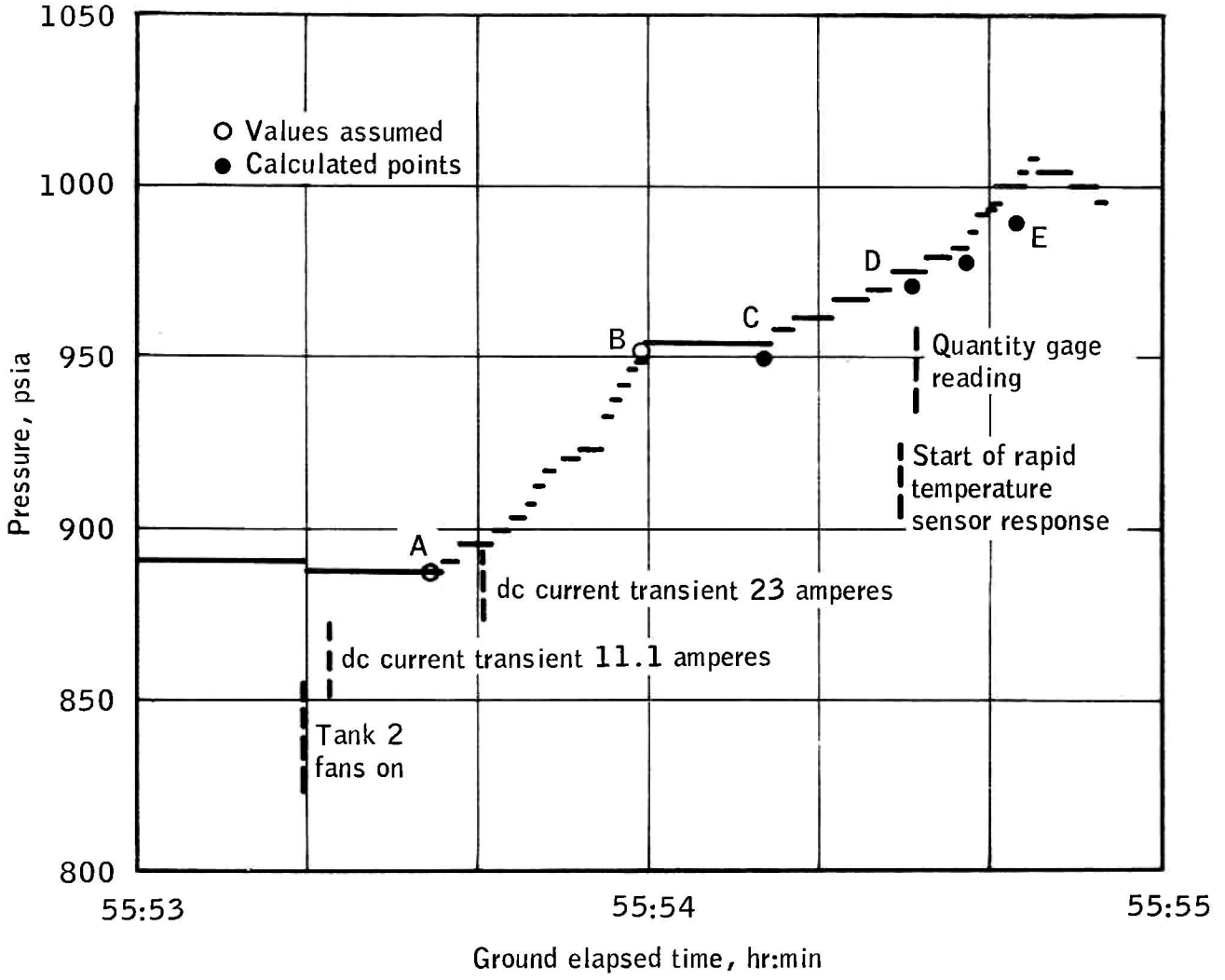

Figure A.17-1.- Significant flight data.

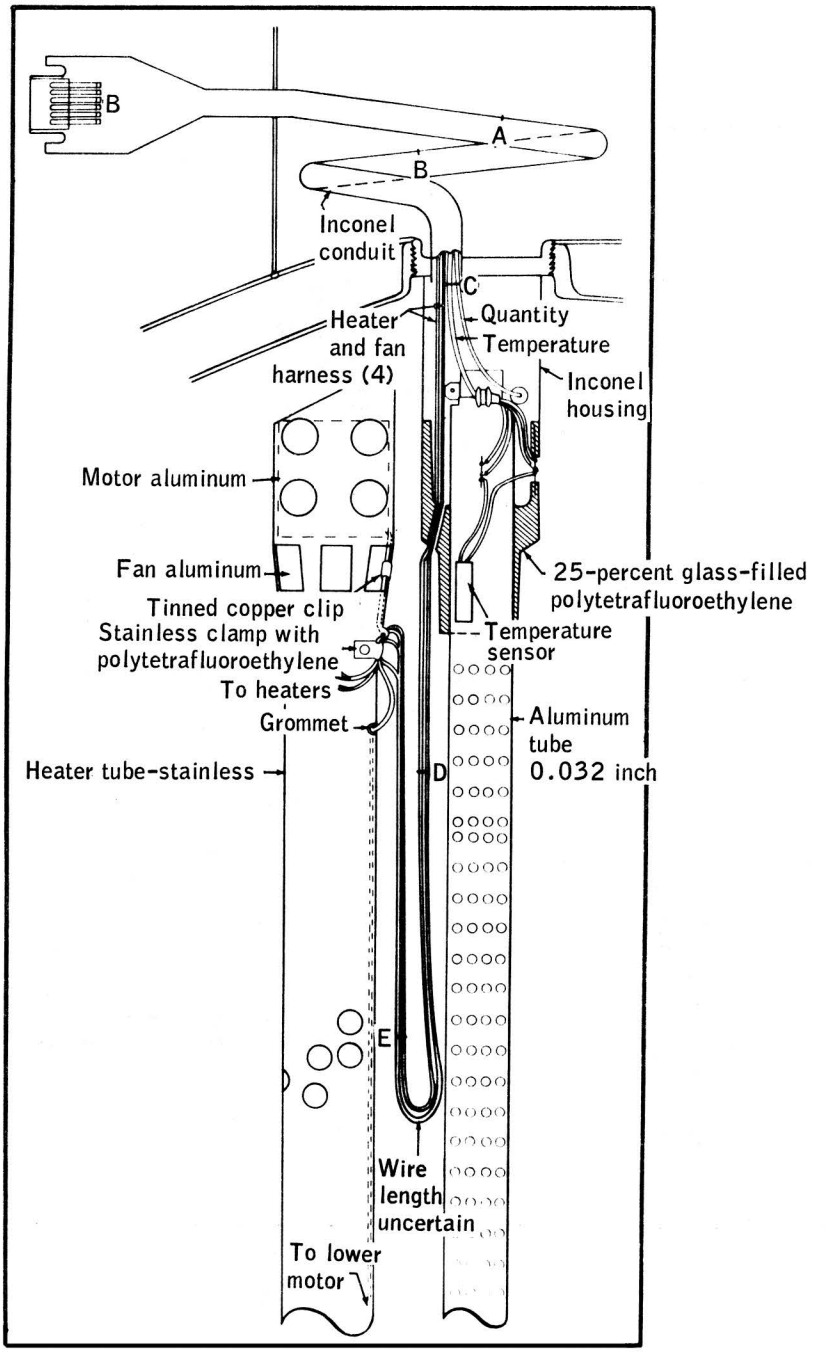

Figure A.17-2.- Upper oxygen tank configuration.

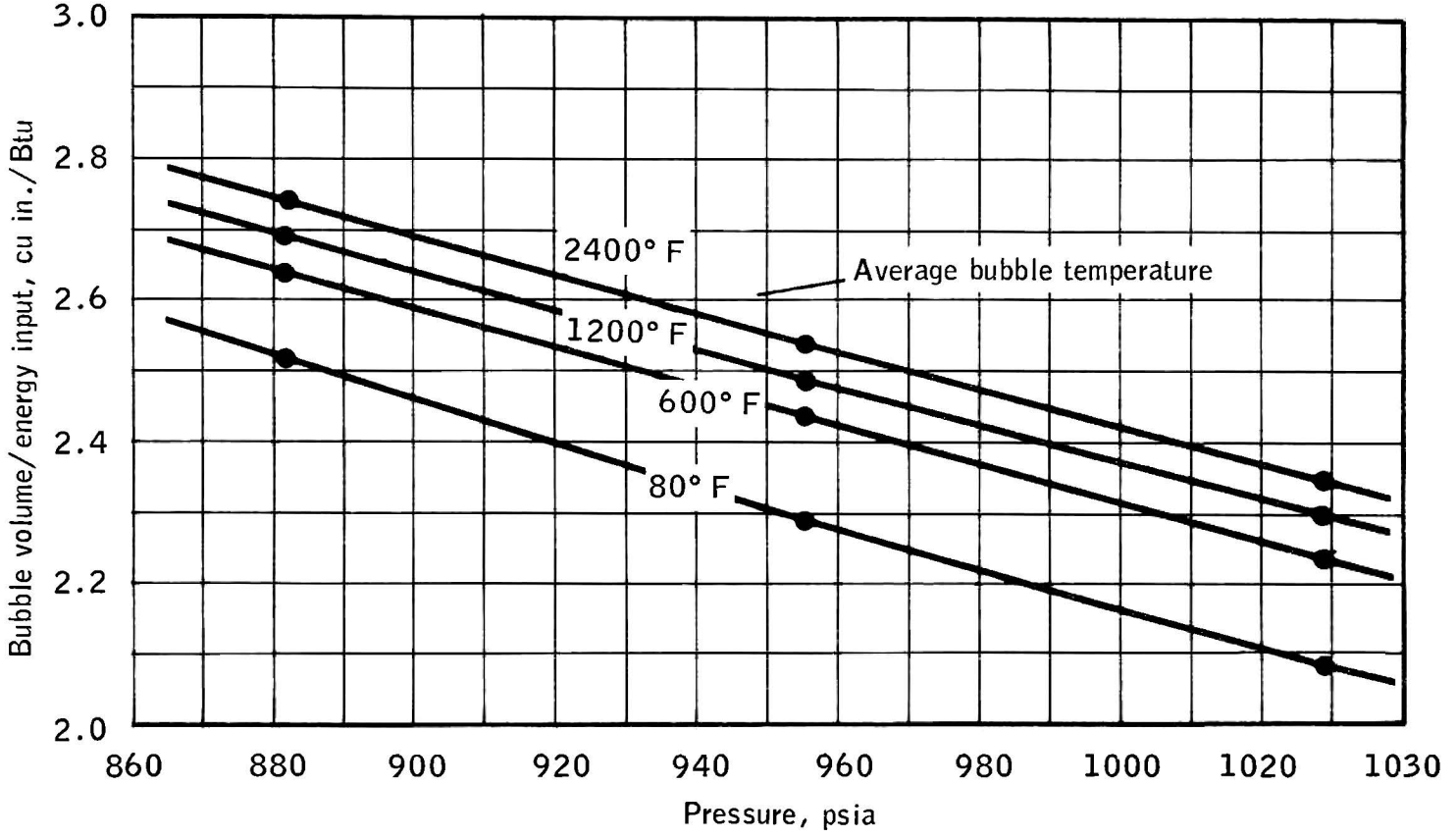

Figure A.17-3.- Gas bubble properties.

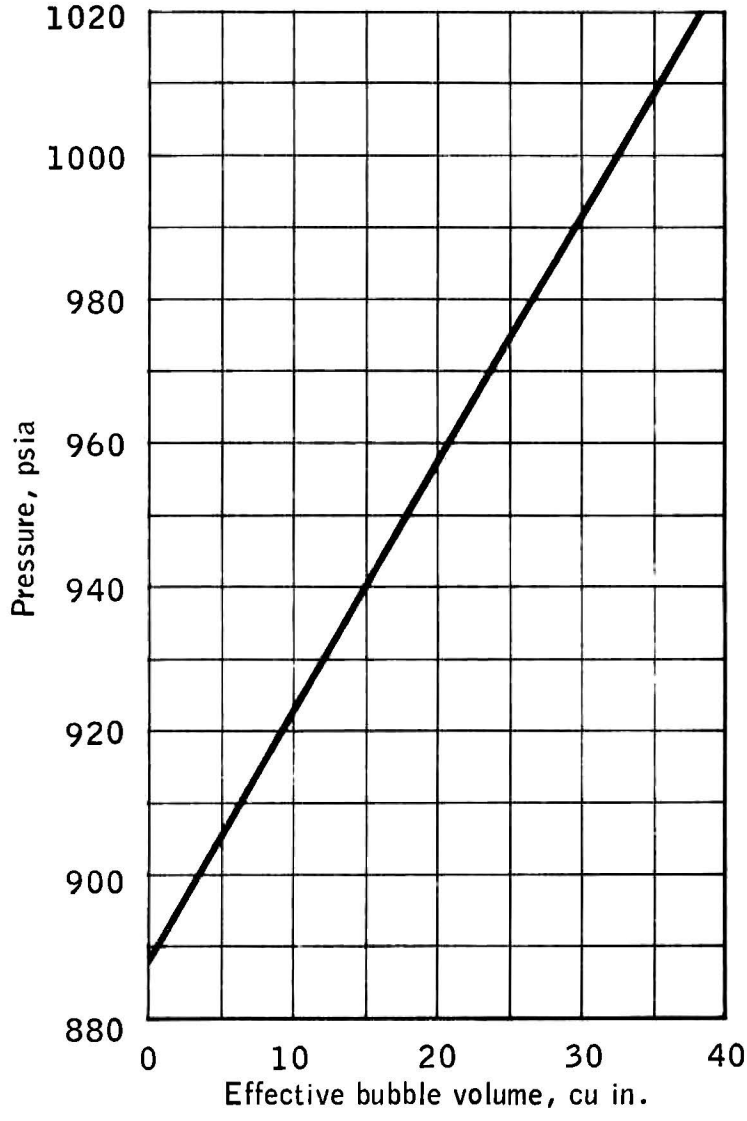

Figure A.17-4.- Isentropic compression and tank stretch effects.

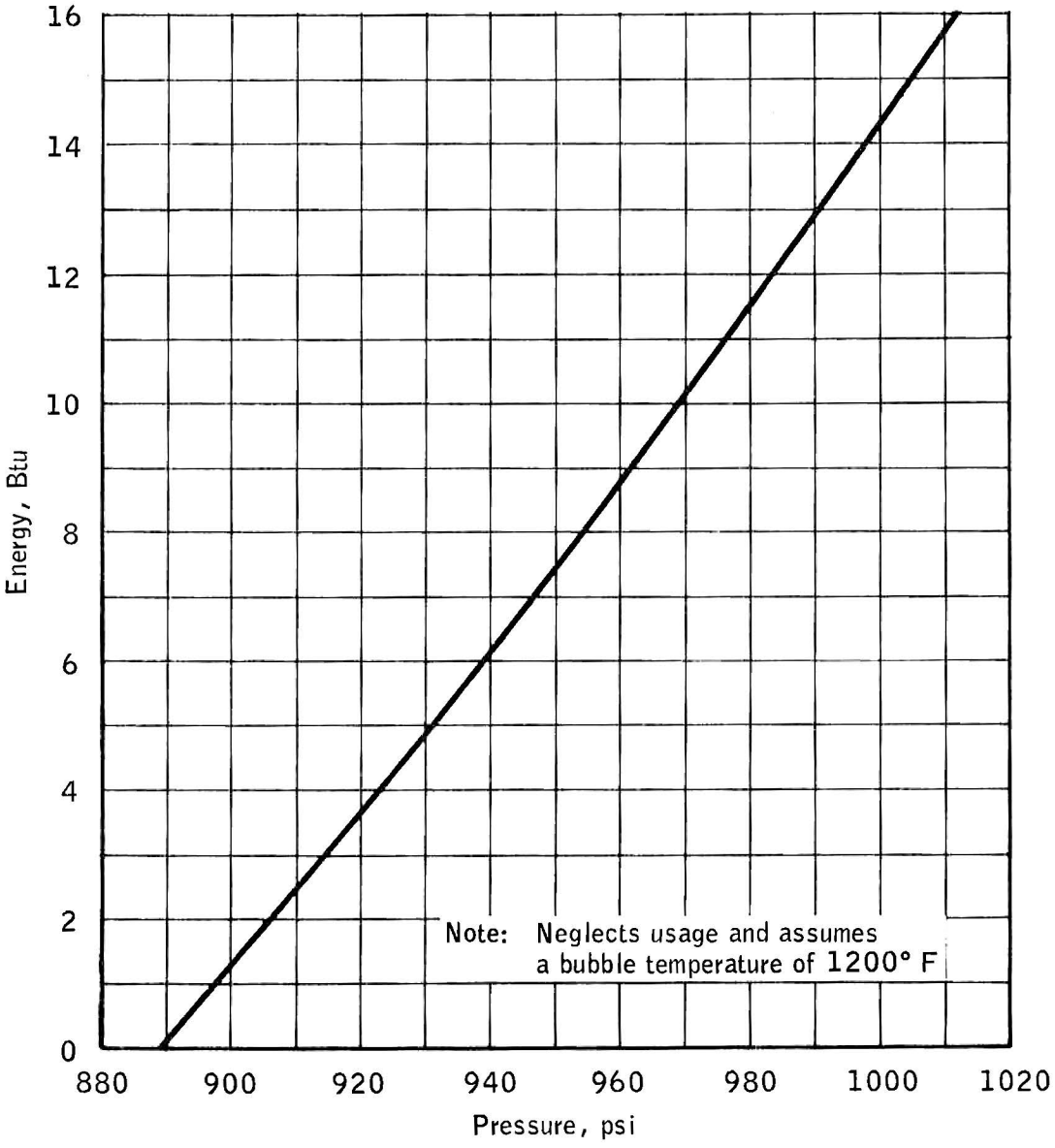

Figure A.17-5.- Net heat in bubble versus tank pressure.

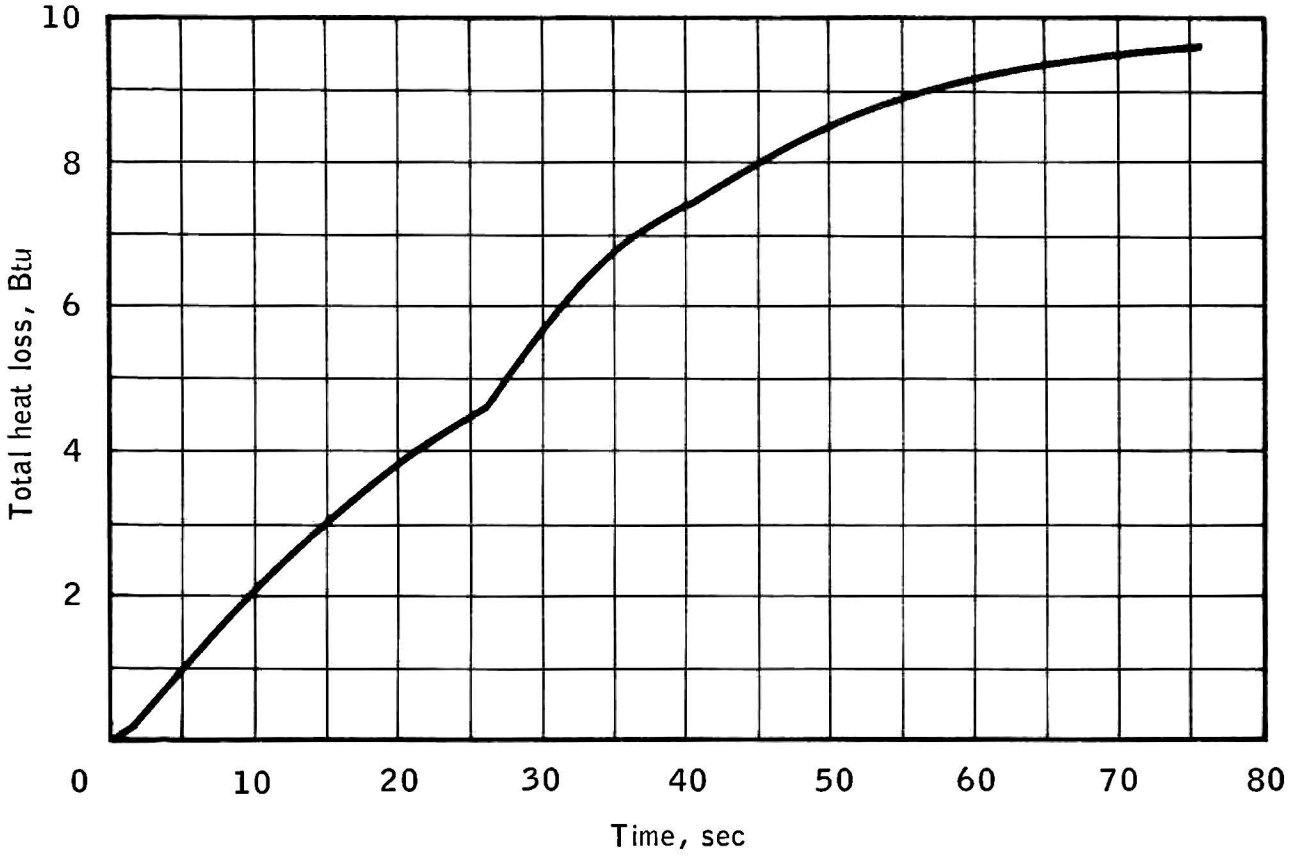

Figure A.17-6.- Heat loss from hot gas to electrical conduit heat sink materials.

A.18 CALCULATION OF FLAME TEMPERATURES AND REACTION-PRODUCT COMPOSITIONS FOR THE POLYTETRAFLUOROETHYLENE-OXYGEN SYSTEM

Equilibrium chemical calculations were performed for the chemical system using the numerical technique of reference 1. The thermochemical data necessary for this analysis were taken from the JANAF tables, reference 2. The enthalpies of formation for the polytetrafluoroethylene and oxygen under the Apollo 13 oxygen system conditions, referenced to 298° R, are

$$\Delta H_{f_{O_2}}^{298} = -66.7 \text{ cal/gm (reference 3)}$$

$$\Delta H_{f_{(C_2F_4)_P}}^{298} = -2004.56 \text{ cal/gm}$$

The enthalpy of formation of the polytetrafluoroethylene represents the best estimate as obtained from the combination of data taken from several references.

A range of conditions were run for which the stoichiometry of the mixture was varied as well as the total mixture enthalpy to investigate the effects of non-ideal conditions on the mixture flame temperature and composition. The effects of additional oxygen or diabatic conditions lowers the flame temperature and pushes the composition away from the ideal stoichiometric mixture conditions:

$$C_2F_4 + O_2 \rightarrow 2CO\ F_2$$

By extrapolation the diabatic conditions back to the -298° R initial system conditions, the total heat available from the equilibrium chemical reaction is approximately 2300 Btu/lb of polytetrafluoroethylene.

A.19 CALCULATION OF FLAME TEMPERATURES AND REACTION PRODUCT COMPOSITIONS FOR THE MYLAR-OXYGEN SYSTEM

Equilibrium chemical calculations were performed for the Mylar-oxygen chemical system using the numerical technique of reference 1. The thermochemical data necessary for this analysis were taken from the JANAF tables, reference 2. The heat of combustion for the Mylar and oxygen are:

$$\Delta H_R = 9850 \text{ Btu/lb}$$

A range of conditions were run for which the stoichiometry of the mixture was varied as well as the total mixture enthalpy to investigate the effects of non-ideal conditions on the mixture flame temperature and composition. The effects of additional oxygen or diabatic conditions lowers the flame temperature and pushes the composition away from the ideal stoichiometric mixture conditions:

$$C_{10}H_8O_4 + 10\ O_2 \rightarrow 10\ CO_2 + H_2O$$

By extrapolation the diabatic conditions back to the 540° R initial system conditions and using the total heat available from the equilibrium chemical reaction, 9850 Btu/lb Mylar, the adiabatic flame temperature decreased from approximately 5700° R to 2700° R at 2 atmospheres and from 5100° R to 2700° R at 0.1 atmosphere.

REFERENCES

1. Kendall, R. M.: A General Approach to the Thermochemical Solution of Mixed Equilibrium-Nonequilibrium, Homogeneous or Heterogeneous Systems, Aerotherm Corp. Report No. 66-7, Part V, March 1967.

2. Anon: JANAF Thermochemical Tables, Contract No. AF33(616)-6149, Thermal Laboratory, The Dow Chemical Co., June 30, 1962.

3. Weber, L. A.: Thermodynamic and Related Properties of Oxygen from the Triple Point to 300° K at Pressures to 330 Atmospheres, U. S. Department of Commerce, National Bureau of Standards, NBS Report 9710, June 1968.

PART B

REPORTS OF TESTS PERFORMED IN SUPPORT OF THE CRYOGENIC OXYGEN TANK 2 ANOMALY INVESTIGATION

B.1 INTRODUCTION

An extensive experimental program was performed in support of the Apollo 13 cryogenic oxygen tank 2 anomaly investigation. This experimental effort consisted of tests at the Manned Spacecraft Center, at other National Aeronautics and Space Administration centers, and at various contractor and subcontractor facilities. Part B of Volume III is a compilation of the reports from these tests.

A tabulation of the reports, including the report number and subject, is shown in the table of contents.

The tests provided supporting data for accepting or rejecting the various mechanisms postulated for the anomaly. For example, tests supporting the most likely of the failure mechanism include those determining energy requirements for the various ignition mechanisms, energies available, propagation rates of various tank materials, and various failure modes. Other tests determined the functional and transient response characteristics of various components and instrumentation for nominal and off-nominal operations. Still other tests determined the stimulus and conditions required to duplicate those observed in the spacecraft and oxygen system.

A master file of all test and supporting data concerning the anomaly investigation will be maintained by the Apollo Spacecraft Program Office, Manned Spacecraft Center, Houston, Texas 77058. If required, more detailed information concerning each test may be obtained by contacting the manager of that office.

B.2 CRYOGENIC OXYGEN DENSITY AND TEMPERATURE SIGNAL CONDITIONER TEST

B.2.1 OBJECTIVE

The objectives of this test were to determine the output characteristics of the signal conditioner when subjected to hot and cold temperature extremes and to establish the transient and steady state energy levels that could be transmitted to the density and temperature sensor probes under fault conditions.

B.2.2 TEST EQUIPMENT AND CONDITIONS

The location of the probe assembly within the cryogenic oxygen tank and a simplified schematic of each signal conditioner are shown in figure B.2-1.

The signal conditioners for the density and temperature probes for each cryogenic tank are contained within a single hermetically sealed unit but are isolated electrically from each other through independent power supplies.

The signal conditioner was subjected to hot and cold temperature extremes during three separate test sequences. The first sequence was from ambient temperature (plus 70° F) to minus 125° F for 7 minutes. The second sequence was from ambient temperature to plus 180° F for 7 minutes. The third sequence was from ambient temperature to immersion in liquid nitrogen at minus 125° F for 1 minute. The signal conditioner was operating during these tests, and the equipment case temperature reached the extremes of plus 180° and minus 125° F within 30 seconds. The case temperature, when immersed in liquid nitrogen, reached minus 315° F within 10 seconds.

Tests were conducted to determine the transient and steady state energy levels that could, by any possible fault condition or combination of instrumentation wiring, be transmitted to the density and temperature sensors. During these tests, signal conditioner output wave forms were also noted in order to correlate known fault conditions with those of mission telemetry data.

B.2.3 RESULTS

The test sequences from ambient to hot and cold temperature extremes indicated no effects greater than those predicted from temperature data obtained during steady state qualification tests. The immersion of the signal conditioner in liquid nitrogen did not affect the signal output; however, the Nylon potting boots of the electrical connectors did crack.

The maximum transient energy that could have been provided by the temperature circuitry was calculated (at nominal temperature) to be 0.1×10^{-6} joules. The measured energy was 0.006×10^{-6} joules. The maximum steady state energy which could be supplied was by the density circuit under a fault condition of the low Z lead to ground through a 500-ohm resistance. This steady state energy was measured at 4.8×10^{-3} watts.

The following is a list of the more significant fault conditions and their effects on the signal conditioner output signal:

Fault	Effect
Density probe intermittent short circuit (low Z to high Z)	Output rapidly decreased to zero, remained approximately 0.7 second, then slowly (1.5 seconds) increased to correct value
Density probe high Z short circuit to ground	Output decreased to zero with positive spikes every 1.5 seconds
Density probe low Z short circuit to ground	Output decreased to zero
Density probe open circuit	Output increased to full scale
Density probe intermittent short-circuit period less than 1.5 seconds	Output oscillated
Temperature sensor short circuit	Output decreased to zero
Temperature sensor short circuit to ground	Output decreased to zero

Temperature sensor ground side open circuit	Output increased to full scale
Temperature sensor high side (+) open circuit	Output decreased to zero
Short circuit temperature sensor ground side to density probe high Z	Density output increased to full scale, temperature output did not change
Short circuit temperature sensor ground side to density probe low Z	Density output decreased to zero, temperature output decreased slightly
Short circuit temperature sensor high side to density probe high Z	Density output oscillated, temperature output did not change
Short circuit temperature sensor high side to density probe low Z	Density output decreased to zero, temperature output oscillated

B.2.3 CONCLUSIONS

The temperature tests performed had no effect on signal conditioner output. The energy levels provided to the density and temperature sensor were insufficient to create or support combustion within the cryogenic tank. The observed signal conditioner signal output wave forms indicated that the most probable failure modes were associated with an intermittent or short circuit of the density probe leads.

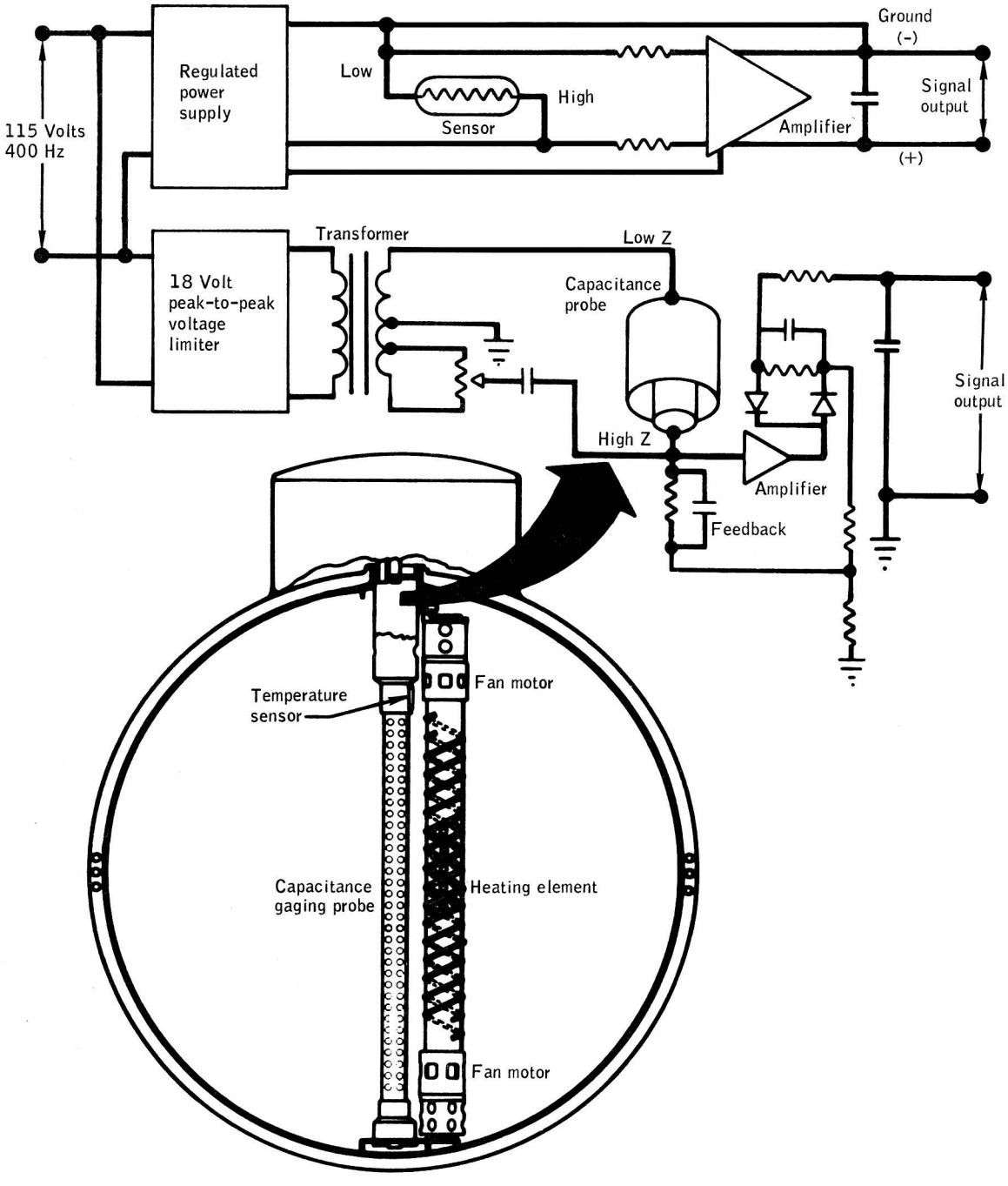

Figure B.2-1.- Cryogenic density and temperature location and simplified signal conditioner schematic.

B.3 PRESSURE TRANSDUCER RESPONSE TEST

B.3.1 OBJECTIVE

One objective of this test was to determine the differential pressure between a simulated oxygen tank and the flight transducer as a function of mass flow through the relief valve assembly when the entire system is conditioned to the actual Apollo 13 oxygen tank pressure and temperature. Another prime objective was to determine the response of the flight transducer to a step pressure stimulus.

B.3.2 TEST EQUIPMENT AND CONDITIONS

The test fixture was a modification of the system used during the ambient condition tests (fig. 3-1). A blowdown test, using gaseous oxygen at minus 130° F was completed by first pressurizing the system to 985 psig and allowing it to temperature stabilize. Then as rapidly as possible, the shock tank was used to dynamically pressurize the simulated oxygen tank to 1060 psig. To increase the pressure from 985 to 1060 psig required 32 milliseconds.

B.3.3 RESULTS

A maximum difference of 9.0 psi (fig. B.3-2) was observed between the oxygen tank pressure and the relief valve assembly inlet pressure (flight transducer reading) at a relief valve flow rate of 182 lb/hr. The differential pressure between the two ground support equipment transducers was 4 psi at the same flow rate. The pressure stimulus of 75 psi required 24 milliseconds (fig. B.3-3) to transmit from the simulated oxygen tank through the equivalent spacecraft line length to the relief valve assembly. The flight transducers responded to the pressure stimulus at the same time as the ground support equipment relief valve transducer. Each achieved 100-percent of the step input in 57 milliseconds, corrected for the inability to produce a step pressure stimulus at the simulated oxygen tank.

B.3.4 CONCLUSIONS

This test indicates that, within the measurement range, the pressure transducer is capable of following any change in pressure that may occur between sample times.

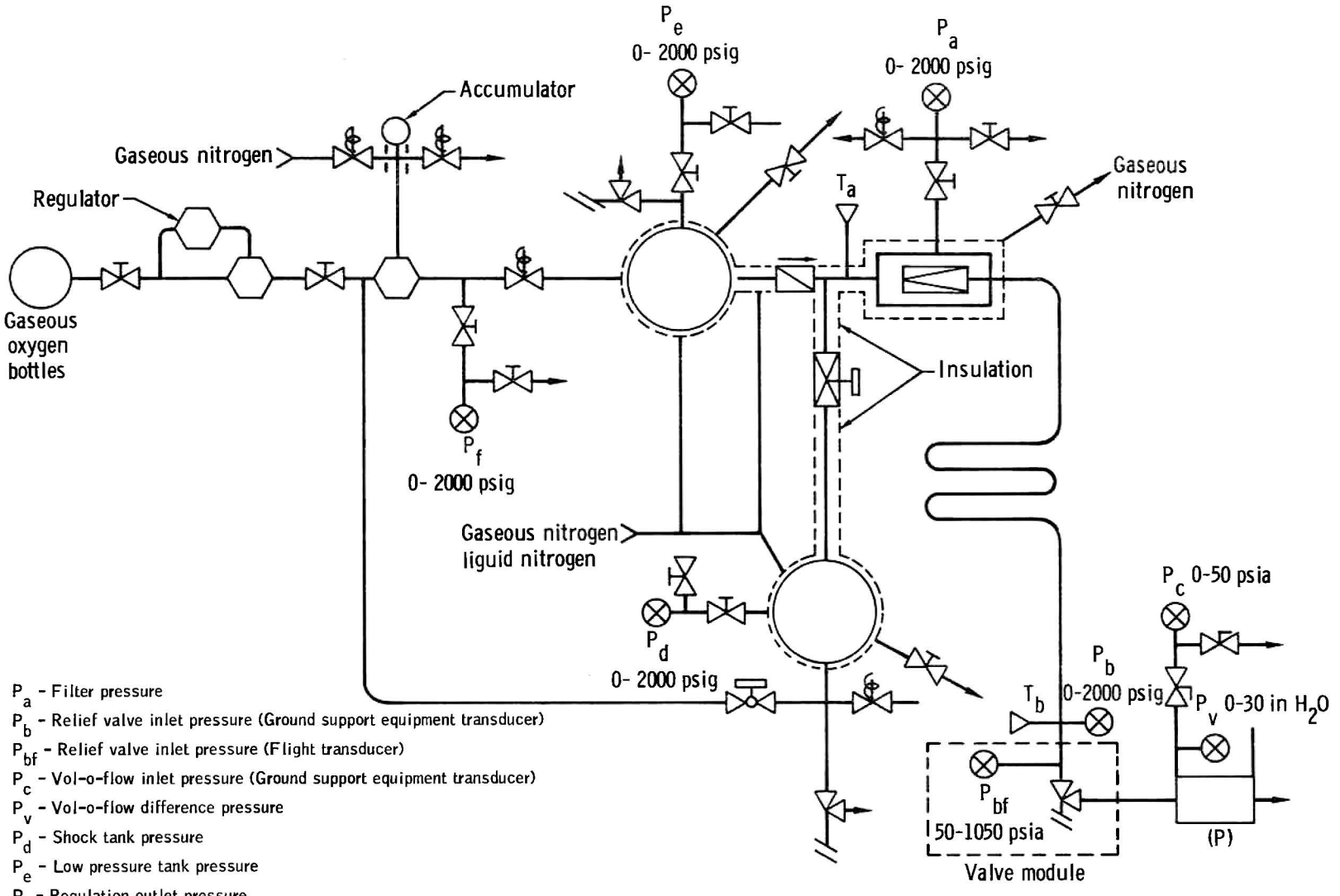

P_a - Filter pressure
P_b - Relief valve inlet pressure (Ground support equipment transducer)
P_{bf} - Relief valve inlet pressure (Flight transducer)
P_c - Vol-o-flow inlet pressure (Ground support equipment transducer)
P_v - Vol-o-flow difference pressure
P_d - Shock tank pressure
P_e - Low pressure tank pressure
P_f - Regulation outlet pressure
T_a - Filter inlet temperature
T_b - Relief valve inlet temperature

Figure B.3-1. - Pressure transducer test setup.

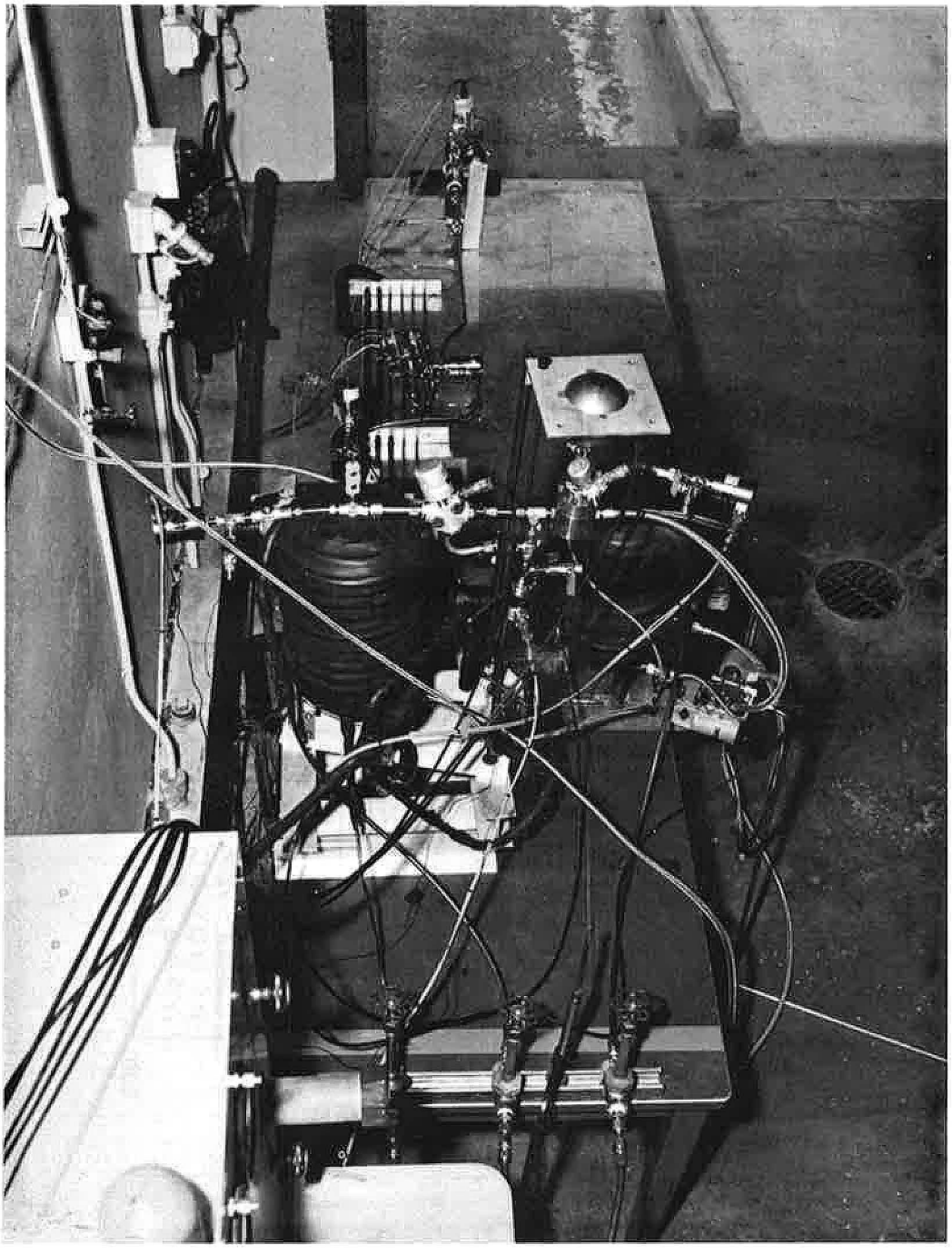

b) Test stand

Figure B.3-1.- Concluded.

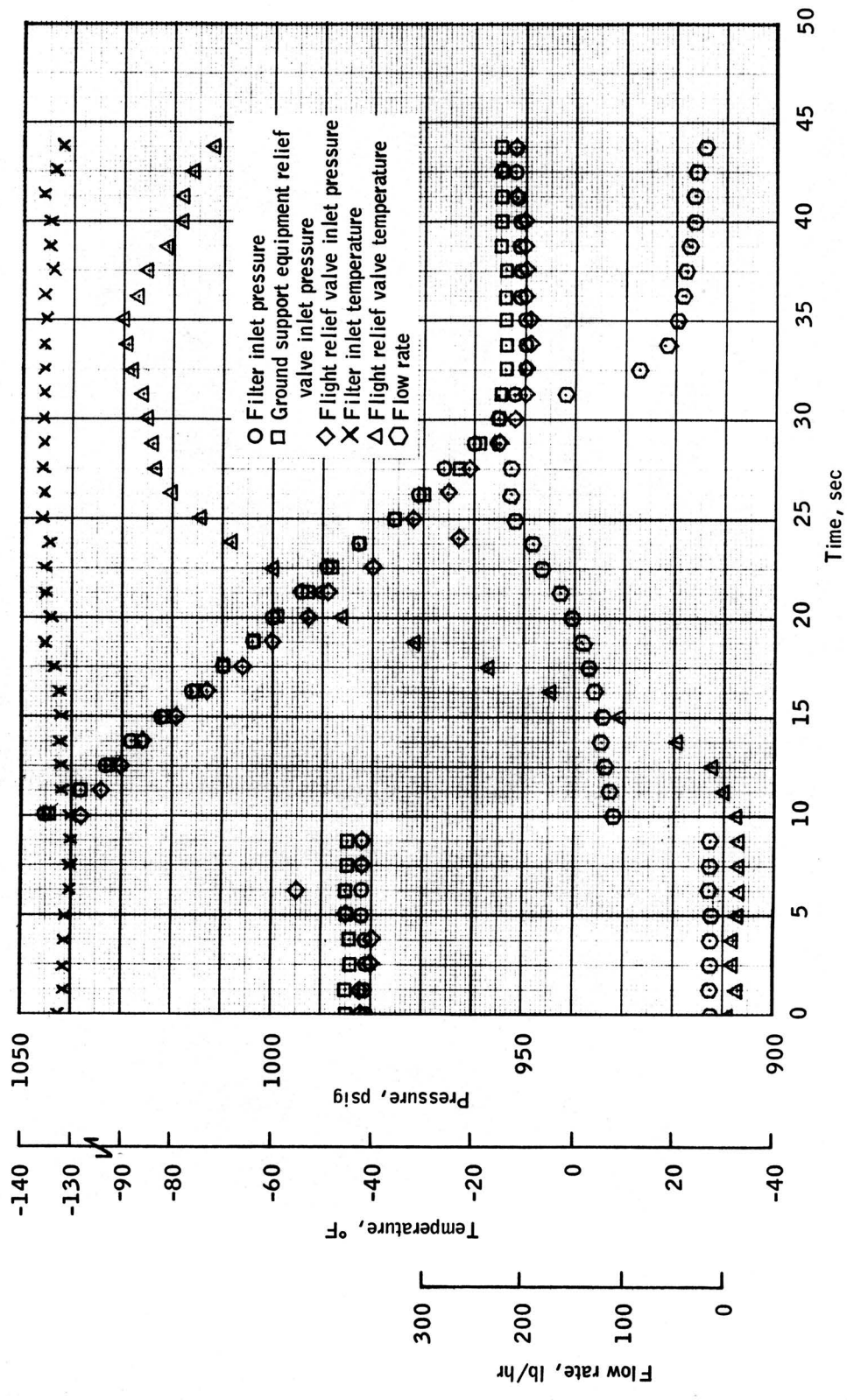

Figure B.3-2.- Liquid oxygen relief valve blowdown test data.

B.4 PRESSURE TRANSDUCER RESPONSE TEST

B.4.1 OBJECTIVE

The objective of this test was to determine the differential pressure between a simulated oxygen tank and the flight pressure transducer (mounted on the valve module) as a function of mass flow through the oxygen relief valve assembly at ambient conditions.

B.4.2 TEST EQUIPMENT AND CONDITIONS

The spacecraft plumbing was simulated (fig. B.4-1), using the Darcy equation for calculation of equivalent line lengths. A flight-configured oxygen filter and valve module assembly were used. All blowdown tests were conducted with ambient gaseous oxygen. Six test sequences were accomplished by first pressurizing to 950 psig and allowing the temperature to stabilize. Then the system was dynamically pressurized at a rate of approximately 2 psi/second until predetermined relief valve inlet pressures of 1001, 1020, 1028, 1028, 1038, 1046, and 1048 psig were achieved.

B.4.3 RESULTS AND CONCLUSIONS

The maximum difference observed between the oxygen tank pressure and the relief valve assembly inlet pressure (flight transducer reading) was 18 psi at a relief valve flow rate of 82.3 lb/hr.

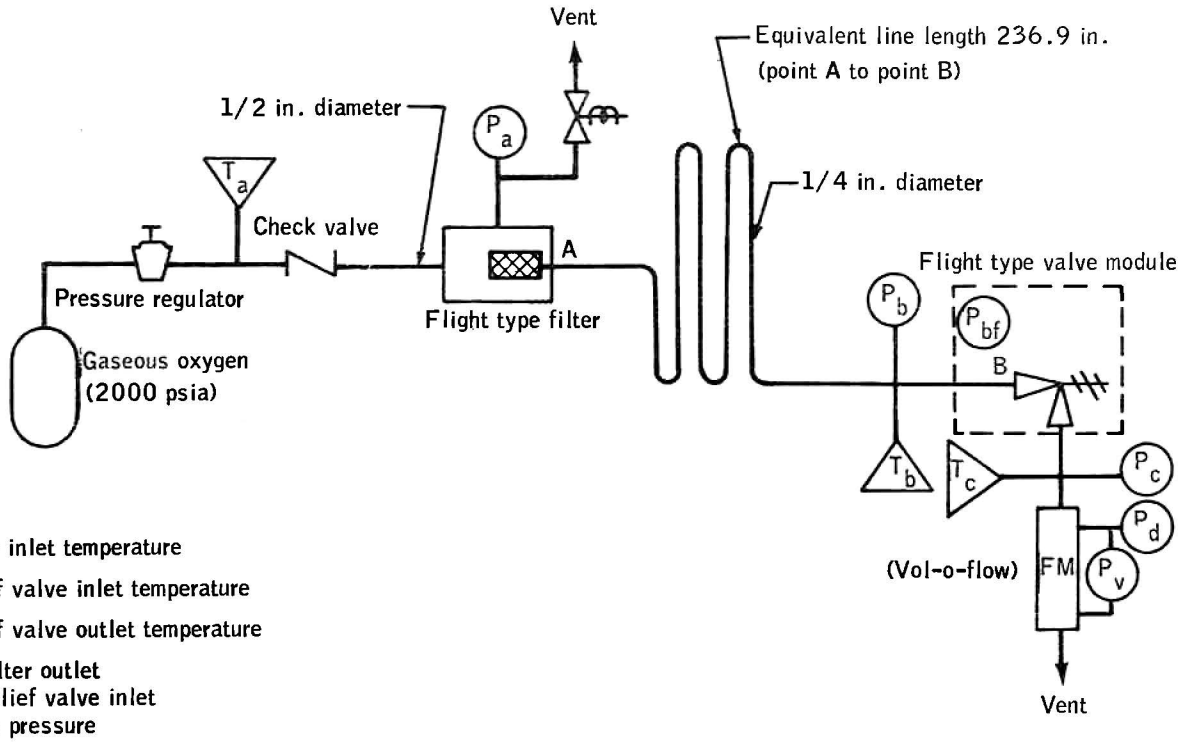

Legend:

T_a - Filter inlet temperature
T_b - Relief valve inlet temperature
T_c - Relief valve outlet temperature
Pt. A - Filter outlet
Pt. B - Relief valve inlet
P_a - Filter pressure
P_b - Relief valve inlet pressure (ground support equipment transducer)
P_{bf} - Relief valve inlet pressure (flight transducer)
P_c - Relief valve outlet pressure (ground support equipment transducer)
P_d - Vol-o-flow inlet pressure
P_v - Vol-o-flow differential pressure
All pressures and temperatures recorded on digital system.

Figure B.4-1.- Oxygen relief valve blowdown apparatus.

B.5 OXYGEN VALVE PRESSURE TRANSDUCER RESPONSE TESTS

B.5.1 OBJECTIVE

The objective of this test was to determine the response of the oxygen pressure transducer to a 500 psi step change after the oxygen relief valve was open and flowing.

B.5.2 TEST EQUIPMENT AND CONDITIONS

Two dynamic pressure response tests of the oxygen valve module pressure transducer. The system used for the previous test (fig. B.4-1) was modified (fig. B-5-1) to provide a step pressure input to the simulated oxygen tank for determining the response of the flight-type transducer to such a step pressure stimulus. As in the previous tests, the oxygen system was pressurized to 950 psig and allowed to temperature stabilize. The system was then dynamically pressurized at a rate of 2 psi/second until the oxygen relief valve opened and the flight transducer had stabilized at approximately 1015 psig. After pressure stabilization, the simulated oxygen tank was subjected, as rapidly as possible, to a step pressure input of about 500 psig (that is, pressurized from approximately 1040 to 1540 psig).

B.5.3 RESULTS AND CONCLUSIONS

The step pressure increase at the simulated oxygen tank was achieved in 4 milliseconds (fig. B.5-2). The pressure stimuli required 16 milliseconds to transmit from the simulated oxygen tank through the equivalent spacecraft line length to the oxygen valve module assembly. The flight transducer located on the valve module assembly responded to the pressure stimuli at the same time as the ground support equipment transducer and in 45 milliseconds, including the 16 milliseconds delay, had reached a steady state 6 V dc output, which is the electrical output limit of the transducer and corresponds to approximately 1300 psig. The ground support equipment pressure transducer, which is located at the valve module, and is redundant to the flight transducer, responded to the full step pressure in 96 milliseconds, including the 16 milliseconds delay.

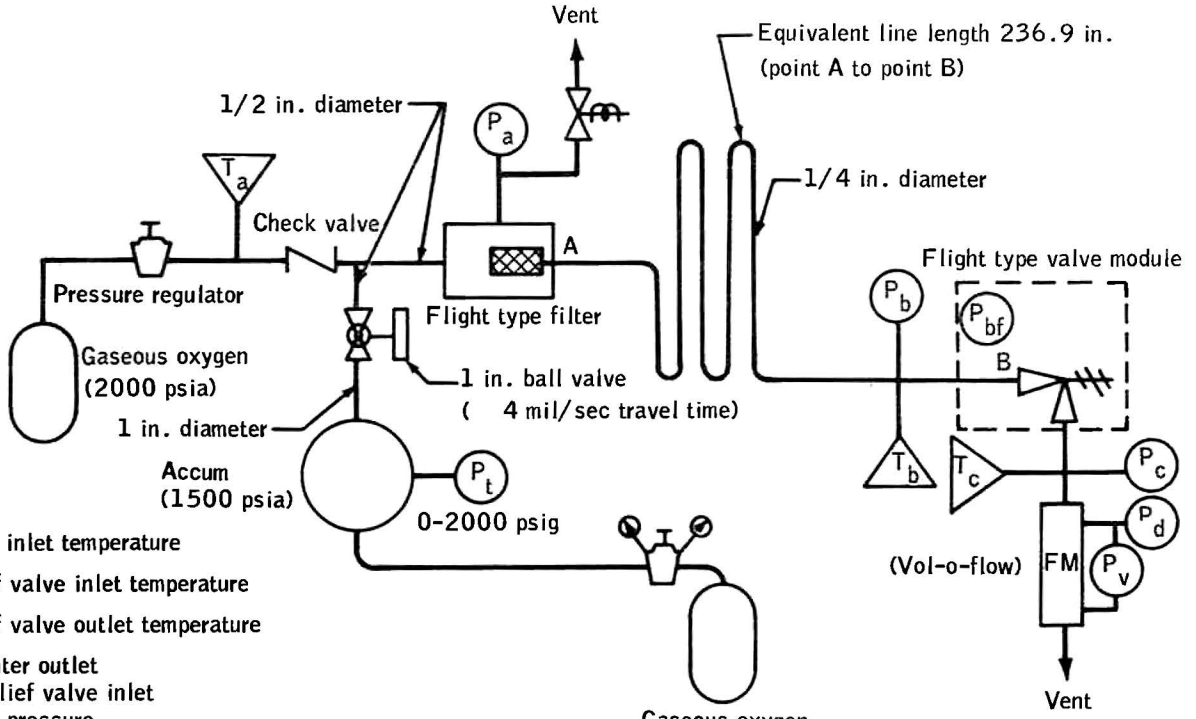

Legend:

T_a - Filter inlet temperature
T_b - Relief valve inlet temperature
T_c - Relief valve outlet temperature
Pt. A - Filter outlet
Pt. B - Relief valve inlet
P_a - Filter pressure
P_b - Relief valve inlet pressure (ground support equipment transducer)
P_{bf} - Relief valve inlet pressure (flight transducer)
P_c - Relief valve outlet pressure (ground support equipment transducer)
P_d - Vol-o-flow inlet pressure
P_v - Vol-o-flow differential pressure

All pressures and temperatures recorded on digital system.

Figure B.5-1.- Transducer response apparatus schematic.

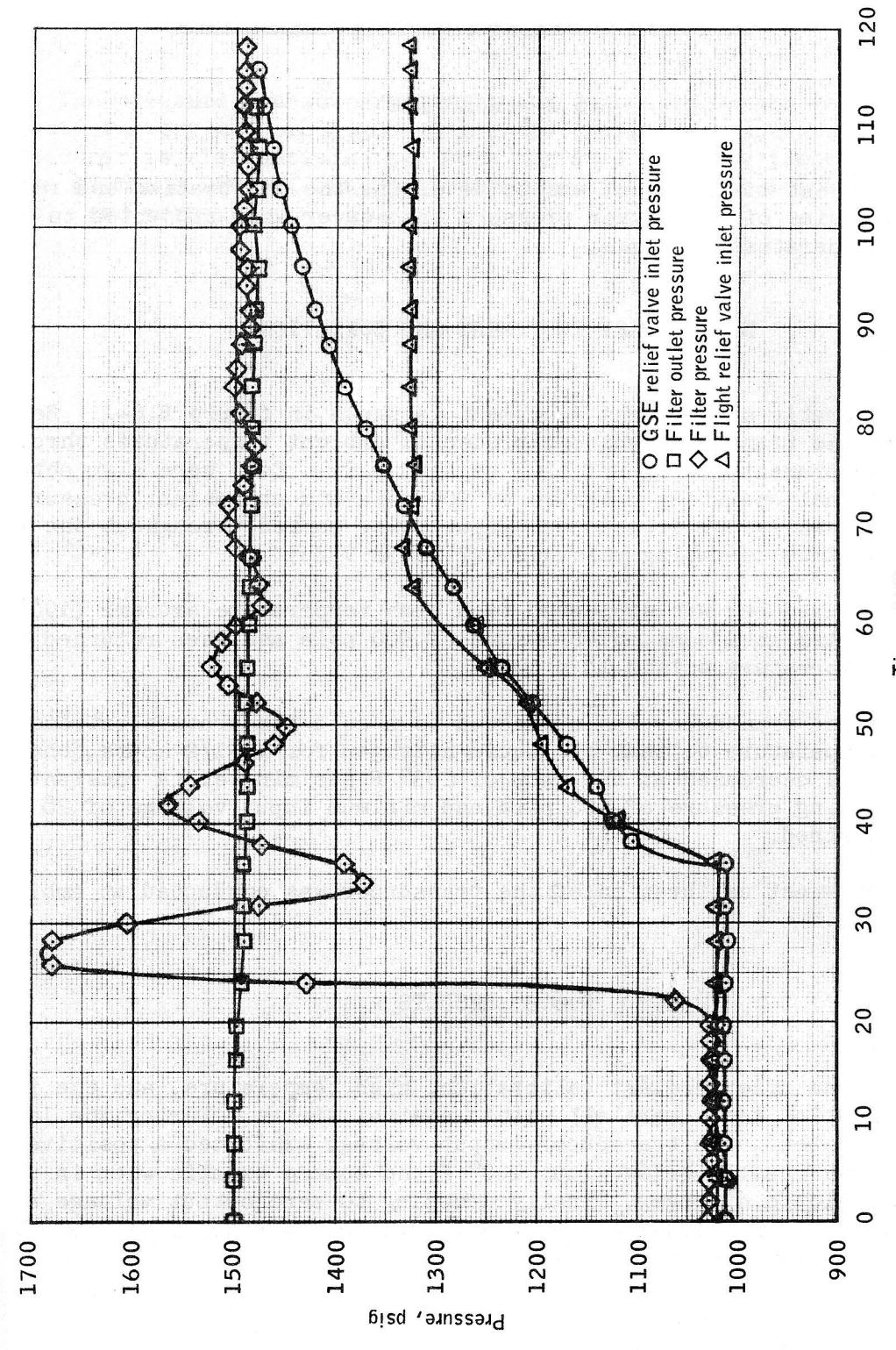

Figure B.5-2.- Transient response plots for transducer response investigation.

B.6 CRYOGENIC OXYGEN PRESSURE TRANSDUCER TEST

B.6.1 OBJECTIVE

The object of this test was to determine the calibration and response characteristics of the oxygen pressure transducer when subjected to high and low temperature extremes.

B.6.2 TEST EQUIPMENT AND CONDITIONS

A schematic of the test equipment is shown in figure B.6-1. Before the test, the transducer was calibrated at ambient temperatures throughout its instrumented range of 11.7 to 1100 psia. Data were also obtained at the nominal operating pressure of 900 psia and at ambient pressure (14.7 psia) while the transducers input power varied throughout the minimum and maximum operating voltages (22 to 32 V dc).

The transducer was subjected to a high temperature extreme (190° F) for 25 minutes at a constant pressure of 900 psia and then returned to ambient temperature within 18 minutes.

When the transducer was subjected to a cold temperature extreme from ambient temperature to that of liquid nitrogen for 10-1/2 hours, the temperature was decreased at the rate of 283° F per minute. A constant nominal operating pressure of 900 psia and minimum input voltage of 28 V dc, were maintained.

A post-test calibration of the transducer was conducted at ambient temperature.

B.6.3 RESULTS

The transducer pretest calibration, high temperature, and the input power variation tests were all within nominal limits. During the low temperature test, the transducer output voltage exhibited a positive increase significantly below minus 160° F and became erratic when in contact with liquid nitrogen, finally dropping to zero output voltage at minus 305° F. The post-test calibration indicated a positive bias of approximately 30 psi (fig. B.6-2).

B.6.4 CONCLUSION

The pressure transducer used in the cryogenic oxygen valve module is satisfactory at both high and ambient operating temperatures. The transducer is also satisfactory when operated to a low temperature extreme of minus 160° F, but below that temperature, the transducer is unstable and erratic.

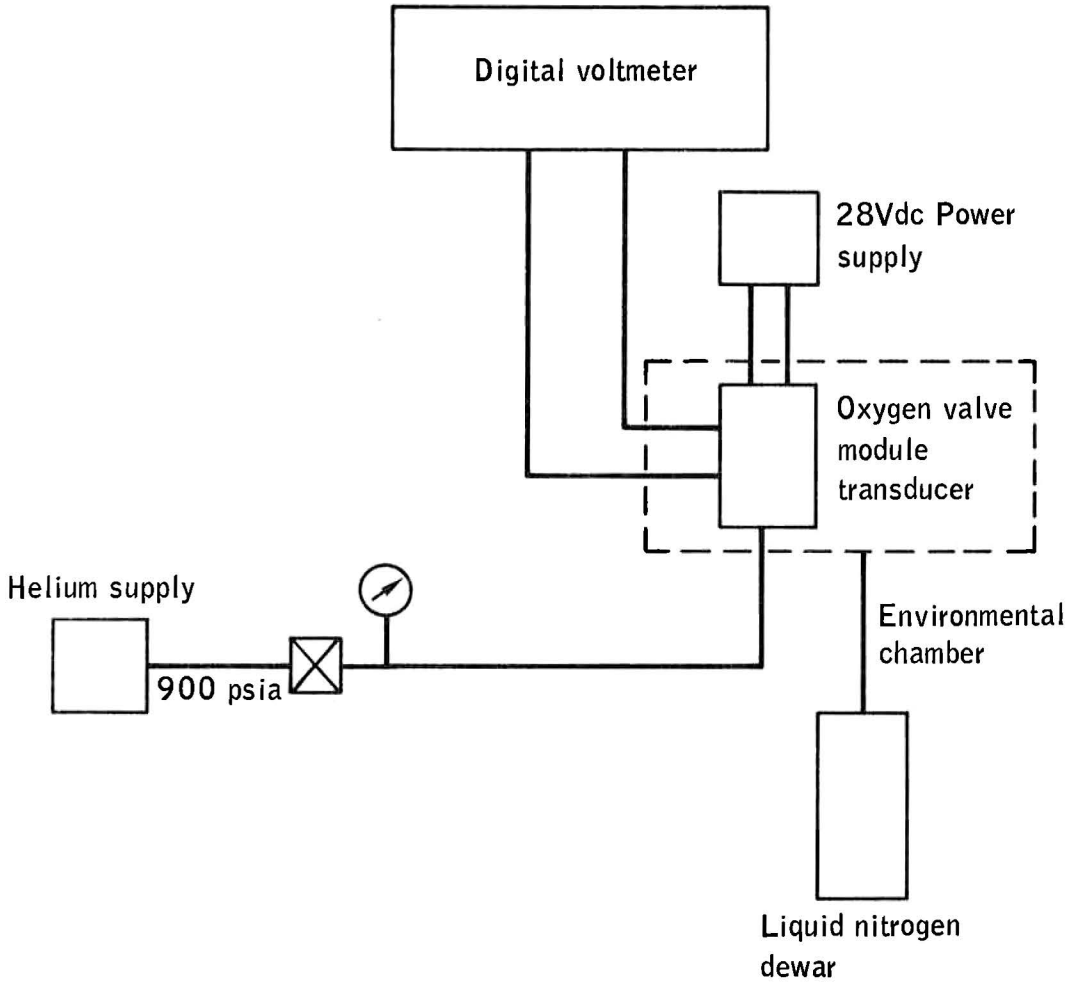

Figure B.6-1.- Pressure transducer temperature effects test equipment.

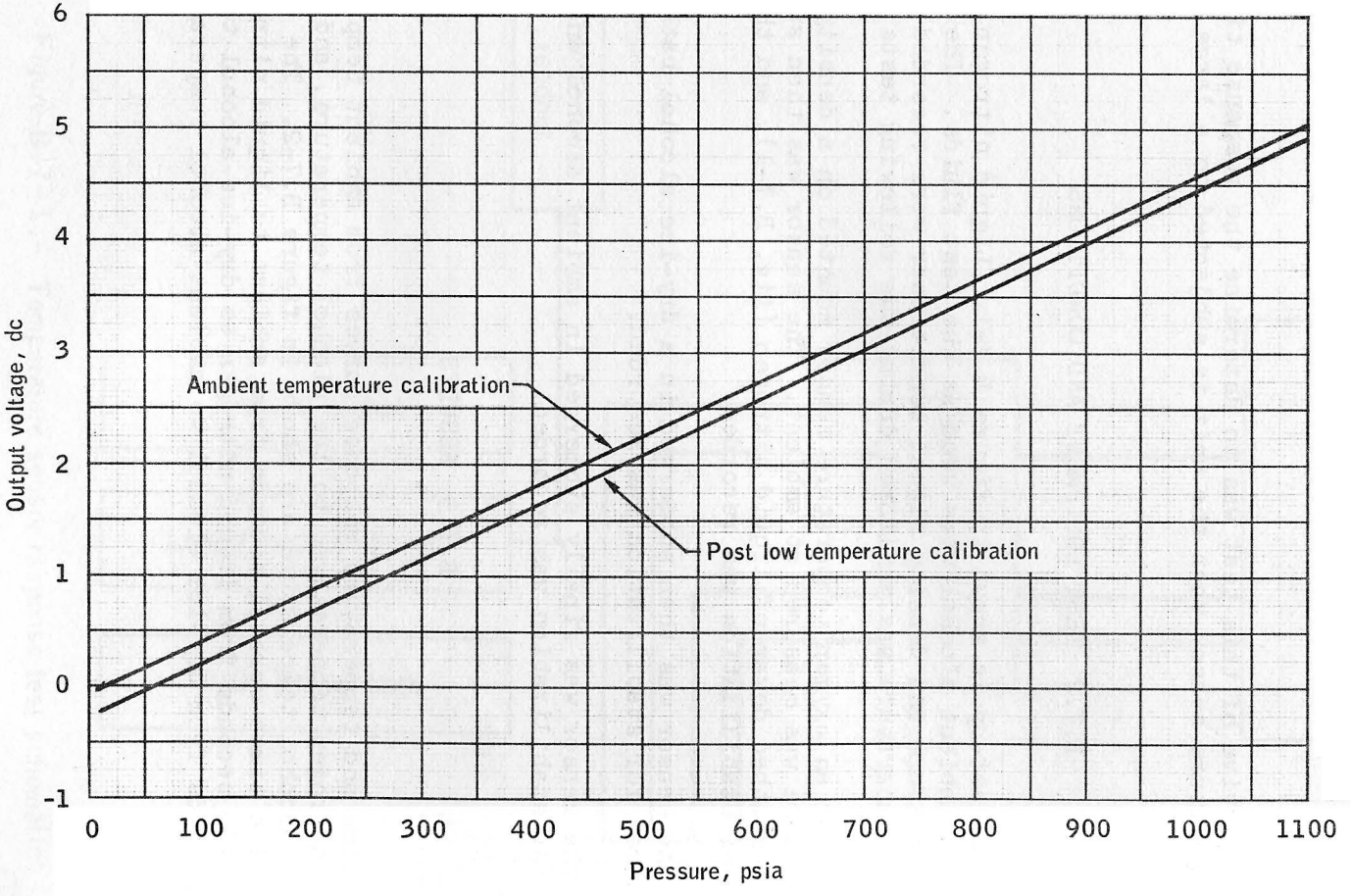

Figure B.6-2.- Pressure transducer calibration curve.

B.7 OXYGEN TANK TEMPERATURE SENSOR RESPONSE TEST

B.7.1 OBJECTIVE

The objective of this test was to determine the response time of the oxygen temperature sensor when the unit is subjected to a large change in temperature.

B.7.2 TEST EQUIPMENT AND CONDITIONS

The test set-up is shown in figure B.7-1. Liquid nitrogen, dry ice alcohol, and ambient alcohol were used as the test fluids. The outputs of the temperature and density signal conditioner were recorded and the test fluid temperature was monitored during the following tests.

a. Using an oxygen temperature sensor mounted on a density probe, the temperature was measured at ambient. The sensor was then submerged in an open-mouthed dewar of liquid nitrogen (fig. B.7-1), and the time required for stabilization was recorded.

b. The sensor was then submerged in a dry-ice alcohol bath and the time required for stabilization was recorded.

c. The sensor was finally submerged in ambient alcohol and the time required for stabilization was recorded.

B.7.3 RESULTS

The time and temperature response curves from ambient temperature to liquid nitrogen temperature, to ice alcohol temperature, and finally to ambient alcohol temperature are shown in figure B.7-2. The approximate stabilization times were 31 seconds from ambient to liquid nitrogen temperature, 100 seconds from liquid nitrogen to dry-ice alcohol temperature; and 110 seconds from dry-ice alcohol to ambient alcohol temperature.

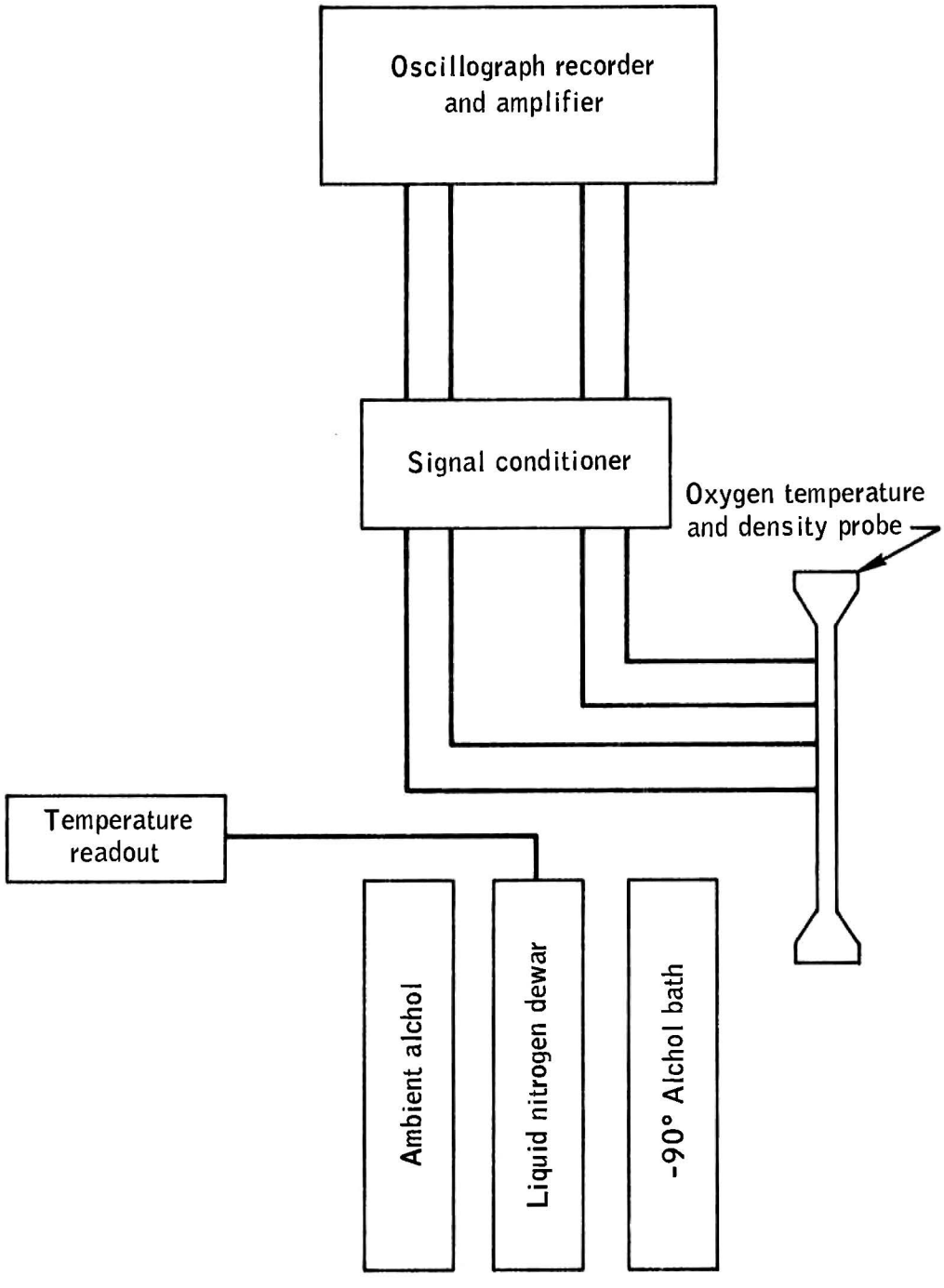

Figure B.7-1.- Temperature sensor response test schematic.

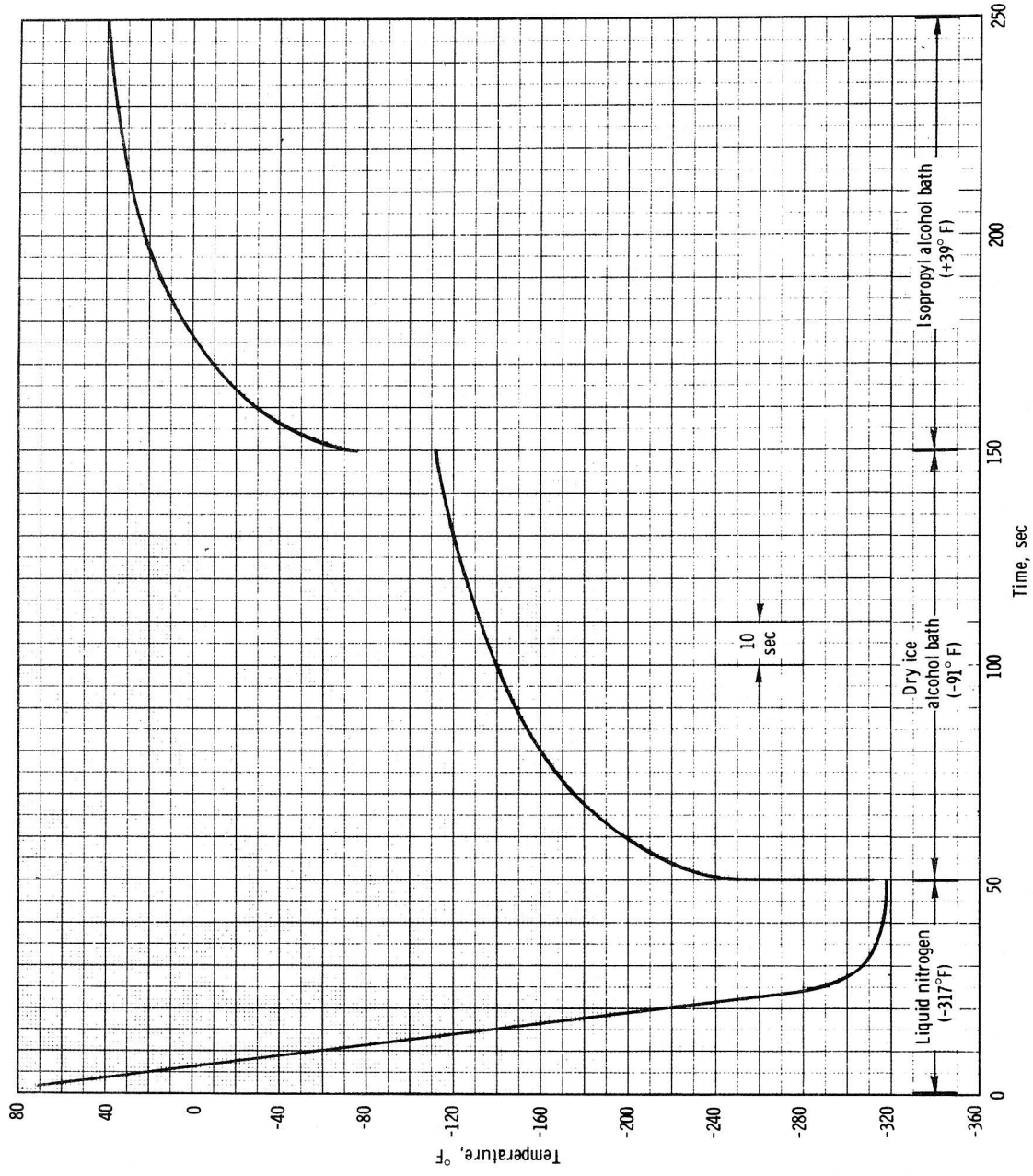

Figure B.7-2.- Response capability of cryogenic oxygen tank temperature sensor.

B.8 FUEL CELL RADIATOR INLET TEMPERATURE SENSOR RESPONSE TEST

B.8.1 OBJECTIVE

The objective of this test was to determine the conditions that would be required to duplicate the observed thermal response of the temperature sensor installed on the Apollo 13 fuel cell water/glycol line.

B.8.2 TEST EQUIPMENT AND CONDITIONS

The test set-up (figs. B.8-1 to B.8-5) consisted of a flow bench, a radiant heating system, and instrumentation to record temperature and heat rate. Tests were conducted with heat applied under both flow and no-flow conditions. A series of test sequences were conducted in an effort to reproduce the 1.4 deg/sec slope recorded in flight.

B.8.3 RESULTS

Test results indicated that the flight profiles could not be reproduced under no-flow conditions. However, under conditions of a flow of 80 lb/hr, a water/glycol temperature of 94° F, and a radiant heat rate of 0.92 Btu/ft^2-sec, the flight profile with a slope of 1.4 deg/sec was reproduced, the initial response of the temperature sensor occurred in 0.25 second after the application of heat (fig. B.8-6).

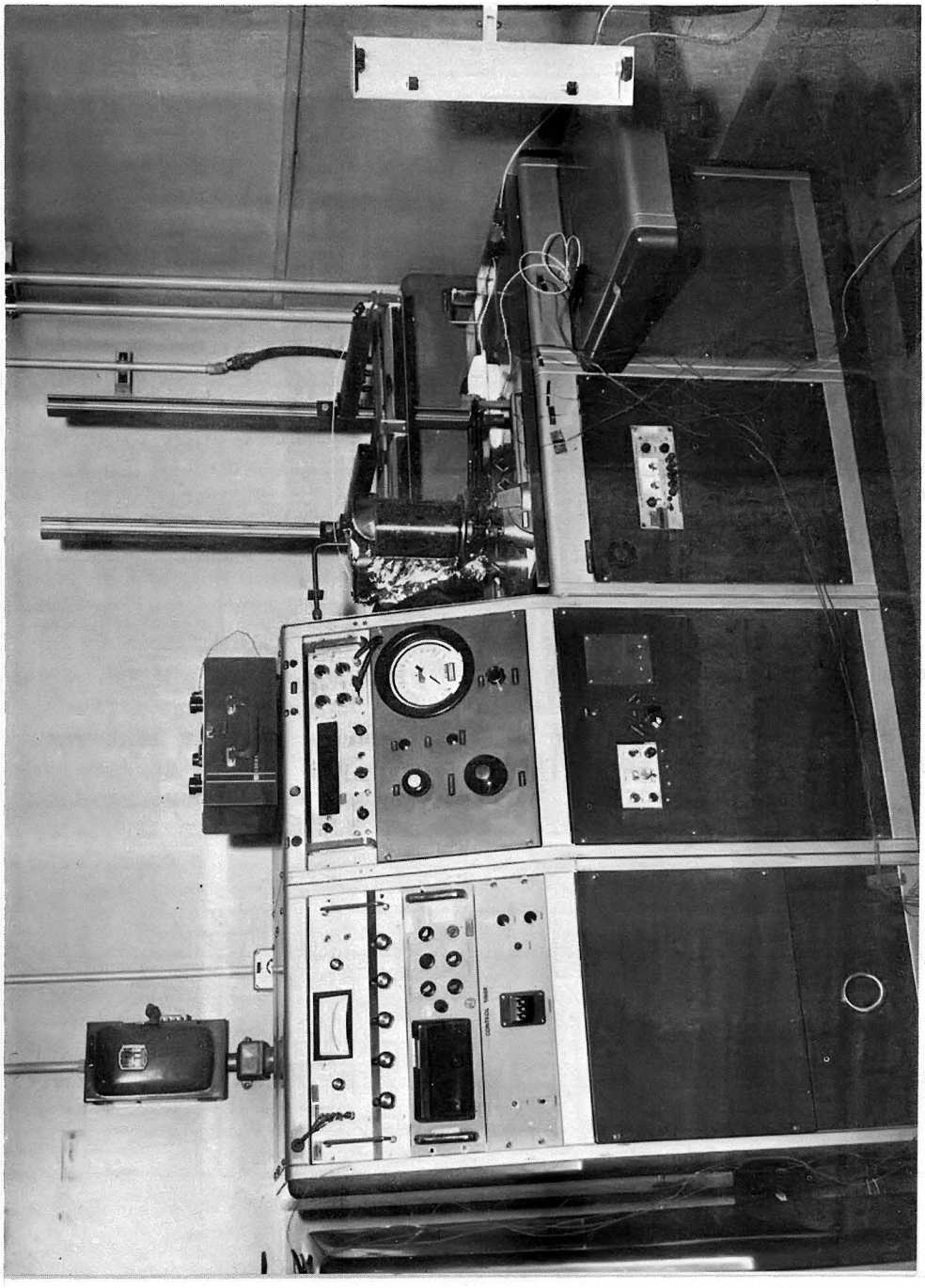

Figure B.8-1.- Flow bench.

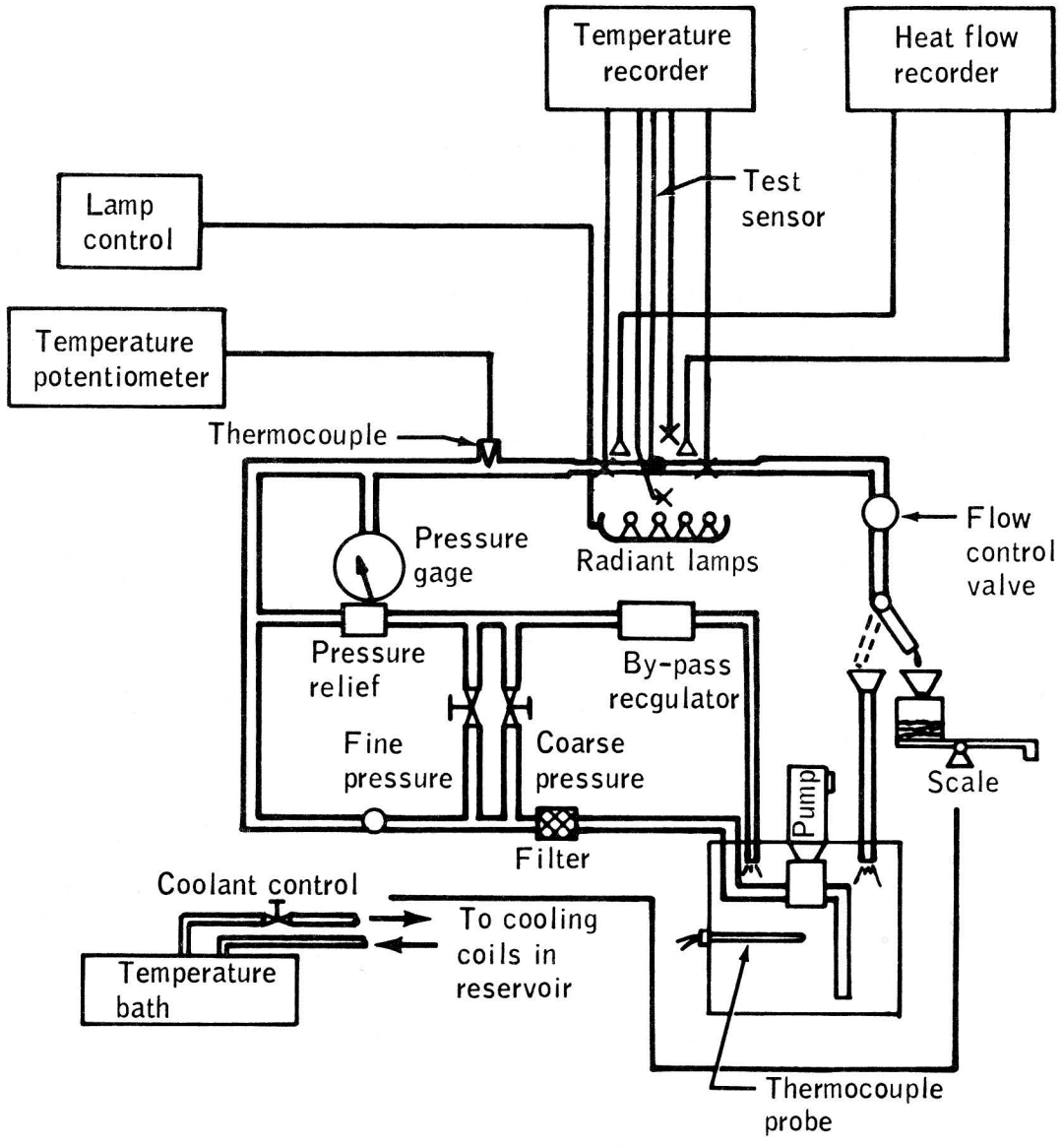

Figure B.8-2.- Schematic of water/glycol flow bench and instrumentation.

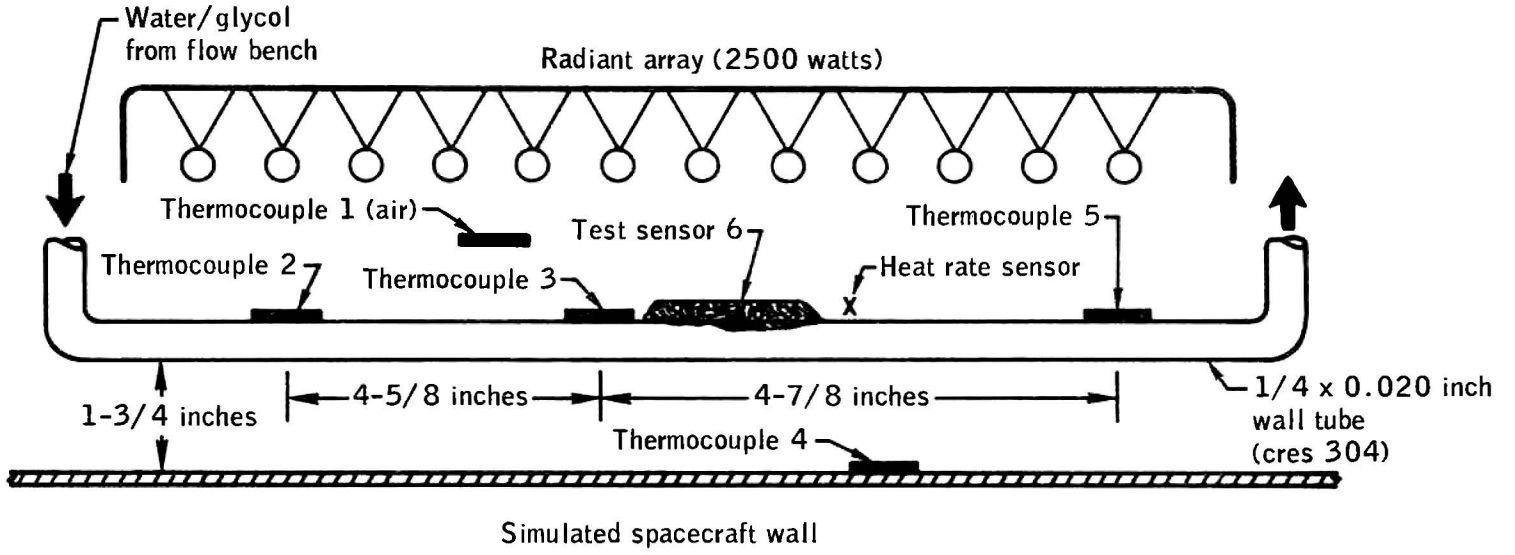

Figure B.8-3.- Radiant heating array test set-up.

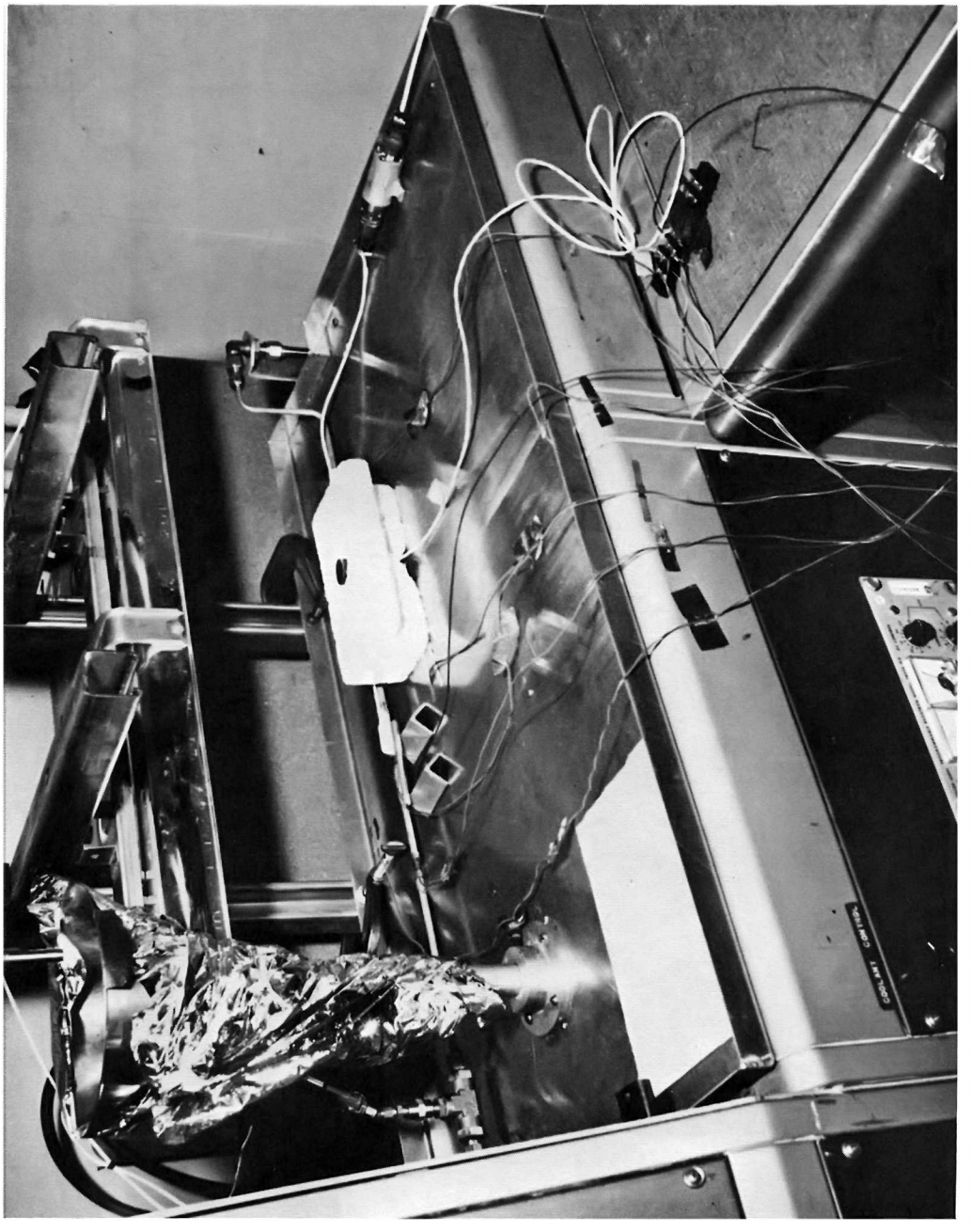

Figure B.8-4.- Test specimen and radiant heating array.

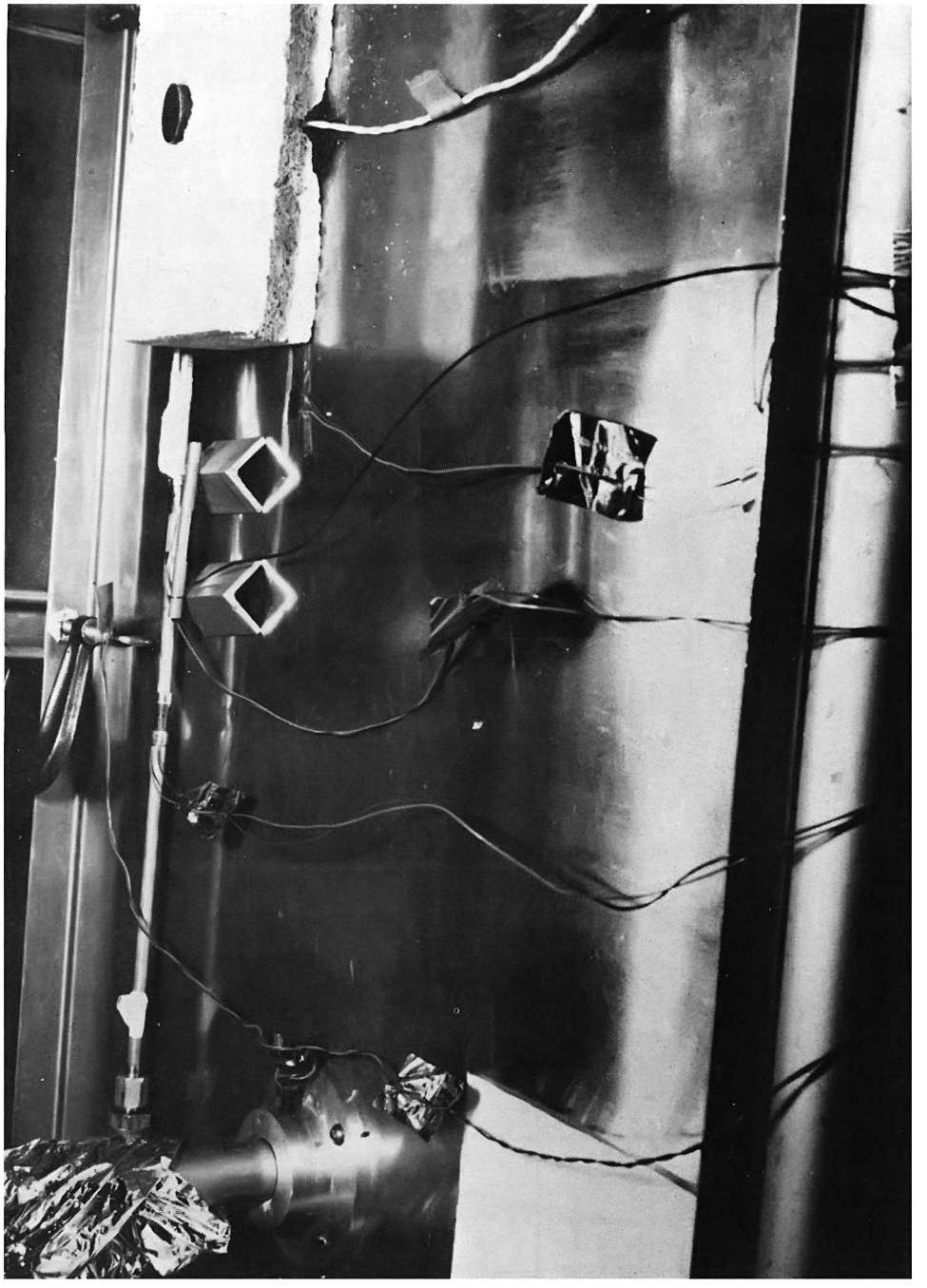

Figure B.8-5.- Detailed view of test specimen.

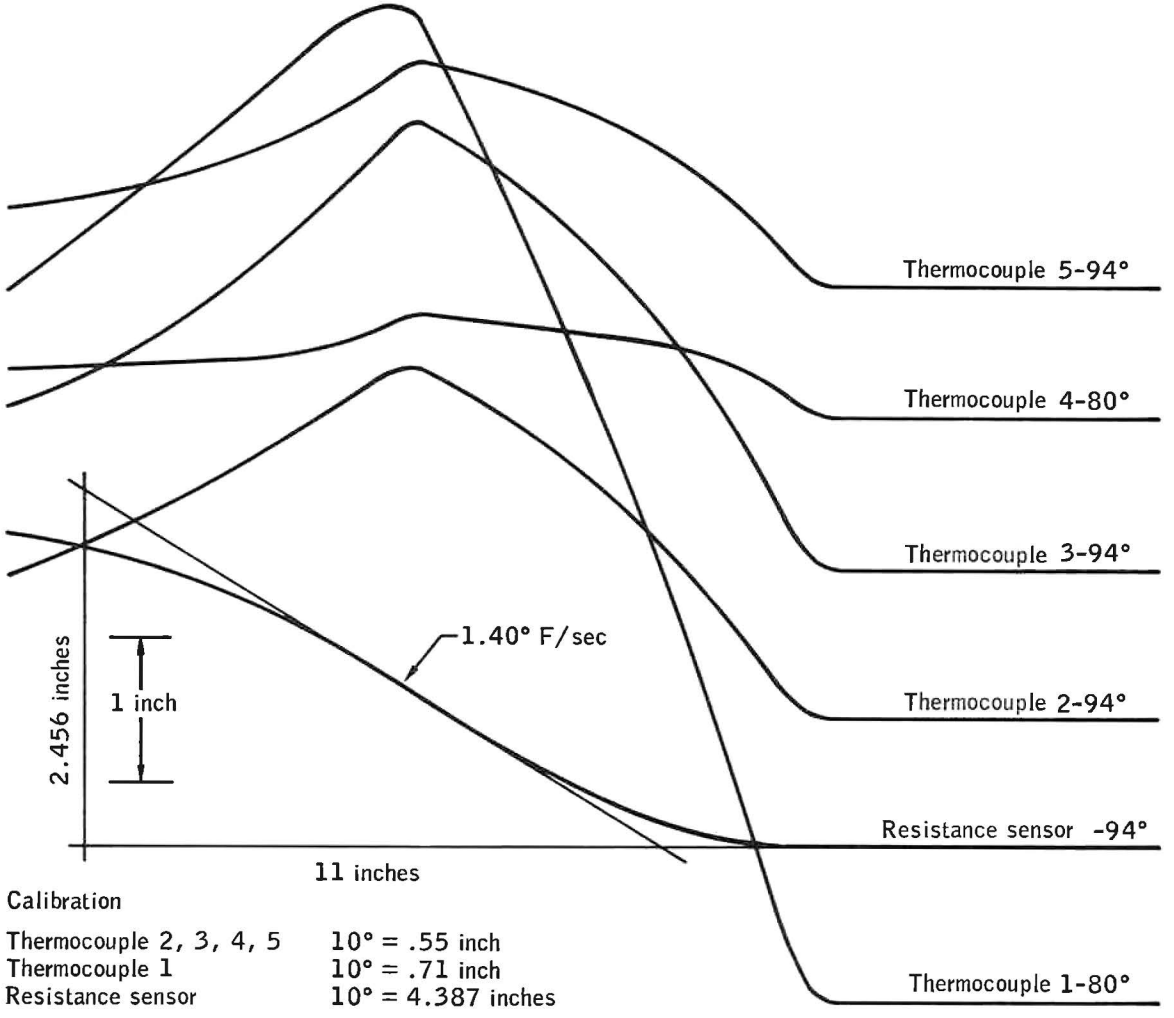

Figure B.8-6.- Thermocouple response history for 80 lb/hr flow rate and 0.92 Btu/ft^2 sec heat rate.

B.9 AC BUS 2 VOLTAGE TRANSIENT TEST

B.9.1 OBJECTIVE

The objective of this test was to determine the amplitude and time duration of an ac bus 2 transient that could cause the thrust vector control gimbal command signal disturbances observed on telemetry data from the Apollo 13 stabilization and control system.

B.9.2 TEST EQUIPMENT AND CONDITIONS

Two sets of three variable-frequency power supplied were used to create 400-Hz, 3-phase power for both ac bus 1 and ac bus 2. Using a precision pulse generator and a modified control oscillator, a glitch with a controlled voltage drop and pulse width was placed on ac bus 2. The response of the pitch and yaw gimbal command telemetry signals, and other pertinent signals, to a matrix of ac bus 2 voltage drops and pulse widths were recorded on strip charts.

The gyro assembly used to represent gyro assembly 2 in this test was a nonflight production unit that had been modified to the electrical configuration of the Apollo 13 gyro assembly. Two electronic control assemblies were used. One was a modified nonflight production unit, but contained a lunar-module-on notch filter of the Apollo 8 configuration, which had a different frequency response than the Apollo 13 lunar-module-on notch filter. The rate signal wave shape and magnitude were affected accordingly. The Apollo 8 type electronic control assembly was replaced in the test setup by an Apollo 13 type electronic control assembly breadboard. Tests using the Apollo 13 type electronic control assembly accurately reflected the difference in lunar-module-on notch filter frequency response between the two electronic control assemblies. All data used in this report were taken from the test set using the electronic control assembly Apollo 13 type lunar-module-on notch filter.

B.9.3 RESULTS

Performing the ac bus 2 transient test without the gyro assembly powered up showed that the ac bus 2 transient did not cause the gimbal command signal disturbances until ac bus 2 voltages dropped below 60 V rms for relatively long pulse widths. Voltages below this level overtaxed the dc supply regulation capability within the electronic control assembly. When the test was performed with the gyro assembly 2 powered

up, the output of the gyro assembly 2 (rate) was significantly affected by ac bus 2 voltage transients. It was therefore concluded that, for transients above 60 V rms, the gimbal command signal disturbances resulted from the rate output of this gyro being disturbed by ac bus 2 transients and that this rate signal was passed and amplified by the electronic control assembly without additional bus transient induced disturbances.

A test matrix of ac bus 2 voltage drops versus pulse widths and the peak responses of the thrust vector control gimbal command signal disturbances for each combination of voltage drop and pulse width are given in table B.9-I. Approximately 10 response samples of the signal disturbances were made for each transient voltage drop/pulse width combination. Of the 10 response samples, only the largest and smallest samples were used to establish the response range. The maximum zero-to-peak magnitudes of these two response samples are recorded in table B.9-I. Maximum zero-to-peak magnitudes of the signal disturbances observed on Apollo 13 flight telemetry are shown in figure B.9-1.

Data interpolated from the constant pulse widths were used to plot a bounded area of transient pulse width versus transient voltage drop for a constant signal disturbance response. Figures B.9-2 and B.9-3 show the bounded area for signal disturbances of 0.12 deg/sec, which corresponds to the largest disturbance observed on Apollo 13 flight telemetry and shown in fig. B.9-1, disturbance number 3, pitch axis, and 0.09 deg/sec, which corresponds to figure B.9-1, disturbance number 3, yaw axis. Figures B.9-2 and B.9-3 indicate that the transient pulse width could have been as much as 150 milliseconds. The test data showed that the first half cycle time of the thrust vector control gimbal command response could be correlated to the pulse width of the ac bus 2 voltage transient. Curves of constant transient voltage drop relating first half cycle time to pulse width are shown in figure 9-4. Based on these curves and on the first half cycle times of pitch and yaw signal disturbance number 3, the predicted corresponding ac bus 2 voltage transient pulse width was 20 milliseconds. For a 20-millisecond transient, the ac bus 2 voltage must drop to between 65 and 90 V rms to cause a 0.12 deg/sec signal disturbance. A comparison of flight telemetry and laboratory duplicated disturbances is shown in figure B.9-1.

Test data also showed a 15-millisecond delay between the leading edge of the ac bus 2 voltage drop and the start of the induced signal disturbance.

B.9.4 CONCLUSIONS

The Apollo 13 telemetry thrust vector control gimbal command signal disturbances were successfully duplicated using a stabilization and control system in the Systems Dynamics Laboratory. An ac bus 2 transient voltage drop from 115 V rms to between 90 and 65 V rms for approximately 20 milliseconds duplicated the largest thrust vector control gimbal command signal disturbance observed on Apollo 13 stabilization and control system telemetry data.

TABLE B.9-I.- TEST MATRIX OF VOLTAGE DROPS AND PULSE WIDTHS AND GIMBAL COMMAND RESPONSES

Time, Milliseconds	Potential, ac volts	Pitch TVC gimbal command		Yaw TVC gimbal command	
		Minimum deg/sec	Maximum deg/sec	Minimum deg/sec	Maximum deg/sec
10	95	0.02	0.044	0.036	0.062
10	85	0.048	0.056	0.098	0.056
10	75	0.04	0.064	0.048	0.056
10	65	0.056	0.072	0.048	0.088
20	95	0.056	0.104	0.076	0.084
20	85	0.069	0.136	0.076	0.124
20	75	0.08	0.16	0.128	0.152
20	65	0.12	0.192	0.144	0.16
30	105	0.036	0.088	0.048	0.076
30	95	0.064	0.16	0.088	0.128
30	85	0.096	0.184	0.12	0.18
30	75	0.14	0.26	0.18	0.25
40	105	0.048	0.10	0.052	0.088
40	95	0.112	0.152	0.12	0.144
40	85	0.128	0.16	0.16	0.18
40	75	0.2	0.26	0.256	0.316
50	105	0.128	0.164	0.068	0.10
50	100	0.14	0.2	0.064	0.128
50	95	0.18	0.28	0.064	0.20
60	105	0.088	0.128	0.096	0.20
60	100	0.22	0.26	0.104	0.192
60	95	0.36	0.40	0.16	0.22
75	105	0.112	0.176	0.104	0.16
75	100	0.30	0.34	0.18	0.20
75	95	0.44	0.50	0.28	0.34
100	105	0.088	0.152	0.096	0.144
100	100	0.28	0.38	0.22	0.32
100	95	0.60	0.64	0.46	0.50
125	105	0.096	0.144	0.048	0.096
125	100	0.22	0.30	0.16	0.22
125	95	0.44	0.60	0.18	0.48
150	105	0.12	0.144	0.096	0.144
150	100	0.18	0.24	0.14	0.18
150	95	0.32	0.44	0.30	0.40

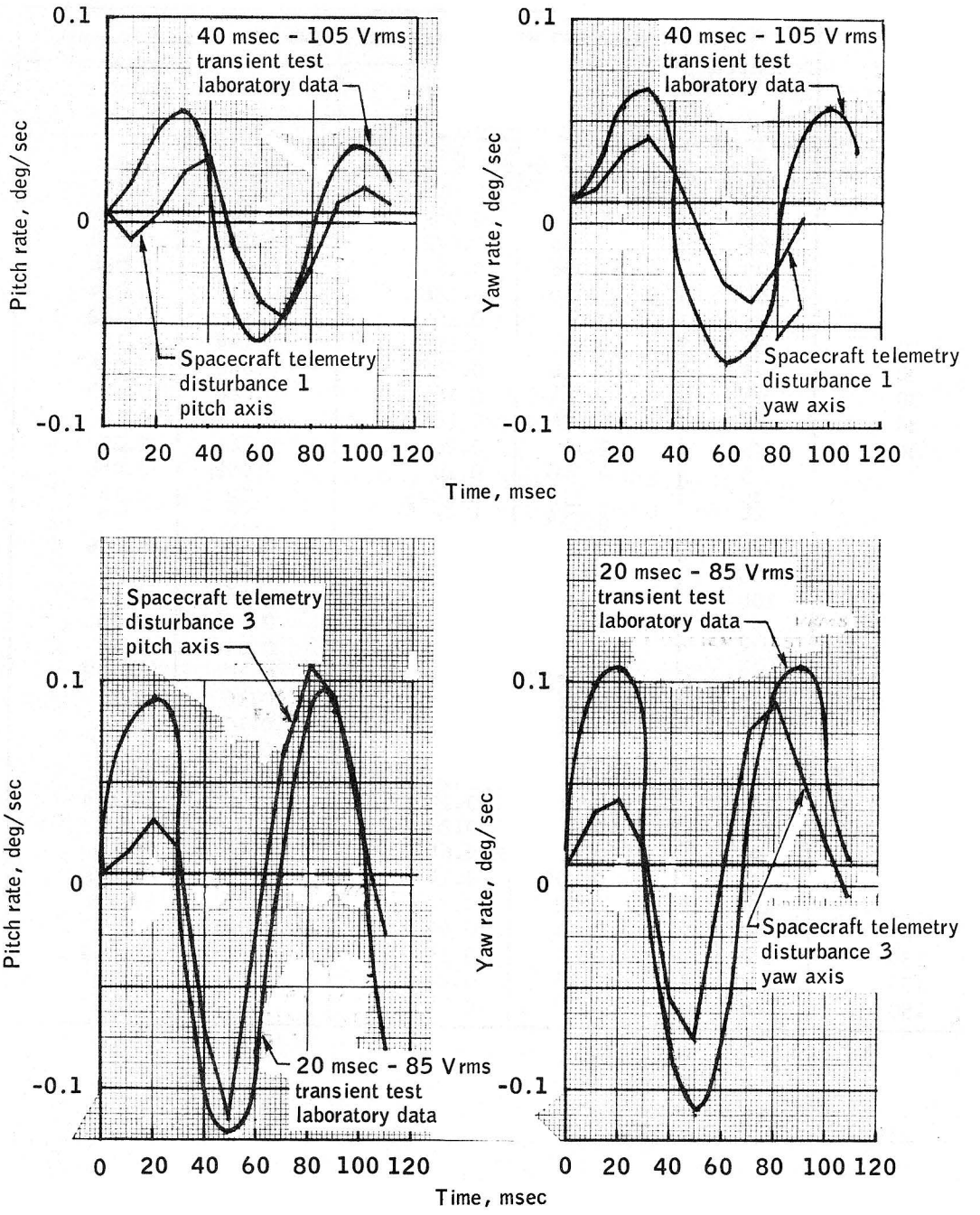

Figure B.9-1.- Spacecraft and laboratory duplicated thrust vector control gimbal command signal disturbances.

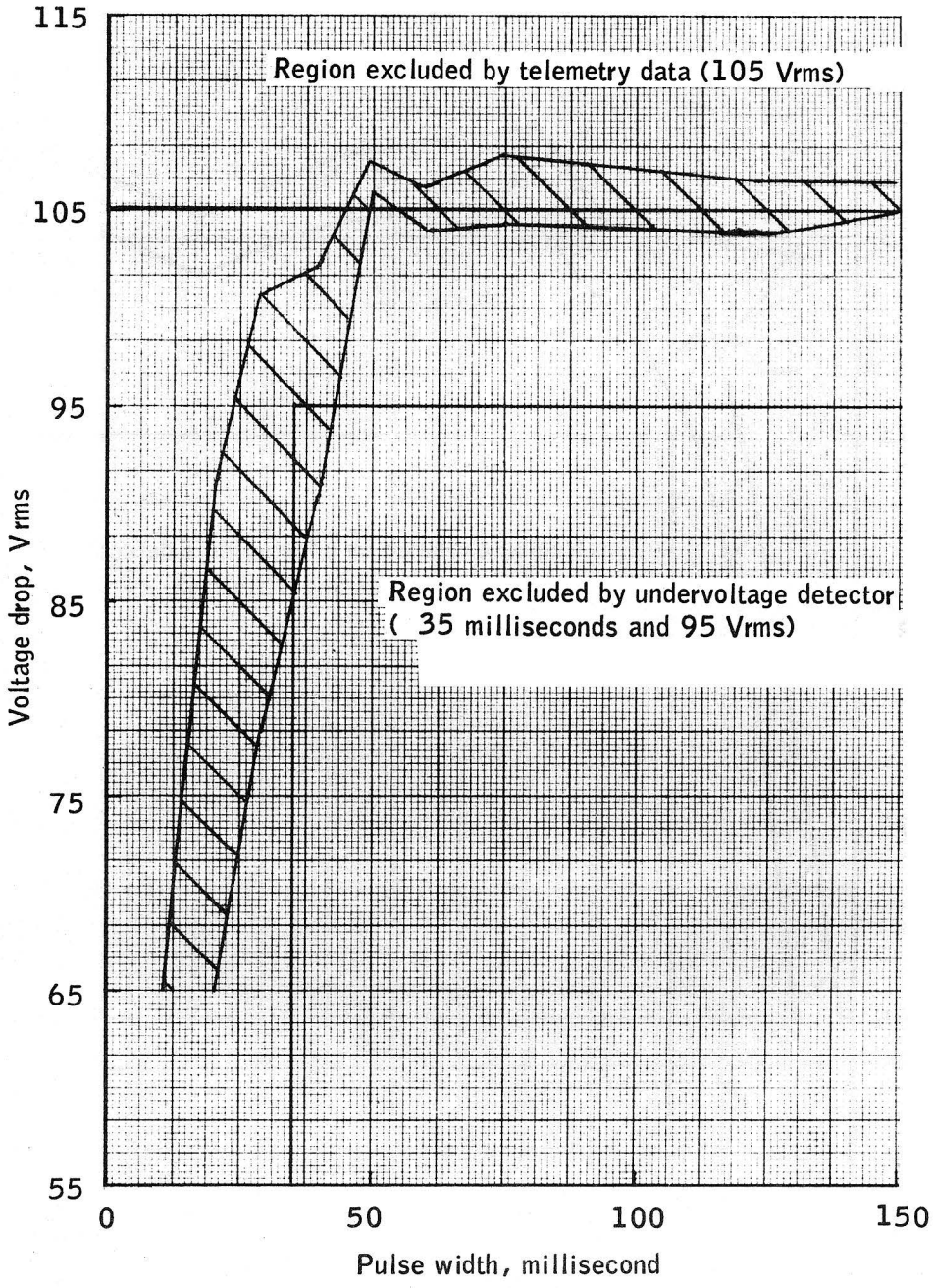

Figure B.9-2.- Region for 0.12 deg/sec pitch thrust vector control gimbal command response.

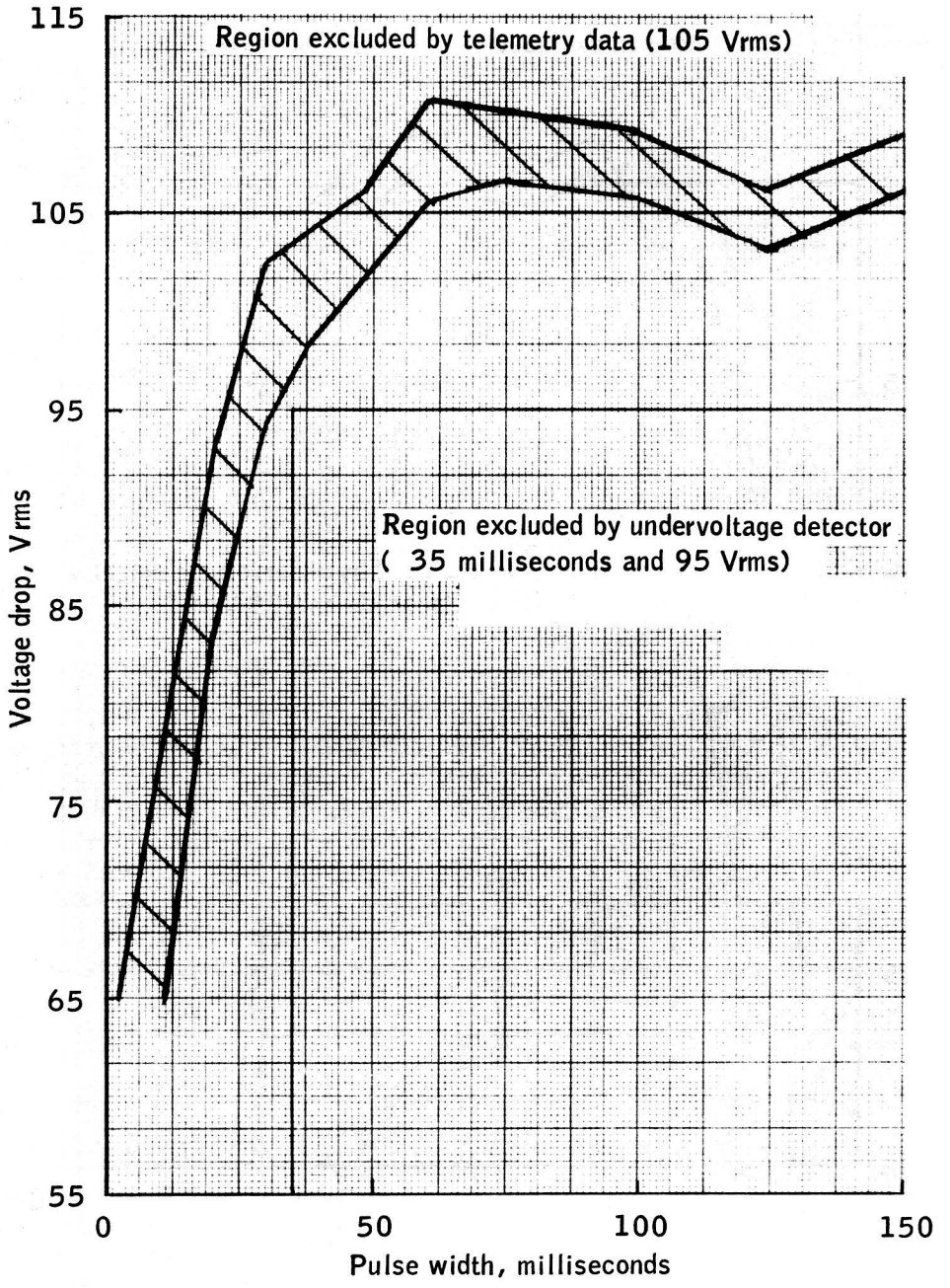

Figure B.9-3.- Region for 0.09 deg/sec yaw thrust vector control gimbal command response.

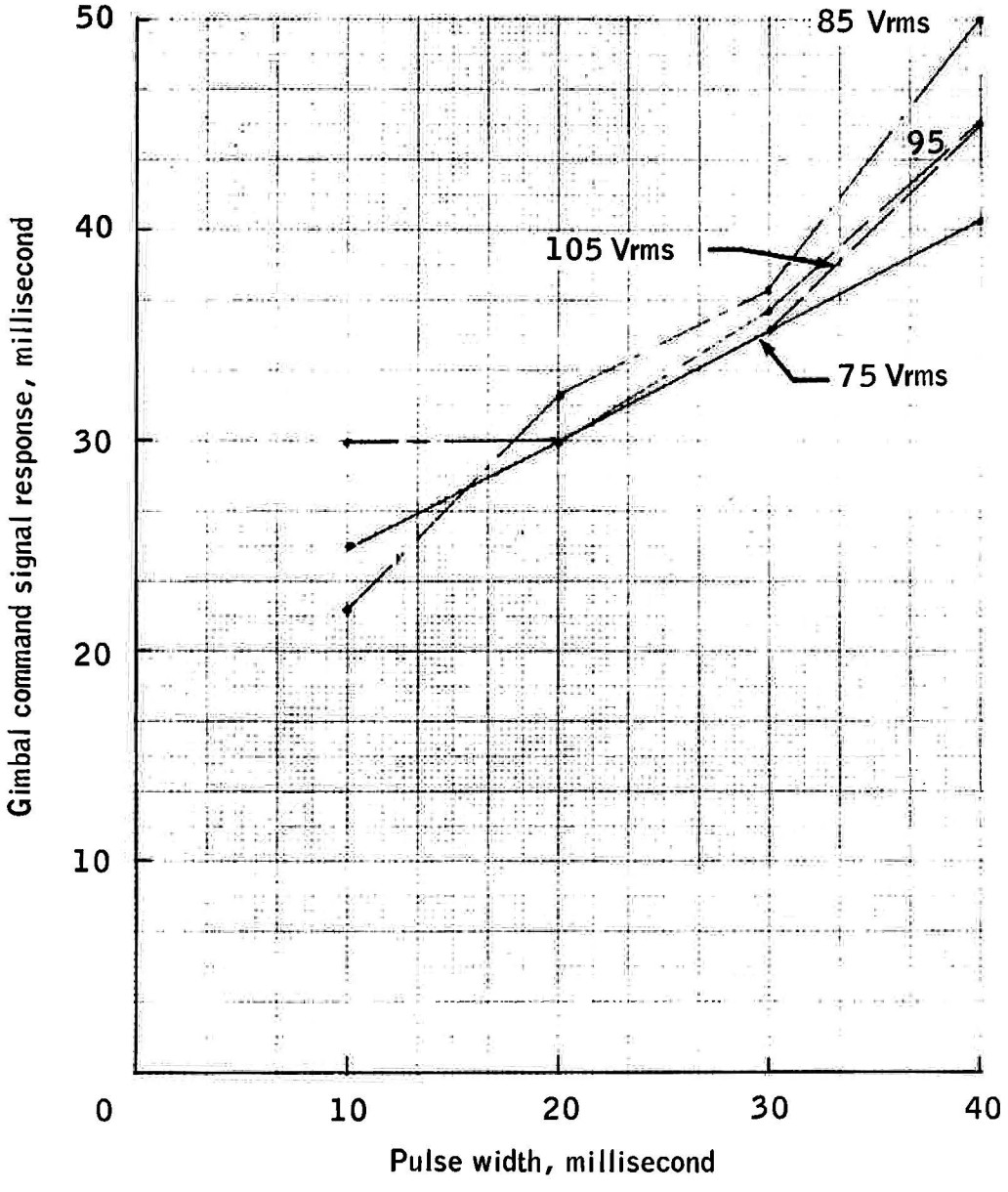

Figure B.9-4.- Transient pulse width versus disturbance first half cycle time.

B.10 VARIATIONS IN OXYGEN PRESSURE ON FLOWMETER OUTPUT TEST

B.10.1 OBJECTIVE

The objective of this test was to define the effect that variations in oxygen pressure and temperature would have on flowmeter output.

B.10.2 TEST EQUIPMENT AND CONDITIONS

A test stand (figs. B.10-1 and B.10-2) simulated the spacecraft volumetric and pressure drop characteristics beginning with the check valves at the fuel cell assembly valve modules and included the flowmeter, fuel cell assembly pressure regulators, flow control valve (fuel cell assembly load simulation), and a facility flowmeter. The gaseous oxygen facility supply provided the necessary pressure regulation and step pressure changes together with a heat exchanger capable of cooling the 0.5 lb/hr gas flow to minus 125° F. The flow rate through the simulated fuel cell was held constant for all operations. The system operating procedures were as follows:

a. Test A - Cool the flowing oxygen gas upstream of the flowmeter as rapidly as possible and observe flight flowmeter output.

b. Test B - With oxygen gas flowing at a relatively constant cold temperature, observe flowmeter outputs at increased and decreased operating pressures.

c. Test C - Warm the flowing oxygen gas upstream of the flowmeter as rapidly as possible and observe the flight flowmeter output.

d. Test D - While oxygen gas is flowing at ambient temperatures, provide step increases and decreases in pressure and observe flowmeter output.

B.10.3 RESULTS

Throughout the test, the step pressure increases resulted in the flowmeter output showing a spike due to increased flow during pressure equalization of the downstream line volume. At ambient temperature, a pressure change resulted in no change in indicated flow rate, except for the spike.

At low temperatures, an increase or decrease in pressure resulted in a corresponding increase or decrease in indicated flow. At constant pressures, an increase or decrease in gas temperature resulted in a corresponding increase or decrease in indicated flow. However, these changes in indicated flow occur slowly because of the thermal mass of the flowmeter.

B.10.4 CONCLUSIONS

The changes in flowmeter output as a function of pressure and temperature are the result of the specific heat characteristics of oxygen. The flowmeter is sensitive to the specific heat of the flowing gas; oxygen specific heat varies little with pressure and temperature changes in the ambient temperature range but varies greatly with pressure and temperature in the minus 100° F range. The flowmeter behavior was as expected, based upon specific heat characteristics.

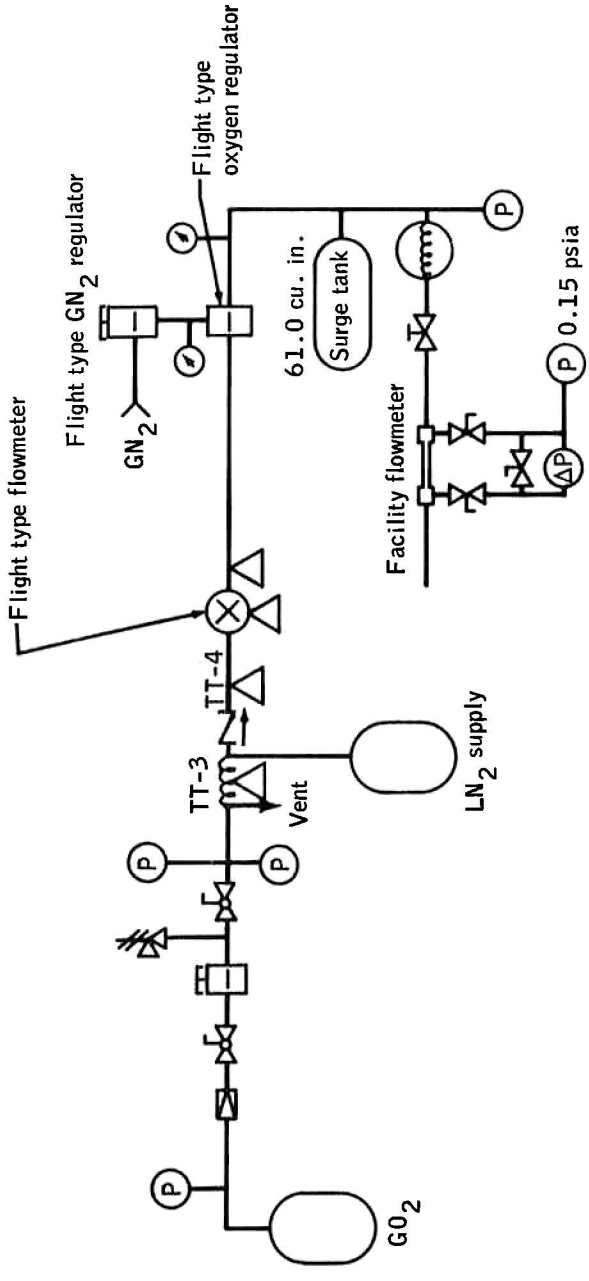

Figure B.10-1.- Flowmeter transient test set-up.

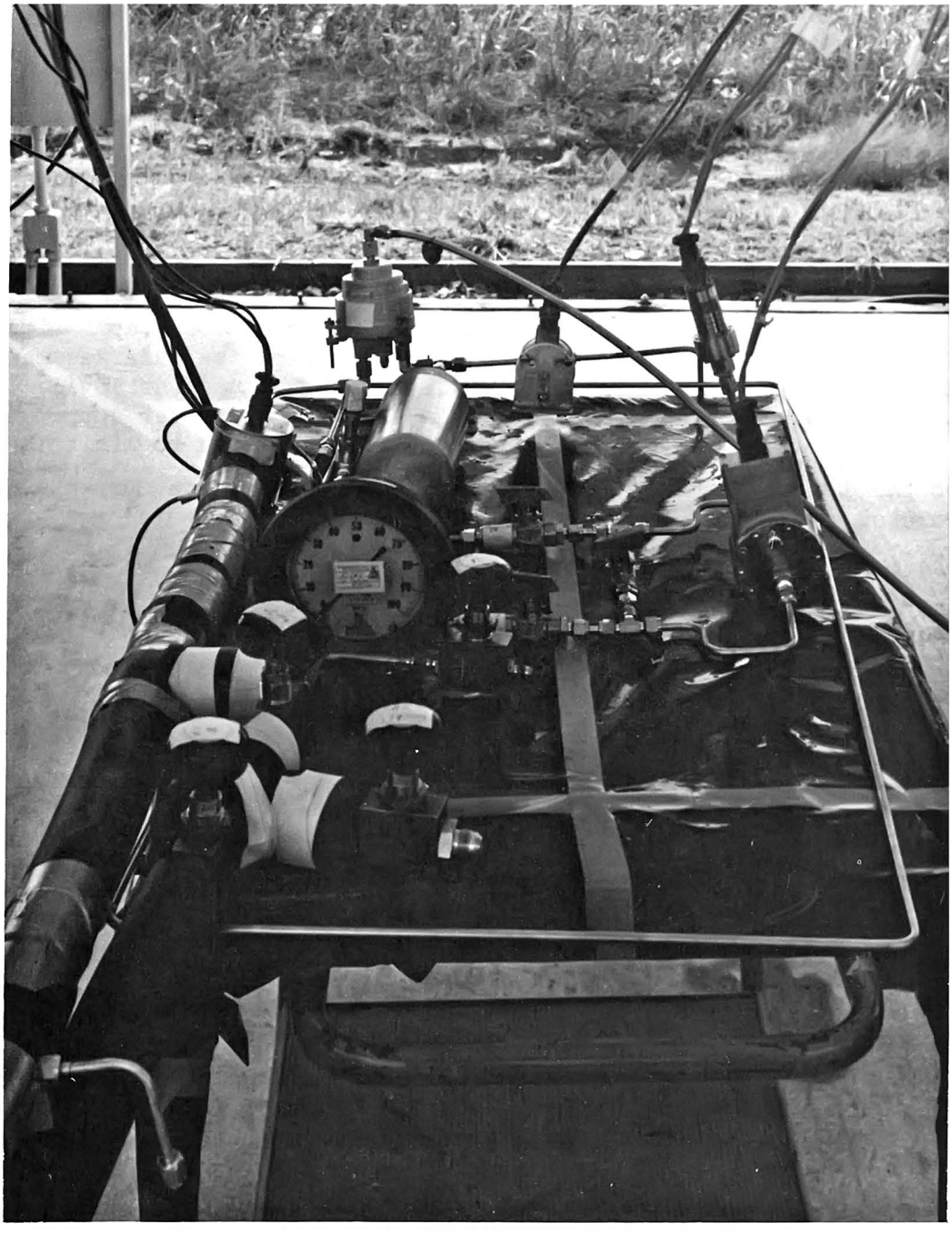

Figure B.10-2.- Flowmeter transient flow table test stand.

B.11 OXYGEN TANK FAN MOTOR FUSE BLOW CHARACTERISTIC TEST

B.11.1 OBJECTIVE

The objective of this test was to determine the current/time characteristics of the fuse for the oxygen tank fan motor.

B.11.2 TEST EQUIPMENT AND PROCEDURES

The test was performed in room ambient conditions (approximately 72° F and 14.7 psia). The time required to blow the fuse was measured at five current levels using three fuses at each current level. The test setup was as illustrated in figure B.11-1 with the power supply set at approximately 25 V dc and the resistor R_L adjusted to limit the current to the desired level. The data were recorded, and the currents were calculated by dividing the recorded voltages by the measured resistances.

B.11.3 RESULTS

The results are plotted in figure B.11-2.

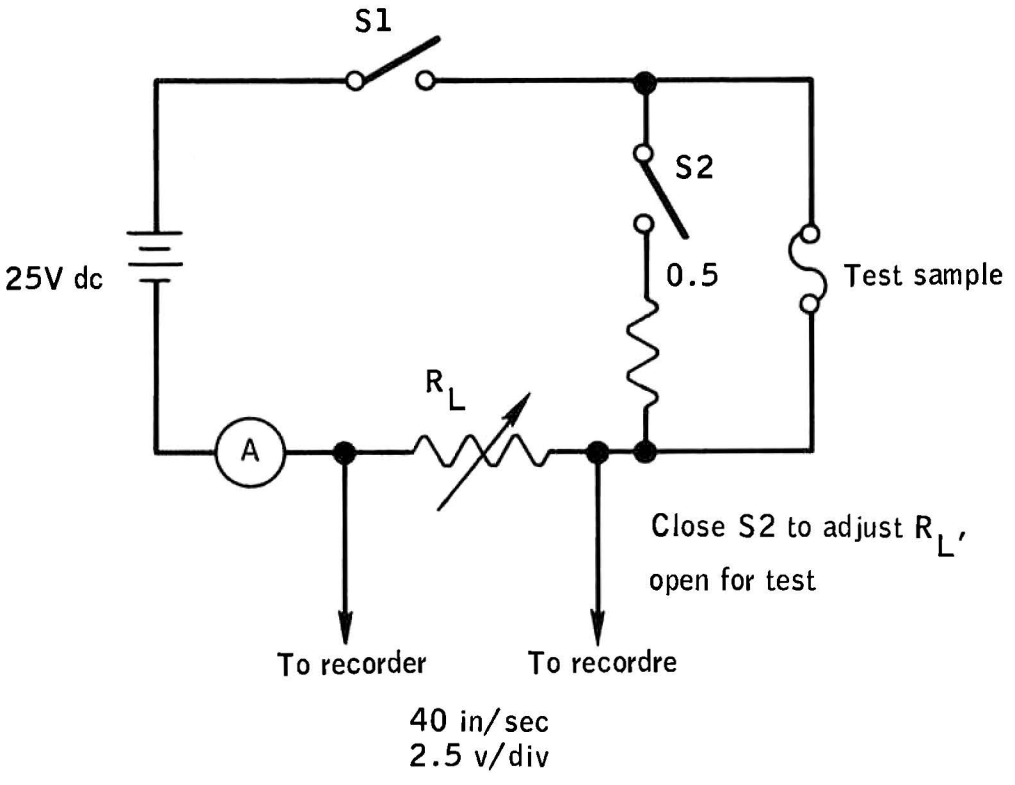

Figure B.11-1.- Test apparatus.

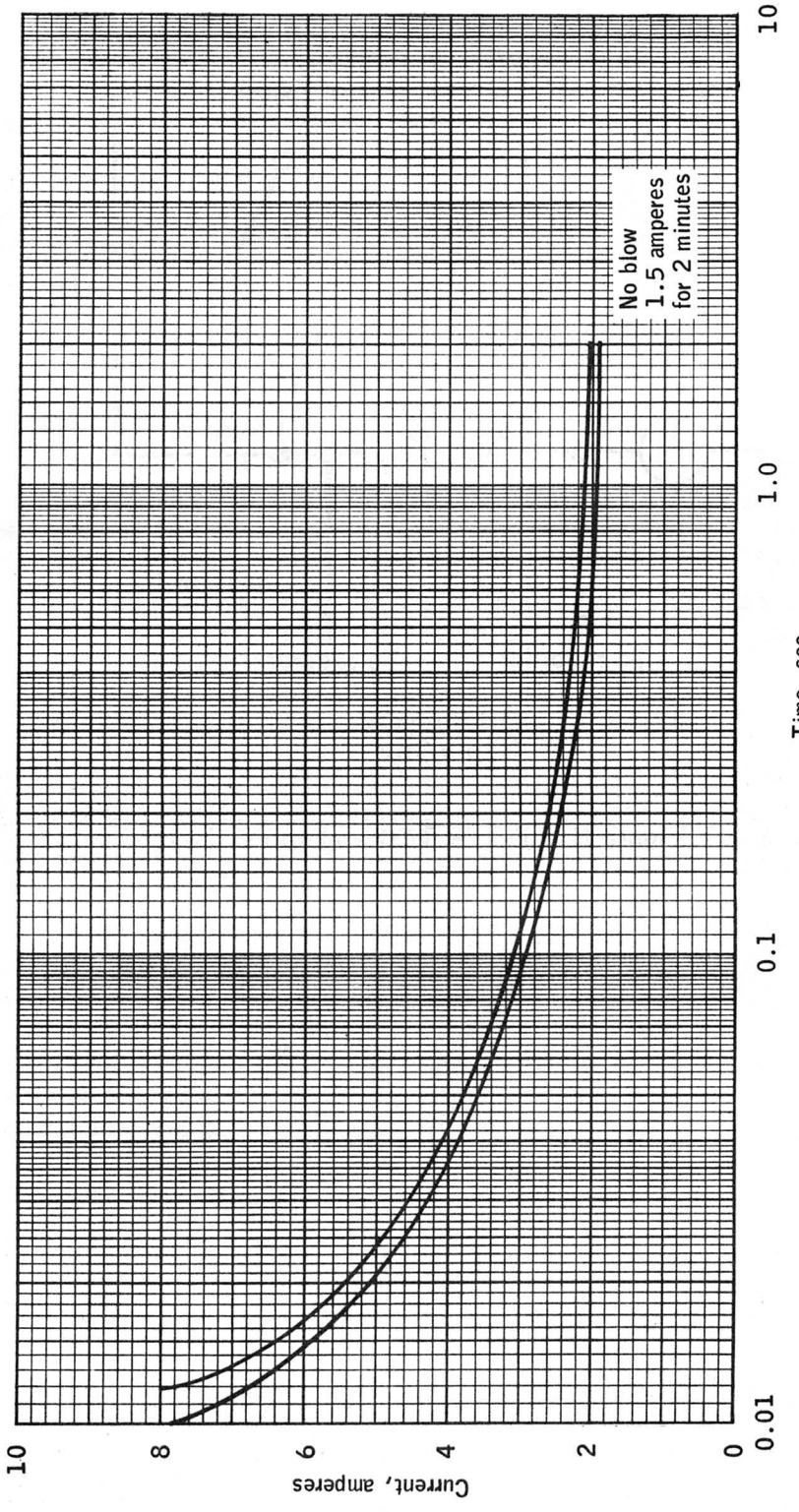

Figure B.11-2.- Fuse blow data.

B.12 INVERTER TESTS

B.12.1 OBJECTIVE

The objective of these tests was to determine the Apollo inverter performance parameters under specified load conditions.

B.12.2 TEST EQUIPMENT AND CONDITIONS

The tests were divided into four classifications.

a. Test A - Three-phase increasing balanced step loads in about 1-ampere steps

b. Test B - Line-to-line (phase A to phase B) increasing unbalanced step loads in about 1-ampere steps

c. Test C - Single-phase (phase C to neutral) increasing unbalanced step loads in about 1-ampere steps

d. Test D - Fused line tests.

Tests A, B, and C were conducted with the resistive load current steps starting from a steady-state balanced condition of about 0.75 ampere per phase at a 0.81 lagging power factor. These tests were repeated with the resistive load current steps starting from a steady-state balanced condition of about 1.0 ampere per phase at a 0.9 lagging power factor.

Test D was conducted for a steady-state load of about 1.0 ampere at a 0.9 lagging power factor with the following resistive loading current steps:

a. Four amperes, 8 amperes, and short-circuit loads through a 1-ampere fuse in each phase

b. Four amperes, 8 amperes, and short-circuit loads through a 1-ampere fuse in phase C only, with phases A and B remaining at the steady-state load conditions.

All tests were conducted with a 28 V dc input to the inverter. Figure B.12-1 is a schematic diagram of the test setup. The inverter was mounted on a water-cooled heat sink. The input voltage was monitored with

a digital voltmeter. The input current was measured through a 100-ampere shunt with its output displayed on a millivoltmeter and recorded on an oscillograph. The output was monitored with an ammeter, voltmeter, and power factor meter in each phase. A load bank was connected to the output through two three-pole relays to control separately the application of the steady-state loads (relay 1) and the step loads (relay 2). The voltage across the loads was recorded on the same oscillograph as the dc current measurement. An ohmmeter was connected to the resistance thermometer that monitors the critical temperature within the inverter.

Test B involved line-to-line loading and required a separate load bank that was series-connected to facilitate the higher voltage levels of this mode of operation. This load was switched through the contacts of relay 2 for A phase and B phase. This load bank was disconnected during all other tests. Line-to-line voltage was measured with a separate voltmeter, and current was measured with an ammeter and a calibrated current transformer.

B.12.3 RESULTS

The results are presented in table B.12-I, which also includes the nominal step loads (currents that were preset into the load bank before each step and based on resistors of about 10-percent accuracy and a voltage of 115 V rms). The actual current was measured through the ammeters during the application of the steps until the current exceeded 5 amperes. Beyond 5 amperes, the actual currents were computed for each phase, except for test B. The computations were based on the measured voltage on each phase and the impedances preset into the load bank for each phase. During test B, a direct measurement of the line-to-line current at all load settings was obtained. The transient voltages recorded are the maximum change in peak voltage. The surge current values shown are the peak change in input current over the steady-state value of the current. The temperature measurement did not vary significantly or become a critical factor throughout the tests.

The inverter did not appear to have been damaged in any way from the tests. It returned to a normal operating condition after each step.

TABLE B.12-I.- TEST DATA

TEST A — 4-19-70

Step	Nominal AC Amps/θ (Load Bank Switch Setting)	AC Amps (Actual)			AC Volts (rms) (Steady-State)			ΔAC Volts (Peak) (Maximum Transient)			Δ Amps DC (Maximum Transient)
		A	B	C	A	B	C	A	B	C	
Steady State	0.08 P.F. lag 0.74 Amp	0.74	0.74	0.74	115.0	115.3	116.0				13.2 Steady State
1	Δ=1 amp/θ	1.70	1.70	1.70	115.5	115.0	115.2	-22 12ms	-18 18ms	-22 18ms	13.0 / 12.0 20ms
								Missed Recovery			
2	Δ=2 amp/θ	2.60	2.60	2.60	115.0	114.5	115.0	-33 22ms +48 15ms	-37 22ms +48 13ms	-38 22ms +45 18ms	29 / 27 30ms
3	Δ=3 amp/θ	3.55	3.55	3.55	115.0	114.5	114.5	-35 28ms +50 15ms	-55 28ms +52 20ms	-48 28ms +52 12ms	40 / 38 40ms
4	Δ=4 amp/θ	4.55	4.55	4.55	115.0	114.5	114.5	-55 33ms +60 40ms	-60 35ms +55 40ms	-60 3ms +57 40ms	60 / 58 50ms
5	Δ=5 amp/θ	* 5.88	* 5.85	* 5.85	114.5	114.3	114.0	-75 40ms +68 40ms	-75 35ms +77 40ms	-68 38ms +60 40ms	84 / 80 65ms
6	Δ=6 amp/θ	* 6.75	* 6.75	* 6.80	112.5	112.5	113.0	-65 45ms +75 50ms	-58 45ms +68 50ms	-82 50ms +65 50ms	97 / 94 90ms
7	Δ=7 amp/θ	* 7.40	* 7.35	* 7.35	108.0	107.0	107.0	-53 40ms +75 50ms	-52 40ms +78 50ms	-55 40ms +80 50ms	105 / 103 43ms

*Indicates calculated data

TABLE B.12-I.- TEST DATA - Continued

TEST A — 4-19-70

Step	Nominal AC Amps/θ (Load Bank Switch Setting)	AC Amps (Actual)			AC Volts (rms) (Steady-State)			ΔAC Volts (Peak) (Maximum Transient)			Δ Amps DC (Maximum Transient)
		A	B	C	A	B	C	A	B	C	
8	Δ =8 amp/θ	* 7.95	* 7.60	* 7.60	100.0	98.0	98.0	-55 33ms / Missel +85 ---	-67 40ms / +85 55ms	-58 40ms / +85 55ms	105 / 105 } 33ms
9	Δ =9 amp/θ	* 8.20	* 8.15	* 8.15	96.5	95.5	95.5	-85 38ms / +95 50ms	-87 35ms / +95 50ms	-98 35ms / +95 50ms	105 / 103 } 45ms
10	Δ =10 amp/θ	* 8.55	* 8.40	* 8.35	90.0	88.5	88.0	-100 35ms / +102 50ms	-110 30ms / +90 55ms	-98 30ms / +92 48ms	110 / 108 } 35ms
11	Δ =11 amp/θ	* 8.60	* 8.50	* 8.40	83.0	83.3	82.0	-118 30ms / +112 50ms	-95 30ms / +108 50ms	-120 30ms / +102 50ms	115 / 110 } 40ms
12	Δ =12 amp/θ	* 8.67	* 8.54	* 8.48	77.5	76.3	75.5	-90 50ms	-105 50ms	-110 50ms / Missing Recovery	125 / 105 } 40ms
13	Δ =13 amp/θ	* 8.85	* 8.60	* 8.75	73.0	73.3	74.0	-115 60ms ←	-115 55ms	-92 55ms / Missing Recovery	115 / 110 } 38ms

*Indicates calculated data

TABLE B.12-I.- TEST DATA - Continued

TEST A — 4-19-70

Step	Nominal AC Amps/θ (Load Bank Switch Setting)	AC Amps (Actual)			AC Volts (rms) (Steady-State)			ΔAC Volts (Peak) (Maximum Transient)			ΔAmps DC (Maximum Transient)
		A	B	C	A	B	C	A	B	C	
14	Δ =14 amp/θ	9.00*	8.80*	8.80*	69.0	67.3	68.0	-65 45ms / Missing	Missed	115 55ms / ——	120 / 110 } 35ms
15	Short Circuit				0	0	0	Shut Off To Zero			130 / 20 } 15ms

*Indicates calculated data

TABLE B.12-I.- TEST DATA - Continued

TEST B April 19, 1970

Step	Nominal AC Amps/θ (Load Bank Switch Setting)	AC Amps (Actual)			AC Volts (rms) (Steady-State)			ΔAC Volts (Peak) (Maximum Transient)			ΔAmps DC (Maximum Transient)
		A	B	C	A	B	C	A	B	C	
Steady State	0.74 amps @ 0.81 P.F. lag A to B	.74	.74	.74	115	115	115.5	—	—	—	12.0 Steady State
1	Δ= 1.15 Amp V=200 I=1 amp	1.45	1.7	.75	* 115	* 114	* 115.5	-20 26ms missed recov.	-15 26ms	-15 26ms	7.0 5ms
2	Δ=2.3 Amp V=190 I=2 amp	2.25	2.62	.75	* 116	* 116.2	* 116.5	-20 32ms +22 28ms	-22 32ms +30 30ms	-20 32ms +25 24ms	15.4 20ms
3	Δ=3.45 V=180 I=2.7	3.08	3.48	.75	* 116	* 116.2	* 118.5	-30 44ms +35 30ms	-20 37ms +34 30ms	-22 36ms +36 30ms	23.8 20ms
4	Δ=5 V = 180 I = 3.9	4.25	4.65	.75	* 116	* 110	* 121.5	-42 42ms +46 32ms	-50 42ms +47 32ms	-31 42ms +45 32ms	38.2 36ms
5	Δ=6.5 V=180 I=5.0				118.1*	107*	121.5*	-50 48ms +51 42ms	-48 46ms +50 42ms	-41 46ms +48 45ms	48.8 44 ms
6	Δ=8 V=180 I=5.9				115.2*	104*	121.5*	-54 58ms Missed Recovery	-56 57ms	-51 56ms	59.4 53 ms
7	Δ=9.5 V=162 I=6.6				111.0*	98.4*	119.5*	-57V 57ms Missed Recovery	-59 58ms	-54 57ms	66.0 66 ms

*Indicates calculated data

TABLE B.12-I.- TEST DATA - Continued

TEST B April 19, 1970

Step	Nominal AC Amps/9 (Load Bank Switch Setting)	AC Amps (Actual)			AC Volts (rms) (Steady-State)			ΔAC Volts (Peak) (Maximum Transient)			Δ Amps DC (Maximum Transient)
		A	B	C	A	B	C	A	B	C	
8	Δ=12 V=146 I=7.4				* 101	* *86.5	* 112.5	-75 55ms +55 57ms	-80 56ms +52 58ms	-55 56ms +49 56ms	72.6 54ms
9	Δ=16.5 V=120 I=8.4				* 85.6	* 74.3	* 105.5	-77 58ms +45 67ms	-94 59ms +46 66ms	-61 58ms +53 66ms	79.2 53ms
10	Short Circuit V=0 I=10.7				* 26.9	* 26.9	* 51.6	-130 29ms +130 77ms	-139 30ms +131 77ms	-109 30ms +95 77ms	101 28ms
								LAST VALUE DID NOT OVERSHOOT.			
								VALUES ARE FOR RECOVERY TO STEADY STATE.			

*Indicates calculated data

TABLE B.12-I.- TEST DATA - Continued

TEST C April 19, 1970

Step	Nominal AC Amps/θ (Load Bank Switch Setting)	AC Amps (Actual)			AC Volts (rms) (Steady-State)			ΔAC Volts (Peak) (Maximum Transient)			ΔAmps DC (Maximum Transient)
		A	B	C	A	B	C	A	B	C	
Steady State	0.75A/0 at .81 P.F.										
	Δ = 1 amp θ "C" only		EXAMINATION OF THIS TEST DATA								
			INDICATED SOMETHING ERRATIC IN THE TEST SETUP . ALL DATA								
			IS INVALID								

*Indicates calculated data

TABLE B.12-I.- TEST DATA - Continued

TEST A April 20, 1970

Step	Nominal AC Amps/θ (Load Bank Switch Setting)	AC Amps (Actual)			AC Volts (rms) (Steady-State)			ΔAC Volts (Peak) (Maximum Transient)			ΔAmps DC (Maximum Transient)
		A	B	C	A	B	C	A	B	C	
Steady State	1 amp 0.9 P.F.	1.05	1.0	1.0	115.2	115.0	116				15.0 (steady state)
1	Δ = 1 amp/θ	1.95	1.93	1.92	115.2	114.7	115.0	-20 10ms +20 20ms	-20 12ms +20 20ms	-18 10ms +20 20ms	16.5 16.0 } 20 ms
2	Δ = 2 amp/θ	2.92	2.88	2.89	115.1	114.5	115.0	-38 23ms +55 37ms	-40 20ms +50 37ms	-38 23ms +45 37ms	33.0 31.0 } 37 ms
3	Δ = 3 amp/θ	3.85	3.82	3.83	115.0	114.2	114.5	-45 25ms +55 44ms	-40 25ms +50 44ms	-50 22ms +55 44ms	49.5 46.2 } 40 ms
4	Δ = 4 amp/θ	4.9	4.87	4.85	115.0	114.0	114.0	-60 25ms Missed Recovery	-60 30ms	-58 33ms	70.0 66.7 } 54 ms
5	Δ = 5 amp/θ	5.88*	5.82*	5.82*	114.5	113.2	113.2	-70 33ms +60 40ms	-65 42ms +55 40ms	-70 37ms +60 40ms	92.4 87.1 } 47 ms
6	Δ = 6 amp/θ	6.75*	6.74*	6.81*	112.5	112.2	113.2	-80 40ms +60 46ms	-70 50ms +55 46ms	-70 40ms +60 46ms	107 105 } 65 ms
7	Δ = 7 amp/θ	7.31*	7.25*	7.25*	106.5	105.5	105.5	-80 45ms Missed Recovery	-80 45ms	-85 40ms	109 106 } 54 ms NOTE: Shifted galvo

*Indicates calculated data

TABLE B.12-I.- TEST DATA - Continued

TEST A April 20, 1970

Step	Nominal AC Amps/θ (Load Bank Switch Setting)	AC Amps (Actual)			AC Volts (rms) (Steady-State)			ΔAC Volts (Peak) (Maximum Transient)			ΔAmps DC (Maximum Transient)
		A	B	C	A	B	C	A	B	C	
8	Δ = 8 amp/θ	7.67*	7.62*	7.58*	99.0	98.5	98	-90 32ms +60 53ms	-85 35ms +60 53ms	-80 35ms +60 53ms	115.5 108 55 ms
9	Δ = 10 amp/θ	8.24*	8.17*	8.15*	87.0	86.2	86.0	-80 30ms +65 45ms	-95 28ms +55 45ms	-90 30ms +55 45ms	115.5 108 53 ms
10	Δ = 12 amp/θ	8.65*	8.54*	8.52*	77.2	76.2	76.0	-120 25ms +60 50ms	-105 25ms +55 50ms	-90 25ms +55 50ms	122 108 45 ms
11	Δ = 15 amp/θ	9.05*	8.92*	8.92*	65.5	64.5	64.5	-110 15ms +60 50ms	-85 17ms +55 50ms	-120 17ms +55 50ms	128 102 45 ms
12	Short Circuit				0	0	0	Shut Off to "0"	Shut Off to "0"	Shut Off to "0"	124 16.5 10 ms

*Indicates calculated data

TABLE B.12-I.- TEST DATA - Continued

TEST B April 20, 1970

Step	Nominal AC Amps/θ (Load Bank Switch Setting)	AC Amps (Actual)			AC Volts (rms) (Steady-State)			ΔAC Volts (Peak) (Maximum Transient)			ΔAmps DC (Maximum Transient)
		A	B	C	A	B	C	A	B	C	
Steady State	1 amp/θ @0.9 PF A to B	1.06	1.00	1.00	115.5	115.0	115.5	-	-	-	15.0 (steady state)
1	V=193 I=1a Δ= 1.15 amp	1.75	1.95	1.00	114	112	119	-10 12ms / +12 20ms	-15 12ms / +10 22ms	-10 10ms / +10 22ms	10.0 / 9.5 } 20 ms
2	V=188 I=1.84 Δ= 2.3	2.55	2.8	1.00	114.2	110.2	121.5	-20 18ms / +25 23ms	-20 20ms / +20 22ms	-18 15ms / +25 20ms	15.0 / 14.5 } 25 ms
3	V=183 I=3.2 Δ= 4	3.82	4.15	1.05	114.2	107	123.5	-35 20ms / +40 30ms	-40 23ms / +35 28ms	-25 20ms / +40 28ms	30.0 / 29.0 } 28 ms
4	V=180 I=4.05 Δ= 5.2	4.65	4.98	1.05	114.5	104.5	124.5	-40 20ms / +40 28ms	-48 25ms / +40 27ms	-40 20ms / +50 26ms	37.0 / 36.0 } 30 ms
5	V=176 I=4.95 Δ= 6.5			1.05	114.5	102.5	125.8	-45 20ms / +50 32ms	-60 25ms / +45 34ms	-35 18ms / +45 33ms	47.0 / 46.2 } 37 ms
6	V=170 I=5.9 Δ= 8			1.05	113.0	98.5	125.5	-40 25ms / +50 37ms	-60 25ms / +45 37ms	-45 20ms / +55 37ms	57.0 / 53.0 } 42 ms
7	V=141 I=7.4 Δ= 12			.9	100.0	82.5	115.0	-60 25ms / +50 43ms	-80 25ms / +45 43ms	-45 20ms / +40 43ms	60.0 / 58.0 } 43 ms

*Indicates calculated data

TABLE B.12-I.- TEST DATA - Continued

TEST B April 20, 1970

Step	Nominal AC Amps/θ (Load Bank Switch Setting)	AC Amps (Actual)			AC Volts (rms) (Steady-State)			ΔAC Volts (Peak) (Maximum Transient)			ΔAmps DC (Maximum Transient)
		A	B	C	A	B	C	A	B	C	
	A to B										
8	V=126 I=8.0 Δ = 15			.8	92.0	73.0	108.0	-70 20ms +50 43ms	-90 20ms +45 43ms	-55 20ms +40 43ms	64.0 59.4 37 ms
9	V=0 Short I=10.25			0	15.0	15.0	50.0	-130 20ms +130 70ms	-120 20ms +130 70ms	-90 25ms +80 70ms	84.0 13.0 23 ms
	V= I=							NOTE: Last transient did not overshoot steady state. Transient values given are recovery to steady state.			
	V= I=										
	V= I=										

*Indicates calculated data

TABLE B.12-I.- TEST DATA - Continued

TEST C — 4-20-70

Step	Nominal AC Amps/θ (Load Bank Switch Setting)	AC Amps (Actual)			AC Volts (rms) (Steady-State)			ΔAC Volts (Peak) (Maximum Transient)			ΔAmps DC (Maximum Transient)
		A	B	C	A	B	C	A	B	C	
Steady State	1 amp /θ @ 0.9 P. F. lag	1.05	1.00	1.00	115.5	114.8	115.5				(Steady State) 15 amps
1	Δ=1 amp, θC	1.05	1.00	1.86	118.0	116.0	112.5	-7 10ms +5 15ms	-10 10ms +5 15ms	-10 10ms +5 15ms	6
2	Δ=2 amp, θC	1.08	1.00	2.75	119.5	116.0	110.0	-10 15ms +15 24ms	-15 12ms +15 24ms	-15 12ms +15 24ms	10
3	Δ=3	1.10	1.00	3.62	121.0	116.0	108.0	-15 10ms +20 24ms	-20 12ms +20 24ms	-25 12ms +20 24ms	13.5 13.0 } 20ms
4	Δ=4	1.10	1.00	4.50	122.0	116.2	106.0	-20 15ms +25 27ms	-20 20ms +30 25ms	-25 15ms +25 28ms	20 19.5 } 26ms
5	Δ=5	1.15	1.00	5.28*	123.0	117.0	105.7	-20 20ms +30 20ms	-30 20ms +30 20ms	-35 18ms +35 20ms	24 23 } 25ms
6	Δ=8	1.12	1.00	7.43*	123.0	113.5	96.0	-30 18ms Missed Recovery	-35 20ms	-50 18ms	33 31 } 34ms
7	Δ=6	1.10	1.00	6.12*	124	116.5	102.0	-25 18ms +35 22ms	-30 20ms +35 22ms	-40 15ms +35 22ms	27 26 } 29ms

*Indicates calculated data

TABLE B.12-I.- TEST DATA - Continued

TEST C 4-20-70

Step	Nominal AC Amps/9 (Load Bank Switch Setting)	AC Amps (Actual)			AC Volts (rms) (Steady-State)			ΔAC Volts (Peak) (Maximum Transient)			ΔAmps DC (Maximum Transient)	
		A	B	C	A	B	C	A	B	C		
8	Δ =7	1.10	1.00	6.70*	124.2	116.0	99.0	-22 25ms +40 24ms	-35 25ms +40 24ms	-40 20ms +40 24ms	28 26	30ms
9	Δ =10	1.05	.95	8.36*	119.0	109.0	88.2	-30 20ms +35 25ms	-45 20ms +40 25ms	-45 20ms +40 27ms	36 33	32ms
10	Δ =12	1.05	.90	9.08*	115.2	104.0	81.0	-42 13ms +35 34ms	-42 13ms +40 34ms	-70 18ms +40 35ms	36 34	32ms
11	Δ =15	1.00	.85	10.2*	110.0	98.0	72.5	-10 10ms +40 37ms	-45 15ms +30 37ms	-70 10ms +35 37ms	40 33.5	32ms
12	Short Circuit	.60	.2	13**	63.0	49.5	0	-60 28ms 170 70ms	-85 28ms 170 70ms	Zero 28ms 170 70ms	74 6.7	27ms

*Indicates calculated data

** MAX INVERTOR SHORT-CKT AMPS

TABLE B.12-I.- TEST DATA - Concluded

TEST D April 20, 1970

Step	Nominal AC Amps/θ (Load Bank Switch Setting)	AC Amps (Actual)			AC Volts (rms) (Steady-State)			ΔAC Volts (Peak) (Maximum Transient)			Δ Amps DC (Maximum Transient)
		A	B	C	A	B	C	A	B	C	
Steady State	1 amp/θ @ 0.9 P.F. lag	1.05	1.00	1.00	115.2	115.0	116.0	-	-	-	15.0 (Steady State)
1	Steady State + Δ4A/θ through 1A fuse/θ				115.2	115.0	116.0	-70 34ms +60 38ms	-50 34ms +50 36ms	-60 34ms +55 38ms	66 Δ T = 50ms
2	Steady State + Δ 8A/θ through 1A fuse/θ				115.5	115.0	115.5	-90 25ms +55 40ms	-75 25ms +50 40ms	-85 25ms +55 40ms	96 Δ T = 25ms
3	Steady State + Δ4A, θC thru 1A fuse				115.5	115.0	115.5	-20 15ms +20 20ms	-20 15ms +20 20ms	-30 15ms +25 20ms	20 Δ T = 75ms
4	Steady State + Δ 8A, θC thru 1A fuse				115.5	115.0	115.5	-25 10ms +40 20ms	-40 25ms +40 20ms	-50 25ms +45 20ms	30 Δ T = 25ms
5	3θ Short Ckt through 1 amp fuse				115	115	115.7	-160 7.5ms +30 30ms	-160 5ms +40 40ms	-160 5ms +30 40ms	120 Δ T = 7.5ms
6	1θ Short Ckt through 1 amp fuse				115	115	115.7	-30 7ms +20 22ms	-60 5ms +15 24ms	-160 5ms +100 24ms	33 Δ T = 7ms

*Indicates calculated data

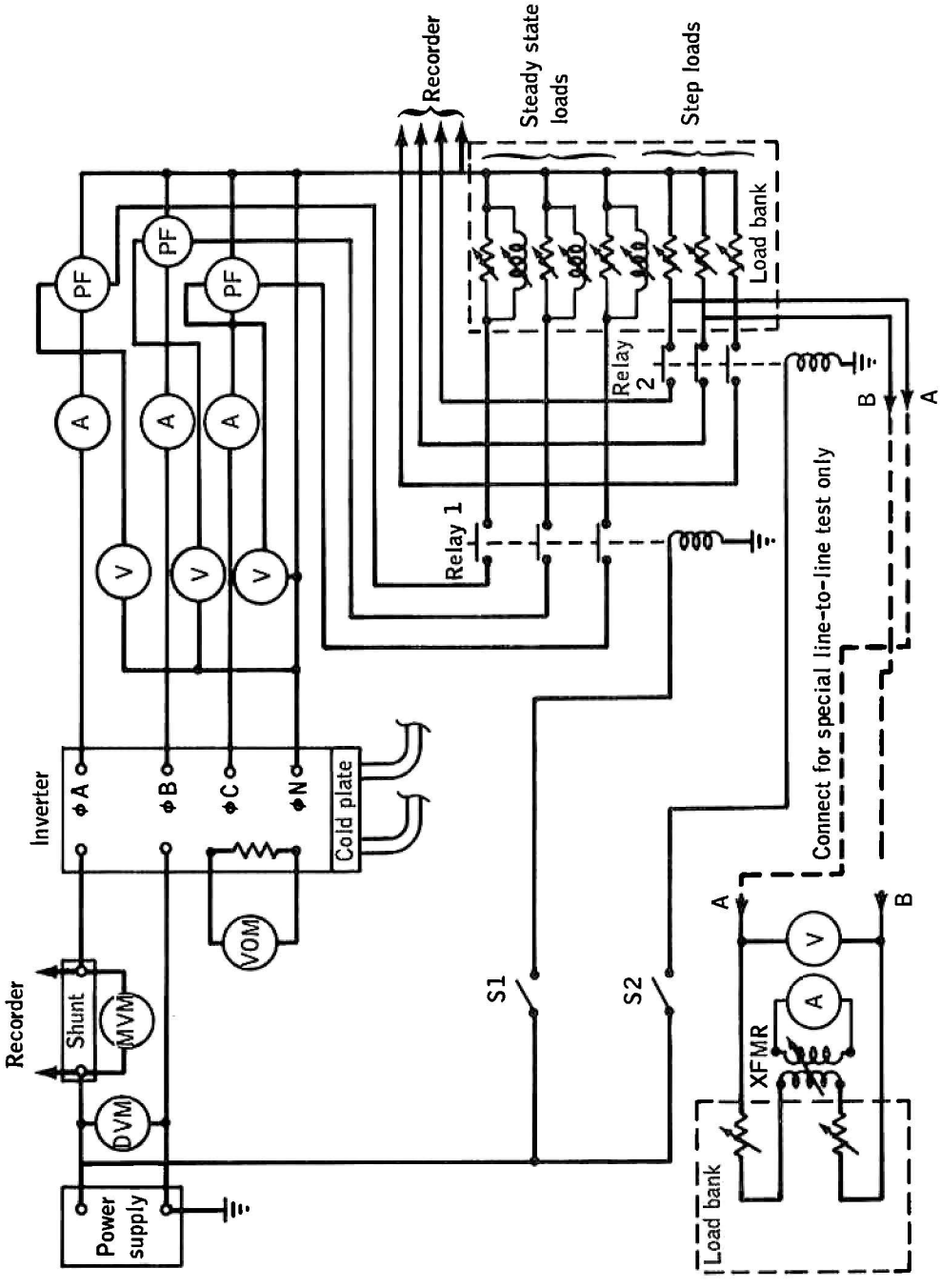

Figure B.12-1.- Test setup schematic.

B.13 FAN MOTOR STATOR WIRE OVERLOAD TEST

B.13.1 OBJECTIVE

The objectives of this test were to determine whether the type of wiring used in cryogenic oxygen tank 2 would ignite and burn in an overload condition and to determine what conditions are necessary to produce an overload of the fan motor stator wire.

B.13.2 TEST EQUIPMENT AND CONDITIONS

The tests were conducted in a reaction vessel (fig. B.13-1) at minus 170° (± 10°) F with 940 psig oxygen. Figure B.13-2 is a schematic of the test apparatus. The vessel was modified to accept thermocouple insertion probes through the walls and base, and electrical feedthroughs were made from thermocouple insertion probes through the walls (fig. B.13-3).

Attempts were made to overload the motor stator wire in the configuration shown in figure B.13-4, using a 115-volt, 400-hertz generator. The maximum current available from this generator was 5 amperes, which was insufficient to fuse the wire. A 24 V dc power supply was then substituted for the 115-volt, 400-hertz generator, and the wire was overloaded to fusion. Post-test examinations were made to determine if the wire or insulation would ignite and the burning propagate.

B.13.3 RESULTS

The results from a total of 14 tests indicate that 8 amperes are necessary to fuse the motor stator wire at environmental conditions of 940 psig and minus 180° F. The wire fuses in approximately 200 milliseconds at 10 amperes. A post-test examination of the test specimens indicated that no insulation ignition occurred in any of the tests. The discoloration evident in figure B.13-5 was apparently the result of the conductor overheating and was not caused by interaction with the oxygen environment. Tests conducted in a high pressure nitrogen gas environment revealed similar discoloration.

B.13.4 CONCLUSIONS

The results of these tests indicate that the motor stator winding wire is difficult to ignite by an electrical overload of the conductor. Propagation of the burning is also very unlikely. The currents and durations required to fuse the motor stator wire are not within the capabilities of the electrical systems in the oxygen tank.

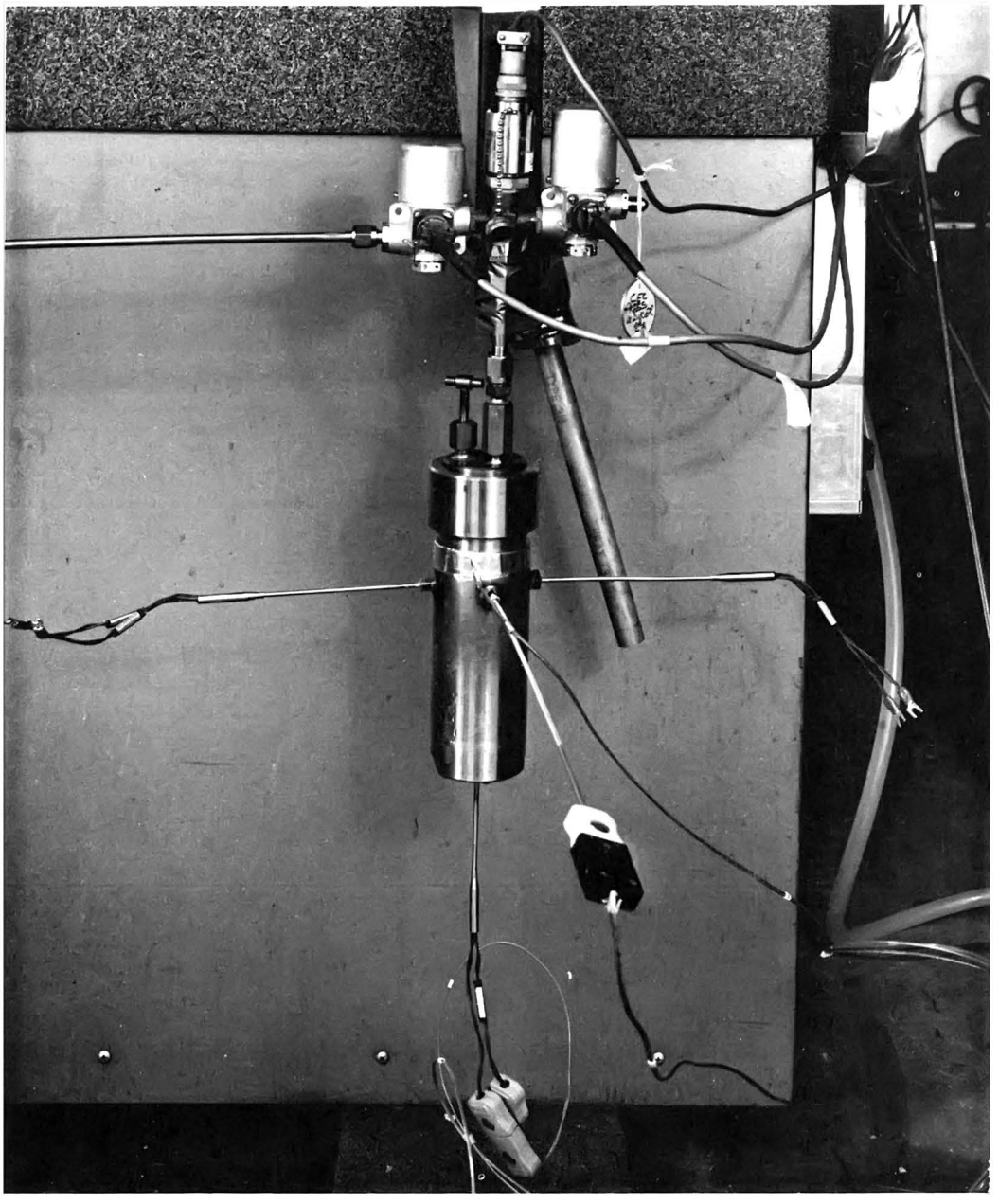

Figure B.13-1.- External view of test chamber.

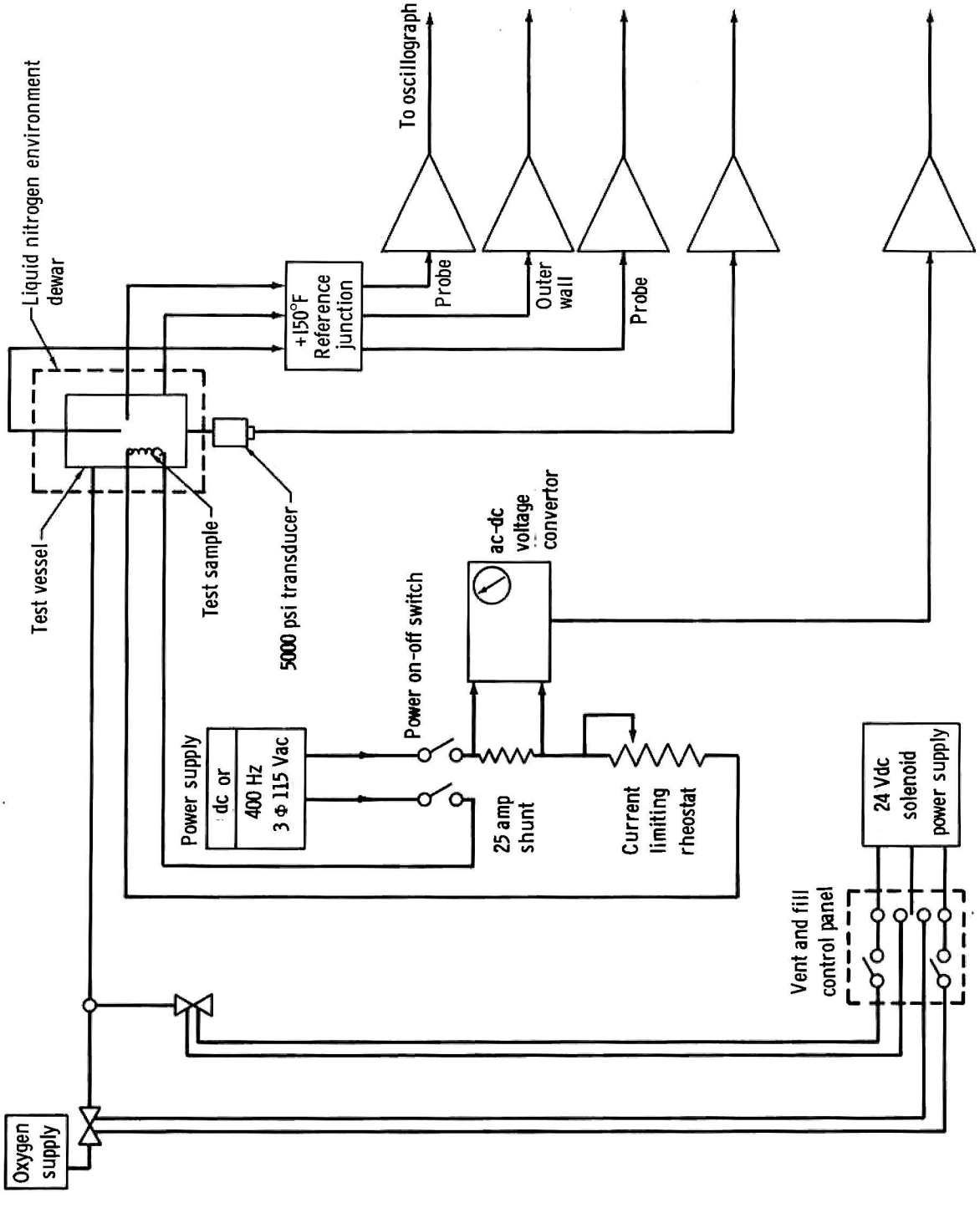

Figure B.13-2. - Schematic of high pressure oxygen test apparatus.

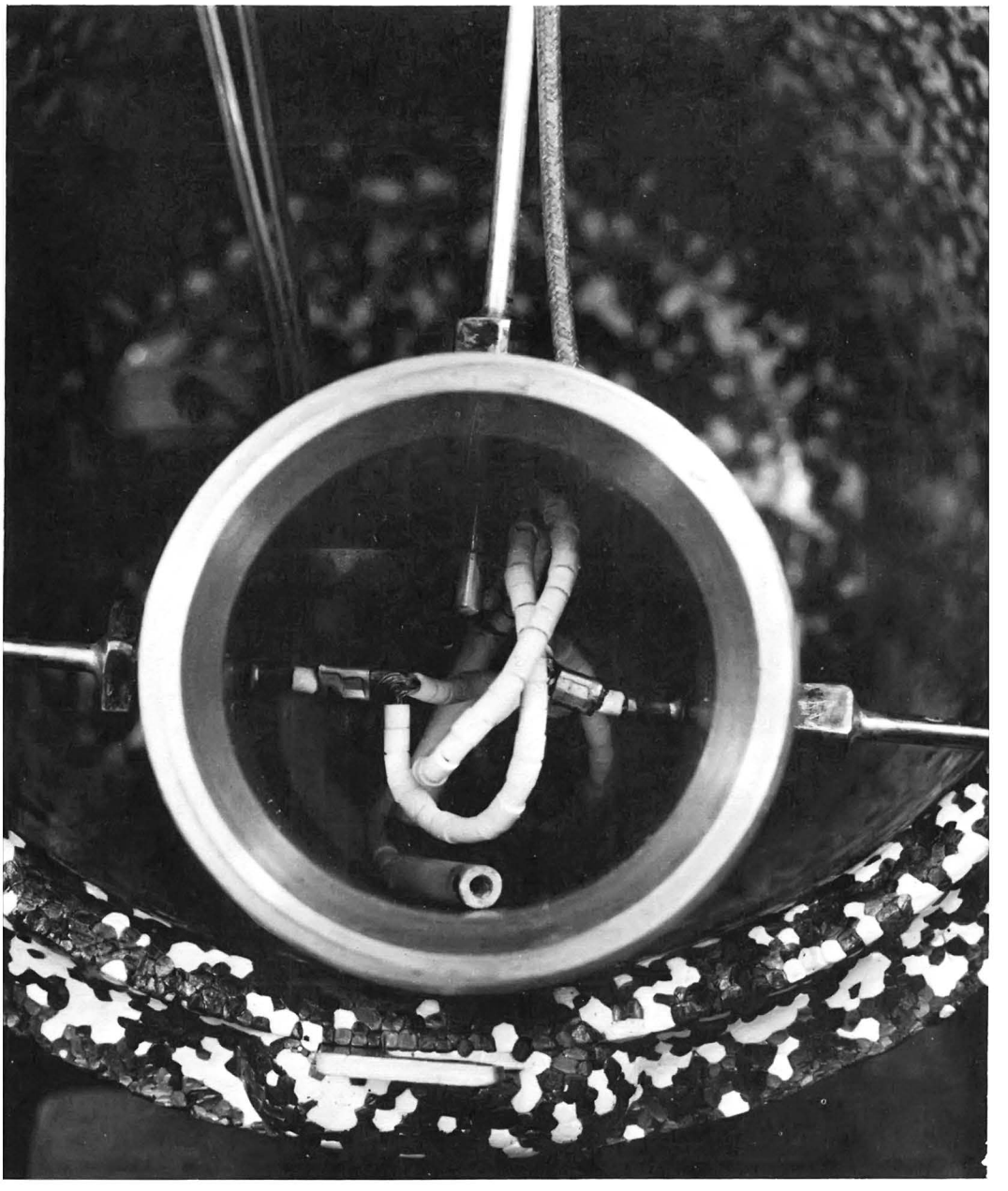

Figure B.13-3.- Internal view of test chamber.

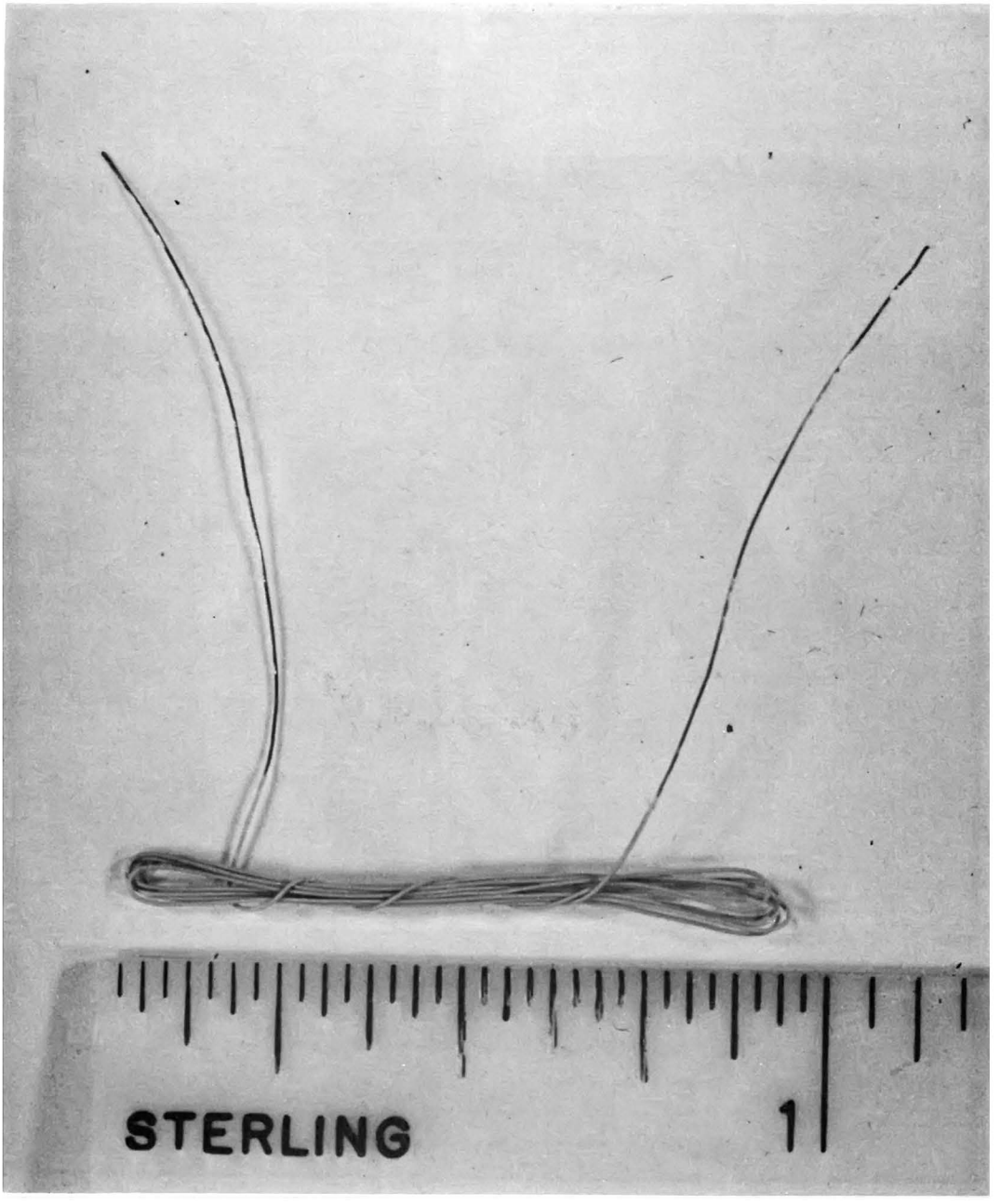

Figure B.13-4.- Wire after dc test.

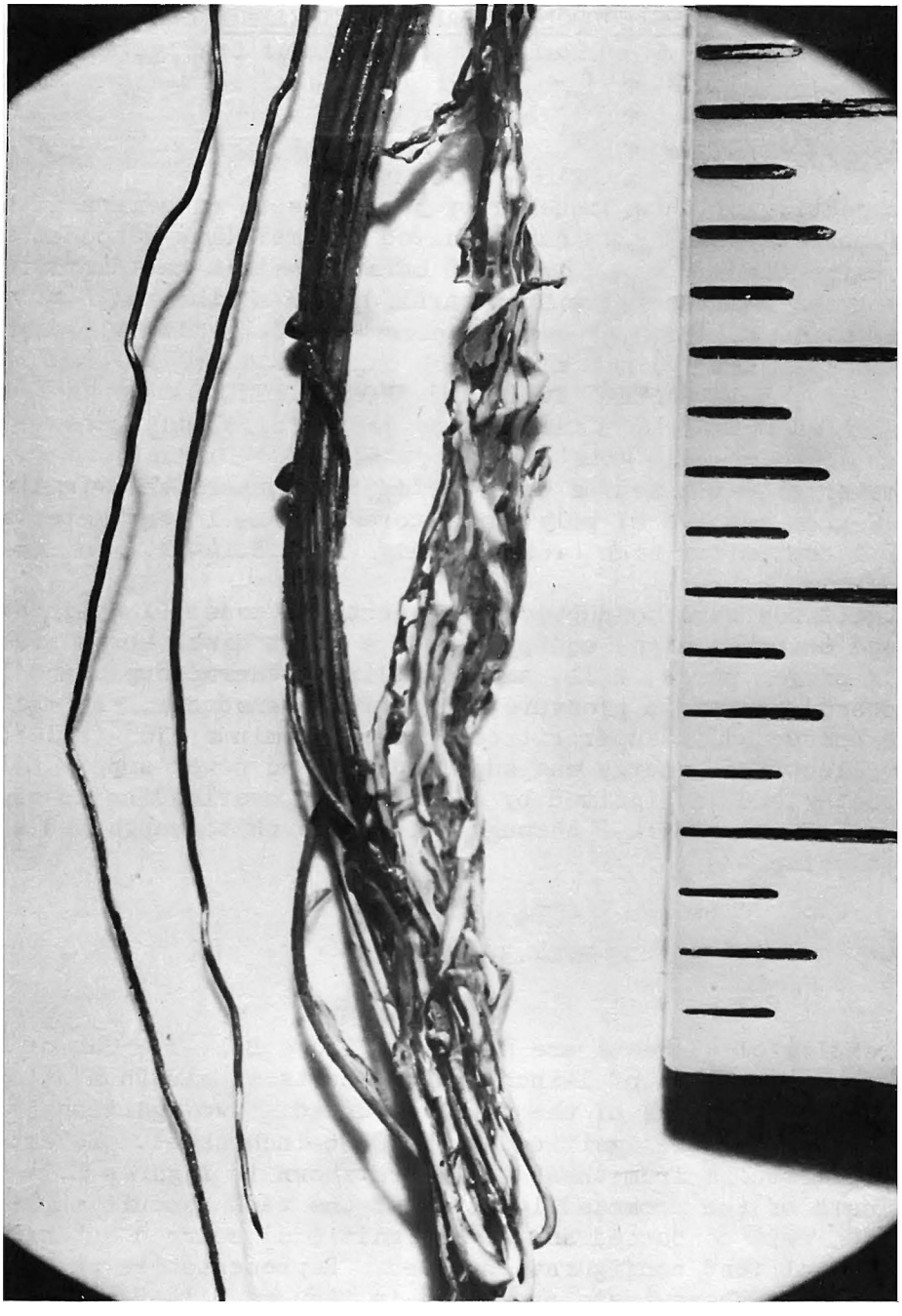

Figure B.13-5.- Wire after dc test.

B.14 PROMOTED IGNITION TEST OF METALS BY BURNING POLYTETRAFLUOROETHYLENE

B.14.1 OBJECTIVE

The objective of this sequence of tests was to determine if burning polytetrafluoroethylene could have ignited the metallic components in cryogenic oxygen tank 2. The ignition of such metals could provide additional energy as well as cause structural damage of the tank.

B.14.2 TEST EQUIPMENT AND CONDITIONS

The materials selected as possible energy sources were ignited with 1-gram or 2-gram samples of polytetrafluoroethylene 1 centimeter square and 0.5 or 1 centimeter high, respectively (fig. B.14-1).

The ignitions were conducted in a reaction vessel (1.75-inch inside diameter and 6 inches high) equipped with a burst disk (burst pressure 3500 psig); oxygen purge, fill, and vent lines; thermocouple and igniter power feedthroughs; and a pressure monitering transducer. In most cases, tests were conducted in supercritical oxygen at minus 170° (± 10°) F and 940 psig. Electrical energy was supplied by a dc power supply. The polytetrafluoroethylene was ignited by electrically overloading 26-gage nichrome wire. Figures B.14-2 through B.14-4 are photographs and a schematic of the test setup.

B.14.3 RESULTS

The results of 45 tests are shown in figure B.14-1. Out of 23 tests of the promoted ignition of 1-inch square sheets of aluminum alloy 2024 and 5052, three ignitions of the metal occurred: two ignitions of the 0.012-inch sheet and one ignition of the 0.06-inch sheet. Selected photographs of the results from these tests are shown in figures B.14-5 through B.14-8. Tests of the promoted ignition of the tank conduit material, Inconel X750, were conducted and seven ignitions occurred out of ten tests, with the several test configurations used. Representative photographs of the residues from these tests are shown in figures B.14-9 and B.14-10. To determine if ignition of the motor stator iron core was probable, seven tests of motor stator segments were conducted. The segments were sectioned from an oxygen tank fan motor and were ignited as indicated in figure B.14.1.

The segments were partially consumed in all tests and photographs of the residues are shown in figures B.14-11 and B.14-12. Five tests were conducted on specimens simulating the electrical feedthrough region of the fan motor housing, and ignition of the aluminum occurred. A photograph of a specimen after test is shown in figure B.14-13.

B.14.4 CONCLUSIONS

The results of these promoted ignition tests indicate that aluminum can only be ignited by burning polytetrafluoroethylene in certain configurations. Aluminum sheets having thicknesses similar to those used in tank applications did not ignite during the tests. All of the motor stator core tests shown that the core segments are easily ignited by burning polytetrafluoroethylene in this test environment. Similar conclusions can be drawn from the Inconel tube tests, particularly when the tube is configured with a wire bundle similar to that used on the spacecraft.

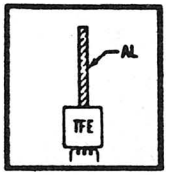

VERTICAL - CONTACT

SAMPLE AL	SIZE TFE	NO. TESTS	RESULTS
0.03135	1 g	1	NO IGNITION
0.0135	1 g	1	NO IGNITION
0.006	1 g	1	NO IGNITION

(a)

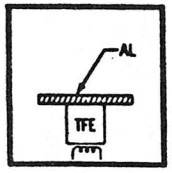

I HORIZONTAL - CONTACT

SAMPLE AL	SIZE TFE	NO. TESTS	RESULTS
0.006	1 g	1	NO IGNITION
0.006	2 g	3	ONE IGNITION (MELTING INDICATED ON OTHERS)
0.012	2 g	6	TWO IGNITIONS OUT OF 6 TESTS

(b)

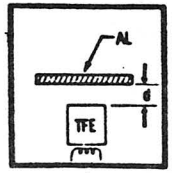

H HORIZONTAL - SEPARATED

SAMPLE AL	SIZE TFE	NO. TESTS	RESULTS
0.012	2 g	1	d = 1/4", NO IGNITION
0.006	2 g	2	d = 1/4", NO IGNITION (MELTING INDICATED)
0.006	2 g	1	d = 1/2", NO IGNITION

(c)

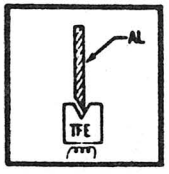

VERTICAL - KNIFE EDGE

SAMPLE AL	SIZE TFE	NO. TESTS	RESULTS
0.063	2 g	6	NO IGNITION (MELTING INDICATED)

(d)

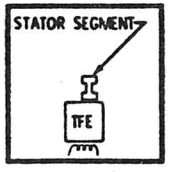

HORIZONTAL - CONTACT

SAMPLE	SIZE TFE	NO. TESTS	RESULTS
MOTOR STATOR SEGMENT	2 g	3	ALL SAMPLES IGNITED AND 60-95% OF SEGMENTS BURNED

(e)

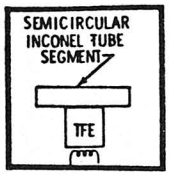

HORIZONTAL - CONTACT

SAMPLE	SIZE TFE	NO. TESTS	RESULTS
0.5 g INCONEL TUBE SEGMENT	2 g	4	ONE IGNITION OUT OF 4 TESTS

(f)

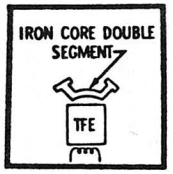

SAMPLE	SIZE TFE	NO. TEST	RESULTS
3.3, 3.4, 3.6 g SEGMENTS	2 g	4	4 SEGMENTS IGNITED

(g)

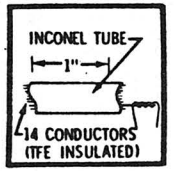

SAMPLE	SIZE	NO. TESTS	RESULTS
MOCKUP CABLE ASSY IN INCONEL TUBE. 14 CONDUCTORS		3	2 SAMPLES IGNITED AND PARTIALLY BURNED

(h)

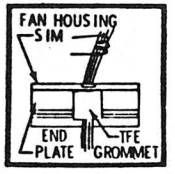

SAMPLE SIZE AL	TFE	NO. TESTS	RESULTS
3.8 g SIMULATED FAN MOTOR HOUSING AND END PLATE	2 g	5	NO IGNITION

(i)

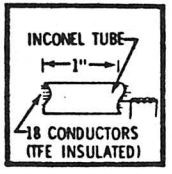

SAMPLE	SIZE	NO. TESTS	RESULTS
6.62 g, 18 CONDUCTORS IN 1-INCH		3	ALL SAMPLES IGNITED AND BURNED OR MELTED COMPLETLY

(j)

TFE = Polytetrafluoroethylene
g = Weight of test item in grams

Figure B.14-1.- Ignition configurations and results.

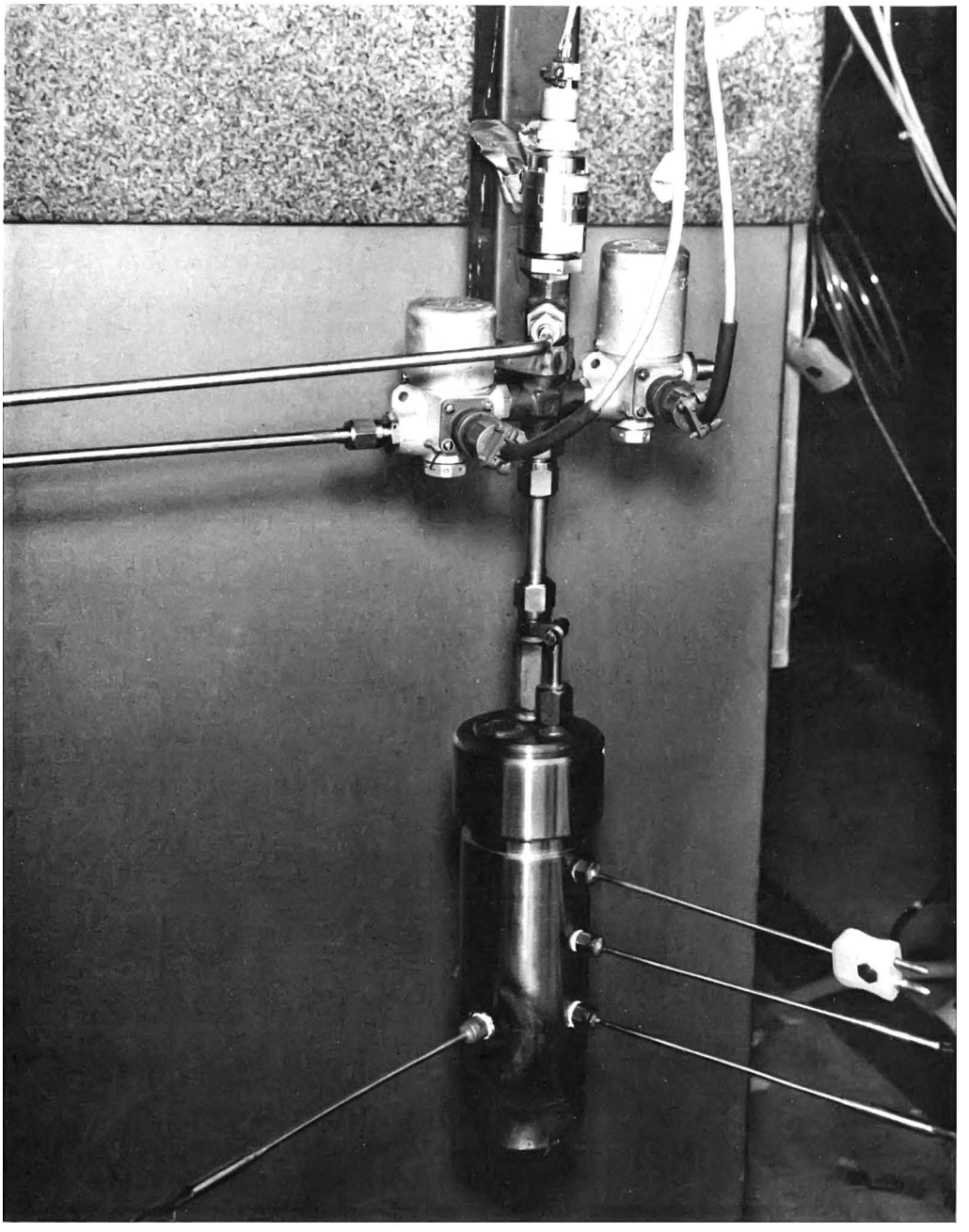

Figure B.14-2.- External view of test chamber.

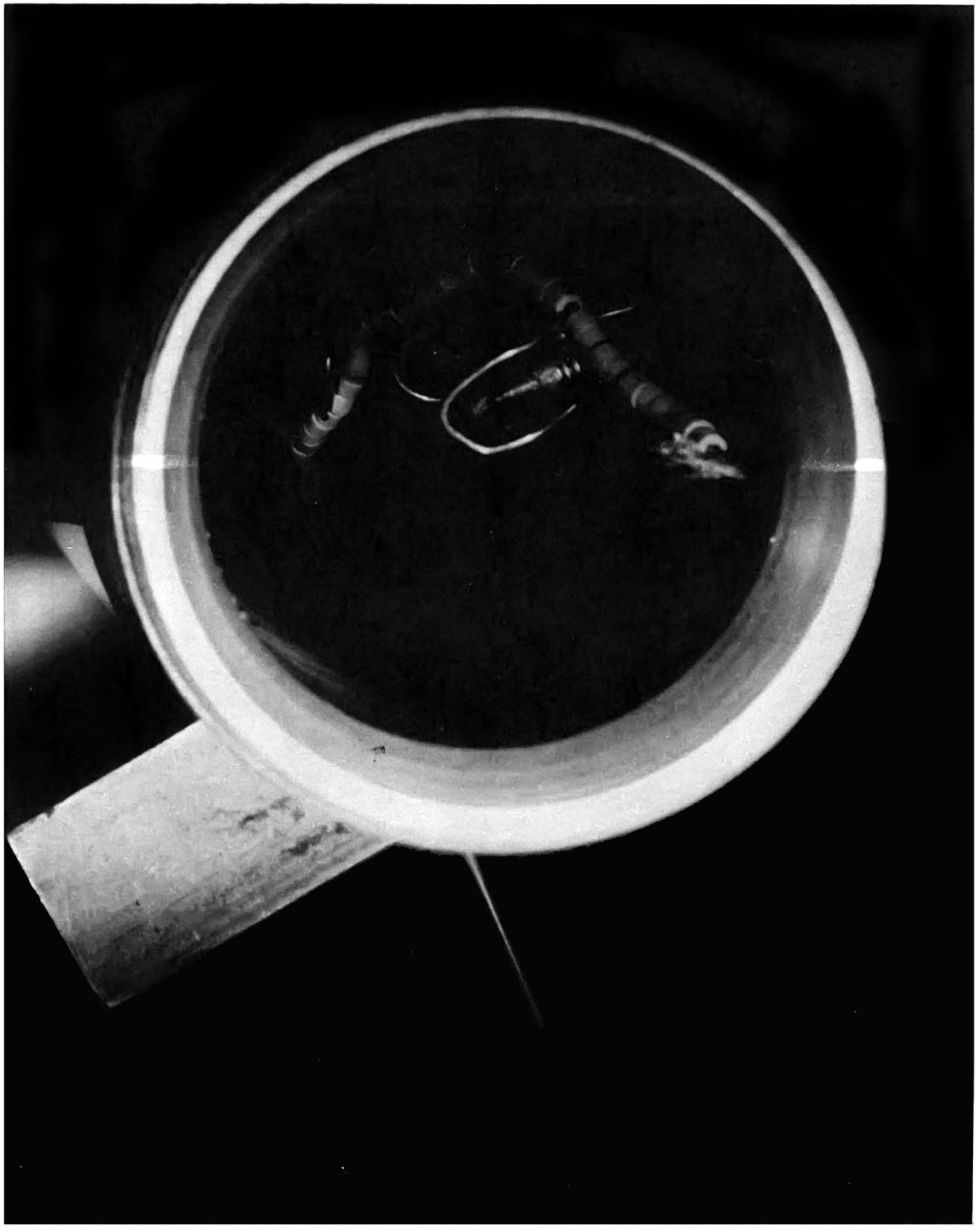

Figure B.14-3.- Internal view of test chamber.

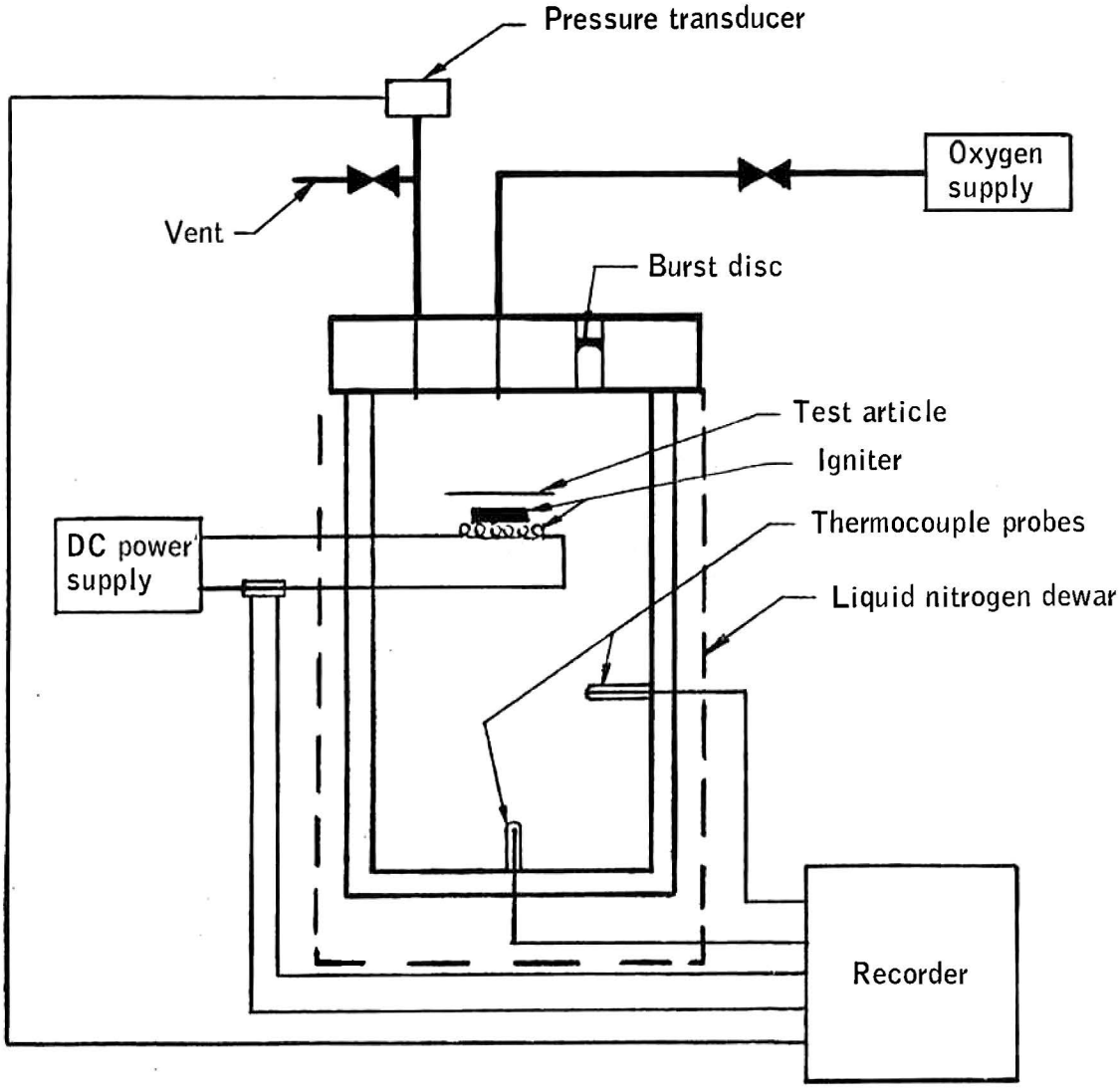

Figure B.14-4.- Schematic of test apparatus.

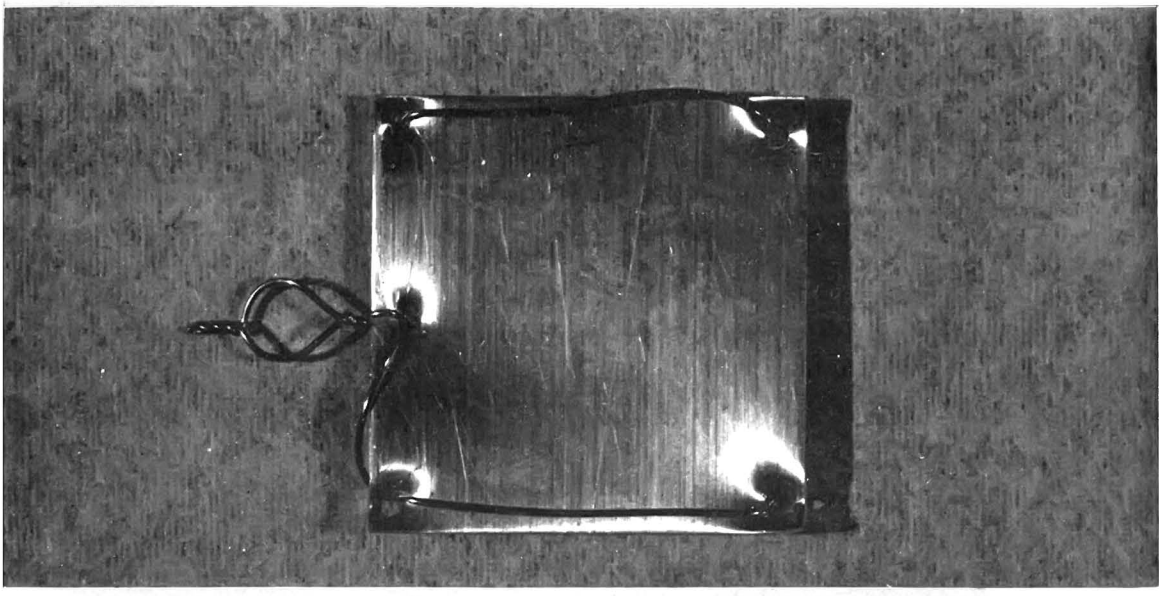

Figure B.14-5.- Post test residue from aluminum with no ignition.

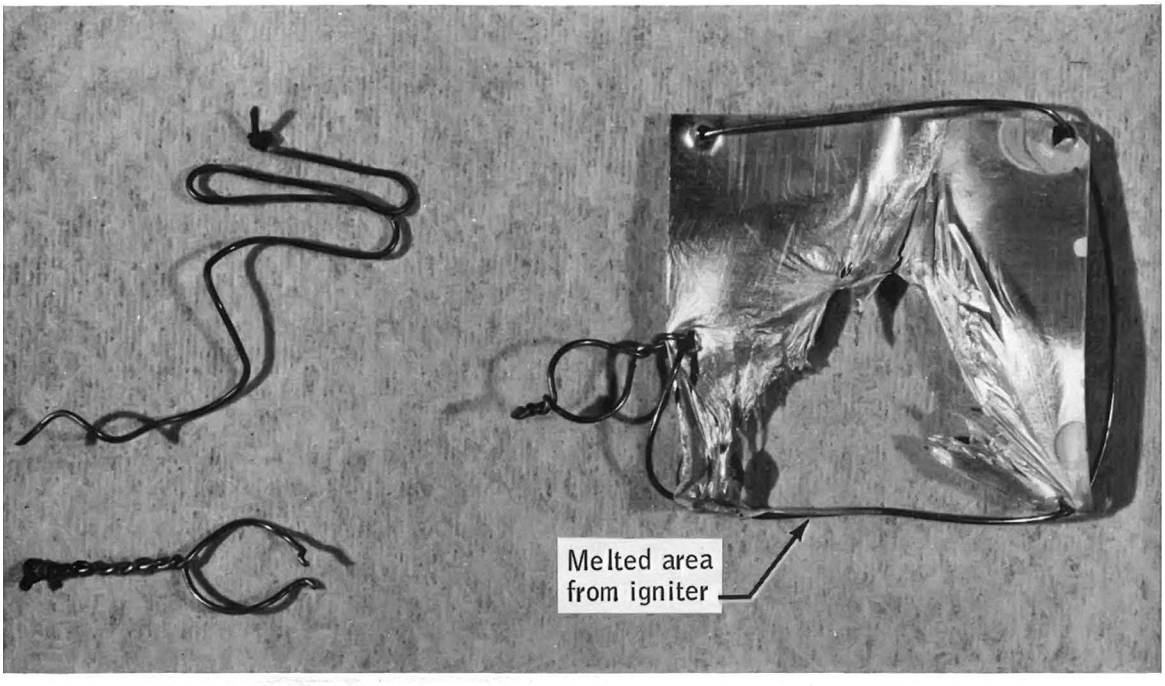

Figure B.14-6.- Post test residue from aluminum - no ignition.

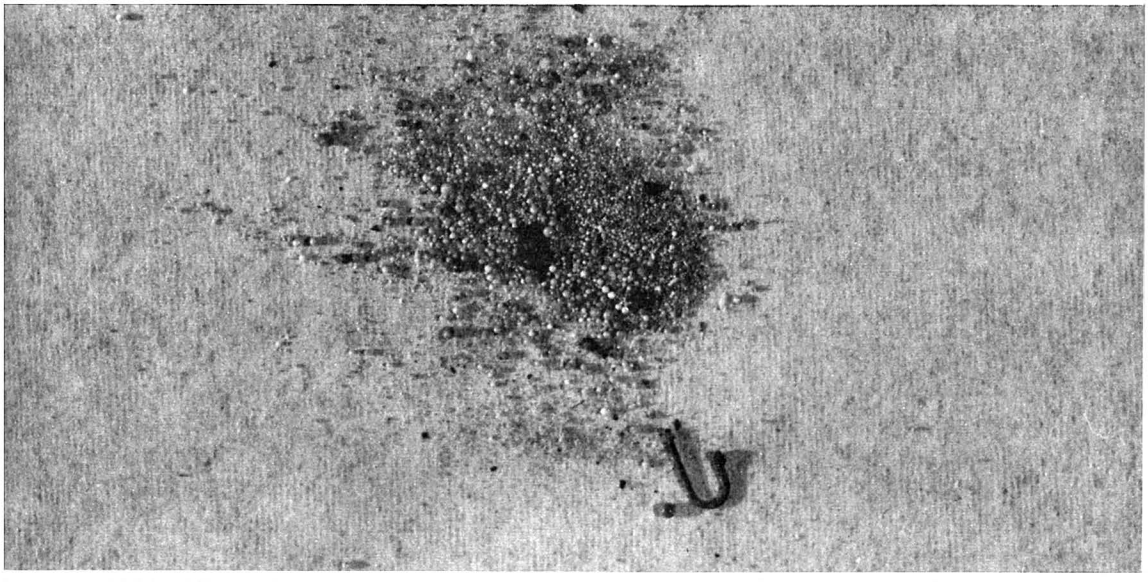

Figure B.14-7.- Post-test residue from aluminum ignition and complete combustion.

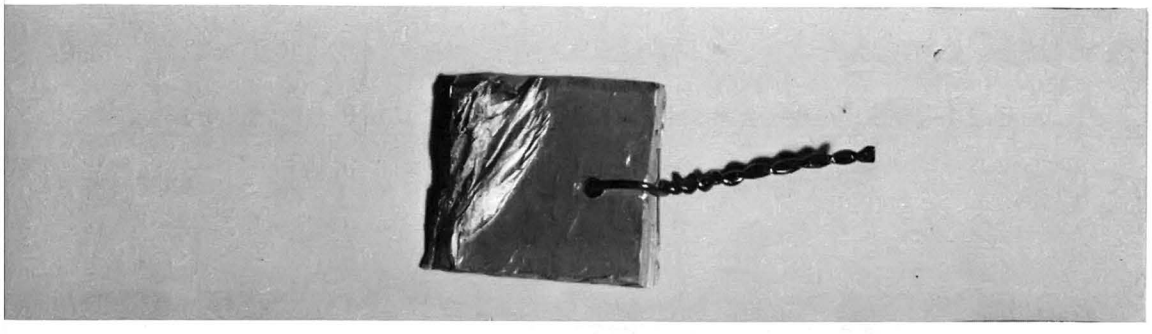

Figure B.14-8.- Post-test residue from knife edge aluminum specimen no ignition.

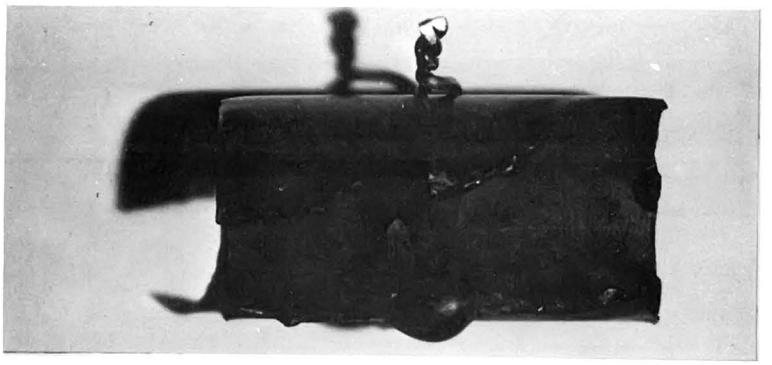

Figure B.14-9.- Post-test residue from Inconel X750 with wire bundle ignition.

Figure B.14-10.- Post-test residue from Inconel X750 with wire bundle ignition.

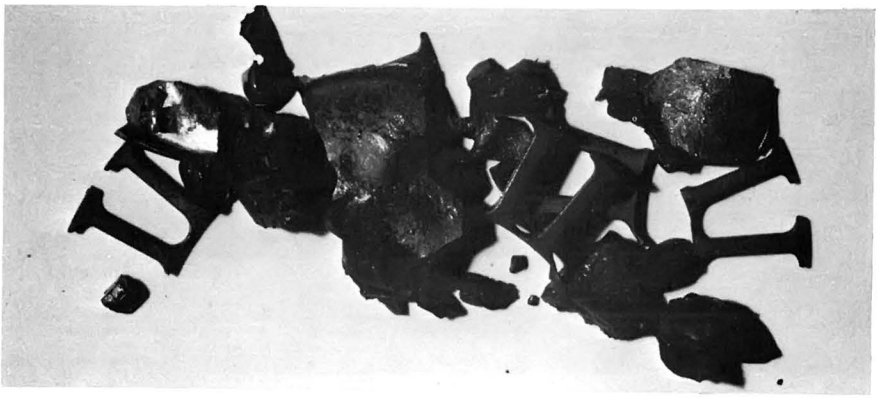

Figure B.14-11.- Post-test residue from motor stator core ignition.

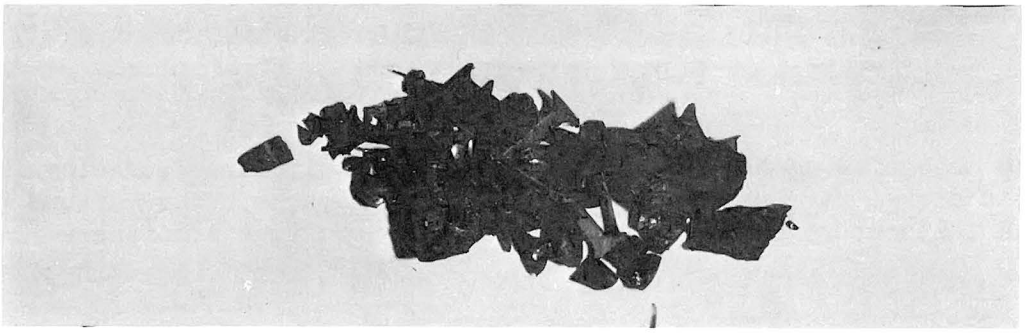

Figure B.14-12.- Post test residue from motor stator core ignition.

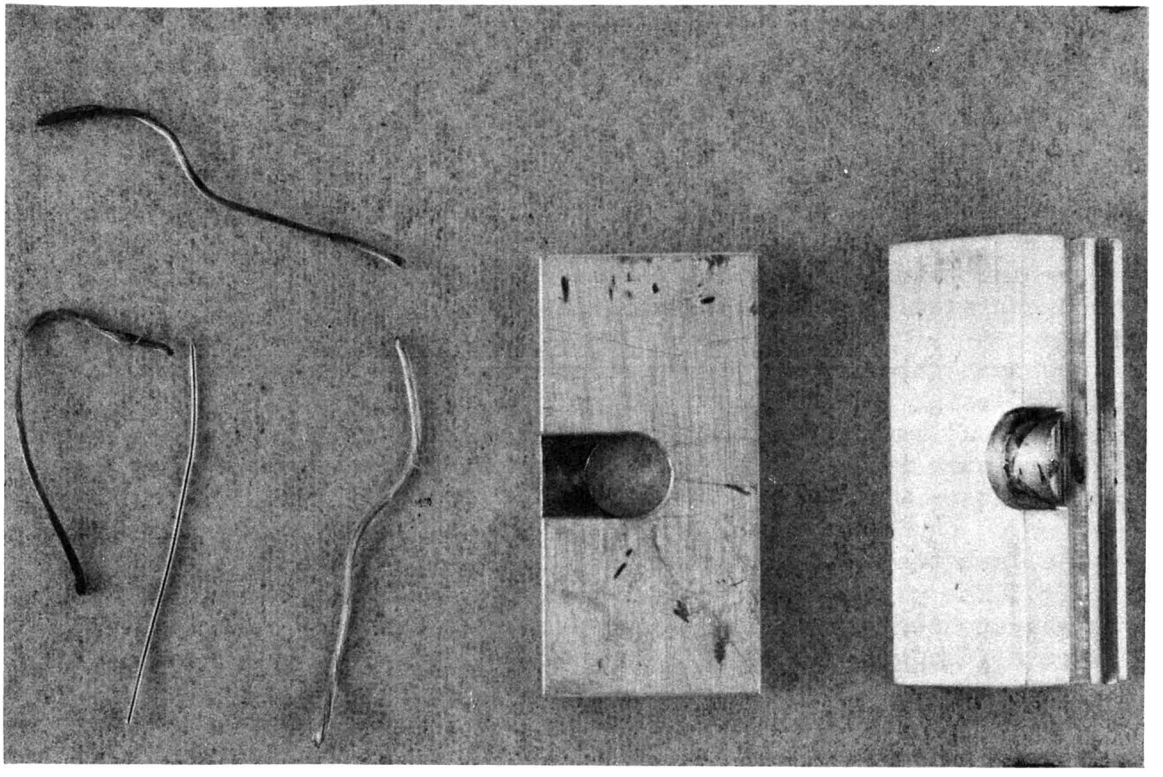

Figure B.14-13.- Post test residue from simulated motor housing ignition.

B.15 SPARK IGNITION TESTING OF POLYTETRAFLUOROETHYLENE-INSULATED NICKEL WIRE

B.15.1 OBJECTIVE

The objective of these tests was to ignite polytetrafluoroethylene-insulated nickel wire using 115-volt, 60-hertz, sparks under various pressure and temperature conditions in a 100-percent oxygen atmosphere.

B.15.2 TEST CONDITIONS

The test specimen consisted of a 1-inch length of polytetrafluoroethylene-insulated wire mounted vertically in a Pyrex holding fixture. A 2-1/2- to 3-inch length of contact wire, identical to the test specimen, was frayed at one end with a single strand in contact with the conductor through a nick in the test specimen insulation (fig. B.15-1).

B.15.3 RESULTS

The first tests were conducted under laboratory ambient pressure and temperature conditions with the test vessel purged with oxygen prior to spark initiation. Ignition of the polytetrafluoroethylene insulation was not achieved under these conditions.

The next three tests were conducted at pressures greater than atmospheric (50 psig, 500 psig, and 940 psig) and at laboratory ambient temperature. In all instances, the insulation was burned from both lengths of wire. Pressure rises and slight temperature increases were observed on all the tests.

The last test was conducted in 100-percent oxygen at minus 190° F and 940 psig. The circuit was protected with a 1.0-ampere slow blow fuse. Power was applied with no temperature or pressure rise indicated. The 1.0-ampere fuse was blown. The fuse was replaced and power reapplied. A pressure rise of approximately 138 psi was indicated with no noticable rise in temperature. A post-test inspection revealed essentially the same results as the ambient temperature tests, that is, the insulation was completely burned from both lengths of wire (fig. B.15-2).

B.15.4 CONCLUSIONS

These tests indicate that ignition of tank wiring insulation, with 1-ampere fuse protection, can occur at cryogenic conditions.

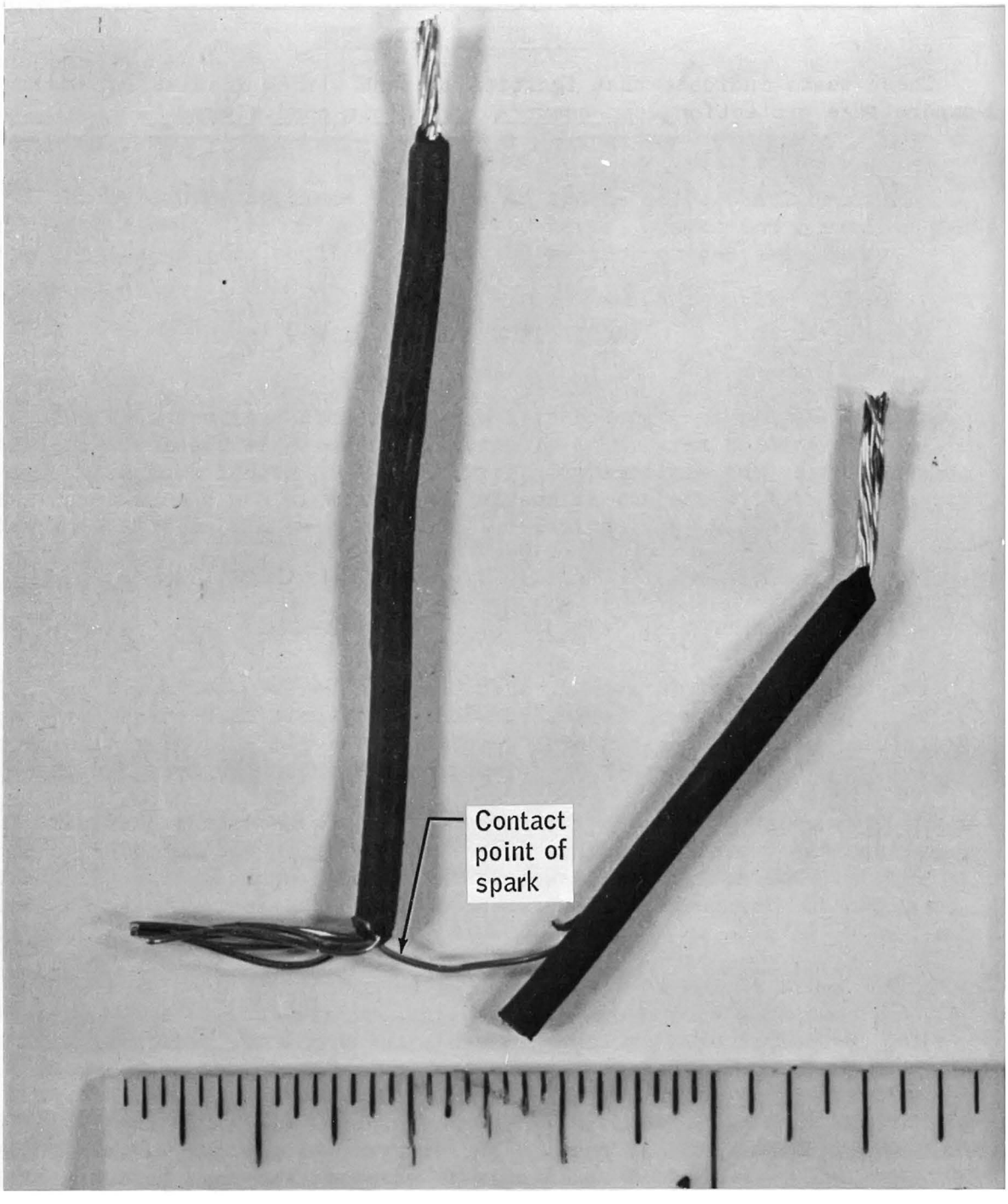

Figure B.15-1.- Typical pre-test configuration of wire sample.

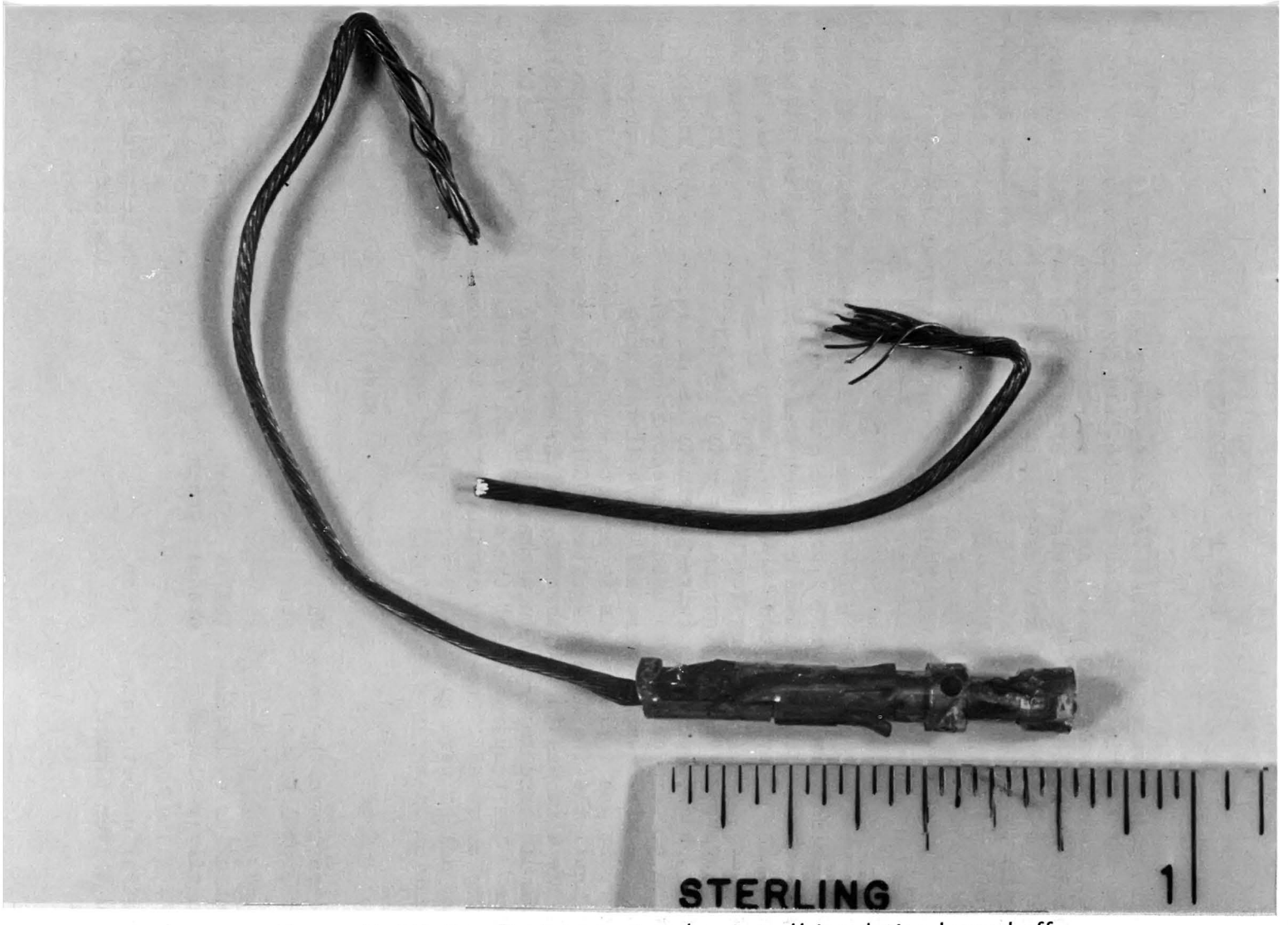

Figure B.15-2.- Post-test wire showing all insulation burned off.

B.16 LOW PRESSURE IGNITION AND COMBUSTION TESTS

B.16.1 OBJECTIVE

The objective of this test was to investigate the ignition and combustion characteristics of selected materials in a pure oxygen environment at low-pressure (20 psia) and ambient-temperature. The sample materials selected were representative of materials used in an Apollo cryogenic storage system, such as various sizes of wire, dry lubrication, and 60-40 lead-tin solder.

B.16.2 TEST EQUIPMENT AND CONDITIONS

The test set-up (fig. B.16-1) consisted of a small chamber fitted with a camera view port; an oxygen gas management system capable of charging the vessel with 20-psia oxygen and vacuum purging it; electrical feedthroughs to provide power to the wire samples and to the liquid sample heaters; and provisions for the measurement of current (through the wire or heater), voltage (across the wire or heater), pressure (in the chamber), and temperature (wire proximity or immersion in the liquid). A motion picture camera was used to record the events through the view port. The wire samples were all 2-1/4 inches long. For all samples, the current was increased in increments with a 30-second pause between steps until the insulation ignited. Current was sustained on the wire until the wire was burned through. Nichrome wire was substituted for wire samples and immersed in a small cup of solder or dry lubrication samples. The temperature of the sample was increased slowly until ignition was observed. One-gram samples of dry lubrication and 1/2-cc samples of solder were used. The wire types and sizes used and their application in the cryogenic supply system vessel are as follows:

Type	Colors	Size, AWG	Use
Polytetrafluoroethylene-coated nickel plated copper	White with brown stripe	20	Heater
Polytetrafluoroethylene-coated silver plated copper	Yellow, black orange, green	20	Temperature probe
Polytetrafluoroethylene-coated silver plated copper	Clear	18	Capacitance probe low side

Polytetrafluoroethylene-coated silver plated copper	Clear + shield + red polytetrafluoroethylene	Capacitance probe high side

B.16.3 RESULTS

Between 16.4 and 19.0 amperes were required to ignite the insulation on the temperature probe wires. The shielded capacitance probe wires ignited between 27 and 34 amperes and the unshielded capacitance probe wire between 21 and 25 amperes. The heater wire required the maximum current for ignition, from 62 to 68 amperes. An additional 15 to 50 percent increase in current was necessary to burn through the conductor portion of the wires. The brown stripe on the heater wire tended to ignite sooner than the white polytetrafluoroethylene and the flame propagated faster. The dry-lubrication samples ignited at temperatures between 300° and 400° F and continued to burn to completion after interruption of heater power. The one-gram samples required from 100 to 110 seconds to complete the combustion process. Temperatures as high as 800° F failed to ignite the solder.

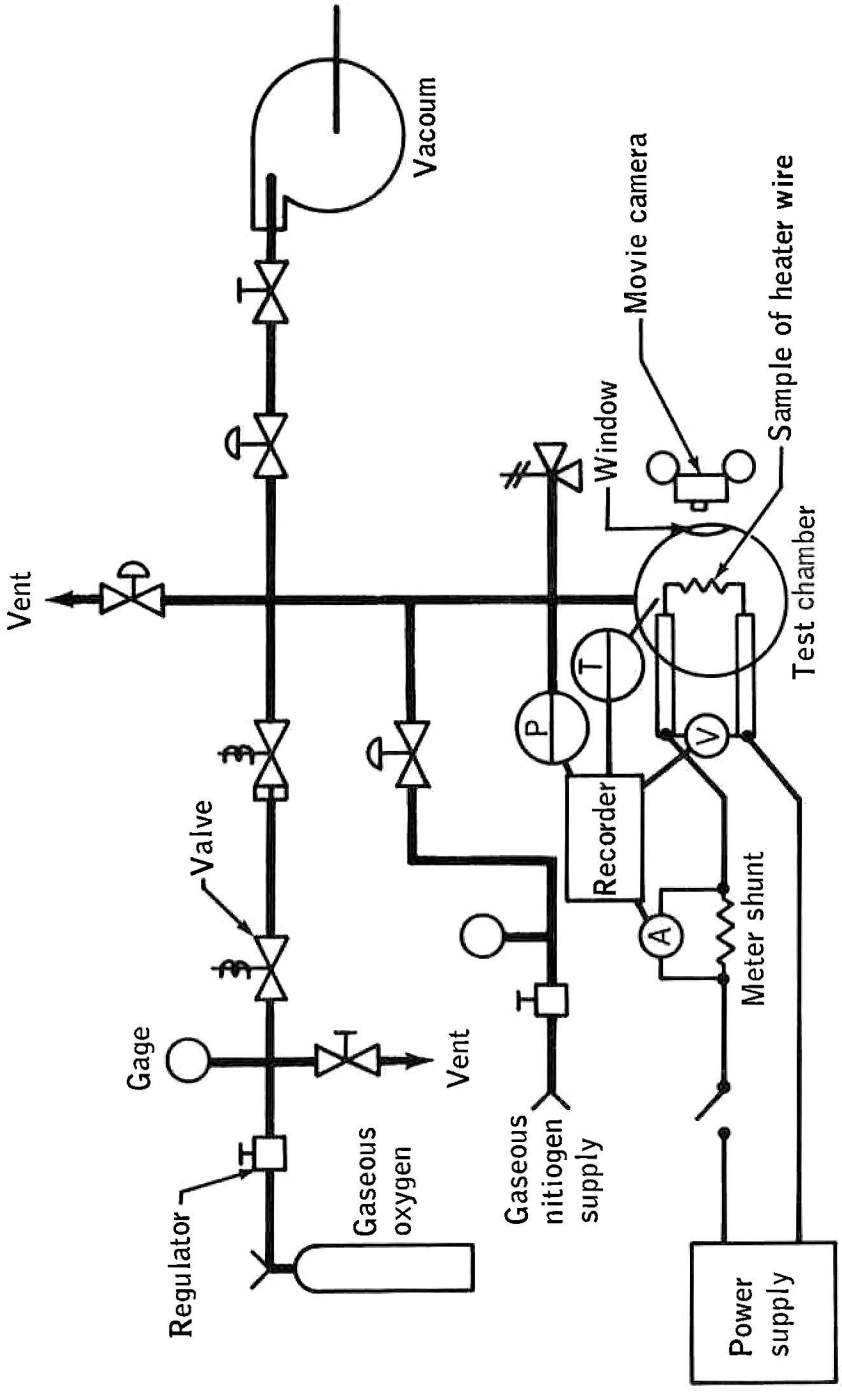

Figure B.16-1.- Low pressure gaseous oxygen ignition schematic.

B.17 HIGH PRESSURE IGNITION AND COMBUSTION TESTS

B.17.1 OBJECTIVE

The objective of this test was to determine the ignition and burning characteristics of dry lubrication, polytetrafluoroethylene-insulated wire, and 60-40 lead-tin solder in high pressure gaseous oxygen.

B.17.2 TEST EQUIPMENT AND CONDITIONS

A small chamber (Parr oxygen bomb) (fig. B.17-1) was modified to provide a means for supporting the non-metallic samples in contact with a length of Nichrome heater wire heated by a controlled electrical current. The tests were performed at pressures of 0, 500, 1000, 1500, and 2000 psi. The heater current was increased in 0.25-ampere steps with approximately 15 seconds duration each step. Ignition of the samples was detected by means of a thermocouple placed near the sample. The configuration for the tests were:

a. One-half gram samples of dry lubrication in ceramic crucibles

b. Polytetrafluoroethylene insulation removed from the conductors and threaded over the Nichrome heater wire

c. Individual strands of the copper wires and nickel wires were used in place of the Nichrome wire

d. Small amounts of the solder in ceramic crucibles in contact with the heater wire.

B.17.3 RESULTS

a. The samples of dry lubrication ignited at all pressures with power input levels to the heater wire from 4.15 to 8.25 watts.

b. The samples of polytetrafluoroethylene insulation ignited and burned at all test pressures with power input levels from 6.4 to 11.2 watts.

c. Six samples of copper wire (single strand, 31 gage) were tested, however, none of these samples ignited at a current level of 5 amperes through the wire. (Five amperes was the maximum current capability of the test fixture.) Three samples of 36-gage copper wire ignited at current levels from 2.6 amperes at atmospheric pressure to 3.95 amperes at

2000 psi. At atmospheric pressure the wire was approximately 60 percent consumed, and at 1000 and 2000 psi the wire was approximately 90 percent consumed. Three samples of nickel wire ignited at 4.4 to 4.8 amperes, all at atmospheric pressure, and were approximately 50 percent to 80 percent consumed. Two samples did not ignite with 5 amperes at 1000 and 2000 psi.

d. None of seven samples of solder ignited with input power levels up to 15 watts.

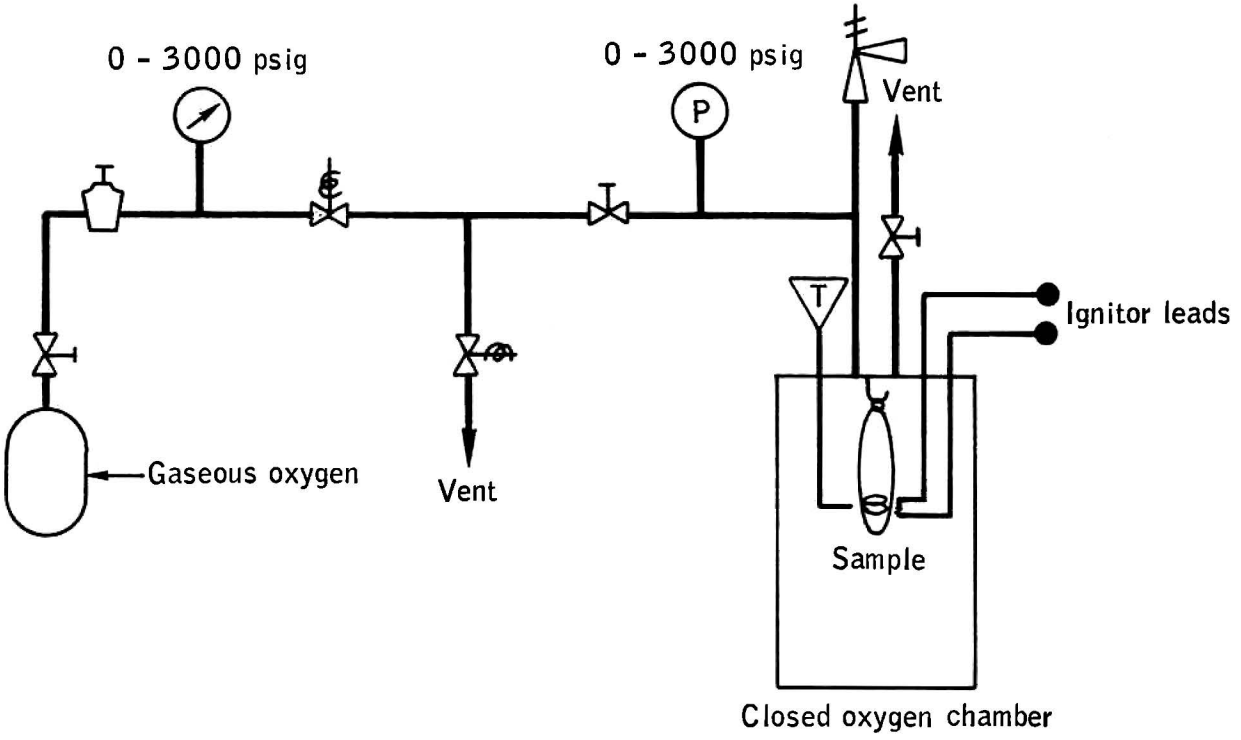

Figure B.17-1.- Closed chamber gaseous oxygen ingition investigation.

B.18 IGNITION AND COMBUSTION TESTS IN LIQUID OXYGEN

B.18.1 OBJECTIVE

The objective of this test was to investigate the ignition and combustion characteristics of materials immersed in liquid oxygen at atmospheric pressure. These materials were representative of those used in the Apollo cryogenic storage system, such as various sizes of wire, dry lubrication, and 60-40 lead-tin solder. The results of the liquid oxygen test were to provide a comparison with the gaseous oxygen test relative to ignition and flame propagation characteristics.

B.18.2 TEST EQUIPMENT AND CONDITIONS

The test setup (fig. B.18-1) consisted of a small vacuum-jacketed bottle for the liquid oxygen, a liquid oxygen management system, electrical feedthroughs for the current heaters on the liquid samples, and a temperature thermocouple. Motion pictures were used to record the events through the glass dewar. The current through the wire samples (all 2-1/4 inches long) was increased gradually until ignition occurred. In one portion of testing, a wire sample was subjected to a sustained 2-ampere load and then was shorted by cutting the insulation with a knife edge and allowing a 50-ampere surge to flow through 60 percent of the sample length. Nichrome wire was substituted for the wire samples and immersed in the dry lubrication samples for the ignition source. The current was increased until ignition was observed. One-gram samples of the dry lubrication were used. The wire sizes and types tested and their application in the cryogenic storage system vessel are shown in the table in section B.16.2.

B.18.3 RESULTS

The current required to ignite the insulation in liquid oxygen was significantly higher than for gaseous oxygen tests, apparently due to the high energy removal rate from the sample. The cryogenic storage system heater wire required 106 amperes, the cryogenic storage system temperature probe wire 38 to 44 amperes, the capacity probe low side 57 to 59 amperes, and the capacity probe high side 46 to 50 amperes. During the liquid oxygen tests, the insulation and the wire separated simultaneously, with virtually no burning of the insulation. The shorting tests with the knife blade only resulted in the wire rapidly burning in two at

the point of contact with the knife, and no burning of the insulation was apparent. A small notch was burnt in both the stainless steel and aluminum cutter at the point of contact. The dry lubrication samples burned to completion upon ignition, but the duration of combustion was only 13 to 14 seconds as compared to the 100 to 110 seconds in gaseous oxygen. There was no recorded increase in the bulk sample temperature, above liquid oxygen temperature, until ignition had occurred. The ignition area was apparently only at the heater wire sample interface.

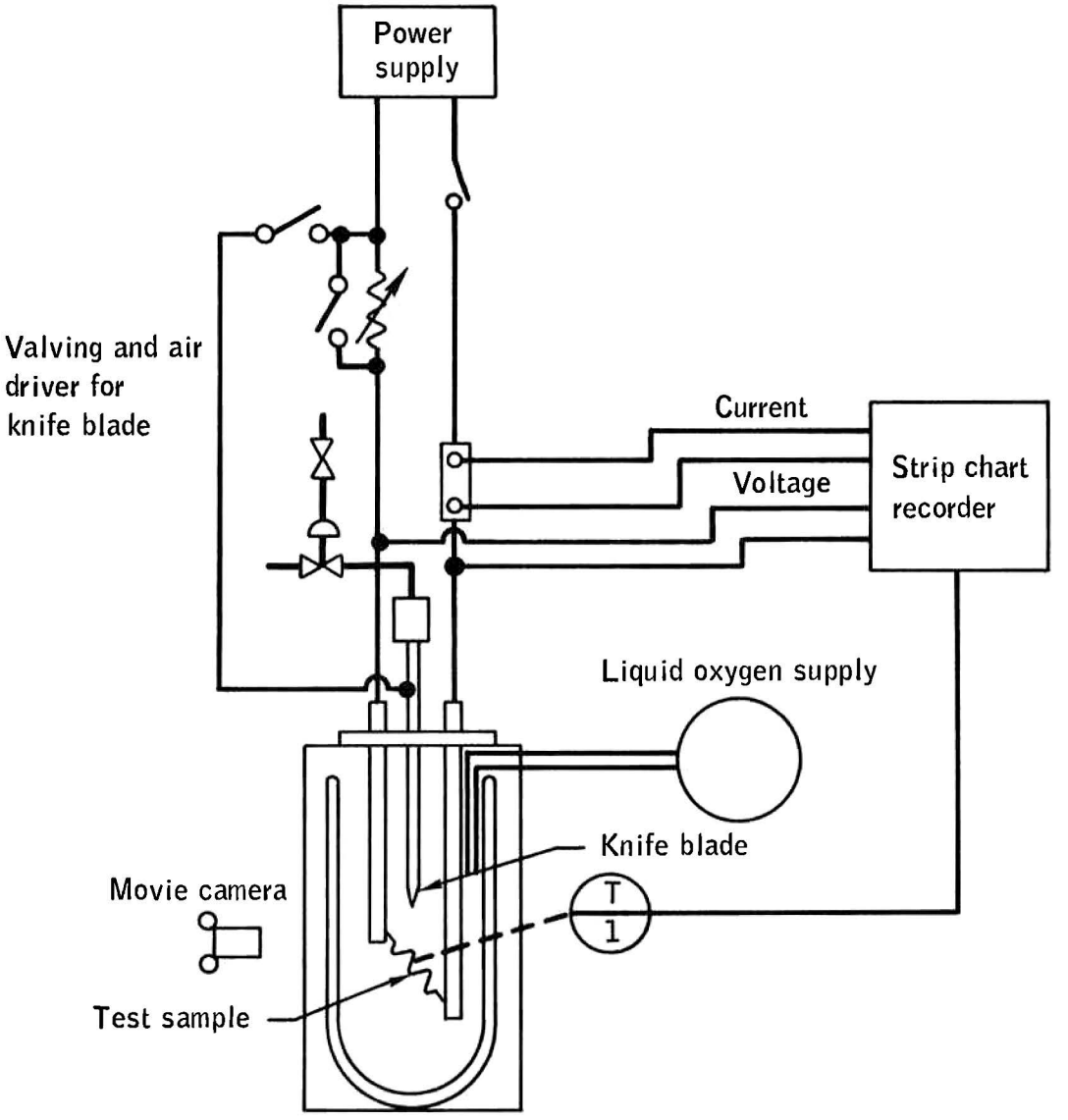

Figure B.18-1.- Liquid oxygen ignition test stand.

B.19 LOCKED ROTOR TESTS

B.19.1 OBJECTIVE

The objective of this test was to determine the effects of a locked rotor on an oxygen destratification fan motor while it is powered up and submerged in liquid oxygen.

B.19.2 TEST EQUIPMENT AND CONDITIONS

The test setup and motor configuration are shown in figures B.19-1 and B.19-2. One motor was subjected to 2.3 hours and the other motor to 1.0 hour of locked rotor operation in liquid oxygen.

B.19.3 RESULTS

The currents and voltages for each motor phase remained constant throughout the test. A comparison of pre-test and post-test phase resistances indicated no effect from the locked rotor operation. Following the test, the motor winding-to-case resistance was measured and no insulation degradation was indicated. A slight temperature increase of the motor was indicated by monitoring the phase resistance readings immediately after the motor was deenergized. A slight decrease in the phase resistance was indicated as the deenergized motor reached thermal equilibrium with the liquid oxygen. Rotation of the motor in air was verified following the locked rotor operation.

The following is a summary of the motor data.

	Motor 1			Motor 2		
Phase	A	B	C	A	B	C
Pre-test resistance (70° F), ohms	82	84	85	83	86	87
Pre-test resistance (-297° F), ohms	13.4	13.8	13.8	13.5	14.0	14.2
Phase current (-297° F), amps	0.353	0.361	0.335	0.307	0.306	0.291
Phase neutral voltage, volts	121.1	121.0	121.0	121.4	121.4	121.4
Post-test resistance (-297° F), ohms	13.3	13.6	13.7	13.6	14.0	14.2
Post-test resistance (70° F), ohms	81	84	84	85	88	90

B.19.4 CONCLUSIONS

The two motors tested indicated no problems as a result of locked rotor operation. No indication of high current or overheating was experienced.

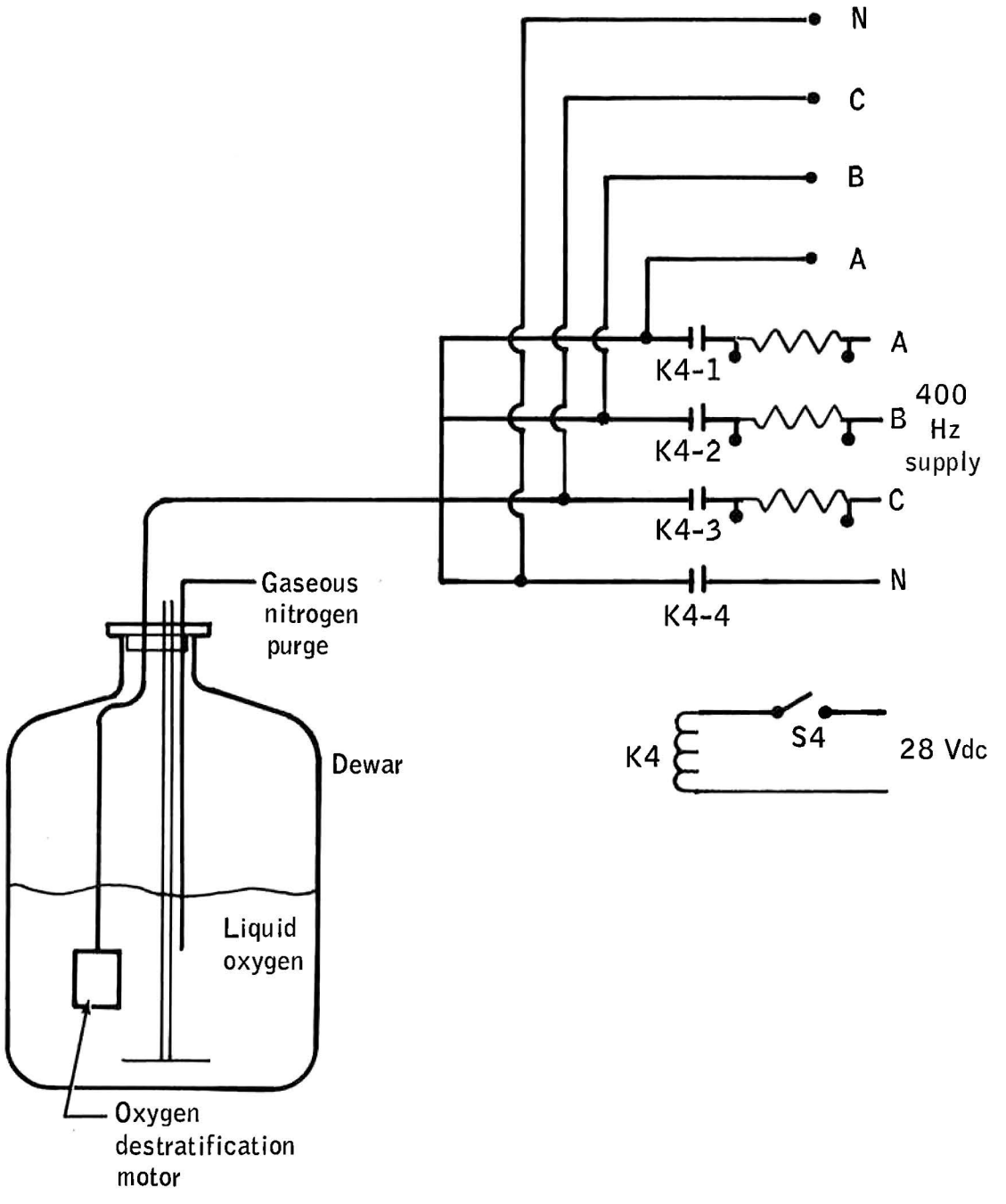

Figure B.19-1.- Schematic of destratification motor stall test in liquid oxygen.

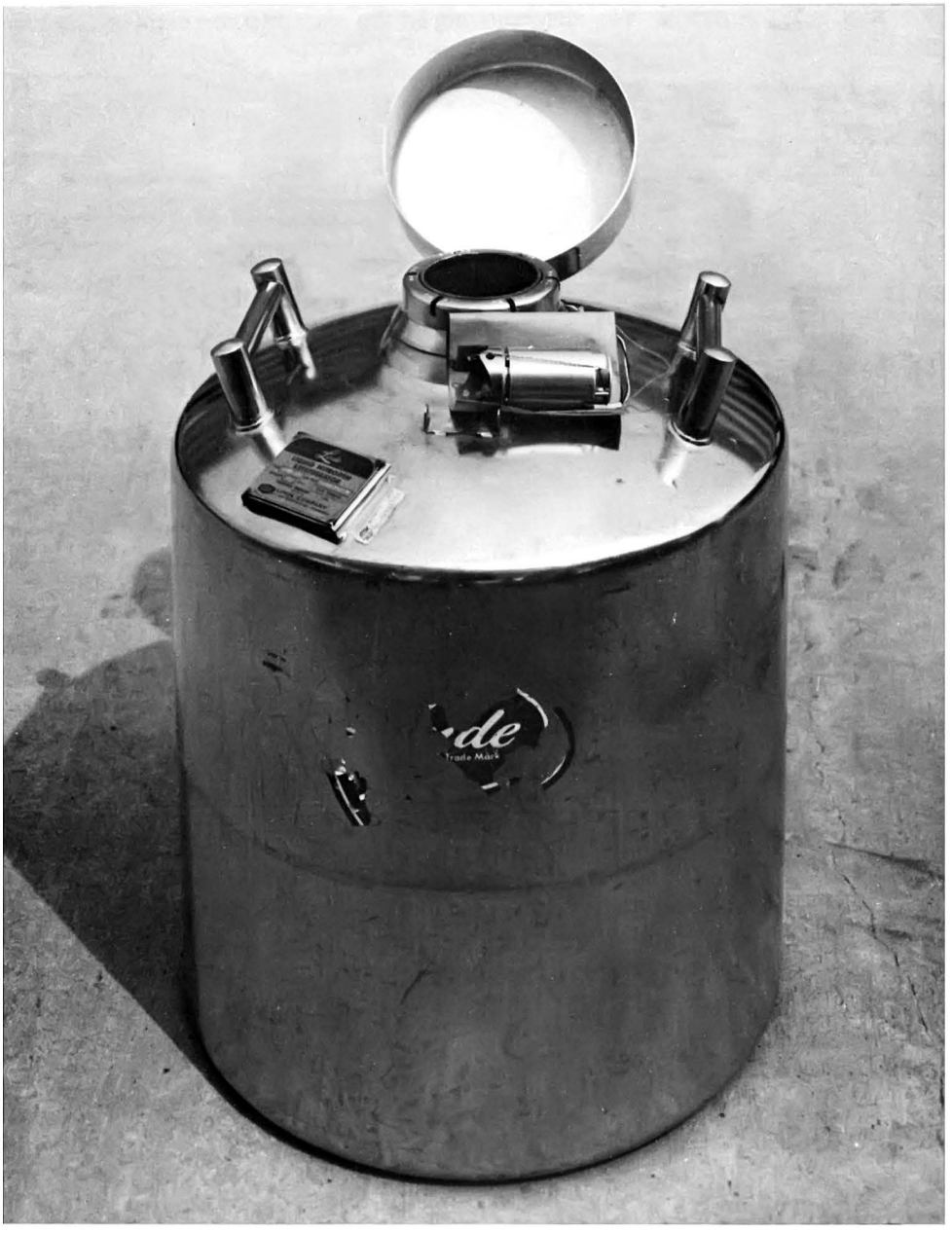

Figure B.19-2.- Destratification locked rotor investigation (motor shown with safety wire lock).

B.20 SPARK IGNITION TEST (COMPONENT IGNITION SOURCES)

B.20.1 OBJECTIVES

The objective of this test was to determine the spark (electric arc) ignition characteristics of polytetrafluoroethylene and other non-metallic materials in a liquid oxygen/gaseous oxygen environment by simulating specific component failures which could serve as possible ignition sources.

B.20.2 TEST EQUIPMENT AND CONDITIONS

The test fixtures and equipment used are shown in figures B.20-1 through B.20-4. Each fixture was essentially a prototype that had been fabricated from available components with very little design analysis. Wall effects, thermocouple placement, resistance of feed-throughs, and other factors contributed to data distortions.

Since each test was exploratory, the sensor components and calibrations were selected for very wide ranges. Additionally, no concerted effort was made to optimize interfaces between the data acquisition system and the test fixtures.

Values presented for electric power and time duration are reasonably accurate (10 percent range), but flux ranges are largely unknown, particularly at the instant of wire burn-through when arcing and the associated ionization effects would be pronounced. The contribution of wire combustion towards ignition appears low compared with ohmic heating values; however, it should be noted that the heat-of-combustion values for the wire used represent net rather than gross heat, which would be much higher if high-temperature combustion had been achieved.

B.20.3 RESULTS

Open-Bath Spark Series

Thin (1/8-mil) polytetrafluoroethylene films lying on a plate electrode subjected to a spark or arc from a needle electrode moved to penetrate the specimen while immersed in liquid oxygen at minus 297° F and 1 atmosphere. Electrical energy was supplied by circuits that duplicated or simulated spacecraft sources for the capacitance probe, the motors, and the heaters. The purpose of the open-bath series was to provide immediate

information on ignition and flame behavior to guide design of experiments for the more difficult case of subcritical compressed liquid oxygen at minus 190° F and 900 psig. It was postulated that the higher density at minus 297° F would compensate for latent heat effects and that the ignition requirements would approximate the requirements at minus 190° F and 900 psig. Initial testing quickly proved the postulated similarity was unlikely and that the open-bath series could not fulfill their purpose. Severe sparking and arcing produced no ignition. Table B.20-I contains the results of this test.

B.20.4 CONCLUSIONS

In compressed liquid oxygen, polytetrafluoroethylene will ignite at wire burn-through with moderate ignition energy pulses and will burn rapidly.

TABLE B.20-I.- OPEN BATH SERIES TESTS

Test No.	Energy source	Results and comments
OBCP-1	Actual capacitance probe circuitry (signal conditioner)	No apparent effect
OBCP-2	Actual capacitance probe circuitry (signal conditioner)	No apparent effect Run without specimen in attempt to produce visible discharge
OBM-1	Simulated motor supply (115 V ac, 400 Hz with limiting resistor for 0.75 ampere maximum)	Consistent visible sparks. No ignition.
OBM-2	Same as OBM-1 except no limiting resistor. Fused for 1 ampere.	Blown fuse. Needle welded to plate. No ignition.
OBM-3	Same as OBM-2 except fused for 2 amperes.	Power supply breaker tripped. Needle welded to plate. No ignition
OBM-4	Same as OBM-1 except one leg of a fan motor connected in parallel with spark electrodes.	Consistent visible sparks. No ignition.
OBM-1	Simulated heater supply (28 V dc power supply with limiting resistor for 10 amperes maximum)	Violent sparks. Sustained power arcs prolonged for 5 to 10 seconds. No ignition.

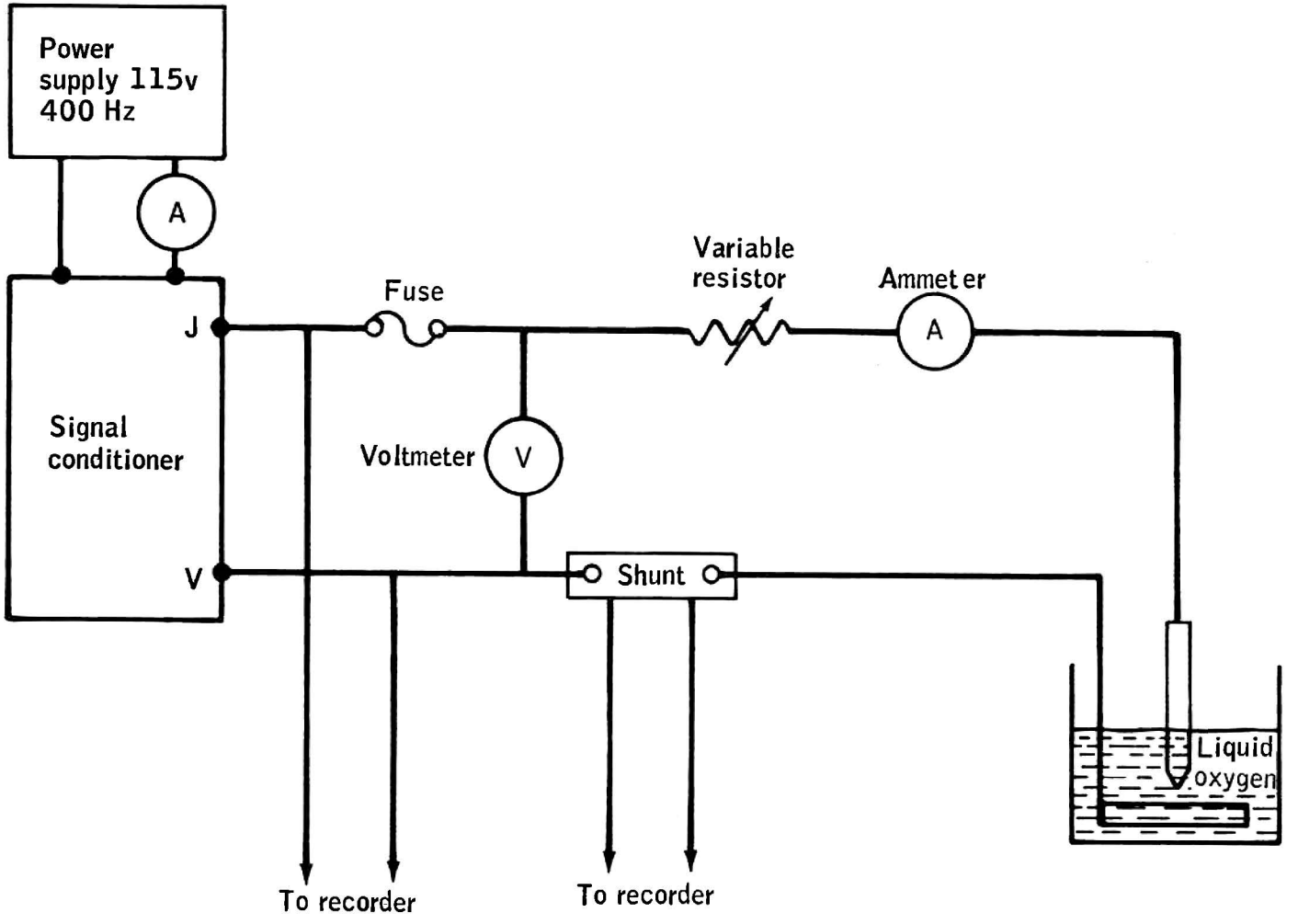

Figure B.20-1.- Simulation of electrical source associated with capacitance probe.

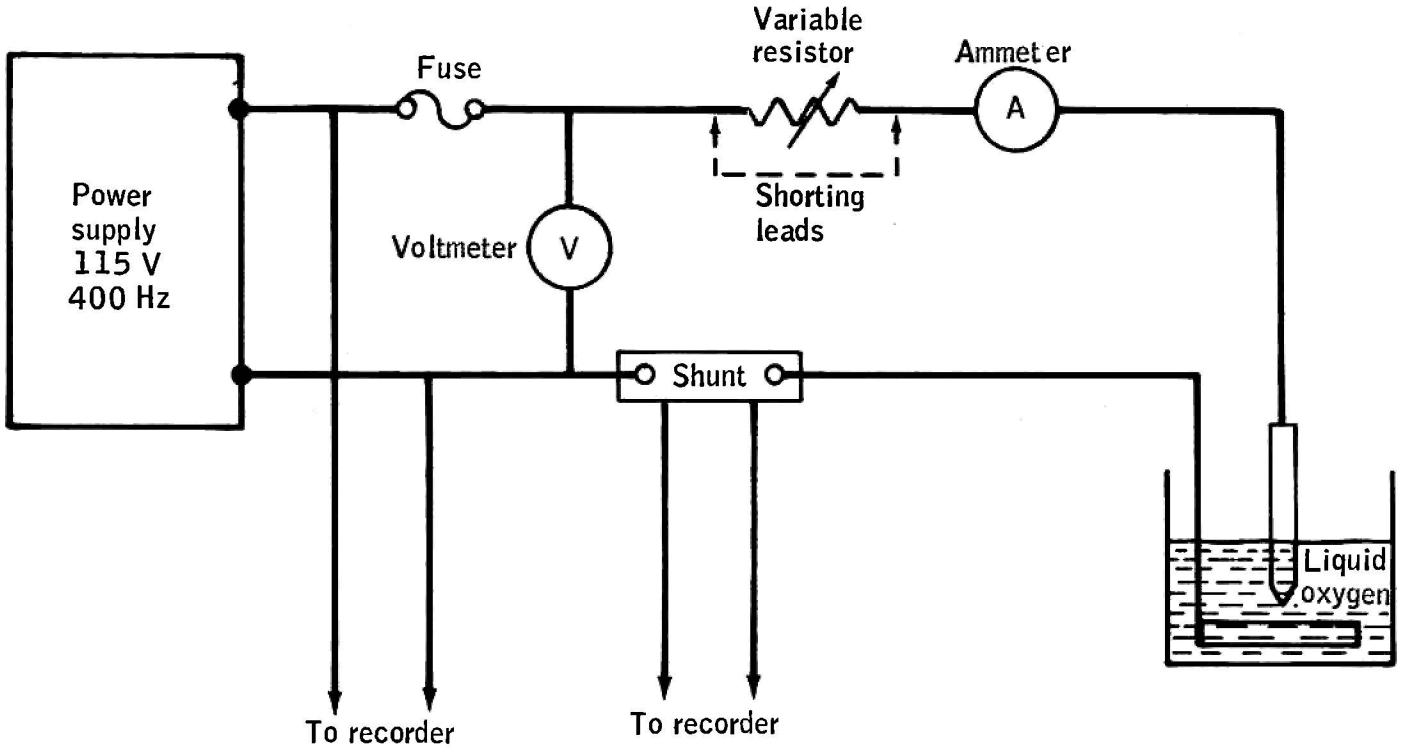

Figure B.20-2.- Power to simulate fan motor circuit ignition sources without motor.

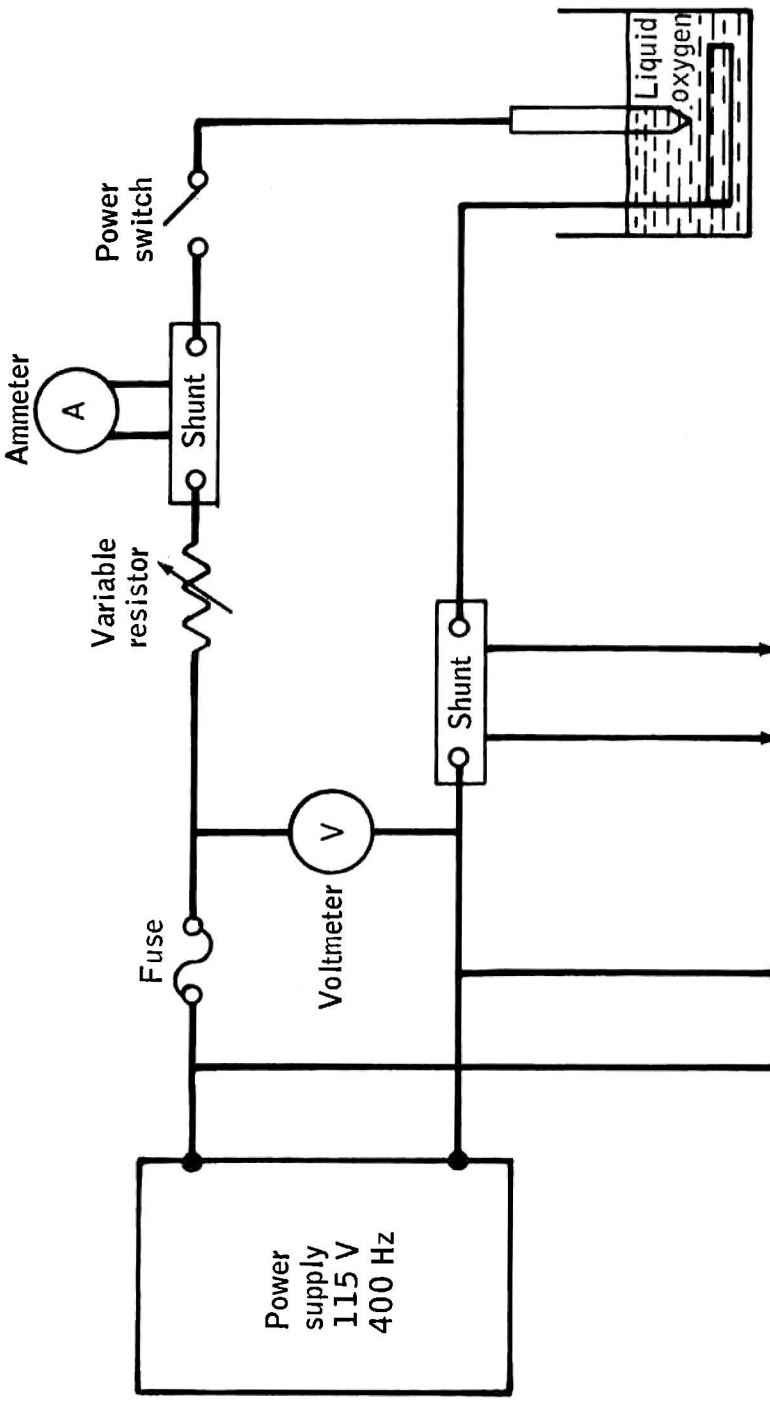

Figure B.20-3.- Simulation of heater circuit ignition sources.

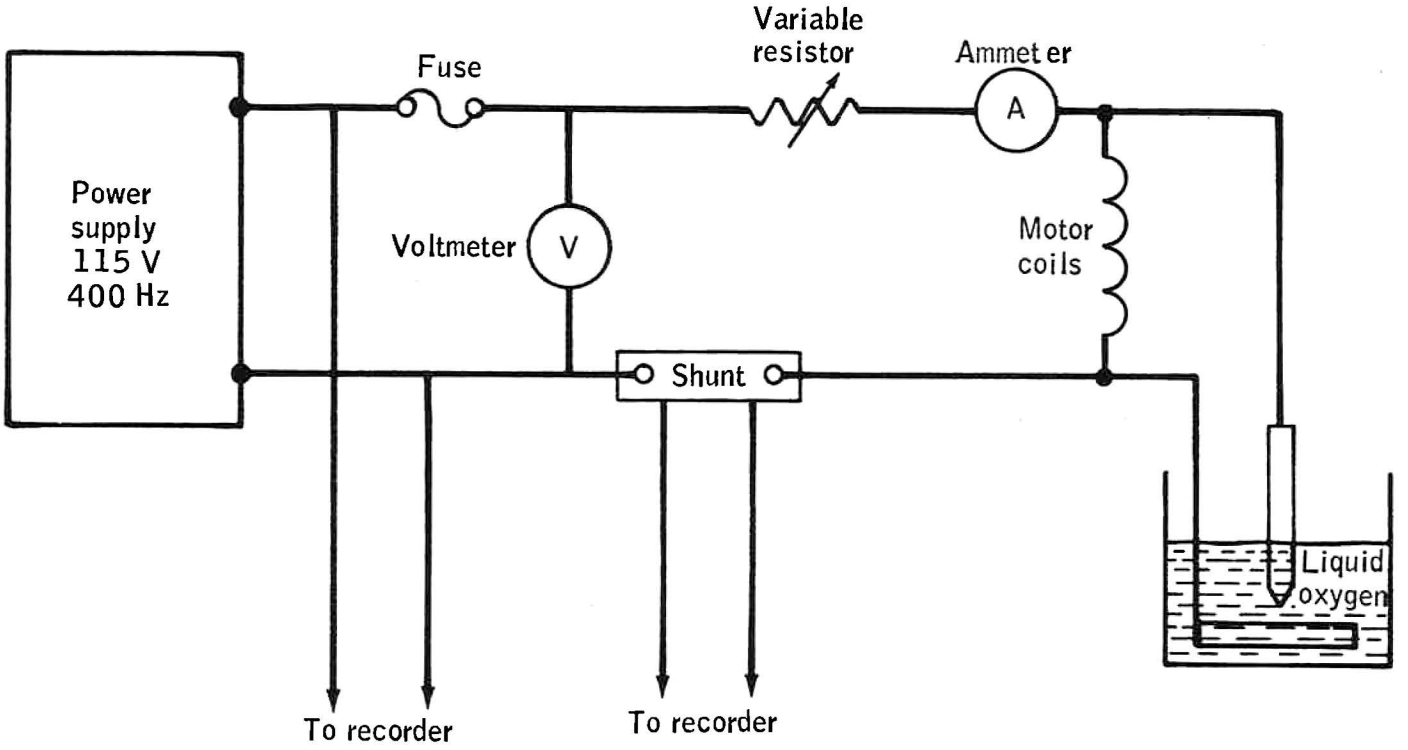

Figure B.20-4.- Simulation of fan motor circuit ignition sources with motor operating.

B.21 CLOSED CHAMBER SPARK IGNITION TEST

B.21.1 OBJECTIVES

The objective of this test was to determine the threshold spark energy for ignition of polytetrafluoroethylene.

B.21.2 TEST EQUIPMENT AND CONDITIONS

A motor lead shorting test was conducted and was intended to demonstrate ignition with a fairly close simulation of postulated inflight conditions. Prior circuit analysis information indicated that the most likely concentrated energy release and highest probability for a fire would be associated with a short of one motor lead to ground such as might occur if the lead insulation was penetrated by a grounded sharp edge or point.

The test setup is shown in figure B.21-1. The flat electrode was used to support a short section of wire and also acted as an anvil. Electrical feed-throughs were brought in on each side of the anvil support post. The actuator was made from a pneumatically operated valve by removing the seat assembly, tapping the ram to accept chisel or knife edge rods, and machining a special fitting to mate with the chamber body. The electrical schematic is shown in figure B.21-2. The chamber body (and thus the chisel) was connected to both earth ground and inverter neutral. The fixture was equilibrated with minus 190 F, 600 psig liquid oxygen. The actuator was then pressurized with helium to actuate the chisel.

B.21.3 RESULTS

Two tests were aborted because of problems in achieving electrical continuity and proper stroke length. In the third test the apparatus functioned properly, but no ignition occurred. The wire and sleeving were severed completely and cleanly with no evidence of fused metal. The fuse for the affected leg of the motor circuit was blown.

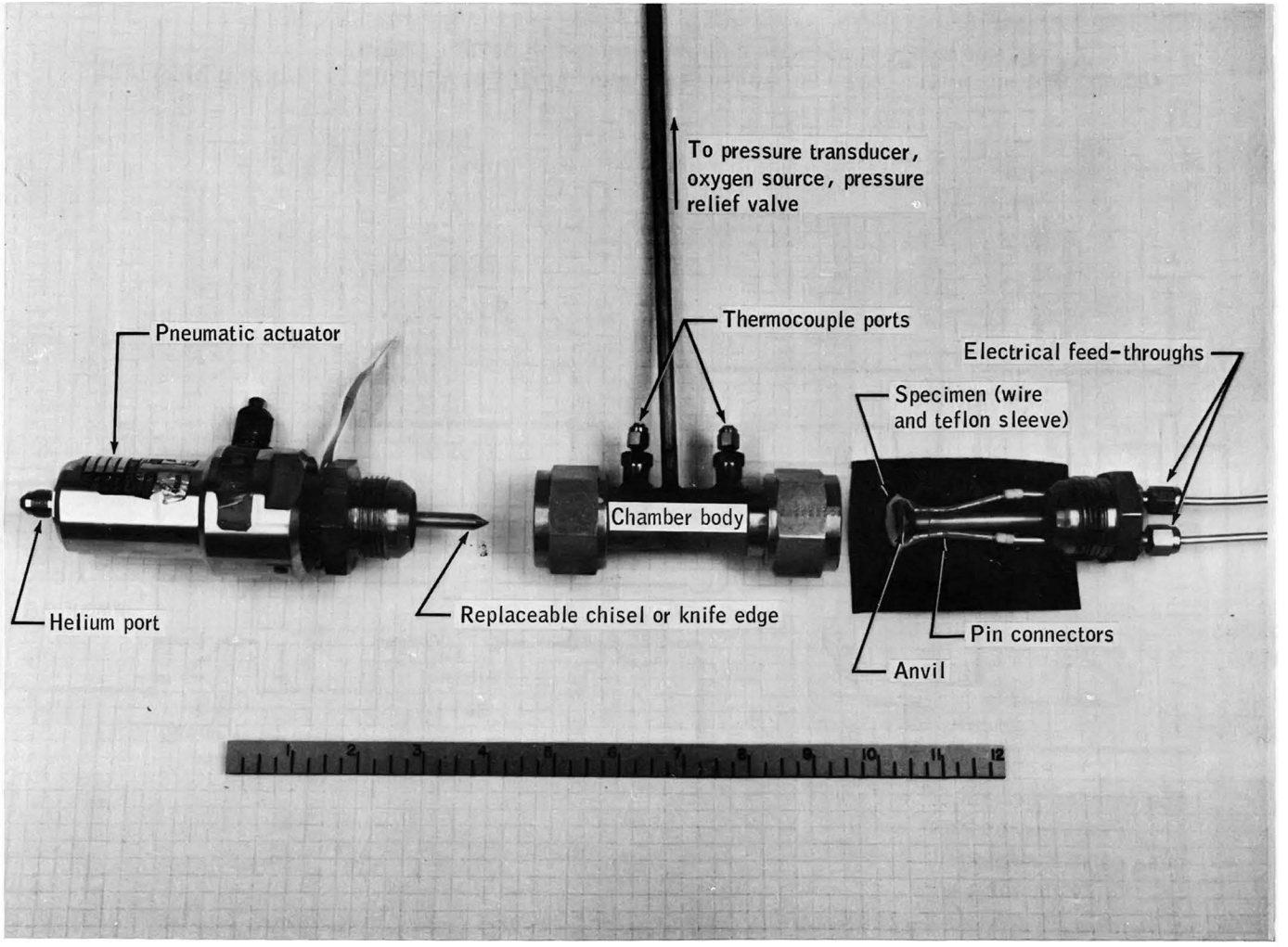

Figure B.21-1.- Pneumatic ram spark ignition test fixture for minus 190° F, 600 psig liquid oxygen.

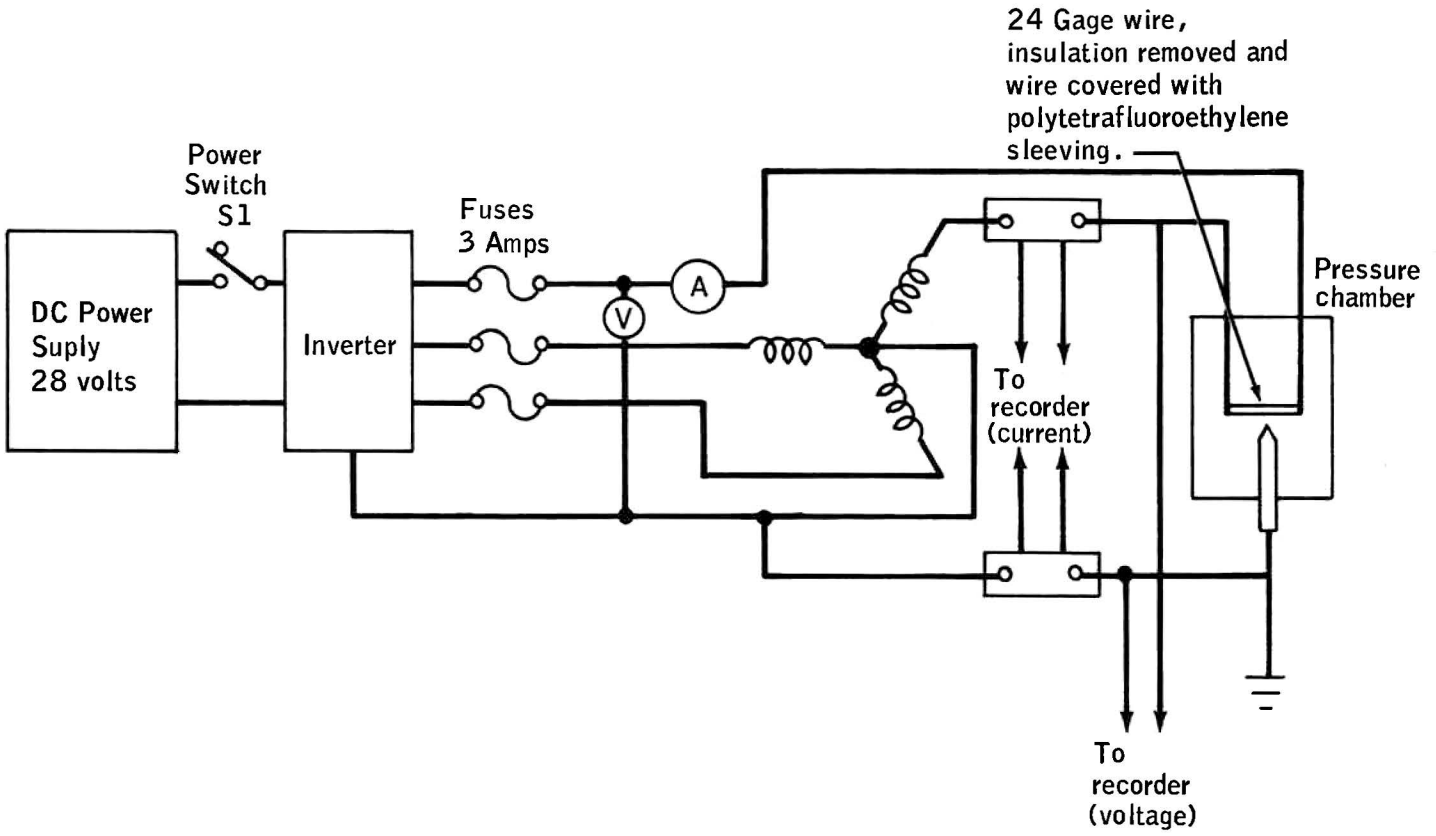

Figure B.21-2.- Circuitry to supply power to simulate fan motor circuit ignition sources with 3 motors in operation using a spacecraft static inventer.

B.22 HOT WIRE IGNITION TESTS

B.22.1 OBJECTIVE

The objectives of this test series were to demonstrate that ignition of polytetrafluoroethylene could be achieved at ignition energy levels within the range of tank electrical circuitry and to observe the physical effects of the fire in a closed chamber environment (minus 190° F, 900 psig).

B.22.2 TEST EQUIPMENT AND CONDITIONS

The test apparatus consisted of a pressure vessel fabricated from 1-inch corrosion resistant steel tubing with both welded joints and modified fittings to incorporate electrical feed-throughs, thermocouple probes, and a standpipe for oxygen fill, vent, and pressure sensing. The plumbing schematic is shown in figure B.22-1. For the test, a convenient length of fuse wire was used to bridge between the internal electrodes and to support the test specimen (polytetrafluoroethylene sleeve). A typical arrangement is shown in figure B.22-2. The vessel was then closed, mounted in the minus 190° F chamber, flushed with oxygen, filled with oxygen, and equilibrated at 900 psig. The power supply was then energized until burn-through and ignition occurred.

The experiments were essentially non-simulative in that the wire used for a fuse was a nickel-chromium alloy that probably has a different melting point, heat-dissipation capability, and combustion temperature than the exposed current carriers in the oxygen tank. The specific fuse wire had been previously used for reliable ignition of polytetrafluoroethylene at room temperature and 700 psi (to study combustion products) and seemed well suited for the present purpose. Cursory circuit analysis did indicate that electrical energy inputs were not drastically different from those postulated for the Apollo tank.

Since each test was exploratory, the sensor components and calibrations were selected for very wide ranges. Additionally, no concerted effort was made to optimize the interfaces between the data acquisition system and the test fixtures.

Values presented for electric power and time duration are reasonably accurate (10-percent range), but flux ranges are largely unknown, particularly at the instant of wire burn-through when arcing and the associated ionization effects would be pronounced. The contribution of wire combustion towards ignition appears low compared with ohmic heating values;

however, it should be noted that heat of combustion values for the wire used represent the net rather than the gross heat values, which would be much higher if high temperature combustion was achieved.

B.22.3 RESULTS

Ignition of polytetrafluoroethylene sleeving specimens was reliably achieved and combustion was essentially complete. Burn time and pressure excursions were affected by direction of propagation. High local temperatures were observed, but excursions of bulk temperature appeared to be moderately low. The results are summarized in figures B.22-3 through B.22-6.

Ceroc T hot-wire ignition tests.- Two hot-wire tests in minus 190° F. 900 psig liquid oxygen were made with a section of Ceroc T polytetrafluoroethylene/ceramic-insulated magnet wire removed from a fan motor. For the first test a single 3-inch length of Ceroc T wire was wrapped for a portion of its length around a fuse wire loop in the chamber as shown in figure B.22-2. The free end of the sample wire was allowed to stand upward from the ignition wire. The electrical power supplied was 12 V dc, 6.3 amperes, 0.11 second to burn-out. No ignition occurred. Post-test examination of the specimen indicated that the only effect was a darkening of the insulation surface and formation of a molten metal ball at the point where heating was highest.

For the second test, 10 strands, 3.2 inches long, of magnet wire were bundled together. Fuse wire was wrapped around the bottom 1/4-inch of the bundle. Electrical power supplied was 18 V dc, 4.2 amperes for 1.05 seconds. No ignition occurred. Post-test examination again showed darkening of insulation and formation of a fused metal ball.

A supplementary study indicated that the magnet wire is a single-strand copper wire with an extruded, filled polytetrafluoroethylene insulation. The filler is principally zinc oxide. The total insulation weight if 117 microgram per centimeter with 65.4 percent being polytetrafluoroethylene and the remainder a filler composed of a mixture of zinc oxide and silica.

Glass-filled polytetrafluoroethylene grommet hot-wire ignition test.- A single glass-filled polytetrafluoroethylene grommet was burned in a hot-wire ignition test in minus 190° F, 900 psig liquid oxygen. The specimen, weighing 483 milligrams, was held by two turns of fuse wire between the terminals of the hot-wire test chambers shown in figure B.22-2. Electrical power was 19 V dc, 3.8 amperes for 0.27 second. Ignition and nearly complete burning resulted. Chamber pressure peaked at 1518 psi in 9 seconds. The chamber temperature, as measured approximately 1 inch

from specimen, peaked at minus 145° F in 9 seconds. A post-test examination of the thermocouple yielded approximately 35 milligrams of white powdery residue. Spectrographic analysis of the residue revealed heavy major calcium,; major iron, chromium, and aluminum; and light major silicon, magnesium, and titanium. X-ray diffraction analysis revealed substantial amounts of calcium and aluminum fluorides.

Analysis of glass-filled polytetrafluoroethylene.- A rod sample of glass-filled polytetrafluoroethylene was analyzed to verify nominal composition and to provide base data for interpretation of combustion residue. Determination of polytetrafluoroethylene content yielded an average percent by weight value of 75.4 percent. Density measurement results were 2.253 gm/cm^3 (0.0814 lb/in^3).

B.22.4 CONCLUSION

Polytetrafluoroethylene in compressed liquid oxygen will ignite at wire burn-through with moderate ignition energy pulses and will burn rapidly.

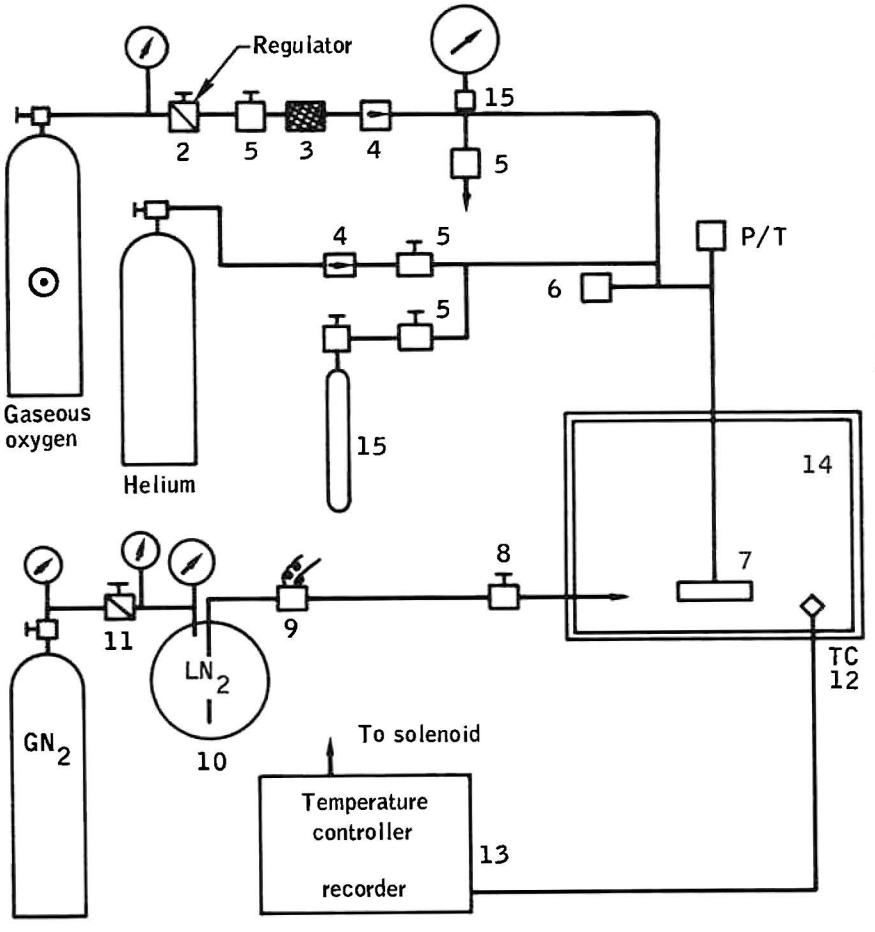

Item	Description
1	Gaseous oxygen
2	Regulator, 3000 psig in and 2000 psig out
3	5 micron filter - 3000 psig
4	Check valve - 6000 psig
5	1/4-inch valve - 10 000 psig
6	Pneumatic relief valve - 3000 psig
7	Test fixture - proof pressure (4500 psig)
8	3/8-inch ball valve
9	3/8-inch liquid nirtogen solenoid valve
10	100-liter liquid nitrogen dewar
11	Regulator - 3000 psig in and 100 psig out
12	Copper constantan thermocouple
13	Temperature recorder/controller
14	Insulated environmental chamber
15	500-cc bottle

Figure B.22-1.- Test fixture for hot-wire ignition.

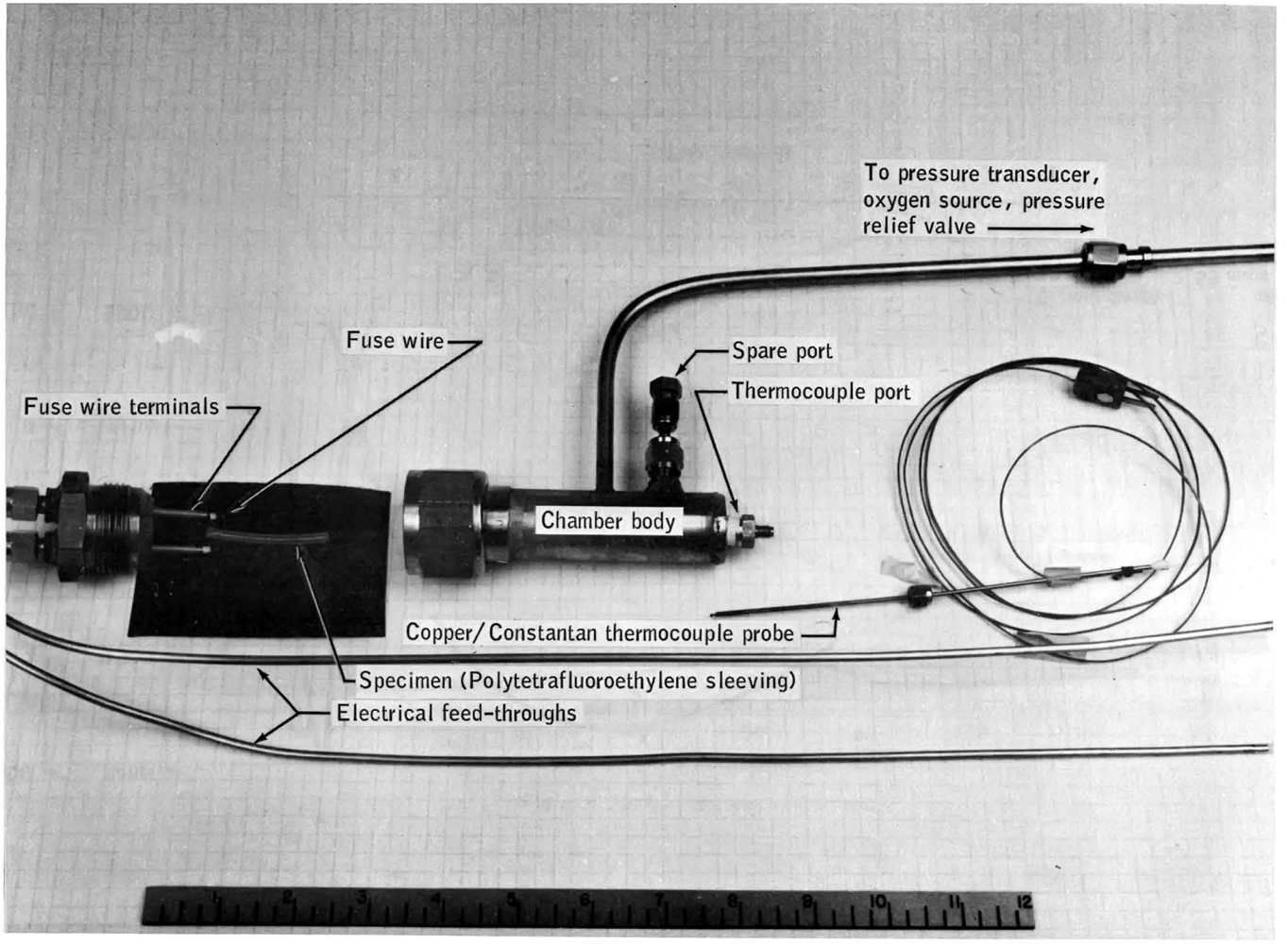

Figure B.22-2.- Hot-wire ignition test fixture for minus 190° F, 600 psig liquid oxygen.

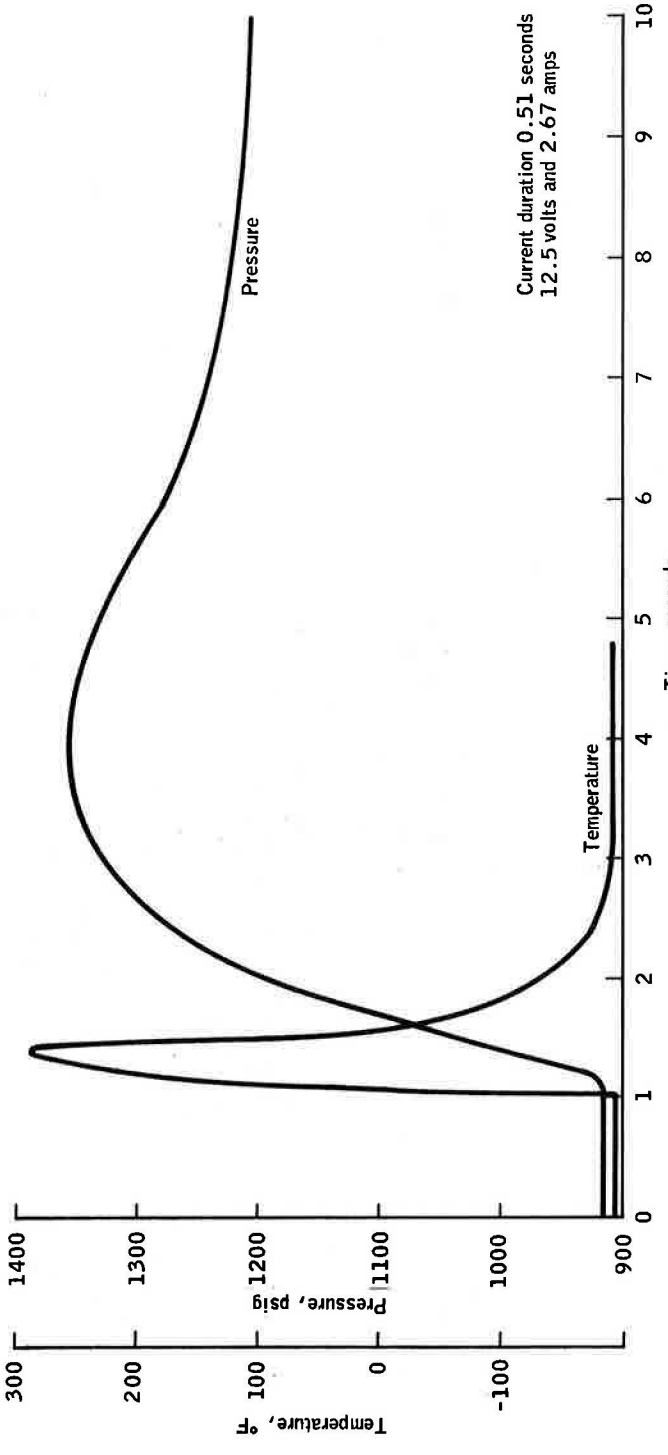

Figure B.22-3.- Hot wire ignition test.

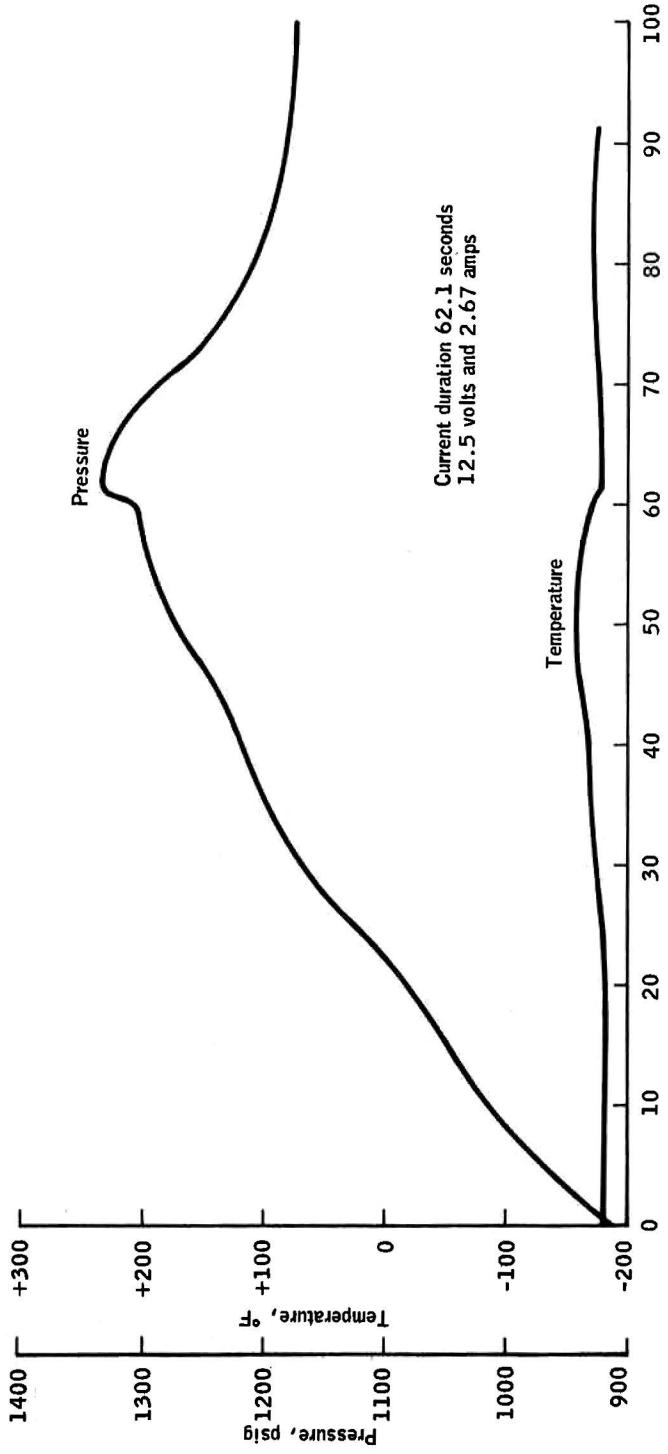

Figure B.22-4.- Hot wire ignition test.

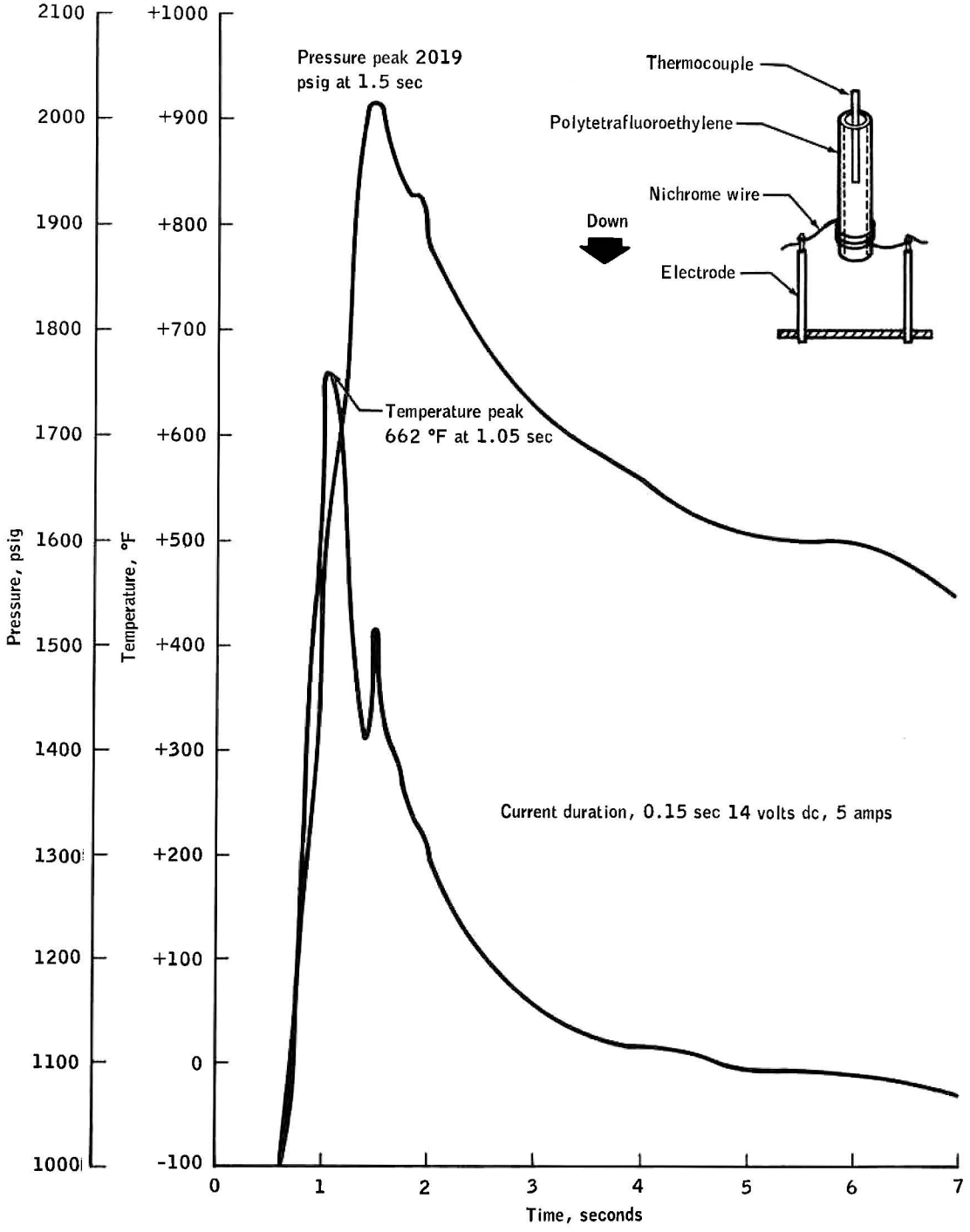

Figure B.22-5.- Hot wire ignition test.

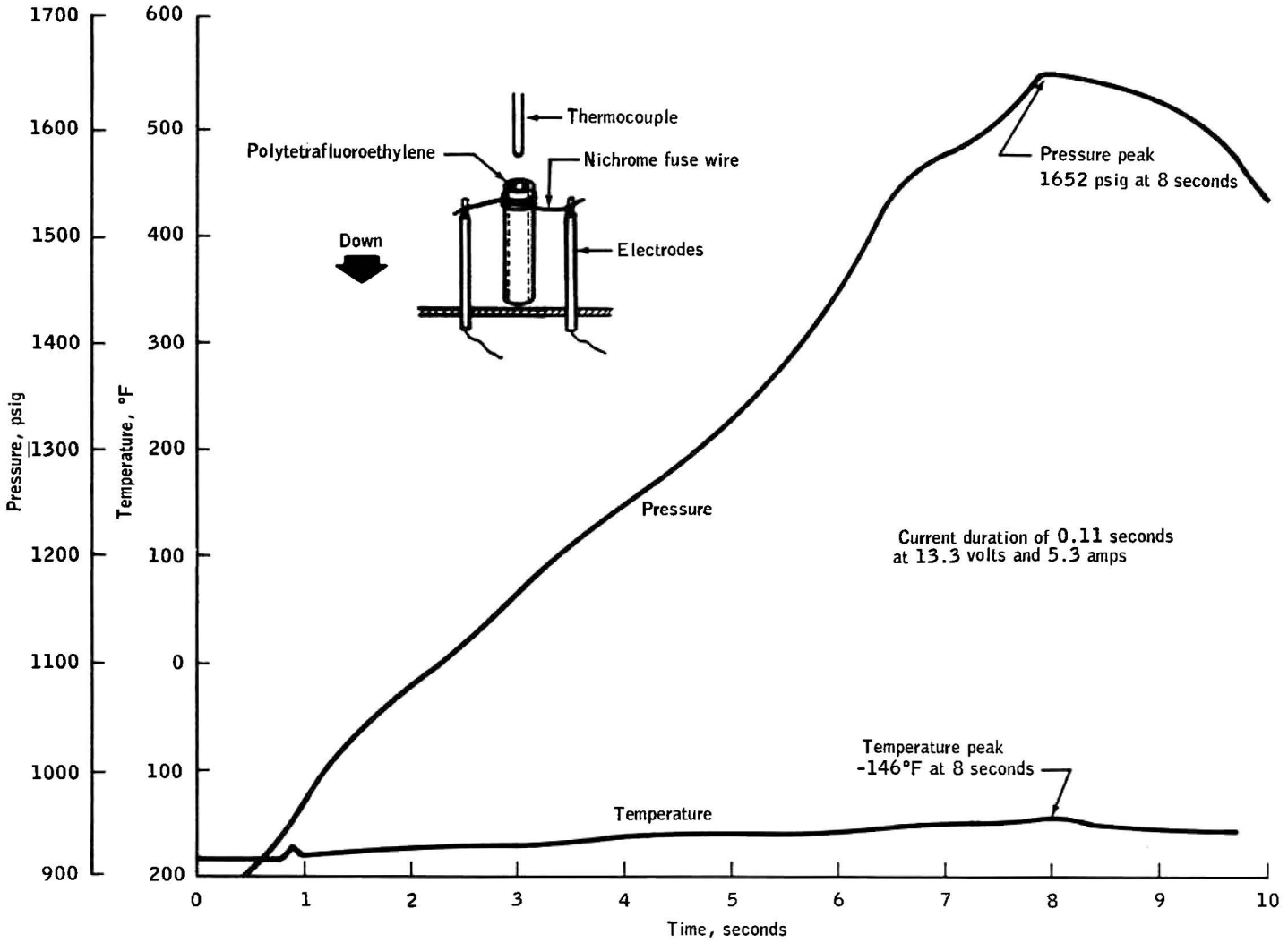

Figure B.22-6.- Hot wire ignition test.

B.23 IGNITION OF DAMAGED WIRE BY ELECTRICAL OVERLOAD TEST

B.23.1 OBJECTIVE

The objectives of this test were to determine if a damaged wire, both insulation and conductor, could have been electrically overloaded by the spacecraft electrical system at the time of the Apollo 13 anomaly and to determine if such an overloaded condition would ignite polytetrafluoroethylene wire insulation.

B.23.2 TEST CONDITIONS

Since the first consideration was to determine under what conditions damaged wires could be overloaded, a series of tests were conducted at ambient conditions. During these tests, a 400-hertz generator was used to electrically load single strands of nickel motor lead wire. The motor lead wire was chosen because it has the smallest single strand diameter and is used in the electrical system which can provide the most energy. The effects were determined for various conditions of current and fuse time on the single strands of wire and damaged single strands.

B.23.3 RESULTS

The test results are presented in table B.23-I. It is significant that at currents up to 5 amperes, failure (fusion) only occurred when slow blow fuses were used. Indication of overheating of the wire occurred on only one test.

B.23.4 CONCLUSIONS

The test results indicate that it is not possible to fuse single strands of the fan motor wire of reduced diameter with the Apollo 13 spacecraft electrical system. Although overheating was indicated in one test, it was not sufficient to cause damage to the insulation. This overheating, as well as fusion, should be less likely to occur at low temperatures.

TABLE B.23-I.- WIRE OVERLOAD TEST AT AMBIENT CONDITIONS

Test No.	Sample Material	Test Conditions Current (amps)/ Fuse (amp)	Test Results
1	.004 nickel motor wire	1 amp	Held specimen at 1 amp for 1 minute. No fusion. Single strand.
2	.004 nickel motor wire	1 amp	Cut through one-half diameter of wire, specimen will now be .002" diameter. Held at 1 amp for 1 minute. No fusion.
3	.004 nickel motor wire	1 amp	Cut and reduce .004 diameter motor wire to .001 diameter. Held for 1 minute at 1 amp. No fusion.
4	.004 nickel motor wire	3 amps/ 3amp	Single strand of wire held for 1 minute at 3 amps. No fusion.
5	.004 nickel motor wire	3 amps/ 3 amp	Cut through one-half diameter of wire to .002" diameter. Held for 1 minute at 3 amps. No fusion.
6	.004 nickel motor wire	3 amps/ 3 amp	Cut through three-fourths diameter of wire to .001" diameter. Held for 1 minute at 3 amps. No fusion. Specimen broke during removal from setup.
7	.004 nickel motor wire	3 amps/ 1 amp	Single strand of wire held for approximately .2 before fuse blew. This test was done three times. Specimen broke while being moved.

TABLE B.23-I.- WIRE OVERLOAD TEST AT AMBIENT CONDITIONS - Continued

Test No.	Sample Material	Test Conditions Current (amps)/ Fuse (amp)	Test Results
8	.004 nickel motor wire	3 amps/ 1 amp	Rerun of Test No. 7.
9	.004 nickel motor wire	3 amps/ 1 amp	Rerun of Test No. 8.
10	.004 nickel motor wire (black)	3 amps/ 1 amp slo blo	Single strand of wire held for approximately 0.35 seconds before fusion took place.
11	.004 nickel motor wire (black)	3 amps/ 1 amp slo blo	Rerun of Test No. 10.
12	.004 nickel motor wire (red)	3 amps/ 1 amp slo blo	Single strand of wire held for approximately 0.36 seconds before fusion took place.
13	.004 nickel motor wire (red)	3 amps/ 1 amp slo blo	Rerun of Test No. 12.
14	.004 nickel motor wire (blue)	3 amps/ 1 amp	Single strand of wire. No fusion with regular fuse, 2 runs.

TABLE B.23-I.- WIRE OVERLOAD TEST AT AMBIENT CONDITIONS - Continued

Test No.	Sample Material	Test Conditions Current (amps)/ Fuse (amp)	Test Results
15	.004 nickel motor wire (blue)	3 amps/ 1 amp	Rerun of Test No. 14.
16	.004 nickel motor wire (blue)	3 amps/ 1 amp slo blo	Rerun of Test No. 14.
17	.004 nickel motor wire (white)	3 amps/ 1 amp	Single strand wire .004" diameter. No fusion.
18	.004 nickel motor wire (red)	3 amps/ 1 amp	Single strand wire .004" diameter. No fusion.
19	.004 nickel motor wire (black)	3 amps/ 1 amp	Wire diameter reduced to .002" diameter. No fusion.
20	.004 nickel motor wire (black)	3 amps/ 1 amp	Wire diameter reduced to .001" diameter. No fusion.
21	.004 nickel motor wire (blue)	4 amps/ 1 amp	Single strand wire, 1 amp regular fuse. No fusion.

TABLE B.23-I.- WIRE OVERLOAD TEST AT AMBIENT CONDITIONS - Concluded

Test No.	Sample Material	Test Conditions Current (amps)/ Fuse (amp)	Test Results
22	.004 nickel motor wire (blue)	4 amps/ 1 amp	Single strand wire, 1 amp regular fuse. No fusion.
23	.004 nickel motor wire (blue)	4 amps/ 1 amp	Wire strand diameter reduced to .002", 1 amp regular fuse. No fusion.
24	.004 nickel motor wire (blue)	4 amps/ 1 amp	Wire strand diameter reduced to .001", 1 amp regular fuse. No fusion.
25	.004 nickel motor wire (red)	5 amps/ 1 amp	Single strand wire. No fusion
26	.004 nickel motor wire (red)	5 amps/ 1 amp	Single strand wire. No fusion
27	.004 nickel motor wire (red)	5 amps/ 1 amp	Wire strand diameter reduced to .002". No fusion.
28	.004 nickel motor wire (red)	5 amps/ 1 amp	Wire strand diameter reduced to .001". No fusion.

B.24 CONDUIT WIRE BUNDLE IGNITION TEST

B.24.1 OBJECTIVE

The objective of this test was to determine the ignition, combustion, and combustion propagation characteristics of the insulated electrical wiring in a simulated Apollo oxygen tank electrical feedthrough conduit. The conduit carries all the electrical wiring that serves the internal components of the oxygen tank, including the temperature probe, quantity gaging system, fan motors, and heaters.

B.24.2 TEST EQUIPMENT AND PROCEDURE

The test setup is shown in figure B.24-1. A pressure vessel and a flight-type conduit containing the normal wiring assembly was installed in a vacuum chamber. Figures B.24-2 and B.24-3 show the thermocouple locations on the conduit. Electrical loads simulating the oxygen tank internal components were connected to the conduit wires. A relief valve, (1050 psig) was attached to the pressure vessel. The chamber was then evacuated. Gaseous oxygen was fed to the pressure vessel while liquid nitrogen was flowed through copper coils wrapped compactly around the vessel. When the desired conditions of supercritical oxygen, 910 psig and minus 190° F, were reached, 20 volts (20 amperes) were applied to the Nichrome igniter wire in the electrical connector portion of conduit.

B.24.3 RESULTS

At 4.2 seconds after igniter voltage was applied, the thermocouples attached to the outside of the conduit indicated a temperature decrease. At 6.0 seconds, the conduit burst at the first bend after the conical section of the electrical connector portion of the conduit (fig. B.24-4). A brief spurt of flame followed by a rapid discharge of oxygen was observed from the ruptured conduit. The pressure vessel experienced negligible pressure (9 psi) and temperature rise during the combustion phase, figure B.24-5. Conduit temperatures near the rupture area were 1193° to 1507° F at the time of rupture. All three phases of both fan motors electrical power shorted, and the six fuses in the fan circuits blew at approximately 5.2 seconds.

Some of the polytetrafluoroethylene insulation remained within the connector area (fig. B.24-6). Insulation in the ruptured area was nearly all consumed, but the insulation that was more than about 4 inches downstream of the rupture was only slightly damaged (fig. B.24-7).

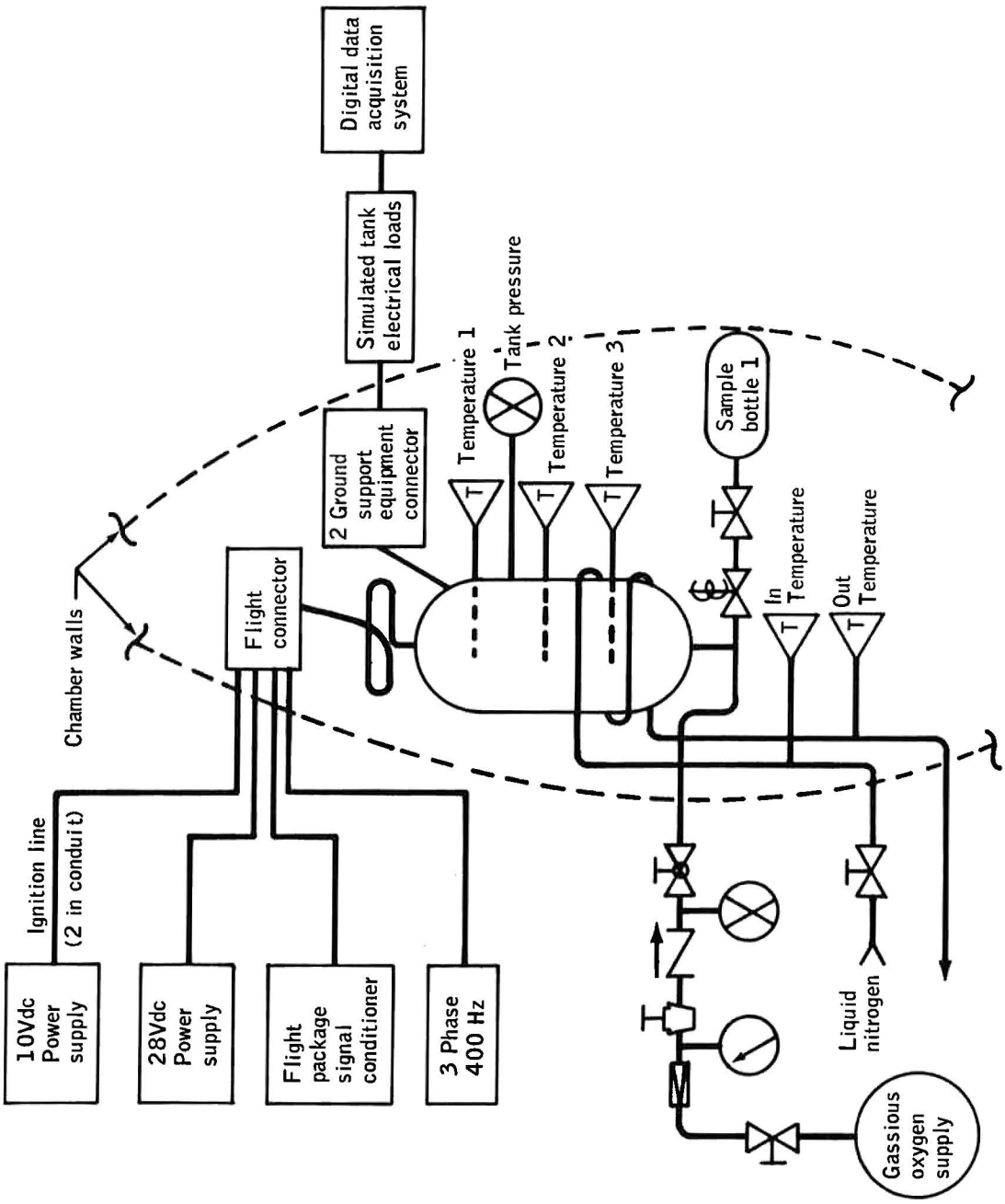

Figure B.24-1.- Schematic for ignition of wire conduit.

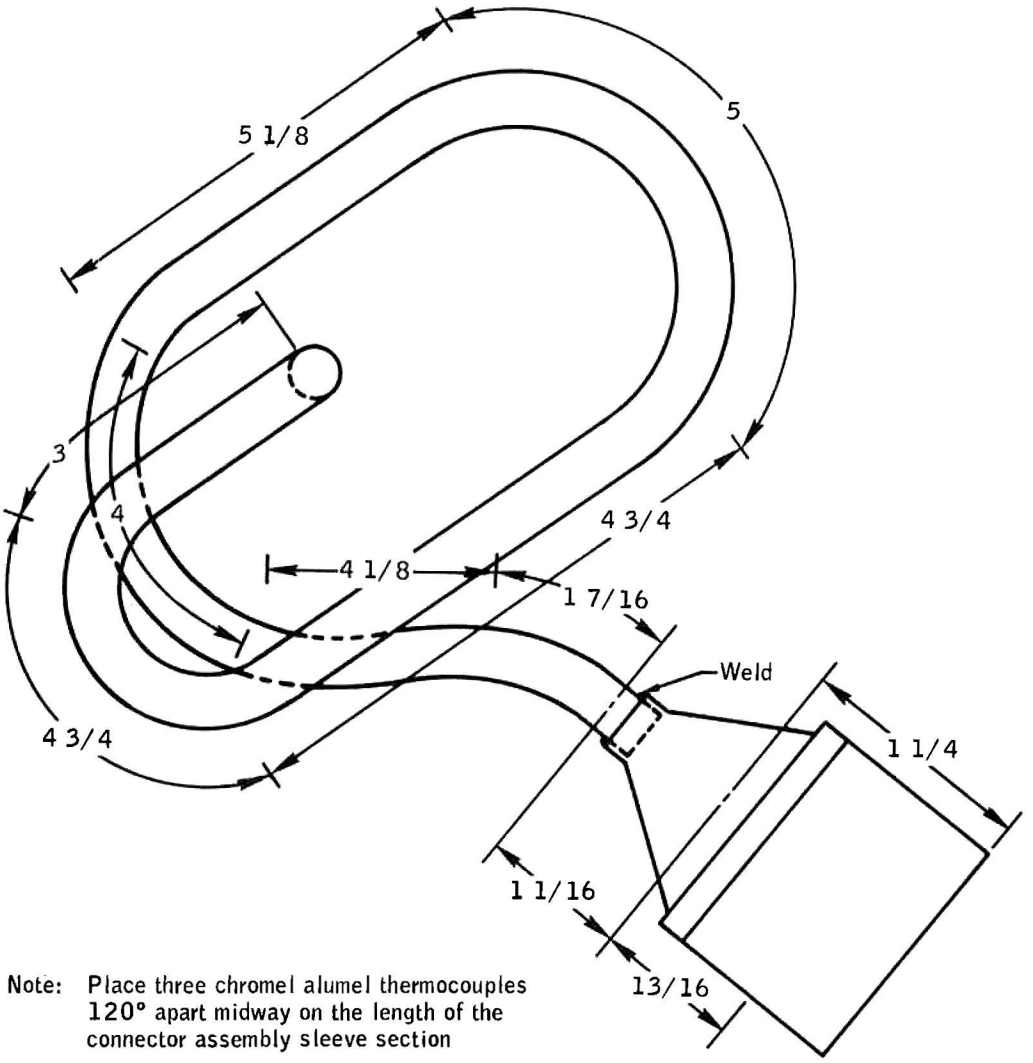

Note: Place three chromel alumel thermocouples 120° apart midway on the length of the connector assembly sleeve section

Figure B.24-2.- Conduit thermocouple set-up.

Figure B.24-3.- Wiring conduit before test.

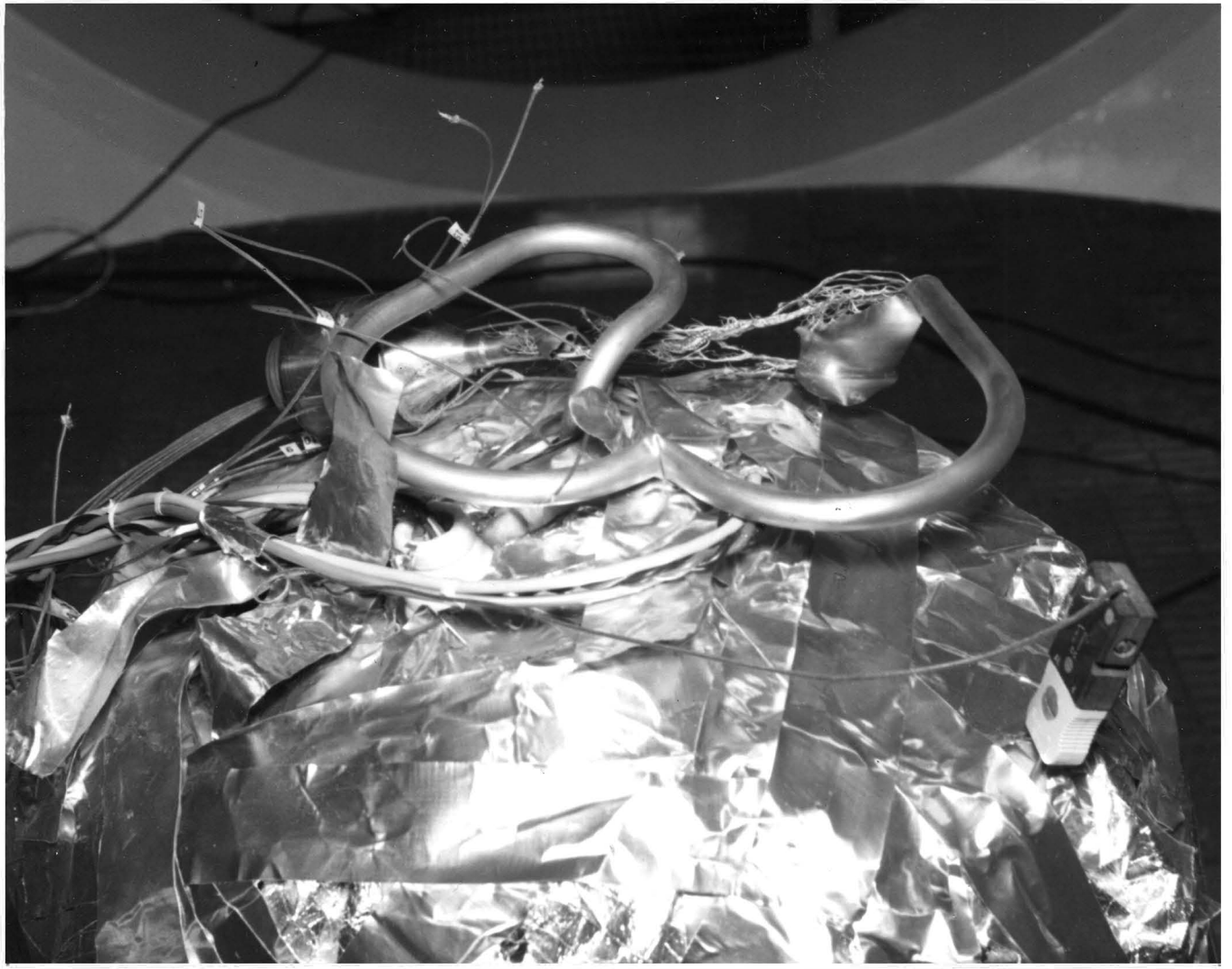

Figure B.24-4.- Wiring conduit after test.

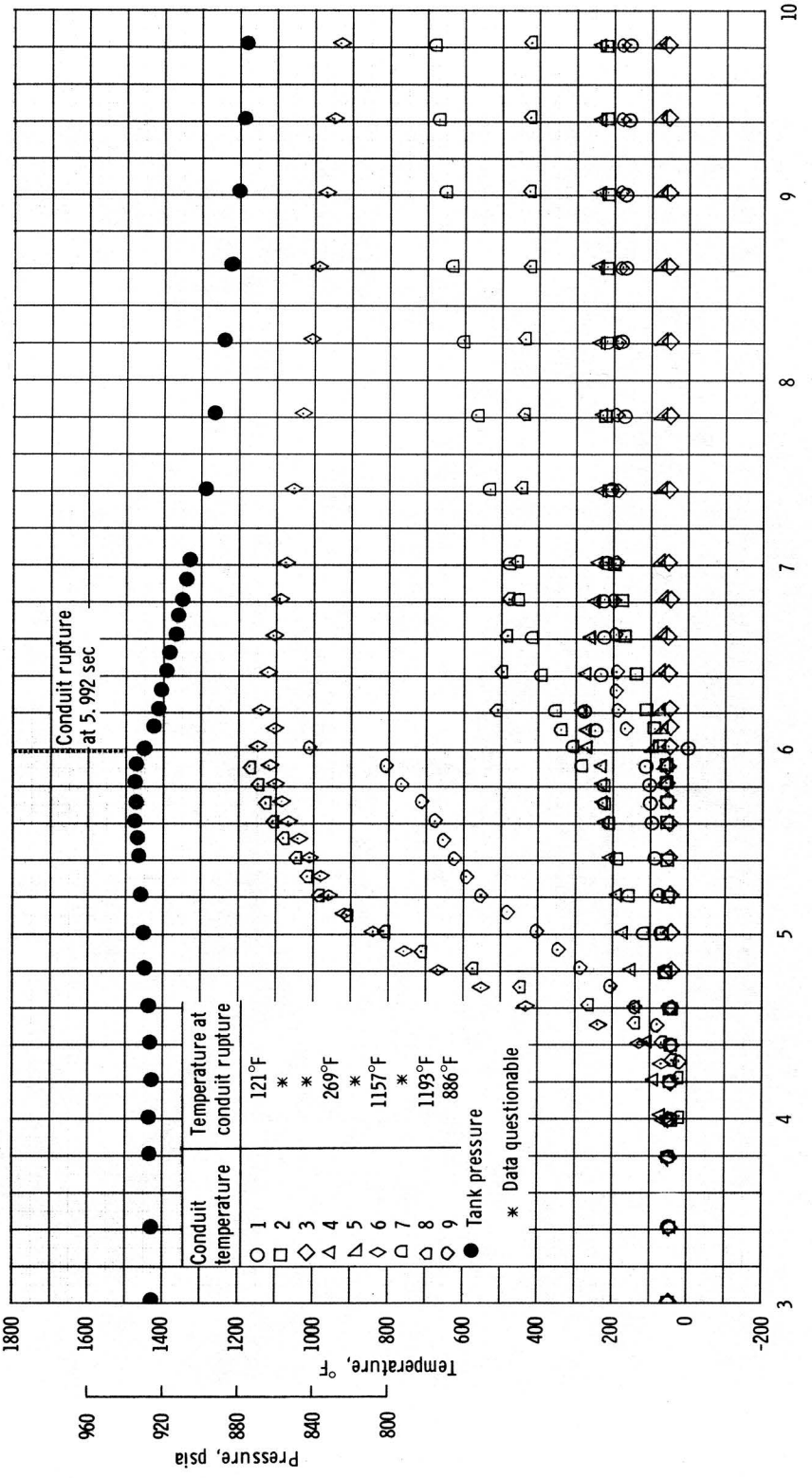

(a) Test point 1 through 9.

Figure B. 24-5. - Conduit wire bundle test data.

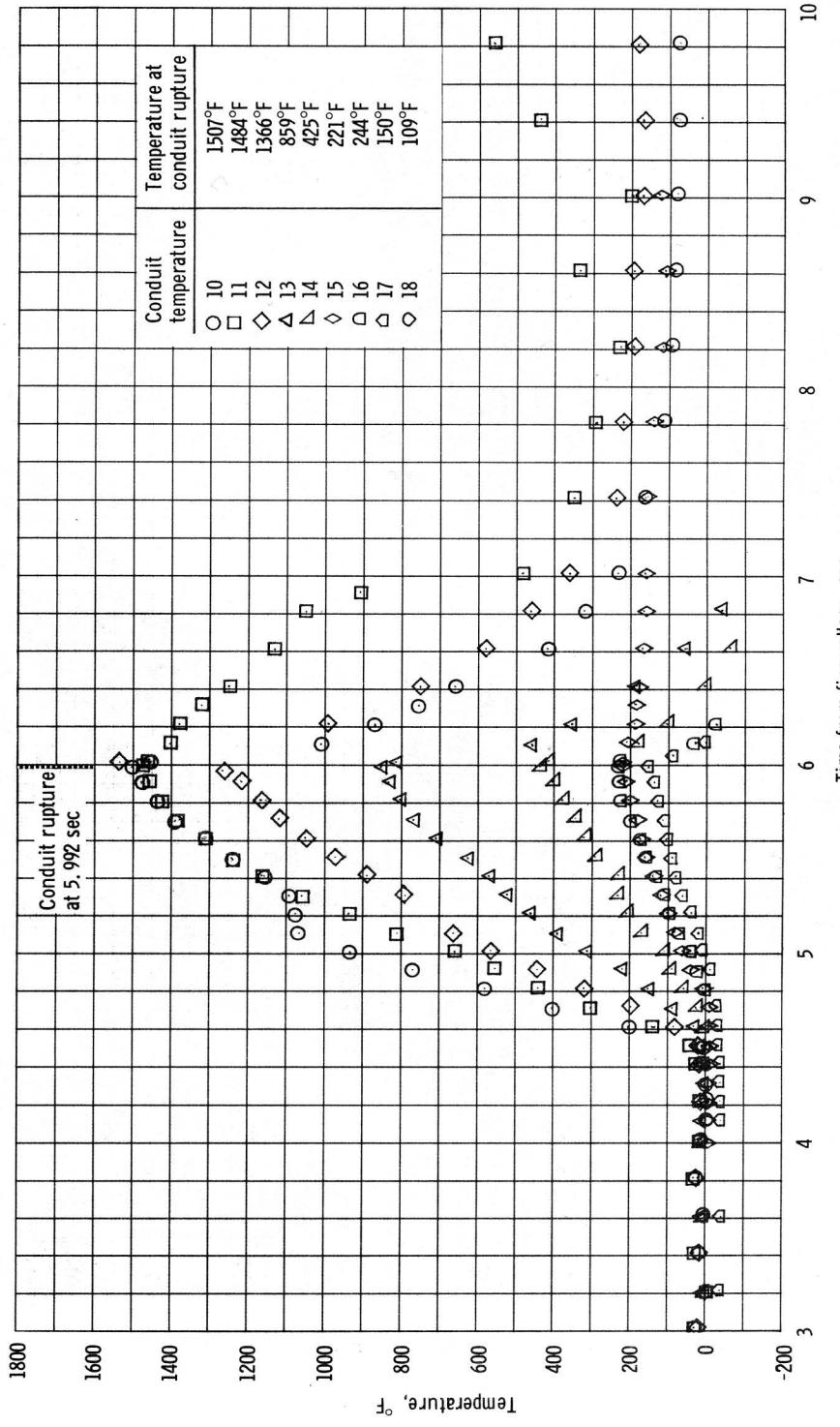

(b) Test point 10 through 18.

Figure B. 24-5. - Concluded.

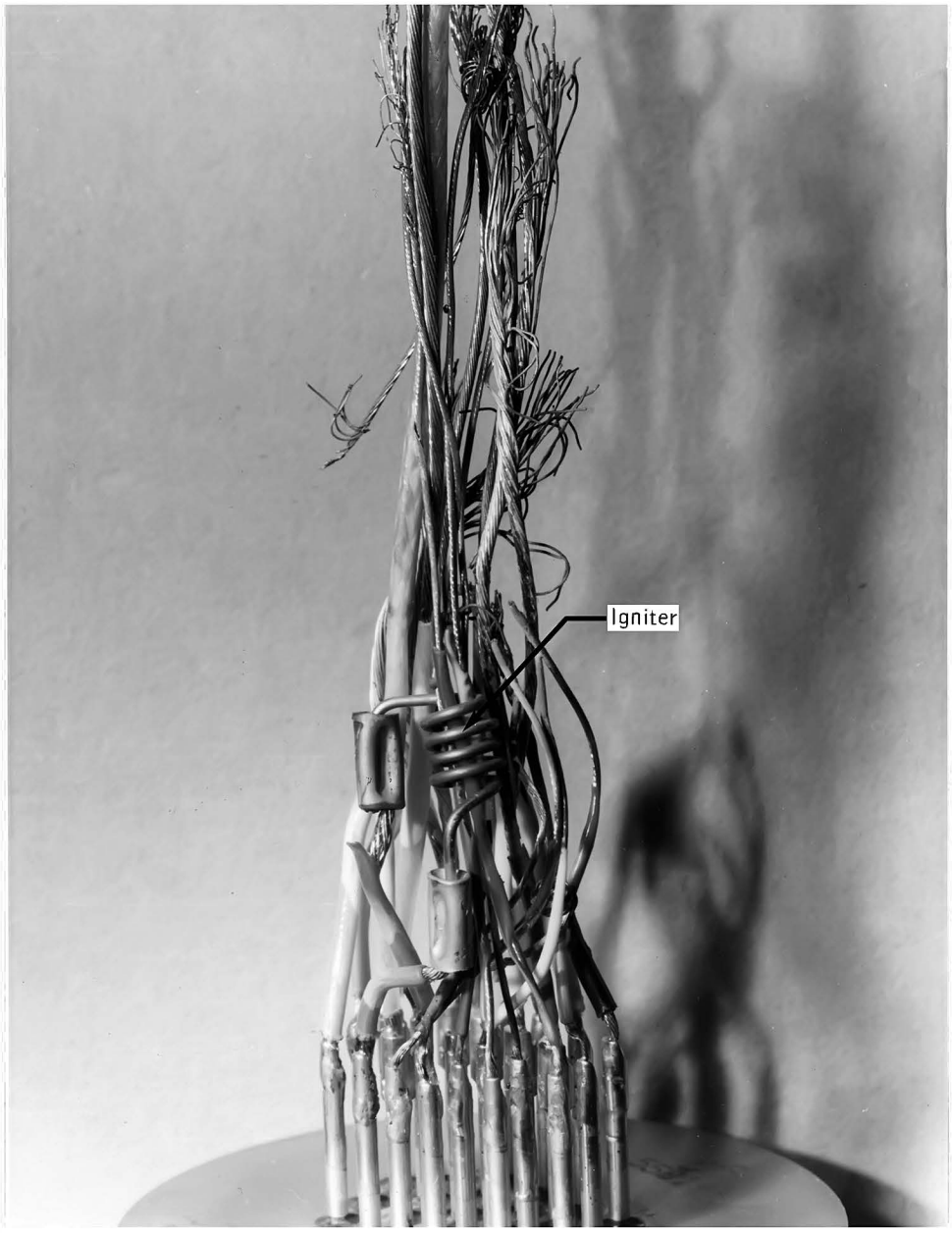

Figure B.24-6.- Disassembled connector after test.

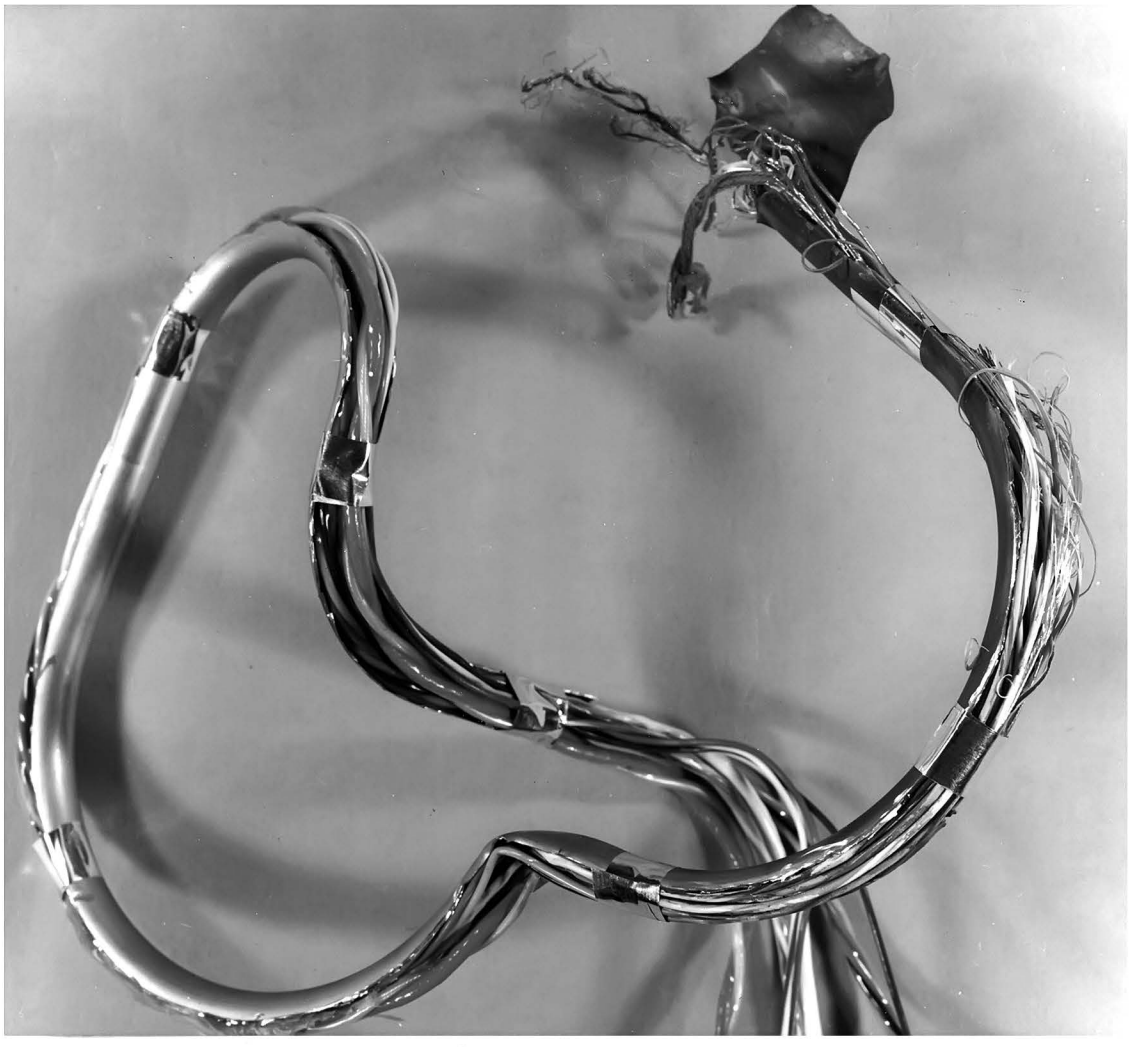

Figure B.24-7.- Wiring of sectioned conduit after test.

B.25 IGNITION TEST OF POLYTETRAFLUOROETHYLENE SUBMERGED IN LIQUID OXYGEN

B.25.1 OBJECTIVE

The objective of this test was to determine the possibility of igniting of polytetrafluoroethylene by an electrical short while submerged in liquid oxygen.

B.25.2 TEST CONDITIONS

A section of 28-gage polytetrafluoroethylene-insulated copper wire was wrapped on a carbon steel spool about 0.3-cm by 1.5-cm, and a fabricated sparking device was provided. A thermocouple was imbedded in the spool, and a polytetrafluoroethylene collar was placed over the assembly. This assembly was put into a pressure vessel and filled with oxygen at 930 psia at 150° K. Several tests were run, and in some cases, the assembly was covered by an aluminum sleeve over the polytetrafluoroethylene collar.

B.25.3 RESULTS

A spark of 5 (±3) joules from a 115 V 60 hertz power supply caused the pressure to rise to 1100 psia within 9.5 seconds and the temperature rose to 400°F (off scale) in less than 1 second. Upon opening the chamber it was noted that all of the polytetrafluoroethylene was consumed, and when aluminum was included, it too was burned. In one case, combustion proceeded to include the pressure vessel which failed and vented to atmosphere.

B.26 ARC TEST OF TANK MATERIALS SUBMERGED IN LIQUID OXYGEN AT ONE ATMOSPHERE

B.26.1 OBJECTIVE

The objective of this test was to determine the ignition energy required from an electrical short and polytetrafluoroethylene burning to cause ignition of tank materials in atmospheric liquid oxygen.

B.26.2 TEST PROCEDURES

This test was performed in conjunction with those discussed in section B.25.

B.26.3 RESULTS

All materials could be ignited, but burning was very marginal. Ignition energy under these conditions was not determined.

B.27 IGNITION TEST OF TANK MATERIALS IN HIGH PRESSURE LIQUID OXYGEN

B.27.1 OBJECTIVE

The objective of this test was to determine the ignition energy required from an electrical short and polytetrafluoroethylene burning to cause ignition of tank material in high pressure liquid oxygen.

B.27.2 TEST PROCEDURES

This test was performed in conjunction with those discussed in section B.25.

B.27.3 RESULTS

Spark energies of 2.5 joules would ignite polytetrafluoroethylene and initiate a metal-polytetrafluoroethylene reaction.

B.28 FAN MOTOR OPEN CIRCUIT TRANSIENT TEST

B.28.1 OBJECTIVE

The objective of this test was to investigate the potential ignition energies present if a power wire to either tank fan motor should break. This was accomplished by measuring the induced voltages and current transients that resulted from interrupting one phase of power to a tank fan motor.

B.28.2 TEST EQUIPMENT AND CONDITIONS

An electrical schematic of the test fixture is shown in figure B.28-1. Two tank fan motors were powered in parallel from a 400-hertz, 3-phase power supply. The rotor was removed from each motor shaft so that the motors could achieve the maximum revolutions. The fans were immersed in liquid nitrogen. One phase of power to each motor was interrupted and the potential ignition source energy was measured. The energy levels were recorded for each phase.

B.28.3 RESULTS

The power interruptions resulted in voltage spikes as high as 1800 volts with a duration of about 0.05 millisecond. However, the phase current transients were extremely small, indicating that very little energy was available.

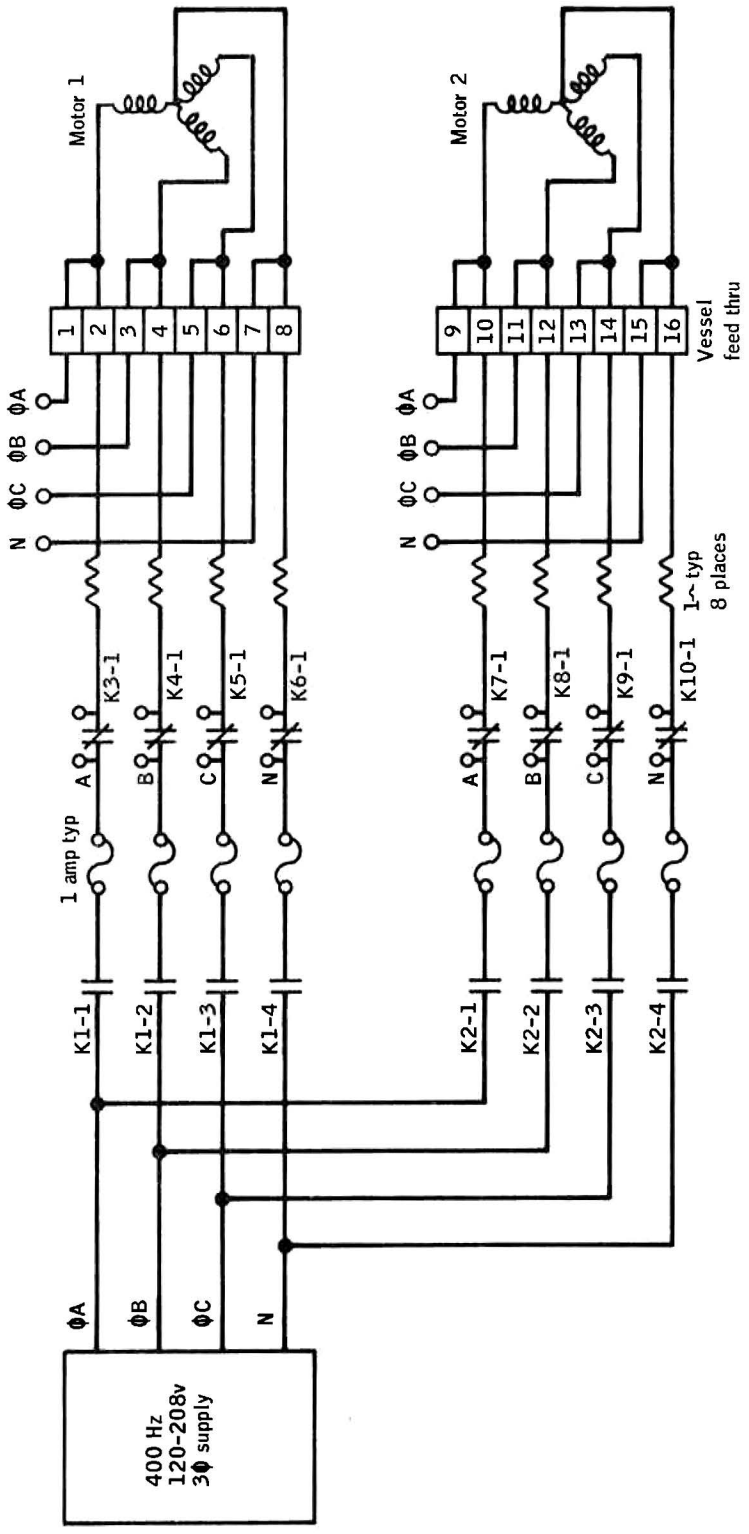

Figure B.28-1.- Fan motor test fixture schematic.

B.29 SPARK IGNITION TEST OF POLYTETRAFLUOROETHYLENE IN LIQUID OXYGEN AT SUPERCRITICAL TEMPERATURES

B.29.1 OBJECTIVES

The primary objectives of this test series were to determine the minimum electrical spark required to ignite polytetrafluoroethylene wire insulation in high pressure gaseous and supercritical oxygen environment and determine the burning characteristics of the insulation in these environments. A secondary objective was to determine if the combustion would propagate through a length of stainless steel tubing and wire clamps used in the spacecraft oxygen tank.

B.29.2 TEST EQUIPMENT AND CONDITIONS

A test fixture with a 0.18 cubic foot tank was installed in a 6-foot vacuum chamber (fig. B.29-1). This fixture (fig. B.29-2) had two view ports which allowed photographic coverage of the test specimens in either gaseous or liquid oxygen at pressures up to 1200 psig. An ignition system provided variable capacitance, in steps, from 8000 microfarads maximum to 25 microfarads minimum at a potential of 50 volts. The energy used to generate the spark was determined by recording the voltage across the capacitance during discharge. Photographic coverage was provided by a motion picture camera running at 64 frames per second.

A total of 44 test runs were made using various samples of wire, including that used in the spacecraft cryogenic oxygen tank, and with various capacitances for the initial charge. Sixteen runs were made in gaseous oxygen with the remaining 28 runs in liquid oxygen. The test conditions were 900 to 950 psig and minus 180° to minus 200° F for the liquid oxygen testing. All gaseous oxygen tests were performed at the same pressure but at ambient temperature.

B.29.3 RESULTS

Combustion was initiated in both gaseous and liquid oxygen with less than 0.45 joule of energy in the electrical arc.

Typical propagation rates in liquid oxygen were 3 in/sec vertical up, 1/4 in/sec vertical down, and 0.4 in/sec horizontal. Propagation rates were higher in gaseous oxygen, particularly in the vertical up direction.

The burning of polytetrafluoroethylene insulation down a 0.155-inch inside diameter stainless steel tube and propagation under a copper clamp holding the electrical wire to a steel tube was also demonstrated.

B.29.4 CONCLUSION

Polytetrafluoroethylene wire insulation is easily ignited in gaseous or liquid oxygen and in most cases combustion is maintained until all the polytetrafluoroethylene is consumed.

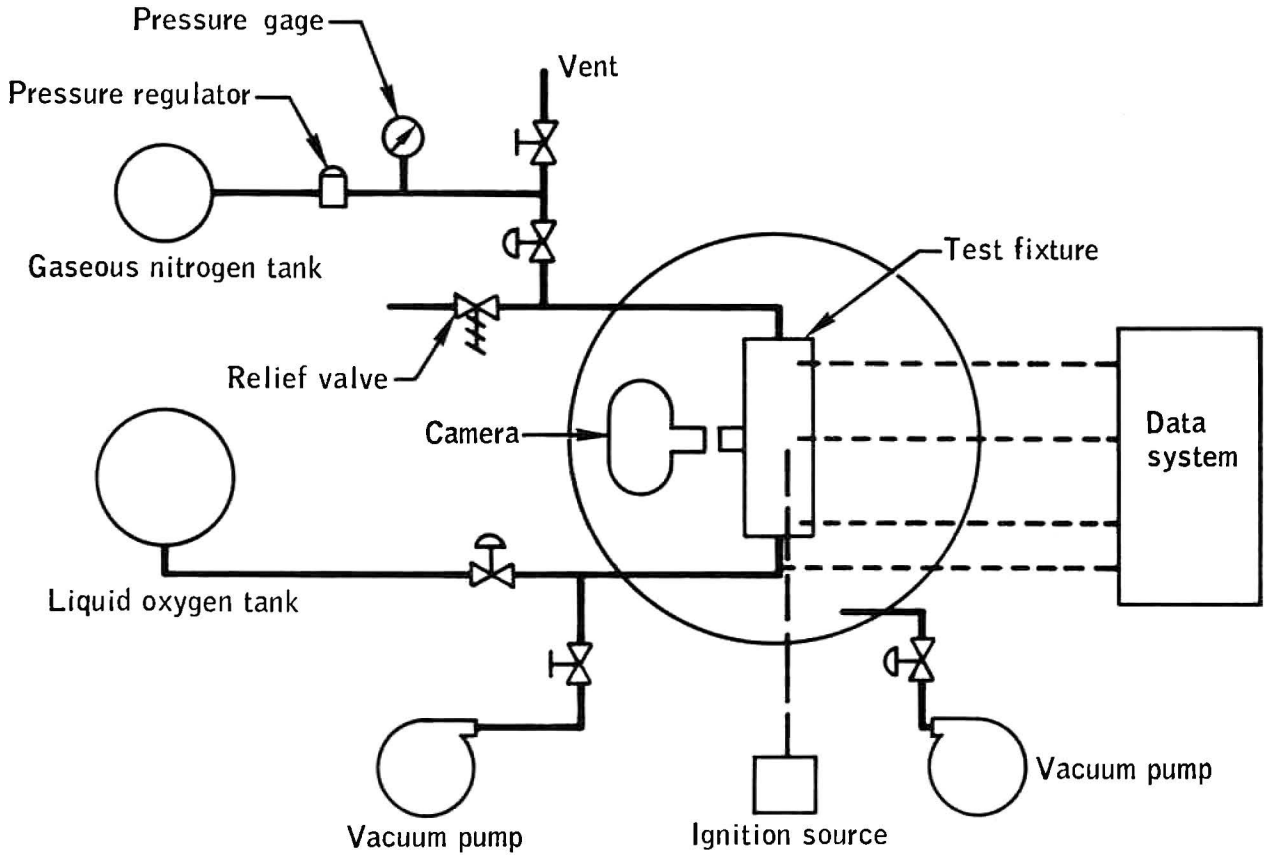

Figure B.29-1.- Schematic of test setup for spark ignition of polytetrafluorethylene in liquid oxygen.

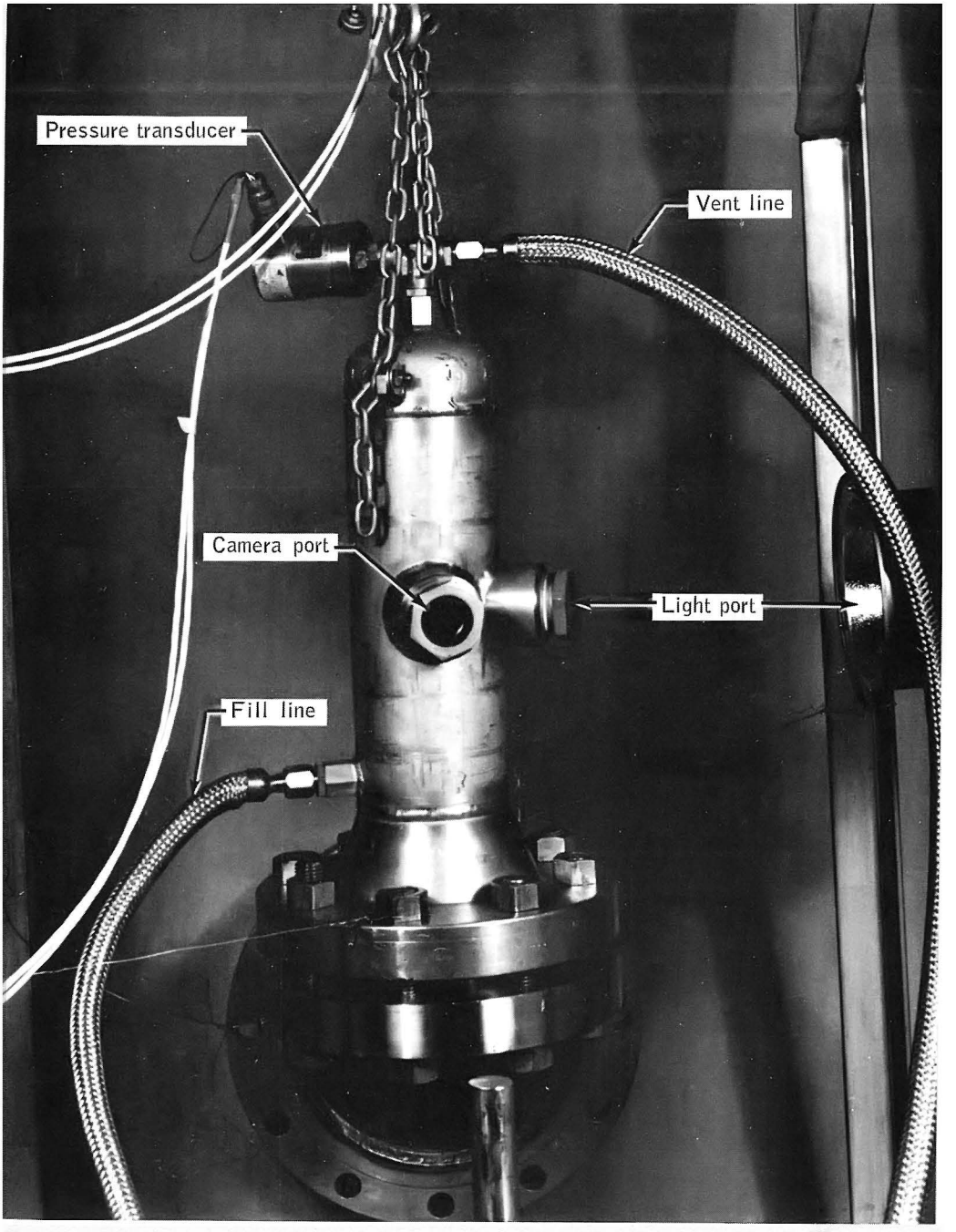

Figure B.29-2.- Test fixture for spark ignition of polytetrafluorethylene in liquid oxygen.

B.30 FAN MOTOR IGNITION TESTS

B.30.1 OBJECTIVE

The objective of these tests was to examine the ignition and combustion characteristics of the cryogenic oxygen tank fan motors under realistic operating conditions.

B.30.2 TEST EQUIPMENT AND CONDITIONS

Two fan motors were installed correctly within the heater probe assembly mounted in a test fixture in liquid oxygen at 900 psia and minus 190° F. Ignition was accomplished by the vigorous heating of a Nichrome wire wrapped around the fan motor wire insulation. The tests were classified as downward or upward burning ignition and, in some cases, included the observance of fire propagation through the 3/16-inch motor wire conduit which passes through the heater assembly. Strategically located temperature instrumentation (fig. B.30-1) allowed tracking of the combustion flame front.

B.30.3 RESULTS

The results of these tests were as follows:

a. Downward propagation of the flame on the wire insulation in the 3/16-inch conduit self-quenched approximately 1/4 inch from the bottom conduit exit grommet.

b. Downward propagation rate through the conduit averaged 0.25 in./sec

c. The downward burning motor ignition had the following combustion results (fig. B.30-2):

1. 90 percent of lead wire
2. 100 percent of polytetrafluoroethylene grommet
3. 75 percent of strain relief
4. No other motor parts burned

d. Upward propagation rate through the motor wire conduit was several in./sec and had no tendency to self quench.

e. The upward burning motor ignition was more vigorous and had the following results (figs. B.30-1 and B.30-3):

1. 100 percent of lead wire
2. 100 percent of polytetrafluoroethylene grommet
3. 100 percent of strain relief
4. 100 percent of terminal polytetrafluoroethylene shrink tubing
5. 90 percent of stator insulator strips
6. Less than 5 percent of stator wire insulation
7. No other parts burned

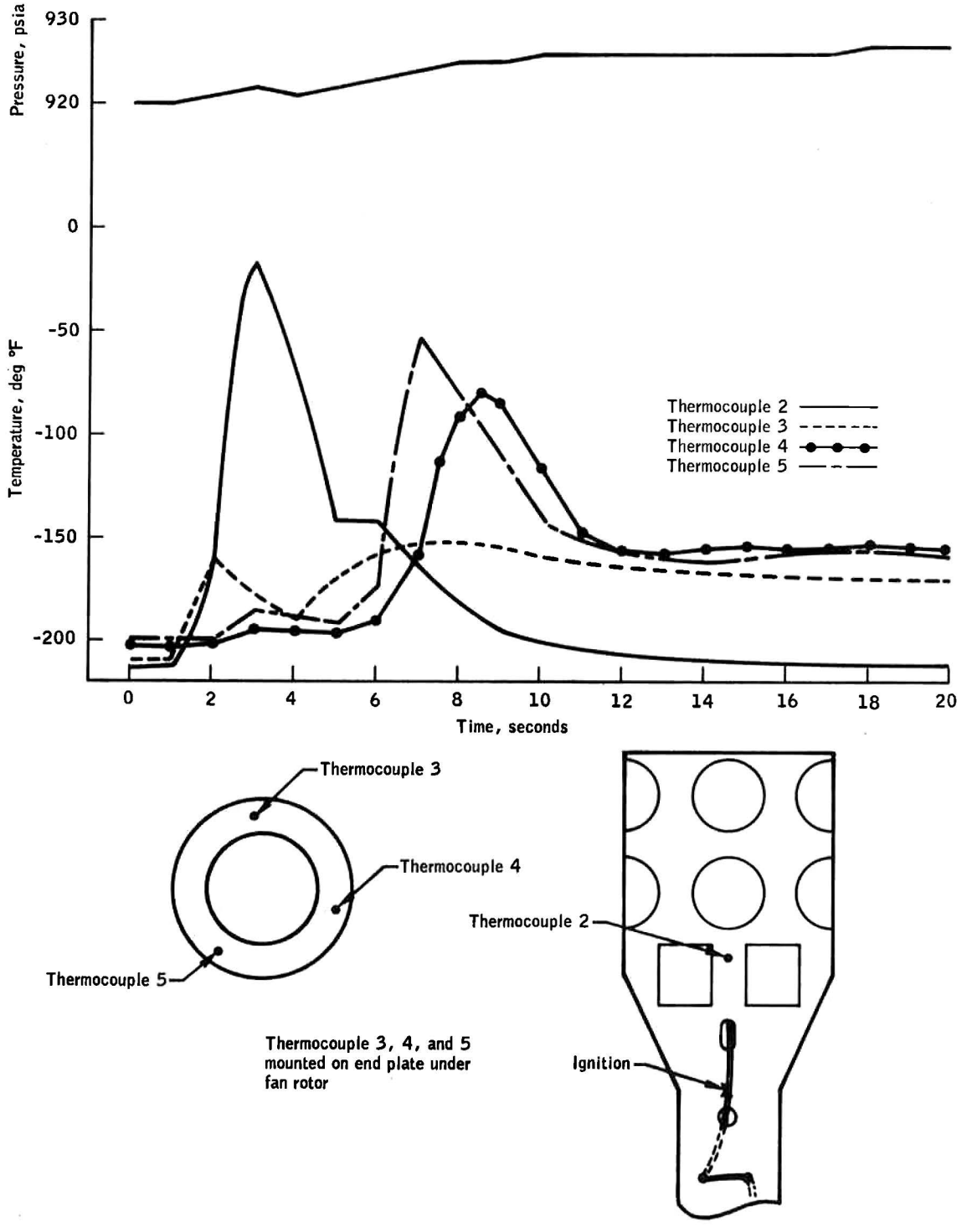

Figure B.30-1.- Comparison of temperature and pressure with time during fan motor ignition tests.

Figure B.30-2.- Effects of downward combustion during fan motor ignition tests.

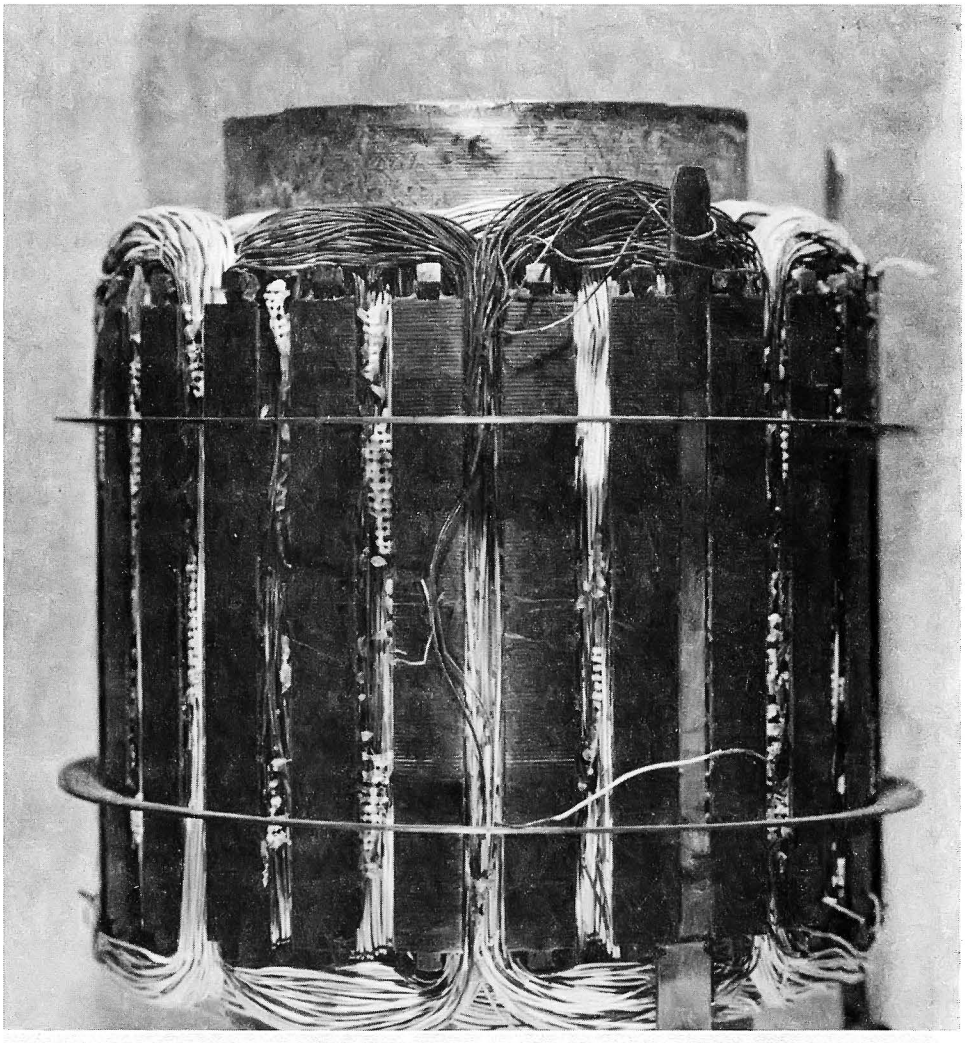

(a) Stator

Figure B.30-3.- Effects of upward combustion during fan motor ignition tests.

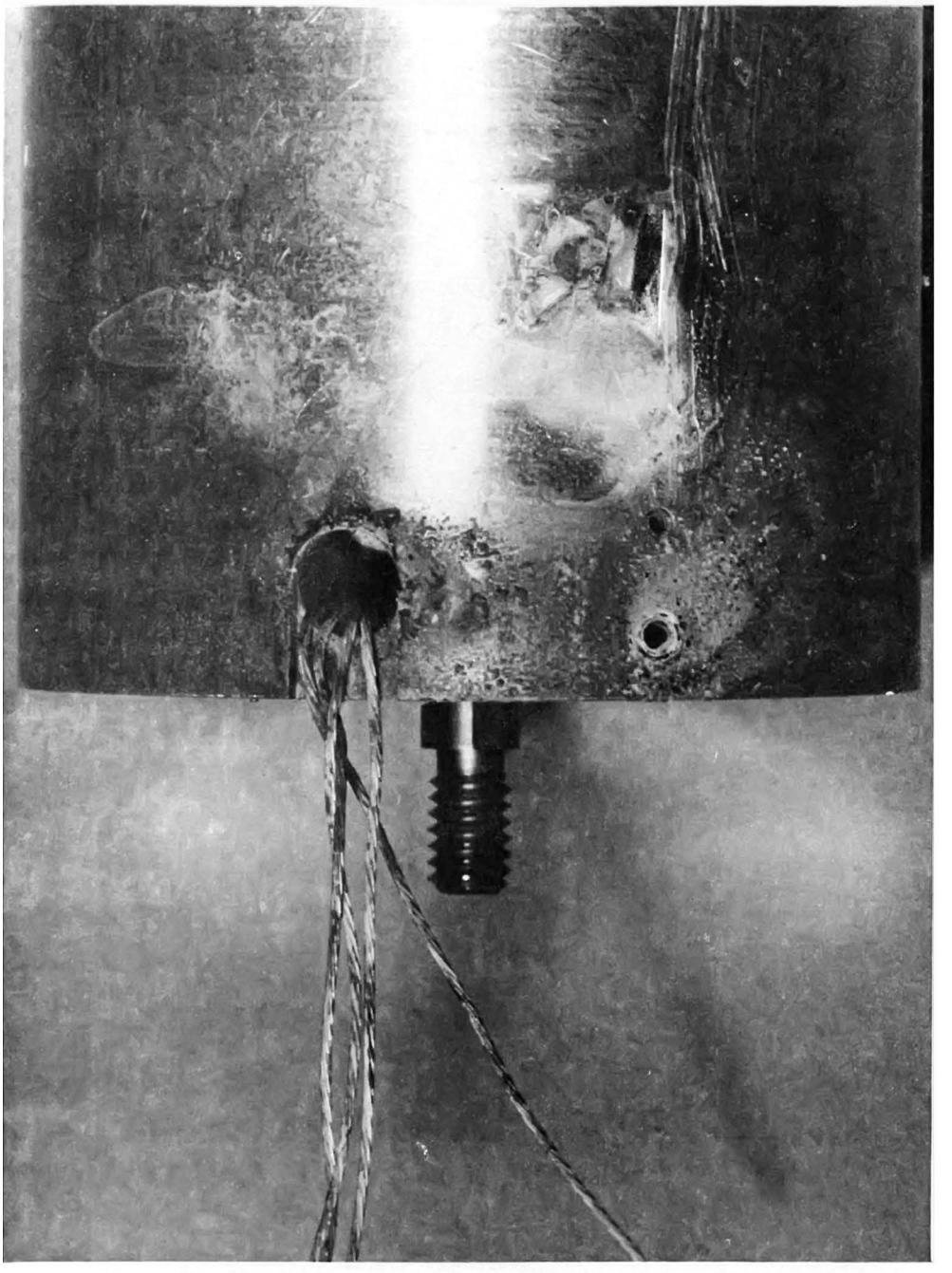

(b) Wire exit area

Figure B.30-3.- (Continued)

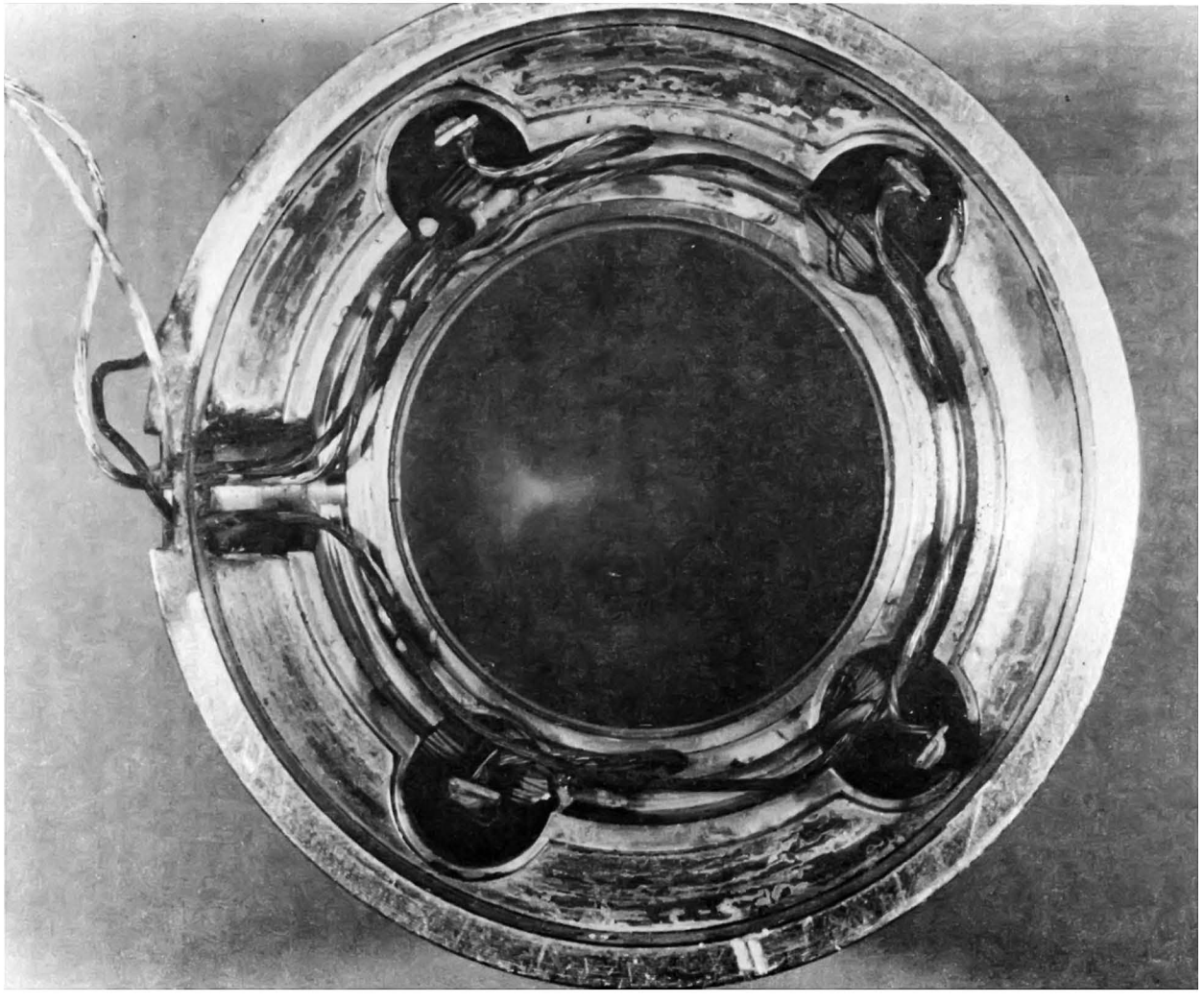

(c) End view of fan motor case

Figure B.30-3.- (Continued)

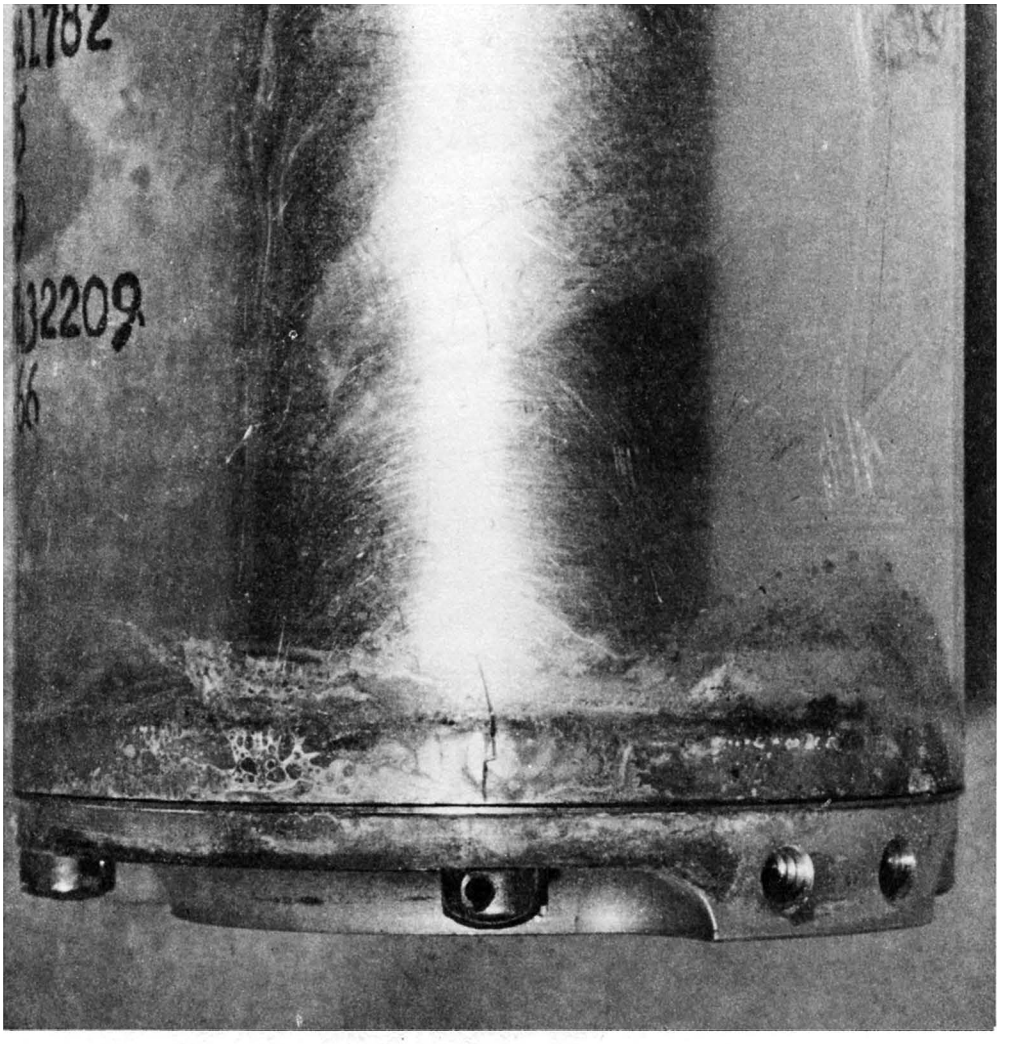

(d) External view of fan motor case

Figure B.30-3.- (Concluded).

B.31 IGNITION TEST AND CHEMICAL ANALYSIS OF BAKED POLYTETRAFLUOROETHYLENE INSULATION

B.31.1 OBJECTIVE

One objective of this test was to determine if the polytetrafluoroethylene insulation on fan motor wires which had been "baked" at approximately 750° F in a gaseous nitrogen atmosphere would ignite and burn in the same manner as normal insulation. Also, another wire sample was to be baked in a 750° F oxygen environment (15 to 20 psia), and determination made as to whether this condition had an effect on the polytetrafluoroethylene insulation.

B.31.2 TEST EQUIPMENT AND CONDITIONS

Two ignition tests were performed on the insulation which had baked in the nitrogen environment. These ignition tests were performed in liquid oxygen at 900 to 950 psig and minus 180° to minus 200° F. Then a 6-inch length of four-conductor fan motor wire (fig. B.31-1) was placed in a closed vessel with gaseous oxygen at 15 psia and heated to 750° (±10°) F for 5 hours. Gaseous pressure was then increased to 20 psia and maintained at that pressure. A sample of the gaseous oxygen, taken at completion of the 5-hour heat soak was analyzed for carbon dioxide, carbon tetrafluoride, and carbonyl fluoride content and was also tested for ignition and burning characteristics in liquid oxygen.

B.31.3 RESULTS

The baked insulation ignited and burned with the same characteristics of new insulation. Neither the nitrogen nor oxygen baking had any apparent effect on the burning characteristics in liquid oxygen. The insulation did not become brittle or crack in the 750° F oxygen soak, indicating that the temperature during the nitrogen soak was probably above 750° F. During the soak a red wire was bleached to virtually a white color. The insulation also pulled back (shrank) from each end of the wire by 3/8 inch (fig. B.31-1).

An analysis of the gases from the high temperature oxygen soak showed 1.3 percent carbon dioxide with no indication of other constituents, indicating little or no oxidation of the polytetrafluoroethylene at this temperature.

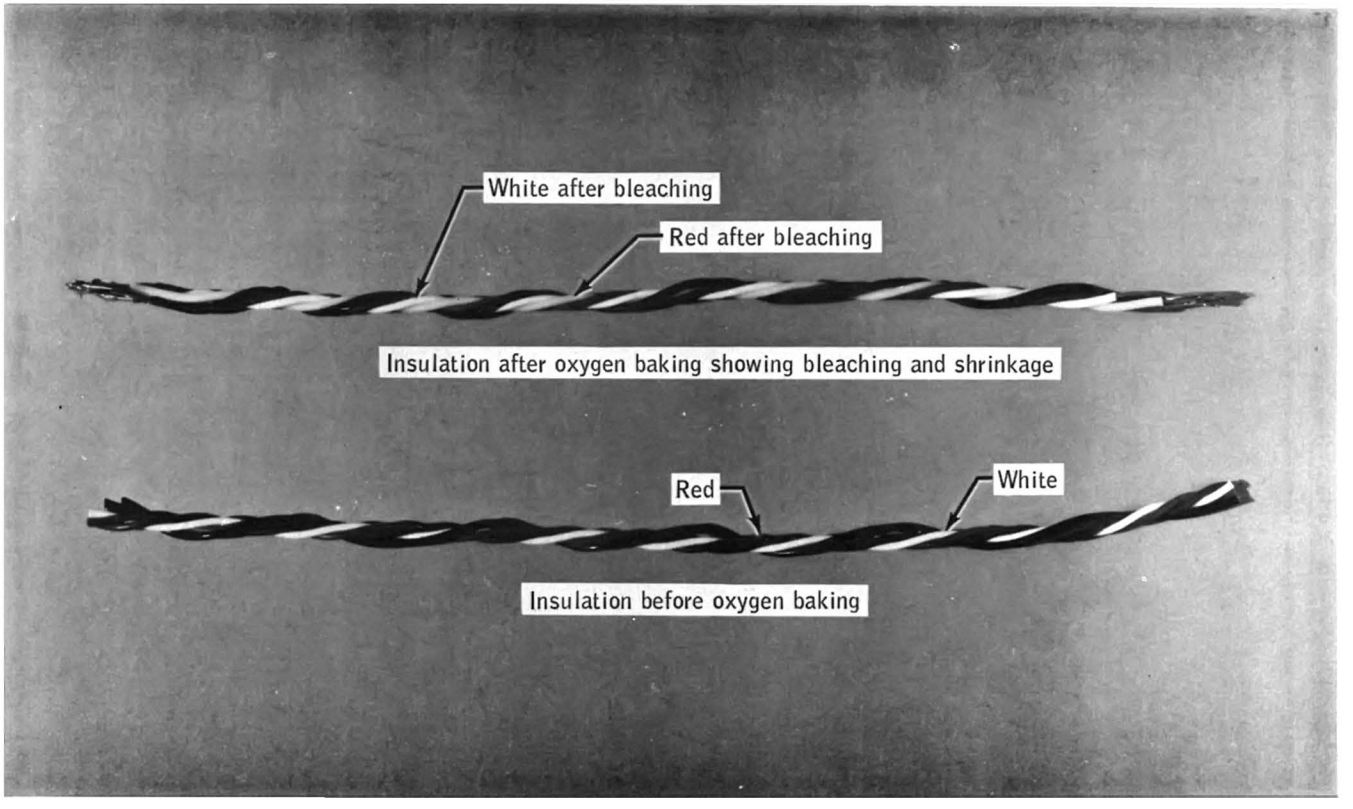

Figure B.31-1.- Fan motor wire before and after oxygen baking.

B.32 CRYOGENIC OXYGEN TANK WIRE SELF-HEAT TEST

B.32.1 OBJECTIVE

The objective of this test was to determine if the detanking procedure used at the Kennedy Space Center during the countdown demonstration test could cause damage to the wire bundle in the oxygen tank entry conduit.

B.32.2 TEST EQUIPMENT AND CONDITIONS

The test setup is shown in figure B.32-1. An oxygen tank wire bundle with flight-type conduit and electrical interface connector was interfaced to a thermal vacuum chamber with the connector located outside the chamber. The other end of the conduit was interfaced to a pressure vessel located in the thermal vacuum chamber. In this configuration, the connector environmental pressure was ambient, the conduit environment was 2 x 10-5 torr at 70° to 80° F, and the wire bundle and conduit internal pressure were set at the same elevated pressure as the pressure vessel. Some of the wires protruding from the conduit were interfaced to electrical feedthroughs mounted on the pressure vessel end plate and connected to simulated oxygen tank heaters, fan motors immersed in liquid nitrogen, and a quantity gage sensor. The oxygen tank internal temperature sensor wires were interfaced to a simulated sensor inside the pressure vessel. The flight-type connector was interfaced to facility heater power supplies, a facility 400-Hz power supply, and a signal conditioning unit. The pressure vessel was pressurized with gaseous oxygen and vented in accordance with the schedule recorded for the detank operations during the countdown demonstration test; the heaters and fan motors were also operated in accordance with the countdown demonstration test schedule. Temperatures along the conduit outer wall and on the connector recorded. Post-test inspection was accomplished by sectioning the conduit at the maximum temperature point.

B.32.3 RESULTS

The maximum conduit temperature recorded was 327° F at a point 14.5 inches from the pressure vessel end of the conduit (fig. B.32-2). The conduit temperature achieved equilibrium approximately 5 hours after start of the test. A visual inspection at the location of the highest indicated temperature showed no insulation degradation. The wire bundle continuity and insulation resistance tests indicated no anomalies. Pressurizing and venting the pressure vessel with gaseous oxygen in accordance with the countdown demonstration test schedule had little effect on the conduit temperature.

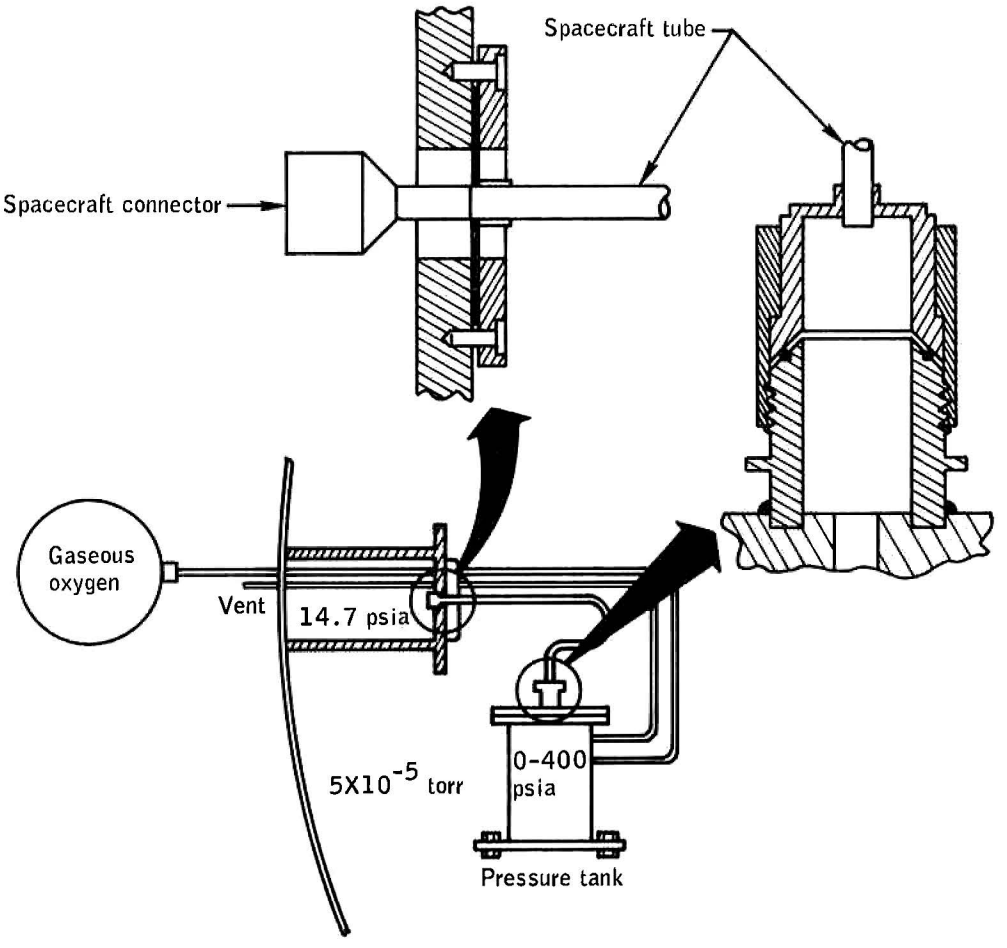

Figure B.32-1.- Setup for cryogenic oxygen tank self heat test.

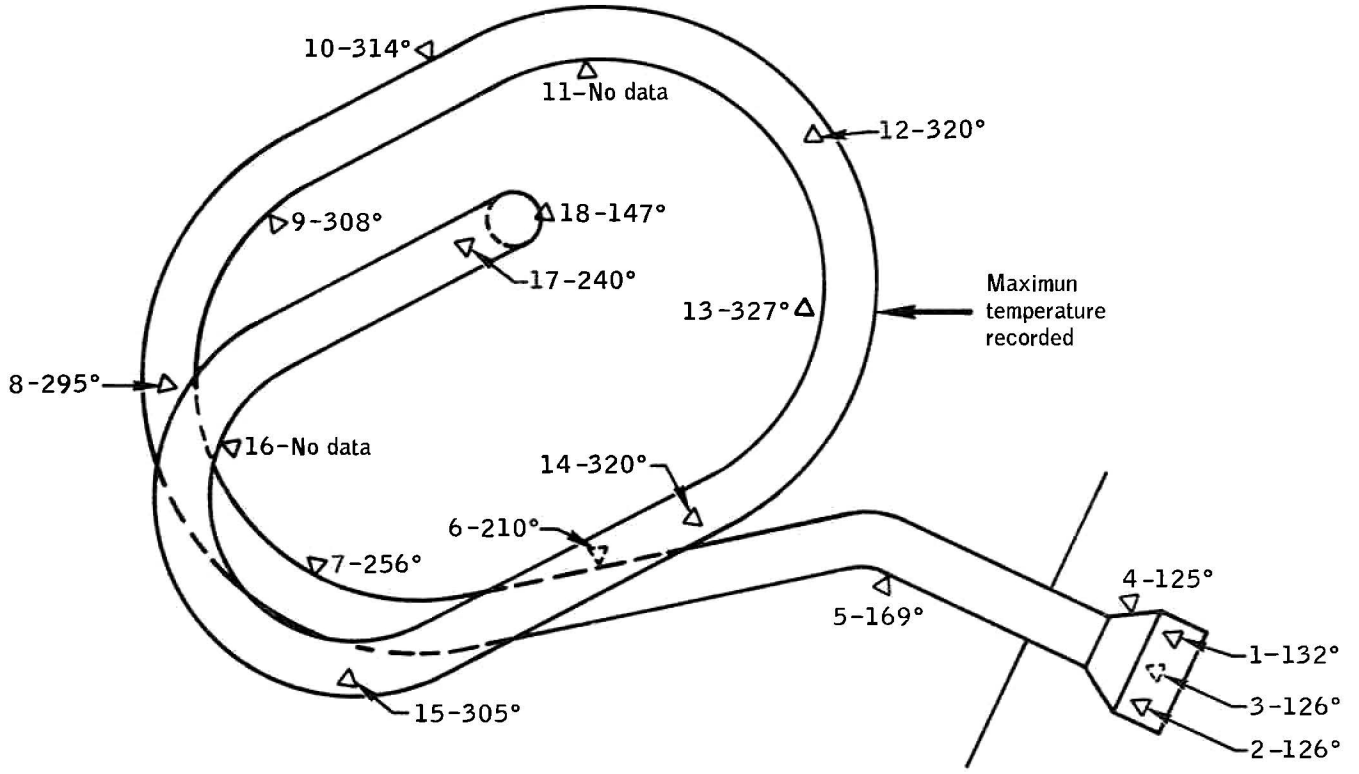

Δ = Thermocouple, all temperature in degrees F°

Figure B.32-2.- Highest conduit temperature profile achieved.

B.33 CAPACITANCE PROBE SIGNAL CONDITIONER ENERGY TEST

B.33.1 OBJECTIVE

The objective of this test was to determine if the capacitance probe signal conditioner could provide sufficient energy in the cryogenic oxygen tank to cause ignition of any of the tank materials.

B.33.2 TEST EQUIPMENT AND CONDITIONS

Two different methods of conducting this test were completed. In addition, a mathematical analysis was made to determine the maximum spark energy available.

In the first method, the signal conditioner was placed in a vacuum environment and the lead wires that normally are connected to the capacitance probe were shorted for 9 hours with the signal conditioner energized. The open-circuit voltages and short-circuit currents were measured at the signal conditioner sensing leads prior to, during, and after the 9-hour shorting period.

In the second method, the signal conditioner was placed in a dark room, the unit energized, and the output leads were intermittently short circuited in an attempt to visually observe a spark.

B.33.3 RESULTS

The maximum open-circuit voltage measured from the signal conditioner sensing leads was a 400-cycle square wave at a potential of 160 vac peak-to-peak. In addition, there was no observable change in the signal conditioner after 9 hours of shorted signal lead operation.

During intermittent short-circuit operations in the dark room, no sparking was visible from the sensing leads. The approximate threshold of spark visibility is 0.03 millijoules.

The maximum calculated spark energy available at the sensing leads is 0.0875 millijoules.

B.33.4 CONCLUSIONS

Polytetrafluoroethylene insulation requires greater than 0.1 joule of energy for ignition. The maximum calculated energy available is in millijoules and no sparking was observed.

B.34 QUANTITY PROBE AND CONDUIT ASSEMBLY FLAMMABILITY PROPAGATION TEST

B.34.1 OBJECTIVES

The objectives of this test were:

a. Determine if burning wire insulation would propagate through the upper quantity probe insulator wire bundle penetrations

b. Determine the failure mode of the conduit resulting from propagation of the burning polytetrafluoroethylene insulation from the region of the quantity probe into the lower conduit.

B.34.2 TEST EQUIPMENT AND CONDITIONS

The chamber used for this test consisted of a schedule 80 weld-neck tee equipped with three flanges to provide a viewport, electrical and hard line feedthroughs and conduit to the quantity probe interface. The chamber (fig. 34-1), had a volume of approximately one-third cubic foot. A pressure relief valve was provided to maintain chamber pressure at 1050 psia during the test; and, in addition, the chamber contained a rupture disk to prevent chamber failure. Five thermocouple penetrations were provided through the chamber wall. Color motion pictures were taken through the chamber viewport at a speed of 24 frames a second. An additional camera provided external color motion pictures of the conduit-chamber interface.

The test item consisted of an upper portion of the quantity probe interfaced with a conduit assembly (fig. 34-2). The quantity probe used was Block I hardware modified to the Block II configuration and the wire was routed through it and the conduit assembly to represent the Apollo 13 configuration. Insulated wiring extended beyond the polytetrafluoroethylene insulator approximately 4 inches. This wiring was also routed through the conduit and connected to the feedthrough pins through which 400-hertz 115-volt power was supplied to both fan motor bundles. One of the fan motor bundles had a Nichrome ignitor installed on it.

Thermocouples were located as shown in figure 34-1.

After filling the chamber to 925 psia with gaseous oxygen, the chamber was cooled to minus 138° F. Power was applied to the ignitor until fusion occurred.

B.34.3 RESULTS

A pressure history of the chamber is shown in figure 34-3. The first relief valve opening occurred at approximately 28 seconds. It subsequently reopened 15 times before failure occurred.

Temperature histories of both the internal and external portions of the test apparatus are shown in figures 34-4 and 34-5.

The propagation observed in the motion picture coverage proceeded from the ignition site vertically downward. Burning progressed down the fan motor wire bundle, then began burning other wire bundles progressing to the polytetrafluoroethylene insulator. The fire became more subdued after the fire progressed deep into the upper probe region.

Figure 34-6 shows the conduit and chamber interface burnthrough scenes taken from the external movie photographic coverage. The small amount of external burning observed resulted from ignition of the Mylar film used to insulate the test chamber.

Visual observation of the failure of the conduit through a test cell window revealed that a flame front resulted as far away as three or four feet from the chamber.

After the test, the section of conduit was found approximately eight feet from the chamber. Several pieces of the polytetrafluoroethylene insulator, two pieces of the conduit swedgelock nut, and one piece of conduit tubing were gathered from a 20-foot radius around the test area. The only item remaining in the test chamber was a portion of the Inconel section of the capacitance probe (fig. 34-7). The stainless steel portion was completely gone and a portion of the Inconel was burned. No remains of the aluminum portion of the probe could be found. The conduit-chamber interface was torched out to a maximum diameter of 1-7/8 inches.

B.34.4 CONCLUSIONS

The results of this test show that the insulation burning on the electrical conductors did propagate through the probe insulator even in downward burning and did proceed into the conduit. It is difficult to determine if the insulator was ignited and what time was required for the burning had proceeded to the insulator-wire bundle interface. After the initial failure of the conduit, the contents of the tank (1/3 cubic foot) were vented in approximately 0.5 second with a major portion of the burning of metal occurring in 0.25 second. Venting of larger amounts of oxygen would not necessarily take longer since continued oxygen flow should produce considerably larger "torched out" sections. In order to produce the heat necessary for the effects observed here, metal burning must have occurred.

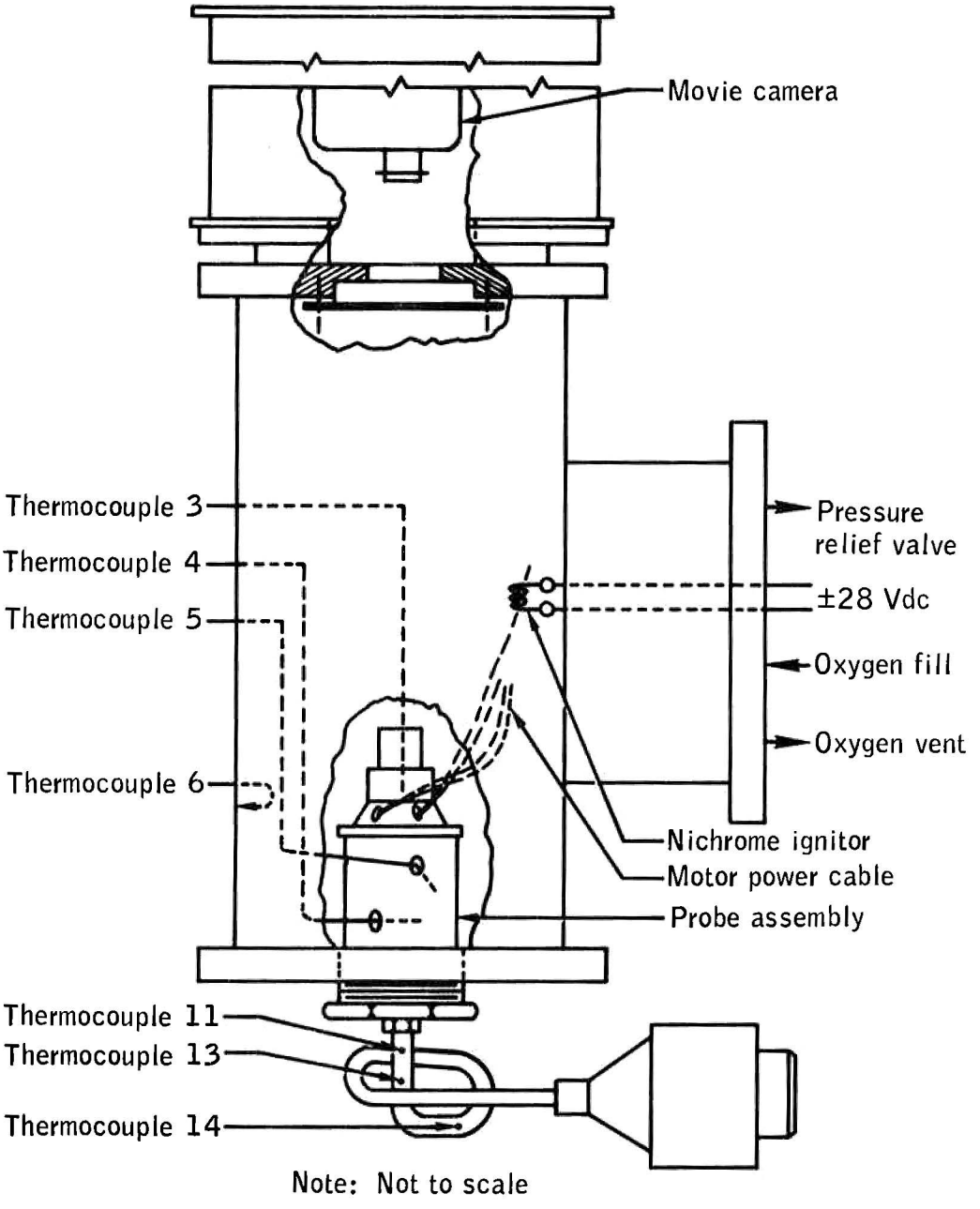

Figure B.34-1.- Quantity probe and conduit assembly apparatus.

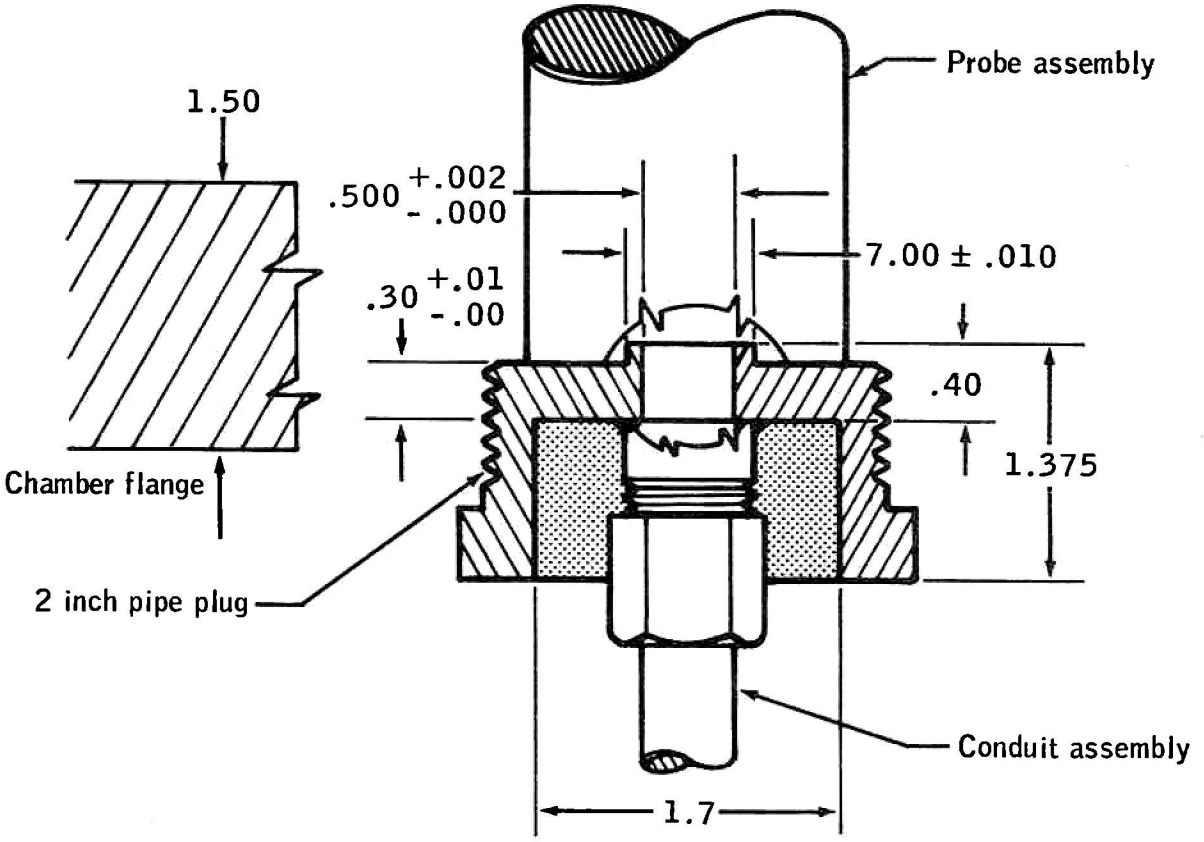

Figure B.34-2.- Upper quantity probe - conduit interface.

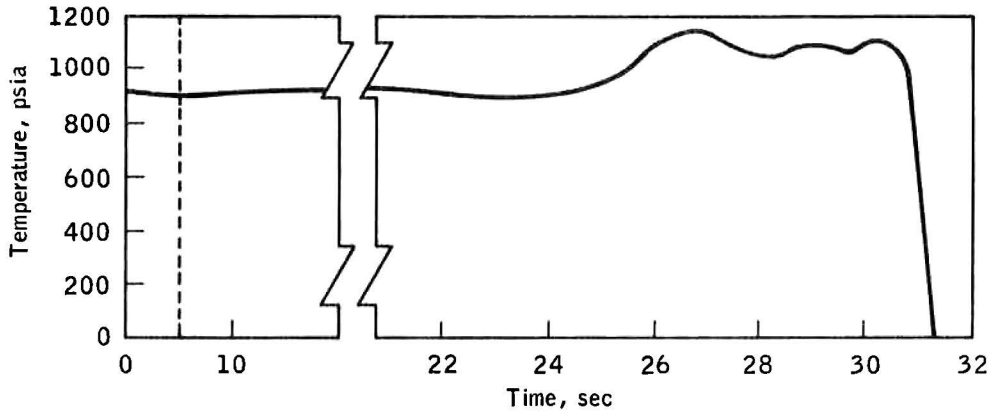

Figure B.34-3.- Quantity probe and conduit assembly test pressure history.

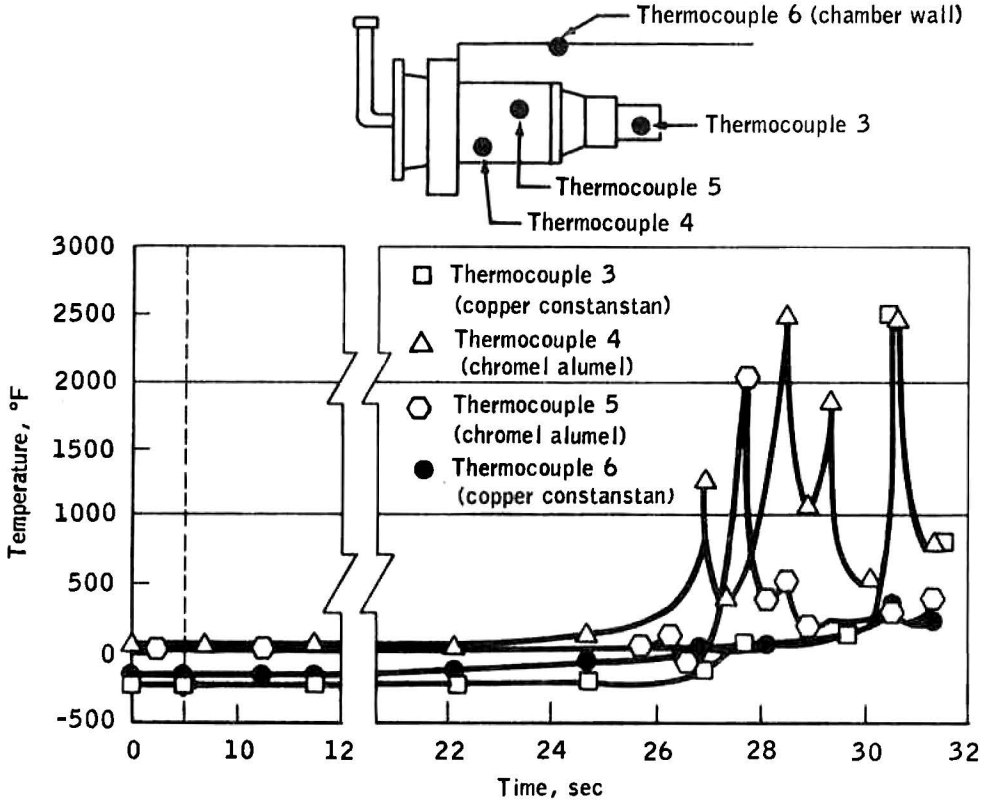

Figure B.34-4.- Temperature history of quantity probe and chamber wall.

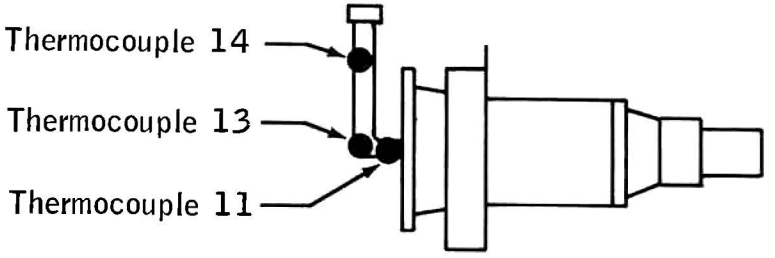

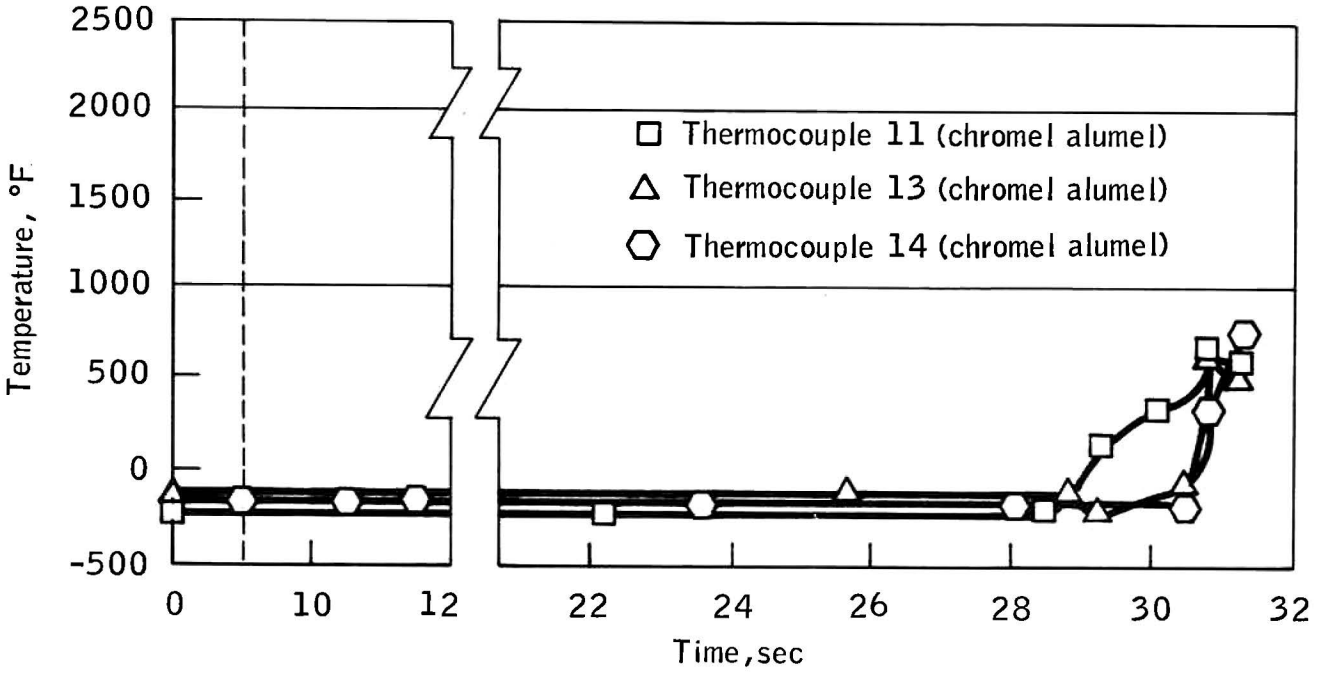

Figure B.34-5.- Temperature history of conduit.

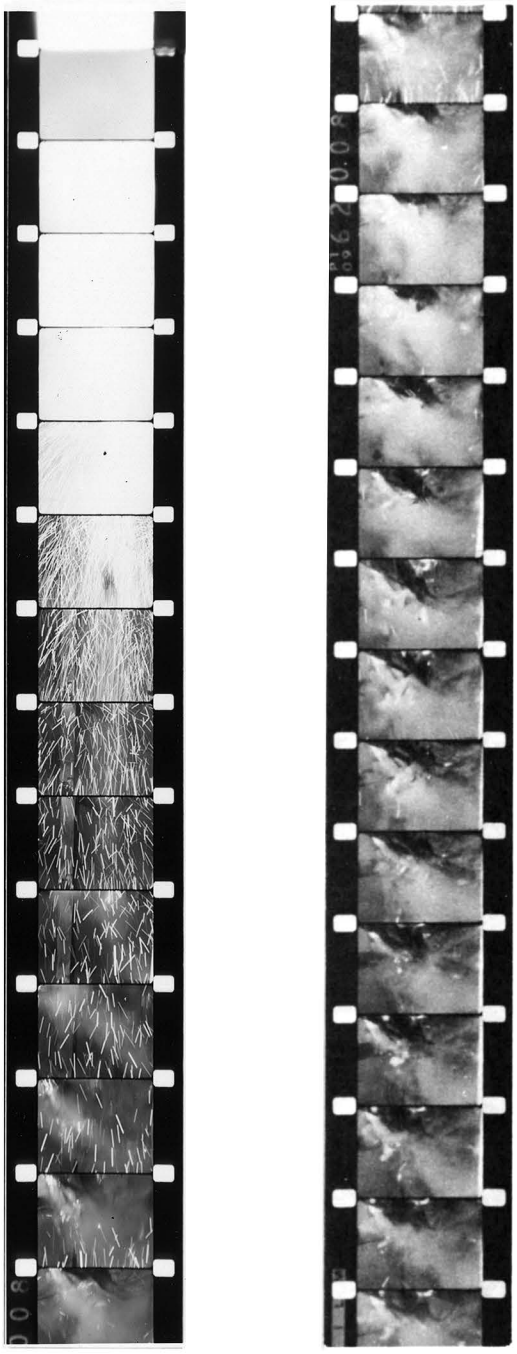

Figure B.34-6.- External views of chamber-conduit interface at time of failure.

Figure B.34-7.- Portion of probe which remained in the test chamber.

B.35 WIRE INSULATION PROPAGATION-RATE TEST

B.35.1 OBJECTIVE

The objective of this test series was to determine the downward and upward limits of propagation rates for the various wire configurations used in cryogenic oxygen tank 2 operating conditions.

B.35.2 TEST EQUIPMENT AND CONDITIONS

Both downward and upward propagation rates were measured for each of the individual wires used in cryogenic oxygen tank 2. In addition, separate tests were conducted on specific wire bundles and on the poly-tetrafluoroethylene used as an insulator in the probe assembly.

The ignitions were conducted in a reactive vessel (1.75-inch inside diameter by 6-inch long) equipped with a burst disk (3500-psig burst pressure); oxygen purge, fill, and vent lines; thermocouple and igniter power feedthroughs; and a pressure transducer (fig. B.35-1). Tests were conducted under ambient conditions and also at minus 170° (±10°) F and 940 (±20) psig.

The configurations for determining the upward and downward burning rate are shown in figure B.35-2. The wires used to hold the sample in contact with the thermocouples were placed in such a manner as not to interfere with the propagation. The propagation rate was determined from the time required for the flame to propagate the distance between thermocouples. Two propagation rate measurements were obtained during each test.

B.35.3 RESULTS

Propagation rate results for each of the wires and insulations used in cryogenic oxygen tank 2 are shown in table B.35-I. Photographs of selected residues are shown in figures B.35-3 through B.35-8. Propagation rates for selected wires were determined in several tests to investigate the reproducability of the data. The results of these repeated tests indicate that the downward rates are reproducible to ±0.1 in./sec. The upward burning rates are difficult to reproduce under test conditions and should be considered as representing the upper range.

TABLE B.35-I.- WIRE PROPAGATION RATE TEST

(a) Downward at ambient temperature

Test No.	Test Article		Cable	Test Pressure, (psig)	Propagation Rate			Discussion
	Color	Gauge AWG			1 (in/sec)	2 (in/sec)	Avg. (in/sec)	
1	white	26	Wh-B-Bl-R	980	-	-		Insulation burned. Temperature rise on CTR and lower T/C's insignificant. See Test #57.
2	black	26	Wh-B-Bl-R	970	-	-	-	Wire burned through and fell. Data not available.
3	blue	26	Wh-B-Bl-R	985	1.00	0.40	0.70	Insulation burned.
4	red	26	Wh-B-Bl-R	980	0.47	0.35	0.41	Insulation burned.
5	orange	22	O-Y-G-B	980	2.5	0.34	1.42	Insulation burned. Repeated in Test 55.
6	yellow	22	O-Y-G-B	980	0.46	0.50	0.48	
7	black	22	O-Y-G-B	920	0.41	0.43	0.42	
8	green	22	O-Y-G-B	955	0.47	0.35	0.41	
9	violet	20	W-V	940	0.68	0.43	0.56	
10	white	20	W-V	960	0.49	0.54	0.52	
11	red	20	coaxial	950	0.70	1.07	0.88	Burned #2 T/C away (ΔP = 200 psig)
12	transparent	20	coaxial	980	0.36	0.42	0.39	Tested several times to determine reproducability of data.

TABLE B.35-I.- WIRE PROPAGATION RATE TEST - Continued

(b) Downward at ambient temperature

Test No.	Test Article		Cable	Test Pressure (psig)	Propagation Rate			Discussion
	Color	Gauge AWG			1 (in/sec)	2 (in/sec)	Avg. (in/sec)	
30	transparent	20	coaxial		-	-	-	No data. Void run.
31	transparent	20	coaxial	970	0.43	0.33	0.38	
32	transparent	20	coaxial	960	0.42	0.38	0.40	
33	transparent	20	coaxial	980	0.40	0.41	0.41	
34	transparent	20	coaxial	935	0.33	0.38	0.35	
39	transparent	20	coaxial	967	0.54	0.71	0.62	
40	transparent	20	coaxial	970	1.00	0.68	0.84	
41	red	20	coaxial	950	0.75	0.94	0.85	
42	red	20	coaxial	960	0.86	0.79	0.825	Partially burned shield.
55	orange	22	O-Y-G-B	970	0.41	0.38	0.39	
57	white	26	R-W-Bl-B	975	0.77	0.64	0.71	

TABLE B.35-I.- WIRE PROPAGATION RATE TEST - Continued

(c) Upward at ambient temperature

Test No.	Test Article		Cable	Test Pressure (psig)	Propagation Rate			Discussion
	Color	Gauge AWG			1 (in/sec)	2 (in/sec)	Avg. (in/sec)	
13	yellow	22	Y-O-G-B	925	2.50	1.88	2.19	Did not fuse igniter.
14	black	22	Y-O-G-B	985	2.00	4.29	3.14	
15	orange	22	Y-O-G-B	980	-	-	-	Data unreadable.
16	orange	22	Y-O-G-B	980	6.25	12.5	9.38	
17	black	26	R-B-Bl-Wh	930	3.12	-	-	T/C #1 data lost.
18	white	26	Bl-B-R-Wh	980	5.00	2.14	3.57	
19	red	26	Bl-B-R-Wh	975	7.5	3.75	5.62	
20	green	22	Y-O-G-B	960	1.67	3.00	2.33	
21	violet	20	W-V	965	3.33	7.5	5.42	
22	white	20	W-V	950	15.00	7.5	11.25	
23	transparent	20	coaxial	960	10.00	7.50	8.75	Several tests of this item conducted to determine reproducability of data.
24	transparent	20	coaxial	960	4.28	15.00	9.64	
35	transparent	20	coaxial	975	5.00	15.00	10.00	
36	transparent	20	coaxial	975	4.41	7.50	5.96	
37	transparent	20	coaxial	960	3.75	10.00	6.88	

TABLE B.35-I.- WIRE PROPAGATION RATE TEST - Continued

(d) Upward at ambient temperature

Test No.	Test Article		Cable	Test Pressure (psig)	Propagation Rate			Discussion
	Color	Gauge AWG			1 (in/sec)	2 (in/sec)	Avg. (in/sec)	
38	transparent	20	coaxial	970	5.00	8.82	6.91	
43	red	20	coaxial	965	3.00	-	-	
44	red	20	coaxial	960	5.36	4.69	5.03	Partially burned shield.
45	red	20	coaxial	960	4.84	2.21	3.53	Partially burned shield on igniter end.
46	red	20	coaxial	950	6.52	1.85	4.19	Partially burned shield on igniter end.
54	blue	26	980	3.57	7.50	5.50		

TABLE B.35-I.- WIRE PROPAGATION RATE TEST - Continued

(e) Downward at cryogenic temperatures

Test No.	Test Article		Cable	Test Conditions		Propagation Rate			Discussion
	Color	Gauge AWG		Pressure (psig)	Temp. (°F)	1 (in/sec)	2 (in/sec)	Avg. (in/sec)	
25	yellow	22	O-G-B-Y	970	-150	0.22	0.20	0.21	
26	black	22	O-G-B-Y	970	-159	0.21	0.21	0.21	
27	transparent	20	coaxial	950	-164	0.22	0.20	0.21	
28	orange	22	O-G-B-Y	1025	-171	0.24	0.23	0.24	
29	green	22	O-G-B-Y	1050	-200	0.26	0.23	0.25	
47	red	20	coaxial	910	-165	0.39	-	-	Partially burned shield on igniter end.
56	red	20	coaxial	975	-170	0.47	0.34	0.40	
58	white	26	R-W-Bl-B	970	-190	0.37	0.46	0.41	4 conductor in white shrink tubing.
59	clear	26	R-W-Bl-B	975	-172	0.30	0.40	0.35	4 conductor in clear shrink tubing.
63	violet/ white	20	V-W	950	-158	0.29	0.31	0.30	
64	brown/ white	20	B-W	940	-155	0.36	0.36	0.36	
65	brown	20	brown	950	-160	0.33	0.33	0.33	

TABLE B.35-I.- WIRE PROPAGATION RATE TEST - Continued

(f) Downward at cryogenic temperatures

Test No.	Test Article		Cable	Test Conditions		Propagation Rate			Discussion
	Color	Gauge AWG		Pressure (psig)	Temp. (°F)	1 (in/sec)	2 (in/sec)	Avg. (in/sec)	
66	violet	20	violet	950	-160	0.27	0.25	0.26	
73	vlack	26	R-W-Bl-B	950	-170	0.26	0.22	0.24	
74	red	26	R-W-B;-B	950	-170	0.24	0.26	0.25	
75	white	26	R-W-Bl-B	975	-175	0.21	0.21	0.21	
76	blue	26	R-W-Bl-B	980	-158	0.24	0.23	0.24	

TABLE B.35-I.- WIRE PROPAGATION RATE TEST - Continued

(g) Upward at cryogenic temperatures

Test No.	Test Article		Cable	Test Conditions		Propagation Rate			Discussion
	Color	Gauge AWG		Pressure (psig)	Temp. (°F)	1 (in/sec)	2 (in/sec)	Avg. (in/sec)	
48	yellow	22	G-B-Y-O	950	-170	6.00	2.50	4.25	
49	orange	22	G-B-Y-O	960	-155	1.88	3.75	2.82	
50	black	22	G-B-Y-O	960	-170	6.00	4.29	5.15	
51	green	22	G-B-Y-O	960	-165	1.36	7.50	4.43	
52	clear	20	coaxial	940	-170	4.29	3.33	3.81	
53	clear	20	coaxial	950	-170	3.75	2.14	2.95	
60	clear	26	R-W-Bl-B	940	-175	2.5	2.0	2.25	4 conductor in clear shrink tubing.
67	violet	20	violet	940	-155	1.11	1.25	1.18	
68	brown	20	brown	940	-156	1.20	1.30	1.25	
69	white/ violet	20	W-V	950	-170	3.0	2.5	2.75	
70	white/ brown	20	W-B	950	-170	2.73	3.75	3.24	
71	white/ brown	20	W-B	950	-170	1.00	2.31	1.66	Repeat of Test 70.
72	white/ violet	20	W-V	950	-170	1.25	-	1.25	Repeat of Test 69.

TABLE B.35-I.- WIRE PROPAGATION RATE TEST - Concluded

(h) Special material downward propagation rate tests at cryogenic temperatures

Test No.	Test Article		Cable	Test Conditions		Propagation Rate			Discussion
	Size	Weight (gms.)		Pressure (psig)	Temp. (°F)	1 (in/sec)	2 (in/sec)	Avg. (in/sec)	
61	1/4" x 1 9/16"	0.93	Quality Probe Material 25% Filled Teflon	980	-168	0.094	-	0.094	
62		0.93	Simulated Quantity Probe Material Teflon Only	1000	-162	0.37	-	0.37	Plain teflon strip.
77	1/4" x 1 9/16"	1.5	Quantity Probe Material 25% Filled Teflon	965	-159	0.12	-	0.12	
78	1/4" x 1 9/16"	1.5	Quantity Probe Material 25% Filled Teflon	960	-160	0.17	-	0.17	

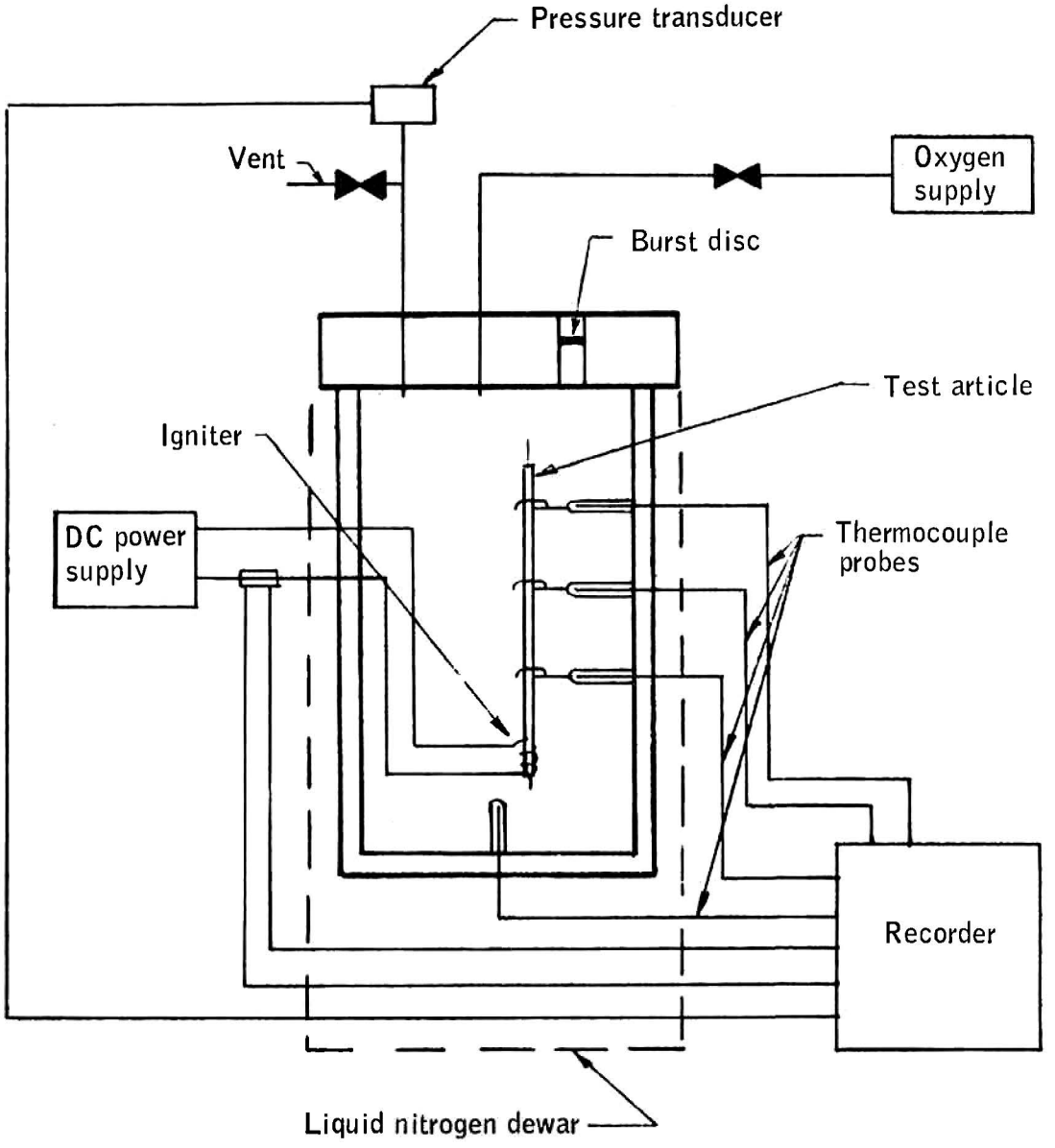

Figure B.35-1.- Schematic of propagation rate test chamber.

Initial chamber conditions:
Pressure, 925 to 1125 psig
Temperature, 148 to -210° F

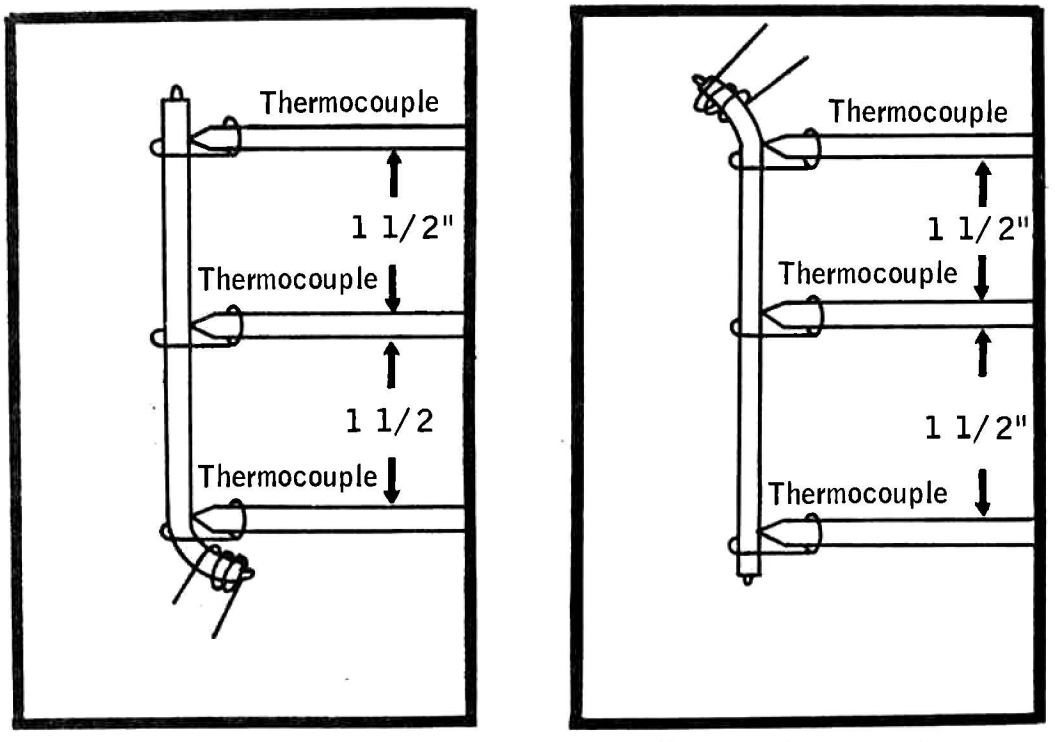

Upward propagation

Downward propagation

Figure B.35-2.- Propagation rate test setup.

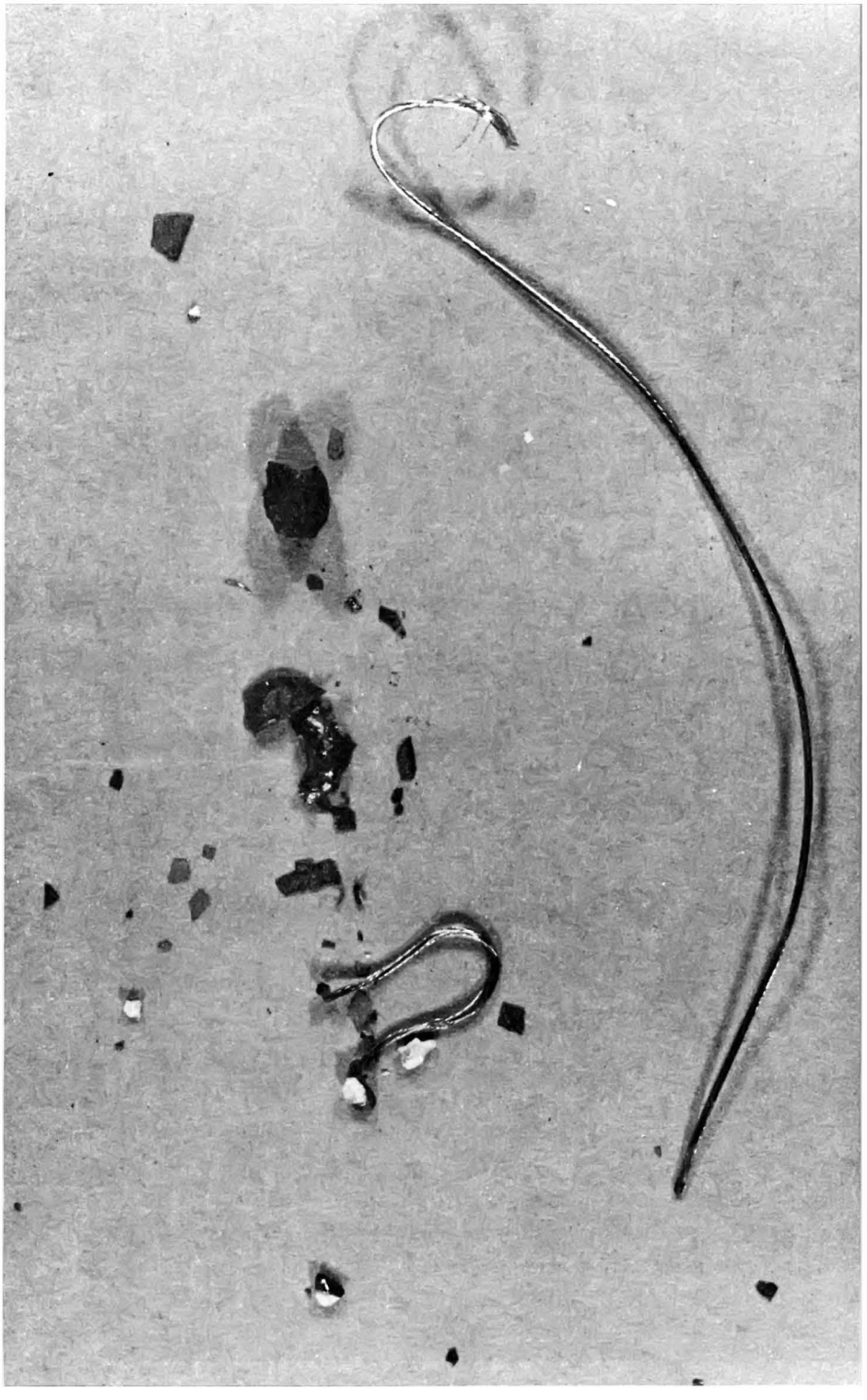

Figure B.35-3.- White wire from brown, white, blue, and red cable.

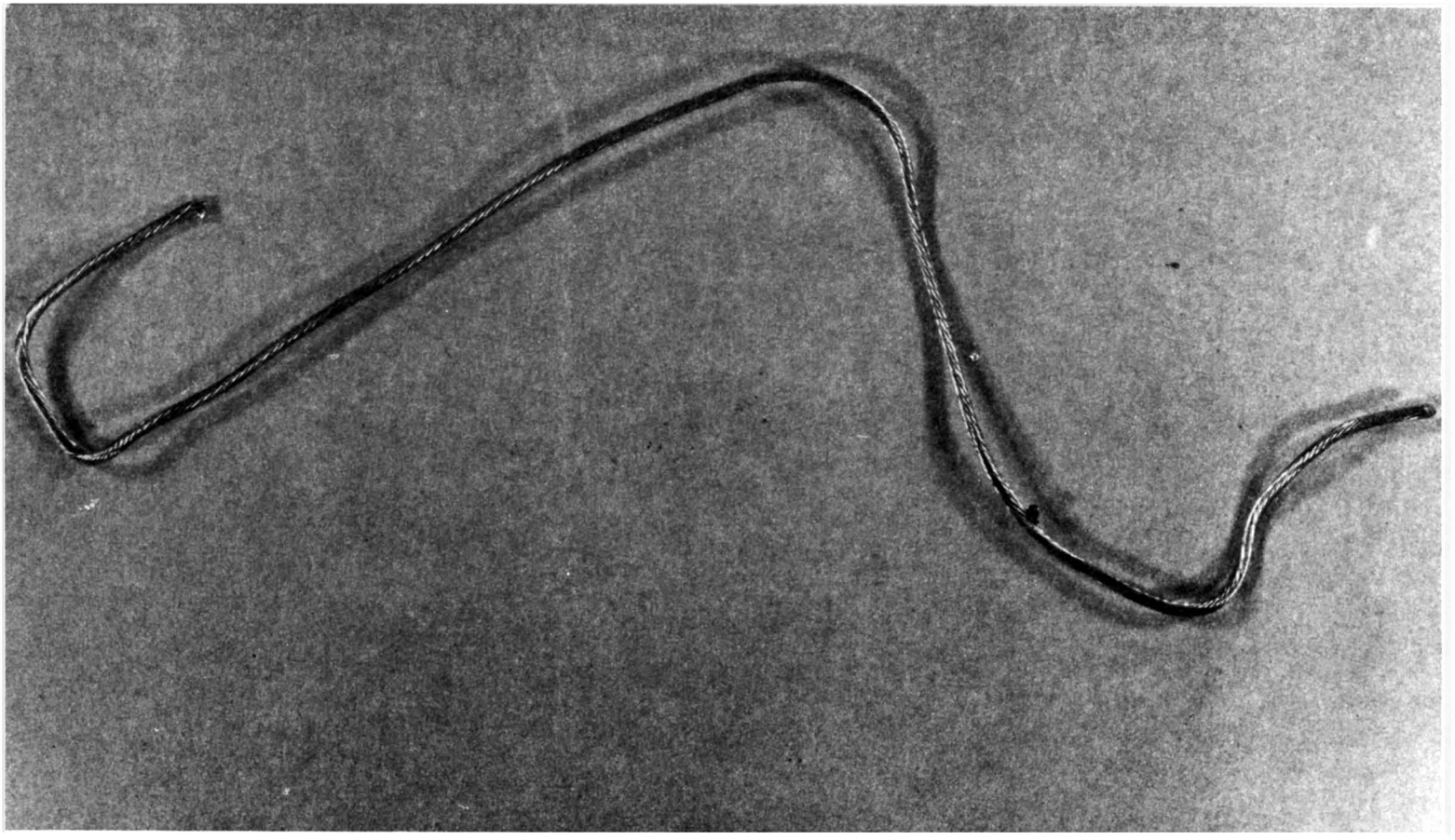

Figure B.35-4.- Orange wire from orange, yellow, green, and brown cable.

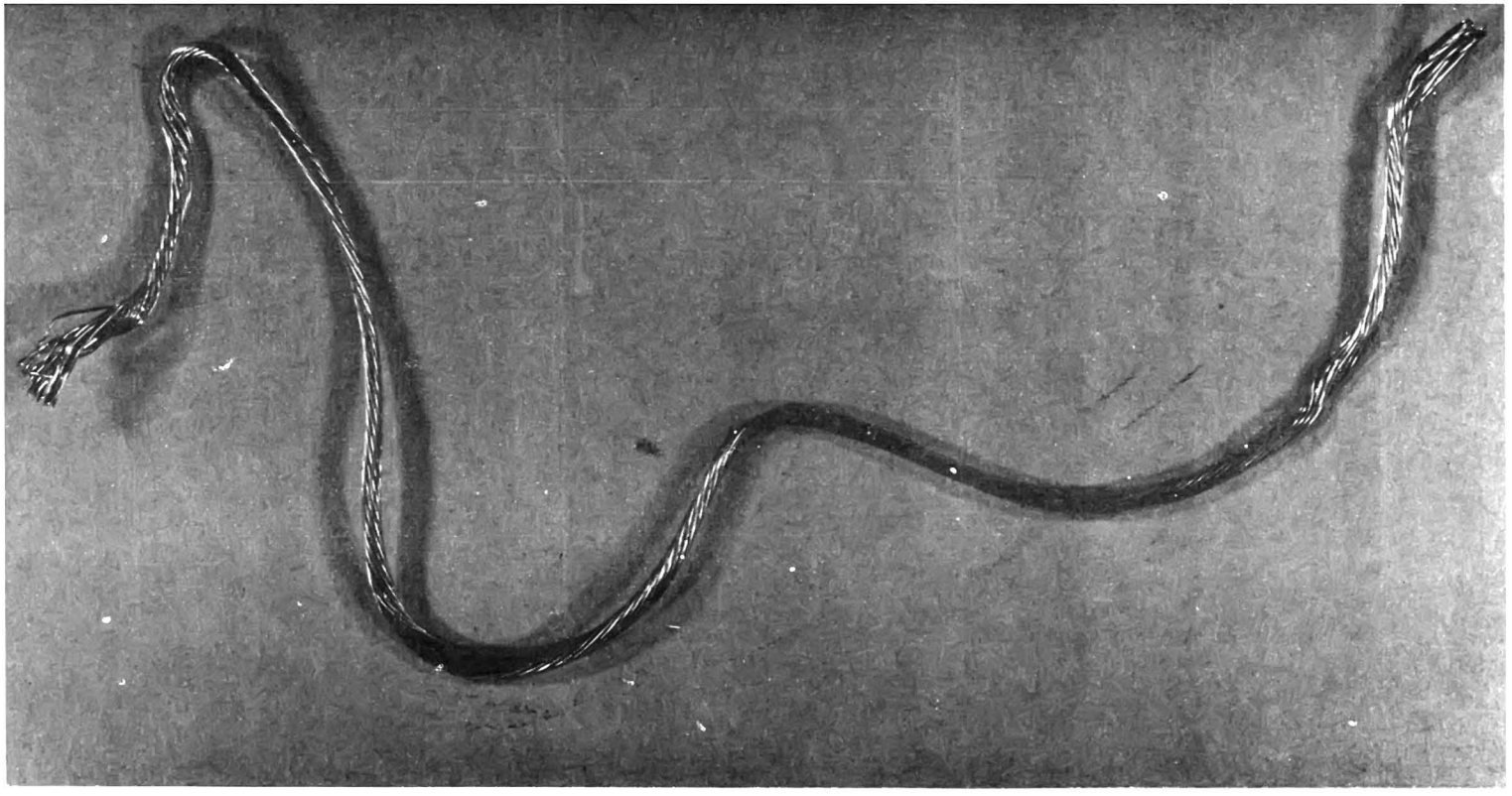

Figure B.35-5.- Violet wire from a violet and white cable.

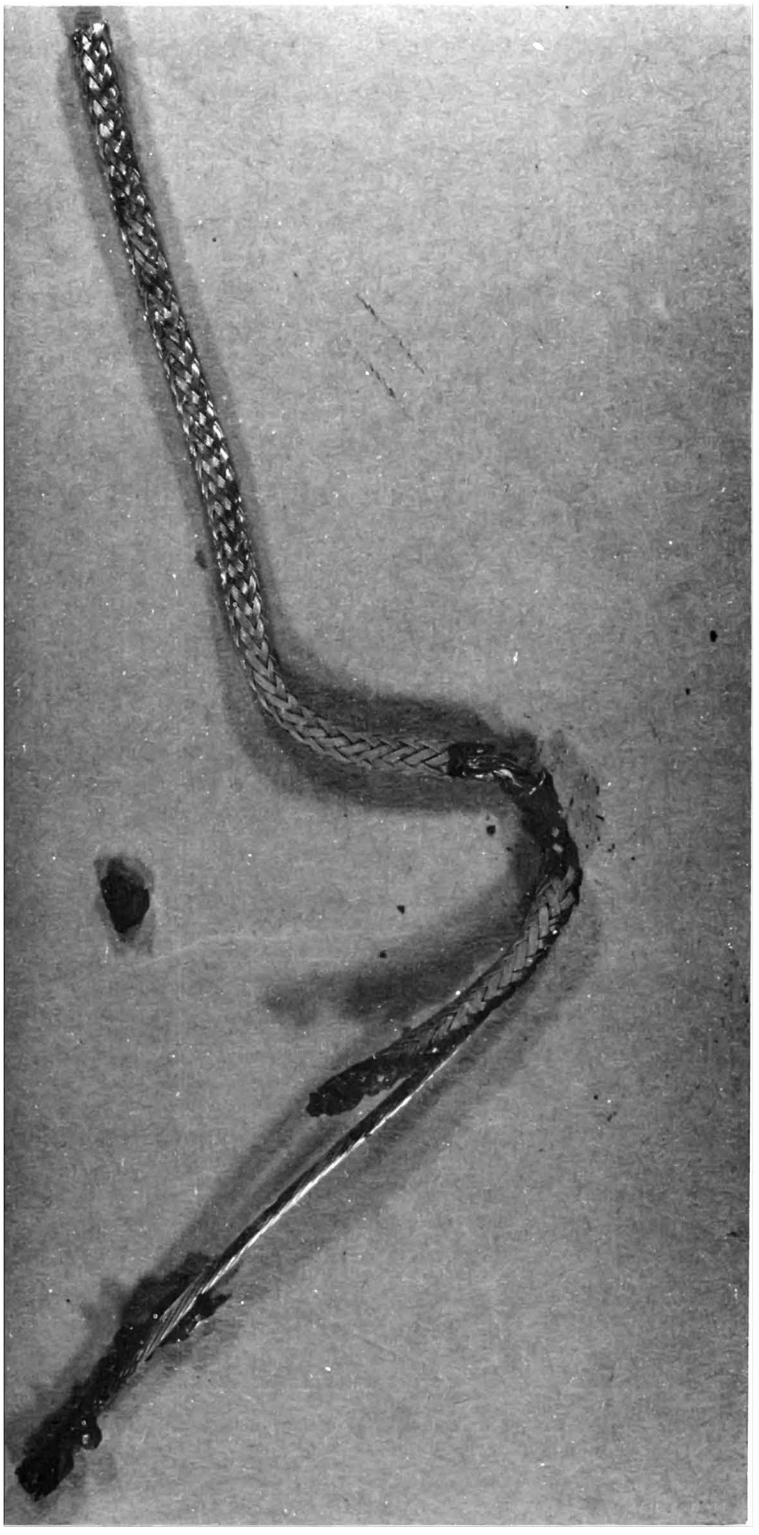

Figure B.35-6.- Red wire from a red and clear coaxial cable.

Figure B.35-7.- Four conductor wire in white tubing.

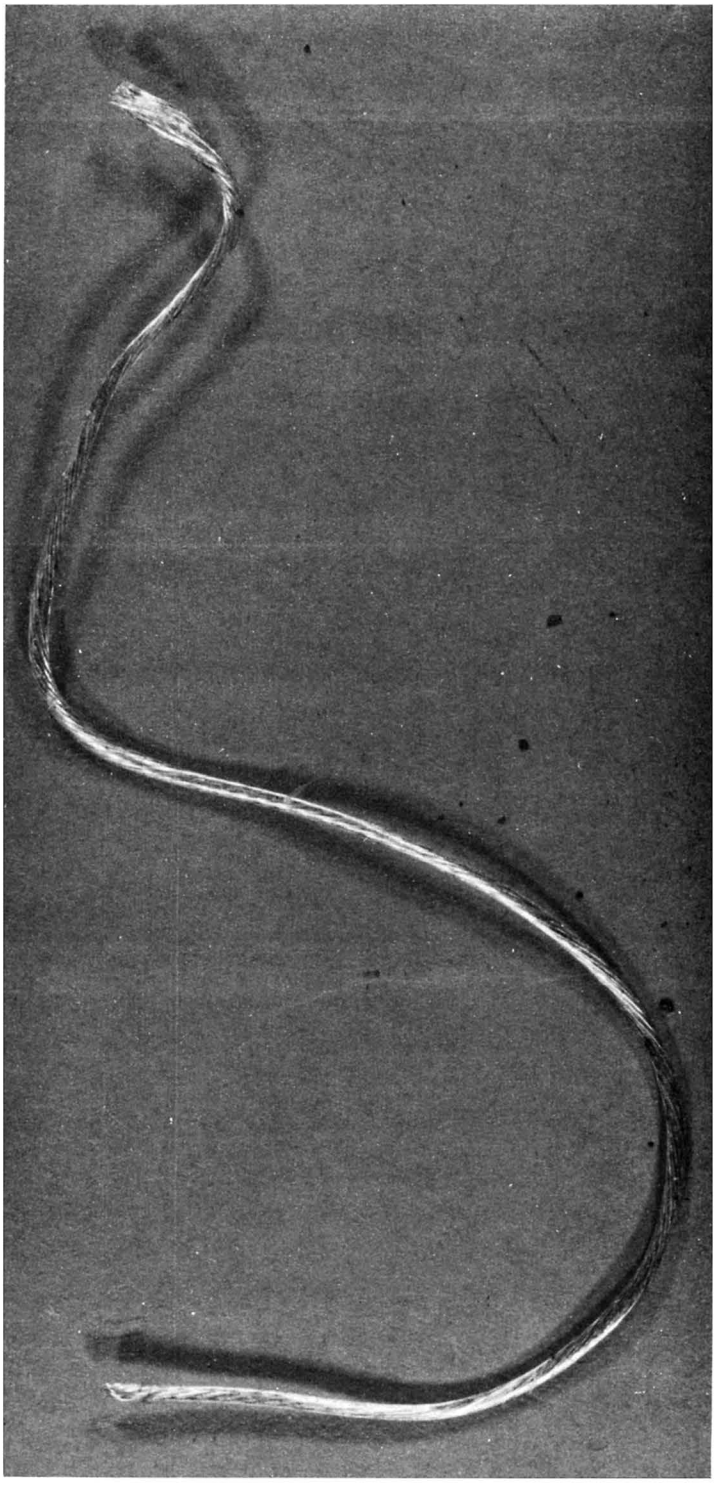

Figure B.35-8.- Brown wire from a brown-brown/white-violet-violet/white cable.

B.36 HEAT OF COMBUSTION OF POLYTETRAFLUOROETHYLENE, MYLAR, ALUMINIZED MYLAR, AND ALUMINIZED KAPTON SAMPLES TEST

B.36.1 OBJECTIVE

The objective of this test was to determine the heat of combustion of samples of polytetrafluoroethylene, Mylar, aluminized Mylar, and aluminized Kapton.

B.36.2 TEST PROCEDURES AND CONDITIONS

The tests were made using a Parr series 1200 adiabatic oxygen bomb calorimeter apparatus with a Parr 1101 double-valve bomb for combustion. The method is considered a standard for heat of combustion measurements over a broad range of combustible materials. Briefly, the method involves the ignition of samples up to 1.5 grams in a pure oxygen atmosphere pressure and the subsequent measurement of heat units liberated. The ignition source used was a 34 gage (AWG) Nichrome wire, 10 centimeters long, electrically heated, and partly consumed in the combustion. The ignition of the materials in the oxygen bomb is rapid, less than 0.2 second.

B.36.3 RESULTS

The results of the analyses are as follows:

	Heat of combustion, Btu/lb			
Sample	Test 1	Test 2	Test 3	Average
Mylar, no coating, 0.25 mil	9853	9857	9842	9851
Mylar, single aluminized, 0.25 mil	9840	9843	9882	9885
Mylar, double aluminized, 0.25 mil	9873	9869	9833	9859
Polytetrafluoroethylene	2180	2194	-	2187
Kapton, single aluminized, 0.5 mil	10 715	10 676	10 714	10 701

B.36.4 CONCLUSIONS

The results of the analyses show no significant differences in heat of combustion values obtained for Mylar and aluminized Mylar materials. Since the thickness of the aluminimum coating is approximately 1000 to 1200 Angstroms, the contribution to the heat of combustion values would be minimal. The aluminized Kapton material yielded heat of combustion values of about 900 Btu/lb higher than those for the Mylar samples. The results obtained for polytetrafluoroethylene showed heat of combustion values of approximately one-fourth those obtained for the Mylar.

The test data show that Mylar and Kapton yield relatively high heat of combustion values, comparable to the heat of combustion of methyl alcohol (9759 Btu/lb).

B.37 PRODUCTS OF COMBUSTION OF POLYTETRAFLUOROETHYLENE IN OXYGEN

B.37.1 OBJECTIVE

The objective of this test was to determine the principal products of combustion of polytetrafluoroethylene in oxygen.

B.37.2 TEST EQUIPMENT AND CONDITIONS

Samples of polytetrafluoroethylene were burned in one atmosphere of oxygen and in 20 atmospheres of oxygen plus aluminum powder and analyses of the residue were made using a mass spectrometer and a gas analyses.

B.37.3 RESULTS

The analyses identified the following compounds at the indicated relative concentration.

Possible species	One atmosphere, oxygen	Twenty atmospheres, oxygen plus aluminum
CF_3	100	100
CF	16.1	4.3
C_2F_5	13.6	--
CF_2	5.1	10.6
C_2F_4	.5	--
COF_2	.3	--
C_2F_2O	.3	1.7

B.38 FLOW REACTOR TEST

B.38.1 OBJECTIVE

The objective of this test is to determine the effect of flowing oxygen over a heated polymer.

B.38.2 TEST PROCEDURE

This test was performed by flowing gaseous oxygen through a heated flow reactor filled with polytetrafluoroethylene shavings.

B.38.3 RESULTS

The initial stages of degradation follows a first order equation, $K = 6.3 \times 10^{18} e^{-78000/RT}$ second. The temperature at which spontaneous ignition occurs is 500° C.

B.39 FLAME SPREADING STUDIES OF POLYTETRAFLUOROETHYLENE INSULATED WIRE

B.39.1 OBJECTIVE

The objective of this test was to determine the effect of a zero-gravity environment on the burning characteristics of polytetrafluoroethylene-insulated wire.

B.39.2 TEST EQUIPMENT AND CONDITIONS

The tests were conducted in an oxygen environment of 920 (±20) psia and minus 180° (±10°) F. The experimental apparatus was installed on a standard drop test vehicle (figs. B.39-1 and B.39-2) capable of providing the necessary supporting functions. The basic components of the experimental apparatus were the combustion chamber with a sapphire window to permit high-speed photography and an expansion tank as a safety feature in the event of an excessive pressure rise. The apparatus was equipped with a fill and vent system, pressure relief system, and liquid nitrogen cooling coils. The test specimen was installed in the combustion chamber in a horizontal position (fig. B.39-3), and ignition was caused by heating a 26-gage Nichrome wire wrapped around the specimen. The chamber pressure and temperature were monitored throughout the test. High-speed (400 frames per second) photographic data were obtained using a register pin Milliken camera with Ektachrome MS 2256 (Estar Base) film. Standard film processing was used.

A total of eight tests were conducted on three test specimens. Each specimen was tested in a one-gravity and a zero-gravity environment, and a one-gravity and a zero-gravity test were repeated on two specimens to examine repeatability of the data. The three specimens were:

a. Type 1 - Fan motor conductor bundle - four wires and white sleeving

b. Type 2 - Fan motor conductor bundle - four wires and clear shrink sleeving

c. Type 3 - Aluminum polytetrafluoroethylene feedthrough assembly - four wires and no sleeving.

B.39.3 RESULTS

A brief summary of the results is presented in table B.39-I.

B.39.4 CONCLUSIONS

The major conclusion from this study is that the flame spread rate in zero gravity is less than that observed in one gravity.

TABLE B.39-I.- SUMMARY OF RESULTS

Run number	Test specimen	Gravity level	Average flame spread rate - cm/sec	Comments
A-1-1 A-1-2 A-1-6	Type 1 Type 2 Type 1	One One One	1.4 1.4 1.4	The specimens burned vigorously. The flame progressed along the specimens in a pulsating fashion.
A-1-3 A-1-5 A-1-7	Type 2 Type 1 Type 2	Zero Zero Zero	.4 .3 .8	The specimens burned in zero gravity but not as vigorously as in normal gravity. The flame pulsated along the specimens in a similar way as in normal gravity but at a slower overall rate.
A-1-8	Type 3	One	-	The flame propagated through the aluminum holder but did not ignite it.
A-1-4	Type 3	Zero	-	The flame could not be clearly defined on the film. The aluminum holder did not ignite.

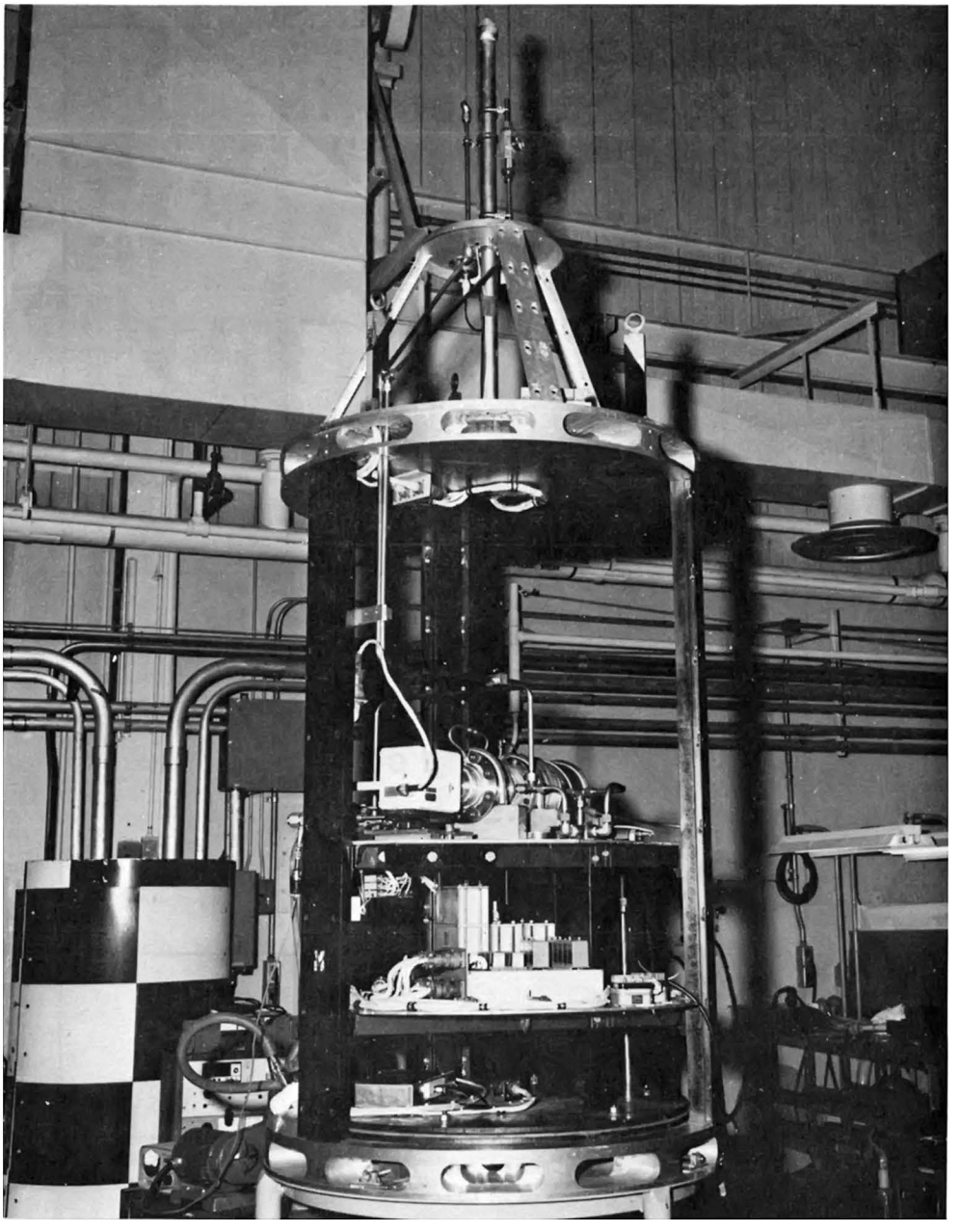

Figure B.39-1.- Five-second drop vehicle.

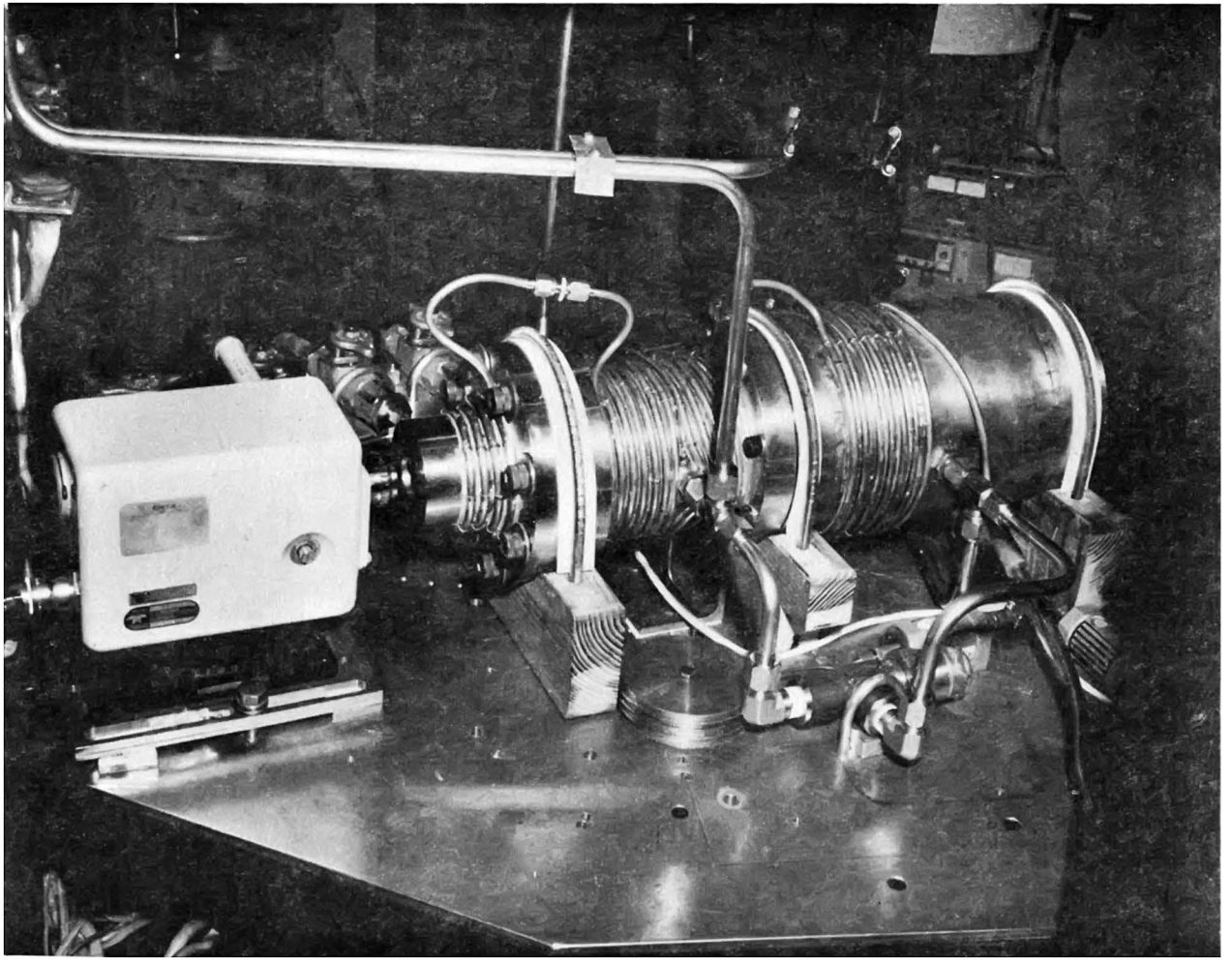

Figure B.39-2.- Experimental combustion apparatus.

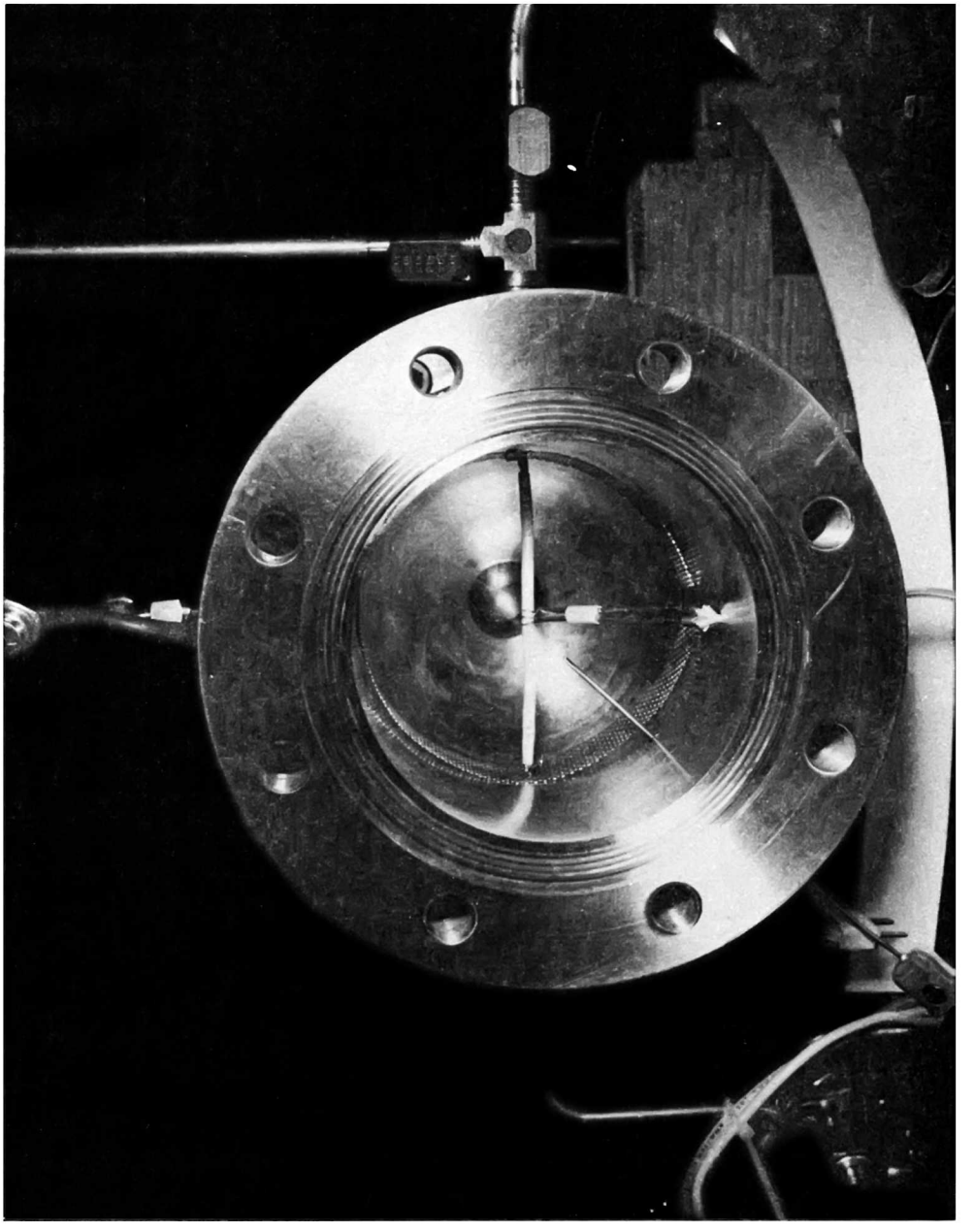

Figure B.39-3.- Typical test specimen installation in combustion chamber.

B.40 CRYOGENIC OXYGEN TANK BLOWDOWN TESTS

B.40.1 OBJECTIVE

The objective of this test was to determine the temperature, pressure, and density profile during sudden venting of cryogenic oxygen tank. Three individual tests were conducted, one each through the fill, vent, and feed lines.

B.40.2 TEST EQUIPMENT AND CONDITIONS

For each test, the tank was loaded with liquid oxygen to approximately 78 percent, pressurized with ground support equipment heaters to 900 psia, and allowed to stabilize at normal heat leak flow rate for a minimum of 10 hours prior to the following venting tests:

a. With the fill line and vent line valves closed, the feed line valve was placed in the full open position, and the internal tank pressure and temperature were recorded until pressure was depleted (fig. B.40-1).

b. The vessel was refilled with liquid oxygen, the fill line valve was fully opened, and the internal tank temperature and pressure were recorded until pressure was depleted (fig. B.40-2).

c. The vessel was refilled with liquid oxygen, the vent line valve was fully opened, and the internal tank pressure and temperature were recorded until pressure was depleted (fig. B.40-3).

B.40.3 RESULTS

None of the tests resulted in any abnormal pressure surges of unexpected depletion rates. The feed line blowdown depleted the tank to 65 percent quantity; the fill line blowdown to 0.43 percent, and the vent line blowdown to 38 percent.

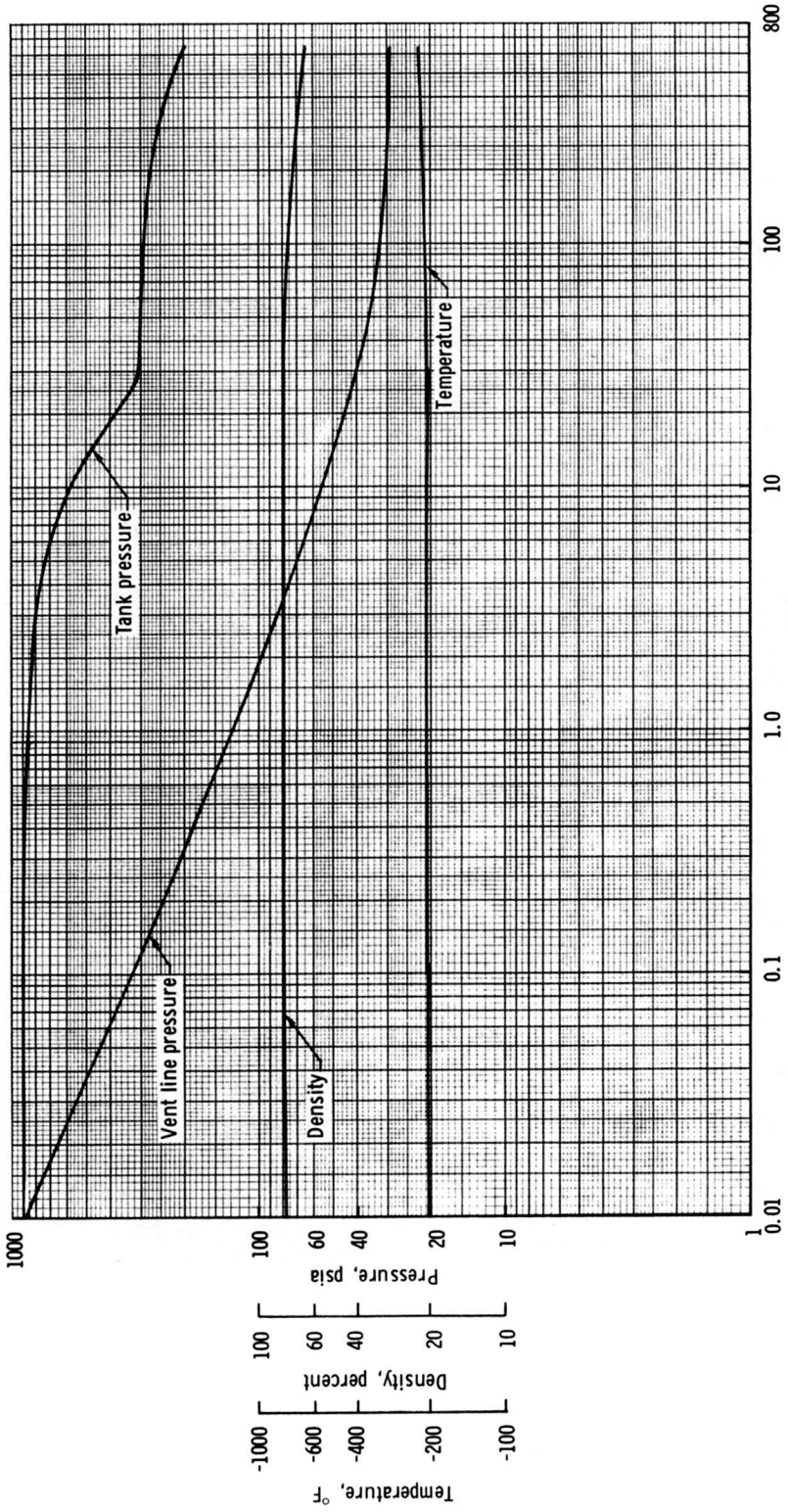

Figure B.40-1. - Tank pressure, temperature and quantity during feed line blowdown test.

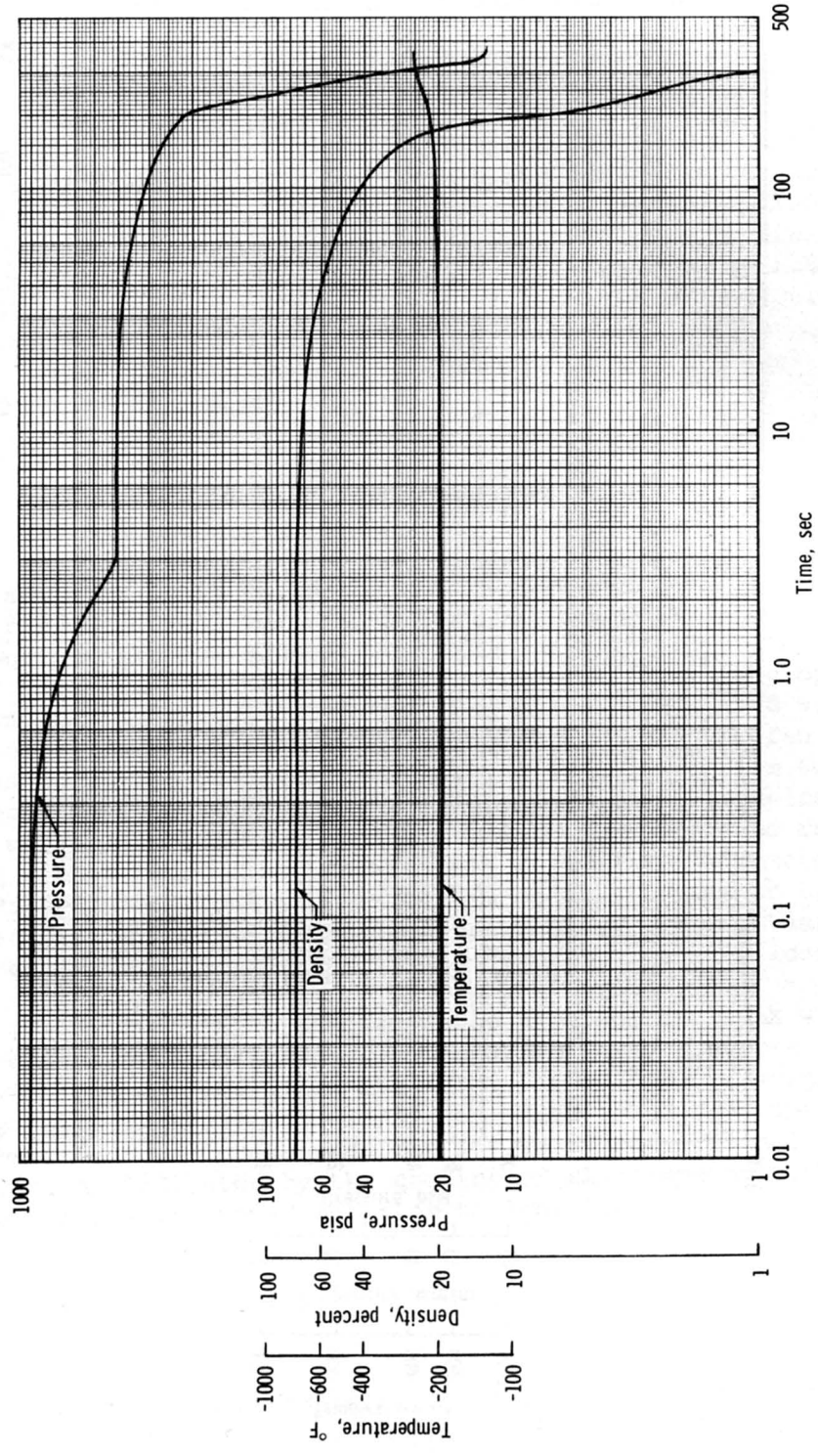

Figure B.40-2. - Tank pressure, temperature and quantity during fill line blowdown test.

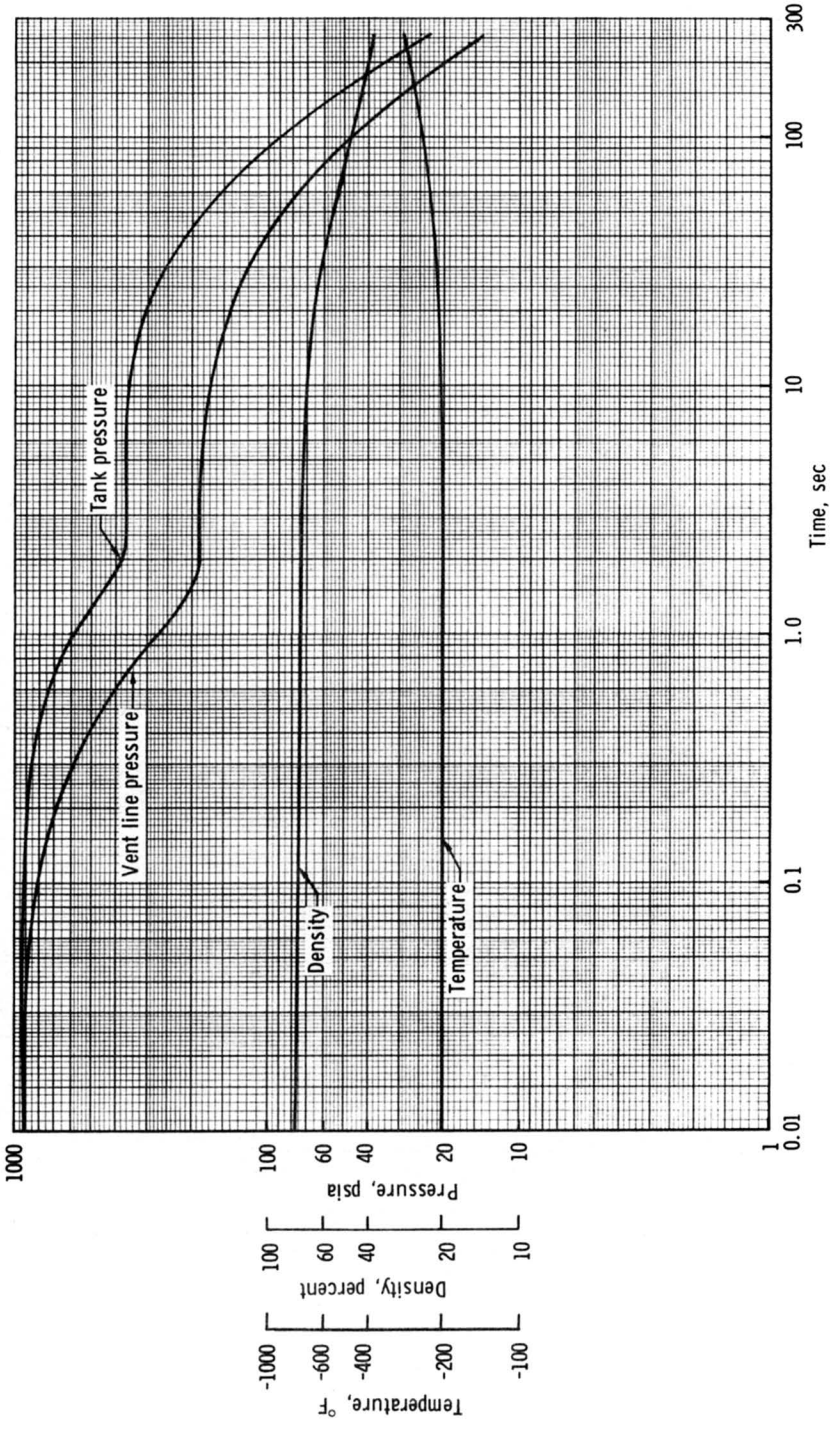

Figure B.40-3. - Tank pressure, temperature and quantity during vent line blowdown test.

B.41 ALL-UP CRYOGENIC OXYGEN STORAGE SYSTEM

B.41.1 OBJECTIVE

The primary objective of this test was to determine the pressure and temperature time history of the combustion of polytetrafluoroethylene wire insulation and the extent of propagation to other materials when the wire insulation was forcibly ignited near the lower fan motor in a flight configured cryogenic oxygen tank. The secondary objective was to measure the performance characteristics of the oxygen system components, such as the relief valve, pressure transducers, and flowmeters, during and immediately after combustion.

B.41.2 TEST EQUIPMENT AND CONDITIONS

The test setup is shown in figure B.41-1. The test was conducted on a cryogenic oxygen storage system that was near flight configuration, including equivalent flow line sizing. The only modifications were the addition of three internal temperature measurement and three optional internal ignition locations. The ignition location selected was at the point the lower fan motor wiring where it exits the heater/fan assembly. The test was conducted with the tank rotated 90 degrees from the normal vertical position (fig. B.41-2). Two additional glass-bead-insulated thermocouples were installed in the tank, and the wiring was routed out of the tank via the vent line, terminating in pressure connectors capable of withstanding the operating pressures. The existing temperature sensor was modified from a four wire system to a two wire system, thereby providing two conductors for an additional sensor at the wire loop mid-point.

After the altitude test chamber was evacuated, the tank was filled to 100 percent and the desired fluid temperature and pressure conditions were achieved (900 psi and minus 190° F). In addition, a supply line flow rate of approximately 0.50 lb/hr was established from the tank. Data were recorded continuously during the test and until all combustion was completed, as indicated by the cooling of all temperature measurement points. The fans were turned on prior to ignition.

B.41.3 RESULTS

The electrical conduit ruptured about 1/4-inch from the electrical conduit/pressure vessel interface at 58 seconds after ignition (fig. B.41-3).

A time history plot of tank pressure and temperature recorded during the ignition and an identification of the significant events is shown in figure B.41-4. Discrete geometric locations and linear distances between these discrete locations are shown in figure B.41-5.

The electrical conduit ruptured at 58 seconds after ignition, but this was an expected failure mode and demonstrated that the combustion phenomena and time history relationships predicted for this test were in agreement with results obtained from prior component level tests. The flight relief valve relieved at 1006 psia and indicated a maximum flowrate of 100 lb/hr (tank pressure 1170 psia) approximately 1 second before conduit rupture. There was no significant differential pressure observed between the tank pressure, as measured by the ground support equipment transducer located in the tank vent line, and the flight pressure transducer during the dynamic tank pressurization history. The average burning rate from ignition location to flight position temperature sensor going off scale was 0.585 in./sec.

A visual inspection of the tank interior revealed the following:

a. All internal wiring insulation was burned.

b. The top glass-filled polytetrafluoroethylene sleeve insulator, in the density sensor probe, was approximately 98 percent consumed (fig. B.41-6).

c. Both the upper and lower polytetrafluoroethylene fill tube adapters within the density sensor probe were totally consumed.

d. The bottom polytetrafluoroethylene sleeve insulator on the density sensor was not damaged.

e. There was no indication of metal burning except some minor wire fusing.

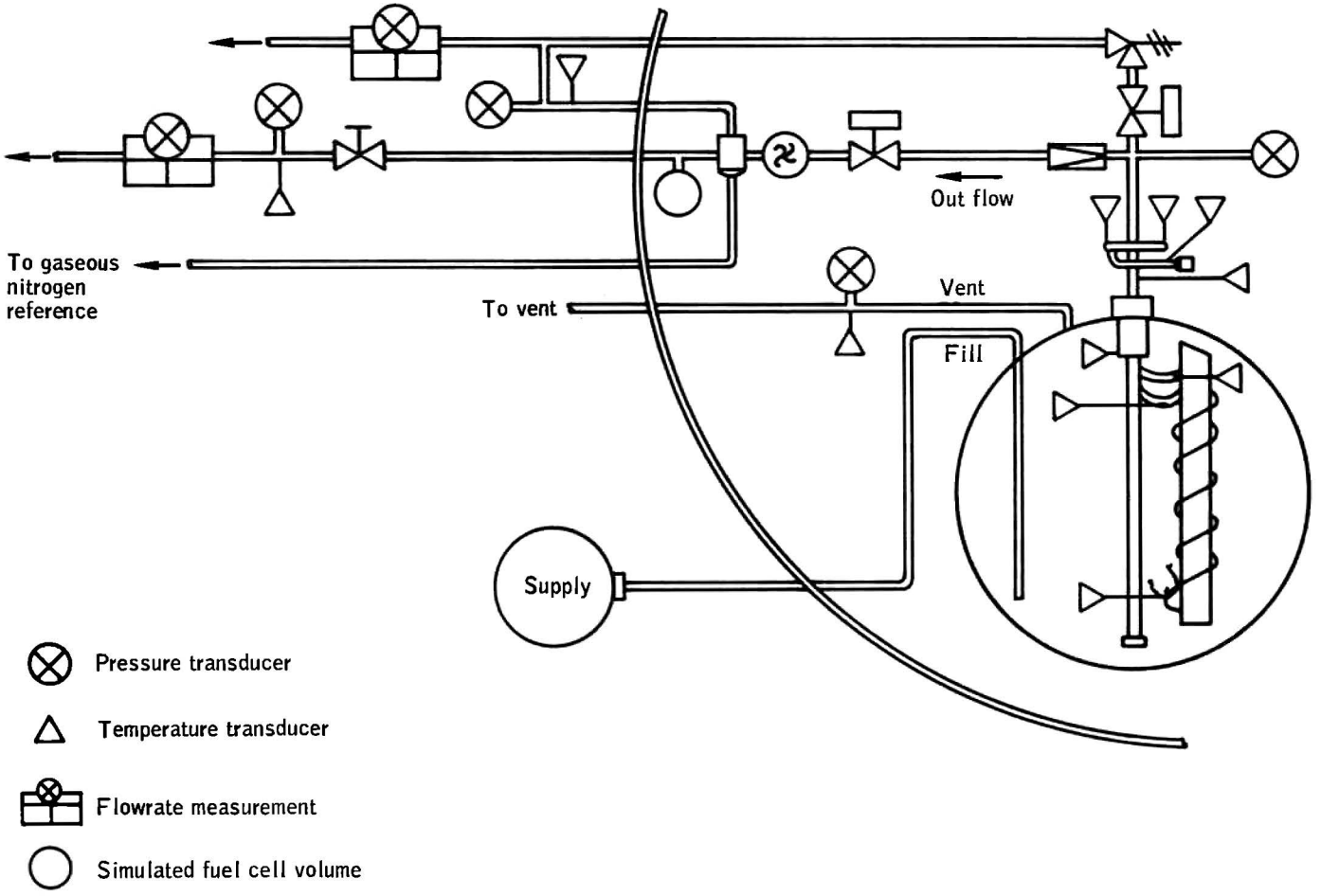

Figure B.41-1.- All-up cryogenic oxygen storage system test setup.

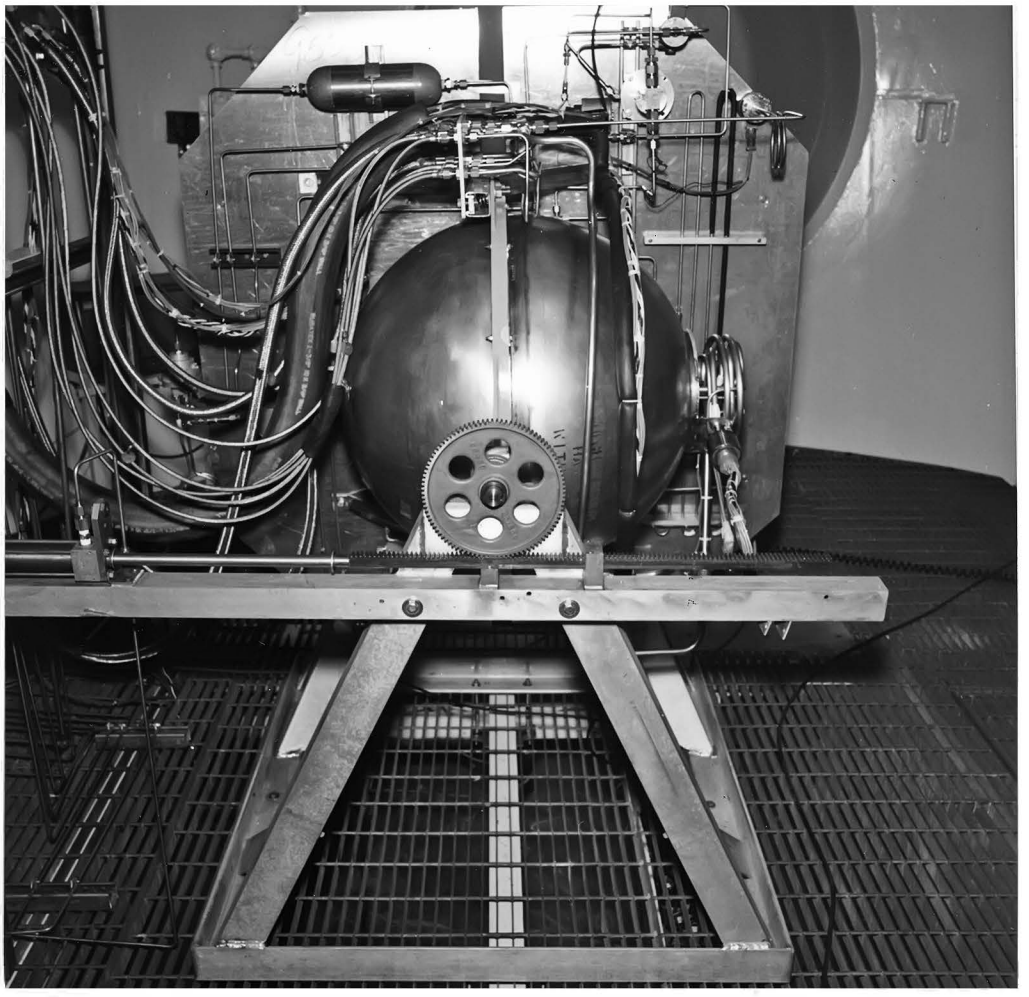

Figure B.41-2.- Orientation of oxygen tank during test.

Figure B.41-3.- Electrical conduit rupture.

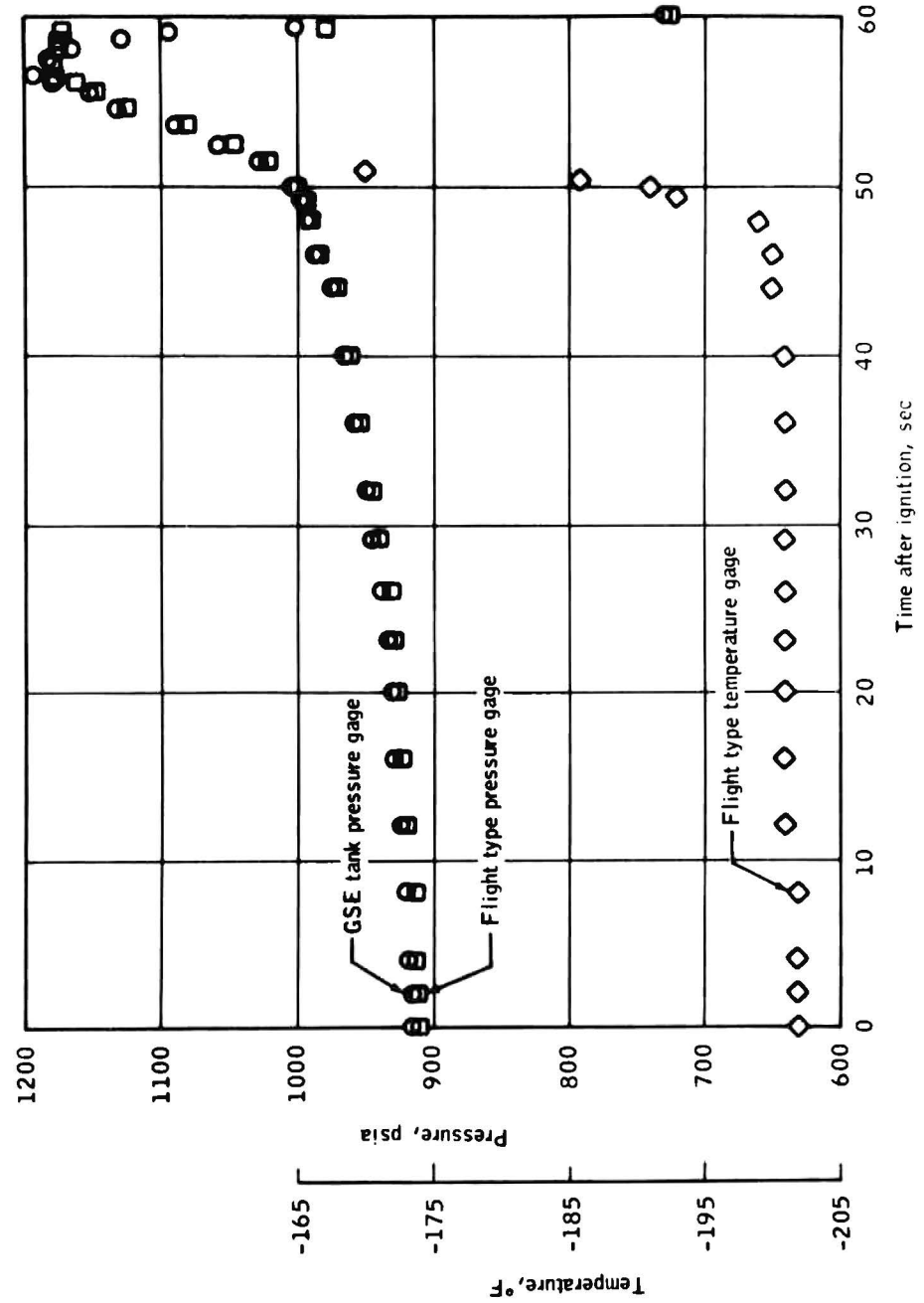

Figure B.41-4.- Time history of tank pressure and temperature plotted against time.

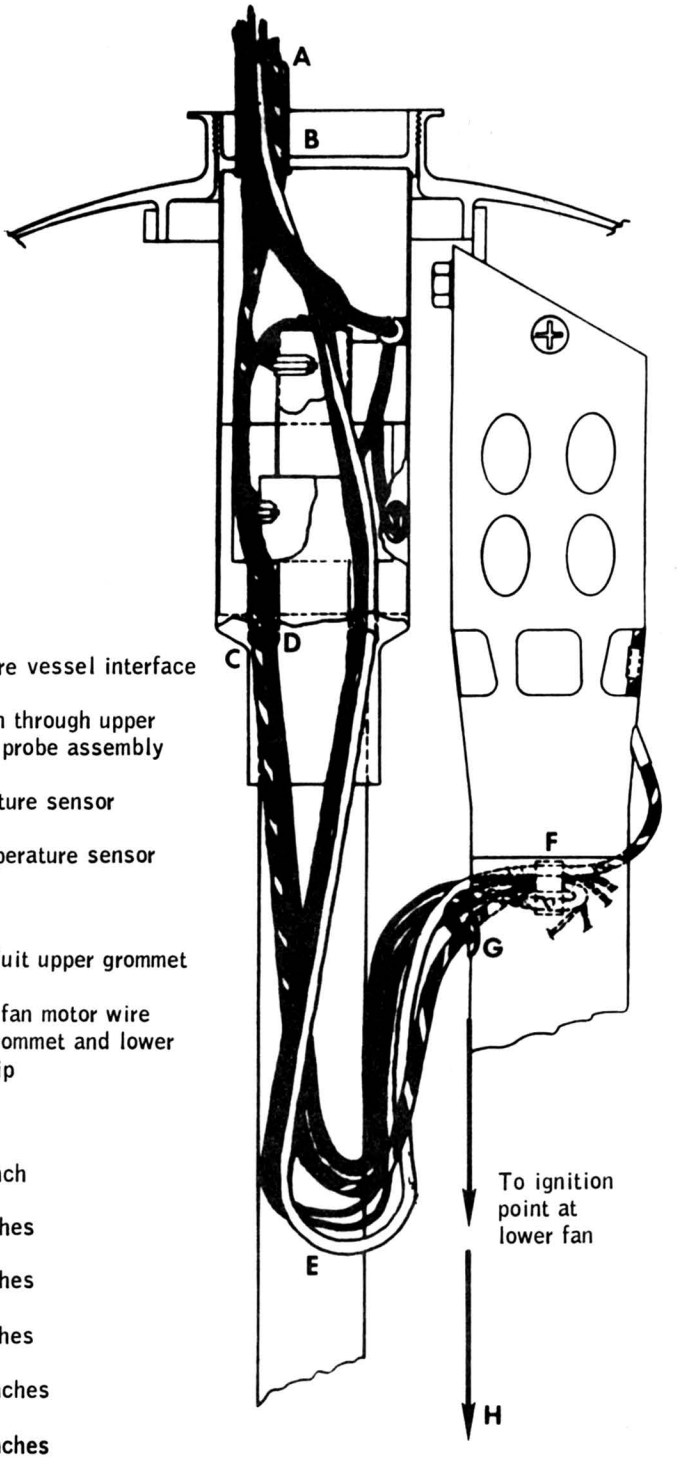

Identification	
Point	Description
A	Point of conduit rupture
B	Electrical conduit/pressure vessel interface
C	Electrical wire penetration through upper insulator of capacitance probe assembly
D	Location of flight temperature sensor
E	Location of wire loop temperature sensor
F	Clamp
G	Lower fan motor wire conduit upper grommet
H	Ignition location on lower fan motor wire between conduit lower grommet and lower fan motor copper wire clip

Distances	
A to B	Approximately 0.25 inch
B to C	Approximately 4.0 inches
C to E	Approximately 5.0 inches
E to F	Approximately 6.0 inches
F to G	Approximately 1.75 inches
G to H	Approximately 12.5 inches

Figure B.41-5. - Significant point location.

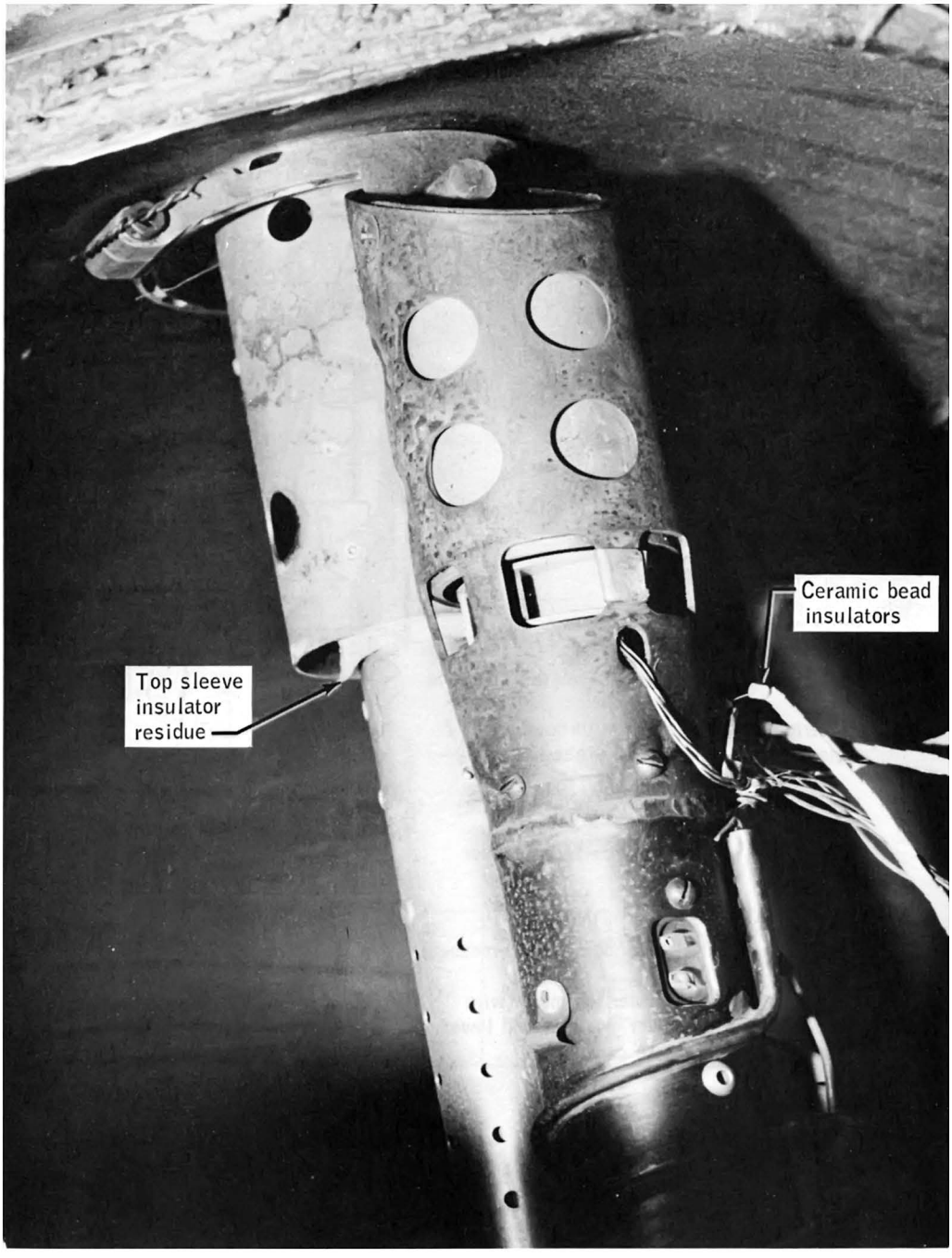

Figure B.41-6.- Top glass-filled polytetrafluorethylene sleeve insulator (post-test).

B.42 HEATER GROUND POWER SUPPLY VOLTAGE TESTS

B.42.1 OBJECTIVE

The objective of this test was to determine if the voltage data would indicate whether the thermal switches in the cryogenic oxygen tank 2 opened while the heaters were on during the special detanking procedure prior to the Apollo 13 mission.

B.42.2 TEST CONDITIONS

During this test, the ground power supply was set to provide 75 V dc to the cryogenic oxygen tank heater, with no load; then a 12.5-ampere load was applied.

B.42.3 RESULTS

The resulting voltage drop at the ground power supply was 5 to 6 V dc. This compares favorably with the following voltage drops measured at launcher umbilical tower 2 during the Apollo 13 detanking procedure:

a. For oxygen tank 1 at 9.5 amperes, the voltage differential between the ground power supply and spacecraft was 13.8 V dc

b. For oxygen tank 2 at 9.25 amperes, the voltage differential was 13.5 V dc.

B.42.4 CONCLUSIONS

It is concluded that during the special detanking procedures prior to the Apollo 13 mission the heaters were on for the times shown on table B.42-I.

TABLE 42-I.- HEATER AND FANS RUN TIME - CRYOGENIC OXYGEN TANK 2

Date	Heater on	Heater off	Total on time heater, hr:min	Fans on	Fans off	Total on time heater, hr:min:sec
March 27	2147	0603 (3/28)	8:15	23:20:57	06:02:04	6:41:8
March 30	1652	1724	0:32	16:53:30	17:50:04	0:56:24

NOTES: 1. ON March 28 at 0050, temperature transducer reached upper limit of +84° F. It remained at this level until 0402. It remained on scale through the remainder of the test.

2. Review of voltage strip charts (A14-052) indicates heaters remained on during the period that the temperature read off scale (March 28 at 0050 to 0402 on March 28).

B.43 PANEL SEPARATION TESTS

B.43.1 OBJECTIVE

The objective of these tests was to demonstrate the separation sequence of the service module bay 4 cover panel in a manner that could be correlated with flight conditions. The panel failure mechanism and the pressure distribution that resulted in separation were also to be determined.

B.43.2 TEST EQUIPMENT AND CONDITIONS

An experimental and analytical program utilizing one-half scale dynamic models of the service module bay 4 cover panel was conducted. Panels were attached through replica-scaled joints to a test fixture that simulated pertinent service module geometry and volume. Venting was provided between compartments and to space. A high pressure gas system was used to rapidly build up pressure behind the cover panel as the input force leading to failure. Similarity laws for the response of structures led to scale factors of one-half for model time and one-eighth (one-half cubed) for model mass. Some of the derived model to full-scale ratios are:

Displacement	= 1/2	Force	= 1/4
Velocity	= 1	Pressure	= 1
Acceleration	= 2	Stress	= 1
Area	= 1/4	Energy	= 1/8
Volume	= 1/8	Momentum	= 1/8

Initial tests were conducted on isotropic panels that scaled only membrane properties while more completely scaled sandwich panels were being fabricated. While preparations for vacuum testing were underway, testing started at one atmosphere. The first tests concentrated on determining the pressure input required for separation and deferred to later tests the simulation of internal flow required to produce these distributions.

Two computer programs were used for analysis of the one-half scale models of the bay 4 cover panel. The initial dynamic response calculations using a non-linear elastic finite difference program indicated that panel response was essentially static for the class of pressure loadings with a nonlinear elastic finite element representation and the NASTRAN computer program.

Figure B.43-1 shows cross sections of the full scale and model panels. The full scale panel was a honeycomb sandwich structure with a Z-bar edge closeout attached to the service module with 1/4-inch bolts around the edges and to each of the bay 4 shelves. The first one-half scale panel models, designated DM on figure B.43-1(b), scaled membrane properties of the full-scale sandwich panel inner and outer face sheets with a single isotropic panel having the correct nominal ultimate tensile strength. The Z-bar was simulated by a flat bar that represented the shear area of the outer Z-bar flange. Fastener sizes, bolt patterns, and bonding material were duplicated from full scale.

One-half size honeycomb sandwich panels, designated HS in figure B.43-1(c), scaled both bending stiffness and membrane stiffness. Although core density of the sandwich models was slightly high, the dimensions, materials, bonding, and Z-bar closeout were scaled. Some alloy substitutions were made, but nominal strength requirements were met.

Test fixture.- The test fixture (figs. B.43-2 and B.43-3) was a one-half size boilerplate mockup of the service module bay 4 and central tunnel. Vent areas connected the bay 4 shelf spaces to the central tunnel and to each other. The tunnel also had vents to space and to a large tank simulating the remaining free volume of the service module. Vent areas were adjusted in initial tests to obtain desired pressure distributions but were scaled from the best available data for final testing. The fixture also held the pressurization system and instrumentation. True free volume was approached by adding several wooden mockups of equipment.

Pressurization system.- The pressurization system is shown in figure B.43-2. A 3000-psi accumulator was discharged, on command, through an orifice by mechanically rupturing a diaphragm. The gas expanded into the oxygen shelf space of bay 4 through a perforated diffuser. In order to obtain uniform pressure over the entire panel for some tests, the diffuser was lowered so that it discharged into both the oxygen and hydrogen shelf spaces. For these particular tests, extra vent area was provided between all shelves to insure uniform pressure throughout bay 4. For most tests, a shelf was placed between the diffuser and panel to minimize direct impingement.

Other.- Instrumentation consisted of strain gages, fast response pressure sensors, and high speed motion picture cameras. Atmospheric tests were conducted in a rocket test cell and vacuum tests at 1 mm Hg pressure in a 60-foot vacuum sphere.

B.43.3 RESULTS

Presentation of results.- The test program is summarized in table B.43-I. Typical failures and pressure time histories are illustrated in figure B.43-4. Figure B.43-5 is a sequence of prints from high speed movie cameras that demonstrate separation of the sandwich panel models. Results of NASTRAN calculations on the one-half scale models are presented in figure B.43-6 and B.43-7.

Demonstration of panel separation.- Panel separation was demonstrated with both membrane and sandwich panels. Two sandwich panels separated completely from the test fixture during vacuum tests. Two membrane panels, although less representative of flight conditions, also separated completely in vacuum tests. However, similar tests with membrane panels in atmosphere left portions of panels attached to the test fixture (figs. B.43-4(b) and B.43-4(c)). Complete separation in atmosphere could not be achieved due to mass and drag of the air.

Pressure distributions.- Complete membrane panel separation was achieved only with nearly uniform pressure distribution over the entire bay 4 panel cover (fig. B.43-4(d)). When just the oxygen shelf space experienced high pressures, membrane panel separation was localized to the area of the panel over the oxygen shelf space (fig. B.43-4(a)). This type of local failure occurred in both atmosphere and vacuum. When scaled internal venting was introduced, model DM-10 lost a slightly larger portion of panel due to high pressure experienced by both the oxygen shelf and fuel cell shelf spaces, while the rest of bay 4 was at low pressure.

Complete separation of sandwich panels has been obtained with both uniform and non-uniform pressure distributions. Figure B.43-8 shows the type of pressure time histories experienced by various sections of the panels. The pressure predictions are based on the internal flow model of the Apollo 13 service module (fig. B.43-2) and have been verified in these experiments. Peak pressure levels were varied from test to test, but the curve shape was always similar. One sandwich panel separated after about 0.2 second during the initial pressure rise in the oxygen shelf space while overall panel loading was highly non-uniform (fig. B.43-4(f)). The other sandwich panel did not separate until about 0.19 second after all bay 4 compartments had time to fill with gas and arrive at a much more uniform loading (fig. B.43-4(e)).

The effect of pressure distribution on peak pressures required for failure is shown by the NASTRAN calculation in figure B.43-6. Included for reference is the linear membrane result, $N = pR$. The load required for edge failure was determined from tensile tests on specimens of the

DM model joints. The peak uniform pressure at failure initiation was only 75 percent of peak pressure at the failure load with just the oxygen shelf space pressurized.

Failure mechanism.- The failure mechanism for complete separation of a membrane panel is demonstrated by the photographic sequence in figure B.43-5(a). Failure was probably initiated by a localized high pressure near the edge of the oxygen shelf space. A crack formed where a shelf bolt head pulled through and rapidly propagated through the panel. Expansion of the pressurizing gas through the openings accelerated panel fragments to very high velocities. Inertia loads from the high acceleration completed the separation. Membrane panels were observed to separate in three pieces — one large and two small fragments.

The failure of a sandwich panel under uniform loading in vacuum is shown in the picture sequence of figure B.43-5(c). Failure started at the edge of the oxygen shelf space by pull-through of the edge bolts through the upper sandwich face sheet. Very rapid tearout along three edges followed, primarily by tension in the face sheets and tearing of the core material from the Z-bar at the edge. The panel then rotated like a door from the test fixture in one piece.

Non-uniform loading of a snadwich panel led to the failure shown in figure B.43-5(b). Initial failure was at the panel edge near the fuel cell shelf. Tearout along one edge and the top rapidly followed and was similar to the previous failure. However, the edge tear stopped before reaching the bottom and became a diagonal rip that left the lower third of the panel attached to the fixture. The upper two-thirds of the panel then rotated door-like and separated. Finally, a vertical tear propagated through the center of the remaining fragment, the bottom tore out, and rapid rotation separated the remnants in two pieces.

Figure B.43-7 relates NASTRAM calculations to the observed failures. Predicted edge load direction and magnitude are illustrated for two pressure distributions. In figure B.43-7(a)-1 and B.43-7(b)-1, panel edges are assumed fixed while in figures B.43-7(a)-2 and B.43-7(b)-2 the panel edge joint along the oxygen shelf space is assumed to have failed. Also shown in figures B.43-7(a)-2 and B.43-7(b)-2 are typical observed failure patterns for these types of loadings on membrane panels. An enlargement of the dotted section of figure B.43-7(a)-2 is shown in figure B.43-7(c) to indicate the type of edge failure observed. Arrows indicate the direction of force required to cause the pullout failures. The NASTRAN edge force patterns are consistent with these failures. In addition, figures B.43-7(a)-2 and B.43-7(b)-2 indicate that tears into the membrane panels tend to remain normal to the direction of the edge forces.

Correlation with flight.- Tests with sandwich panels more closely simulate flight conditions than tests with membrane panels due to initial failure characteristics and post-failure separation behavior. The separation behavior of sandwich model HS-3 (figs. B.43-4(f) and B.43-5(b) is also believed to be more representative of flight than the separation behavior of model HS-2 (figs. B.43-4(e) and B.43-5(c)) for two reasons. First, although model HS-2 was tested with scaled internal venting between the compartments of bay 4 and the service module tunnel, the rest of the service module free volume had been closed. In the HS-3 model test, this vent area had been opened to a realistic value of 60 square inches. Second, the slow pressure build-up before separation of model HS-2 allowed service module tunnel pressure to rise well above the 10 psi limitation required to prevent separation of the command and service modules. Pressurization leading to model HS-3 separation was so rapid (20 milliseconds) that service module tunnel pressure remained below the 10-psi limit. The time to failure would scale up to 40 milliseconds for the flight configuration.

Tests with models HS-3 and HS-4 have bracketed the most likely separation conditions. For both tests, internal venting was scaled and diffuser configuration and accumulator pressure were identical. Model HS-3 separated due to an initial air flow of 190 lb/sec through an orifice of 2.85 square inches. Separation was not achieved on model HS-4 when initial air flow was 135 lb/sec through a 2.0 square inch orifice, even though peak pressures of over 35 psi occurred in the oxygen shelf space after 20 milliseconds.

B.43.4 CONCLUSIONS

Complete separation of one-half scale honeycomb sandwich models of the bay 4 cover panel in vacuum has been demonstrated. Separation was achieved by rapid air pressurization of the oxygen shelf space. Internal volumes and vent areas of the service module were scaled. Separations were obtained with both uniform and non-uniform pressure distributions. The separation resulting from a non-uniform loading that peaks 20 milliseconds after start of pressurization (40 milliseconds full scale) correlates best with hypotheses and data from flight. This particular panel separated in three pieces after an initial tear along the sides that allowed it to open like a door. Inertia loads are a major factor in obtaining complete separation after initial failure.

TABLE B.43-I.- PANEL SEPARATION TEST SUMMARY

MODEL	INTERNAL VENTS	VOLUME FIRST PRESSURIZED	DIFFUSER	LOAD CHARACTER	PRESSURE*		FAILURE
					p (psi)	RISE TIME (Sec)	
ATMOSPHERE TESTS							
DM-1-1	NOT SCALED	O_2 SHELF	OPEN	BAND	24-30	0.020	NONE
DM-1-2	"	"	"	"	30-58	.005	O_2 SHELF AREA
DM-2	"	"	"	"	34-52	.006	O_2 SHELF AREA
DM-3	"	BAY 4	"	UNIFORM	15-35	.015	NEARLY TOTAL (FOLDED BACK)
DM-4	"	"	SHIELDED	"	20-26	.016	NEARLY TOTAL (LEFT EDGES)
VACUUM TESTS							
DM-5-1	"	"	"	"	14-20	---	NONE
DM-5-2	"	"	"	"	20-28	.016	TOTAL
DM-6	"	"	"	"	19-27	.018	TOTAL
DM-7	"	O_2 SHELF	OPEN	BAND	25-40	.005	O_2 SHELF AREA
DM-8	"	"	SHIELDED	"	20-37	.012	O_2 SHELF AREA
DM-9	"	"	"	"	18-23	.040	NONE
DM-10	SCALED	"	"	-	21-39	.070	UPPER 2/3 RDS OF PANEL
HS-1	"	"	"	-	-	-	NONE
HS-2	"	"	"	-	23-32	.190	TOTAL
HS-3	"	"	"	-	30-67	.020	TOTAL
HS-4	"	"	"	-	30-44	.020	NONE

*Range of peak pressures in the O_2 shelf space is indicated. Time from pressure release to peak pressure is rise time.

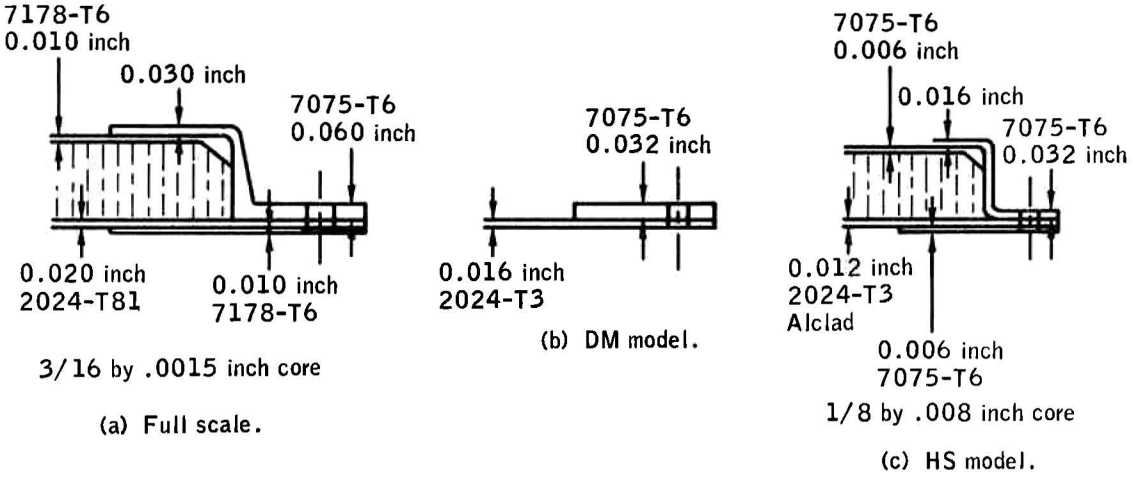

Figure B.43-1.- Panel designs.

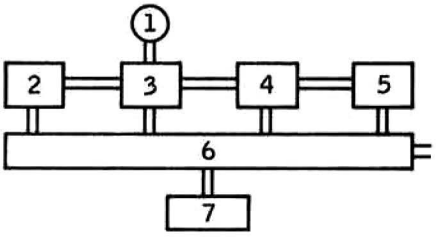

Volume	Description
1	Pressurization tank
2	Fuel cell space
3	Oxygen tank space
4	Upper hydrogen tank space
5	Lower hydrogen tank space
6	Tunnel
7	Other service module free volume

Figure B.43-2.- Schematic of test fixture.

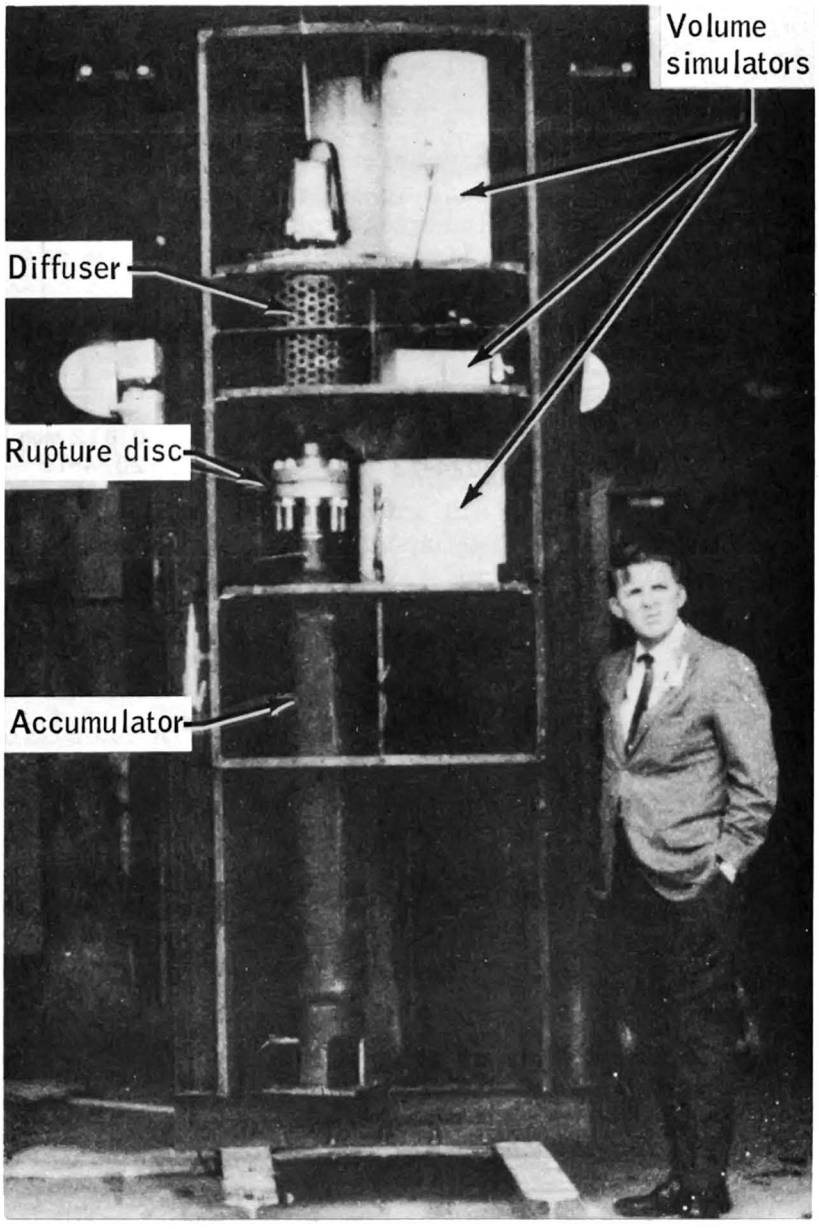

(a) General view.

Figure B.43-3.- Panel separation test fixture.

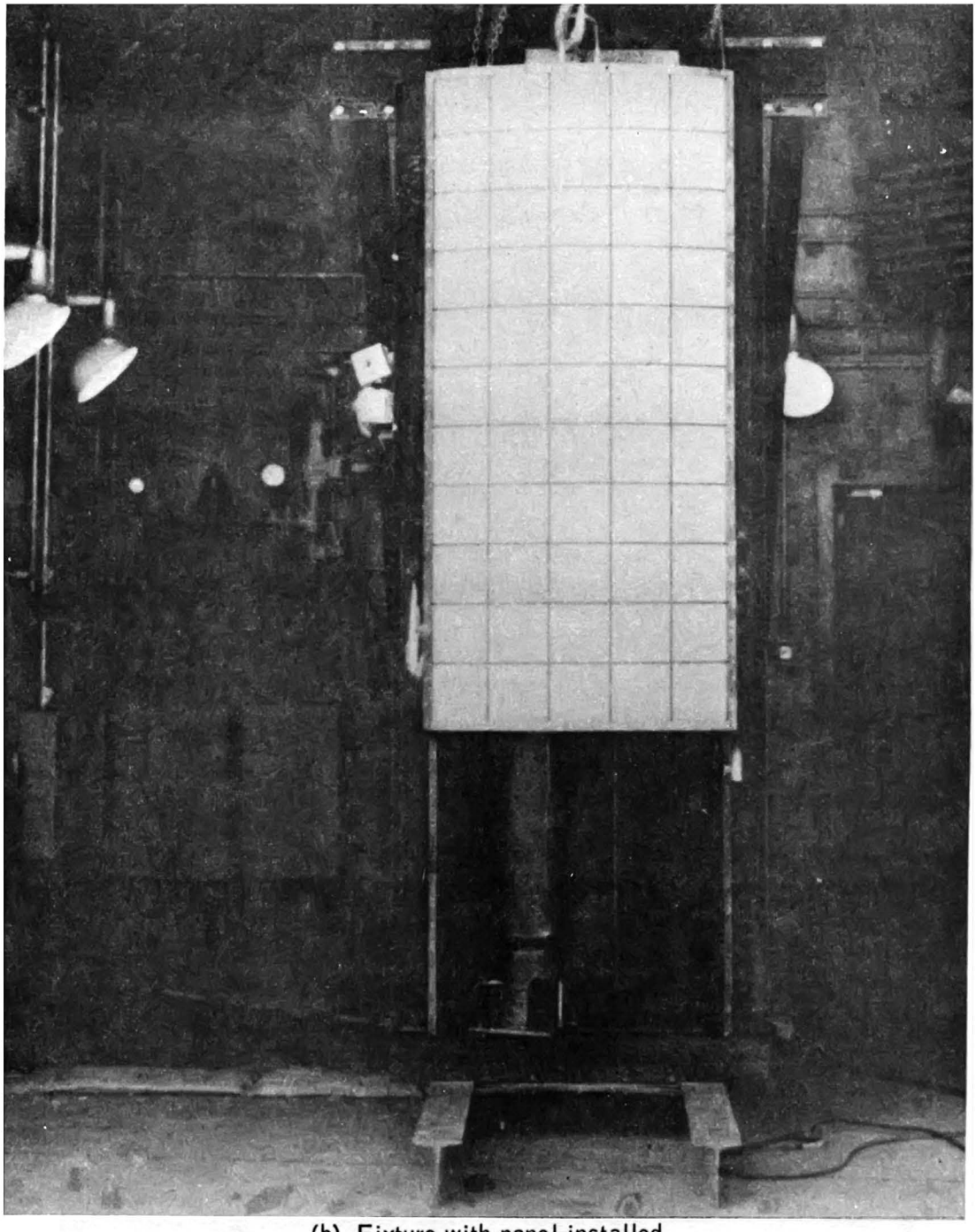

(b) Fixture with panel installed.

Figure B.43-3.- Continued.

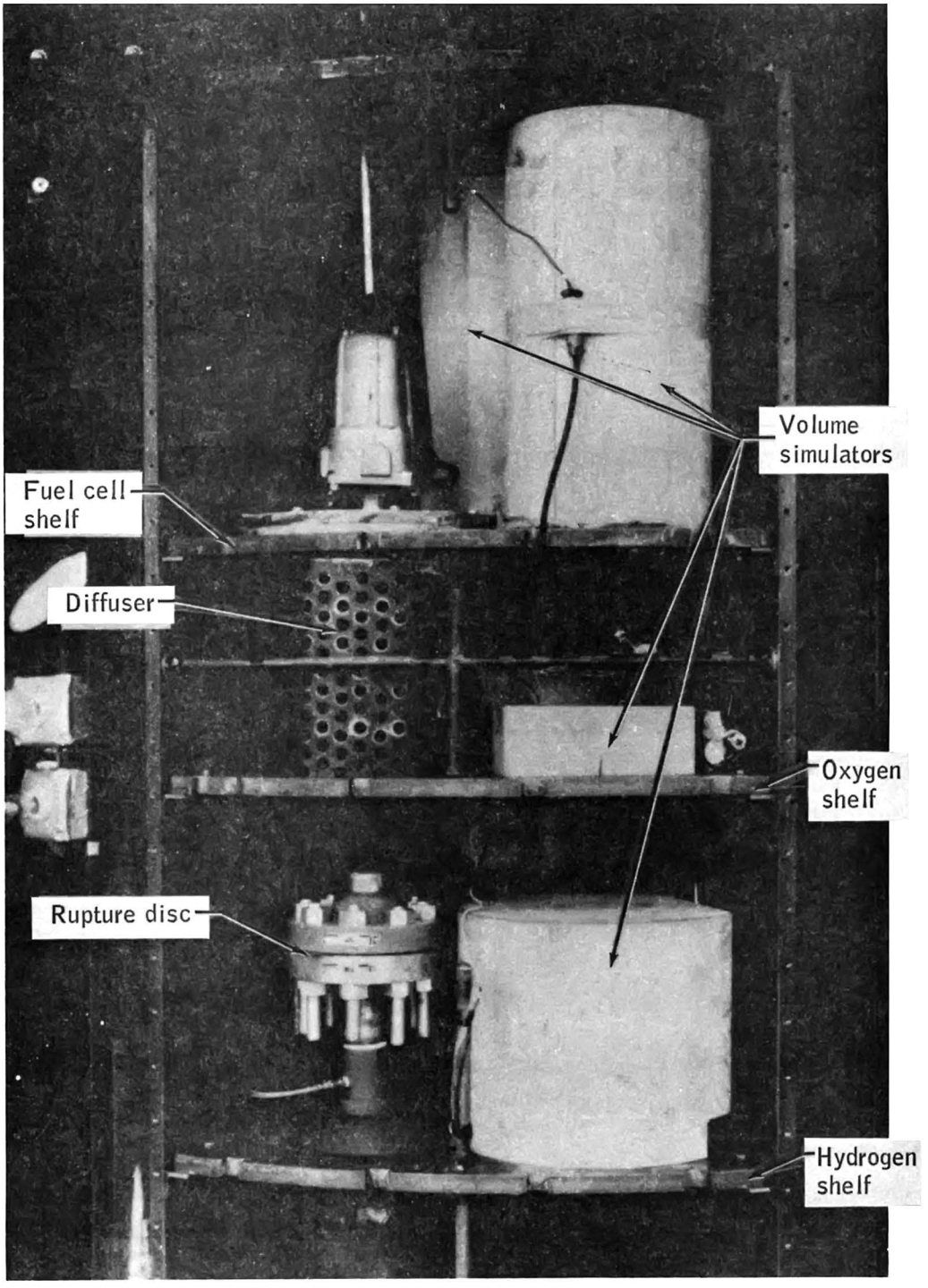

(c) Internal view.

Figure B.43-3.- Concluded.

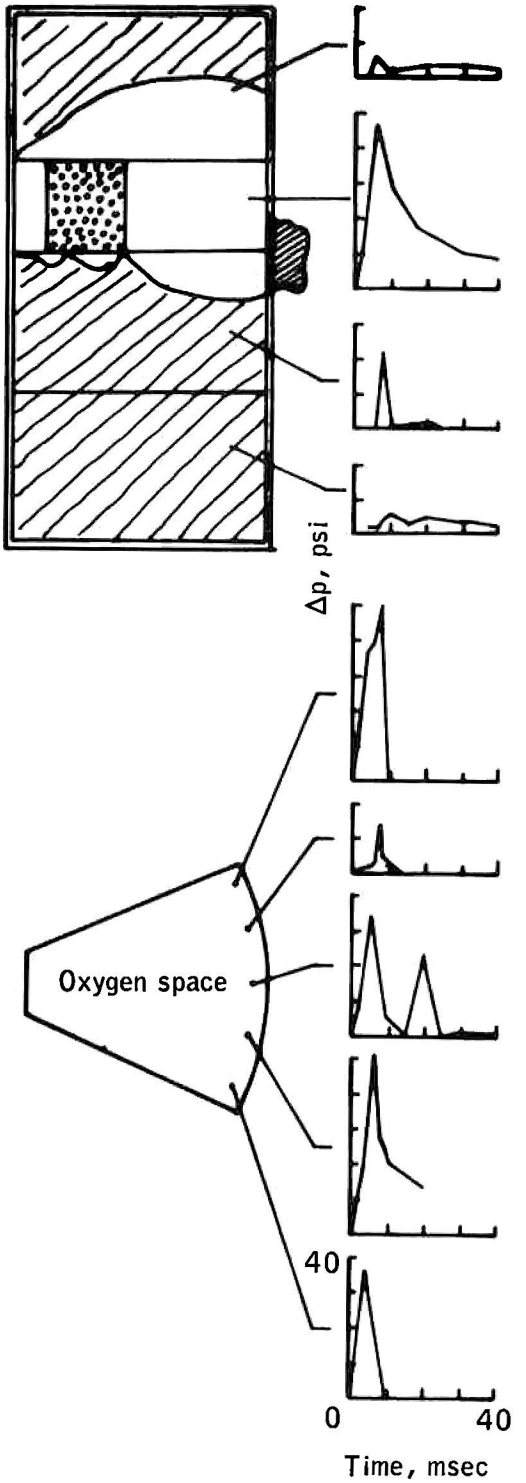

(a) Membrane panel DM-2, atmosphere-band load.

Figure B.43-4.- Separation behavior of sandwich model.

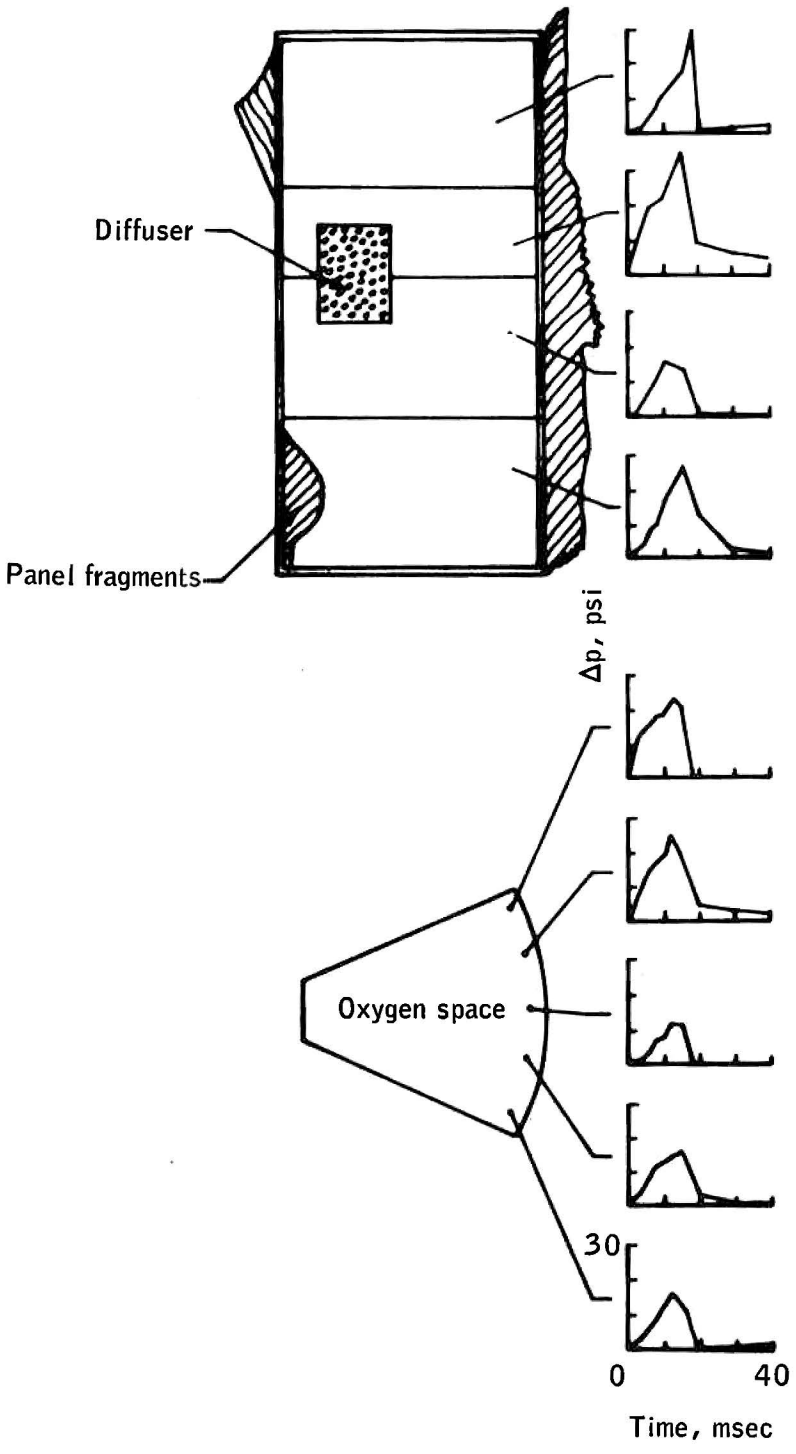

(b) Membrane panel DM-3, atmosphere, uniform load.

Figure B.43-4.- Continued.

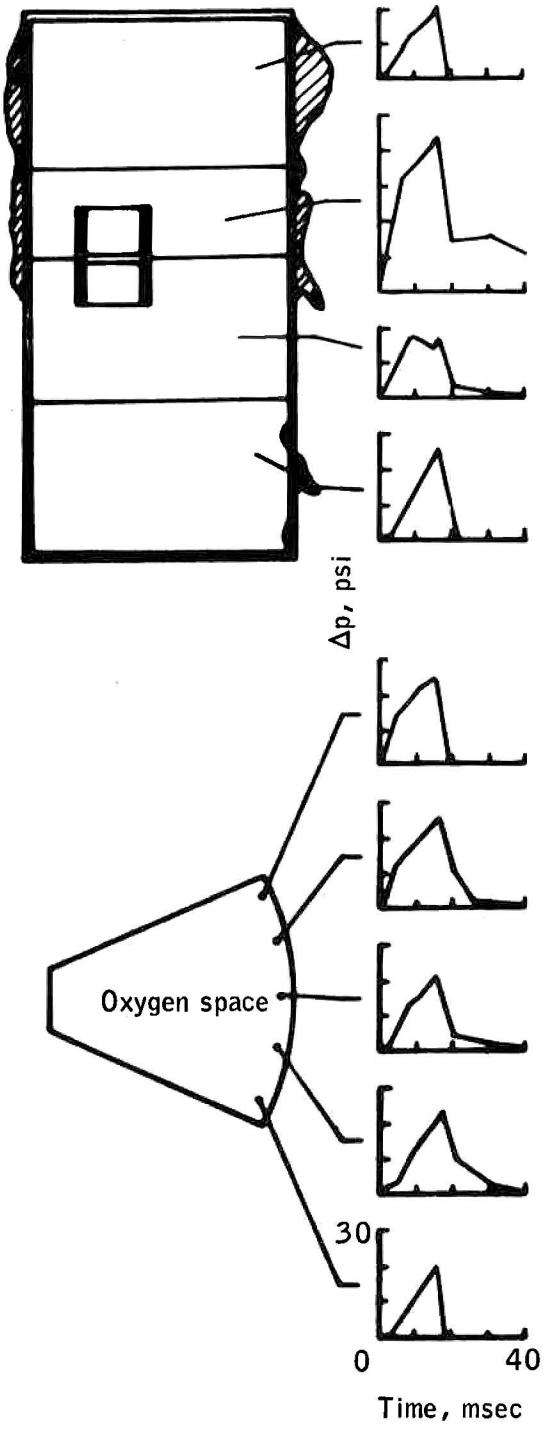

(c) Membrane panel DM-4, atmosphere, uniform load, no direct impingement.

Figure B.43-4.- Continued.

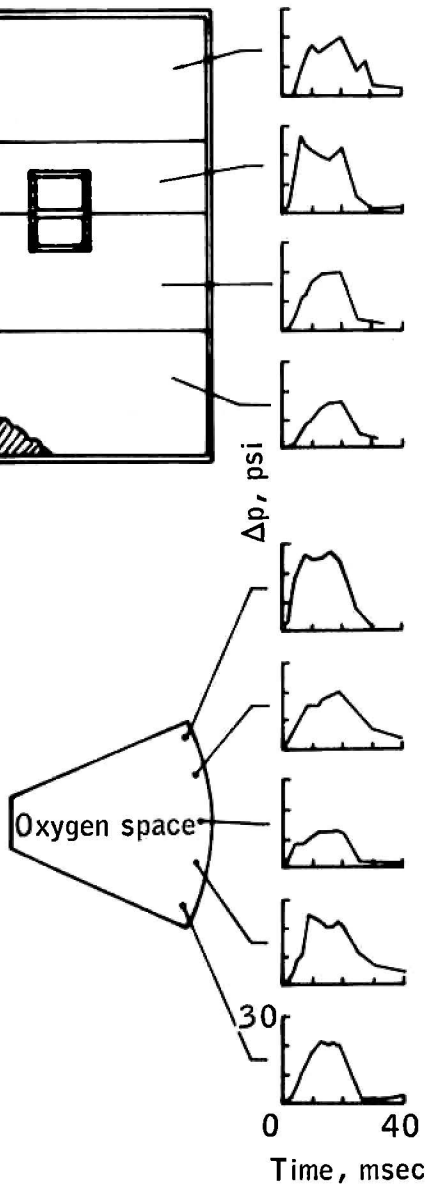

(d) Membrane panel DM-6, vacuum, uniform load, no direct impingement.

Figure B.43-4.- Continued.

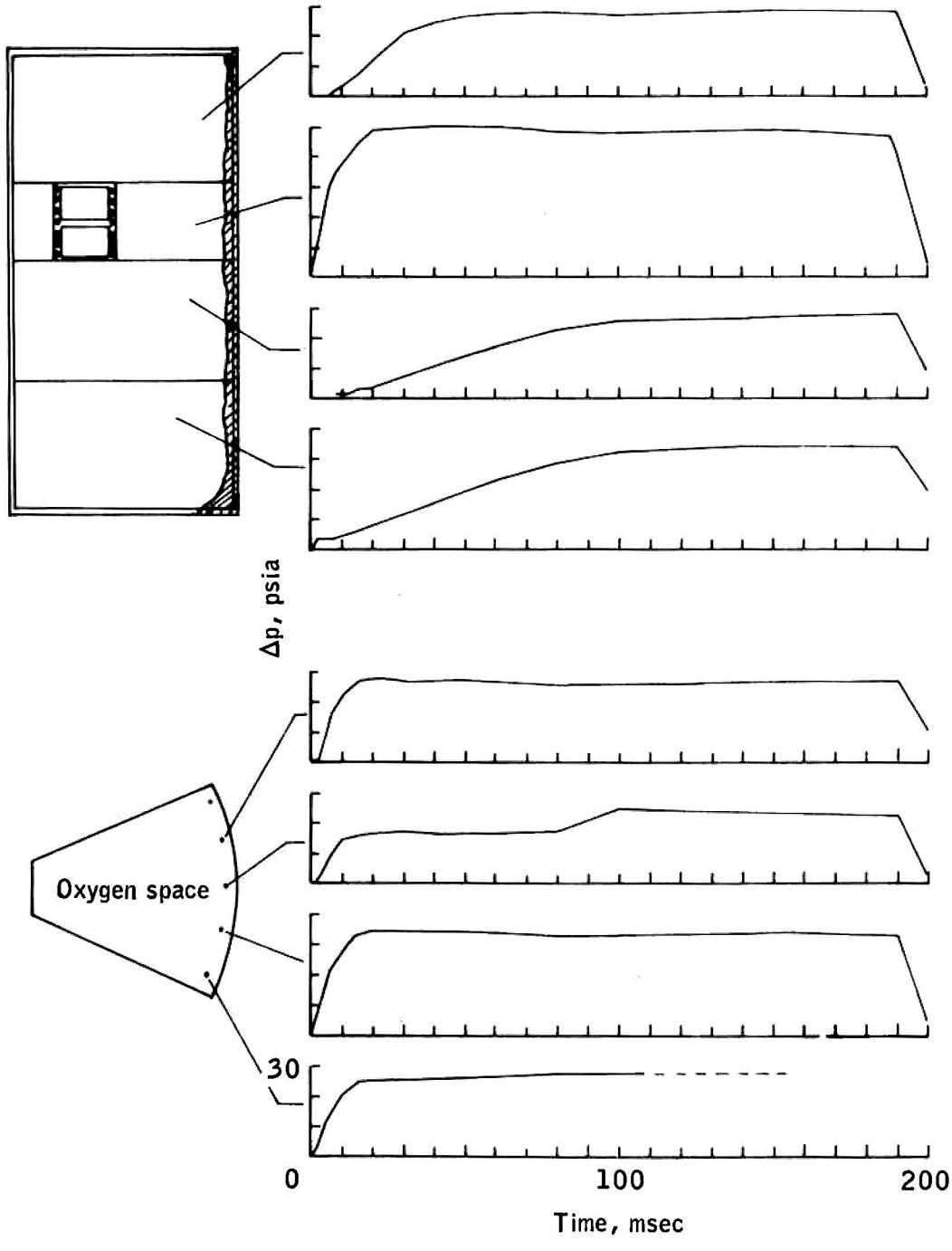

(e) Sandwich panel HS-2, vacuum, no direct impingement.

Figure B.43-4.- Concluded.

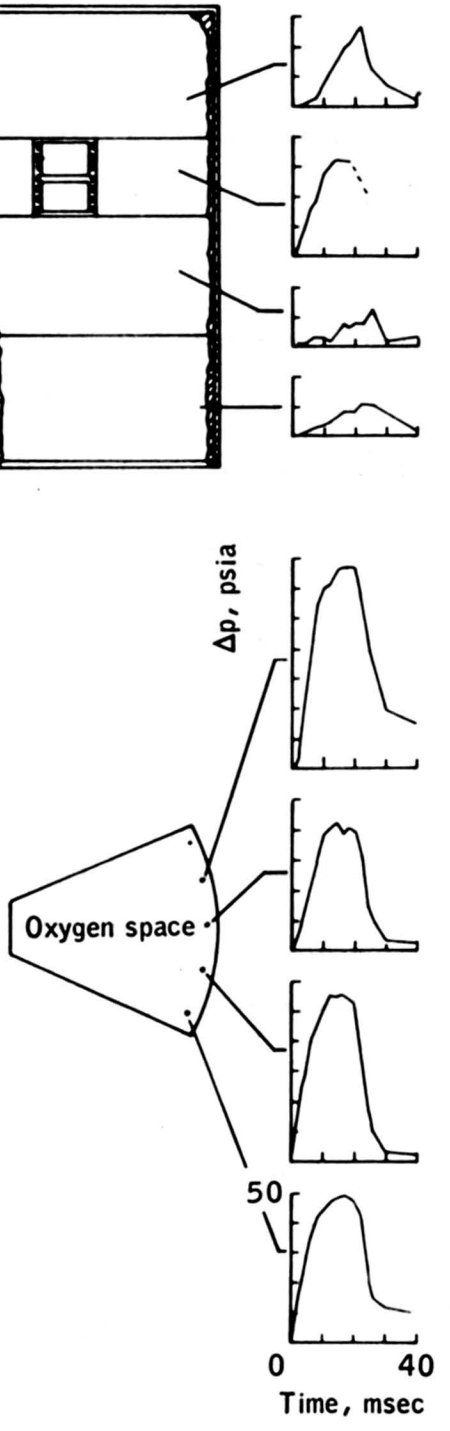

(f) Sandwich panel HS-3, vacum, no direct impingement.

Figure B.43-4.- Continued.

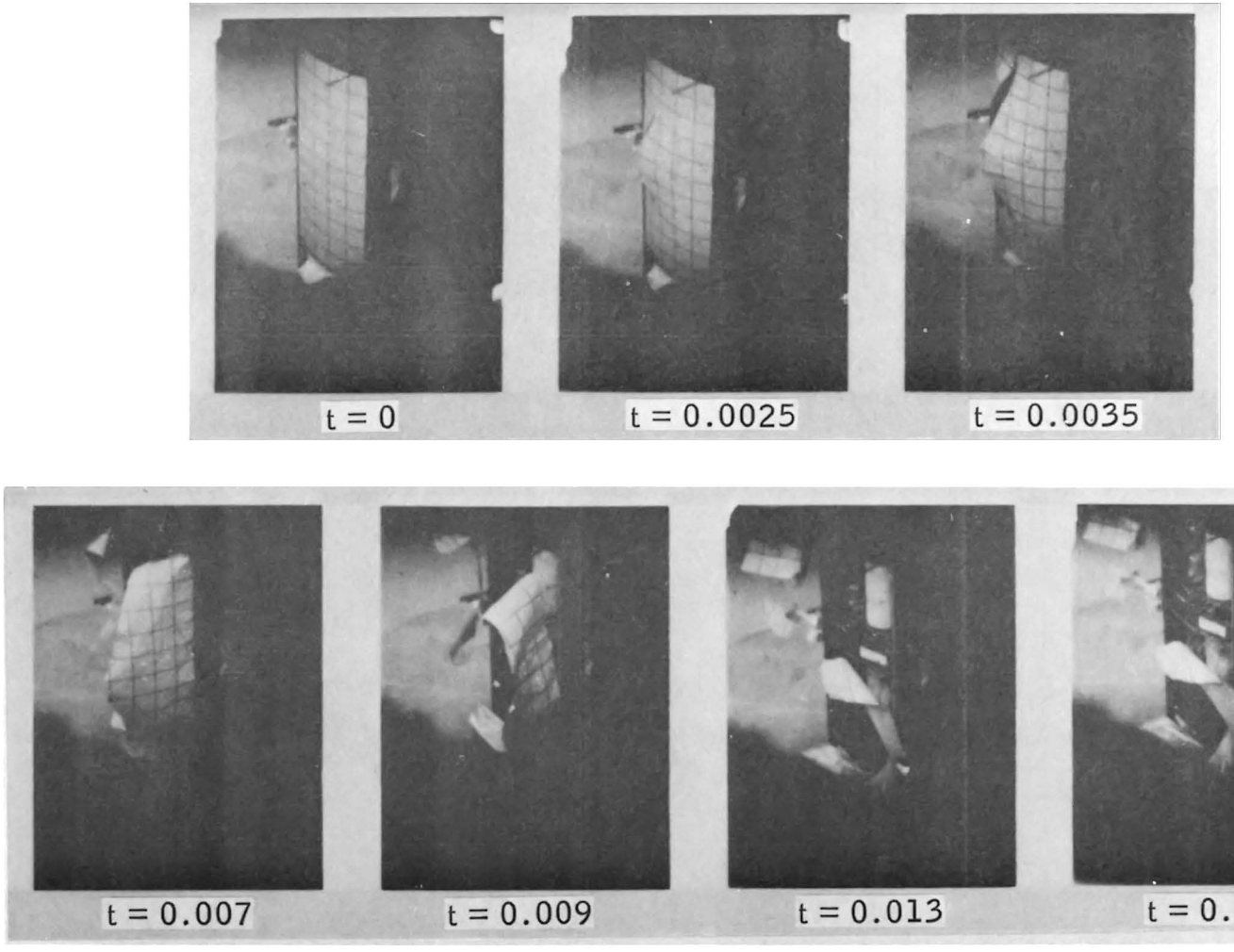

(a) Membrane panel DM-6.

Figure B.43-5.- Sequential failure of two sandwich and one membrane panel.

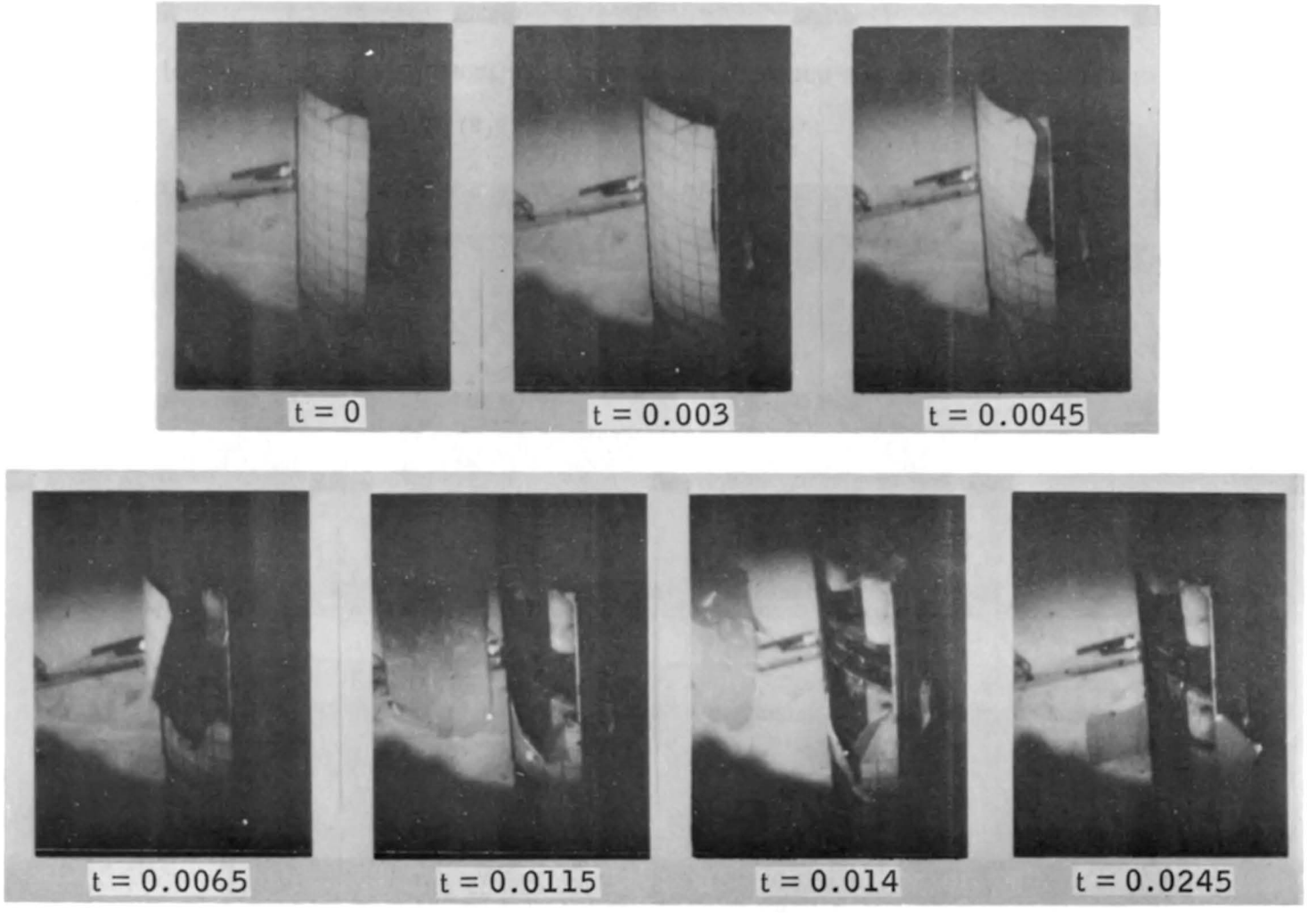

(b) Sandwich panel HS-3.

Figure B.43-5.- Continued.

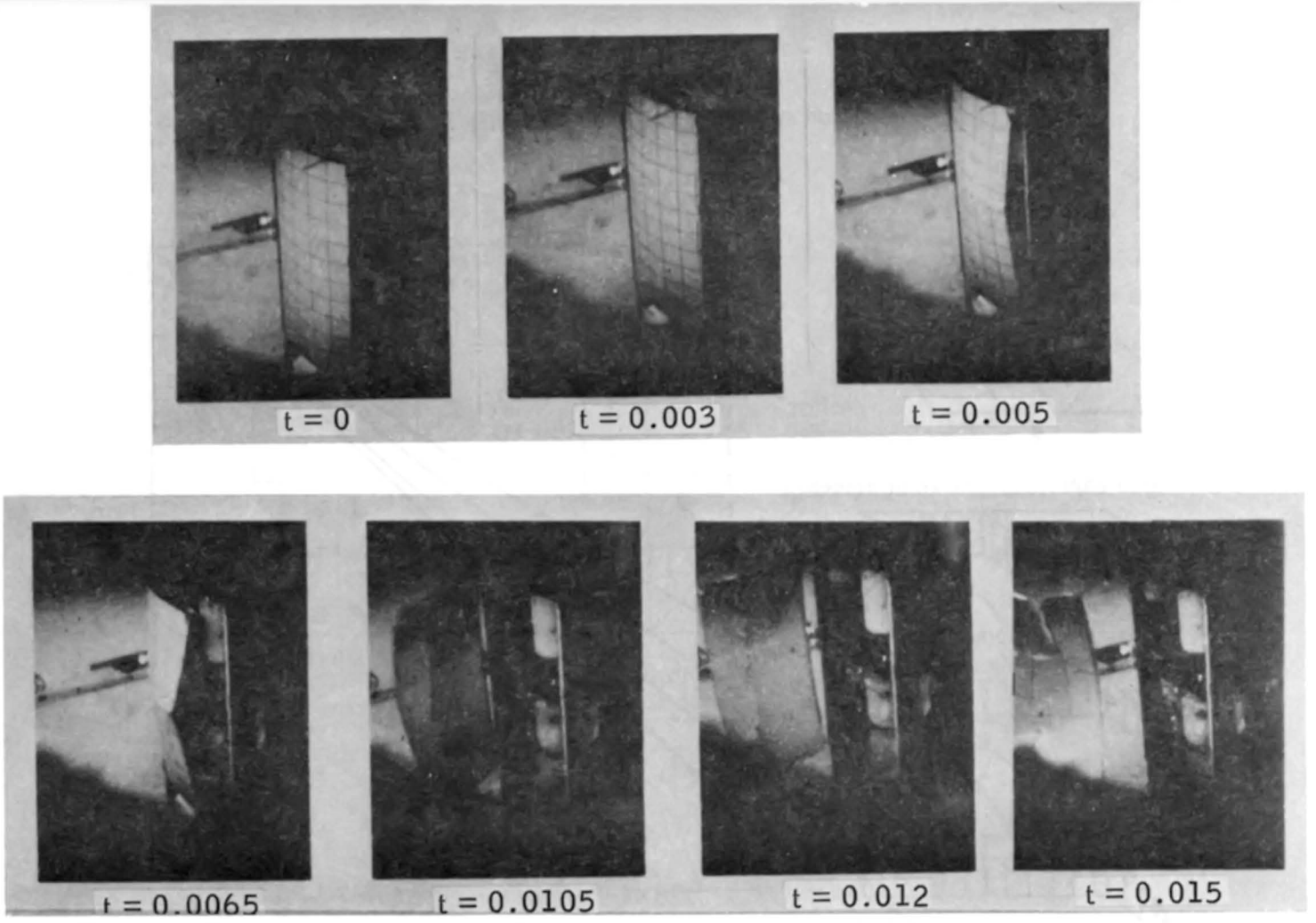

(c) Sandwich panel HS-2.

Figure B.43-5.- Concluded.

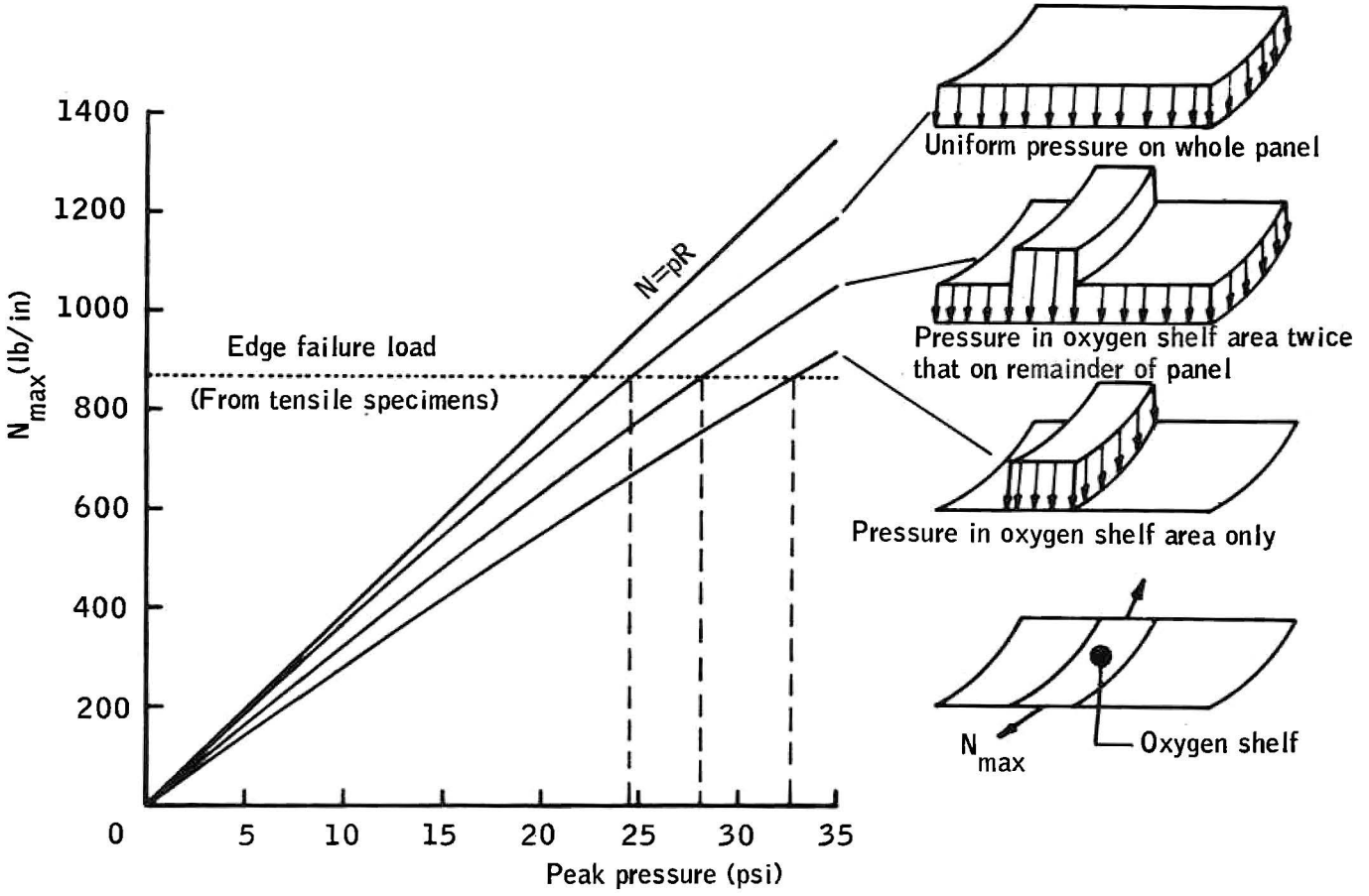

Figure B.43-6.- Maximum edge load on half scale honeycomb panel as predicted by nastran.

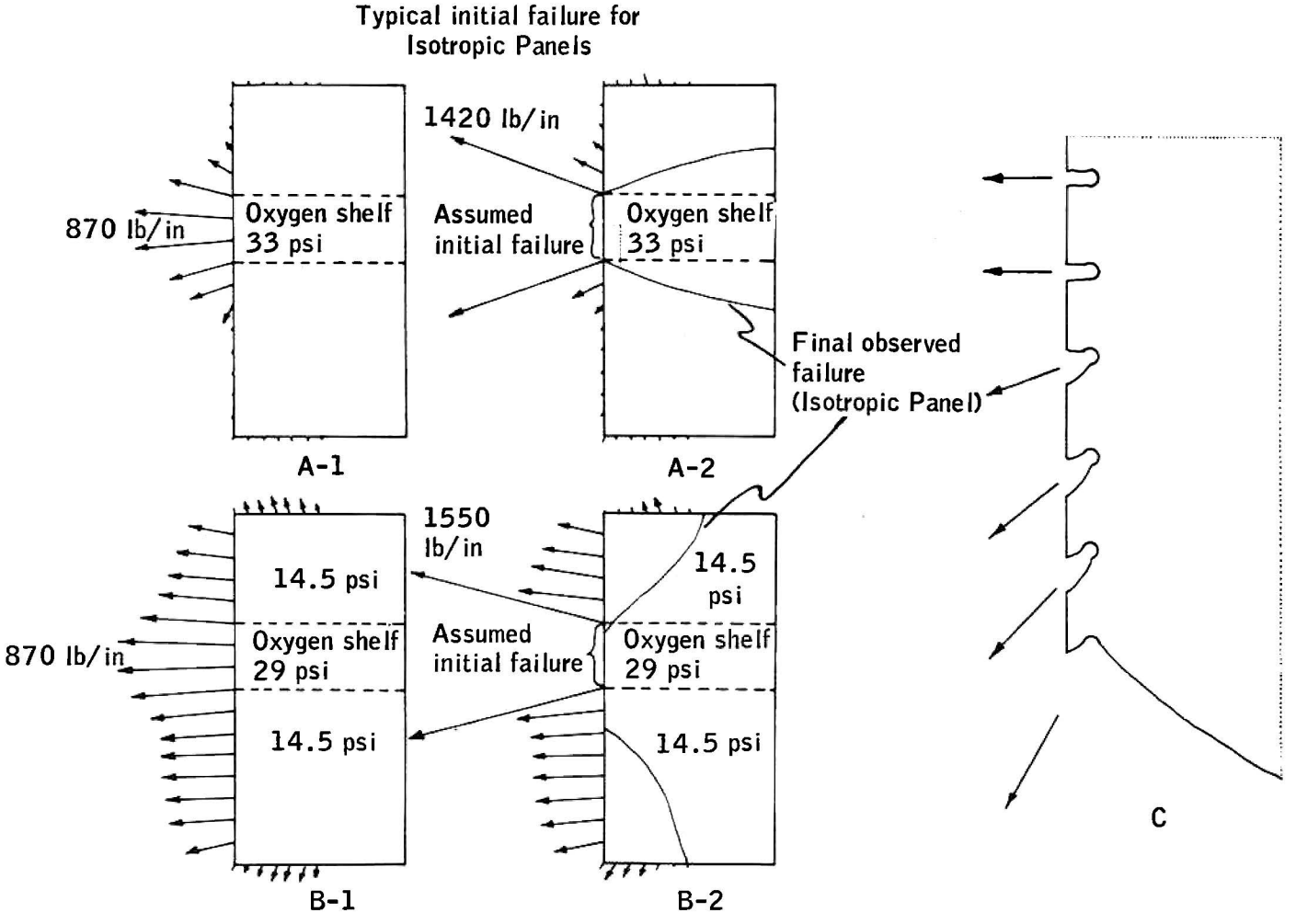

Figure B.43-7.- Distribution of edge loads on half scale Apollo 13 honeycomb panel as predicted by NASTRAN.

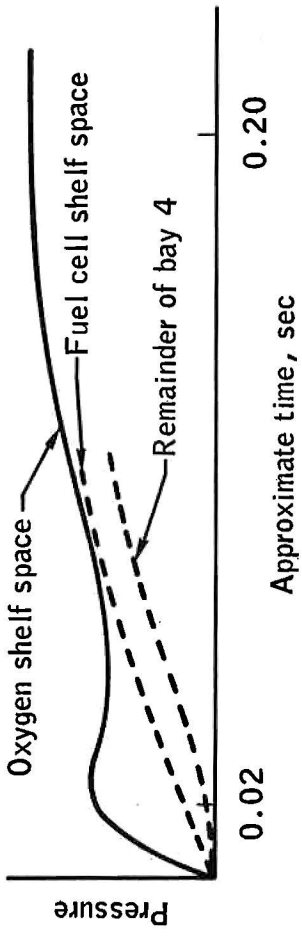

Figure B.43-8.- Pressure buildup in bay 4.

B.44 OXYGEN SENSOR PROBE RIVET FAILURE TEST

B.44.1 OBJECTIVE

The objective of this test was to determine the force required to fail the load rivet in the oxygen quantity gaging probe.

B.44.2 TEST EQUIPMENT AND CONDITIONS

The rest was conducted on an Instron testing machine. The rivet was loaded with a cork (fig. B.44-1) inserted in one end of a tube and a rod inserted in the other end. Radiographs were obtained prior to loading and at each 15 pound increment. Three minutes under each load increment were required to radiograph the rivet (fig. B.44-2).

B.44.3 RESULTS

The following data were obtained during the test and from the radiographs:

Load, lb	Deflection from original position, deg	Remarks
15	0	Load decreased 3-1/2 pounds after 3 minutes
30	1	Load decreased 4 pounds after 3 minutes
45	2	Load decreased 7-1/2 pounds after 3 minutes
60	2	Load decreased 8 pounds after 3 minutes
75	5	Load decreased 9 pounds after 3 minutes
90	8	Load decreased 10-1/2 pounds after 3 minutes
105	10	Load was increased to 105 pounds, but a sudden decrease in load (to 90 pounds) was noted indicating a failure

120	17	The maximum load obtained was 120 pounds, then the rivet end was pulled into the probe tubing. The load decreased to 85 pounds
Last test		Attempts to increase the load were unsuccessful and testing was discontinued. The rivet end was not visible and the rivet head was shearing the outer tube housing. The inner tube of the probe moved with the rivet end approximately 1/2 inch from the original position.

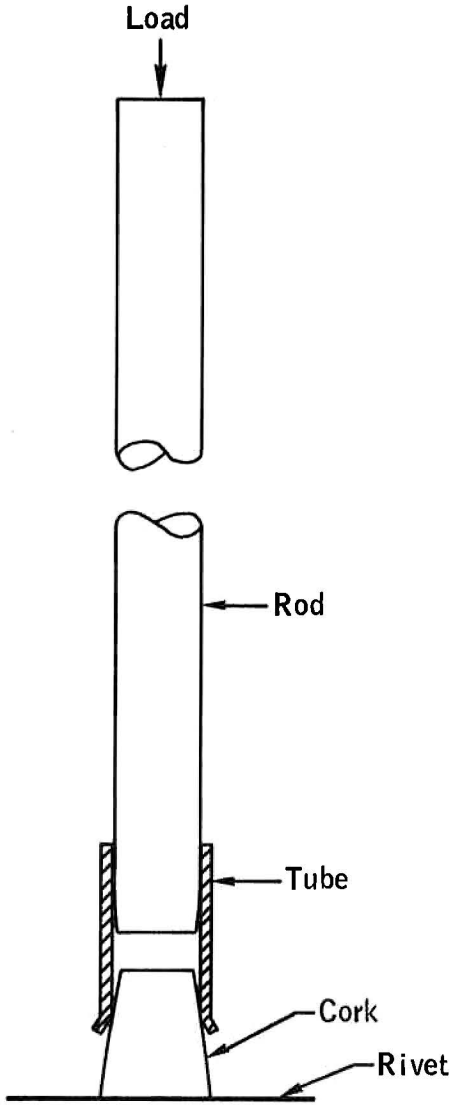

Figure B.44-1.- Capitiance probe load rivet failure test.

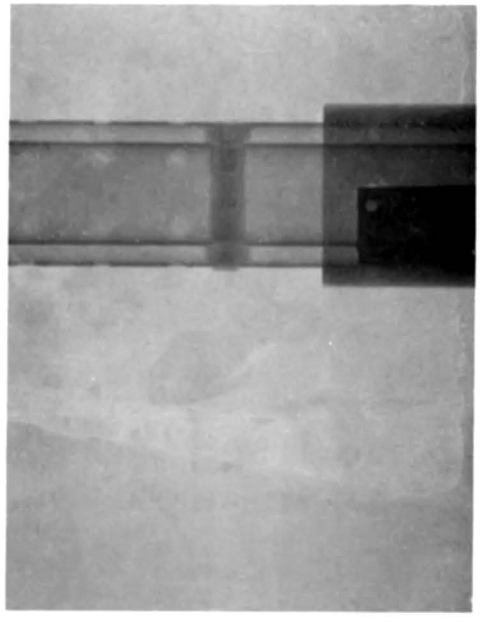

(a) 0 lbs force

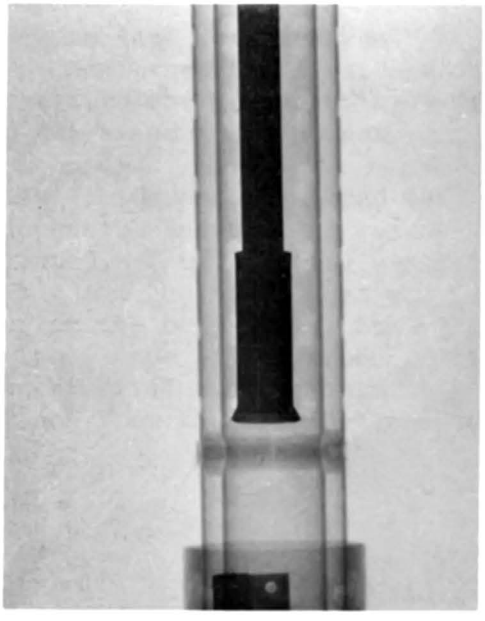

(b) 15 lbs force

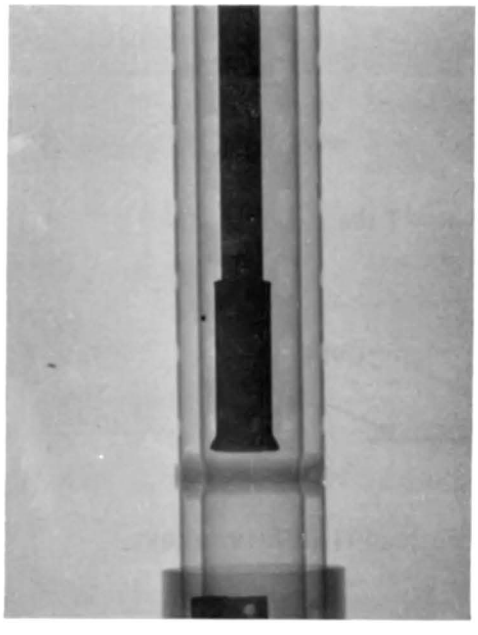

(c) 30 lbs force

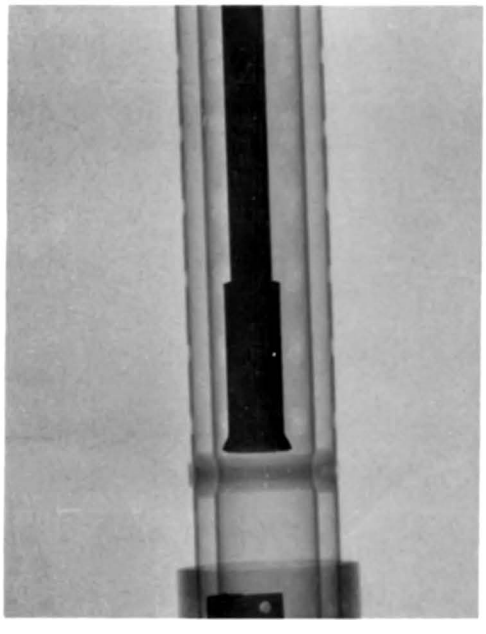

(d) 45 lbs force

Figure B.44-2.- Radiographs of rivet under various loads.

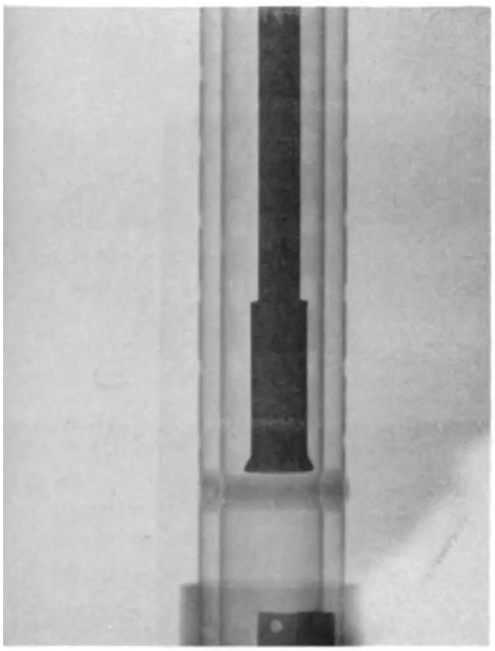

(e) 60 lbs force

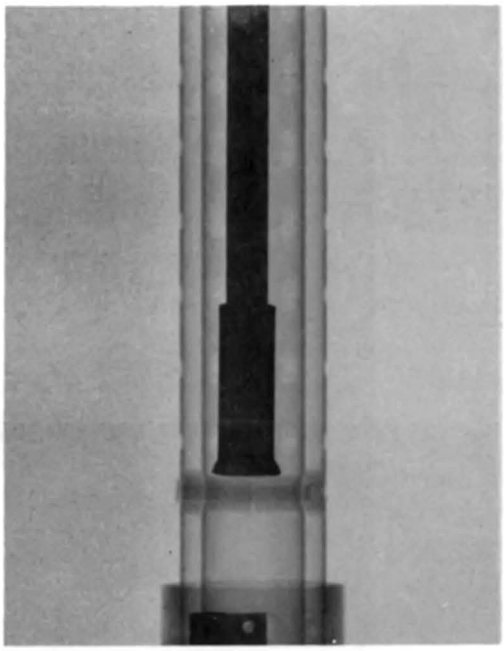

(f) 75 lbs force

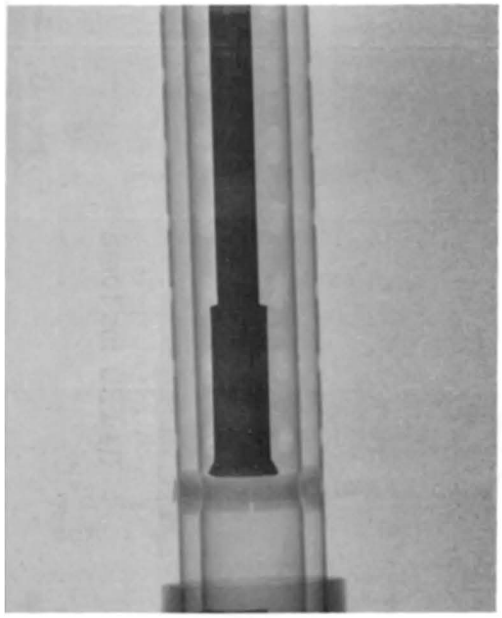

(g) 90 lbs force

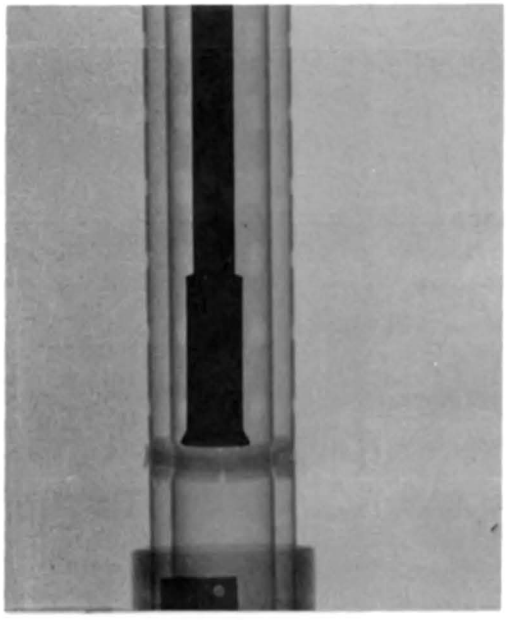

(h) 105 lbs force

Figure B.44-2.- Continued.

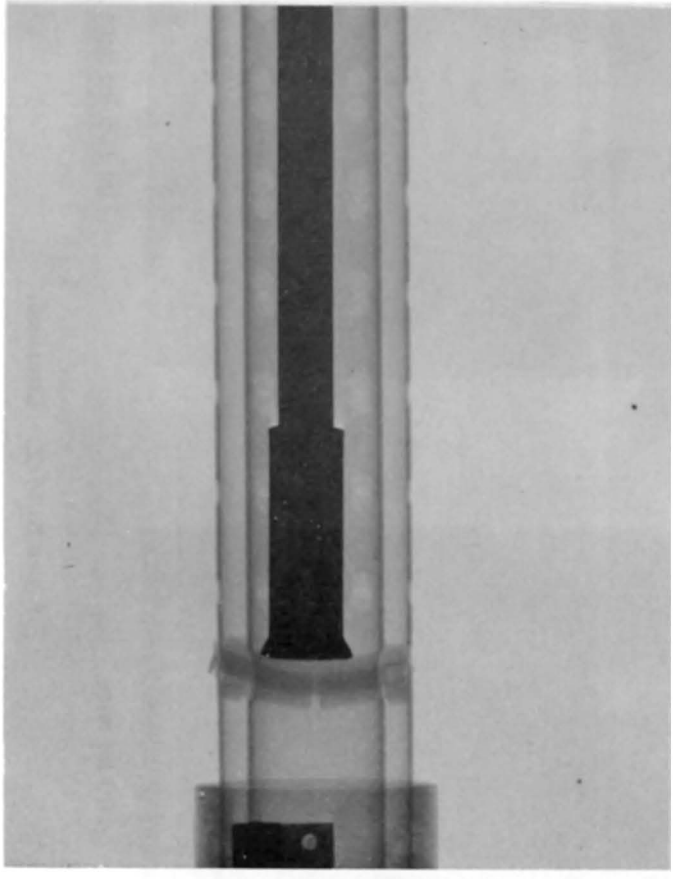

(i) 120 lbs force

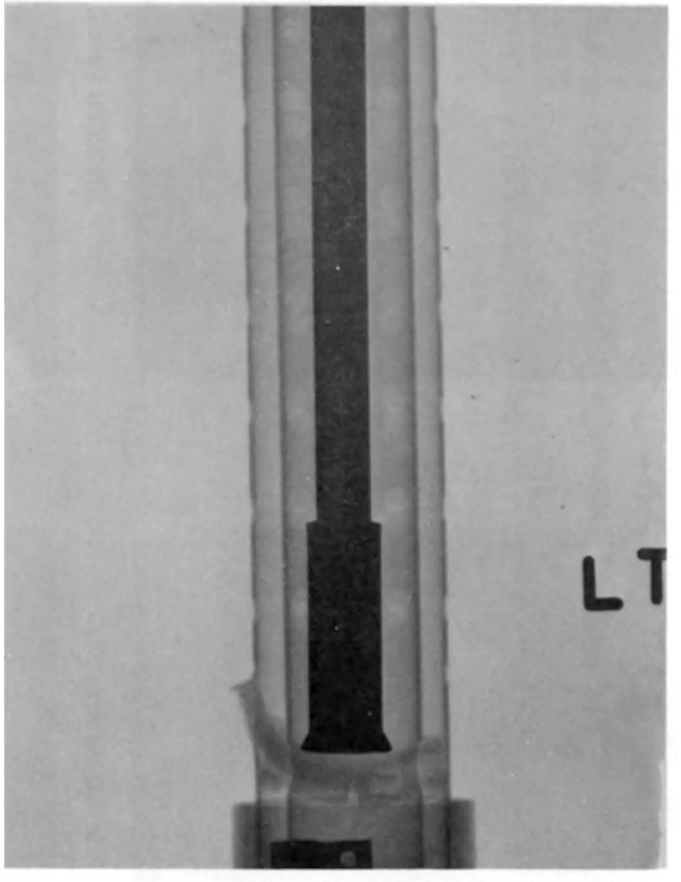

(j)

Figure B.44-2.- Concluded.

B.45 FUEL CELL REACTANT VALVE SHOCK TESTS

B.45.1 OBJECTIVES

The objective of this test was to determine the susceptibility of the valve to move from one position to another as a result of mechanical shock.

B.45.2 TEST EQUIPMENT AND CONDITIONS

Shock tests were performed on two valves in three axes to define the position transfer characteristics of the valve poppets at various g levels. The shock input was accomplished by dropping the valve onto a crushable material; dropping in one axis inputs a shock in the opposite axis. The orientation axes are shown in figure B.45-1.

The voltage and current required to open and close the valve, the leakage through the solenoid valves, and the reverse leakage through the check valves were measured before and after the test and at intervals during the test.

B.45.3 RESULTS

A summary of the shock data is presented in table B.45-I and of the electrical and leakage test data in table B.45-II. Dropping the valve in the direction of the radial inboard axis (fig. B.45-1) tended to close the valve, and dropping in the radial outboard axis tended to open the valve. Shock inputs in the X-axis were normal to the poppet travel and Belleville latch mechanism axis.

The valves, in the open position, were subjected to shocks of 11 milliseconds duration in both the unpressurized and pressurized (935 psig) condition. The lowest unpressurized closing force was 49g, the highest was 78g. With the valves pressurized, an increase in required closing g levels for individual poppets varied from 2 to 16 percent; all further tests were performed with pressure.

Tests in the same axis at a nominal 1 millisecond duration required forces from 88g to 150g to cause a transfer. As noted on table B.45-II, these pulses were filtered from 20 to 2000 Hz for readability.

Tests performed on the valves in the open position with 1/2 ampere load on the opening coils resulted in forces to 285g over a 2-1/2 milliseconds input duration with no transfer of the valves poppets.

Reversing the drop axis and measuring the force required to transfer from closed to open revealed variations from negligible to over a 100-percent increase in required g level. No transfer was effected in the minus X axis even though forces to 236g were measured.

Neither voltage nor current measurement could be used to predict, with any reliability, the relative susceptibility to shock induced transfer among any of the valve poppets. Although some changes in both voltage and current occurred between the pre-test and post-test data, the changes were neither consistent in amplitude nor in direction. Pre-test and post-test leakage comparison also revealed small, inconsistent changes.

After the seventieth drop on one valve, the valve outlets were opened for a leak check. A metal fragment (fig. 45-2), apparently a machining shaving, was observed laying in the B-nut cap of one unit. Since the prior leak check had occurred after the twenty-sixth drop, the fragment must have been dislodged during the interim drops.

The second valve indicated a 0.5 ohm short between the plus 28 V dc side of the switch circuit and the closing coil after a 216g drop in the minus X axis. This was the forty-third drop on the assembly.

B.45.4 CONCLUSION

This test indicated that the fuel cell shutoff valve poppets can transfer from the open to closed position as a result of shocks in excess of 49g, and the valve is more sensitive to shock causing closure than to shock causing opening. The valve will sustain shock levels to 285g without transferring poppet position if drawing 1/2 ampere through the opening coils. The metal shaving found in one valve had no effect on the test.

TABLE B.45-I.- SUMMARY TEST DATA

Fuel Cell Shutoff Valve (ME284-0289)

Shock Summary

Condition	Minimum 'g-level' to Cause Transfer					
	Valve assembly 1			Valve assembly 2		
	Valve A	Valve B	Valve C	Valve A	Valve B	Valve C
Radial inboard axis open to closed						
11 ms 0 psig GN_2	78	72	58	63	49	57
11 ms 935 psig GN_2	86	84	64	68	50	61
1 ms 935 psig GN_2	150	145	88	104	90	99
Radial outboard axis closed to open						
1 ms 935 psig GN_2	146	152	184	128	128	190
Minus X axis open to closed						
1 ms 935 psig GN_2	236 with no transfer			216 with no transfer		
Radial inboard axis open to closed with power-on	285 at 2-1/2 ms with no transfer			240 at 2-1/2 ms with no transfer		

Note: One millisecond pulse data was filtered through a 20 to 2000 Hz band with filter for readability.

TABLE B.45-II.- SUMMARY TEST DATA

Fuel Cell Shutoff Valve (ME284-0289)

Functional Test Summary

Electrical tests	SIN 06553J041024			SIN 06553J040007		
	Valve A	Valve B	Valve C	Valve A	Valve B	Valve C
Pre-test						
Volts to open	17.660	21.785	23.656	17.435	17.571	17.071
Amperes to open	.780	.930	.980	.770	.780	.750
Volts to close	18.973	21.504	18.322	18.673	18.226	17.479
Amperes to close	.818	.910	.785	.815	.800	.780
Post-test						
Volts to open	17.848	22.450	23.388	17.308	17.121	17.309
Amperes to open	.780	.920	.970	.760	.750	.760
Volts to close	18.974	22.920	18.508	18.528	18.152	17.402
Amperes to close	.810	.940	.790	.850	.805	.795
Leakage tests	Leakage in cubic centimeters of GN_2 for 5 minutes at 983 psig					
Pre-test	<0.5	7	10	7	75	41
Post-test	2	8	13	12	61	27

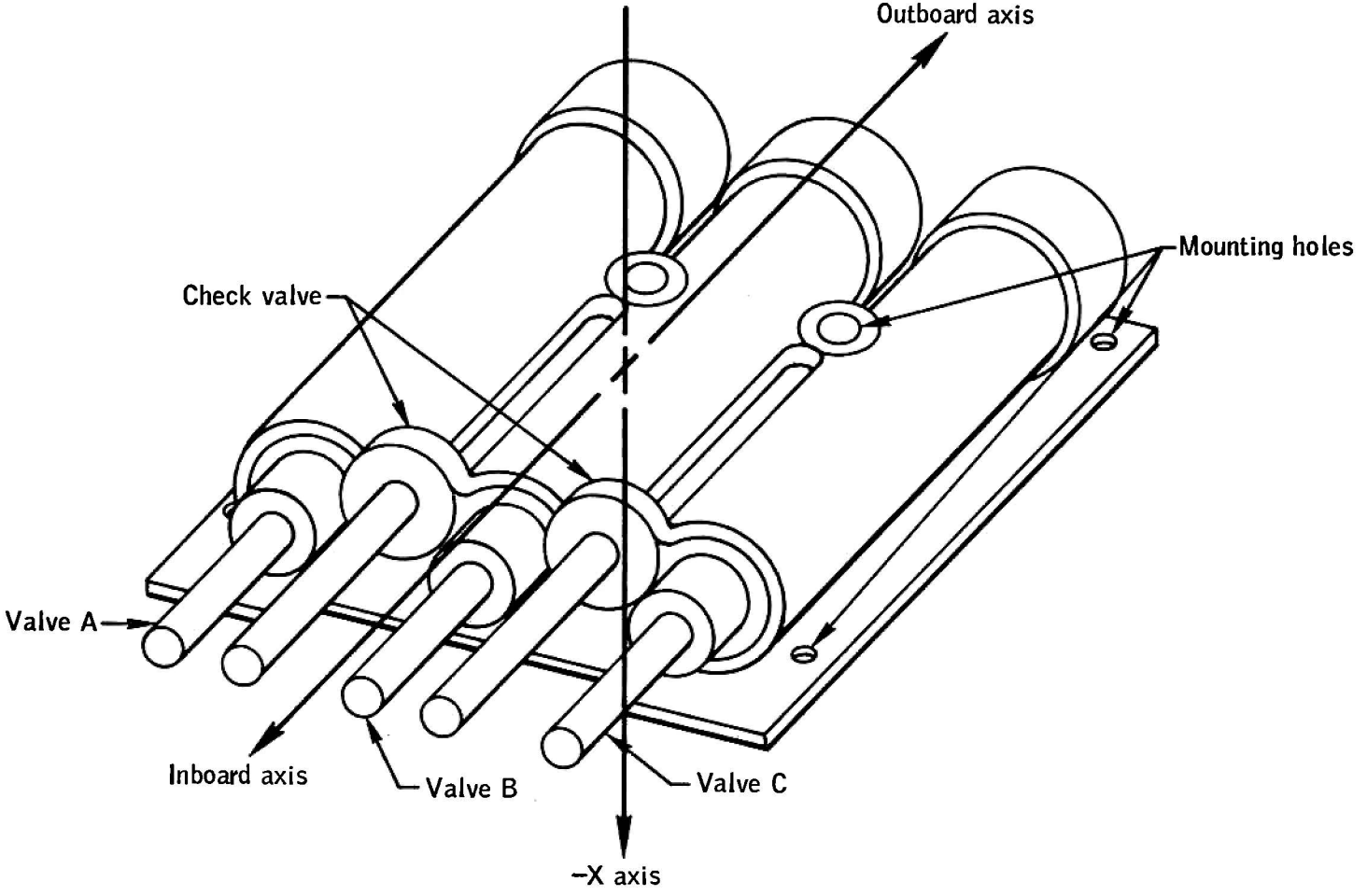

Figure B.45-1.- Fuel cell shutoff valve.

Figure B.45-2.- Metal fragment noted during tests.

B.46 THRESHOLD OXYGEN PRESSURE FOR FLAME PROPAGATION OF MYLAR AND KAPTON

B.46.1 OBJECTIVE

The objective of this test was to determine the threshold pressure of pure oxygen at which combustion of 0.25-mil and 0.50-mil aluminized Mylar and 0.25-mil aluminized Kapton would not occur using the standard nichrome igniter system. The limiting pressure of oxygen required to support combustion of the Mylar and Kapton system in the shelf of the service module was to be hypothesized.

B.46.2 TEST EQUIPMENT AND CONDITIONS

Standard flammability test procedures and equipment were used for these evaluations. The test setup is shown in figure B.46-1. The chamber was evacuated and backfilled with pure oxygen to the desired pressure. This pressure was varied over the range of 5 to 0.5 psia.

The ignition source was a 22-gage nichrome wire with paper insert in coil. The typical energy input was approximately 0.10 Btu, and on selected tests the wire was allowed to fuse.

The combustion characteristics were determined by visual observation through the test cell window and by film coverage.

B.46.3 RESULTS

The test findings(bottom ignition) are as follows:

Oxygen, psia	Results
	Mylar, aluminized NRC_2, 0.25 mil
5	Sample ignited and burned completely.
2.5	Sample ignited and burned completely.
2.0	Sample ignited and burned completely.
1.5	No ignition.
1.0	No ignition.
0.5	Igniter wire fused, ignited and burned completely, Mylar folded around igniter.
1.5	Sample ignited and burned completely.
1.0	No ignition.
1.0	18 gage nichrome wire, sample ignited and burned completely.
0.5	18 gage nichrome, no ignition.
	Mylar 0.5 mil
1	Sample ignited and burned completely.
0.5	No ignition.
	Mylar, aluminized on both sides, 0.25 mil
1.5	Sample ignited and burned completely.
1.0	Sample ignited and burned completely.
0.5	One of two samples ignited and burned completely.
0.3	No ignition.
	Kapton, aluminized, 0.50 mil
1.5	Sample ignited and burned completely.
1.0	No ignition.

In addition to the preceding tests, flammability tests using 18-gage polytetrafluoroethylene insulated wire in liquid oxygen at 14.7 psia were conducted by using overload procedure. Three tests were conducted, and the wire fused at 125 to 145 amperes in liquid oxygen. No ignition was noted at the fusion current of the wire in 14.7 psia liquid oxygen.

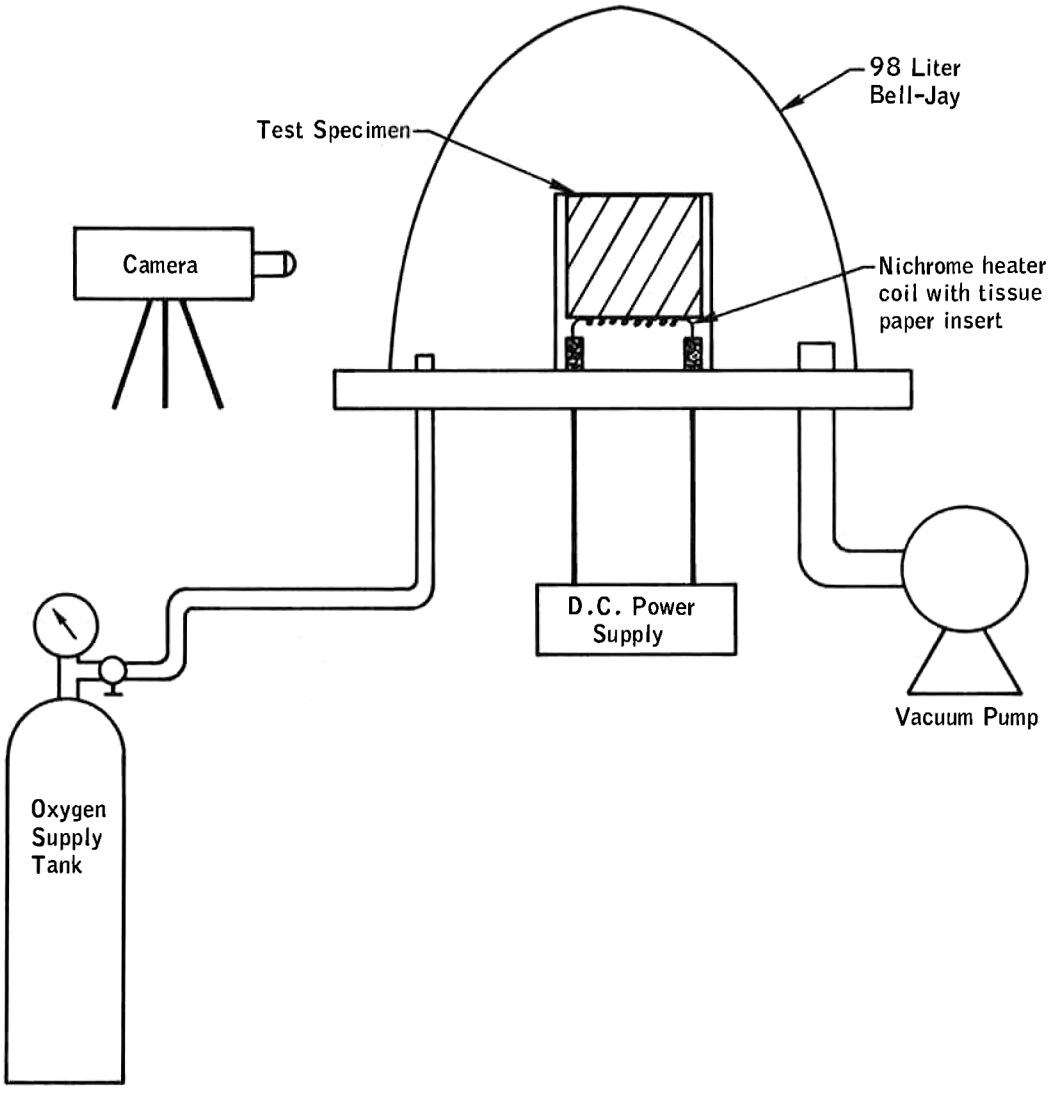

Figure B.46-1.- Test setup for determining threshold oxygen pressure for flame propagation and Mylar and Kapton.

B.47 FILTER ASSEMBLY TEST

B.47.1 OBJECTIVE

The objective of this test series was to determine if the ground support equipment filter assembly contributed to the difficulty in unloading cryogenic oxygen tank 2 during the Apollo 13 countdown demonstration test.

B.47.2 TEST EQUIPMENT AND CONDITIONS

The filter assembly was installed into the test system as noted on figure B.47-1. The inlet pressure to the spacecraft side of the filter was increased from 0 to 3 psig. The effluent gaseous nitrogen was flowed through the sampler to collect any loose particles that might be expelled from the filter assembly as a result of flow. The 0.45-micron membrane filter pad within the sampler was removed, and the particles were measured and counted with a 40-power binocular microscope.

The filter assembly was then installed into a flow system as noted on figure B.47-2. The first test was conducted with the deionized water flow rate of 1.0 gpm, flowing from the spacecraft and ground support equipment to the assembly. The flow rate was varied from 0.75 gpm to 2.0 gpm to determine the gross differential pressure with flows of 0.75, 1.0, and 2.0 gpm. All of the effluent from the entire test was flowed through four samplers connected in parallel. After the flow test was completed, the filter pads were removed from the collectors, dried, and then inspected with a 40-power binocular microscope.

The collectors were reloaded with clean 0.45-micron membrane filter pads, installed into the test system, and the filter assembly was reinstalled into the flow system to permit flow from the ground support equipment to the spacecraft end. The above tests were repeated.

Upon completion of the flow tests, the samplers and the filter assembly were removed from the test set-up and a tare fixture was installed in place of the filter assembly. The system tare differential pressure was measured at 0.75, 1.00, and 2.00 gpm. After the tare pressures were deducted from the gross differential pressures obtained earlier, the net differential pressure of the filter element was derived.

The filter element was removed from the vacuum jacket and subjected to a bubble-point test using isopropyl alcohol (isopropanol) and gaseous nitrogen. The bubble point data were corrected to standard bubble point conditions and were recorded.

B.47.3 RESULTS

The net differential pressure of the element was less than the allowable clean differential pressure of 1 psi specified on the drawing; the actual net differential pressure with 1.0 gpm flow of deionized water was 0.480 psi with the flow from the spacecraft direction and 0.278 psid with flow in the spacecraft direction.

The effluent from the differential tests was collected, filtered, and graded by micron size and quantity of particles. The sizes and amounts of particles were recorded. Three glass beads were found in the effluent from the spacecraft flow direction. There was also a quantity of lubricant on two of the filter pads from the same liquid.

The corrected bubble point of the filter element was 22.3 inches of water. This value is equivalent to a pore diameter of 0.4 microns. The filter as originally delivered had bubble point of 22.8 inches of water which is equivalent to a pore diameter of 9.2 microns.

There were no indications of damage to or degradation of the filter.

An excessive amount of lubricant was used in the bore of the bayonet end (ground support equipment) of the vacuum jacket assembly.

B.47.4 CONCLUSIONS

The ground support equipment filter assembly was not the cause of nor did it contribute to the Apollo 13 cryogenic oxygen system malfunction at the launch site.

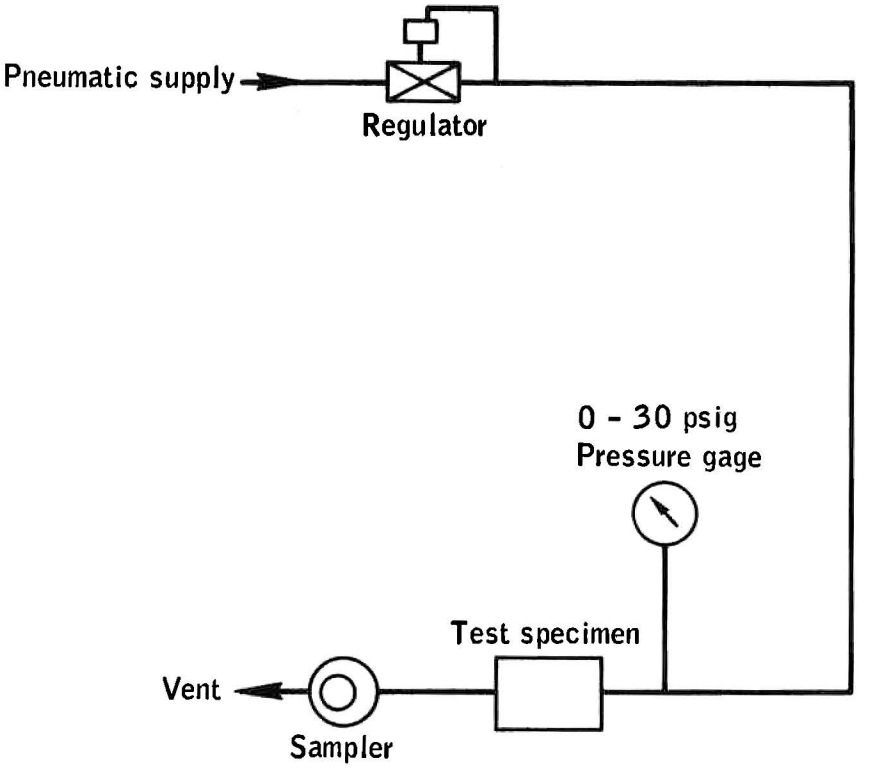

Figure B.47-1.- Pneumatic blown-down system.

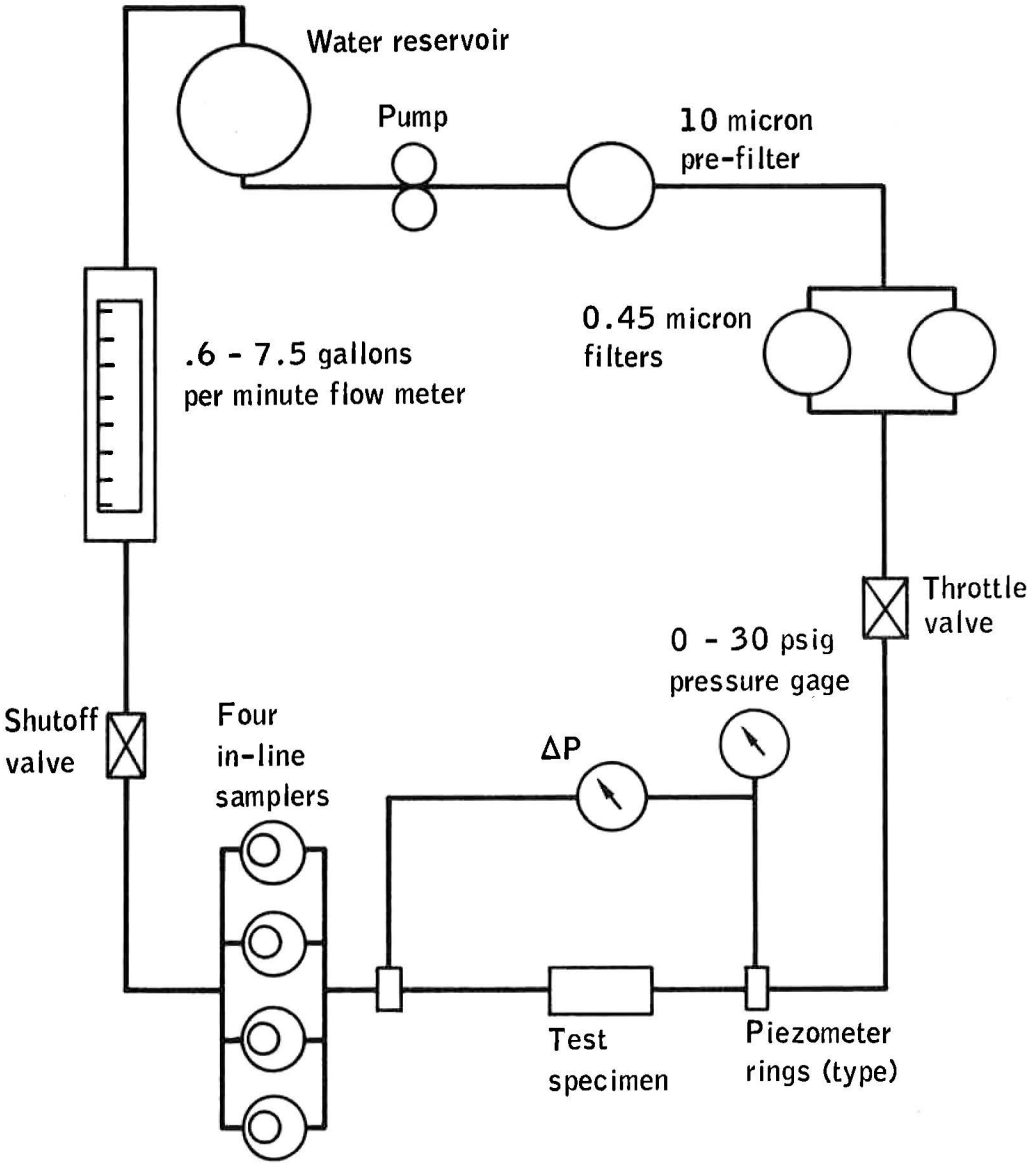

Figure B.47-2.- Flow test system.

B.48 LIQUID OXYGEN IMPACT SENSITIVITY OF VARIOUS MATERIALS

B.48.1 OBJECTIVE

The objective of this test was to determine the liquid oxygen impact sensitivity of various materials used in the Apollo cryogenic oxygen tank.

B.48.2 TEST PROCEDURES AND CONDITIONS

The tests were conducted by the procedures outlined in Marshall Space Flight Center specification 106B, "Testing of Compatibility of Materials for Liquid Oxygen Systems." The amount of Drilube 822 grease and 60-40 solder sent to Marshall Space Flight Center was insufficient to determine threshold values.

B.48.3 RESULTS

Listed below are test results of the materials evaluated or results of previous tests conducted on these materials. These materials were of the same trade names used in the oxygen tank with the exception of the 60-40 solder.

Drilube 822	1/20 audible report
Polytetrafluoroethylene-insulated wire, MIL-W-16878, type X	0/20 at 72.3 ft/lb
Polytetrafluoroethylene-insulated wire, Simmons probe wire	0/20 at 72.3 ft/lb
60-40 solder	7/20 at 72.3 ft/lb

60-40 Solder Data from NASA TMX 53533

Dutch Boy Rosincore Solder

20/20 at 72.3 ft-lb
17/20 at 57.8 ft-lb
17/20 at 43.4 ft-lb
12/20 at 28.9 ft-lb
3/20 at 14.5 ft-lb
0/20 at 7.2 ft-lb

Erskine 5-core Solder

14/20 at 72.3 ft-lb
12/20 at 57.8 ft-lb
7/20 at 43.4 ft-lb
5/20 at 14.5 ft-lb
0/20 at 7.2 ft-lb

Drilube 822 Data from NASA TMX 53533 and TMX 53052

0 to 5 reactions at 72.3 ft-lb

48.4 CONCLUSIONS

The normal acceptance criteria of Marshall Space Flight Center specification 106B dictates that for a material to be used in a liquid oxygen-gaseous oxygen system, it must sustain 20 separate tests at 72.3 ft-lb without a reaction or not more than 1 reaction in 60 separate tests at 72.3 ft-lb. The 60-40 solder would not meet this acceptance criteria. Marshall Space Flight Center ALERT 68-11 requires that each container of Drilube 822 be evaluated prior to use in liquid oxygen.

B.49 EXAMINATION OF MATERIALS IN OXYGEN TANK FAN MOTOR

B.49.1 OBJECTIVE

One objective of this test is to investigate a destratification fan motor of the type used in the Apollo 13 oxygen tank, identify the motor parts, especially non-metallic parts, and provide information concerning their functional usage. A second objective is to identify surfaces where Drilube 822 lubricant is present and report additional information requested or considered important as a result of disassembling the motor.

B.49.2 PROCEDURES

A lower ac fan motor (part number 19A1757 referenced in Beech Aircraft Corporation drawing 325352-2515) from an oxygen tank probe was submitted for disassembly and examination. The motor was manufactured by Globe Industries and is identified as serial number K430031, motor housing 140, and was provided by D/191-202. The fan motor was disassembled and the parts were identified from Globe and Beech drawings and are listed by item numbers in tables B.49-I to B.49-III corresponding to the item numbers on figures B.49-1 to B.49-5. The part name, part number, and materials are listed.

The motor, when received, was attached to the tank heater probe and was removed and disassembled under clean room environment; except when machining was necessary on the housing (item 1) to remove the stator assemblies (item 4). The motor was mounted for examination purposes as shown in figure B.49-1, and the non-metallic materials listed in table B.49-II and shown in figure B.49-5 were retained for testing.

B.49.3 RESULTS

The surfaces of the motor parts were inspected with black-light for hydrocarbons; nothing was detected. Selected parts were analyzed for non-volatile residue and lubricants. The parts were rinsed with Freon TF and the non-volatile residue determined gravimetrically. The non-volatile residue (soluble portion) was taken up in carbon tetrachloride and analyzed for lubricants (Drilube 822) using infrared spectrophotometric methods. Drilube 822 was detected on the threaded areas of the motor housing and mounting hardware. No lubricants were detected on the rotor, bushings, or bearings (table B.49-III).

The magnet wire (item 4C) was tested gravimetrically for coating content using a micro balance and 26 centimeters of wire. The result reported, representing the quantity of coating, includes the polytetrafluoroethylene and ceramic (Ceroc T) materials. The coating was analyzed using X-ray diffraction and emission spectrographic methods and the results are reported in table B.49-III. The results of the analyses would indicate the copper wire is coated with a zinc oxide glass base ceramic mixed with a small amount of polytetrafluoroethylene.

The disassembly of the motor revealed two areas involving the housing and the stator assembly that exhibit mild corrosion. These areas are the housing and the stator yolk ring (item 1). Corrosion was also present on the yolk ring at the shim cover (item 14) location; however, it was less intense and appeared as only a darkening of the surface.

B.49.3 CONCLUSIONS

The corrosion present resulted from the contact of dissimilar metals and was most evident where Cor T (stator laminations, item 7) is in contact with the aluminum housing (fig. B.49-3).

In addition to the corrosion, the examination revealed three other conditions that should be considered.

Several metallic particles were found in the rear bushing (item 11) following the removal of the bearing. They appeared to be contaminants and not a result of damage to the motor bearing.

The Drilube 822 contributed very little to the total non-volatile residue, which would indicate additional contamination was present on the parts tested (items 1B, 13, and 16 to 18).

The insulated conductor (item 6) for the lower motor runs through a tube inside the probe and the sleeving was damaged during removal because of sharp edges.

TABLE B.49-I.- IDENTIFICATION OF MOTOR PARTS

Fan, AC, Cryogenic Destratification, FC, IND. 30, 3-pole, oxygen

Item number	Part name	Part number	Material
1	Housing Assembly	2A830	
1A	Housing	4D1838	Al 2024 T351
1B	Stator Yoke Ring	27D1216	Corlite Insulated Cor T
2	Front Bearing	15D1156	440 CRES
2A	Cage		Rulon A
2B	Balls		440 CRES
3	Rear Bearing	1501156	
4	Stator Assembly		
4A	Insulating Compound	47D113	FEP ptfe/Liquinite Coating
4B	Cell Cover Insulator	9D1462	PTFE Impregnated Glass Cloth
4C	Magnet Wire	405253	Ceroc T ptfe/Ceramic/Copper
4D	Slot Stator Insulator	9D1487	PTFE Impregnated Glass Cloth
4E	Spider Sleeve Spacer	27D1214	303 CRES
4F	Stator Sleeve	37D659	416 CRES
4G	Solder		
5	Stator Retainer	35D635	2024-T351 Al
5A	Insulator	9D1484	PTFE
5B	Insulating Sleeving	9D1489	H/S PTFE Sleeving #31E Natural Color
5C	Terminal	32D794	Brass 1/2 Hard QQ-B-613
5D	Grommet	21D918	PTFE
5E	Strain Relief	27D1253	Armalon, PTFE CTD Glass Fabric
6	Conductor & Extruded Insulation	40D1757 -1, -2, -3, -4	Nickel Plated Grade A PTFE, -1 Black, -2 Red, -3 Blue, -4 White
7	Stator Laminations	27D1215	Corlite Insulated Cor T
8	Impeller Assembly		
8A	Front Impeller Plate	1702255	3003 Al (QQ-A-359)
8B	Impeller Vane	27D1207	Alcoa 12 Brazing Sheet
8D	Impeller Hub	19D1250	1100 F Al (QQ-A-411)
8E	Impeller Back Plate	17D2256	Alcoa Brazing Sheet 12
9A	Bearing Plate	17D2582	303 CRES
9B	Coil Spring Pin	20D807	302 CRES
9C	Coil Spring Pin	20D817	302 CRES
10	Rotor	7A3044	416 CRES (QQ-S-763)
11	Bearing Bushing	15D1173	303 CRES
12	Shims	21D917	302 CRES
13	End Plate	17D2294	2024-T4 Al
14	Shim Cover	21D956	302 CRES
15	Beech Mounting Hardware		
16	Beech Mounting Hardware		
17	Beech Mounting Hardware		
18	Beech Mounting Hardware		
19	Screw	1D1100	MS35275-13

TABLE B.49-II.- IDENTIFICATION OF NON-METALLIC PARTS

Fan, AC, Cryogenic Destratification, FC, IND. 30, 3-pole, oxygen (non-metallics)

Item number	Part name	Part number	Material
[a]2A	Bearing Cage		Rulon A
[a]4A	Insulating Compound Stator Assembly	47D113	FEP PTFE/Liquinite Coating
[a]4B	Cell Cover Insulator	9D1462	PTFE Impregnated Glass Cloth
[a]4C	Magnet Wire Coating		Ceroc T PTFE
[a]4D	Slot Stator Insulator	9D1487	PTFE Impregnated Glass Cloth
[a]5A	Insulator	9D1484	PTFE
5B	Insulating Sleeving	9D1489	H/S PTFE Natural Color
5D	Grommet	21D918	PTFE
5E	Strain Relief	27D1253	Armalon, PTFE CTD Glass Fabric
[a]6	Extruded Insulation	40D1757-1, -2, -3, -4	PTFE

[a]Samples of this material retained for test purposes.

TABLE B.49-III.- LABORATORY TEST RESULTS

Non-Volatile Residue (NVR) and IR Analysis

Item	Part name	NVR	Analysis Results
1B	Stator Yoke Ring	2.1 mg	Drilube 822 (present in threaded areas)
2	Front Bearing	0.1 mg	(None detected)
3	Rear Bearing	0.6 mg	(None detected)
[a]4C	Mg		
10	Rotor	0.2 mg	(None detected)
13	End Plate	3.8 mg	Drilube 822
16 to 18	Beech Mounting Hardware	1.3 mg	Drilube 822

[a]Quantity of coating per unit length of wire: 117 micrograms/cm
Identification of coating materials: X-ray diffraction results indicate PTFE and zinc oxid. Spectrographic results indicate zinc and silica are present in the coating.

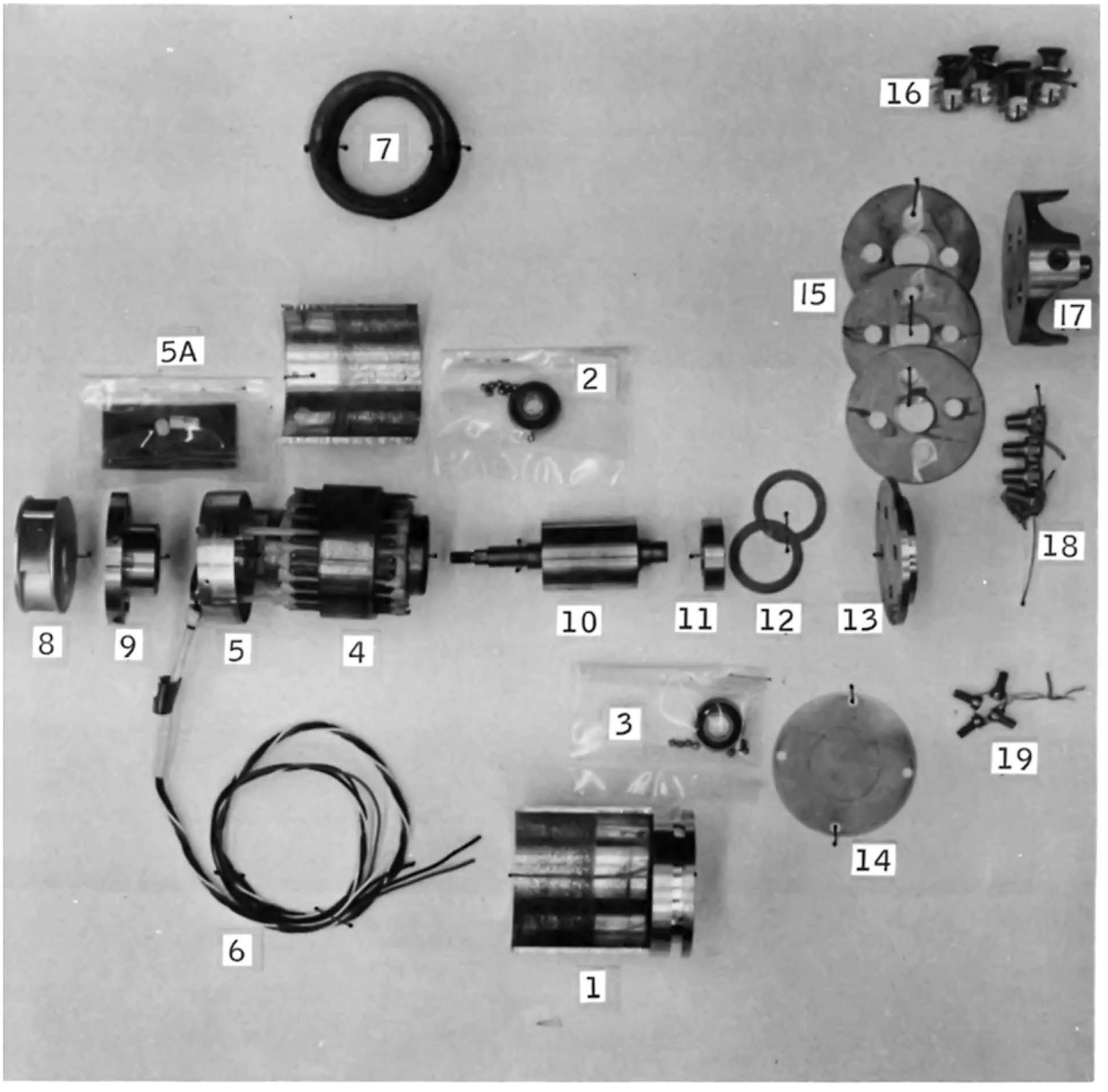

Figure B.49-1.- Disassembled fan motor.

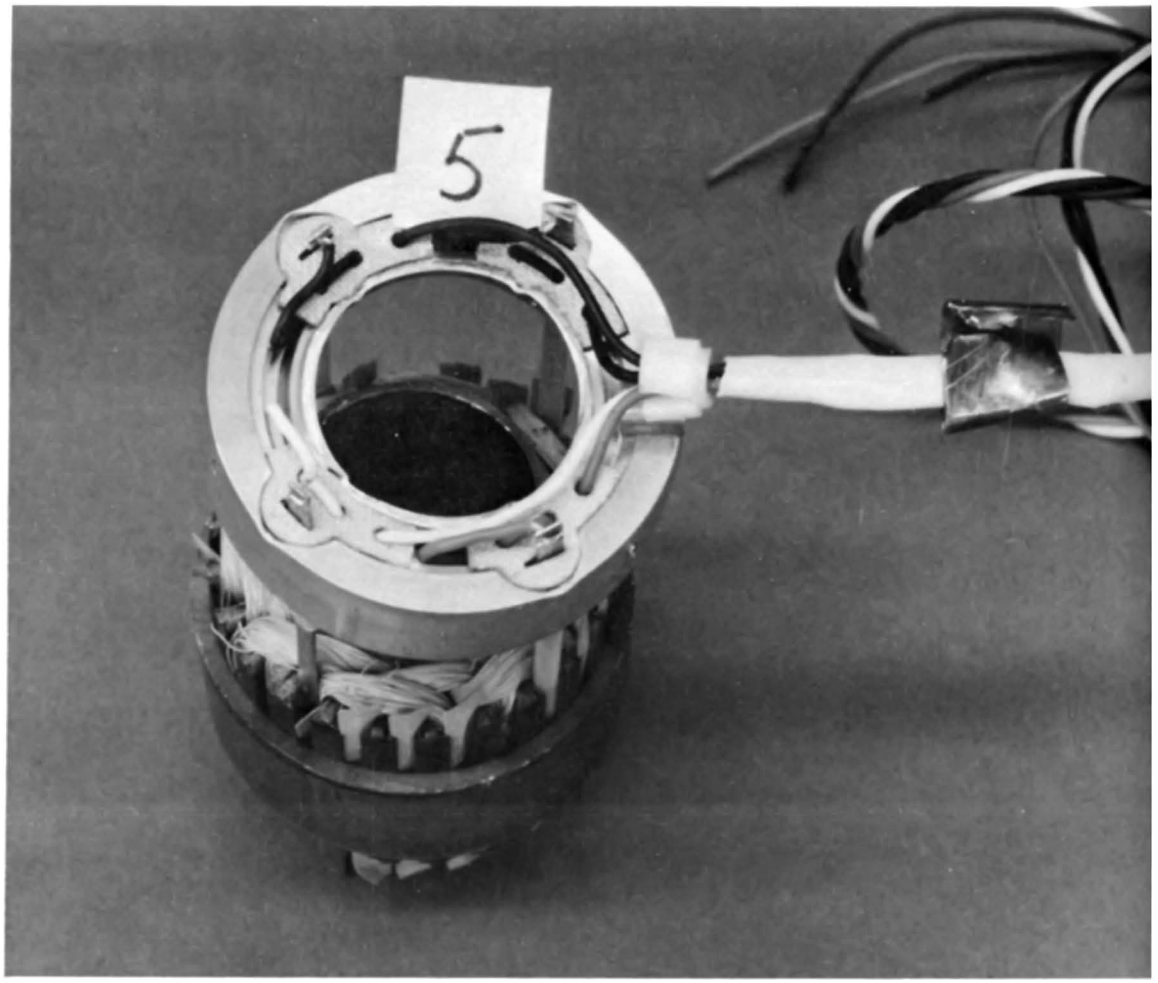

Figure B.49-2.- Stator retainer.

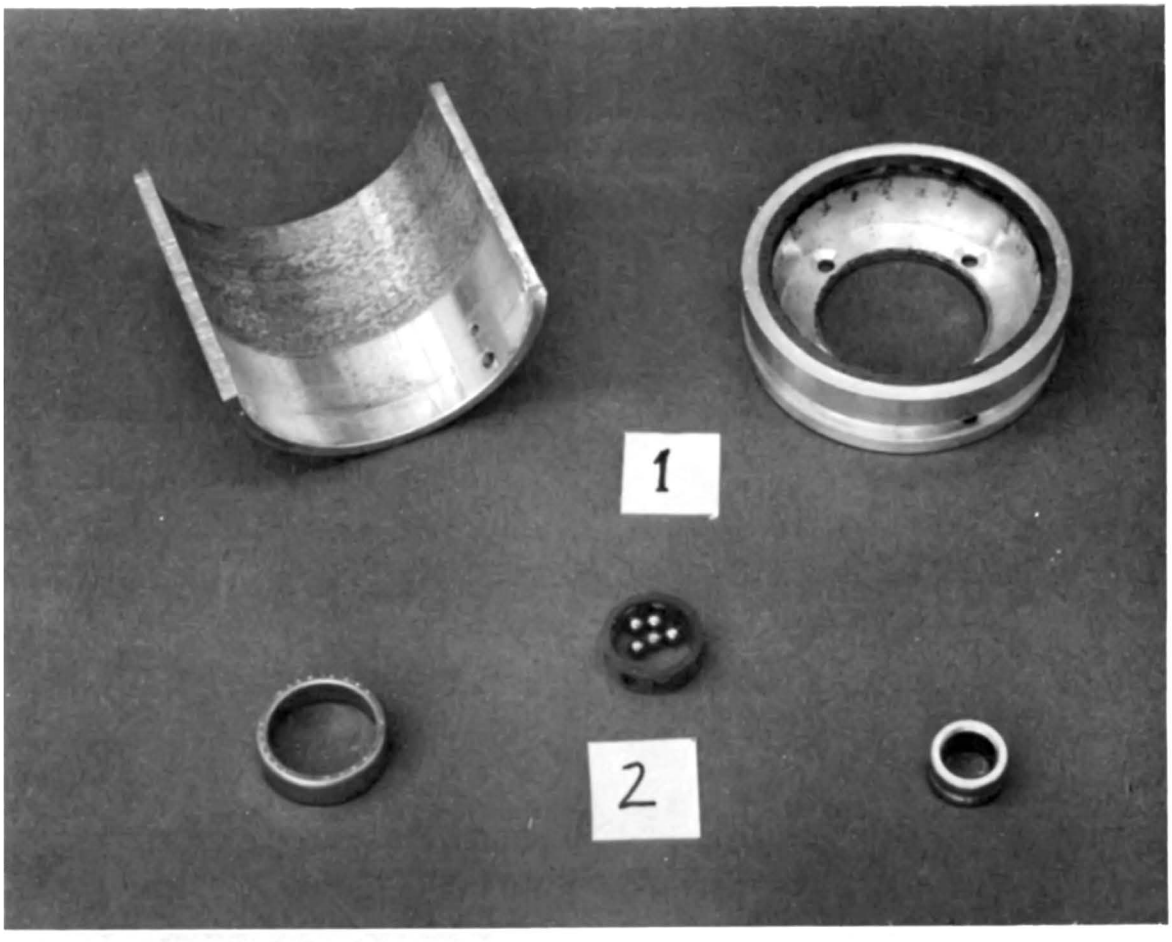

Figure B.49-3.- Housing assembly and bearing.

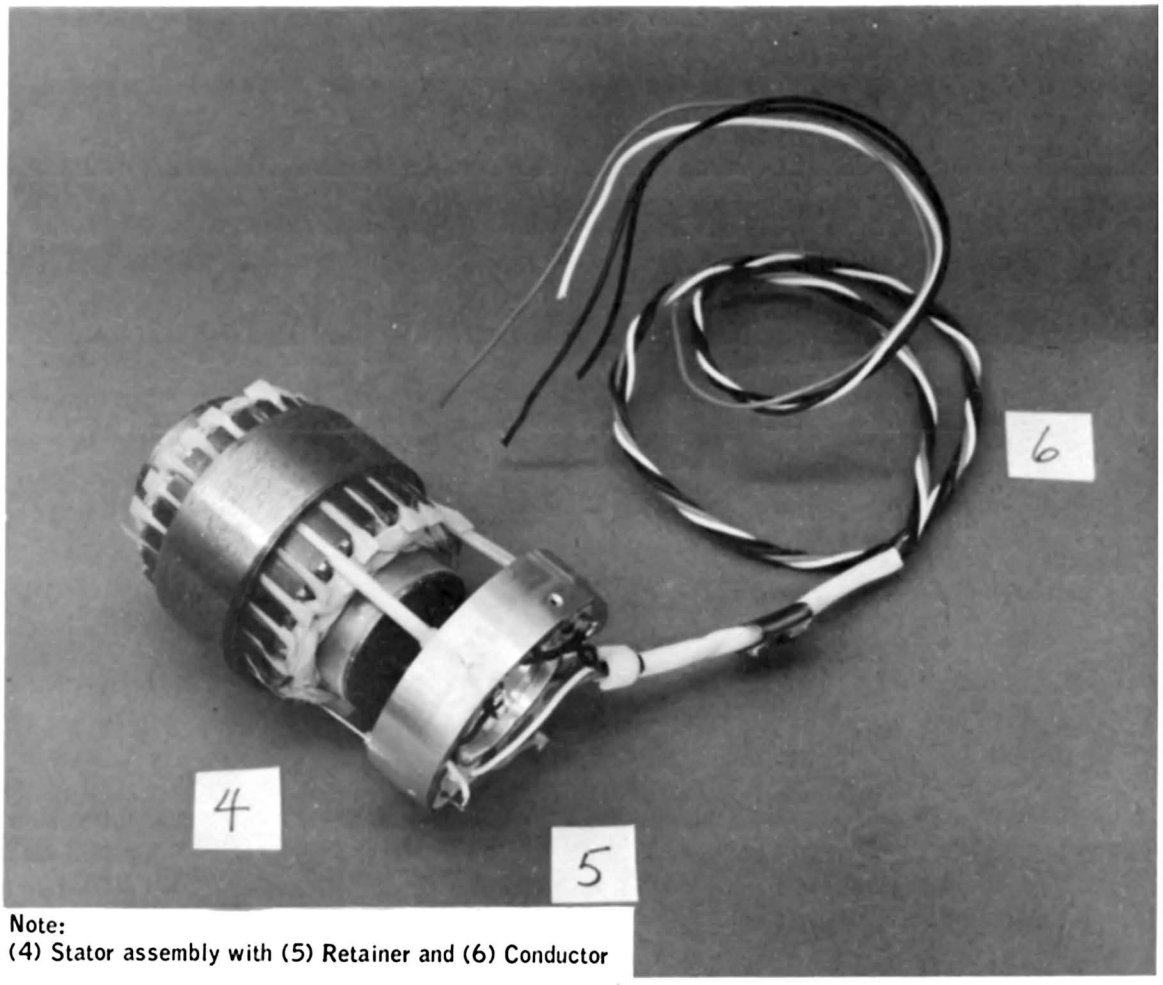

Note:
(4) Stator assembly with (5) Retainer and (6) Conductor

Figure B.49-4.- Stator assemble.

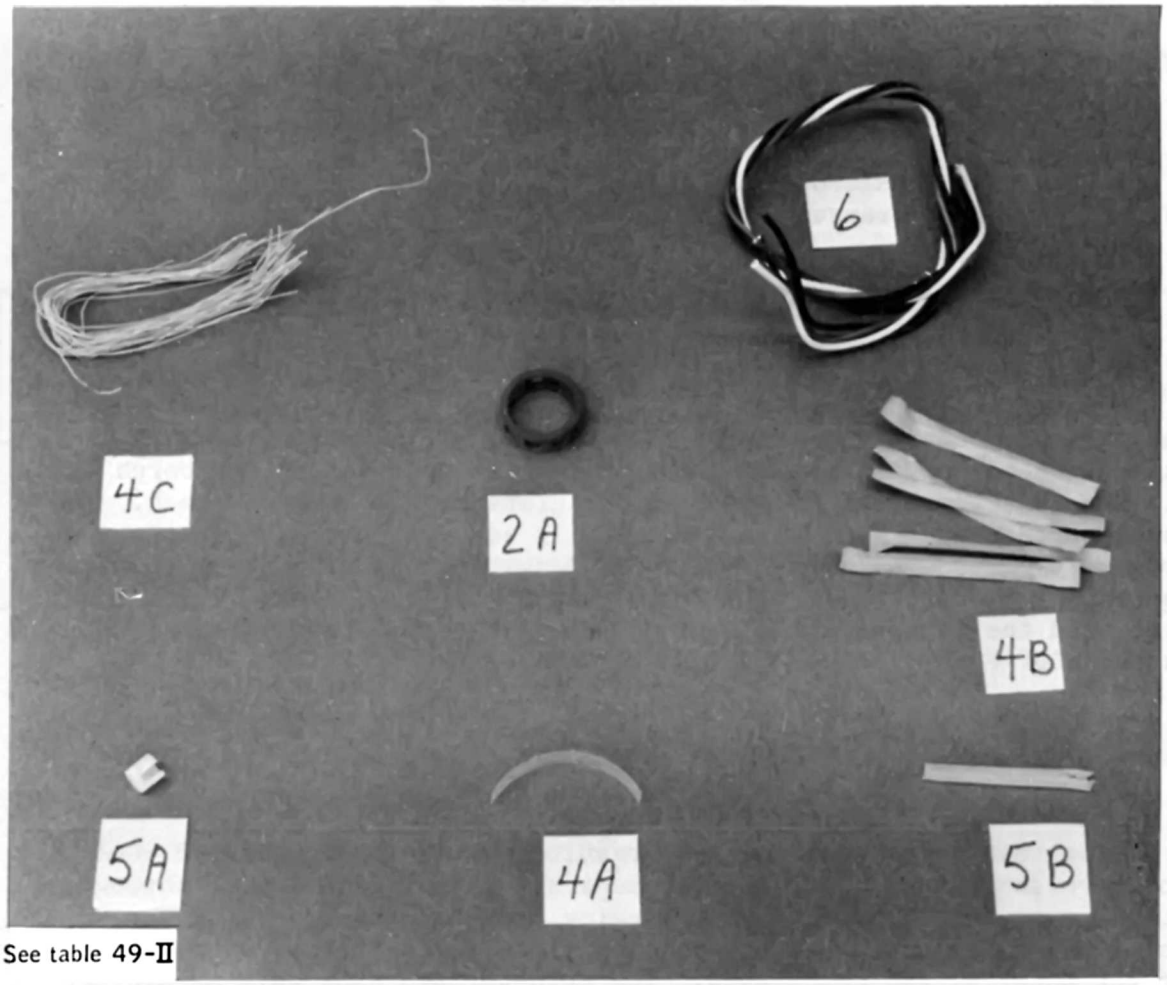

See table 49-II

Figure B.49-5.- Non-metallic materials.

B.50 LONG-FLAW TOLERANCE OF INCONEL 718 THIN SHEET MATERIAL TEST

B.50.1 OBJECTIVE

Three flat panels of Inconel 718 were tested to determine the burn-through damage tolerance.

B.50.2 TEST EQUIPMENT AND CONDITIONS

The test setup is shown in figure B.50-1. The test procedure was to first preload the specimen panels (28 inches long by 0.049 inch thick) in tension to the desired stress level. Then an oxyacetylene torch was lit and quickly set at a predetermined distance from the specimen. The torch horizontal travel was automatically controlled at the speed of approximately 0.13 in./sec. This speed resulted in a relatively localized heating of the specimens. The slot widths were approximately 0.4 inch wide, and the temperature 1 inch from the center of the slots did not exceed 600° F.

B.50.3 RESULTS

The test parameters and test results are listed in table B.50-I. The tarnished surface of the specimens shown in figure B.50-2 through B.50-4, was caused by the 1325° F aging heat treatment. Using the values for slot length and gross stress, the plane stress fracture toughness K_c of the material was calculated. The burn-through slot gave an average fracture toughness of 279 KSI $\sqrt{\text{in.}}$ This value is in reasonable agreement with published values of approximately 300 KSI $\sqrt{\text{in.}}$ for center-cracked specimens of similar thickness.

B.50.4 CONCLUSIONS

The tests indicate that significantly large holes must be burned into Inconel 718 specimens to cause catastrophic failure. The burn-through slot results are similar to published data for through-cracked specimens, both in the critical slot length and in the absence of slow tear before fracture.

A spherical pressure vessel having a diameter and wall thickness similar to the Apollo cryogenic oxygen tank would have a critical slot length approximately 50 percent that of the flat panels used in this test. This would occur primarily because of curvature and lateral pressure effects that were not simulated in the flat specimen tests.

TABLE B.50-I.- BURN-THROUGH TEST RESULTS FOR INCONEL 718 FLAT PANELS

Specimen number	Panel width, inch	Critical slot length, inch	Gross area stress, KSI[b]	Net stress, UTS[c]	Burn time, sec	K_c KSI $\sqrt{\text{in.}}$
1	12.0	5.85	80.0	0.772	41.5	284
2	9.5	3.80	[a]101.0	0.833	31.0	274
3	9.5	2.65	129.0	0.883	22.0	278

[a]Same stress level as in cryogenic oxygen tank at a pressure of 1008 psig.

[b]Kips per square inch.

[c]Ultimate tensile strength.

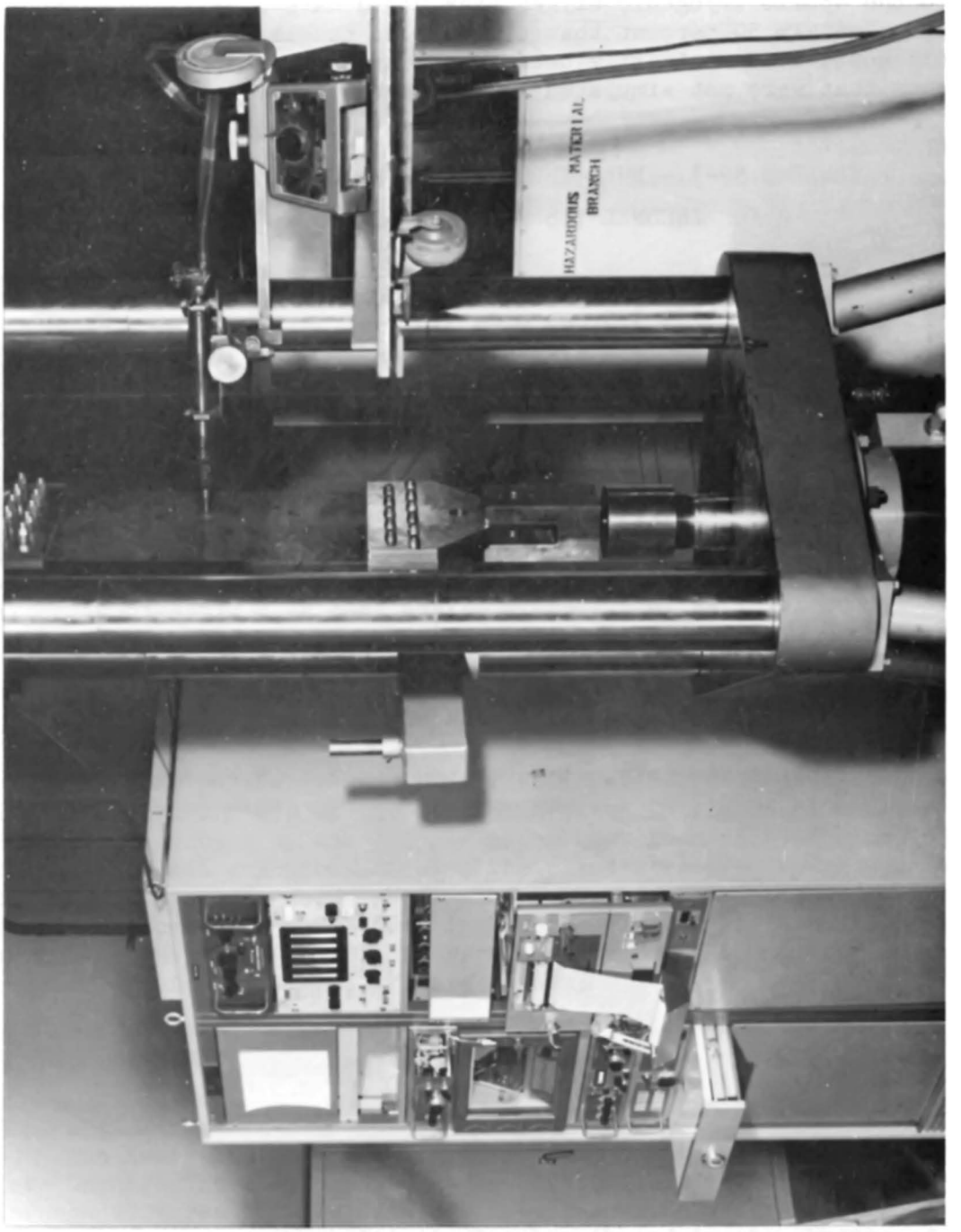

Figure B.50-1.- Test apparatus.

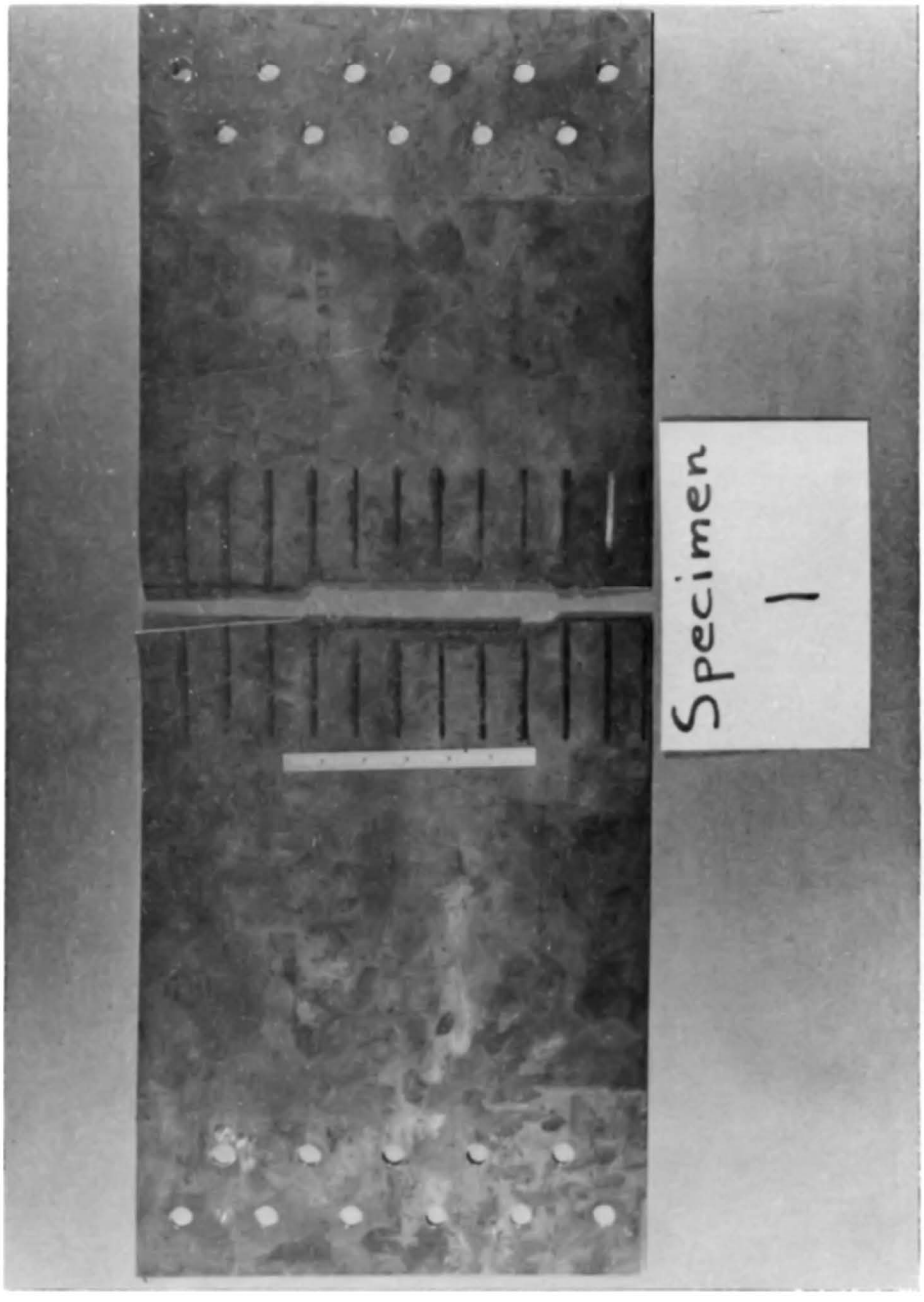

Figure B.50-2.- Condition of specimen 1 after test.

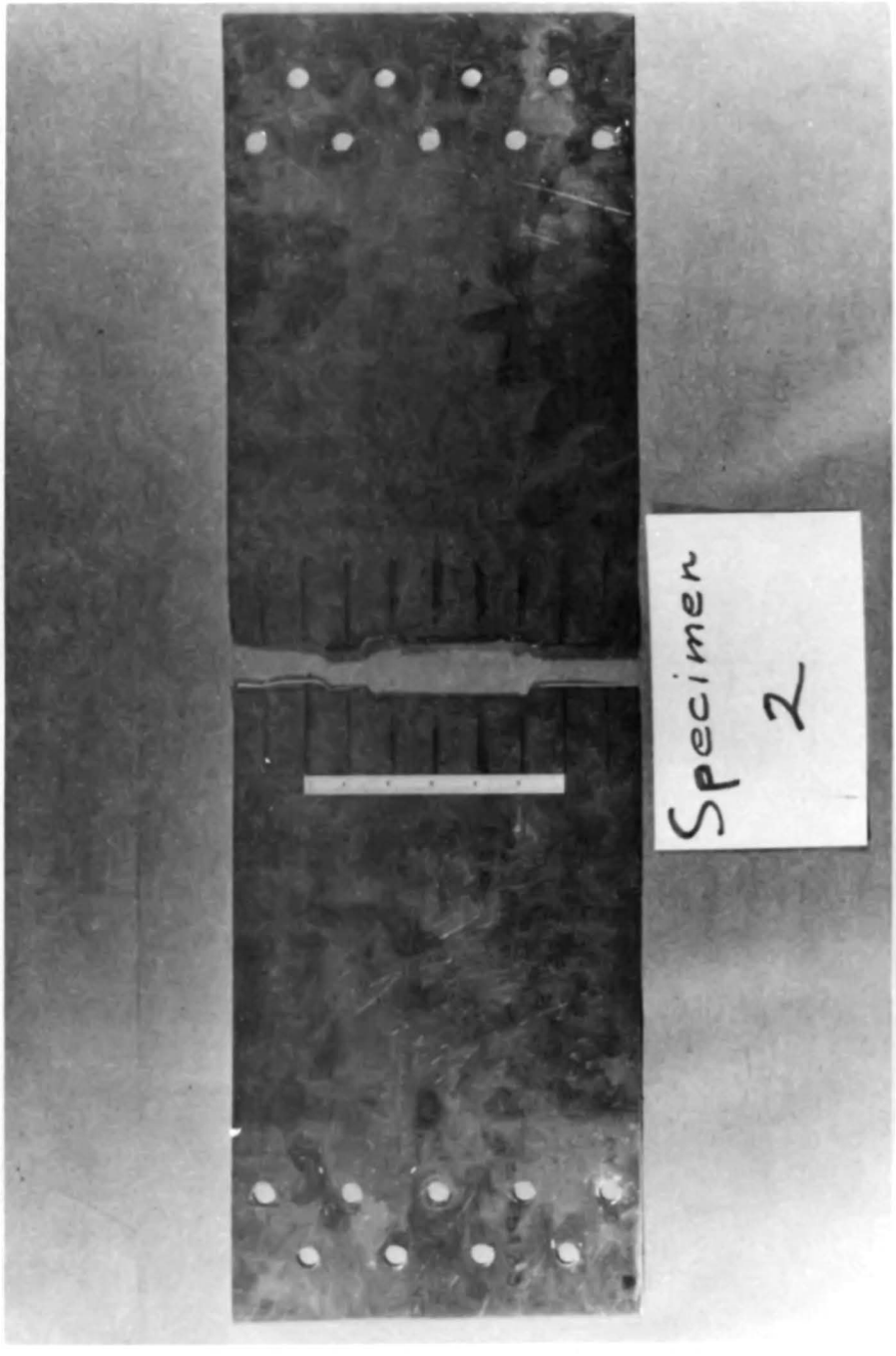

Figure B.50-3.- Condition of specimen 2 after test.

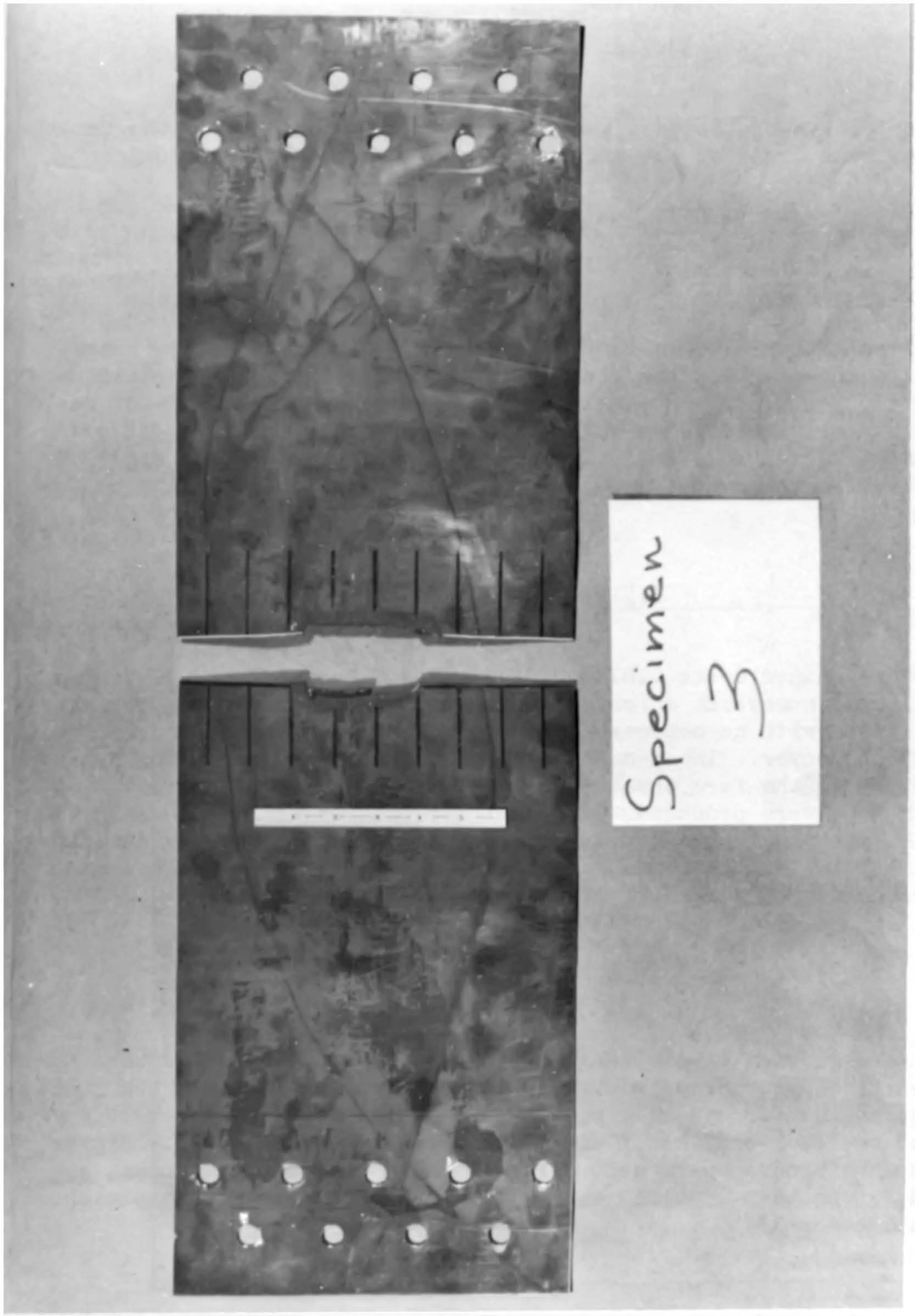

Figure B.50-4.- Condition of specimen 3 after test.

B.51 SERVICE MODULE OXYGEN TANK DOME IMPACT TEST

B.51.1 OBJECTIVE

The objective of the test was to determine the effects of the impact of the fuel cell shelf on the vacuum pinch-off tube cover from oxygen tank 2.

B.51.2 TEST EQUIPMENT AND CONDITIONS

The test setup is shown in figure B.51-1. A 12-inch square honeycomb panel 2 inches thick was clamped to two 1-1/4-inch square aluminum bars with the center of the panel 8 inches from the clamped edge of the bars. An oxygen tank dome was placed on a rod with a total weight of 175 pounds. The cylinder impacting the panel was placed at an angle of 116 degrees from the pendulum rod in a plane perpendicular to the pendulum swing.

B.51.3 RESULTS

Crescent-shaped dents 0.013, 0.026, and 0.033 inch thick deep were produced in the honeycomb at calculated impact velocities of approximately 18 to 28 in/sec with no noticeable damage to the vacuum annulus dome or pinch-off tube cover. These dents scarred the face sheet coating but did not cut into the face sheet aluminum. When dents greater than 0.033 inch deep were produced, permanent deformation was observed in the dome of the vacuum annulus but in no case were the face sheets found to be delaminated. The tests are summarized in table B.51-I, and the results are shown in figure B.51-2.

B.51.4 CONCLUSIONS

The acceleration levels measured in these tests were lower than those predicted by previous analyses. Based on these results, the quantity probe and heater assembly acceleration levels due to impact of oxygen tank 2 and the fuel cell shelf are limited to approximately 7g. Higher energy impacts produce permanent deformation in the vacuum annulus, as indicated by the test results, and restrict the accelerations experienced by the tank assembly.

TABLE B.51-I.- IMPACT TEST SUMMARY

Test run	Initial angle[a] α, deg	Distance[a] A, in.	Distance[a] B, in.	Panel displacement, in.	Tangential acceleration, g	Normal acceleration, g	Panel indentation dimensions, in.			Remarks
							Depth	Width	Length	
1	1	58 5/32	63							Dome indentor did not impact the honeycomb panel.
2	2	59 3/32	63 7/8							Dome indentor did not impact the honeycomb panel.
3	3	59 3/4	64 9/16	0.045	4.5	2.5	0.026	0.83	1.50	
4	2 1/2	59 17/32	64 9/32	0.030	4.25	3.8	0.013	0.72	1.14	
5	3 1/2	60 3/32	64 7/8	0.050	5.1	5.0	0.033	0.91	1.56	
6	4	60 9/16	65 5/16	0.050	6.0	5.8	0.0365	0.99[b]	1.67	
7	5	61 21/64	66	0.056	7.4	8.4	0.024	0.86[b]	1.63	The dome caved in and the indentor was hitting on a flatter angle. This could have occurred on test 6 as is indicated by the maximum depth data.
8	6	62 5/64	66 25/32	0.056	9.5	9.5	0.030	1.12[b]	1.69	

[a]As shown on figure 51-1.

[b]The indentations overlap each other in the width dimension.

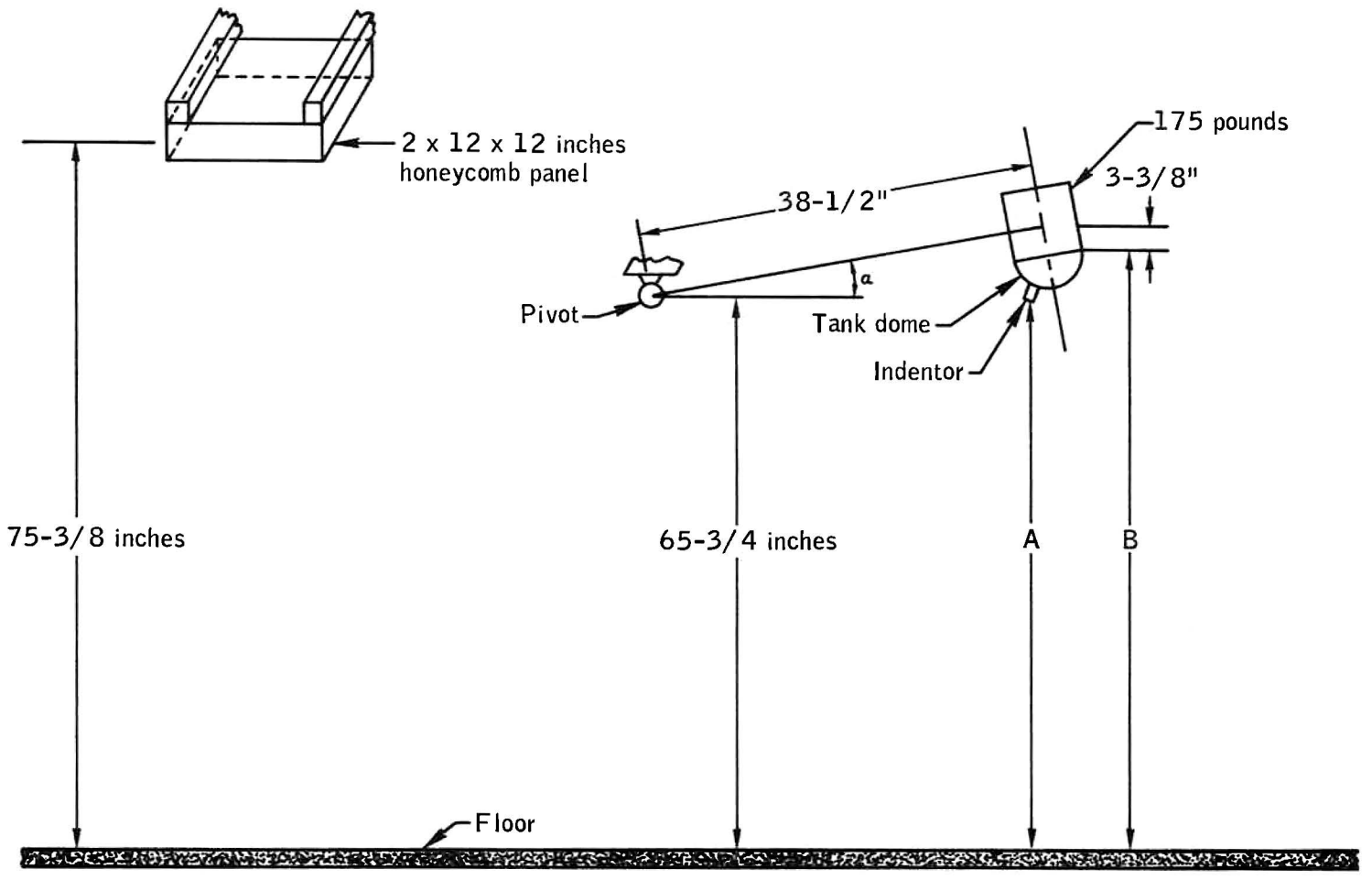

Figure B. 51-1.- Impact test setup.

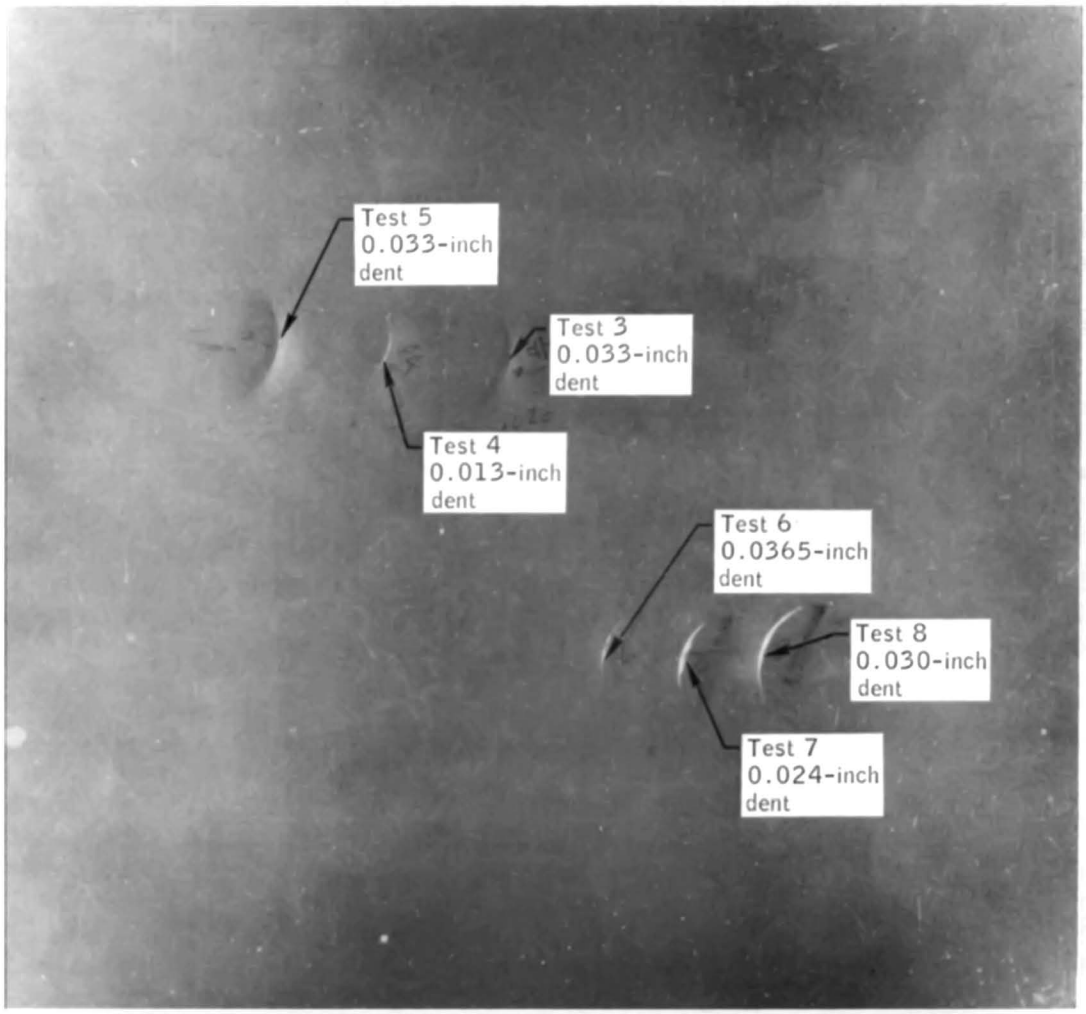

Figure B. 51-2.- Results of impact tests.

B.52 HIGH-TEMPERATURE AND PRESSURE OXYGEN IMPINGEMENT TESTS

B.52.1 OBJECTIVE

The purpose of this test series was to determine the impingement effects of high-temperature, high-pressure oxygen on the service module Mylar/Kapton insulation blankets. The tests were configured to simulate the rupture of the two-inch burst disk in the dome of cryogenic oxygen tank 2.

B.52.2 TEST EQUIPMENT AND CONDITIONS

The tests were conducted in two phases. The first phase investigated the ignition possibilities of Mylar/Kapton from direct impingement of high-temperature oxygen. The second phase investigated the ignition possibilities of Mylar insulation while subjected to the direct impingement of oxygen and burning Kapton.

High Temperature Oxygen Impingement (Phase I)

These tests were designed to investigate the possibility of igniting an aluminized Mylar/Kapton insulation panel while being subjected to the direct impingement of high-temperature oxygen. Three tests were conducted to represent the rupture of the tank-dome burst disk. Approximately one cubic foot of oxygen was preheated to a temperature of 1000° F and a final pressure of 80 psia. A quick-acting, pneumatically actuated valve released the hot oxygen which impinged on a two foot square insulation blanket consisting of 30 layers of aluminized Mylar sandwiched between two layers of aluminized Kapton (fig. B.52-1). This blanket was located 4 inches in front of and at an angle of 19 degrees to the 2-inch diameter nozzle which represented the tank-dome burst disk. The chamber in which this test was conducted was maintained at a vacuum during all tests.

In the third test in Phase I, a Nichrome igniter and a small quantity of Mylar were placed in the nozzle outlet downstream of the release valve. Before release of the high-temperature oxygen, the Mylar temperature was raised to the melting point by applying power to the Nichrome wire.

Burning Kapton Impingement (Phase II)

Three tests were performed to investigate the possibility of igniting a Mylar insulation blanket which was subjected to direct impingement of oxygen and burning Kapton insulation. The test set-up and conditions were similar to Phase I, except that in Phase II, the oxygen was not preheated and the pneumatic valve was replaced by a 2-inch rupture disk. A secondary supply of 1000-psia oxygen was added to maintain gas flow after the burst disk ruptured and the initial cubic foot of oxygen at 80 psia was expended. This condition simulated the opening of the oxygen tank dome and the subsequent continuous flow of gas from the main tank.

A Nichrome igniter and forty-one square feet of Kapton was placed inside the simulated tank dome. The tank was filled with oxygen to a pressure of 30 psia. Power was then applied to the Nichrome wire, causing the Kapton to ignite. This burning caused the tank pressure and temperature to rise very rapidly and rupture the burst disk, thus allowing the oxygen at 80 psia and burning Mylar to impinge upon the insulation blanket. This was immediately followed by the 1000 psia oxygen flowing through a one-half inch line. The design limit of the rupture disk used for these tests was 80 psia at 700° F.

B.52.3 RESULTS

During test 1, approximately one cubic foot of oxygen at 80 psia and 1000° F was released through a two-inch opening onto a service module insulation blanket. Neither high-speed movie coverage nor post-test inspection revealed any evidence of burning. Only minor tearing of the insulation blanket occurred as a result of the gas impingement.

The results of the second test of Phase I were the same as in test 1.

In test 3, a Nichrome wire with a small piece of Mylar insulation was installed downstream of the valve. The Mylar around the Nichrome was preheated to its melting point just before release of the high-temperature oxygen. There was no evidence of burning on the insulation blanket; however, there was a small deposit of melted Mylar which came from the igniter. Again, minor tearing of the insulation occurred as a result of the gas impingement (fig. B.52-2).

Phase II Tests

In test 1 of Phase II, a fire was initiated on 41 square feet of Kapton cut in small pieces and placed inside the simulated dome. The

fire caused the container pressure to rise and rupture the burst disk at 80 psia. A post-test inspection indicated that a substantial amount of burning or melting of the insulation blanket occurred; however, there was no sustained burning. High-speed movies showed momentary impingement of burning Kapton when the rupture disk burst.

Test 2 of Phase II, was a repeat of Test 1 and provided essentially the same results. One observation during this test which was not observed in the preceding test was that the fragments of Kapton and Mylar which were blown off the blanket continued to burn after the oxygen supply was terminated. The chamber pressure increased to 0.3 psia during the test.

During the third test of Phase II, the Kapton inside the simulated dome was ignited and within one-half second the rupture disk burst. Video coverage was lost immediately due to insulation material covering the camera. The pressure inside the test chamber rose to 0.5 psia during the test. Thermocouple data provided no evidence of any burning. A post-test inspection indicated some localized melting or burning of the insulation blanket. Extensive damage was done to the insulation by the high-pressure oxygen impingement (fig. B.52-3). High-speed motion pictures showed momentary impingement of a significant amount of burning material onto the insulation blanket (fig. B.52-4).

B.52.4 CONCLUSIONS

The results of these tests indicate that the Mylar insulation blankets are difficult to ignite by impingement of high-temperature oxygen alone or in conjunction with burning Kapton. Although the duration of flame impingement on the Phase II tests was very short (less than 30 milliseconds), the severity of the tests is indicated by photographic data.

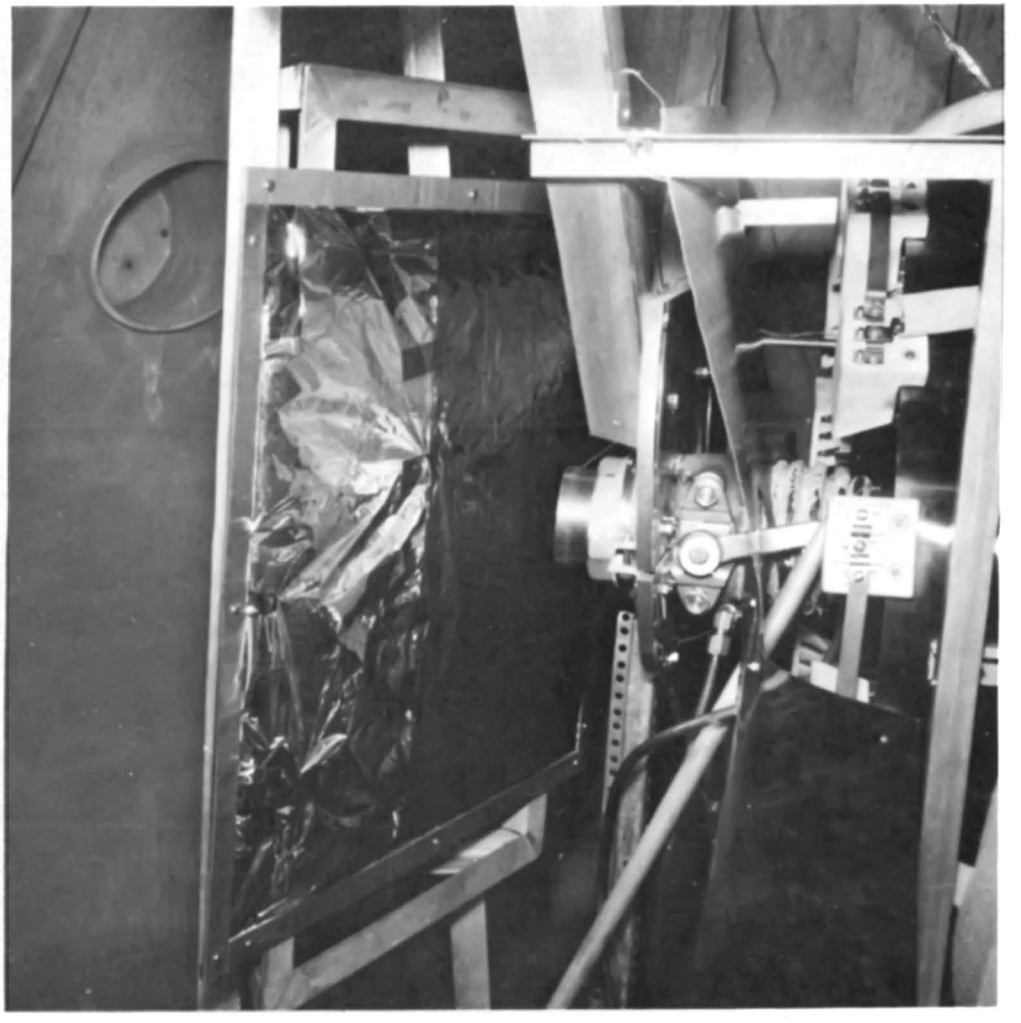

Figure B. 52-1.- Test setup for flowing oxygen at 1000 °F onto multilayer insulation.

Figure B. 52-2.- Tearing of insulation by 1000 °F stream of oxygen. No burning observed.

Figure B. 52-3.- Damage to multilayer insulation by impingement of oxygen stream.

B.53 SHOCK LOAD FAILURE TEST OF MOTOR ASSEMBLY SCREWS

B.53.1 OBJECTIVE

The purpose of this test was to determine the shock load required to fail the four 40 x 1/4-inch motor assembly machine screws.

B.53.2 TEST EQUIPMENT AND CONDITIONS

The tests were conducted at ambient temperature with material properties in critical areas approximating those of the Apollo structural configuration. The test equipment and machine screws are shown in figure B.53-1. The square plate was fabricated from 2024-T4 aluminum and had threaded holes for mounting a simulated equipment mass and mounting plate. The 4-40 x 1/4-inch machine screws used during the tests conform to MIL Spec MS35275.

Both static and dynamic tests were conducted to determine the load at which the machine screws would fail. In the first series of tests, four of the 4-40 x 1/4-inch screws, located at a radius and spacing representative of flight hardware, were statically loaded to failure. In the dynamic tests, the simulated mass and mounting screws were subjected to half-size g-loading of 1-1/2 to 2 milliseconds time duration (fig. B.53-2) at increasing g-levels until failure occurred. Since vibrations could possibly further loosen the screws, new machine screws were inserted and the g-level was then increased until tension failure in three of the four screws occurred.

B.53.3 RESULTS

The results of two static tests indicated that the screws began to yield near 2300 lbf total load (575 lbf per screw) and a complete tension failure occurred at 2950 lbf (735 lbf per screw). For an attached weight of 0.875 lb, the above loads would represent shock loads of 2600 g's and 3450 g's, respectively, for yielding of the screws and for complete tension failure.

Yielding of the machine screws was noted at loadings between 2000 and 2500 g's which is reasonably near the level (2600 g) predicted from the static test results. Although at this point the simulated mass was still restrained, the mounting plate was loose on the fixture and the screws could easily be removed by finger.

Figure B.53-3 presents a time-history of the half-sine shock pulse for which tension failure occurred. The "hash" on the acceleration pulse is indicative of a failure (compare to the clean signal of figure B.53-2). Additional tests also confirmed the 4000 to 4200 g-level for complete failure of the machine screws. The dynamic failure level of about 4000 to 4200 g's is within approximately 15-20 percent of the level predicted from the static data (3450 g's).

B.53.4 CONCLUSIONS

The four 4-40 x 1/4 inch machine screws started yielding between 2000 and 2500 g's and complete failure in tension occurred between 4000 and 4200 g's.

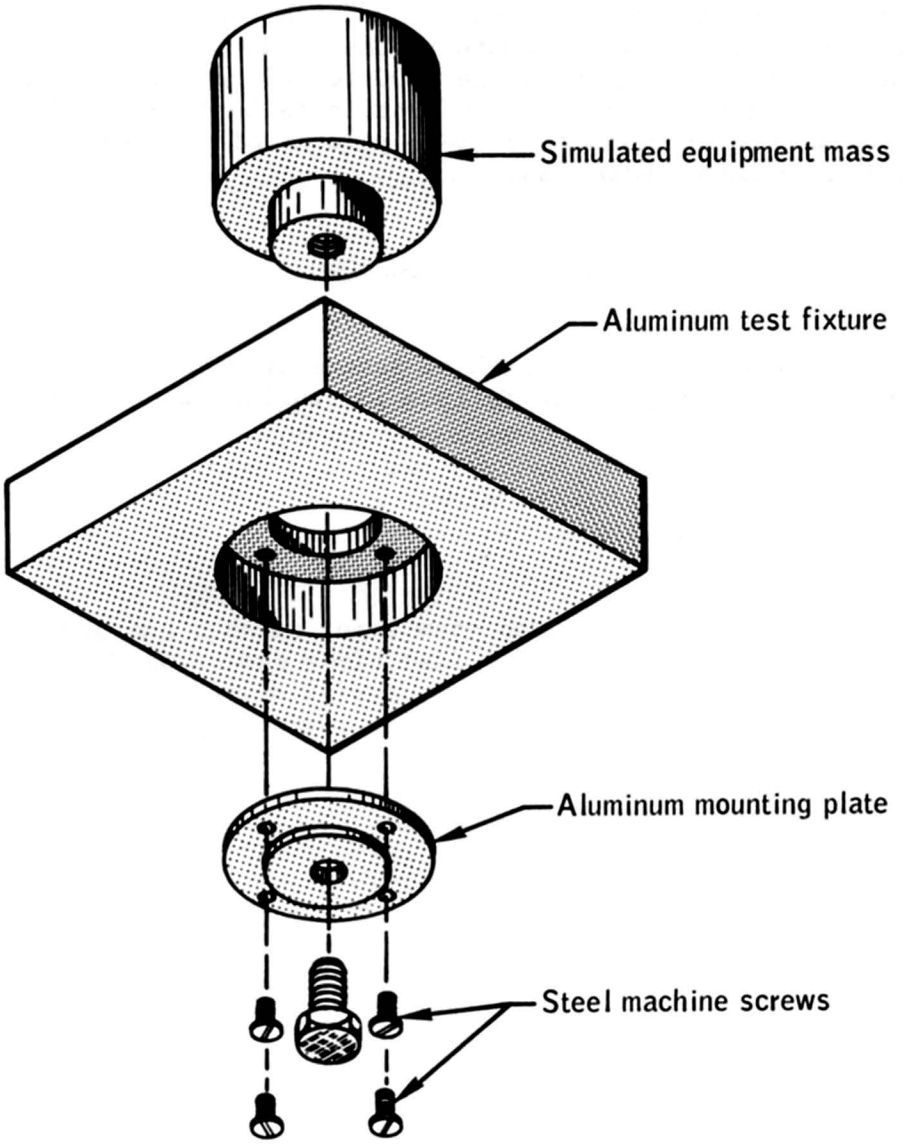

Figure B-53-1.- Exploded view of simulated equipment mass with mounting plate and mounting screws.

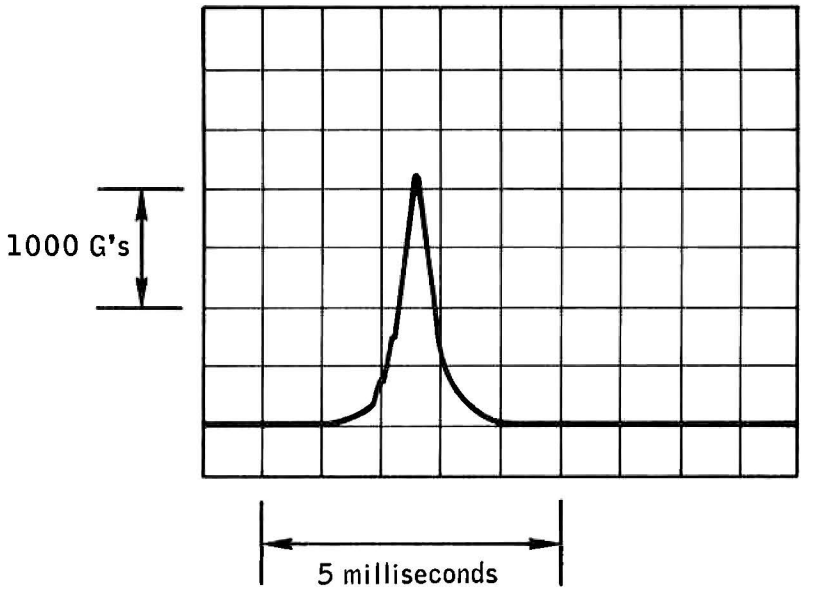

Figure B-53-2.- Typical half-sine acceleration pulse used during dynamic tests.

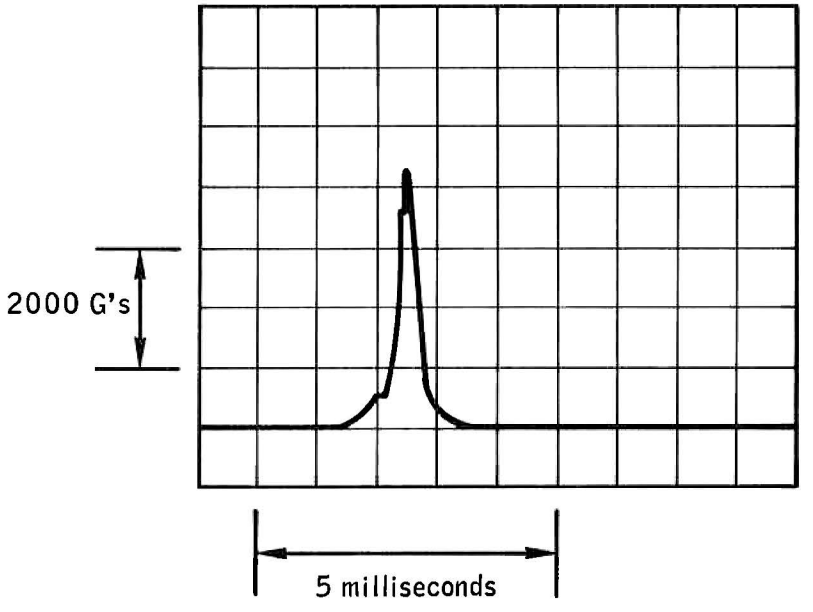

Figure B-53-3.- Half-sine acceleration pulse for which tension failure occurred in the mounting screws.

B.54 DETANKING HEATER ASSEMBLY TEMPERATURE PROFILE TEST

B.54.1 OBJECTIVE

This test was designed to simulate the cryogenic oxygen tank 2 detanking procedure which was performed during the countdown demonstration test. The objectives of the test were to determine the temperature profile along the heater probe assembly as well as determine the effects of increased temperatures on the wire insulation and other parts of the assembly.

B.54.2 TEST EQUIPMENT AND CONDITIONS

A cryogenic oxygen tank heater probe with a fan unit at each end was instrumented with temperature sensors and placed in a single-wall pressure vessel. The pressure vessel was maintained in a vacuum chamber at 75° F.

For the first test phase, the pressure vessel was filled with liquid nitrogen, and the heaters and fans were energized continuously maintaining a back pressure of 20 psi until the liquid nitrogen was depleted to a level below the lower fan motor. In addition, pressure and venting cycles were performed throughout the depletion period to determine their effect on the temperature profile. For the second test phase, the pressure vessel was filled half full with liquid nitrogen, the fan motors were run continuously and the heater power was controlled through the thermal switches.

The heater voltage was 75 V dc at 5.75 amperes for both phases of the test.

B.54.3 RESULTS

The maximum temperatures recorded during the first test phase were as follows:

a. Upper heater element sheath - 1010° F

b. Valley between heater sheath wraps - 895° F

c. Fan motor wire conduit - 735° F (not at the hottest location on the conduit)

d. Assembly near upper fan motor - 345° F

e. In gaseous nitrogen adjacent to upper fan motor - 214° F.

It was also found that the operation of the fan motors which operated continuously throughout the test, tended to keep temperatures lower and that the pressurization and venting cycles had little effect on the average temperatures.

Prior to the second phase, continuity checks verified the heater thermal switches to be functioning properly. However, after the second test phase was initiated, the thermal switches would not operate as required to remove the heater current. The test was terminated after the thermal switches were known to have failed closed. A post-test inspection showed the contacts on both thermal switches had welded closed (fig. B.54-1). Additionally, the insulation on the lower fan motor wiring was degraded (fig. B.54-2).

B.54.4 CONCLUSIONS

Temperatures were of sufficient magnitude to require thermal switch activation. The use of 75 V dc at 5.75 amperes welded the contacts of the switches closed. Section 55 details further testing of the thermal switch.

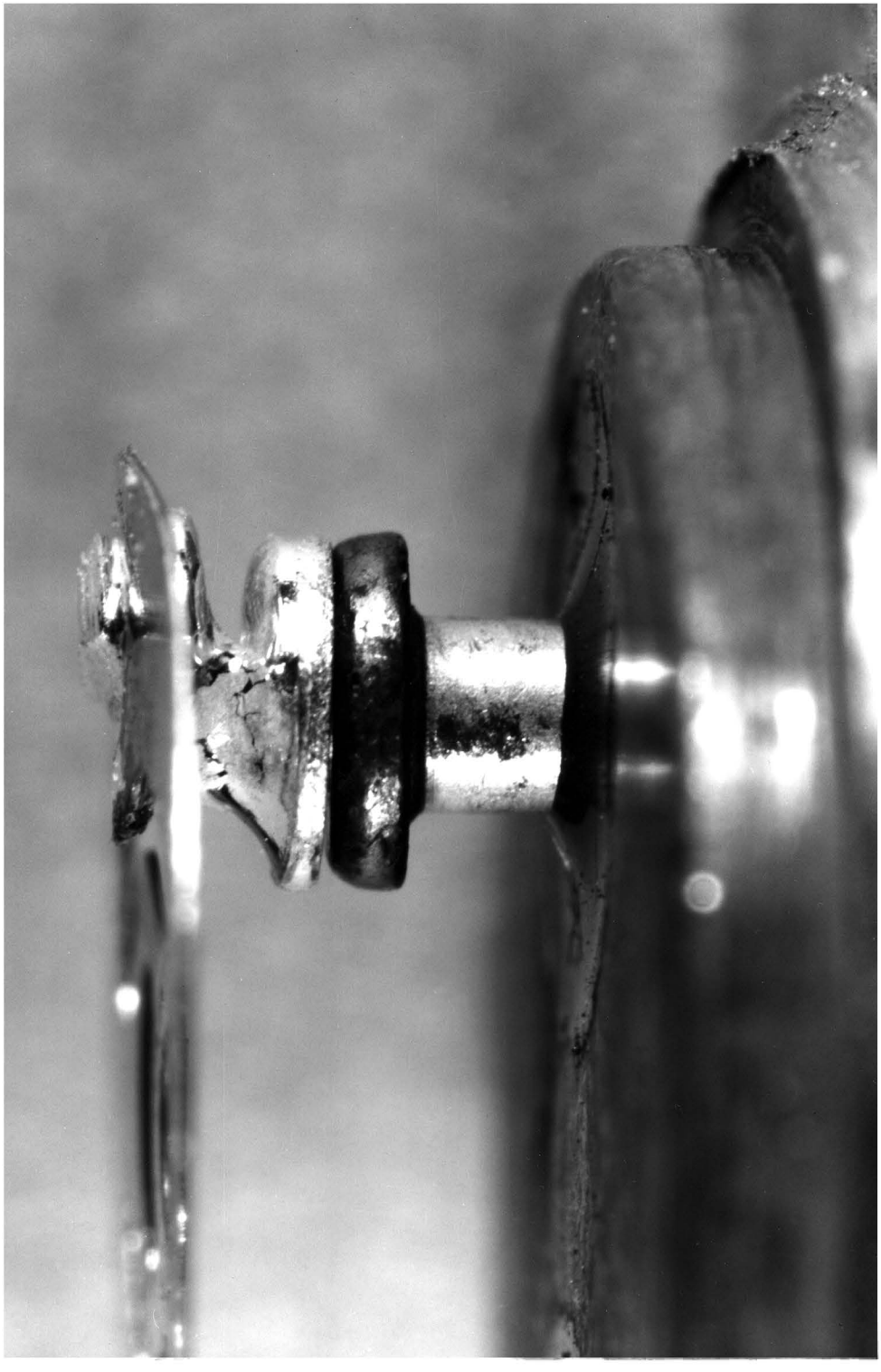

Figure B.54-1.- Welded switch contact.

Figure B.54-2.- Lower fan motor wire degradation.

B.55 HEATER SWITCH FAILURE TEST

B.55.1 OBJECTIVE

The objective of this test was to determine if the voltage-current profiles typical of those used at the launch site and on the spacecraft would overload the thermal switches.

B.55.2 TEST EQUIPMENT AND CONDITIONS

The switches were installed in the test stand shown in figure B.55-1. The test stand was capable of providing voltages of 30 to 65 V dc and 65 V ac at varying current levels.

B.55.3 RESULTS

The following table provides the results of the tests on the two switches:

Voltage	Current range	Remarks
	Switch no. 1	
31 V dc	1.0 to 3.5 amperes	Contact resistance increased from 15.5 to 62.0 milliohms
65 V dc	1.0 to 1.5 amperes	Contacts attempted to weld together at 1.25 amperes. Contacts welded together at 1.5 amperes (final resistance was 3.98 ohms)
	Switch no. 2	
65 V dc	1.0 to 8.0 amperes	Contact resistance increased from 24 milliohms to as much as 2.13 ohms
30 V dc	3.0 to 3.5 amperes	Switch contacts were showing tendencies to weld at 3.25 amperes. Post-test examination revealed appreciable contact pitting

B.55.4 CONCLUSIONS

The switches are not capable of operating with normal heater currents at 65 V dc. With the heaters operating at 65 V ac prior to flight, the switches may be sufficiently degraded to preclude reliable operation at normal spacecraft power levels (30 V dc) (fig. B.54-1).

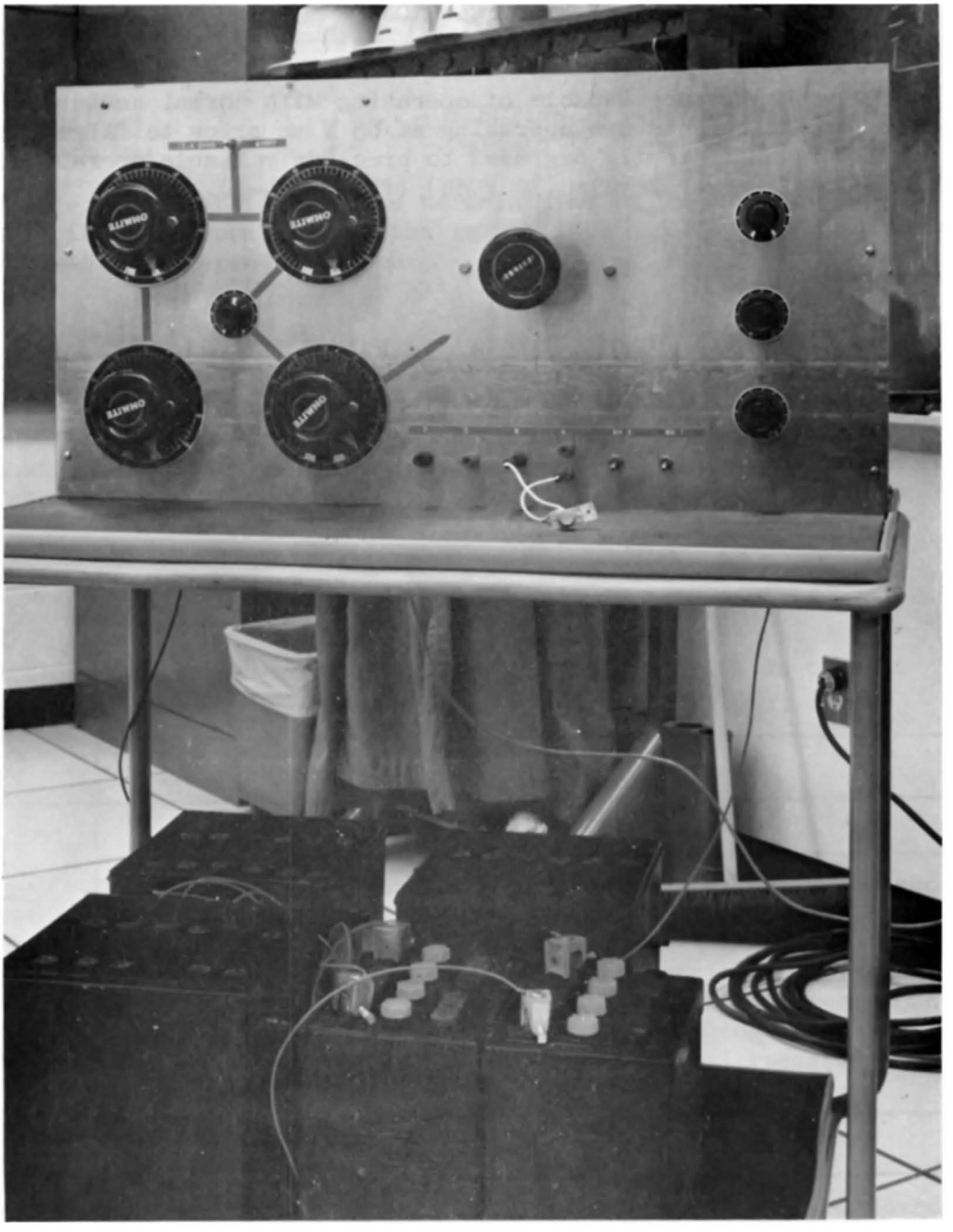

Figure B.55-1.- Electrical test fixture.

B.56 OXYGEN SYSTEM GAS SAMPLING AND ANALYSIS

B.56.1 OBJECTIVE

The objective of this test was to determine what contaminants were present in the residual gas of the 900-psi oxygen system.

B.56.2 PROCEDURE

All hardware directly involved in taking gas samples from the 900-psi oxygen system was cleaned in accordance with approved procedures. This included twelve 0.5-liter cylinders, six 4-liter cylinders, T-assemblies, and associated control valves. No lubricants were used except Teflon tape on pipe threads in the assembly of the valves and cylinders. All assemblies were checked with helium leak detection equipment. Each item was subject to background determination by infrared spectrophotometry, gas chromatography and mass spectrometry. The blanks accompanied the gas sample cylinders throughout the effort.

A practice run was conducted on spacecraft 108 to verify and establish sampling techniques, support equipment requirements, and provide training for personnel.

The gas sampling T-assembly was attached to repressurization package testpoint 27 which is downstream of the emergency breathing oxygen valve. The gas sampling cylinder was attached to the sampling leg; a new VOI-SHAN seal was used for each cylinder. The vacuum isolation valve leg was used to pump-down system/cylinder interfaces or to vent pressure prior to removing the gas sampling cylinder. The sampling setup, except for the vacuum pump, was in a helium-pressurized plastic tent with work access ports.

Gas sampling was accomplished as follows:

a. The T-assembly was evacuated to the gas cylinder and repress urization package interface.

b. The vacuum pump was isolated.

c. The 900-psi oxygen system was equalized by positioning:

1. Surge tank shutoff valve (4.26A) to "ON"

2. Repress urization package valve (4.34) was placed to "FILL"

d. Repress urization package valve was positioned to "OFF."

e. The indicated pressure on repress urization package gage and serial number on attached cylinder were recorded.

f. The gas sampling cylinder valve and emergency breathing oxygen valve were opened.

g. The gas sampling cylinder valve and emergency breathing oxygen valve were closed.

h. The T-assembly pressure was vented and the cylinder removed.

i. The 900-psi system pressure was equalized by positioning the repress urization package valve to "FILL."

The procedure was repeated for each of the 4-liter and 0.5-liter cylinders. Subsequently, an auxiliary pressure gage was installed at the bleed valve vent to verify residual system pressure. The 4-liter cyclinder was liquid-nitrogen chilled prior to drawing off the residual system pressure down to 20 psig as indicated on the repress urization package gage (40 psig on the auxiliary gage).

The 0.5-liter cylinders were used for gas chromatograph and mass spectrometer analyses where lower pressure and smaller volumes would not affect analysis. The gaseous-phase 4-liter cylinders were used for infrared spectrophotometric analyses due to larger volume and higher pressure requirements which could be attained by chill-down prior to introduction into the sample cell.

Prior to analyzing the spacecraft 109 samples, each of the involved laboratories was required to certify that a dry run of the entire procedure was completed with the 4.4-liter cyrogenic dewar obtained from Kennedy Space Center pad loading operations. The first available samples were subjected to a quick-look analysis by the spacecraft contractor. Samples were shipped to Manned Spacecraft Center, Kennedy Space Center, White Sands Test Facility and a subcontractor in Azusa, California for analysis by gas chromatograph, mass spectrometer, and infrared spectrophotometer. The cold-trap sample was subjected to rigorous analysis by North American Rockwell. All laboratories were requested to conserve gas sampling material and to return the sample cylinders to North American Rockwell, Downey, California, for possible contingency testing.

B.56.3 RESULTS

B.56.3.1 Spacecraft Contractor Analyses

The analyses conducted by the spacecraft contractor indicated that the material submitted by Kennedy Space Center from pad loading operations and removed from spacecraft 109 were within specification requirements with the exception of water (48 and 164 ppm with 3 ppm allowed) and carbon dioxide (1.9 ppm with 1.0 allowed).

No oxidative degradation products of polytetrafluoroethylene were found in spacecraft 109 samples. Xenon levels were similar to those found in the Kennedy Space Center sample. The Freon TF would be expected due to the free usage as a solvent during all phases of spacecraft manufacture.

Table B.56-I correlates the spacecraft contractor and subcontractor analyses of Kennedy Space Center and spacecraft 109 gas samples with the requirements of the launch operations fluid servicing specification. Purities were determined only for the spacecraft contractor analyses of the Kennedy Space Center and spacecraft 109 quick look samples. The spacecraft contractor rigorous analysis was based on material from the liquid-nitrogen chilled 4-liter cylinder and combines results from gas chromatograph and infrared analyses. The technique for mass spectrometer analysis of this cylinder would have consumed all of the gas and was not accomplished in order to retain material for contingency testing. Mass spectrometer analysis of 0.5-liter cylinder was comparable and had 164 ppm moisture and 1.9 ppm carbon dioxide with the quantified constituents within specification tolerance.

In addition, the subcontractor analyses (gas chromatograph, infrared spectrophotometer, and mass spectrometer) indicated the following:

Chemical properties	Contaminants, ppm	
	Oxygen from fill facility of launch site	Oxygen from spacecraft 109
Hydrogen	16	16
Helium	(a)	2600
Neon	64	(a)
Nitrogen	680	150
Argon	16	16
Krypton and Xenon	(a)	(a)
Freon	0.03	0.04
Halogenated hydrocarbons	(a)	<0.001

[a]Not detected

B.56.3.2 Kennedy Space Center Analyses

At the Kennedy Space Center, the oxygen samples were analyzed by mass spectrometric methods utilizing two sampling techniques.

a. Direct analysis of samples for contaminants greater than 10 ppm.

b. The pressurized samples were cryogenically trapped for the determination of contaminants less than 10 ppm.

The cryogenically trapped samples were also analyzed by gas chromatography for confirmation analysis.

The results shown in table B.56-II were obtained by the specification methods. All detected components are recorded. Water was not determined due to insufficient sample. The direct analysis of the samples showed no contaminants present greater than 10 ppm except as indicated.

Mass spectrometric results obtained by cryogenically trapping the samples are given in table B.56-III.

The gas chromatographic analysis of both samples confirmed the mass spectrometric results. Seven additional components were observed in spacecraft 109 oxygen that were not found in the oxygen from the launch site facility but could not be identified. The concentration of the unidentified components was found to be less than 5 ppm.

B.56.3.3 Manned Spacecraft Center Analysis

Table B.56-IV lists the contaminants detected during the analyses at the Manned Spacecraft Center.

B.56.3.4 White Sands Test Facility Analyses

The contaminants shown in table B.56-V were detected during the analyses at the White Sands Test Facility.

TABLE B.56-I.- ANALYSIS AT SPACECRAFT CONTRACTOR AND SUBCONTRACTOR

Characteristics	Grade A - fuel cell, requirement, ppm	Contaminants, ppm				
		Spacecraft Contractor Analyses			Subcontractor Analyses	
		Oxygen from fill facility at launch site	Oxygen from spacecraft 109		Oxygen from fill facility at launch site	Oxygen from spacecraft 109
			Quick look,	Rigorous,		
Purity (percent by volume)	(99.995)	(99.998)	(99.994	--	--	--
Methane	10.0	6.4	5.6	5.5	4.0	4.0
Ethane	2.0	<0.02	<0.02	<0.02	<1	<1
Propane	1.0	<0.1	0.2	0.7	<1	<1
Alkyne hydrocarbons	0.05	0.04	0.03	0.03	0.001	0.01
Total hydrocarbons	14.0	6.4	5.8	6.2	4.03	4.01
Moisture	3.0	5.5	48.0	--	1.1	0.8
Nitrous oxide	1.0	<1.0	<1.0	<1.0	(a)	(a)
Halogenated hydrocarbons	1.0	<0.1	0.08	<0.1	0.03	0.04
Odor	None	None	None	None	None	None
CO/CO_2 (total)	1.0	<1.0	1.0	<1.0	0.16	0.36

[a]Not detected

TABLE B.56-II.- ANALYSIS AT KENNEDY SPACE CENTER

FOR CONTAMINANTS GREATER THAN 10 PPM

Chemical properties	Oxygen from fill facility at launch site	Oxygen from spacecraft 109
CO	<1	<1
CO_2	<1	<1
Helium	<15	(≈0.14%)
Argon	8	11
Krypton	5	5
Nitrogen	11	114
Hydrocarbon as methane	8.2	6.1
Methane	7.8	5.2
Hydrocarbon as propane	<1	<1
C_2H_2	<0.05	<0.05
Ethane	0.3	<0.1
N_2O	<0.2	<0.5
Halogenated hydrocarbons	<0.1	<1
CF_4	<0.05	<0.1

[a]Trichloroethylene and 1,1,1-trichloroethane were detected but not quantized since they were <0.5 ppb.

[b]The chemistry of F_2 is such that it would not be expected in the gas phase even if it had originally been in the sample.

TABLE B.56-III.- ANALYSIS AT KENNEDY SPACE CENTER

FOR CONTAMINANTS LESS THAN 10 PPM

Chemical properties	Oxygen from fill facility at launch site	Oxygen from spacecraft 109
Freon 113	0.5	2.4
CS_2	<0.5	7.0
Trichloroethylene	[a]<0.5	0.7
1, 1, 1-trichloroethane	[a]<0.5	1.0
CF_4	<0.5	<0.5
COF_2	<0.5	<0.5
F_2	[b]<0.5	[b]<0.5
Other components found greater than 5 ppb	None	None

[a]Trichloroethylene and 1,1,1-trichloroethane were detected but were not quantized since they were <0.5 ppb.

[b]The chemistry of F_2 is such that it would not be expected in the gas phase even if it had originally been in the sample.

TABLE B.56-IV.- ANALYSIS AT MANNED SPACECRAFT CENTER

Chemical properties	Oxygen from fill facility at launch site, ppm	Oxygen from spacecraft 109[a], ppm
CO	[b]<15.0	[b]<15.0
CO_2	[b]<0.2	[b]<0.2
COF_2	[b]<15 to 150	[b]<15 to 150
CF_4	[b]<0.1	[b]<0.1
CH_4	7.4	5.5
C_2H_6	0.05	0.03
C_2H_4	[b]<0.003	[b]<0.003
C_2H_2	[b]<0.002	[b]<0.002
C_3H_8	[b]<0.008	[b]<0.008
N_2	20.4	202.0
Kr	5.7	1.8
Ar	4.6	9.6

[a]Helium was detected (approximately 0.6 percent) in the sample from the spacecraft surge tank. This finding is not considered significant since helium was used in preparing and cleaning the sample containers.

[b]Detection limit.

TABLE B.56-V.- ANALYSIS AT WHITE SANDS TEST FACILITY

Chemical properties	Oxygen from fill facility at launch site	Oxygen from spacecraft 109
Methane	4.9	2.7
Ethane	[a]<0.05	[a]<0.05
Acetylene	[a]<0.01	[a]<0.01
Ethylene	[a]<0.1	[a]<0.1
Higher hydrocarbons (propane and propylene)	[a]<0.1	[a]<0.1
Nitrous oxide (N_2O)	[a]<0.1	[a]<0.1
Carbon dioxide	0.1	0.1
Carbon monoxide	[a]<0.2	[a]<0.2
Nitrogen	[a]<0.2	60.6
Argon	3.8	5.7
Neon	[a]<2	[a]<2.0
Krypton	4.6	2.4
Hydrogen	[a]<0.2	[a]<0.2
Halocarbons[b]	<0.05	[a]<0.05
Cl_2 FC-CCl F_2 (Freon 113)		0.1

[a]Detection limit

[b]Includes the following materials which were used as standards during gas chromatograph method development:

CF_4 (Freon-14)
CHF_3 (Genetron-23),
F_3CCF_3 (Freon-116)
CCl_2F_2 (Freon-12)
$F_2C=CH_2$
$ClFC=CF_2$
$H_2C=CHCl$ (Vinyl Chloride)
$CClF_3$ (Freon-13)
CCl_2FCF_3
$Cl_2FC-CClF_2$ (Freon-113)

B.57 OXYGEN RELIEF VALVE FLOW TEST

B.57.1 OBJECTIVE

The objective of this test was to operate an oxygen relief valve at full flow at various gas temperatures to determine its flow characteristics.

B.57.2 TEST CONDITIONS AND PROCEDURES

Unless otherwise specified, all testing was conducted with temperature, relative humidity, and barometric pressure at ambient conditions.

Temperature stabilization was considered to have occurred when the temperature of the gas was consistent within ±5° F on two successive readings taken 10 seconds apart.

The test specimen relief valve was set up as shown in figure B.57-1, and tested in accordance with the following procedure.

a. The test specimen relief valve body temperature was stabilized at 70° (±10°) F.

b. Pressure in the vacuum chamber was reduced to less than 100 microns of mercury.

c. Heat exchanger no. 1 was conditioned for the temperature specified in the following table.

Run, no.	Gas temperature at relief valve, degrees F (±10° F)
1	Amb
2	-10
3	-100
4-5	+100
6-7	-140
8	+230
9	+350
10	+550
11	+670

d. The regulator was adjusted to indicate 1010 psia at the inlet to the relief valve.

e. Heat exchanger no. 1 was adjusted to the temperature specified.

f. The inlet pressure was increased until "crack" was obtained. This pressure was maintained until the relief valve inlet gas temperature stabilized.

g. The relief valve inlet pressure was then increased in 5-psi increments. Each pressure was held until the relief valve inlet gas temperature stabilized. The pressure steps were continued until the valve poppet was full open.

h. The relief valve inlet pressure was decreased to 900 psia, and reseat pressure was recorded. Inlet pressure was then increased until crack pressure was indicated.

B.57.3 RESULTS

The oxygen relief valve was operated (in a vacuum environment) with oxygen gas over a gas temperature range of 300° to 1160° R to determine its flow rate characteristics. The results are presented in figures B.57-2 through B.57-6. The flow rate generally follows a theoretical orifice curve (figure B.57-2). The test data were corrected to a base line inlet pressure of 1010 psia.

The effect of relief valve inlet pressure on flow rate is shown in figure B.57-3. Good agreement is demonstrated at normal operating temperatures. Deviations occur at the extreme temperatures with higher flow rates than predicted. The effect of modulating flow rate at pressures below maximum poppet opening is best illustrated at the 549° R gas temperature condition. A rapid rise in flow is obtained with small changes in pressure.

Crack and reseat pressure levels obtained at the various temperatures are shown in figure B.57-4. All nominal temperature points are within specified limits. Some extreme temperature points are slightly higher than the specified maximum.

The relief valve outlet gas temperature and the relief valve body temperature compared with inlet temperature are shown in figure B.57-5. A 50° R temperature drop was experienced through the relief valve. The body temperature was that obtained after about 15 minutes of gas flow through the valve. The relief valve outlet pressures experienced during the test are shown in figure B.57-6. They show that the relief valve orifice flow was sonic under all conditions.

B.57.5 CONCLUSIONS

Flow rate, crack, and reseat pressures were obtained for the oxygen relief valve over an inlet gas temperature range of 300° to 1160° R. Normal operating temperature characteristics were within specified limits. Extreme temperature operation deviated on the high side of projected flow and crack pressures.

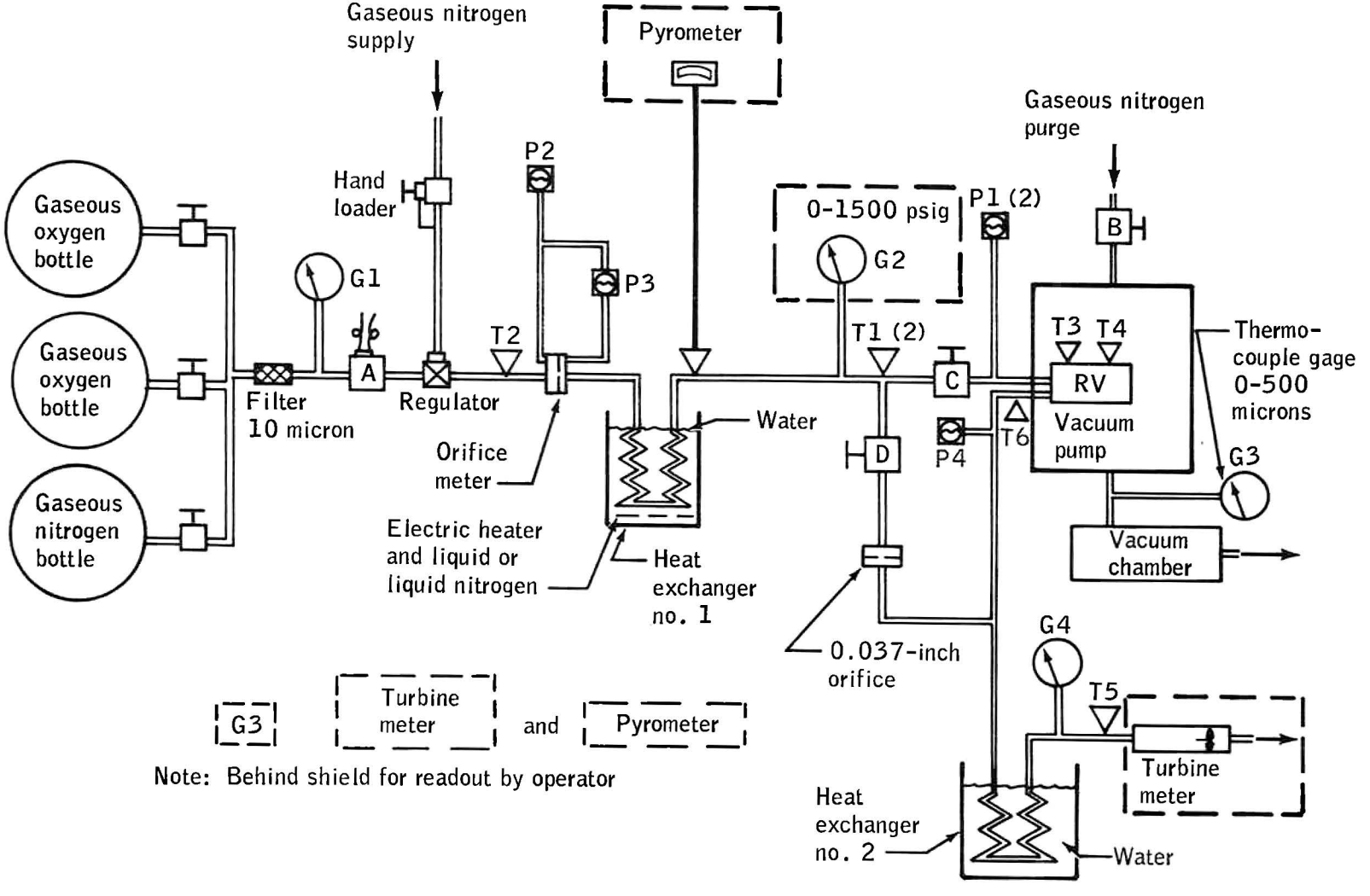

Note: Behind shield for readout by operator

Figure B.57-1.- Test setup - oxygen relief valve.

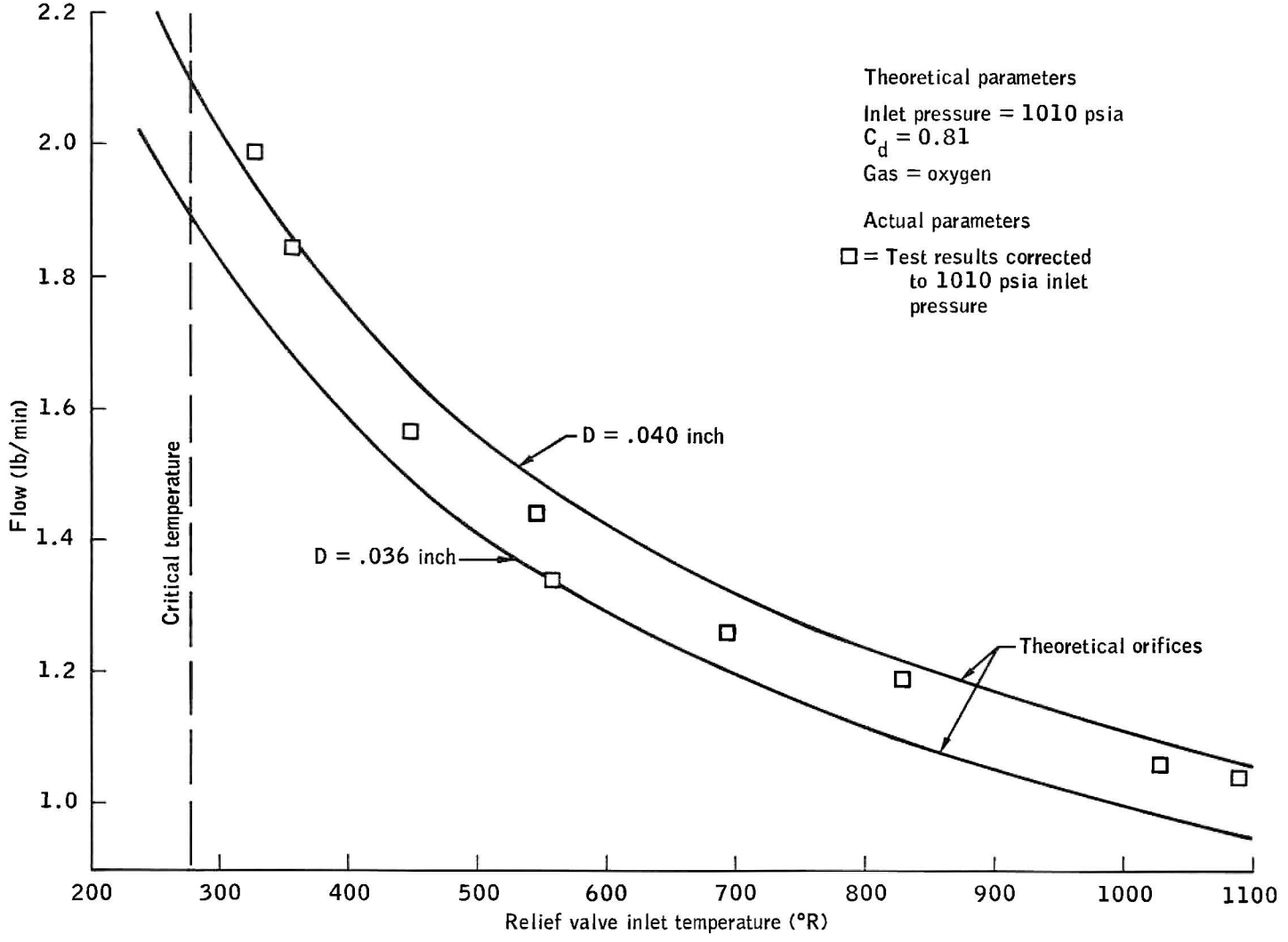

Figure B.57-2.- Inlet temperature versus flow.

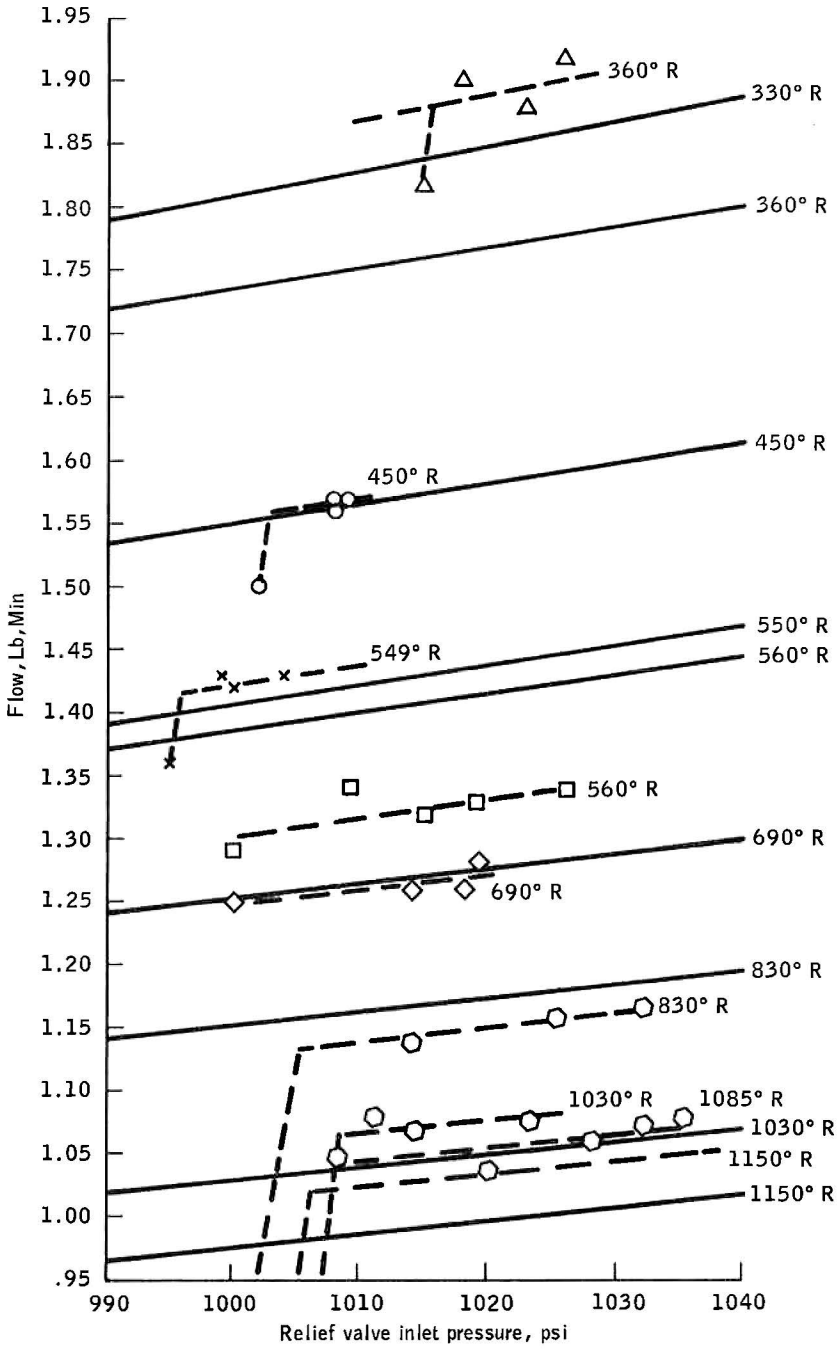

Figure B.57-3.- Effect of relief valve inlet pressure on flow rate.

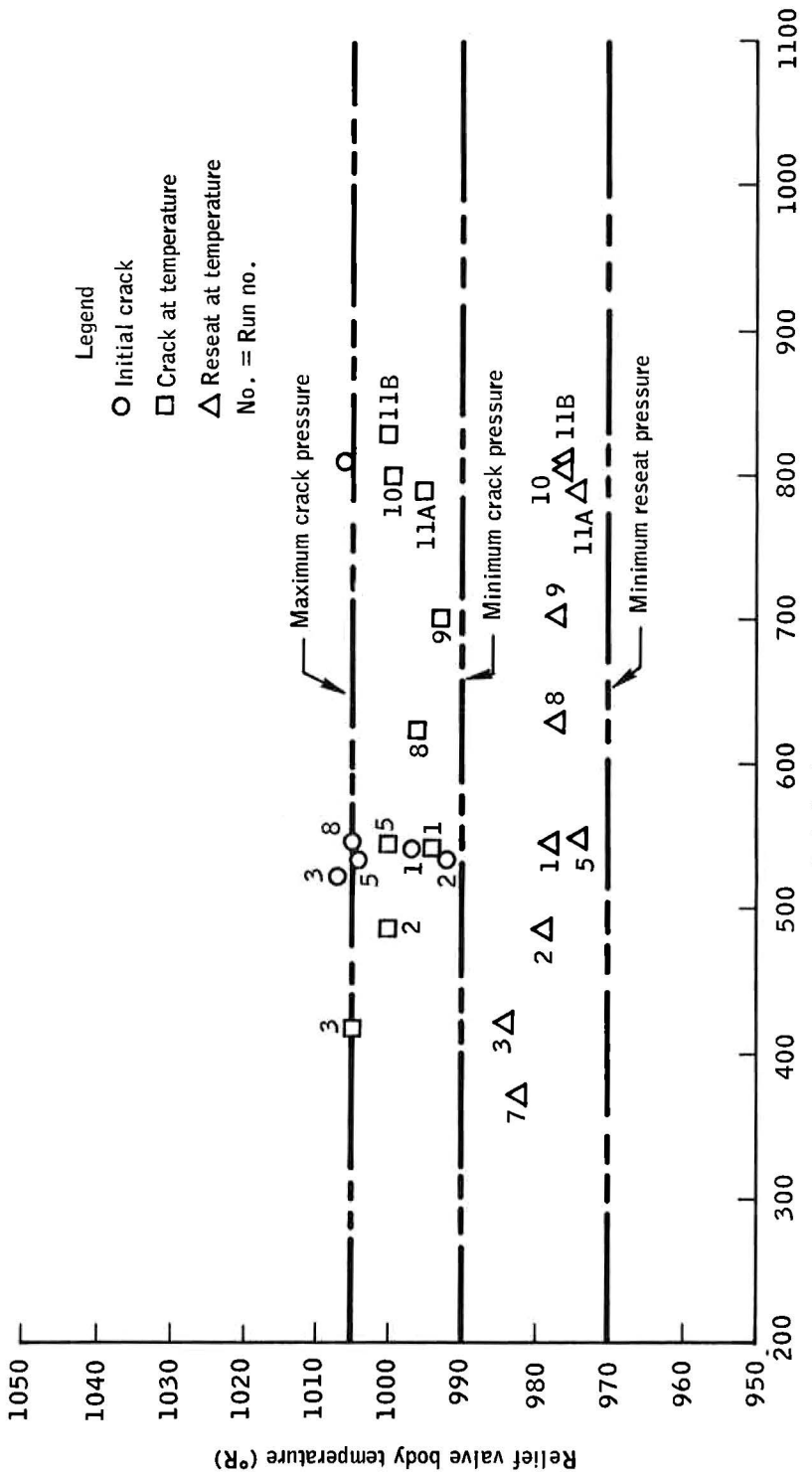

Figure B.57-4.- Crack and reseat pressure versus temperature.

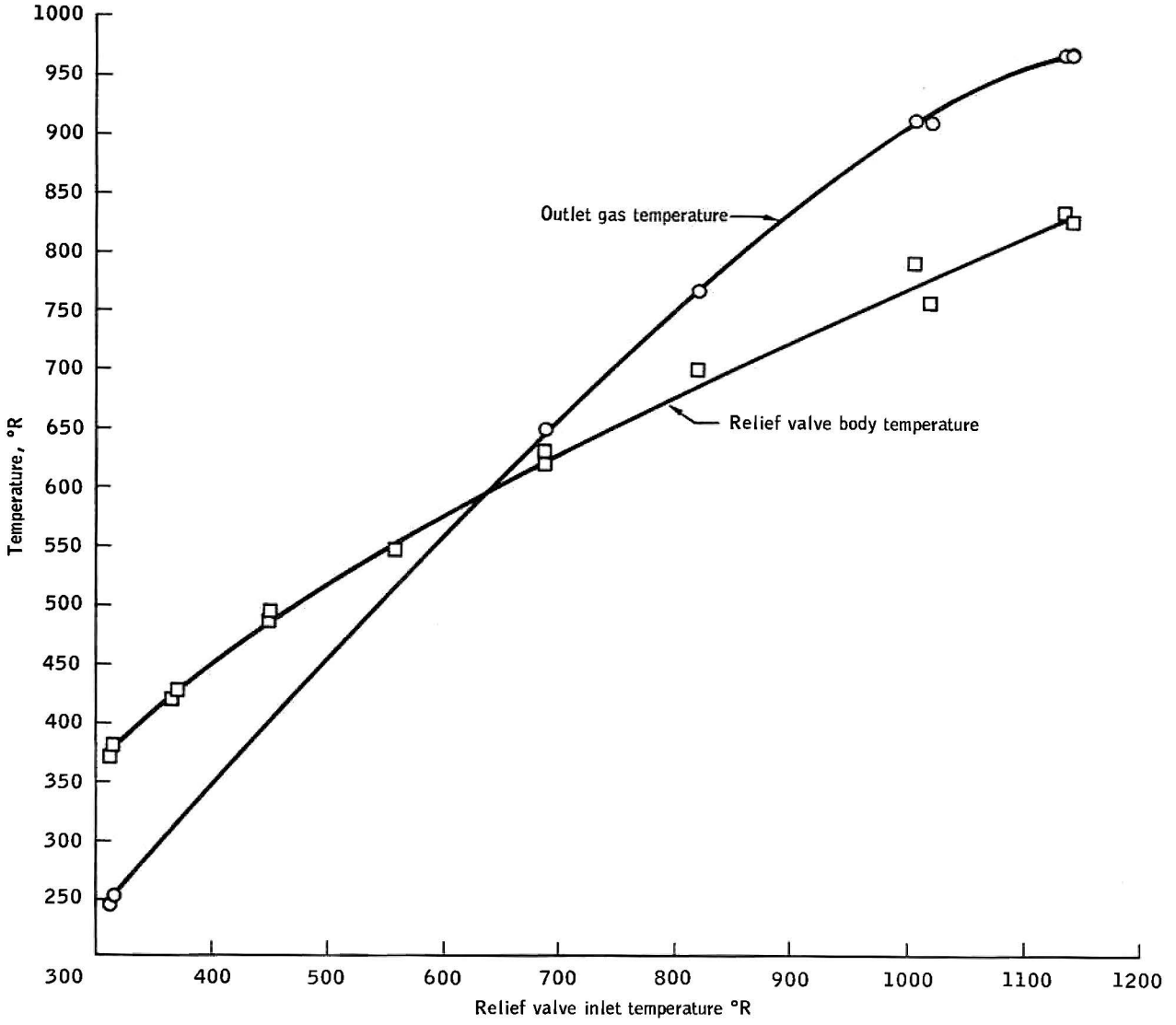

Figure B.57-5.- Inlet versus outlet and body temperature.

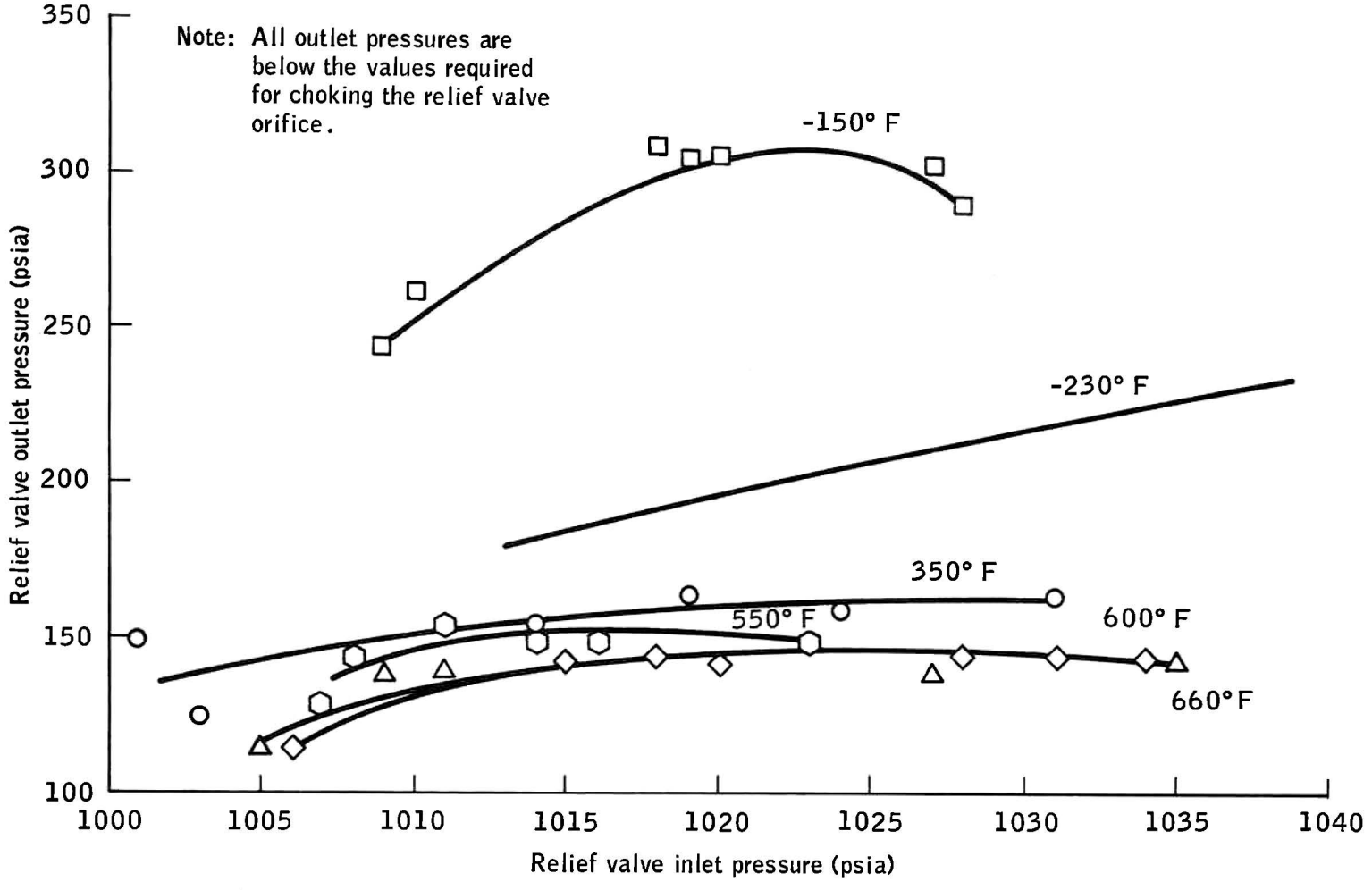

Figure B.57-6.- Inlet pressure versus outlet pressure.

B.58 DIFFERENTIAL THERMAL ANALYSIS OF MOTOR COMPONENTS

B.58.1 OBJECTIVE

The objective of this test was to perform a differential thermal analysis of aluminum and polytetrafluoroethylene in oxygen.

B.58.2 RESULTS

The energy released on reaction of aluminum and polytetrafluoroethylene in oxygen is 138 kilo calories/mole.

B.59 OXYGEN FILTER TEST

B.59.1 OBJECTIVE

The objective of this test was to determine if the pressure drop across the oxygen filter is affected in the presence of condensed particles of carbonyl fluoride from a polytetrafluoroethylene fire.

B.59.2 TEST CONDITIONS AND PROCEDURES

The oxygen filter was installed in a test setup as shown in figure B.59-1. A 6-foot length of polytetrafluoroethylene-insulated wire was multifolded and wrapped with a Nichrome wire igniter. The wiring was placed in chamber which was immersed in a liquid nitrogen bath. The chamber was pressurized to 900 psi and the oxygen flow through the chamber and filter was regulated to 6000 scc/min (1 pound per hour).

Voltage and current levels were gradually increased to 30 volts and 9 amperes at which ignition occurred.

B.59.3 RESULTS

The system pressure rose to 2600 psi before the solenoid valve opened. The pressure then dropped to 2180 psi for about 2 1/2 seconds at which time a fitting about 10 inches downstream of the filter burned out. This burning out resulted in an explosion to atmosphere with oxygen flowing for an additional 11 seconds before the test was terminated.

B.59.4 CONCLUSION

No pressure drop across the filter could be detected. It is doubtful that a significant drop could occur because of the almost complete consumption of the filter.

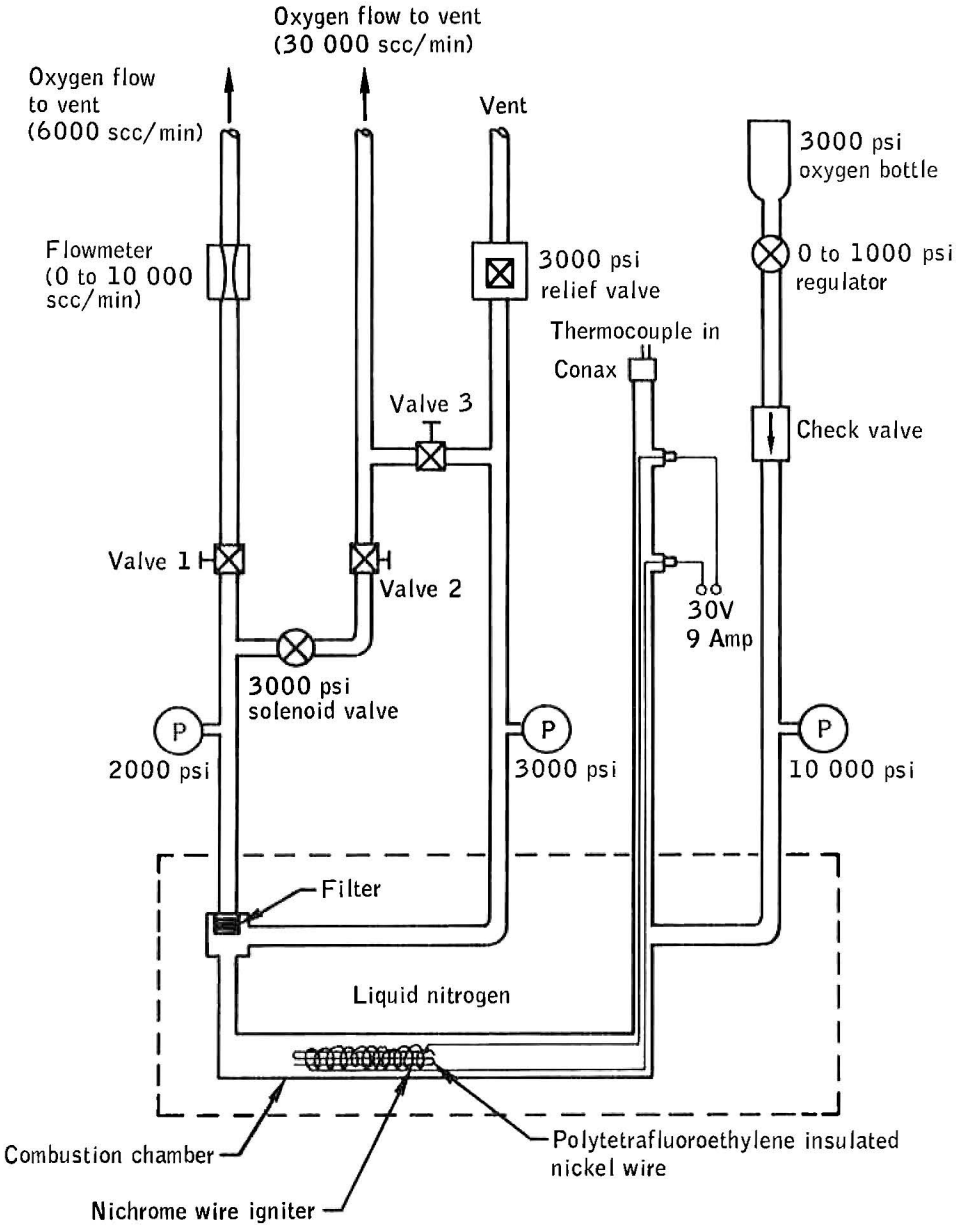

Figure B.59-1.- Filter-test setup schematic.

B.60 LIQUID OXYGEN-MYLAR VACUUM TANK COMBUSTION TESTS

B.60.1 OBJECTIVES

An objective of this series of tests was to determine the combustion rates of liquid oxygen-Mylar in a near-vacuum environment. The second objective was to determine if the release of combustion products from the oxygen tank 2 dome could act as an ignition source for the Mylar insulation in the oxygen tank 2 shelf area as well as on the bay 4 panel.

B.60.2 TEST EQUIPMENT AND CONDITIONS

In developing the test equipment for this test, the following considerations of the oxygen tank shelf geometry were respected:

The free-volume of shelf space, dome to outer panel spacing, spacing between dome top and fuel-cell shelf, and the internal dimensions of the dome. Also the blow-out plug diameter and its location on the dome top, as well as the 80-psi differential blow-out pressure were respected. From flow and thermodynamic considerations, it was essential to duplicate the supercritical conditions for the oxygen in the tank at the time of the anomaly, 900 to 1000 psia and -190° F. A tank size of 2/3-cubic foot was selected to be fabricated from 8-inch pipe with end bells. Flow rate with the restricted volume (and absence of possible "combustion-bubble" in tank) were maintained by flow of gaseous oxygen at tank pressure, but at ambient temperature, into the top of the tank. The estimated flow rate through a 1/2-inch sharp-edged orifice is 16 lbs/sec. Basic dimensions and arrangement of the apparatus are shown in figure B.60-1.

The procedures for the test were as follows:

a. Spray liquid oxygen from a tank at 900 psi and -190° F onto a 1 ft x 1-1/2 ft, 24-layer Mylar blanket, with multiple ignition sources provided at the blanket-surface. For the initial test, flow was about 1 lb/sec.

b. Increase flow-rates and blanket size if pressure-time histories indicated show faster and higher pressure rises as these two parameters increase.

c. If positive results are received in steps a and b, the sealed dome will be loaded with 76 gms of Kapton, a small liquid oxygen leak will be provided with a local ignition source inside the dome, and a 2-inch diaphragm with 80-psi burst pressure will be a part of the dome.

B.60.3 RESULTS

Seven test runs were completed. The results from each test run are discussed in the following paragraphs.

For test run 1, the 1/8-inch diameter orifice in the liquid oxygen line was used. This test provided little data since no liquid oxygen was flowing into the test volume and there was no combustion.

For the second test and all subsequent tests, the 1/2-inch diameter orifice was in the liquid oxygen line just ahead of the simulated dome. The second test run was the first to achieve combustion but data was not valuable because of a leak which developed as the temperature in the liquid oxygen tank was being brought up from its initial value of about -295° F. Rather than abort the run, it was initiated mainly to check ignition which was achieved in 4.84 seconds.

The third test was the first in which the liquid oxygen conditions were satisfactory and all systems operated properly with the exception that no ignition was achieved. This run proved necessary, however, to provide the no-combustion data, (a pressure-rise rate in the test volume of about 6.3 psi/sec is indicated).

For the fourth test, a leak developed as the liquid oxygen tank was being warmed up to -190° F. Thus, the liquid oxygen temperature and pressure were too low. There was a long delay in combustion after valve closing. The pyrofuse current records indicate a corresponding long delay in firing of the pyrofuse after current initiation; the delay is probably due to cooling of the pyrofuse by direct contact with liquid oxygen. A pressure-rise rate in the test volume of about 15 psi/sec was indicated at about 7.3 seconds.

After test 4 it was apparent that the dynamic forces from liquid oxygen flow and Mylar blanket motions on the pyrofuse wires were leading to their breaking before they could fire, thus all possible measures were taken of locate and protect the pyrofuses to minimize chances of their breaking. The results of the fifth test which was the first good test, showed the early ignition of the Mylar-blanket. A pressure rise rate of about 43.5 psi/sec was indicated - a value about seven times that for no combustion with about the same flow rate into the tank.

This sixth test was essentially a repeat of the fifth test with the addition, however, of small solid-fuel rocket motors to provide early and continuous ignition. This was to provide a further means of insuring combustion as soon as "conditions are ripe." A maximum pressure rise rate during combustion of 66 psi/sec was indicated.

For the last test, the large blow-out disc at the top of the test volume was set to lift off at atmospheric pressure, i.e., it sealed off the sub-atmospheric pressure in the tank but was not restrained against super-atmospheric tank pressure. Also, twice the amount of Mylar blanket was used. The data indicated ignition at about the same time as for tests 5 and 6, but a higher pressure rise rate was indicated early after ignition. The combustion was not able to sustain a tank pressure above atmospheric after the lid blew off (the exit diameter was 19 inches).

B.60.4 CONCLUSIONS

The Mylar blanket burns completely when blasted with liquid oxygen at initial conditions such as those that existed in Apollo 13 and locally ignited. The pressure rise rates are not explosive-like, but rather cover a period of several seconds to consume about a pound of the blanket while the pressure changes from, say, 10 psi to 50 psi. If the pressure-rise rates had been explosive-like over this pressure range, it might possibly be concluded that this combustion was the primary energy source for the panel blowoff. Since in the last of the tests where the pressure in the test tank was relieved by a blow-off disc, the pressure rise due to combustion could not be sustained (when such combustion was fed liquid oxygen from a one-half inch hole in the liquid oxygen tank), it must be concluded that the Mylar combustion external to the liquid oxygen could not have been the main source of energy for the panel blowoff.

B.61 CRACK GROWTH TESTS ON INCONEL WELDS WITH LONG CRACKS

B.61.1 OBJECTIVE

If a surface flaw approximately 3 inches or more in length had existed in the Apollo 13 cryogenic oxygen tank 2, the tank could have failed catastrophically, provided the flaw grew through the tank thickness during flight. The specific objective of this test was to determine the maximum flaw depth of a long flaw that would pass the 1276-psig tank pressurization before flight, and the maximum flaw growth that was possible subsequent to the 1276-psig pressurization.

B.61.2 TEST APPARATUS AND TEST PROCEDURE

The test specimens consisted of 12.5-inch wide, 22.5-inch long, and 0.125-inch thick flat panels of Inconel 718 that were electron beam welded with a weld schedule closely simulating that used on the Apollo cryogenic oxygen tanks. Sketches of the specimen configuration and welding procedure are shown in figure B.61-1. The weld schedule is listed in table B.61-I.

Large surface flaws were introduced into the specimens by omitting the full penetration pass over a four-inch distance in the center of the specimens. As shown by the photograph in figure B.61-2, omitting the full penetration pass resulted in a definite sharp-tip surface crack. The crack depth was varied by varying the depth of the partial penetration weld (pass 4), either by changing the voltage or weld speed.

The initial part of the program consisted of pulling panels in ambient temperature air to determine the maximum crack depth that would pass a 71.2 ksi gross area stress level. This stress level corresponds to a 1276 psig tank pressurization. After determining the critical crack depth at 71.2 ksi stress level, two panels were fabricated with slightly shallower crack depths and cyclic loaded. The cyclic loading corresponded to the stress history of the Apollo 13 tank including, and subsequent to, the 1276-psig proof test. Following this, the panels were pulled to failure, and the fracture surfaces studied for indications of fatigue crack growth.

B.61.3 RESULTS

The test results for all nine specimens tested are listed in Table B.61-2. Essentially, the results were that a four-inch long surface crack could not pass a 71.2 ksi proof test stress level if the crack was more than approximately half way through the thickness. Cracks that were shallow enough to pass the proof test did not show indications of fatigue growth during the subsequent cyclic testing. This can be determined from figure B.61-3 which shows the fracture face of specimen 6-A. This specimen had a typical fast fracture type of fracture surface, and no areas of fatigue growth were found.

The two specimens that passed the proof and cyclic load tests required a higher load than expected to cause crack pop-through when pulling to failure. This evidently was due to significant strain hardening of the annealed weld material. The initial proof test would have introduced preferential residual stresses and increased the toughness of the material at the crack tip.

B.61.4 CONCLUSIONS

The essential conclusion from the test program is that the Apollo 13 cryogenic oxygen tank could not have failed catastrophically from a long surface crack growing through the thickness in the girth weld area. Any surface flaw long and deep enough to become catastrophic during the flight could not have passed the proof test of the tank prior to flight. Any fatigue crack growth that occurred due to the known tank pressurization history after the 1276-psig proof test would have been insignificant.

TABLE B.61-I.- WELD SCHEDULE

Test specimens parameter	PASS 1 and 2*	PASS 3*	PASS 4	PASS 5*
Voltage, kV	80	115	**	85
Amperes, mA	1.5	6.0	4.0	3.2
Beam deflection, in.	0.012	.024 -	.040 -	0.110
Travel, in/min	18	18	**	18

Pass 4 specimen	Voltage, kV	Travel, in./min.
1	95	35
2	95	56
3	95	28
4*	95	18
1-A***	115	18
2-A***	105	18
5	115	18
6	105	18
6-A***	110	18

* Same schedule as used for Apollo 13 cryogenic oxygen tank.

** See Table 1b.

*** Specimens 1-A, 2-A, and 6-A were fabricated by shearing off 1/2 inch behind fracture face of Specimens 1, 2, and 6 respectively, and rewelding.

TABLE B.61-II.- SPECIMEN TEST RESULTS

Specimen number	Crack depth		Crack pop-through stress (KSI)	Panel failure stress (KSI)	Remarks
	Inches	% thickness			
1	0.103	81.0	68.2	82.5	Did not pass 71.2 KSI proof test
2	0.098	77.0	52.2	75.8	Did not pass 71.2 KSI proof test
3	0.087	68.5	63.0	78.3	Did not pass 71.2 KSI proof test
4*	0.081	63.8	66.5	76.0	Did not pass 71.2 KSI proof test
1-A	0.061	48.0	74.2	74.9	Passed 71.2 KSI proof test
2-A	0.068	53.5	68.2	70.0	Did not pass 71.2 KSI proof test
5	0.063	49.6	83.0	83.0	Fatigue loaded**, no crack growth occurred
6	0.074	58.3	70.8	77.0	Did not pass 71.2 KSI proof test
6-A	0.065	51.1	88.0	88.0	Fatigue loaded**, no crack growth occurred

* Specimen welded with same weld schedule as used for Apollo 13 cryogenic oxygen tank

** Specimen loaded at following stress levels and then pulled to failure to determine crack pot-through and failure stresses:

Number cycles	Minimum and maximum stress (KSI)	Temperature and environment
1	0 - 71.2	75° F Air
1	0 - 55.9	75° F Air
1	0 - 57.2	75° F Air
1	0 - 51.6	75° F Air
56	48.3 - 52.2	-320° F LN_2

B.62 PROPAGATION RATES OF BURNING POLYTETRAFLUOROETHYLENE IN SUPERCRITICAL OXYGEN

B.62.1 OBJECTIVE

The objective of this test series was to determine the propagation rate of burning polytetrafluoroethylene-insulated electrical wire as well as the associated pressure rise in a fixed volume under 1g conditions.

B.62.2 TEST EQUIPMENT AND CONDITIONS

A schematic of the overall test apparatus is shown in figure B.62-1. The test fixture (Crawford bomb) where the test specimens were contained is shown in figure B.62-2. In each of the three tests for this series, the burning was downward in the one environment.

In test 1, a wire bundle was fabricated from 4-26 gauge polytetrafluoroethylene-coated stranded nickel wires each 5-1/2 inches long to closely resemble the fan motor wires in oxygen tank 2. The wires were twisted together, alternating white and black colored wires, and fitted with a nichrome ignition wire (penetrating through a black wire) and two timing fuse wires (looped once around the same black wire) as illustrated in figure B.61-3. The wire bundle was mounted on the strand burning head and placed in the bomb. Ignition was at the top of the wire sample and burning progressed vertically downward. The bomb and associated piping were pressurized with approximately 2000 psi nitrogen as follows:

Test 2 was a repeat of test 1 to verify the data obtained. The same testing procedure was used as in test 1, and the test was conducted normally.

Test 3 was identical to the previous test with the exception that the twisted wire bundle was placed inside a tube 3/16 outside diameter, 0.016" wall, and 3" long to simulate the combustion of wires inside the oxygen tank heater tube conduit. Figure B.62-4 is a pretest photograph of the wires assembled in the tube. The test was conducted with the same procedure used in the previous test.

B.62.3 RESULTS

The results of test 1 showed a propagation rate of 0.19 in/sec and a pressure rise of 80 psi. The insulation burned cleanly from the wire and no residue was visible. A photograph of the wire is shown in figure B.62-5.

The results of test 2 showed a propagation rate of 0.25 in/sec and a pressure rise of 174 psi. The wire condition after the test was the same as after test 1 and no temperature discoloration could be noted.

The results of test 3 showed a propagation rate of 0.14 in/sec and a pressure rise of 153 psi. The wire had no insulation remaining (fig. B.62-6) and no residue could be found. The tube showed no temperature discoloration.

B.62.4 CONCLUSIONS

Tests of combustion of polytetrafluoroethylene-insulated wire bundles simulating the oxygen tank fan motor wiring in cryogenic oxygen indicate burning rates of 0.22 in/sec (average of two tests) when burning downward in an unrestricted configuration, and 0.14 in/sec (one test) when burning downward through a close fitting stainless steel conduit. Pressure rise measurements seemed to indicate rather complete mixing of combustion products with the oxygen in these one-g tests.

B.63 INVESTIGATION OF CRACK GROWTH THRESHOLD OF INCONEL 718 EXPOSED TO HIGH PRESSURE OXYGEN

B.63.1 OBJECTIVE

The primary objective was to determine whether there was a structural deficiency in the cryogenic oxygen tank which could have contributed to the Apollo 13 incident. The fracture and flaw growth characteristics of forging and EB welded Inconel 718 in an environment of high pressure oxygen were investigated.

B.63.2 TEST DESCRIPTION

The program consisted of testing tensile and surface flawed specimens of Inconel 718 as indicated below:

SPECIMENS TESTED

Environment	Tensiles	Static Fracture	Sustained	Load/ Unload	Cyclic	Sustained/ Cyclic
Air at 70° F	B[1] W[2]	B W			B	
Liquid oxygen at -190° F 1000 psi			B W			B W
Air gaseous nitrogen at -190° F	B W	B W	 W	B W	B W	
Liquid nitrogen at -320° F	B W	B W				

Notes: 1. B = Base metal specimens
2. W = Weldment specimens

Precracked surface flawed specimens were used for all fracture tests including static fracture, sustained load, cyclic, and combined sustained/cyclic load tests. Overall dimensions of the specimens were tailored to the size and shape of the hemispherical cryogenic oxygen tank forging from which specimen blanks were cut.

The weld specimens were electron beam welded in a vacuum using a 60 kV welding machine. The final machined thicknesses of the forging and weldment specimens, which were representative of actual tank wall thicknesses, were 0.059 and 0.111 inch respectively. After final machining, the welded specimens were radiographically inspected. These specimens did not receive any thermal treatment after receipt of the tank forging.

Surface flaws were introduced into the fracture specims by using an electric discharge machine to form a starter notch and then extending the notch by low stress/high cycle tension-tension fatigue. The fatigue extension was accomplished at a maximum gross stress of 40 ksi at 30 hertz. From 2000 to 36 000 cycles were required, depending upon the initial notch dimensions and whether the material was forging or weldment. All precracking was performed in air at room temperature.

All non-hazardous tests were conducted in an environmentally controlled laboratory. This includes all tensile, static fracture, sustained in air, and cycled in air specimens. Where temperatures other than 70° F were required, the environmental control system shown schematically in figure B.63-1 was used. By manual control of gaseous and liquid nitrogen supplies, any temperature between -320° F and 70° F was obtainable. All non-hazardous tests were conducted in a 120 000 pound universal testing machine with a master timing system programmer.

Dead load machines of 10 000 and 30 000 pounds capacity were used for the sustained and sustained/cyclic testing. The sustained/cyclic load profile was accomplished by automatically removing a certain portion of the dead weights for one-half hour and then replacing them for one-half hour.

The first sustained tests were conducted with specimens of flaw depths ranging from 50 to 85 percent of the thickness and loaded to either the operating or proof stress. These stresses were based on a spherically shaped vessel having a 25-inch diameter of the cryogenic oxygen tank. Some of the higher stressed/deeper flawed specimens grew through-the-thickness upon loading and were then unloaded, but generally, the specimens were held at a constant load for about 20 hours. After unloading, the specimens were low-stress cycled in air to mark the flaw front and then pulled to failure. Evidence of growth was then observed by a separation between the initial fatigue crack extension and that of final marking. Depending on whether flaw growth was observed, the next

group of specimens were loaded to lower or higher stress levels. In addition to determining the combinations of stress and flaw depth which caused growth and those which did not, it became necessary to separate growth-on-loading from environmental/time dependent growth. This was accomplished by loading specimens to predetermined stress levels and then immediately dropping the load to zero and observing the fracture face for growth after marking and failing the specimen.

Cyclic flaw growth tests were conducted with a sinusoidal-shaped loading profile whereas the sustained/cyclic tests were performed using the square-wave loading profile. Sustained/cyclic tests were conducted to determine what effect, if any, a high-stress ratio had on flaw growth as compared directly to sustain loaded specimens.

B.63.3 RESULTS

Fracture Tests

Static fracture tests of the Inconel 718 forging and weldment material were conducted in air at 70° F, in air/gaseous nitrogen at -190° F and in liquid nitrogen at -320° F. The weldment specimens either had flaws located in the centerline or in the heat affected zone. The specimens tested at 70° F were visually observed to have the flaws extend through-the-thickness prior to failure in plane stress as a through-the-thickness crack. This condition also existed for the weldments tested at -190° F based on the results of several intended sustain loaded specimens which had flaws that grew through-the-thickness upon reaching maximum load. Based on these data it is assumed that all of the static fracture specimens having very deep flaws (>70 percent of the thickness) did not fail in plane strain but had significant flaw extension prior to failure, to the point of growing through-the-thickness.

Sustained Load and Growth on Loading Tests

Inconel 718 forging and weldment specimens were sustain loaded in liquid oxygen at -190° F and 1000 psi for a minimum of 20 hours. Flaw growth was observed in both the forging and weldment materials for particular combinations of stress and flaw depth, but because of the growth through-the-thickness observed with the static fracture specimens additional tests were conducted to separate time dependent, sustained load flaw growth from growth-on-loading. Key specimens that showed flaw growth after being sustain loaded for a minimum of 20 hours were duplicated with specimens of similar depth flaws and loaded to the same stress level and then immediately unloaded. The load/unload specimen tests were conducted in an air/gaseous nitrogen environment at -190° F. These specimens indicated as much growth as the specimens they duplicated, thereby

proving that what was observed as growth in the sustained specimens was indeed growth occurring during loading the specimen and not environmentally induced.

In summary, within the range of stress levels and flaw sizes tested, the high pressure oxygen environment at -190° F and 1000 psi did not promote flaw growth of Inconel 718 forging or weldment material.

Sustained/Cyclic Tests

Sustained/cyclic tests were conducted to simulate actual in-flight pressure conditions within the cryogenic oxygen tank. The cyclic rate of 1 cycle per hour was slightly higher than the actual rate experienced with the Apollo 13 tank. These tests were intended to determine if high flaw growth rates existed with Inconel 718 in an oxygen environment at high minimum to maximum stress ratios (R = 0.95). For the tests performed at maximum stress levels and flaw sizes below the no flaw growth-on-loading curves, the results showed that flaw growth was less than 0.001 inch, even after 55.5 cycles (55.5 hours). Specimens tested above the growth-on-loading curves, exhibited flaw growth on the same order of magnitude as that observed for the growth-on-loading specimens.

Based on these test results, it appears that sustained/cyclic flaw growth rates at high R values (0.950) with Inconel 718 in oxygen are essentially zero.

Special Flaw Growth Tests

Several special tests were conducted to determine the amount of flaw growth produced by cycling Inconel 718 specimens at high R values (0.950) for 15 000 cycles. The tests were conducted in an air/gaseous nitrogen environment at -190° F. These results, along with those of the sustained/cyclic tests, indicate that essentially zero flaw growth rates are obtained when Inconel 718 is subjected to high R value (0.950) cycles and stress levels below proof in either high pressure oxygen or air/gaseous nitrogen at -190° F.

B.63.4 OBSERVATIONS AND CONCLUSIONS

The following major observations were made from the study conducted:

1. The probable failure mode in the cryogenic oxygen tank is leakage at both proof and operating stress levels.

2. No environmentally induced subcritical flaw growth was observed in testing Inconel 718 in an high pressure oxygen environment.

3. Cyclic flaw growth rates at stress levels and stress ratios applicable to the cryogenic oxygen tank (R = 0.95) are essentially zero.

From these observations the following conclusions were arrived at relative to the Apollo 13 cryogenic oxygen tank:

1. No catastrophic brittle failure occurred.

2. Flaw growth through-the-thickness during flight to produce leakage or a subsequent ductile failure is only a very remote possibility.

Therefore, the cryogenic oxygen pressure vessel material was not directly responsible for the Apollo 13 incident.

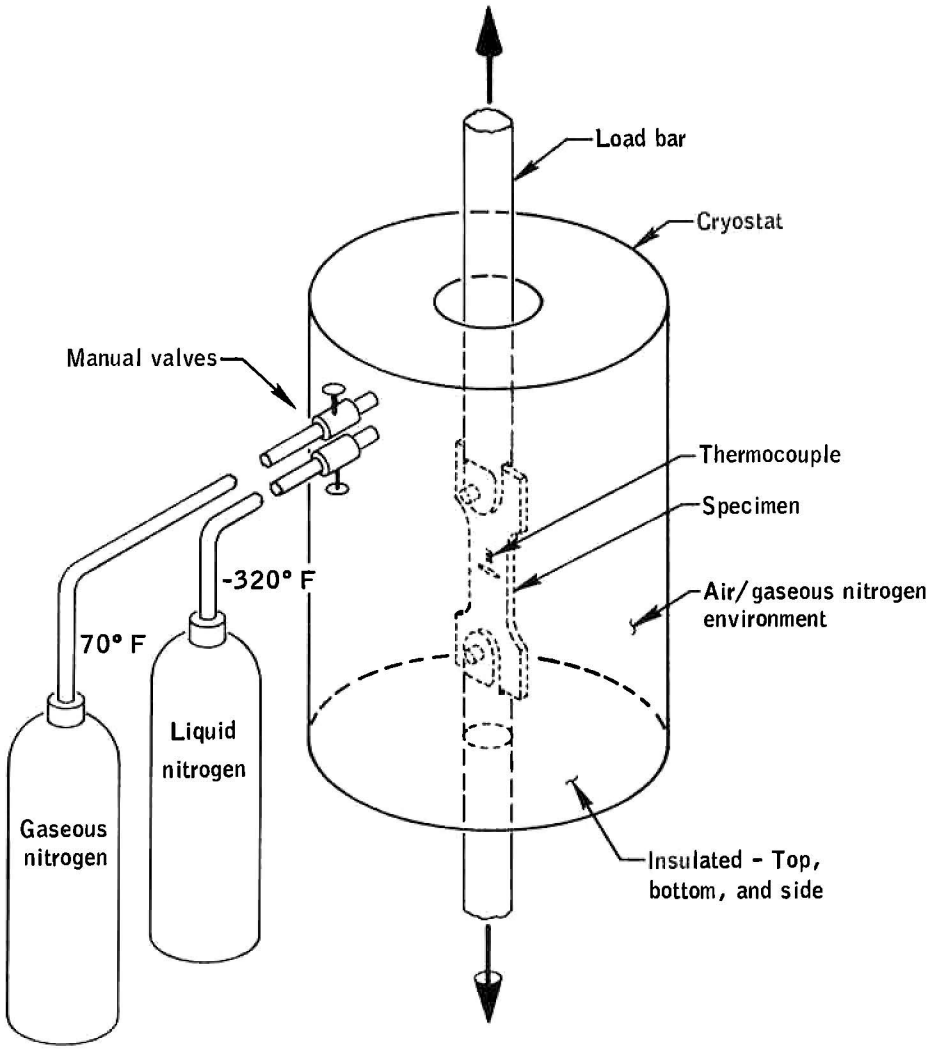

Figure B.63-1.- Environmental temperature control system for non-hazardous tests.